Agenzia nazionale per le nuove tecnologie,
l'energia e lo sviluppo economico sostenibile

MINISTERO DELLO SVILUPPO ECONOMICO



Raccolta delle Lecture del Workshop Tematico "LFR-Gen IV: Stato attuale della tecnologia e prospettive di sviluppo"

Daniele Martelli

Report RdS/PAR2016/069

RACCOLTA DELLE LECTURE DEL WORKSHOP TEMATICO “LFR-GEN IV: STATO ATTUALE DELLA TECNOLOGIA E PROSPETTIVE DI SVILUPPO”

Daniele Martelli (ENEA)

Settembre 2017

Report Ricerca di Sistema Elettrico

Accordo di Programma Ministero dello Sviluppo Economico - ENEA
Piano Annuale di Realizzazione 2016
Area: Generazione di Energia Elettrica con Basse Emissioni di Carbonio
Progetto: Sviluppo competenze scientifiche nel campo della sicurezza nucleare e collaborazione ai programmi internazionali per il nucleare di IV Generazione.
Linea: Collaborazione ai programmi internazionali per il nucleare di IV Generazione
Obiettivo: Comunicazione e diffusione dei risultati
Responsabile del Progetto: Mariano Tarantino, ENEA

Titolo

Workshop Tematico Accordo di Programma MiSE – ENEA

PAR2016 – Progetto B.3.1. LP2

LFR-GEN IV Stato attuale della tecnologia e prospettive di sviluppo

Descrittori

Tipologia del documento: **Rapporto Tecnico**

Collocazione contrattuale: Accordo di programma ENEA-MSE su sicurezza nucleare e reattori di IV generazione

Argomenti trattati: Generation IV reactors, Tecnologia dei metalli liquidi

Sommario

Presso l'Aula Magna della scuola di Ingegneria e Architettura dell'Università di Bologna si è tenuto dal 26 al 27 settembre 2017, un Workshop tematico dal titolo "LFR-GEN IV STATO ATTUALE DELLA TECNOLOGIA E PROSPETTIVE DI SVILUPPO", organizzato da ENEA in collaborazione con le principali università italiane che svolgono attività di ricerca in campo nucleare. Il Workshop, promosso nell'ambito delle attività inerenti la Linea Progettuale 2 "Collaborazione internazionale per il nucleare di IV generazione" dell' AdP MSE-ENEA, assume il duplice obiettivo di condividere lo stato dell'arte dei sistemi LFR tra gli stakeholder italiani definendo al contempo, in maniera condivisa e sinergica con il contesto Europeo, le linee di intervento future in ambito LFR.

Note

Autori: D. Martelli

Copia n. **In carico a:**

2			**NOME**			
			FIRMA			
1			**NOME**			
			FIRMA			
0	**EMISSIONE**	**21/12/2017**	**NOME**	D. Martelli	M. Tarantino	M. Tarantino
			FIRMA			
REV.	**DESCRIZIONE**	**DATA**		**REDAZIONE**	**CONVALIDA**	**APPROVAZIONE**

LIST OF REVISIONS

Revision	Date	Scope of revision	Page
0	21/12/2017	First issue	657

LIST OF CONTENTS

List of Revisions..... 2

1 LFR-GEN IV Stato attuale della tecnologia e prospettive di sviluppo..... 4

2 ALLEGATI..... 6

1 LFR-GEN IV STATO ATTUALE DELLA TECNOLOGIA E PROSPETTIVE DI SVILUPPO

Dal 26 al 27settembre 2017, presso l'Aula Magna della scuola di Ingegneria e Architettura dell'Università di Bologna, si è tenuto il Workshop tematico dal titolo "LFR-GEN IV STATO ATTUALE DELLA TECNOLOGIA E PROSPETTIVE DI SVILUPPO", organizzato da ENEA in collaborazione con le principali università italiane che svolgono attività di ricerca in campo nucleare.

Il Workshop, promosso nell'ambito delle attività inerenti la Linea Progettuale 2 "Collaborazione internazionale per il nucleare di IV generazione" dell' AdP MSE-ENEA, è stato finalizzato ad:

- Analizzare lo stato progettuale della tecnologia dei sistemi LFR partendo dal lavoro svolto in ambito ADP;
- la programmazione delle attività future, definendo le priorità di intervento in ambito italiano in maniera che siano sinergiche al contesto europeo ed internazionale (la Cina sta entrando prepotentemente nel settore)*;*
- armonizzazione le strategie di sviluppo mediante l'incontro di tutti gli stakeholder italiani.



Fig. 1: Ingresso della scuola di Ingegneria e Architettura Bologna

L'Italia, grazie all'ENEA, ANSALDO NUCLEARE e con il contributo fondamentale del CIRTEN, continua a conservare la leadership internazionale sulla progettazione e sullo sviluppo tecnologico dei sistemi LFR, nonostante il sempre più ampio interesse (accompagnato da ingenti investimenti economici) di altri Paesi quali ad esempio la Cina.

Ciò è stato possibile grazie ai continui sforzi fatti da ENEA (che ha sfruttato efficacemente i fondi dell'ADP), sia per accrescere e migliorare le proprie infrastrutture di ricerca (Brasimone e Casaccia), sia per rafforzare le proprie capacità e competenze sulla progettazione dei sistemi nucleari innovativi. (es. gruppo core design di Bologna).

Tutto ciò è stato fatto sinergicamente con ANSALDO NUCLEARE - capofila del progetto – e progettista del Dimostratore ALFRED.

Questi continui sforzi hanno portato all'istituzione del Consorzio Internazionale FALCON (costituito da ANN, ENEA, ICN e CV-REZ e il Consorzio Interuniversitario Italiano), che ha permesso in breve tempo di accrescere la rilevanza internazionale del progetto LFR, di individuare un sito per il DEMO, di coinvolgere un sempre maggior numero di istituti di ricerca europei (es KIT – Germania, GRS – Germania, CRS4 – Sardegna, IIT – Milano), di individuare i possibili canali di finanziamento (fondi ERDF – European Regional Development Fund con il supporto del governo romeno).

Il sistema Italia deve continuare ad investire nel settore, a focalizzare gli sforzi, evitando di disperdere risorse (il progetto di riferimento è ALFRED), cercando di sensibilizzare le istituzioni e coinvolgendo il maggior numero possibile di istituti di ricerca e industrie del settore.

I lavori sono iniziati con i saluti e la presentazione del workshop da parte del Prof. Antonio Peretto direttore del dipartimento di Ingegneria Industriale dell'Università di Bologna. A seguire sono state delineate nel dettaglio le strategie di intervento e sviluppo dal Dr. Mariano Tarantino, Responsabile Divisione Ingegneria Sperimentale Dipartimento Fusione e Tecnologie per la sicurezza Nucleare del Brasimone, attualmente uno dei più vasti ed attrezzati parco impianti a livello internazionale sulla tecnologia dei metalli liquidi pesanti.

Facenti parte del comitato organizzatore troviamo il Dr. M. Tarantino, il Dr. A. Del Nevo il Dr. I. Di Piazza ricercatori FSN-ING ENEA Brasimone ed infine il Prof. Antorio Peretto, direttore del dipartimento di Ingegneria Industriale dell'Università di Bologna.

Gli oltre 30 partecipanti (Allegato 1) di cui 16 rappresentanti delle più prestigiose università italiane (Bologna, Milano, Pisa Roma, Torino e Treviso), 11 rappresentanti dell'Agenzia Nazionale per le Nuove Tecnologie, l'Energia e lo Sviluppo Economico Sostenibile (ENEA), 4 rappresentanti delle eccellenze industriali presenti sul territorio nazionale come Ansaldo Nucleare, CSM S.p.a, Istituto Italiano di Tecnologia (IIT) ed SRS SERVIZI DI RICERCHE E SVILUPPO S.R.L. sono stati accolti presso l'aula Magna della scuola di Ingegneria e Architettura dell'Università di Bologna (Fig. 1).

L'agenda del Workshop (Allegato 2) è stata suddivisa in 6 sessioni. All'interno della sessione di apertura sono state presentate le strategie e prospettive nazionali ed internazionali sui reattori di quarta generazione refrigerati a piombo liquido. Inoltre, è stata fornita un'ampia panoramica sullo stato attuale e sulle problematiche ancora aperte relative alla progettazione del reattore dimostratore ALFRED (Advanced Lead Fast Reactor Demonstrator).

All'interno delle 5 sessioni tecniche, sono stati presentati ben 25 lavori di ricerca sulle tematiche della progettazione di sistema, l'analisi di sicurezza, sviluppo materiali e chimica del refrigerante, termofluidodinamica dei sistemi LFR e lo sviluppo e validazione di codici e modelli multi-fisici per analisi di sicurezza di reattori veloci di iv generazione. Nell'Allegato 3 vengono infine riportati i contributi presentati all'interno delle varie sessioni.

2 ALLEGATI

A1 LISTA DEI PARTECIPANTI AL CONGRESSO

A2 AGENDA

A3 CONTRIBUTI PRESENTATI NELLE VARIE SESSIONI

A1 LISTA DEI PARTECIPANTI AL CONGRESSO

Workshop Tematico

ACCORDO DI PROGRAMMA MISE – ENEA
PAR2016 – PROGETTO B.3.1. LP2

GENERATION IV
LEAD COOLED FAST REACTOR
STATO ATTUALE DELLA TECNOLOGIA E PROSPETTIVE DI SVILUPPO

LISTA PARTECIPANTI

1	SANDRA	DULLA	POLITO
2	LUANA	COGNINI	POLIMI
3	DAVIDE	PIZZOCRI	POLIMI
4	Mariano	Tarantino	ENEA
5	Pierdomenico	Lorusso	UNIROMA1
6	Dario	Diamanti	ENEA
7	Vincenzo	Narcisi	UNIROMA1
8	Sandro	Manservisi	UNIBO
9	Andrea	Baratta	POLIMI
10	Egidio	Zanin	CSM
11	Vincenzo	Peluso	ENEA
12	Massimo	Sarotto	ENEA
13	Massimo	Angiolini	ENEA
14	Morena	Angelucci	UNIPI
15	Giuseppe	Rota	POLIMI
16	Michele	Frignani	ANN
17	Francesco	Lodi	SRS
18	Marco	Beghi	POLIMI
19	Andrea	Subioli	UNIROMA1
20	Antonio	Naviglio	UNIROMA1
21	Fabio	Giannetti	UNIROMA1
22	Alessio	Magni	POLIMI
23	Augusto	Gandini	UNIROMA1
24	Giacomo	Grasso	ENEA
25	Marco	Utili	ENEA
26	Alessandro	Poggianti	ENEA
27	Antonio	Cervone	ENEA
28	Mario	Bragaglia	UNITV
29	Serena	Bassini	ENEA

A2 AGENDA

WORKSHOP TEMATICO

ACCORDO DI PROGRAMMA MISE – ENEA
PAR2016 – PROGETTO B.3.1. LP2

GENERATION IV

LEAD COOLED FAST REACTOR

STATO ATTUALE DELLA TECNOLOGIA E PROSPETTIVE DI SVILUPPO

ADP MiSE-ENEA (PAR2016-LP2)

Aula Magna
Scuola di Ingegneria e Architettura, Università di Bologna
26-27 settembre, 2017

Il Workshop, promosso nell'ambito delle attività inerenti la Linea Progettuale 2 "**Collaborazione internazionale per il nucleare di IV generazione**" dell'AdP MiSE-ENEA, è finalizzato a:

- *analizzare lo stato attuale della tecnologia dei sistemi LFR*
- *supportare la programmazione delle attività future, definendo le priorità di intervento in ambito italiano ed europeo, in sinergia con l'industria del settore*
- *armonizzazione le strategie di sviluppo mediante l'incontro di tutti gli stakeholder italiani.*

Il Workshop assume quindi il duplice obiettivo di condividere lo stato dell'arte dei sistemi LFR tra gli stakeholder italiani definendo al contempo, in maniera condivisa e sinergica con il contesto Europeo, le linee di intervento future in ambito LFR.

Comitato Organizzatore

Ing. Mariano Tarantino (ENEA)	*mariano.tarantino@enea.it*
Prof. Antonio Peretto (UNIBO)	*antonio.peretto@unibo.it*
Ing. Alessandro Del Nevo (ENEA)	*alessandro.delnevo@enea.it*
Ing. Ivan di Piazza (ENEA)	*ivan.dipiazza@enea.it*
Sig.ra Annamaria Masinara (ENEA)	*annamaria.masinara@enea.it*

MARTEDÌ 26 SETTEMBRE, 2017

	Ora	TITOLO	SPEAKER
A	14,00	SESSIONE DI APERTURA	Chair: A. Peretto
A-1	10'	Saluti e Presentazione del Workshop	P. Peretto
A-2	25'	Sviluppo dei Sistemi Gen-IV LFR: strategie e prospettive	M. Tarantino
A-2	25'	DEMO-LFR ALFRED: Technical Overview	M. Frignani
1	15,00	PROGETTAZIONE DI SISTEMA E ANALISI DI SICUREZZA	Chair: M. Frignani
1-1	20'	ALFRED Core Design. Thermo-mechanical analysis of the fuel element	A. Poggianti
1-2	20'	Validation campaign of neutronic codes and recommendations for the correct application to LFR systems	M. Sarotto
1-3	20'	Feasibility studies of an experimental campaign in TAPIRO devoted to the analysis of nuclear database for minor actinides	S. Dulla
	16,00-16,30	Coffe Break	
2	16,30	SVILUPPO E VALIDAZIONE DI CODICI E MODELLI MULTI-FISICI PER ANALISI DI SICUREZZA DI REATTORI VELOCI DI IV GENERAZIONE	Chair: M. Tarantino
2-1	20'	Development of best estimate numerical tools for LFR design and safety analysis	M. Tarantino
2-2	20'	Development/Assessment of models describing the inert gas behaviour in the fuel for application to the TRANSURANUS fuel pin thermo-mechanical code	D. Pizzocri
2-3	20'	Validation of SIMMER code against experimental data	A. Pesetti
2-4	20'	Validation of RELAP53D by CIRCE-ICE experimental tests	F. Giannetti
2-5	20'	Research and development of the FRENETIC code: development of time step adaptivity for the quasi-static method	S. Dulla
2-6	20'	Fuel-coolant chemical interaction	E. Macerata
	18,30	Fine dei Lavori	

Cena (ore 20,30)

MERCOLEDÌ 27 SETTEMBRE, 2017

2	**9,00**	**SVILUPPO E VALIDAZIONE DI CODICI E MODELLI MULTI-FISICI PER ANALISI DI SICUREZZA DI REATTORI VELOCI DI IV GENERAZIONE**	**Chair: A. Cervone**
2-7	20'	Validation of FEM-LCORE/CATHARE by TALL 3D experimental tests	S. Manservisi
2-8	20'	Development of multi-physic code for Lead-cooled Fast Reactor	A. Cammi
2-9	20'	Metodologia HGPT-BU per l'analisi perturbativa nel campo neutroni/nuclidi. Soluzioni analitiche di riferimento per la sua implementazione e validazione nel codice ERANOS	V. Peluso
2-10	20'	Application of RELAP3D on PHENIX experimental tests	F. Giannetti
2-11	20'	Application of RELAPS/mod3.3 – Fluent coupling codes to CIRCE-HERO	M. Angelucci
	10,40-11,00	**Coffee Break**	
3	**11,00**	**SVILUPPO MATERIALI E CHIMICA DEL REFRIGERANTE**	**Chair: M. Angiolini**
3-1	20'	Sviluppo di ricoperture per la protezione di materiali strutturali operanti in sistemi nucleari refrigerati a piombo mediante tecniche di ablazione laser	F. Di Fonzo
3-2	20'	Caratterizzazione meccanica di ricoprimenti prodotti mediante tecnica di ablazione Laser	M. Bragaglia
3-3	20'	Thermomechanical characterization of coatings for nuclear energy applications	M. Beghi
3-4	20'	Controllo della chimica del refrigerante nel reattore DEMO-LFR ALFRED	S. Bassini
3-5	20'	Produzione e caratterizzazione dell'acciaio di guaina del combustibile 15-15 Ti (AIM-1)	M. Angiolini
3-6	20'	Produzione e caratterizzazione di acciai speciali per applicazioni nucleari	C. Cristalli
3-7	20'	Prove di CREEP-RUPTURE su materiali strutturali ricoperti per applicazioni in sistemi LFR	A. Coglitore
	13,20	**Pausa Pranzo**	
4	**14,40**	**TERMOFLUIDODINAMICA DEI SISTEMI LFR**	**Chair: M. Tarantino**
4-1	20'	NACIE Fuel Assembly and System Experiments	M. Angelucci
4-2	20'	Experimental Characterization of Bubble Detection in liquid metal pool	M. Tarantino
4-3	20'	ALFRED SG: HERO Pre-test Analysis	V. Narcisi
4-4	20'	SGTR event in HLM pool and Post Test Analysis	M. Tarantino
5	**16,00**	**CONCLUSIONI E SVILUPPI FUTURI**	**M. Frignani / M. Tarantino**
	16,30	**Fine Lavori**	

A3 CONTRIBUTI PRESENTATI NELLE VARIE SESSIONI

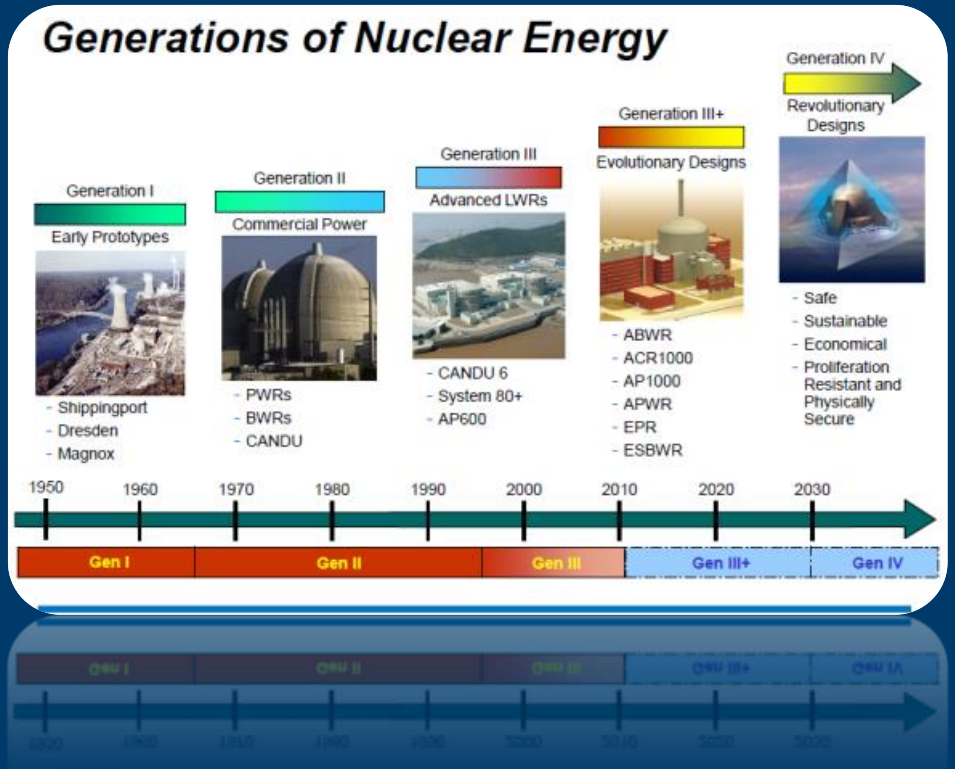
Italian National Agency for New Technologies,
Energy and Sustainable Economic Development

GENERATION IV LEAD COOLED FAST REACTOR
STATO ATTUALE DELLA TECNOLOGIA E PROSPETTIVE DI SVILUPPO

WORKSHOP TEMATICO ACCORDO DI PROGRAMMA MISE – ENEA
PAR2016 – PROGETTO B.3.1. LP2

Scuola di Ingegneria e Architettura, Università di Bologna, 26-27 settembre, 2017

Mariano Tarantino, Responsabile Divisione Ingegneria Sperimentale
Dipartimento Fusione e Tecnologie per la Sicurezza Nucleare



GEN-IV LFR Development

Strategies & Perspectives

Outline





- Why Nuclear?!
- Why Fast Reactor?!
- Why Lead-cooled Fast Reactor?
- Italian Contribution
- International Context
- Final Remarks

Energy Demand





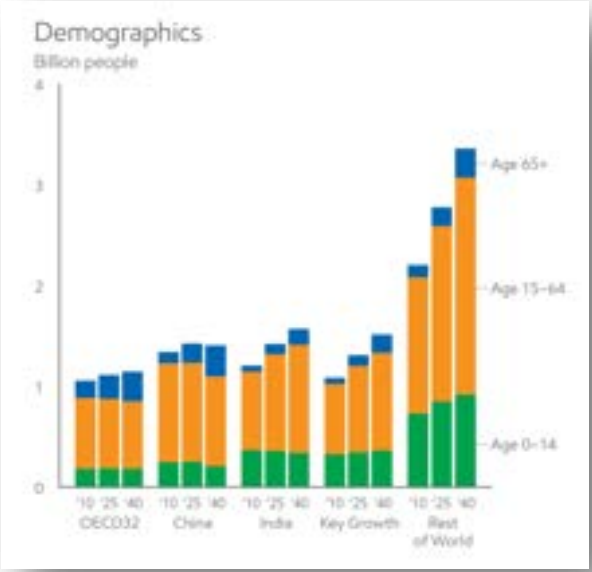
25%

increase in energy demand by 2040.
That's like adding another North and Latin America.



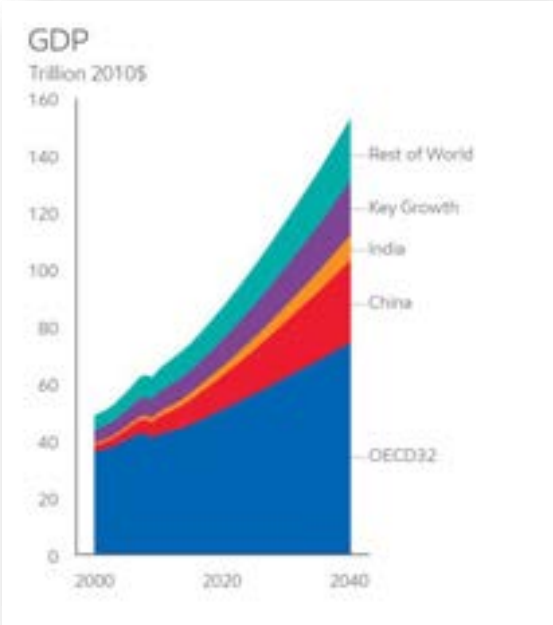
Source: **Exxon Mobil Energy Outlook 2016**

Energy Demand



World population grows 25%, from 7.2 to 9 billion 2014-2040

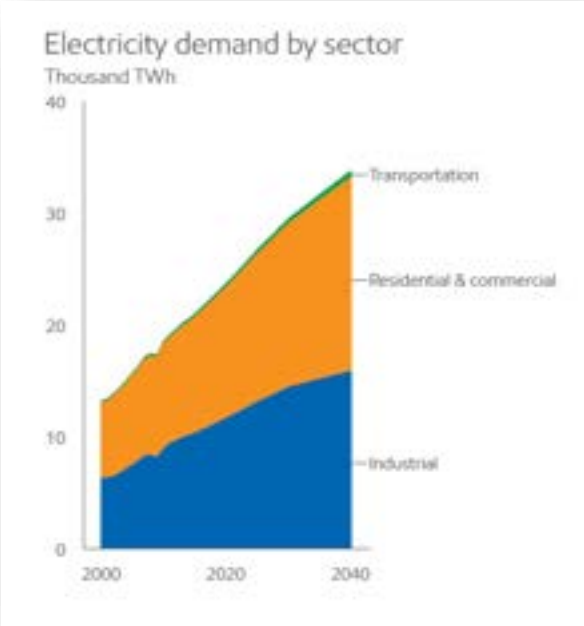
- Economic growth drives increased need for energy
- Global GDP more than doubles 2014-2040; developing countries lead growth
- China rises almost 20% of world GDP, close to US; India exceeds 5%



Source: **Exxon Mobil Energy Outlook 2016**

Electricity Demand

Electricity accounts for nearly all demand growth 2014-2040

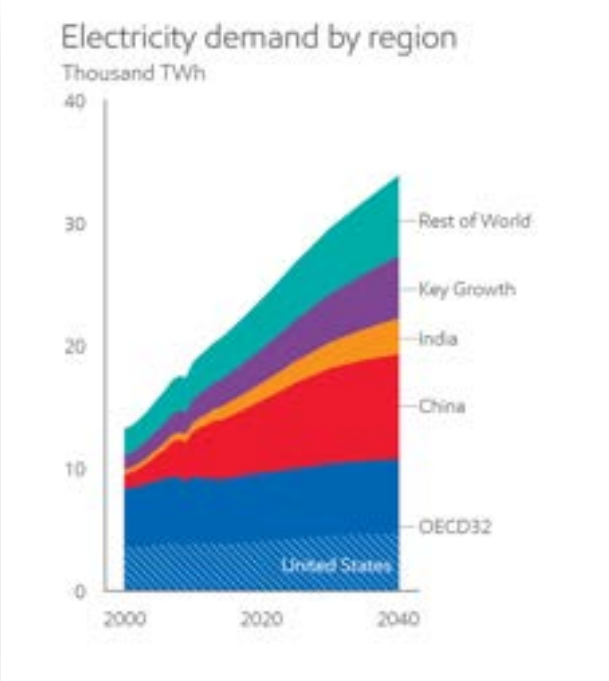


Source: **Exxon Mobil Energy Outlook 2016**

- Global electricity demand seen rising by 65% 2014-2040; 2.5 times more faster than overall energy demand
- Residential and commercial electricity demand rises 70% 2014-2040; industry up to 55%
- Industrial growth eases post-2030 as China's economy shifts from manufacturing
- Transportation electricity demand doubles 2014-2040, but only 2% of the total use

Electricity Demand

Electricity accounts for nearly all demand growth 2014-2040

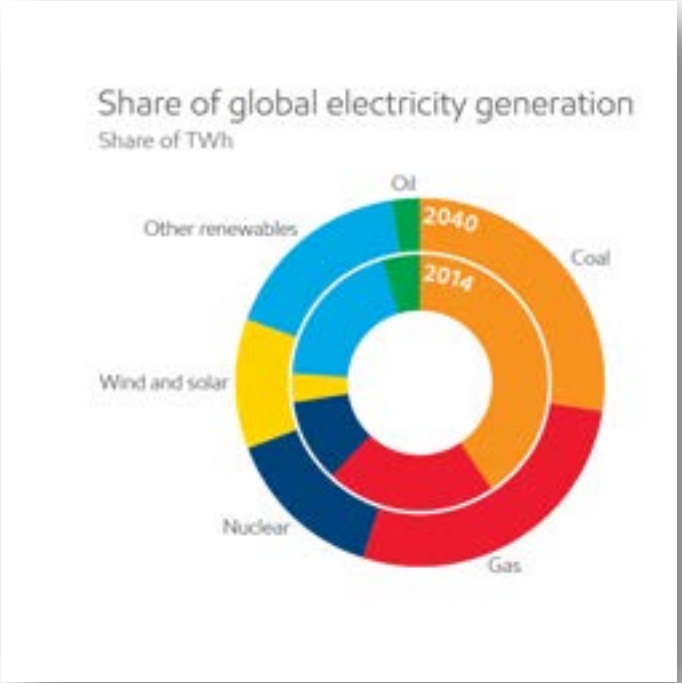




- 85% of the rise electricity demand will come from non-OECD
- China leads growth; will use one-fourth of the world's electricity by 2040
- U.S. share of global electricity demand falls from 20% to 15% 2014-2040

Source: **Exxon Mobil Energy Outlook 2016**

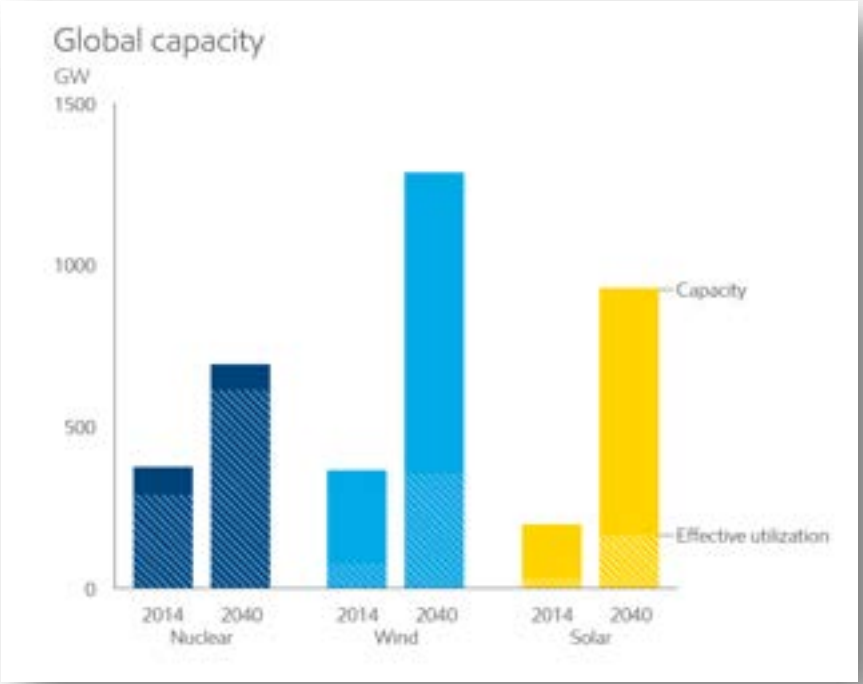
Electricity Generation



- World shifting to cleaner fuels for electricity generation, led by gas
- Coal's share shrink while natural gas, nuclear, wind solar gain
- Coal provides about 30% of world's electricity generation in 2040, versus 40% in 2014
- Wind, solar provide more than 10% of electricity by 2040, 4% in 2014

Source: **Exxon Mobil Energy Outlook 2016**

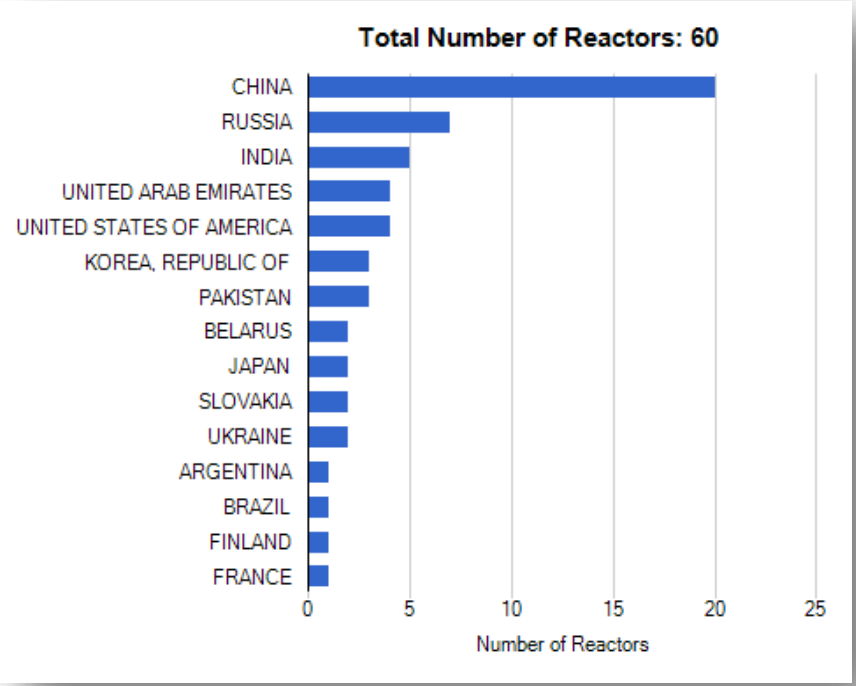
Electricity Generation & Nuclear Role

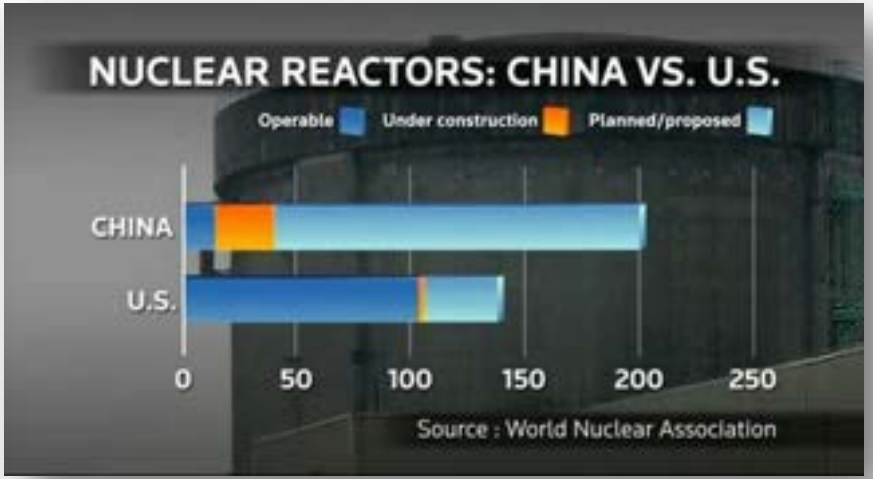


- Global nuclear, wind, solar all see big capacity additions
- **Nuclear capacity to grow 85% 2014-2020, led by China**
- **Intermittency limits the utilization of wind, solar capacity**
- Globally, less than 30% of wind capacity is utilized; solar less than 20%
- **Wind, solar provide less electricity in 2040 than nuclear despite 3 times the capacity**

Source: **Exxon Mobil Energy Outlook 2016**

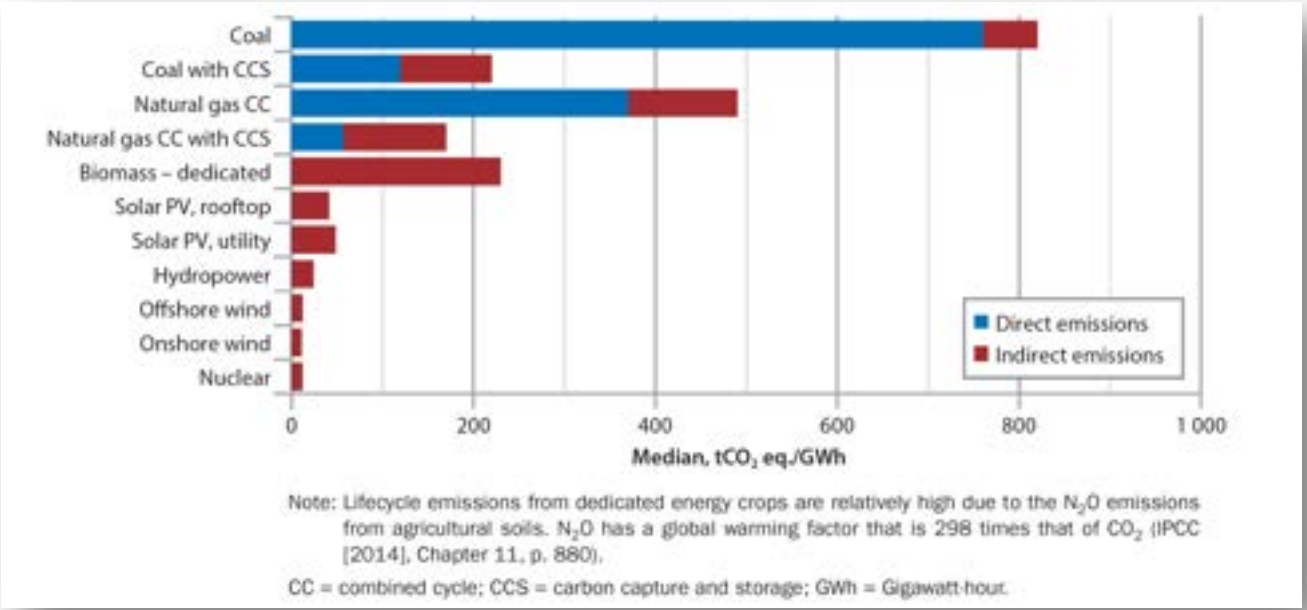
Electricity Generation & Nuclear Role





Source: **IAEA – Power Reactor Information System**

Electricity Generation & Nuclear Role



- Nuclear energy produced **11% of global electricity supply in 2013**.
- This corresponds to 18% of electricity supply in OECD countries and slightly more than 4% in non-OECD countries.
- **Nuclear is the largest low-carbon source of electricity in OECD countries**. Its share in non-OECD countries is still low but is expected to rise substantially in coming years.

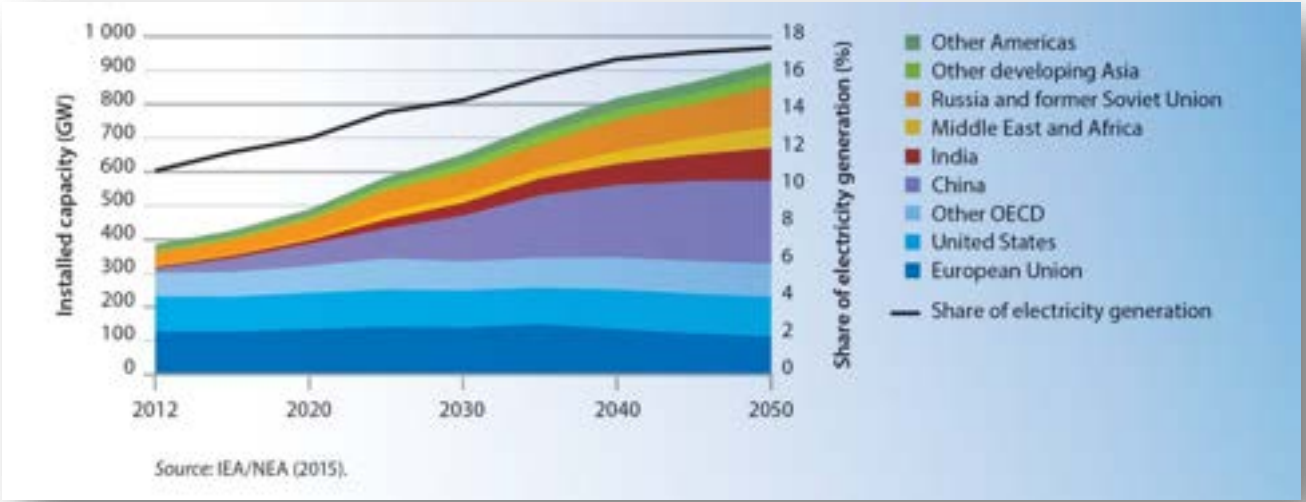
Source: **IPCC (Intergovernmental Panel on Climate Change), 2014**

2°C Scenario

- The 2°C Scenario (2DS) is the main focus of Energy Technology Perspectives.
- The 2DS lays out an energy system deployment pathway and an emissions trajectory consistent with **at least a 50% chance of limiting the average global temperature increase to 2°C**.
- **The 2DS limits the total remaining cumulative energy-related CO2 emissions between 2015 and 2100 to 1 000 GtCO2**.
- **The 2DS reduces CO2 emissions by almost 60% by 2050 (compared with 2013), with carbon emissions being projected to decline after 2050 until carbon neutrality is reached.**
- **COP21 boosted the momentum for accelerating low-carbon technology deployment**

Source: IEA Energy Technology Perspectives 2016

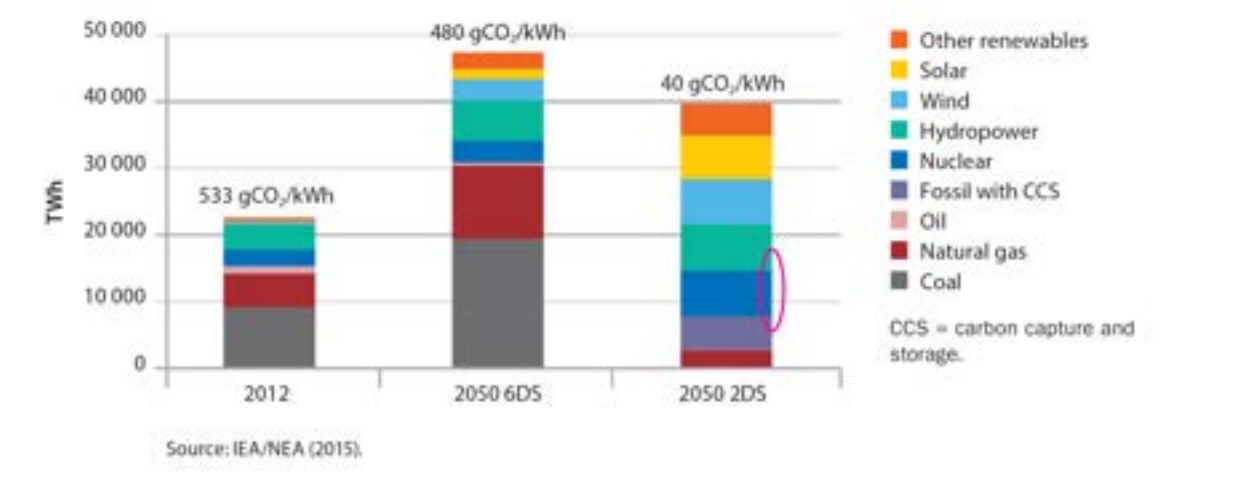
2°C Scenario



Projected nuclear capacity with regional split and share of electricity generation in the IEA *Energy Technology Perspectives* 2015 2°C scenario (2DS)

Source: IEA Energy Technology Perspectives 2016

2°C Scenario



Shares of different technologies in global electricity production until 2050 in the 2DS

- **cumulatively, up to 2050, nuclear power would enable the highest CO2 emission savings in comparison to other technologies**
- **in 2050, nuclear power would represent the largest source of low-carbon electricity.**

Source: IEA Energy Technology Perspectives 2016

Nuclear Open Issues

- Nuclear Energy: good but not good enough

- Improvements
  - Safety

- **Waste**
  - **Too much of it**
  - **Too long lived**

- **Economy**
  - **Once through strata uses less than 0,5% of the fuel**

Nuclear Open Issues



waste minimisation

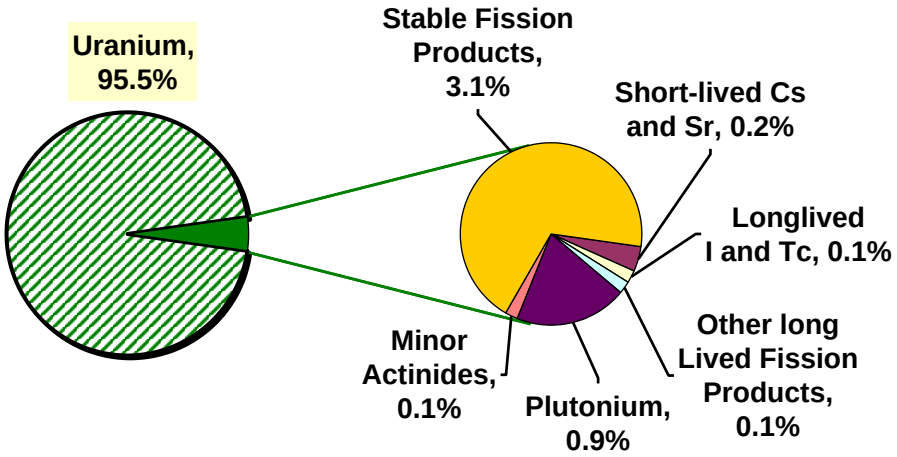
better use of resources

reduced proliferation risks

passive safety

Waste Minimization & Economy

Standard PWR 33GW/t, 10 yr. cooling



Most of the hazard stems from Pu, MA and some LLFP when released into the environment, and their disposal requires isolation in stable deep geological formations.

Source: Phillip Finck and Massimo Salvatores, INL, FUNFI-2, Frascati, October 2016

1 Ton of Spent Nuclear Fuel Contains:

955.4 kg U
8,5 kg Pu

Minor Actinides (MAs)
0,5 kg ^{237}Np
0,6 kg Am
0,02 kg Cm

Long-Lived fission Products (LLFPs)
0,2 kg ^{129}I
0,8 kg ^{99}Tc
0,7 kg ^{93}Zr
0,3 kg ^{135}Cs

Short-Lived fission products (SLFPs)
1 kg ^{137}Cs
0,7 kg ^{90}Sr

Stable Isotopes
10,1 kg Lanthanides
21,8 kg other stable

Partitioning & Transmutation

The Partitioning & Transmutation objectives can be summarized as:

- Minimization of waste mass sent to a repository,
- Reduction of the potential source of radiotoxicity
- Reduction of the heat load in the repository

Strategies making use of P&T can be gathered into three categories:

- Sustainable development of nuclear energy and waste minimization (Pu as a resource)
- Reduction of MA inventory
- Reduction of TRU inventory as unloaded from LWRs

Fast neutron spectrum reactors are the most adapted technology and offer flexible options for implementation.

Waste Minimization & Economy

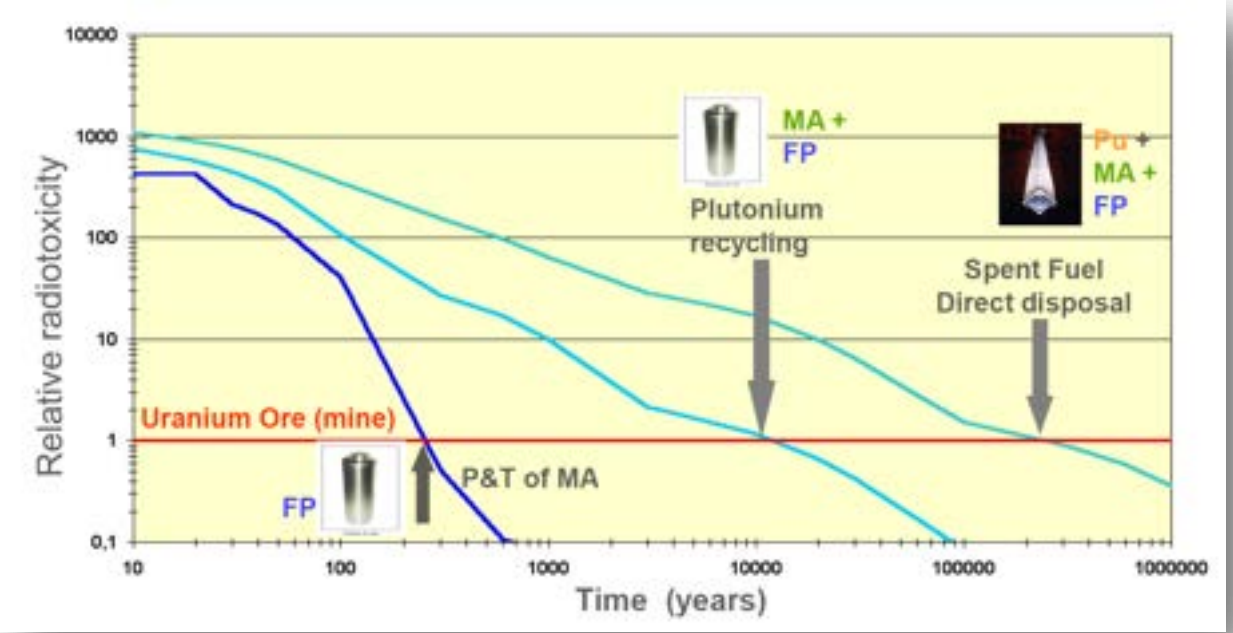
NUCLEAR MATERIALS INVENTORY (TONS) NEEDED TO PRODUCE 100TWH

		1) Present scenario	2) Near term scenario	3) Long term scenario (after 2040)
		Light water reactors	Lead –cooled fast reactors without Minor Actinides recycling.	Lead –cooled fast reactors with Minor Actinides recycling.
Natural Uranium		2100	10,8** *or* a, b, c	10,44** *or* a, b, c, d
Unused uranium, net generated Pu, Nuclear waste	Depleted Uranium from the enrichment facility.	1900 (a)	–	–
	Uranium from the spent fuel.	184 (b)	–	–
	Pu	2,6* (c)	Negligible	Negligible
	Minor Actinides (Np,Am,Cm)	0,38 (d)	0,36	Negligible
	Fission fragments	13	10,43	10,43

* It is possible to reduce the plutonium inventory with increased production of Minor Actinides.
** Reprocessing losses not included

Source: L. Cinotti, "IW on Innovative Nuclear Reactors cooled by HLM: Status and Perspectives, Pisa 2012

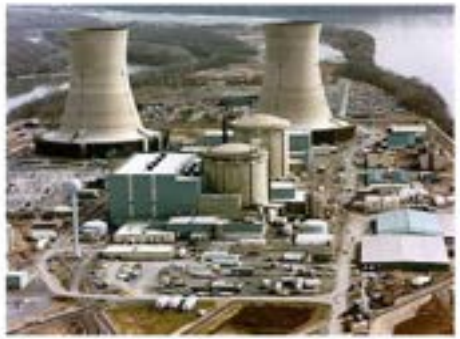
Waste Minimization & Economy



Recycle of all actinides in spent LWR fuel in fast reactors provides a significant reduction in the time required for radiotoxicity to decrease to that of the original natural uranium ore used for the LWR fuel (i.e., man-made impact is eliminated). From 250,000 years down to about 400 years with 0.1% actinide loss to wastes

Safety Improvement

Severe Nuclear Accidents. During the historically short period several low probability NPP accidents occurred with significant radioactivity release into environment and considerable economical losses



Three Mile Island-2
(PWR)
1979



Chernobyl-4
(RBMK)
1986



Fukushima-1
(BWR)
2011

The initial events for these accidents are of extremely low probability

technical failure **human error** **extreme external impact**

Safety Improvement

- Severe Nuclear Accidents occurred due to the **release of various types of potential energy accumulated in various materials**, mainly, in the main coolant.

- Radiotoxicity inventory and decay heat amount are mainly independent from the reactor type, being governed by the fission products.

- **Radiotoxicity release into environment depends strongly on the reactor type and is determined by potential (non-nuclear) energy accumulated in various materials**

  - **Coolant compression energy**
  - **Chemical energy**.

- **Potential energy is an inherent coolant property**

Safety Improvement

Coolant	Water	Sodium	Lead, Lead-bismuth
Parameters	P = 16 MPa T = 300 ºC	T = 500 ºC	T = 500 ºC
Maximal potential energy, GJ/m³, *including:*	~ 21,9	~ 10	~ 1,09
Thermal energy / *including* compression potential energy	~ 0,90 / ~ 0,15	~ 0,6 / None	~ 1,09 / None
Potential chemical energy of interaction	With zirconium ~ 11,4	With water 5,1 With air 9,3	None
Potential chemical energy of interaction of released hydrogen with air	~ 9,6	~ 4,3	None

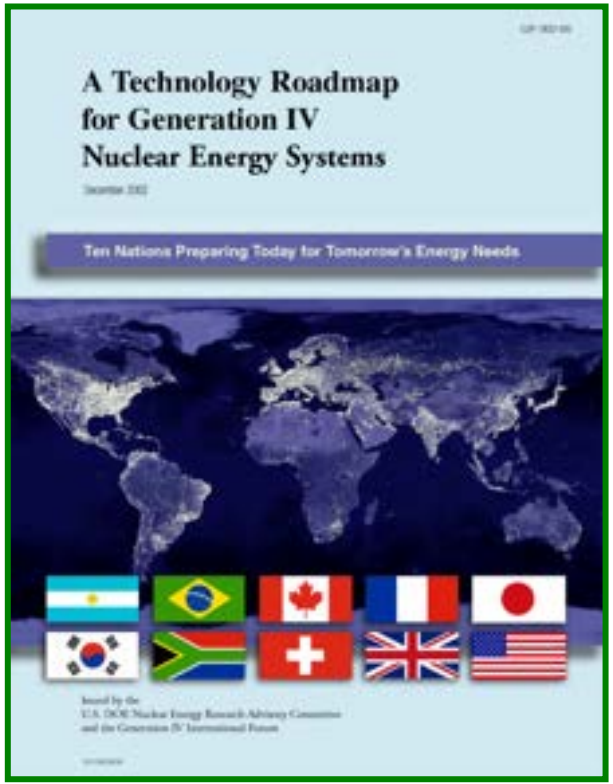
From ICAPP 2011, Paper 11465 "Effect of Potential Energy Stored in Reactor Facility Coolant on NPP Safety and Economic Parameters",

G.I. Toshinsky, O.G. Komlev, I.V. Tormyshev

Safety Improvement

- Upgrading the safety level of NPPs with traditional-type reactors, (in which potential energy is stored in large amounts) requires increasing the number of safety systems and defense-in-depth barriers
- **Such measures can only reduce the probability of severe accidents** and mitigate the consequences, **but cannot eliminate them when there is large potential energy**
- Public opinion has been once more shocked by the loss of control of a nuclear plant
- Convincing demonstration that future reactors can rule out catastrophic scenarios is necessary to recover public acceptance
  - to exploit to the maximum extent solutions that can deterministically exclude scenarios which are potential initiators of accidents leading to severe core damage;
  - to consider the possibility of managing extreme events in degraded plant conditions.

Generation IV



The path from current nuclear systems to Generation IV systems is described in a 2002 Roadmap Report entitled "***A technology Roadmap for Generation IV Nuclear Energy Systems"*** which:

defines challenging technology goals for Generation IV nuclear energy systems in four areas:

- ✓ **sustainability,**
- ✓ **economics,**
- ✓ **safety and reliability, and**
- ✓ **proliferation resistance and physical protection.**

identifies six systems known as Generation IV to enhance the future role of nuclear energy**;**

defines and plans the necessary R&D

Generation IV

Generation IV Systems	*Acronym*
Gas-Cooled **F**ast **R**eactor	**GFR**
Lead-Cooled **F**ast **R**eactor	**LFR**
Molten **S**alt **R**eactor	**MSR**
Sodium-Cooled **F**ast **R**eactor	**SFR**
Super**c**ritical **W**ater-Cooled **R**eactor	**SCWR**
Very-**H**igh-**T**emperature **R**eactor	**VHTR**

Because the capability of fast reactors to meet the sustainability goal and hence to re-position nuclear energy from the present transition-energy role into an inexhaustible source of clean energy

- three out of the six systems selected by GIF (GFR, LFR and SFR) are fast reactors and
- for two systems (MSR and SCWR) studies have been carried out recently to explore the possibility of them to become fast reactors.

Lead cooled Fast Reactor

- For heavy liquid metal coolants (lead-bismuth alloy, lead) the stored thermal potential energy cannot be converted into kinetic energy.
- There is no significant release of energy and hydrogen in an events of coolant contacting with air, water, structural materials.
- There is no loss of core cooling in an event of tightness failure in the gas system of the primary circuit.
- The way to improve the NPP safety and economic performance is to implement reactor facilities with **the lowest stored potential energy**, where the inherent self-protection and passive safety properties are used to the maximal extent.

Lead cooled Fast Reactor

Main advantages and main drawbacks of Lead

Atomic mass	Absorption cross-section	Boiling Point (°C)	Chemical Reactivity (w/Air and Water)	Risk of Hydrogen formation	Heat transfer properties	Retention of fission products	Density (Kg/m^3) @400°C	Melting Point (°C)	Opacity	Compatibility with structural materials
207	Low	1737	Inert	No	Good	High	10580 10580	327	Yes	Corrosive

Lead cooled Fast Reactor

How lead coolant improves the reactor design?

Lead is a low-moderating medium and has a low-absorption cross section

- Fast neutron spectrum: operation as burner of MA and improve resource utilization (Sustainability)
- Long Life Core: unattractive route for Pu procurement (Proliferation resistance and physical protection)
- Large fuel pin lattice (opened/closed): enhanced the passive safety (Safety and Reliability)

Lead does not interact vigorously with air or water

- Improve Simplicity and Compactness of the Plant and reduce the risk of plant damage (Economics)
- Increase the protection against acts of terrorism (Proliferation resistance and physical protection)

Lead cooled Fast Reactor

How lead coolant improves the reactor design?

Lead has a high boiling temperature, high shielding capability and very low vapor pressure

- Un-pressurized primary system (Safety and Reliability, Economics)
- Enhancements in passive safety (Safety and Reliability)

Lead has a high heat transfer, specific heat, and thermal expansion coefficients

- Decay heat removal by natural circulation (Safety and Reliability)

Lead has a density close to that of fuel, and retains fission products

- Reduce the risk of re-criticality and vessel damage in the case of core melt (Safety and Reliability)
- No need of off-site emergency response (Safety and Reliability)

Lead cooled Fast Reactor

A comprehensive R&D program is necessary because of:

- **The use of a new coolant and associated technology, properties, neutronic characteristics, and compatibility with structural materials of the primary system and of the core.**
- **Innovations which require validation programs of new components and systems (the SG and its integration inside the reactor vessel, the extended stem fuel element, the dip coolers of the safety-related DHR system, pump, OCS, …)**
- **The use of advanced fuels (*at least in a further stage*).**

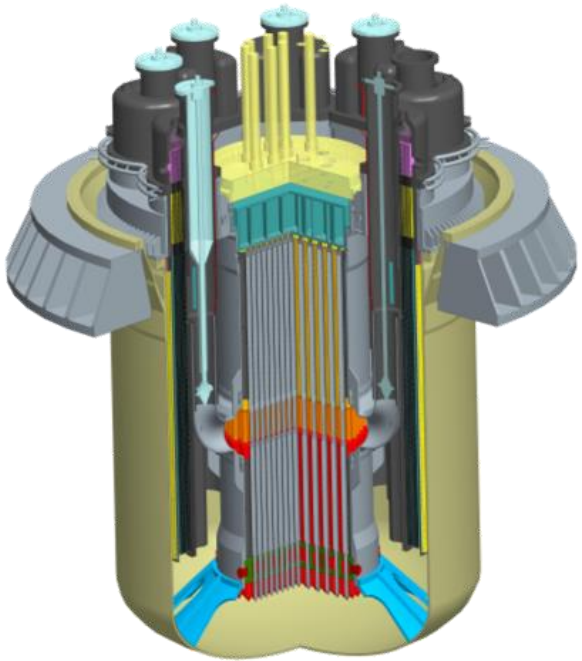
Italian Position

- The **industrial interest on LFR technology increased worldwide**, thanks to the enhanced safety and sustainability performances, the potential for economic competitiveness and the unique flexibility in terms of plant size and potential applications.

- In the European context, the attractive features of the LFR technology are being considered for the industrial deployment of a **lead-cooled Small Modular Reactors (SMR), able to achieve commercial maturity in a short-term.** It will offer a more advanced **alternative to current generation reactors facing retirement between 2035-2040**, while progressively achieving top-scoring performances in economics, safety, sustainability and proliferation resistance in line with the Generation-IV objectives.

- The **ALFRED Project** is framed as a priority to address the challenges of the European Union energy policy. **Italian industries, research centers and academia** have invested in developing and promoting the Project. The ALFRED implementation in Romania will represent an opportunity for the Italian system and is worth support towards the decision makers and European level.

Italian Contribution: ALFRED



Advanced, since integrating innovation-intensive solutions in nuclear technology

Lead, because of its intrinsic properties as primary coolant to achieve superior safety

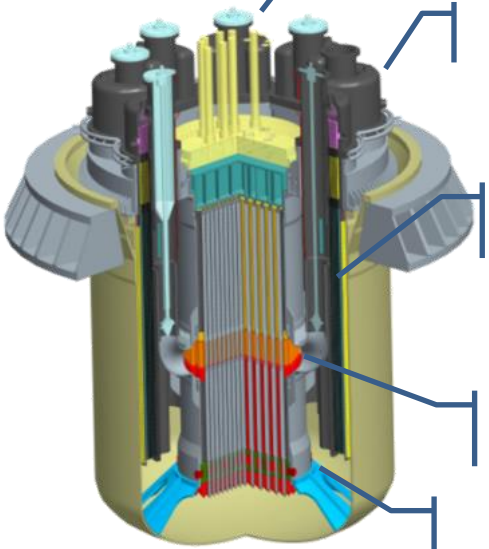
Fast, for the full exploitation of fuel energy and the reduction of long-term radiotoxicity

Reactor, as a representative training system for industry, utilities and safety authorities

European, because conceived and developed by a pan-European collaboration of experts

Demonstrator, to prove the viability LFR for a safe, clean, economic, and sustainable nuclear energy source

ALFRED Conceptual Design



Relatively low power (300 MWth)

Compact design
Removable components
Proven technologies

Simple flow path
Efficient natural circulation

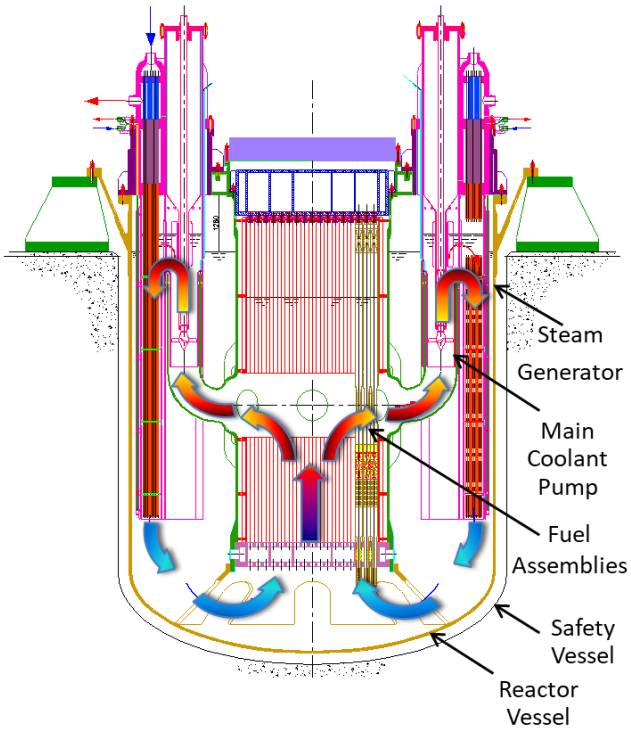
Inner vessel
Enclosing hot pool

Molten lead as coolant
Excellent intrinsic properties.
Manageable negative properties

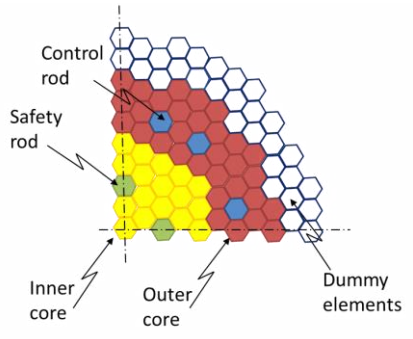
- Pool-type fast reactors have a strongly integrated Primary System.
- Design criteria may look contradictory and trade-offs are typically necessary.
- A design solution is not the best one «per se», but the best integrated in the design.

ALFRED Conceptual Design

Primary system	Pool-type, compact
Coolant circulation	
Normal operation	Forced (8 pumps)
Accident conditions	Natural (pressure drop 0.15 MPa)
Pressure	< 0.1 Mpa
Temparature	400-480°C
Flowrate	26 000 kg/s
Reactor vessel	Austenitic SS, hung
Safety vessel	Anchored to the pit
Inner vessel	Cylindrical, Integral with the core support grid and the hot collectors, Removable
Steam generators	8, bayonet type with double walls, Removable
Primary pumps	4, integrated with the SGs, in hot leg, Removable
Fuel assembly	Closed (with wrapper), Hexagonal, Weighed down/forced in position by springs
Control/Shutdown	System 2 diverse and redundant systems of the same concept derived from MYRRHA
Decay Heat Removal	2 separate and redundant systems of 4 Isolation Condensers connected to the Steam Generator (actively actuated, passively operated)
Refuelling System	No refuelling machine stored inside the Reactor Vessel



FA	171, hexagonal, wrapped
Inner	57 (21,7 at.%)
Outer	114 (27,8 at.%)
Dummy	108 (ZrO_2-Y_2O_3)
FA lattice	Triangular (127 pins)
Pins p/d	1,32
Cladding	15-15 Ti
Fuel	MOX, 25.77 at% (avg)
Residence	5 years
Burnup	73,3 MWd/kg_{HM} avg 103 MWd/kg_{HM} peak
BoC-EoC	2600 pcm swing



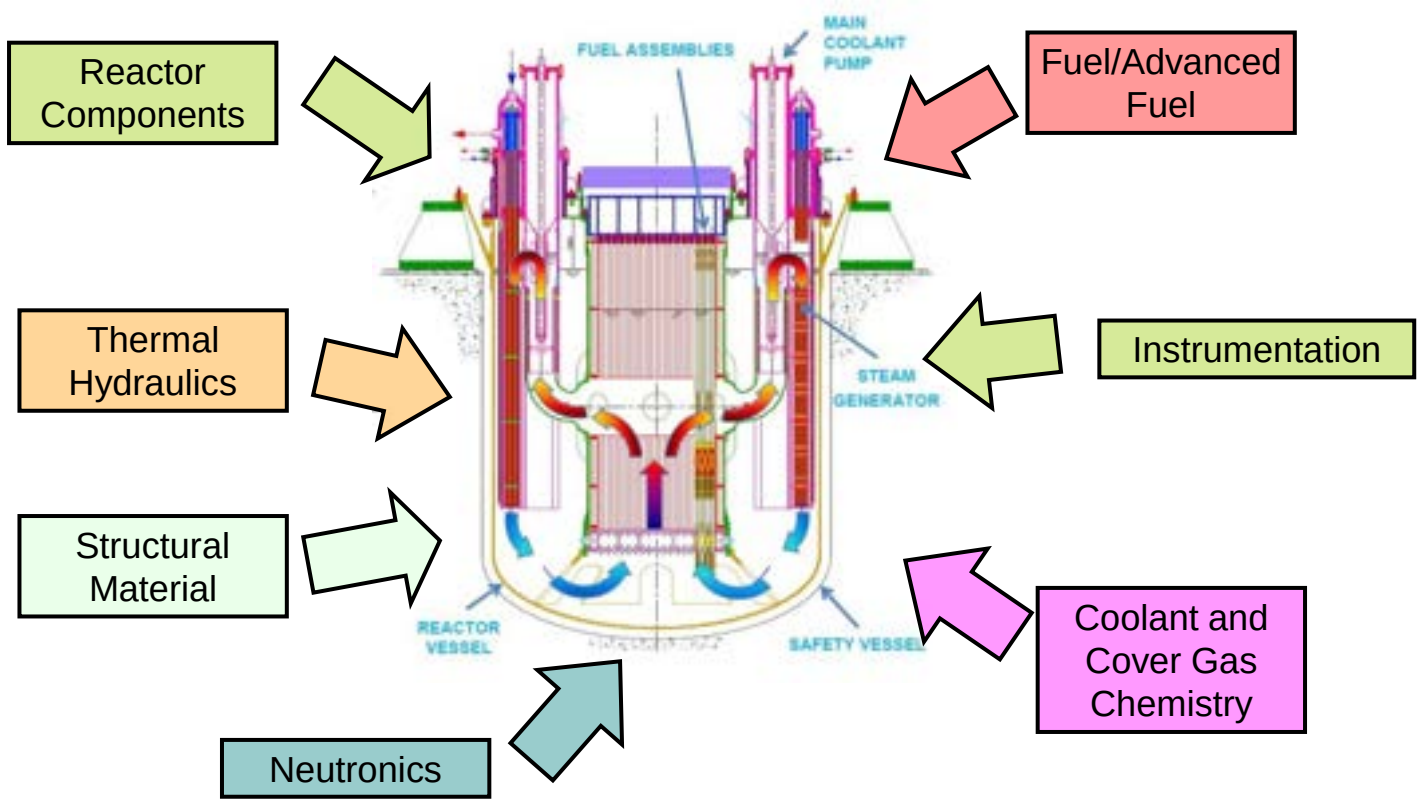
Italian Contribution

Framework Agreement (AdP)
between the Italian Ministry for Economic Development (MiSE) and ENEA.

- **Project B.3.1 → Nuclear Fission**
  - **LP2 "International Collaboration on Gen-IV Nuclear Systems"**

- **Design and Safety Analysis**
- **Structural Materials and Coolant Chemistry**
- **Thermalfluidynamic & Innovative Components**

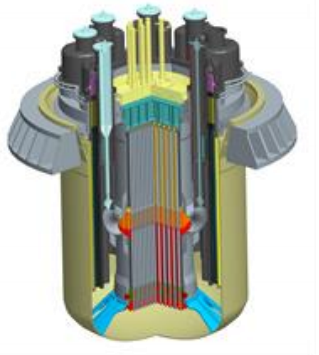
Towards Lead-cooled Fast Reactors



Towards Lead-cooled Fast Reactors

	TRL	TRL Function	Generic Definition	Phase
achieved	1	Technology Down-Selection	•Basic principles definition	Screening
achieved	2		•Technology concepts and applications definition	
Ongoing	3		•Demonstration of critical function •Proof of concept	Pre-qualification
Ongoing	4	Final Process Selections & integration	•Lab-scale component validation	
Ongoing	5		•Component validation in a relevant environment	Qualification
Further Development	6	Full-scale integrated testing	•System/subsystem model or prototype demonstration in relevant environment	
Further Development	7		•System prototype demonstration in prototypic environment	Demo
Further Development	8	Full-scale demo	•Actual system completed and qualified through test and demonstration	
Further Development	9		•Actual system proven through successful operations	

DEMO is needed!



ALFRED

European Scenario

SNETP → Sustainable Nuclear Energy Technological Platform

To ensure the long-term sustainability of nuclear energy, **Gen IV Fast Neutron Reactors should be available for deployment by 2040** or even earlier. Therefore an ambitious yet realistic R&D and demonstration programme is to be put in place.

ESNII → European Sustainable Nuclear Industrial Initiative

ESNII addresses the need for **demonstration of Generation IV Fast Neutron Reactor technologies**, together with supporting research infrastructures, fuel facilities and R&D work.

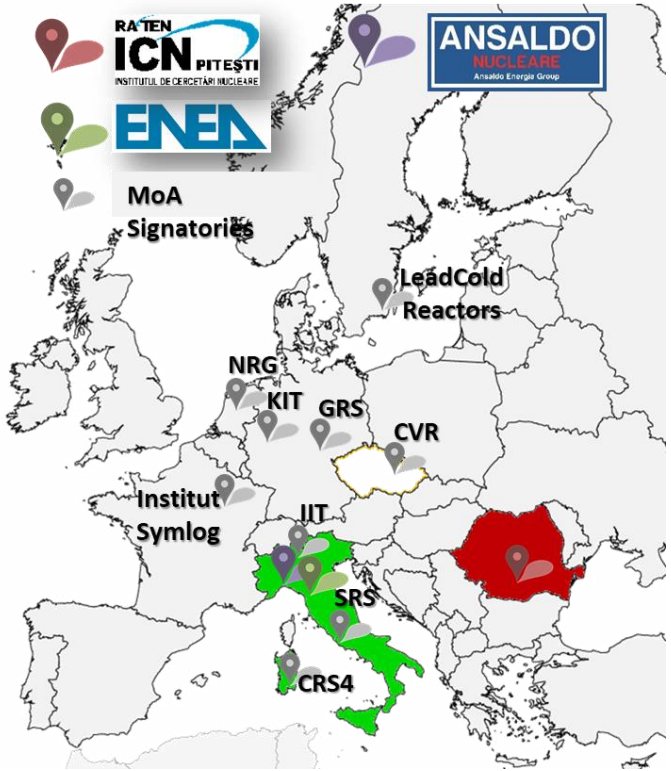
SRIA → Strategic Research and Innovative Agenda (2013)

The **main objective of Europe** is to maintain the leadership in fast spectrum reactor technologies that will **excel in safety** and will be able to achieve a more **sustainable development of nuclear energy**.

"……Lead Fast Reactor technology has significantly extended its technological base and can be considered as the shorter-term alternative technology (to SFR), whereas the Gas Fast reactor technology has to be considered as a longer-term alternative option.

FALCON Consortium

- **FALCON** Consortium Agreement established in **2013** to bring LFR technology to **industrial maturity**.
- **Infrastructures** in Mioveni platform:
  - European "**Lead School**" for E&T and dissemination services,
  - **CoE on HLM** equipped with unique facilities,
  - **ALFRED** playing the role of ETDR of the LFR technology
- New members sharing the **objective** of a rapid deployment of an LFR demonstrator, interested in the R&D supporting **infrastructure** and in the **ALFRED** industrial outcomes are welcome to join.



FALCON Consortium

- The **Romanian Minister of Economy, Trade and Business Environment** expressed in 2011 the interest in **hosting ALFRED** and in supporting the implementation of the demonstrator.
- Taking advantage of the **expertise of ICN** as national nuclear research organization, the **Mioveni nuclear platform** was selected, in the Sud Muntenia region.
- The choice opens to **Romania** the possibility to become the **focal point in the LFR technology** in Europe.
- On **July 15, 2015** as a consequence of the final consultation **of Smart Specialization Strategy** of Romania 3 region, ALFRED was included in **High technology Industry** smart specialization of the region.



An opportunity for Sud Muntenia in Romania

FALCON Consortium (July 2017)

- Prime Minister, Minister of Research and Innovation, State Secretary of the Ministry of Energy declared the **government's firm commitment** to support the **Romanian research** in developing civilian **nuclear** technology.
- **ALFRED** was confirmed to be considered a **strategic research infrastructure** to accelerate the development and use of **LFR technologies**, thus requiring the coordination of **national research efforts** and the project financing support, with the objective of developing the **first fast reactor** within the end of the **next decade**.
- Political support **appreciated by DG-RTD** Commissioner at the Conference.
- Partnership for Research and Education for Advanced Nuclear Systems (CESINA) and the Romanian Atomic Forum Association (ROMATOM).
- **Side events** involving **FALCON**:
  - Panel discussion between FALCON and **ROMATOM**.
  - Technical meeting with **CNCAN** about the licensing process and next steps.

FALCON Consortium

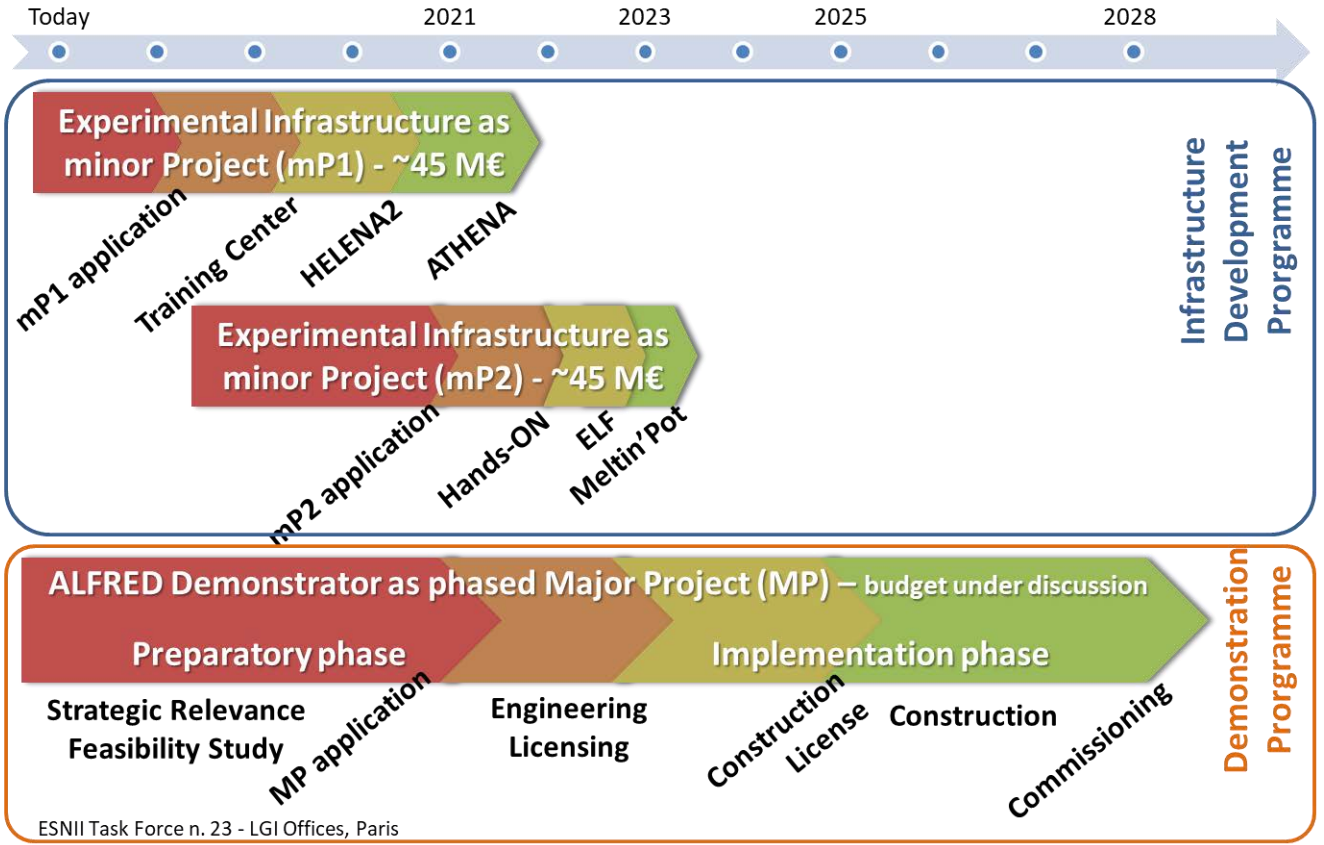
ALFRED General Roadmap



Relying on **45 years** successful nuclear power program in **Romania**

FALCON Consortium

Multi-annual Funding Scheme



FALCON Consortium

Exploiting Potential Synergies in Funds



Synergic Funding Scheme

H2020

Eligible costs: staff, equipment, travel, sub-contracting

Budget: 70% EC + 30% in-kind by Partners (no ESIF!)

ESIF

ERDF

Eligible cost: purchasing R&D equipment and instrastructures

ESF

Budget: ESIF from different Ops + relevant % of Public Funds (no H2020!)

Final Remarks

- Nuclear will play still an important roles in the next years.
- Nuclear energy technology **is among the most reliable and safer technologies**. Nevertheless a in improvement is required about:
  - **Safety**
  - **Waste**
  - **Economy**
- Gen-IV reactors have been conceived to match these goals. Among the others, **Lead cooled Fast Reactors** seems to be the most promising! (but R&D needs are not negligible…)
- In this context the **Italian contribution is significant worldwide**. ENEA and its industrial partners led the technology development.
- International Context is positive (everyday more!!)

Mariano Tarantino
mariano.tarantino@enea.it

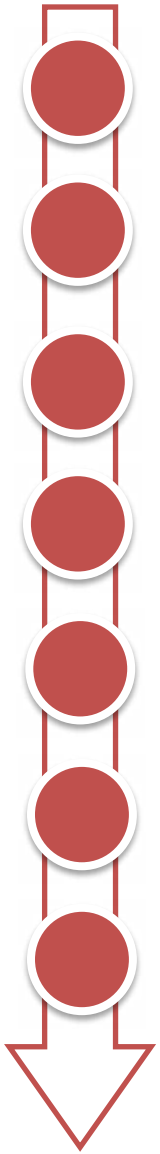


DEMO-LFR ALFRED: Technical Overview

Michele Frignani

Project Engineer – Nuclear Technologies and Safety
Member of Expert Board, FALCON Consortium

ALFRED: Design di riferimento Europeo ed Italiano



2010 Fine del progetto **ELSY**: serve un Dimostratore…

2 mesi dopo KOM di **LEADER**: nasce l'**idea di ALFRED**

2011 La **Romania** si candida per ospitare ALFRED

2013 Fine del progetto LEADER: **ALFRED concept**

2 mesi dopo Firma del Consorzio **FALCON**: inizia la **Technical Review** di ALFRED

2016 FALCON punta sulle potenzialità di ALFRED come **SMFR**

2017 ALFRED viene inserito nella **Strategia nazionale** in Romania

“Academic-Reactor” vs. “Practical-Reactor”

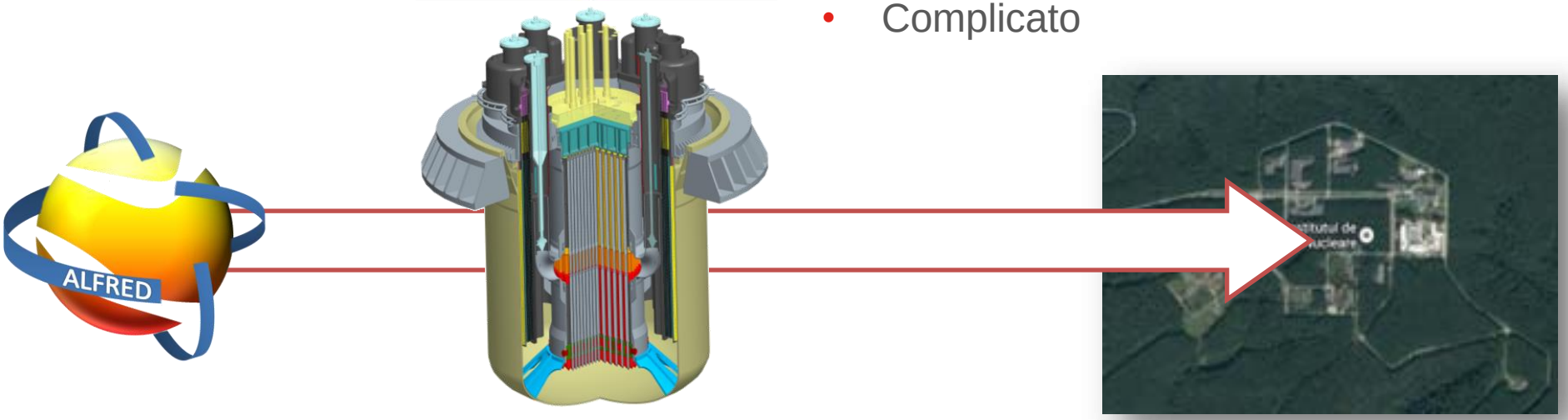
Da una dichiarazione dell’Ammiraglio H. G. Rickover (*the father of the nuclear Navy*), 1953.

Academic Reactor

- Semplice
- Piccolo
- Economico
- Leggero
- Veloce da costruire
- Basato su componenti “off-the-shelf”
- Flessibile
- In fase concettuale

Practical Reactor

- In costruzione
- Già in ritardo
- R&D su argomenti apparentemente triviali
- Molto costoso
- Lungo tempo di costruzione
- Grande
- Pesante
- Complicato



Dimostratore o Prototipo

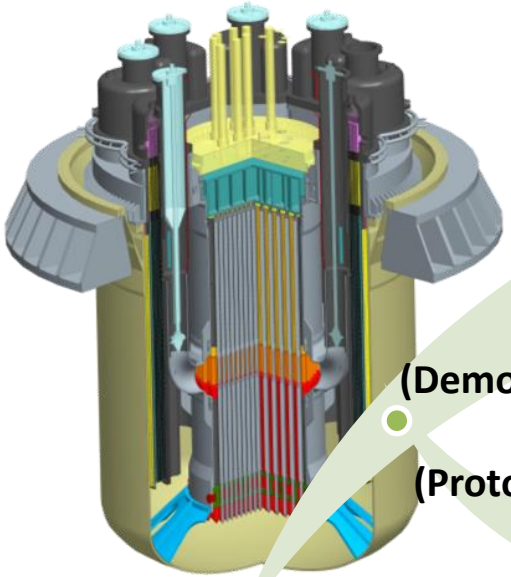
Dimostratore

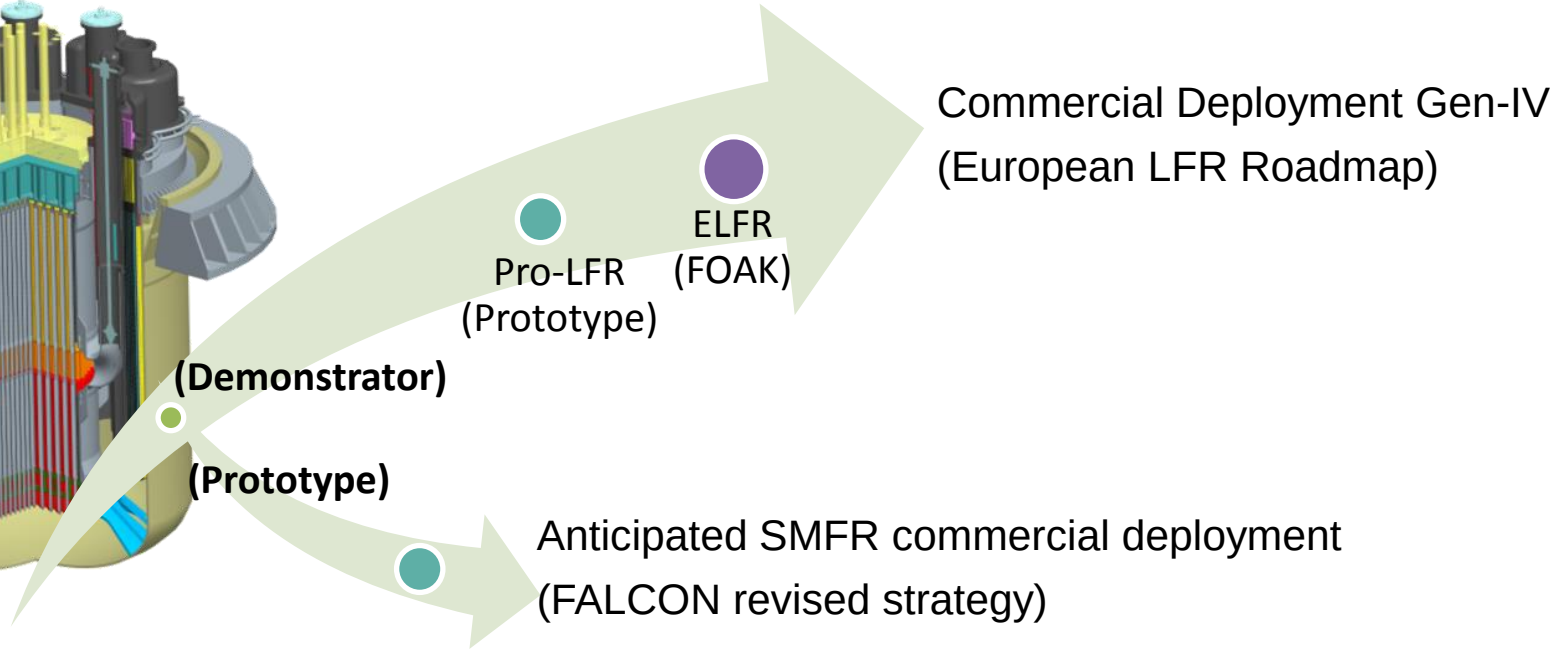
- Usato per mostrare i meriti e le performance di una tecnologia di fronte a potenziali clienti o utilizzatori

Prototipo

- Modello funzionante originale, tipicamente full-scale
- Primo iniziale prodotto usato come campione, facilmente replicabile.
- Usato per testare il concetto come base di standardizzazione

ALFRED
Advanced Lead-cooled Fast Reactor European Demonstrator





ALFRED: i nuovi Obiettivi

- Deve fornire una **dimostrazione** robusta della operazione in **sicurezza** di un LFR in ogni condizione
- Deve consentire un **licensing** in accordo con **standard internazionali**, facendo leva sulle caratteristiche di dimostratore (**elevati margini**, sistemi di sicurezza)
- Deve permettere la **verifica** dei principali parametri progettuali, consentendo di **acquisire esperienza** per **ridurre le incertezze** per futuri LFR
- Deve garantire l'**estrapolabilità** del concetto (principali componenti) su **scala industriale**
- Deve fornire la possibilità di **testare** nuovi combustibili, materiali e componenti
- Deve consentire di supportare la **dimostrazione di sicurezza e sostenibilità** per futuri LFR commerciali
- Deve permettere il **training** di personale di organizzazioni interessate

ALFRED Technical Overview

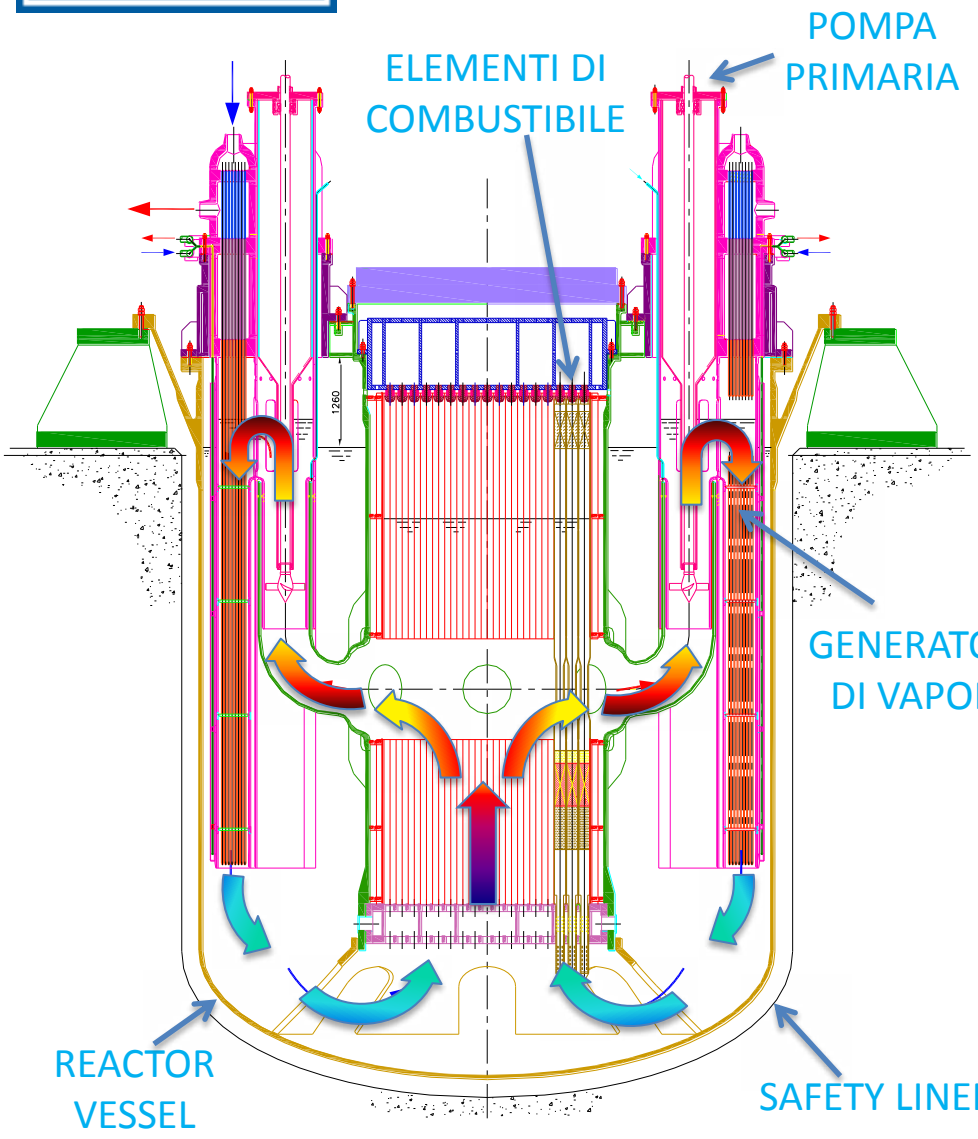
Cosa è stato cominciato in LEADER

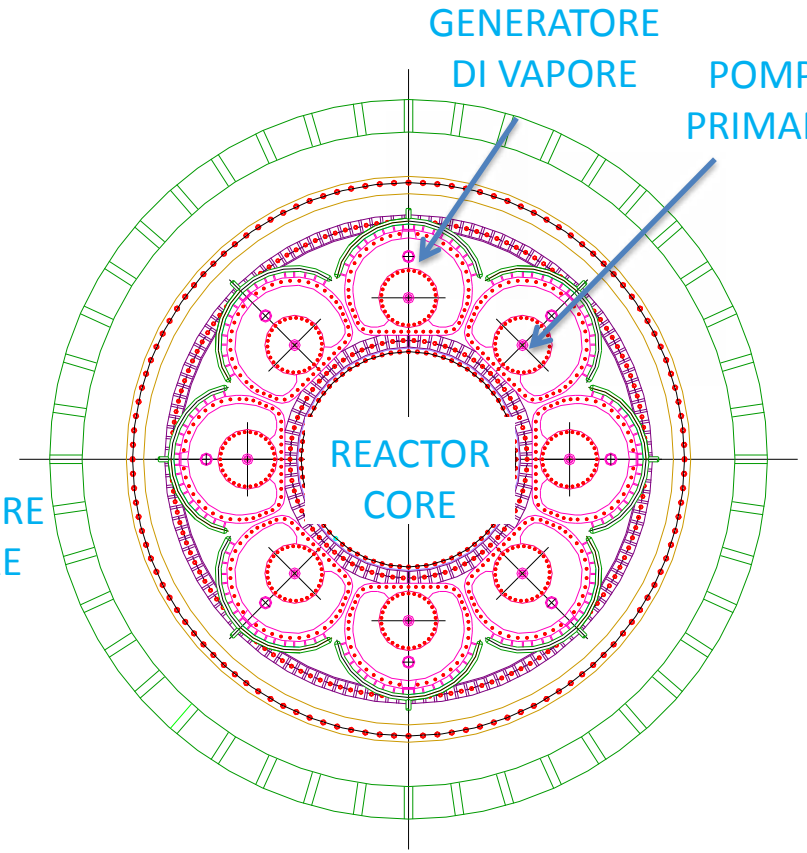
Cosa è stato rivisto in FALCON

Cosa occorre ancora approfondire…



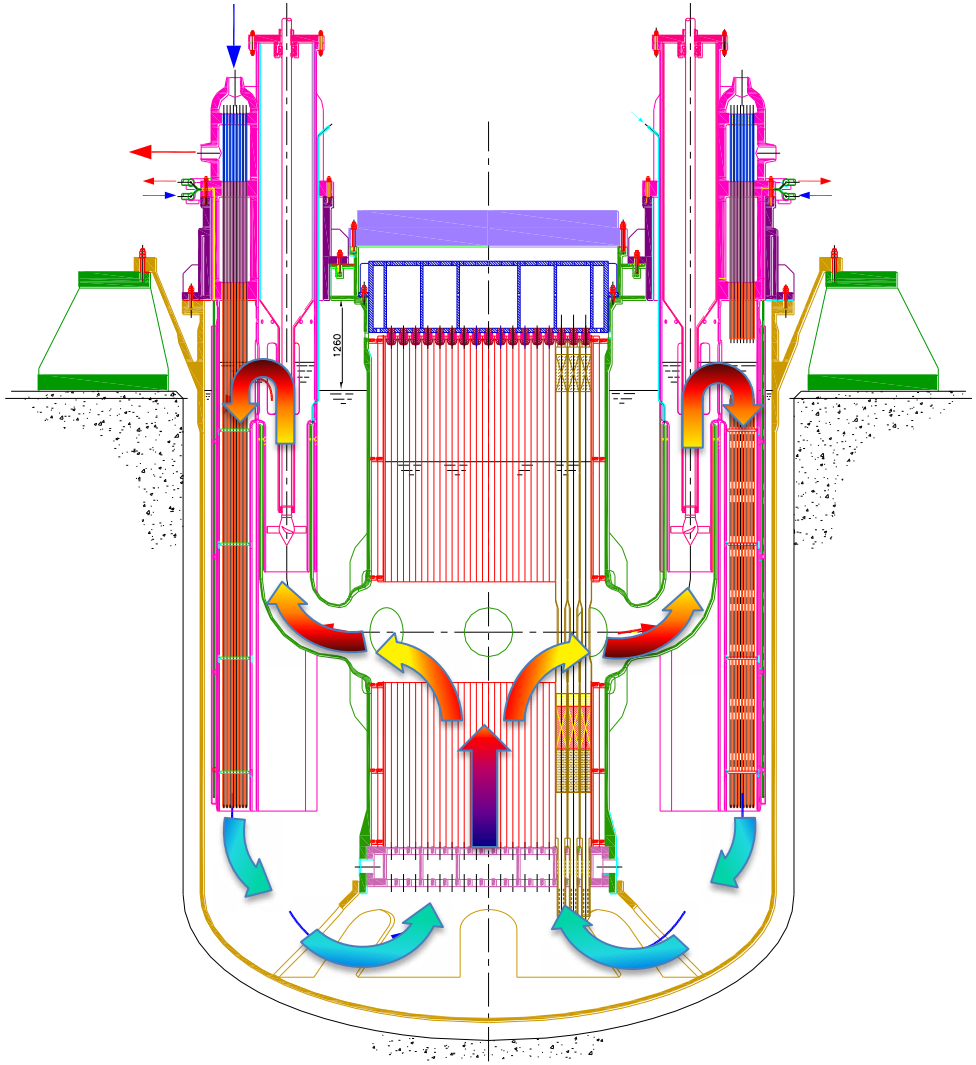
Assieme reattore





Soluzione elegante, **ma**…

Temperature di riferimento



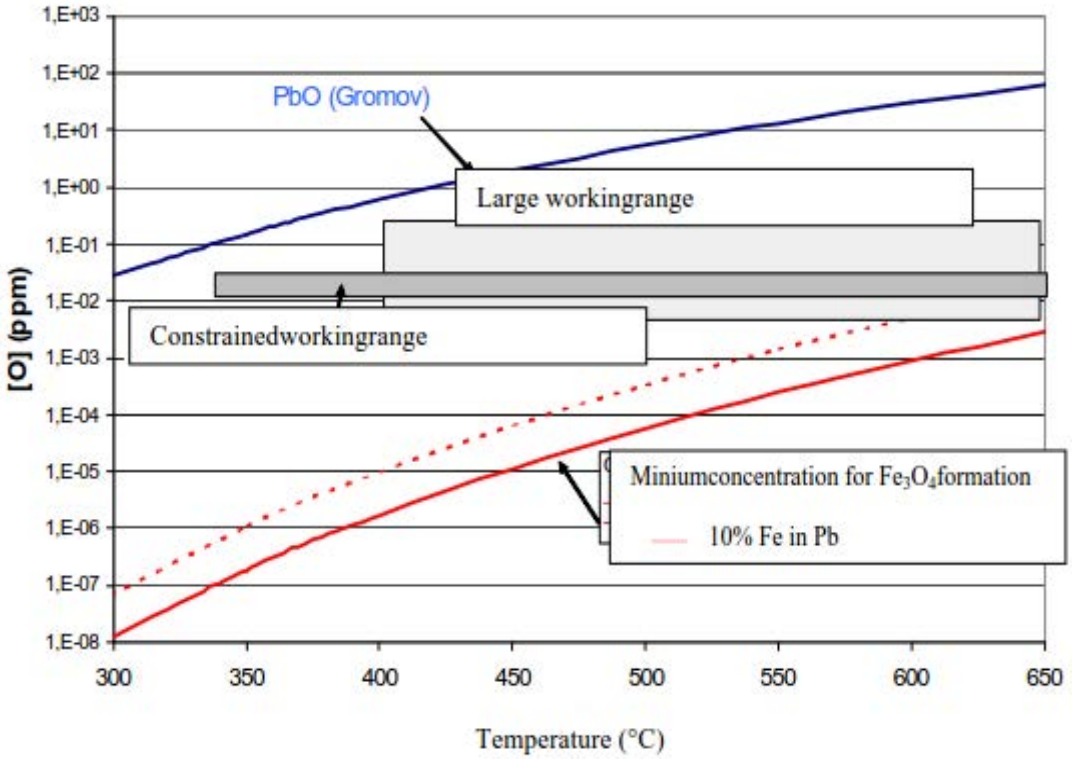
Zona	Temperatura
Core inlet	400°C
Core outlet	480°
Macchia calda	550°C

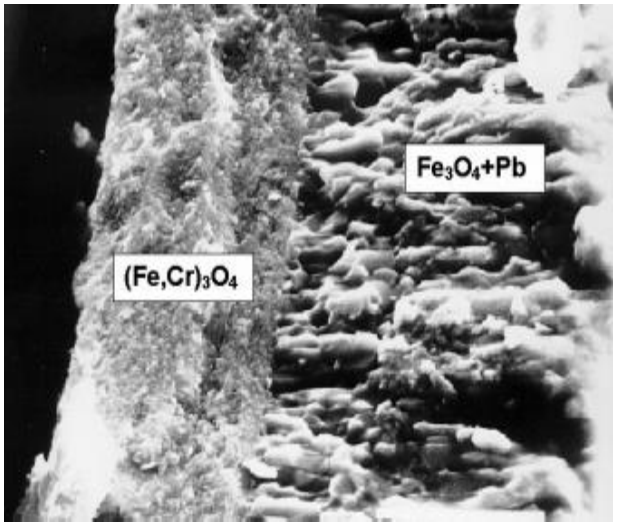
Materiali candidati

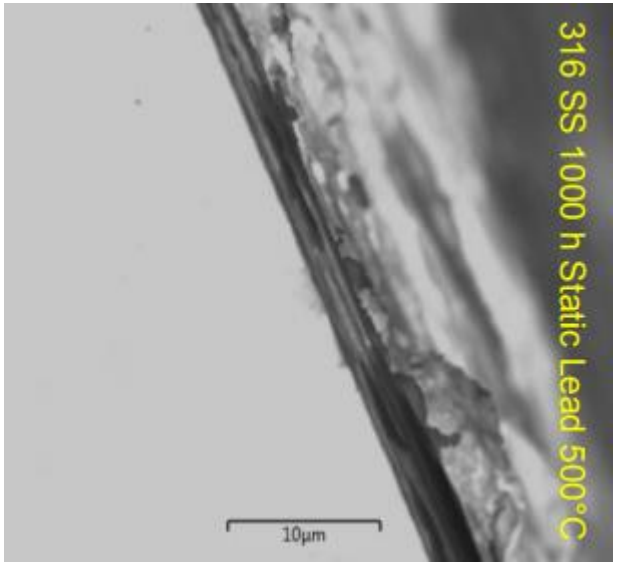
[DEL012] Component	Material	Min/Max Temp. N.O. (°C)	Max lead velocity (m/s)	Max rad. damage (dpa/y)	Max. rad. damage (dpa)
Reactor Vessel	AISI316L	380÷430	0,1	<1E-5	0,0002
Inner Vessel	AISI316L	380÷480	0,2	0,1	0,1
Steam Generator	T91/AISI316L	380÷480	0,6	<1E-5	0,0001
Primary Pumps	MAXTHAL	380÷480	10	<1E-5	0,0001
FA Clad	T91/15-15Ti	380÷550	1	-	(100)
FA Structures	T91/15-15Ti	380÷530			(100)
Dummy Assemblies	T91	380÷480	0,01	-	(100)
Refueling equipment	AISI316L	380÷480	0,2	0,02	0,3
DHR Heat exchanger	T91	380÷430	0,2	<1E-5	0,0001

- Alcuni materiali scartati (T91)
- Incertezze su altri materiali (MAXTHAL)
- Materiali disponibili e normati non resistenti a corrosione ad alta temperatura
- Elevati irraggiamenti non disponibili nelle norme

Controllo della corrosione



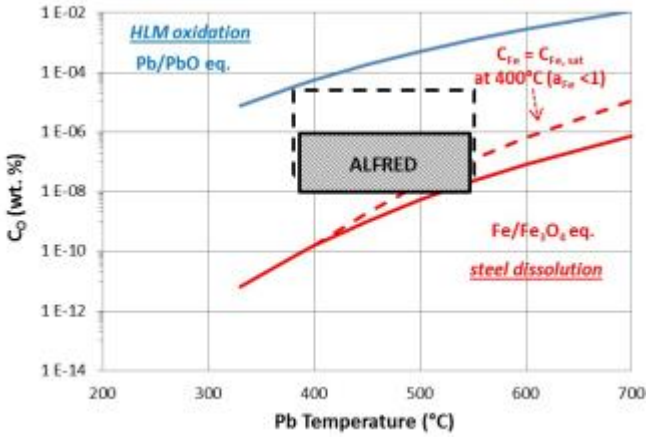




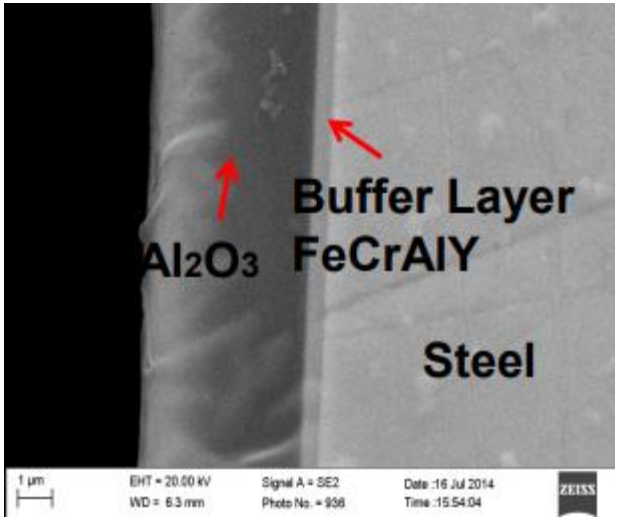
- Rischi connessi alla strategia di controllo dell'ossigeno

Tendenze e linee di ricerca

- T91 sostituito con AISI 316L
- Controllo dell'ossigeno: C_O ~10^{-7} wt%
- Nuove prospettive grazie alla inattaccabilità di Al_2O_3
  - Nuovi coating (PLD-iit, pack cementation-CSM)
  - Nuovi materiali (AFA Steel)



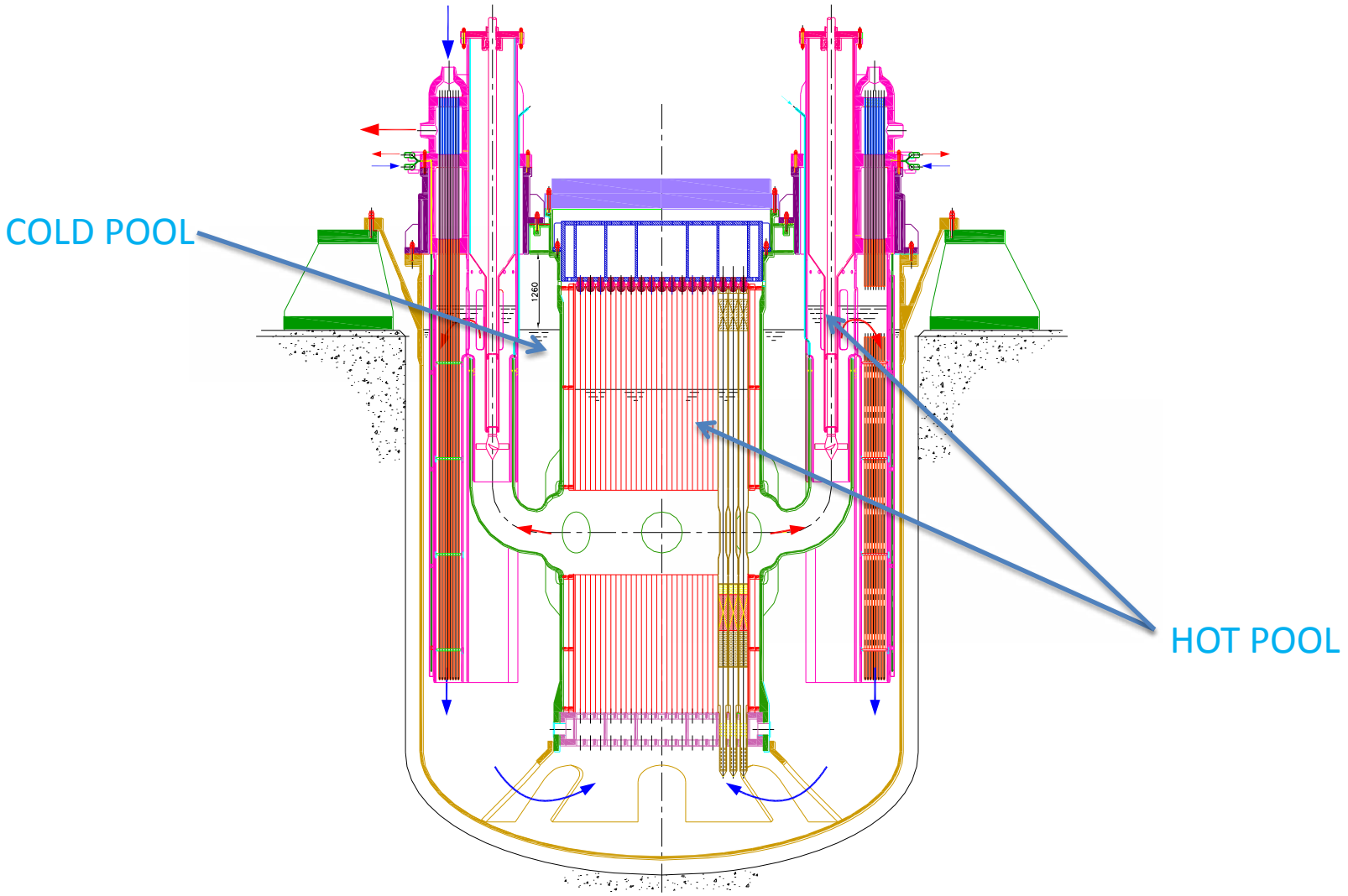
- Approfondimenti necessari in ambito materiali
  - Corrosione + erosione
  - Ciclaggio termico
  - Fatica
  - Creep monoassiale e biassiale
  - Fretting
  - Irraggiamento neutronico



- Soluzione elegante, ma…

Quali sono i tempi e i costi per la qualifica di un nuovo materiale o la standardizzazione industriale e il licensing di un coating?

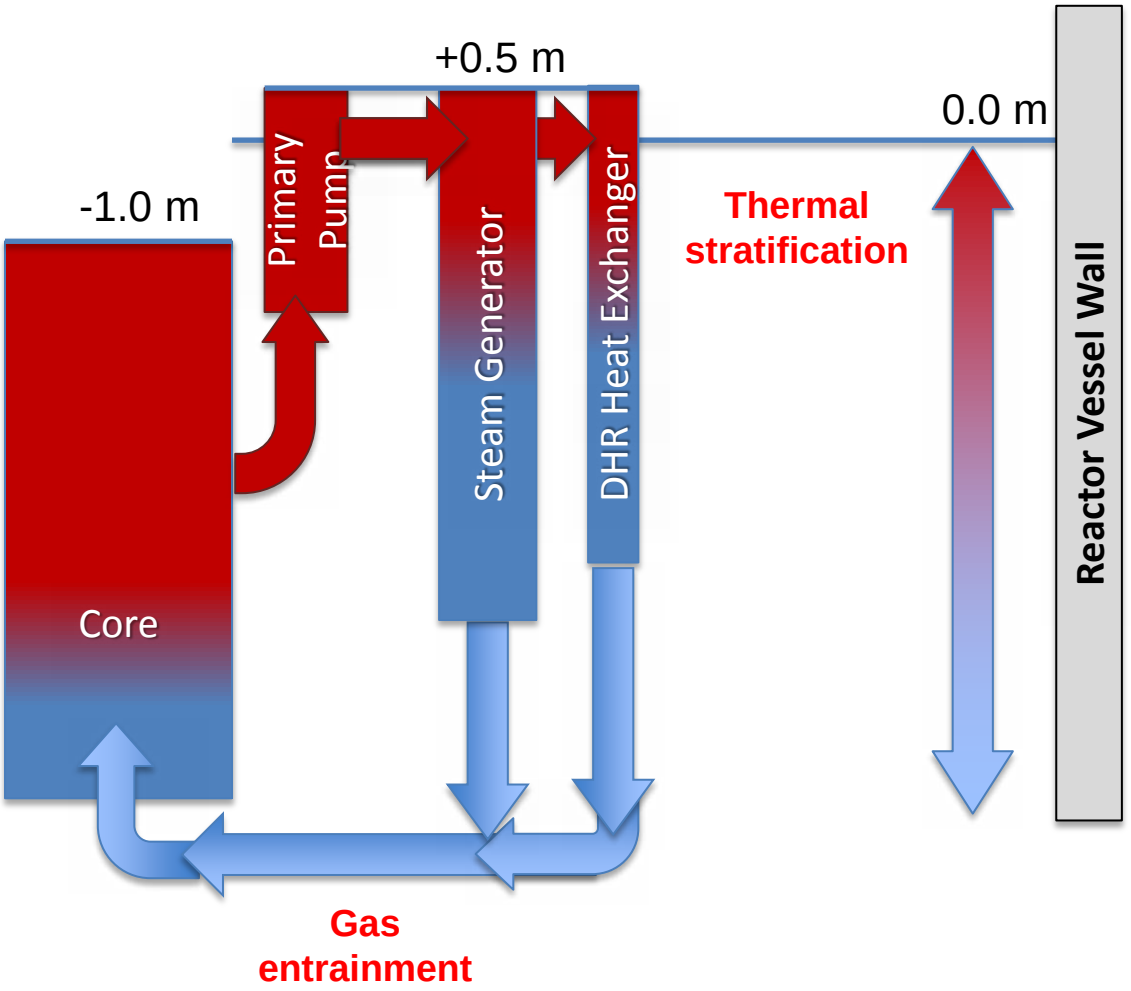
Configurazione termoidraulica



Configurazione termo-idraulica

- Caratteristiche principali
  - Pull-type Primary Pump
  - Primary Pump in Hot Leg
  - Highest level in SG unit
  - Lowest level in the core
  - Small volume of Hot Pool

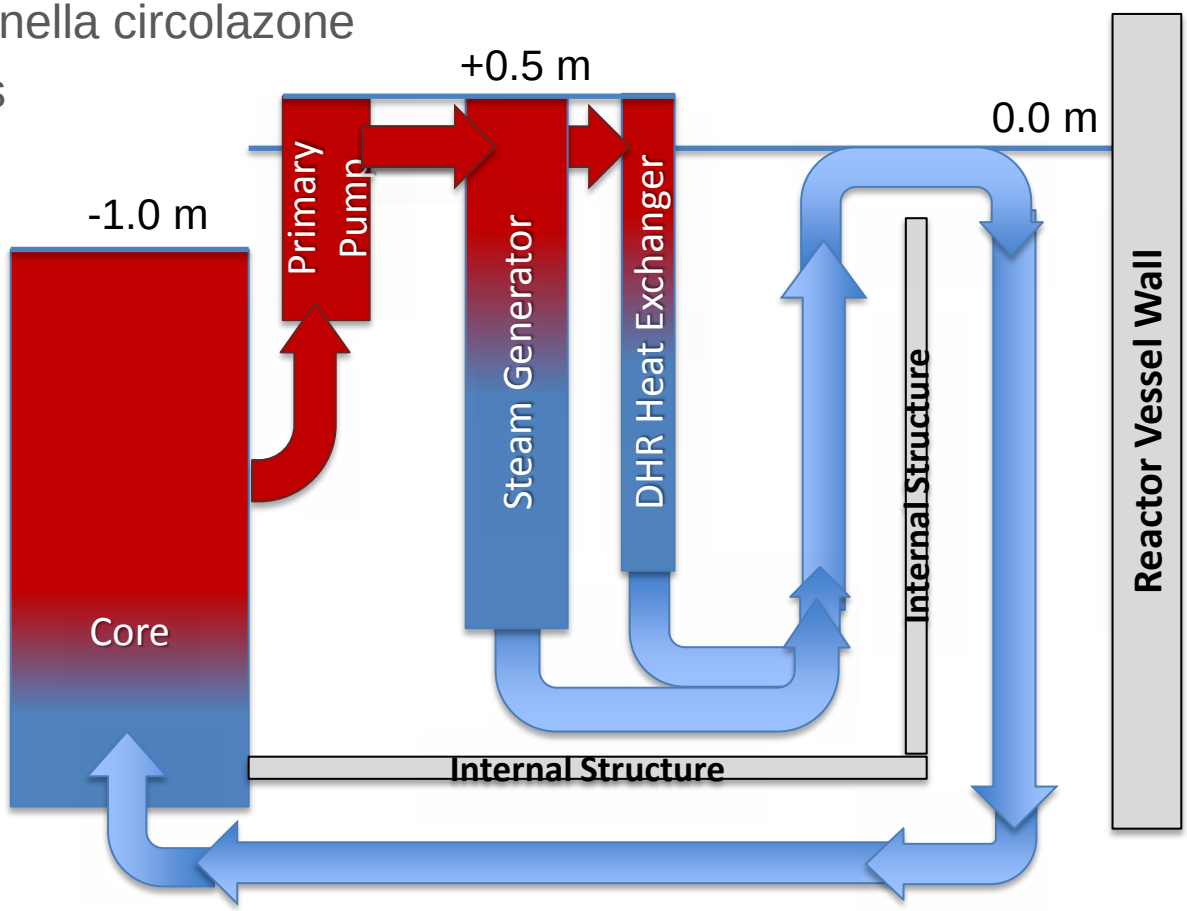
- Soluzione elegante, ma…
  - Soggetta a stratificazione termica in cold pool
  - Possibile gas entrainment in caso di SGTR



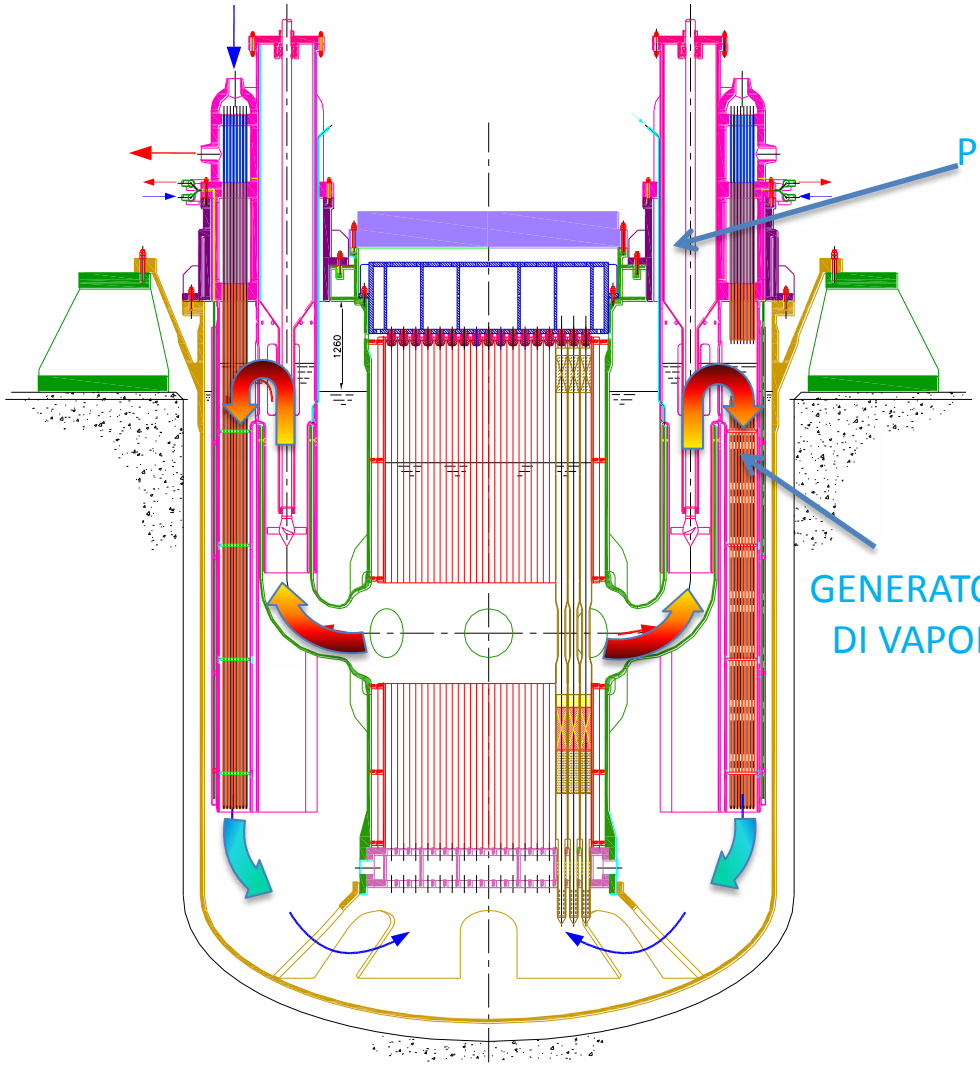
Nuova configurazione investigata

- Inserimento di strutture interne (non safety) per
  - Coinvolgere la cold pool nella circolazone
  - Facilitare il rilascio di gas
  - Mantenere il vessel a bassa temperatura

- Approfondimenti necessari in ambito termo-idraulico
  - Stratificazione in natural circulation
  - Thermal striping
  - Free-level fluctuations
  - Coolant freezing
  - Cellular convection
  - Sloshing

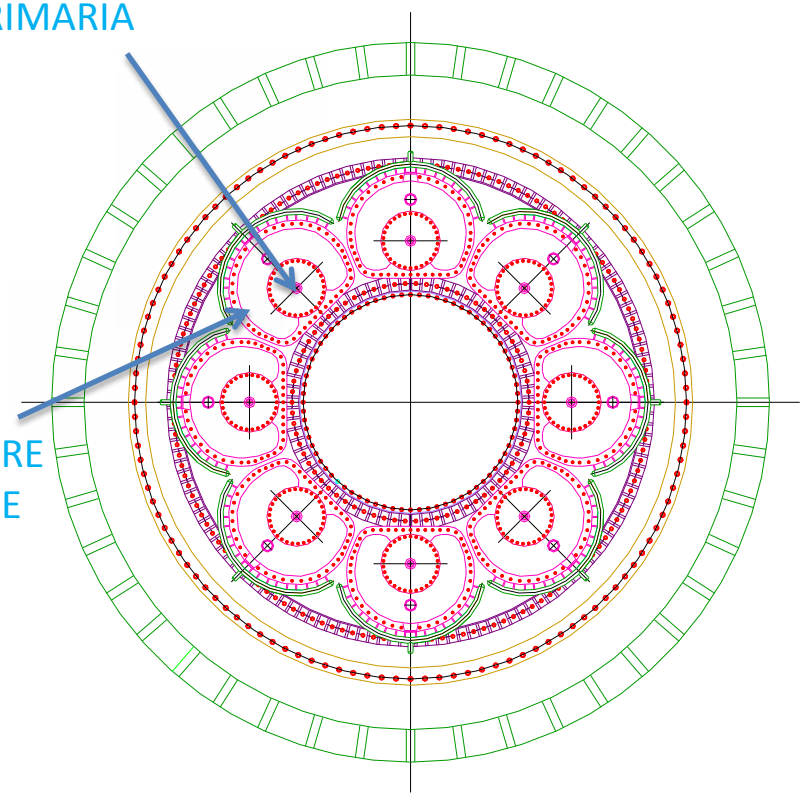


Unità integrata Pompa Primaria e Generatore di Vapore

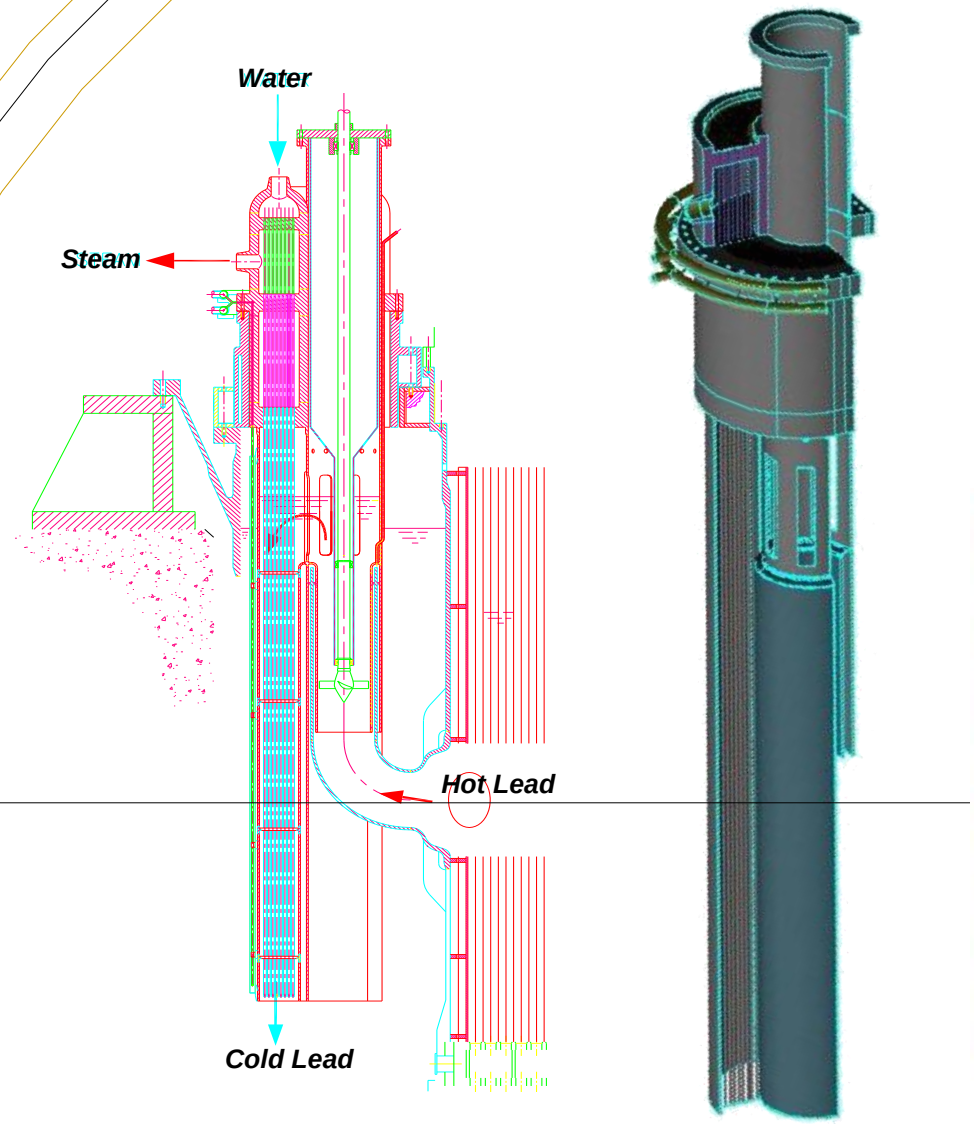


POMPA PRIMARIA

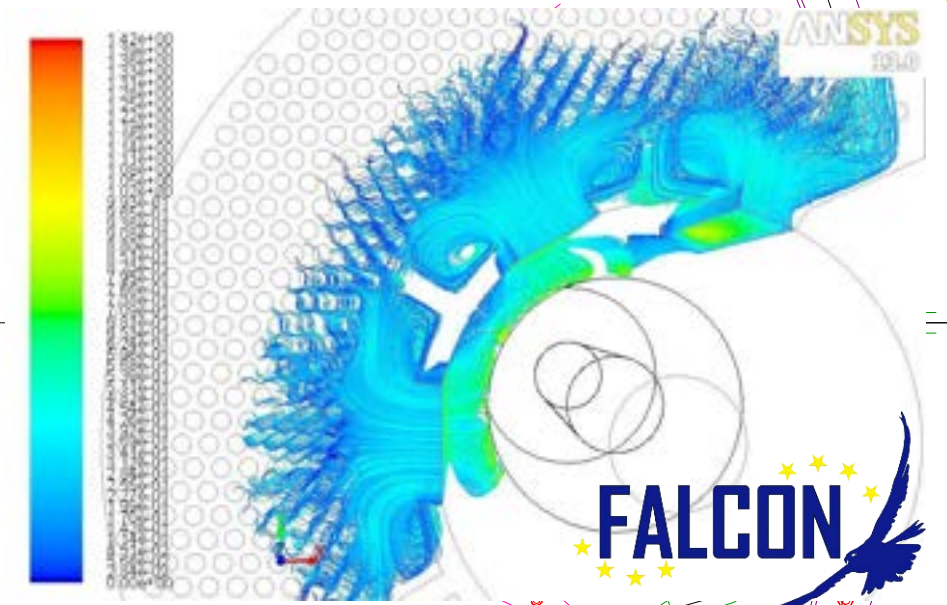
GENERATORE DI VAPORE



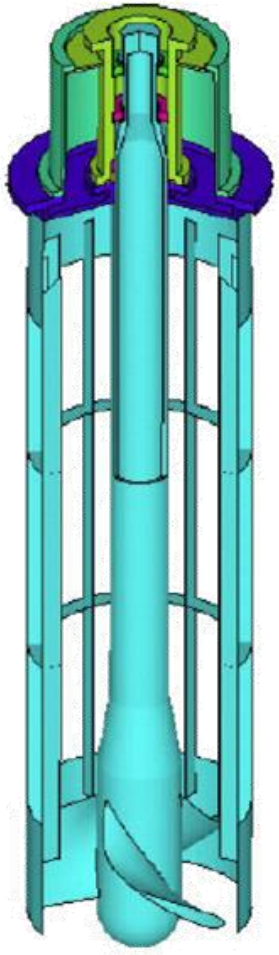
Unità integrata Pompa Primaria e Generatore di Vapore



- Unità integrata (kidney-shape)
- Soluzione elegante, ma…
  - Qualifica dell'upper head
  - Flange non standard
  - Bagnabilità del fascio tubiero

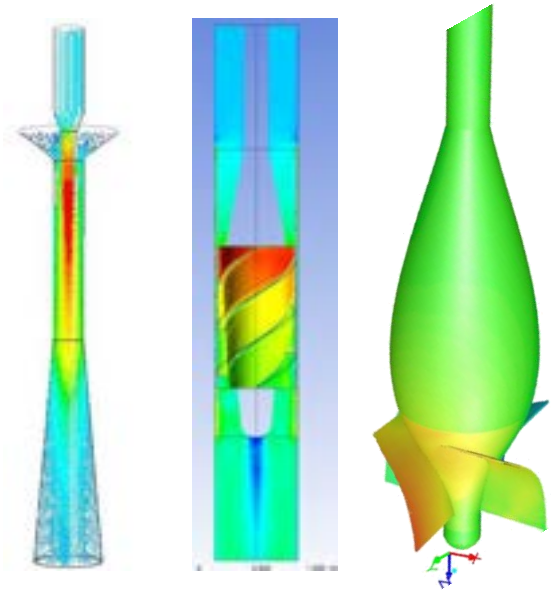


Pompa Primaria



Principali caratteristiche	
Portata	3248 kg/s
Prevalenza	1.5 m
Velocità impeller	315 rpm
Velocità alla tip	~10 m/s
Diametro esterno	~600 mm

Nota: Caduta di pressione minima a rotore fermo

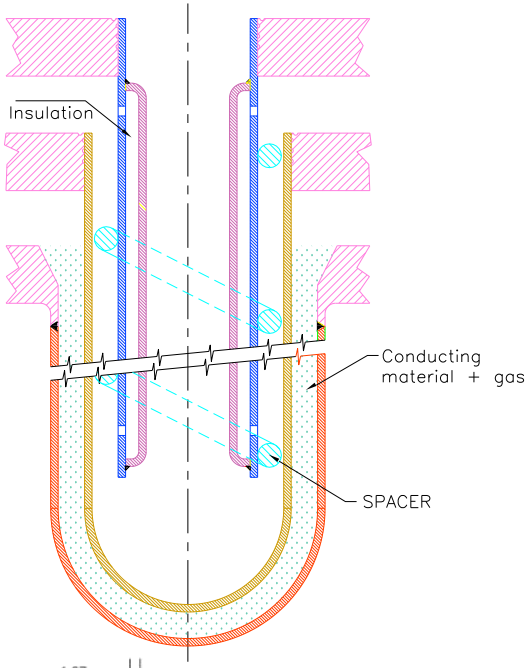


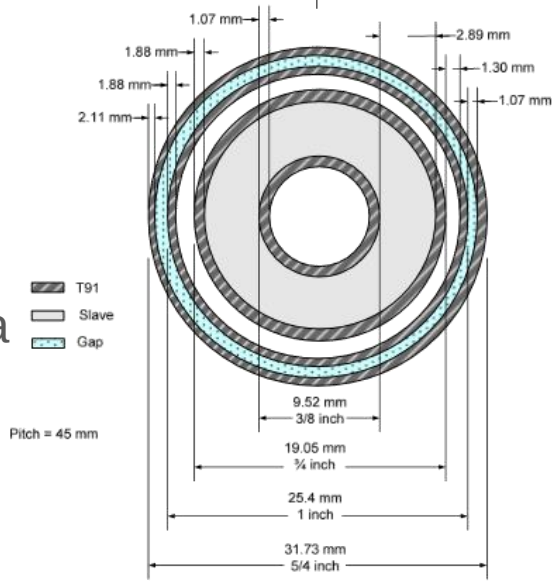
- Altre tipologie
  - Jet pump
  - Screw pump
  - Blade pump

- Approfondimenti necessari
  - Geometria dell'impeller
  - Cuscinetti (idrostatici o auto-lubrificanti)
  - Simulazione CFD delle prestazioni
  - Materiali resistenti a corrosione/erosione
  - Prove sperimentali

Tubo a baionetta con doppia parete

Principali caratteristiche	
Tubi concentrici	4, da 3/8” a 5/4”
Lunghezza di scambio	6 m
Numero di tubi	510
Temperature lato acqua	335°C-450°C
Potenza scambiata	37,5 MW
Rigenerazione attraverso lo sleeve Monitoraggio continuo della integrità	





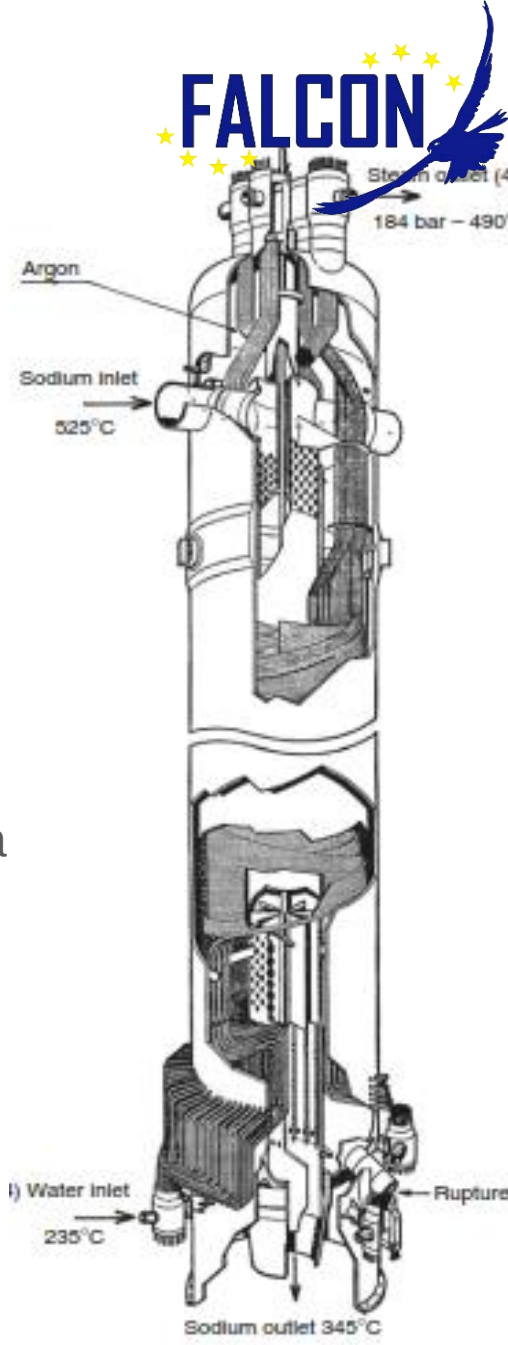
- Soluzione elegante, ma
  - Complessità costruttiva
  - Saldatura inevitabile sul fondo del tubo
  - Problemi di ispezionabilità e plugging
  - Assenza di un materiale di adeguata conducibilità
  - Accettabilità dell’esclusione della rottura a ghigliottina di entrambi i tubi
  - Scarsa efficienza

Opzioni investigate per il Generatore di Vapore

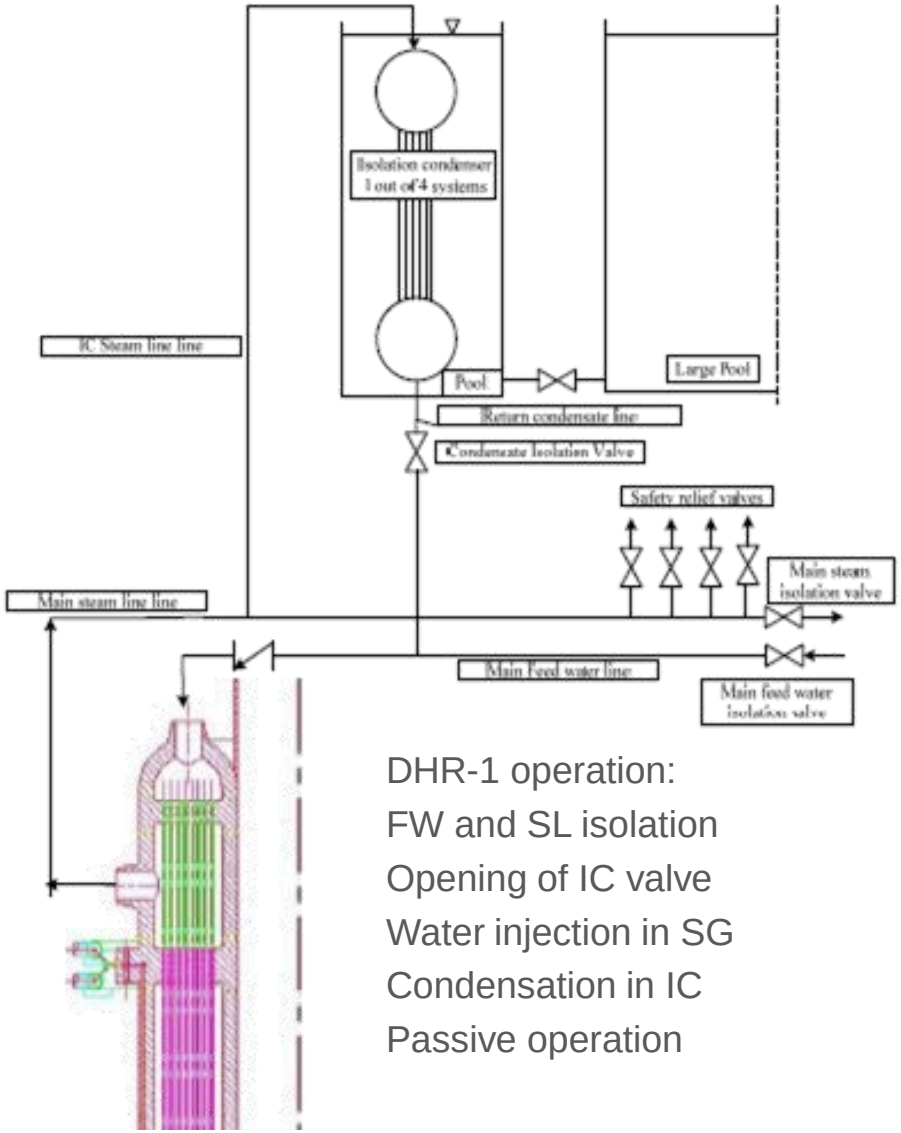


- Disaccoppiamento dei componenti (hot pool)
- Utilizzo di flange standard (componenti a pianta circolare)
- Eliminazione della doppia parete
- Configurazioni alternative rispetto al baionetta

- Approfondimenti necessari
  - Materiale compatibile con piombo e acqua (OTSG con uscita surriscaldata)
  - Coating su tubi non dritti (pack cementation, bending di PLD)
  - Tecniche di ispezione e plugging
  - Analisi in condizioni incidentali (creep)



Sistema DHR



DHR-1 operation:
FW and SL isolation
Opening of IC valve
Water injection in SG
Condensation in IC
Passive operation

- Principi base
  - Secondario usato come DHR attivo
  - SG collegati ad IC (DHR passivo)
  - DHR1 e 2: 4 SG su 8 ciascuno
    - Minimo numero di componenti nella pool
  - Sconto sulla diversificazione, grazie a
    - monitoraggio continuo
    - ridondanza 3 su 4
- Soluzione elegante, ma…
  - Debole diversificazione
  - Non immune al congelamento del piombo

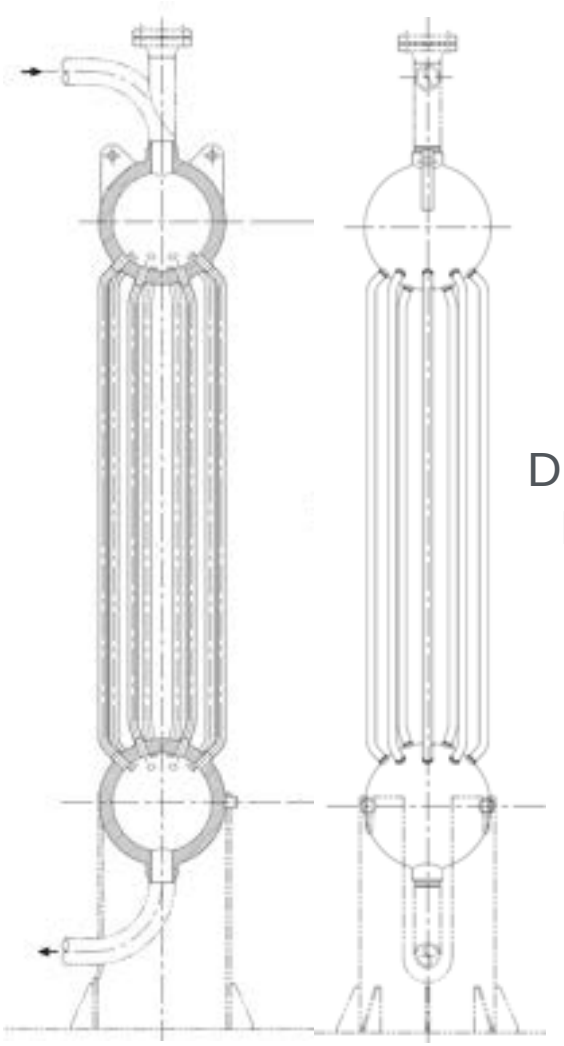
Isolation Condenser: componente chiave del DHR

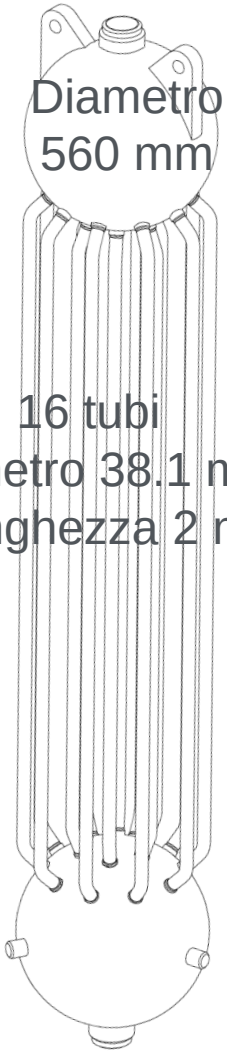
Esperienza italiana (SIET)

ESBWR Isolation Condenser



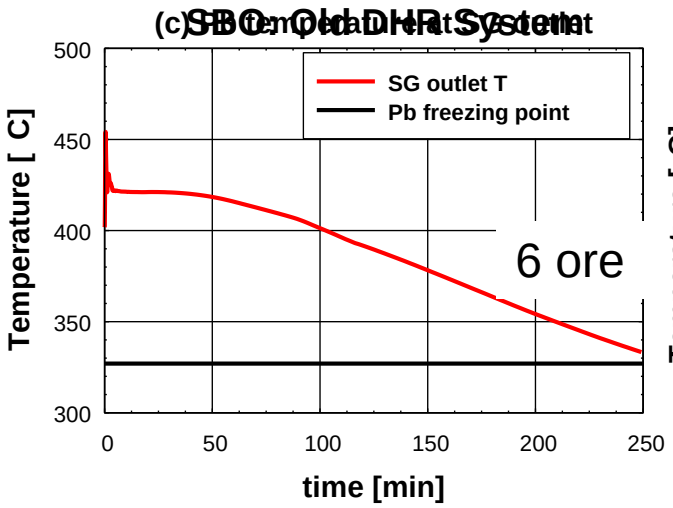
ALFRED Isolation Condenser

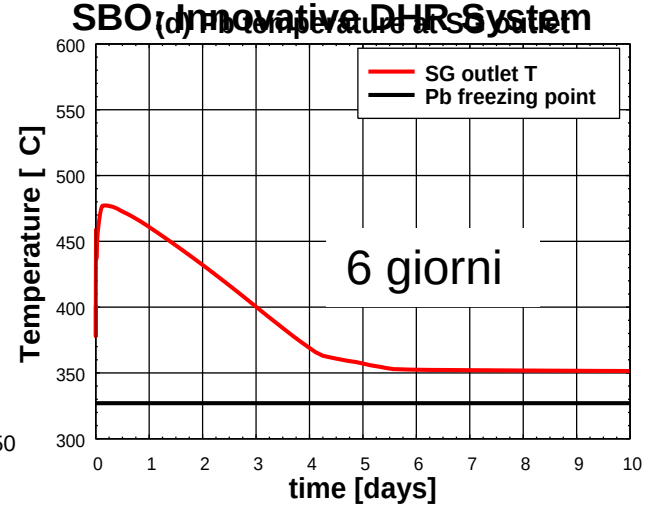




Miglioramenti sul fronte DHR

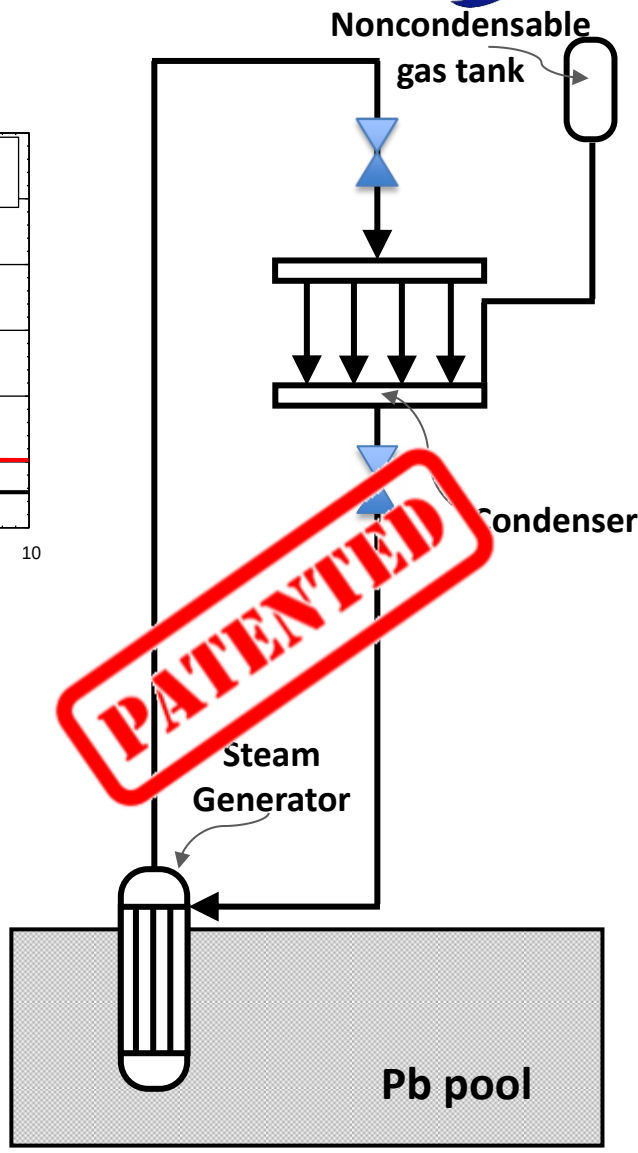
- Anti-freezing system (basato su non-condensabili)



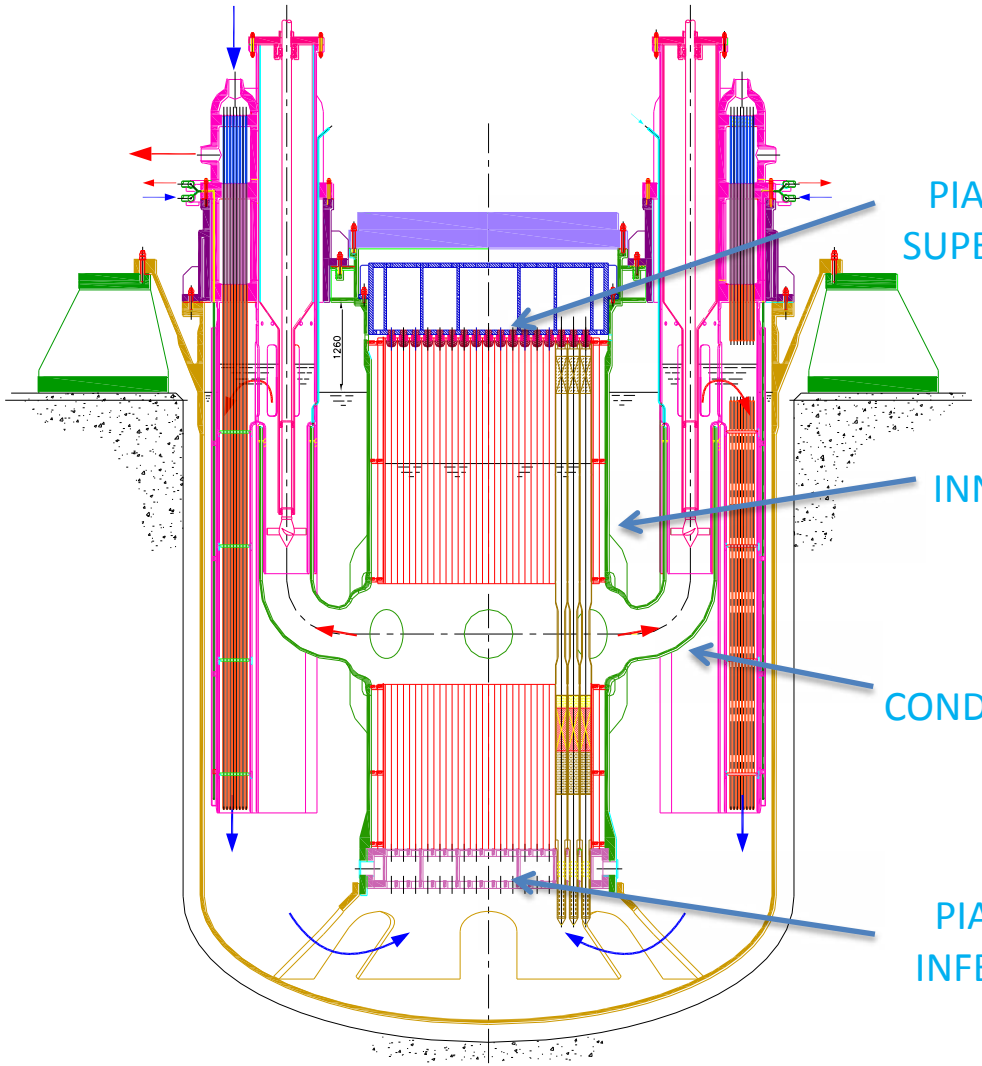


- DHR2 (medesimo principio del DHR1)
  - Dip-cooler con tubo a baionetta a doppia parete
  - Acqua per il funzionamento nell'IC e tank dedicata

- Approfondimenti necessari
  - Test in corso in SIET (ENEA-Ansaldo-SRS)
  - Qualifica codici di calcolo e scalabilità

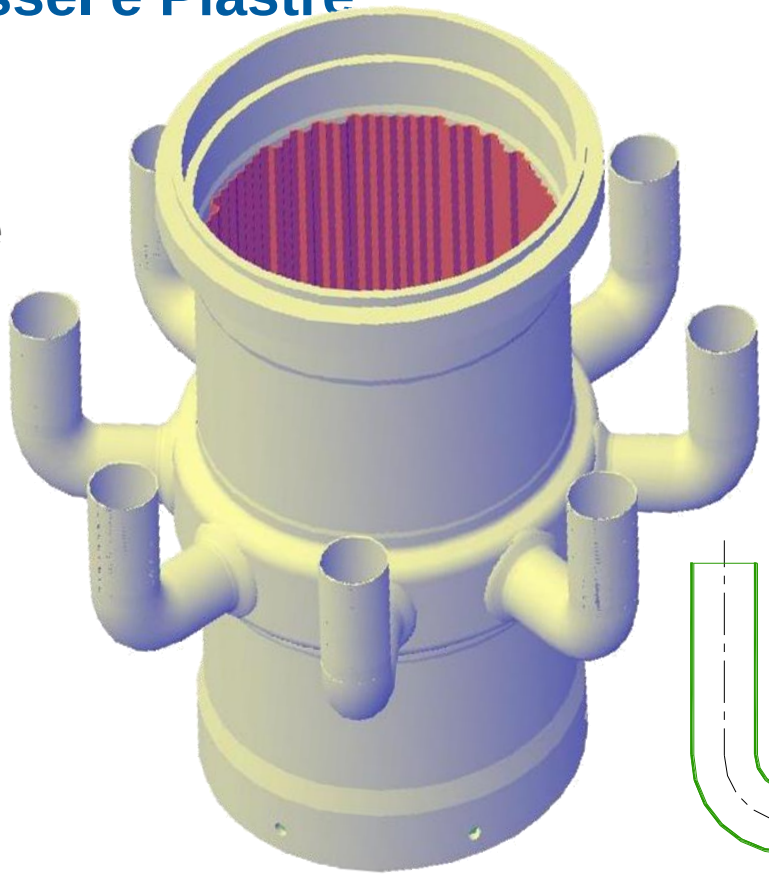


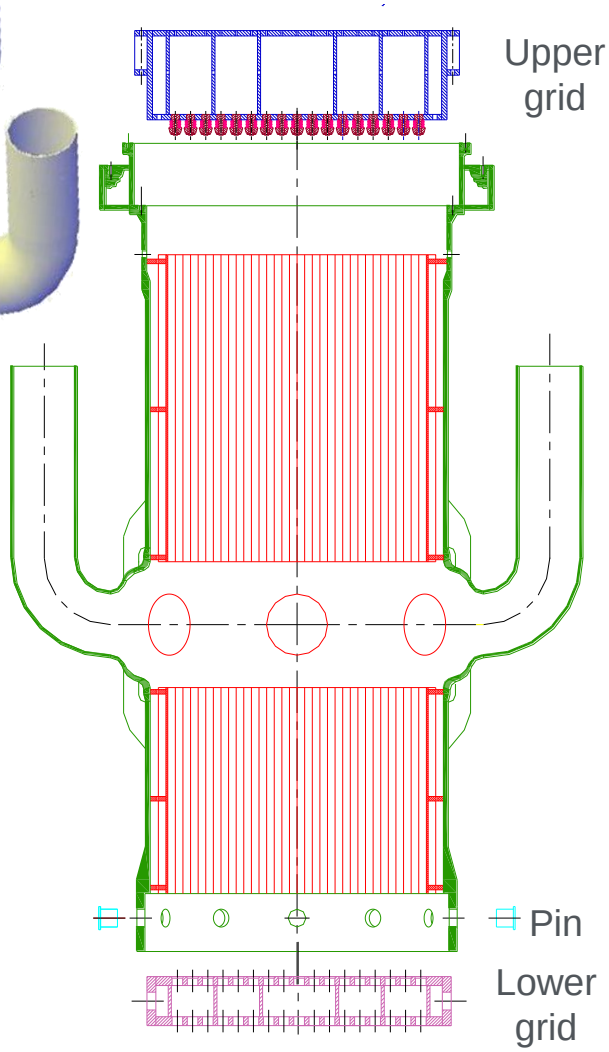
Componenti interni



Inner Vessel e Piastre

- Principali caratteristiche
  - Core restraint
  - Core support
  - “Hot pool”
  - 8 condotti pompa
  - Griglia superiore
  - Griglia inferiore





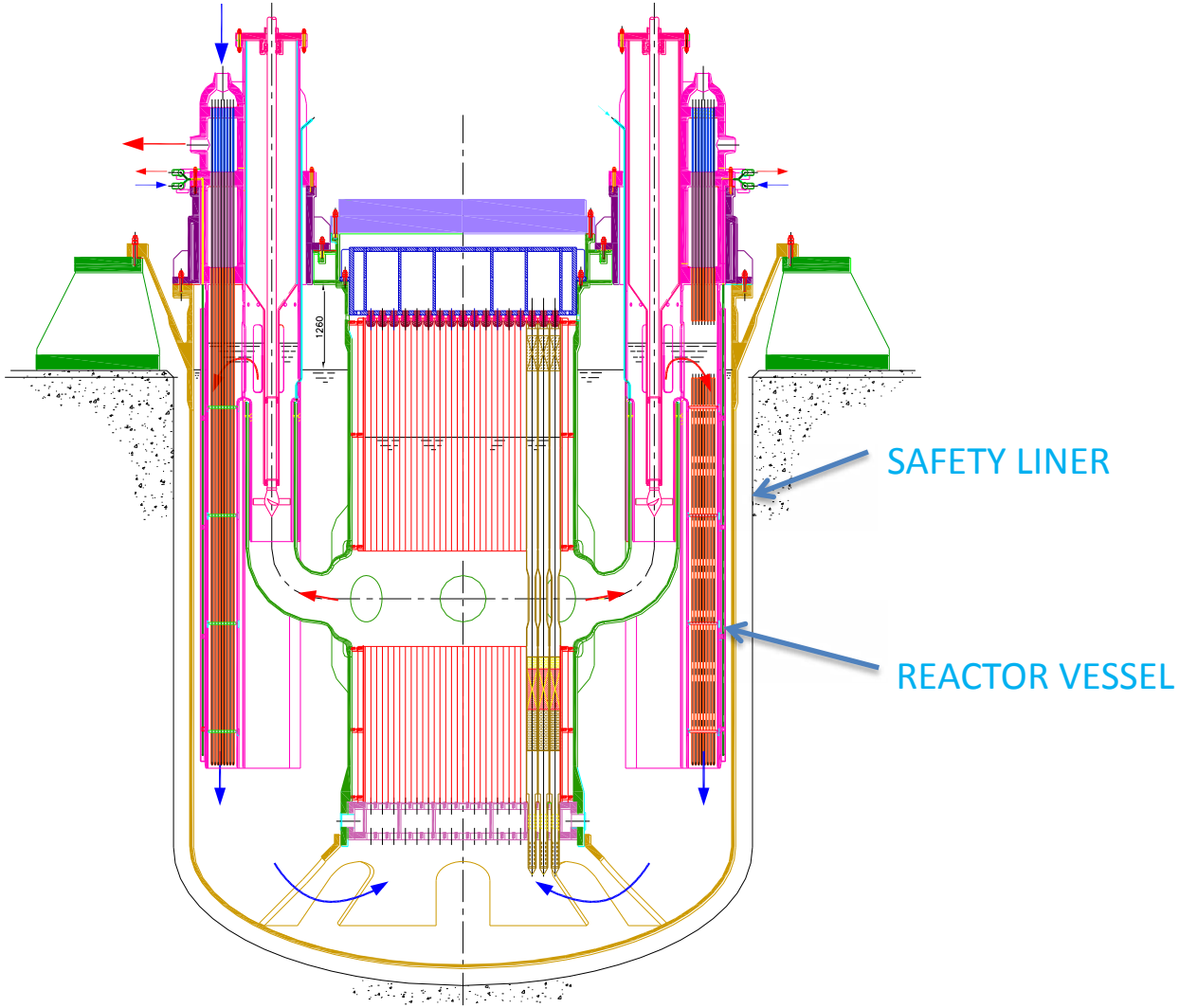
- Soluzione elegante, ma
  - Limitato raggio di curvatura sui condotti pompa
  - Griglia inferiore non ispezionabile
  - Estraibile solo dopo aver rimosso il reactor cover
  - Commistione di funzioni di sicurezza

Opzioni investigate per le strutture interne

- Principali modifiche
  - Separazione della funzioni
  - De-classificazione del flow boundary
  - Estraibilità dell'inner vessel/core barrel
  - Aumentato raggio di curvatura del condotto pompa

- Approfondimenti necessari
  - Requisiti di ispezione imposti dai codici nucleari ed applicabili a FRs
  - Coolability del core anche in caso di leakage dal flow boundary
  - Connessione con il fondo del vessel
  - Connessioni interne
  - Buckling of thin shells, high cycle thermal fatigue, seismic induced forces, design criteria and analysis

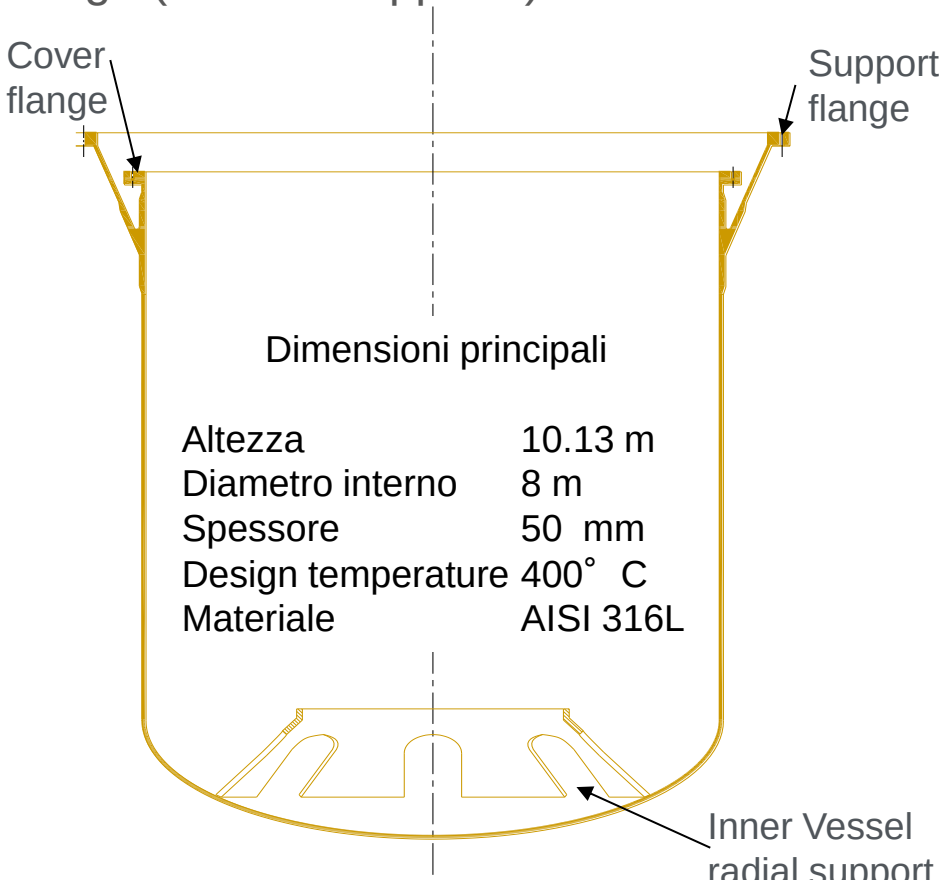
Reactor Vessel e Safety Liner



Reactor Vessel

- Possibili approfondimenti
  - Thin shell buckling (knucle region)
  - Controllo di imperfezioni geometriche (tolleranze di fabbricazione)
  - Massimo diametro disponibile per le flange (cover e supporto)
  - Supporto radiale dell'inner vessel





Safety liner

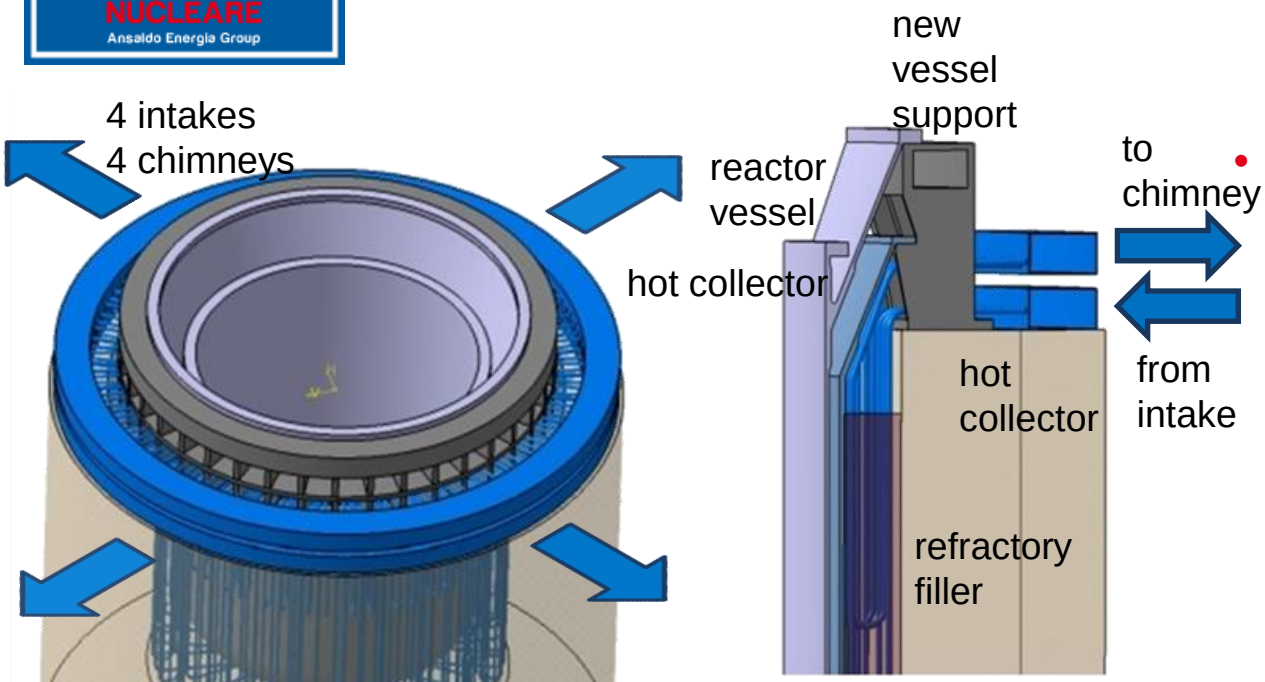
- Principali caratteristiche (design di derivazione ESFR)
  - Liner metallico a contatto con il calcestruzzo della reactor pit
  - Nessuna particolare analisi a supporto
  - Design economico e compatto

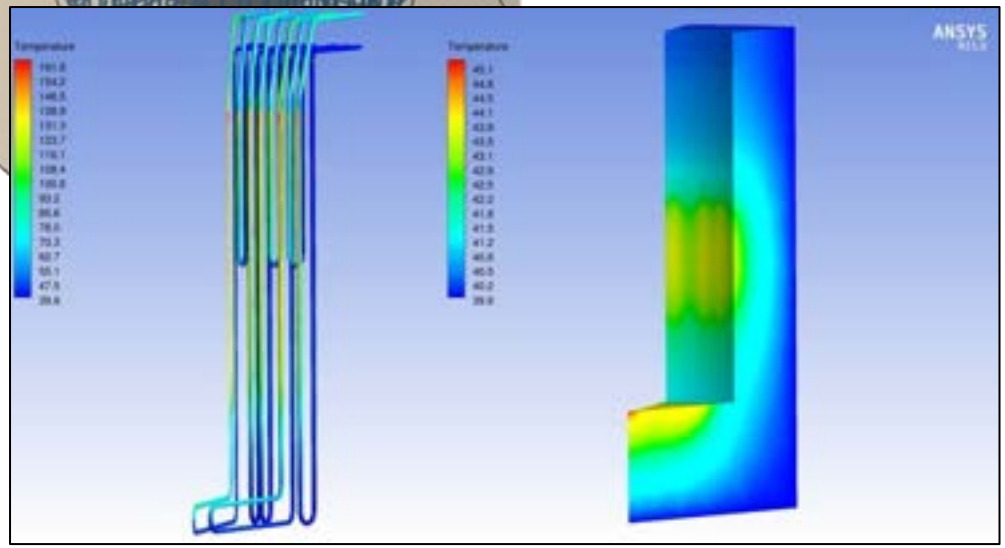
- Soluzione elegante, ma soggetta a requisiti contradditori
  - Minimizzazione delle heat losses: safety liner caldo
  - Compatibilità con il calcestruzzo: safety liner freddo

ACI-349 - Code Requirements (Nuclear Safety related Concrete Structures)

	General (F/°C)	Local areas (F/°C)
Normal operation or any other long term period	150/65	200/93
Accident or any other short term period	350/175 (surface temperature)	650/343

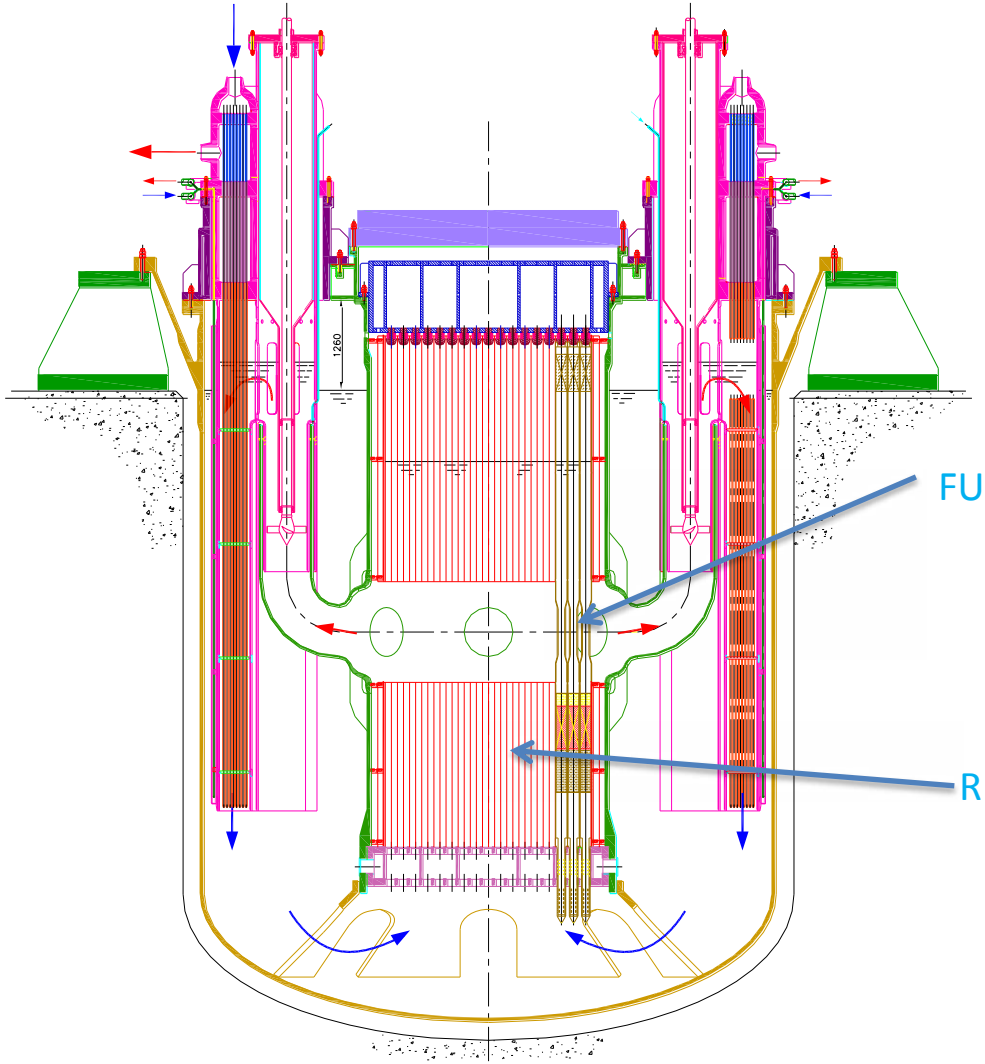
Safety Vessel





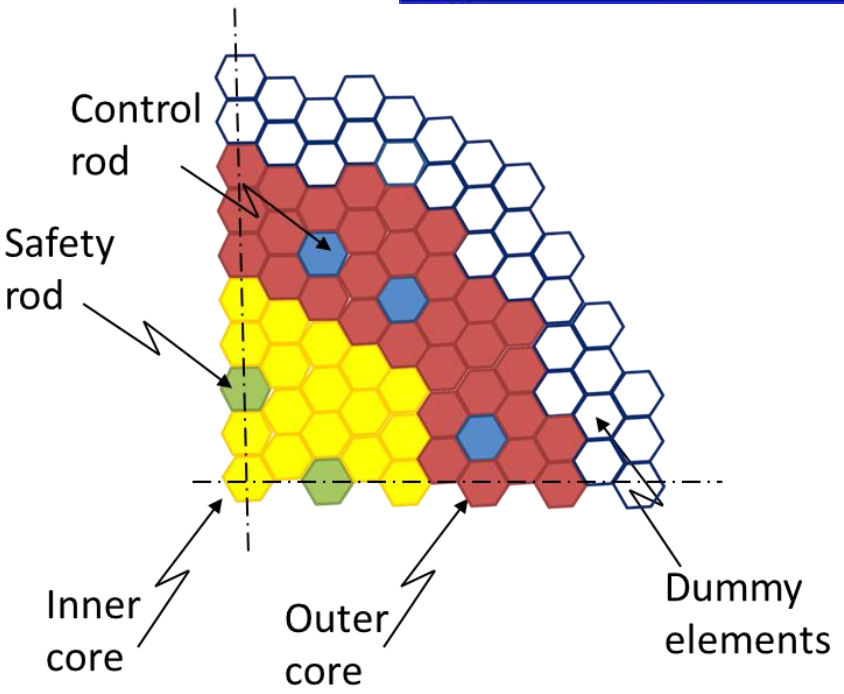
- Principali modifiche
  - Safety vessel
  - Sistema passivo di raffreddamento (cavity cooling)
  - Layer di lightweight concrete
- Approfondimenti necessari
  - Sonde robotizzate per ispezione di vessel e safety vessel
  - Verifiche strutturali della reactor pit (concrete reinforcement)

Reactor Core e Fuel Assemblies



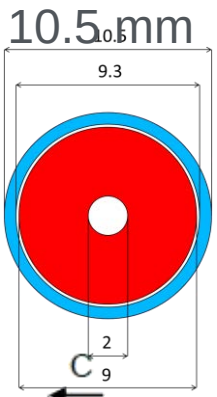
Core e controllo della reattività

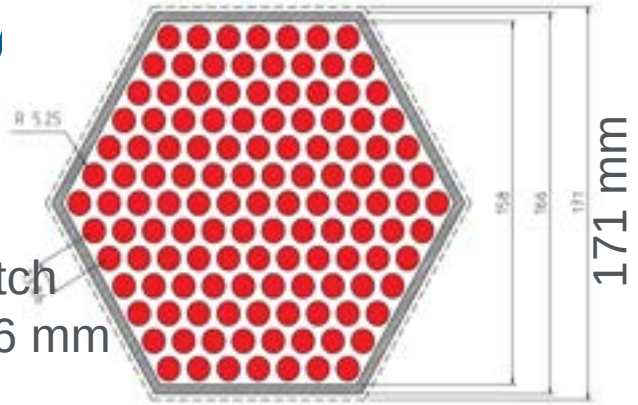
Power (MWth)	300
Fuel Assemblies	171
Fuel type	MOX
Pu enrichment Inn/Out (at %)	21.7/27.8
Control/shutdown Rods	12
Safety Rods	4
Dummy elements	110
Fuel cycle length	365 EFPD
Peak/avg BU (MWd/t)	103/73.3

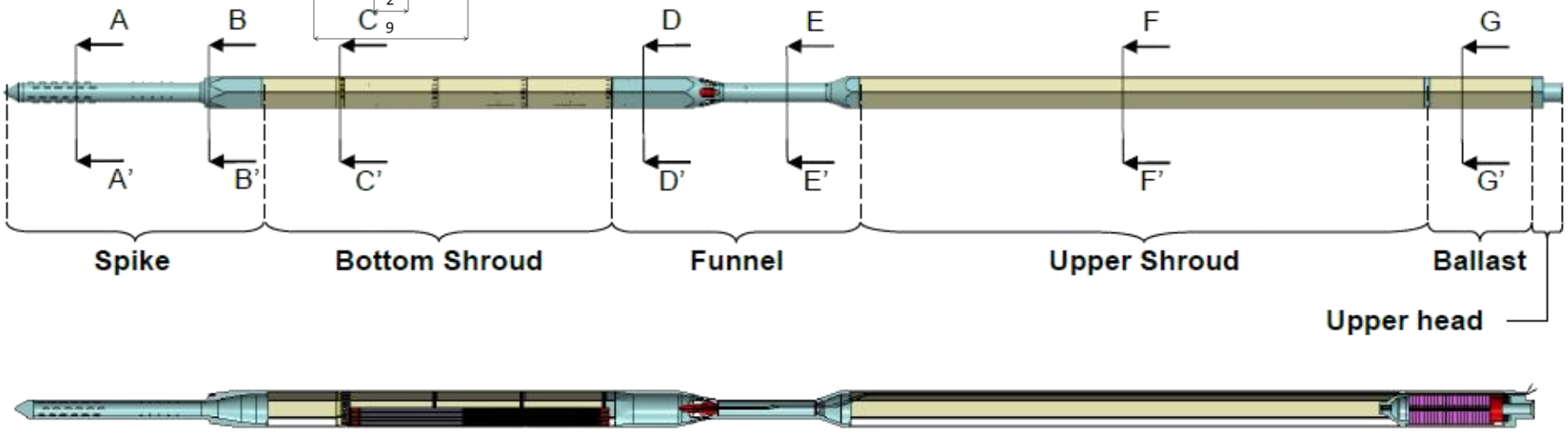


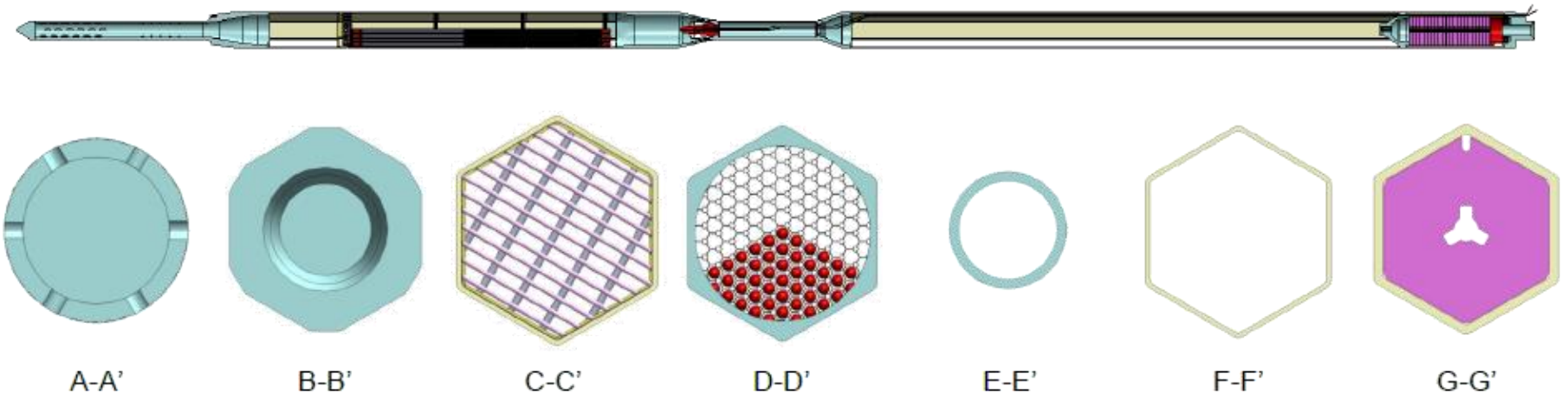
- 2 sistemi ridondanti, indipendenti e diversificati
- CR usate in regolazione e in SCRAM
  - estratte verso il basso, inserite per buoyancy in SCRAM
- SR usate solo per SCRAM
  - completamente estratte, inserite tramite un sistema penumatico
  - mantenute in posizione da un ballast in tungsteno
- Ciascun sistema è efficace anche se la barra più reattiva si blocca
- Durante il refueling entrambi i sistemi sono inseriti

Fuel assembly





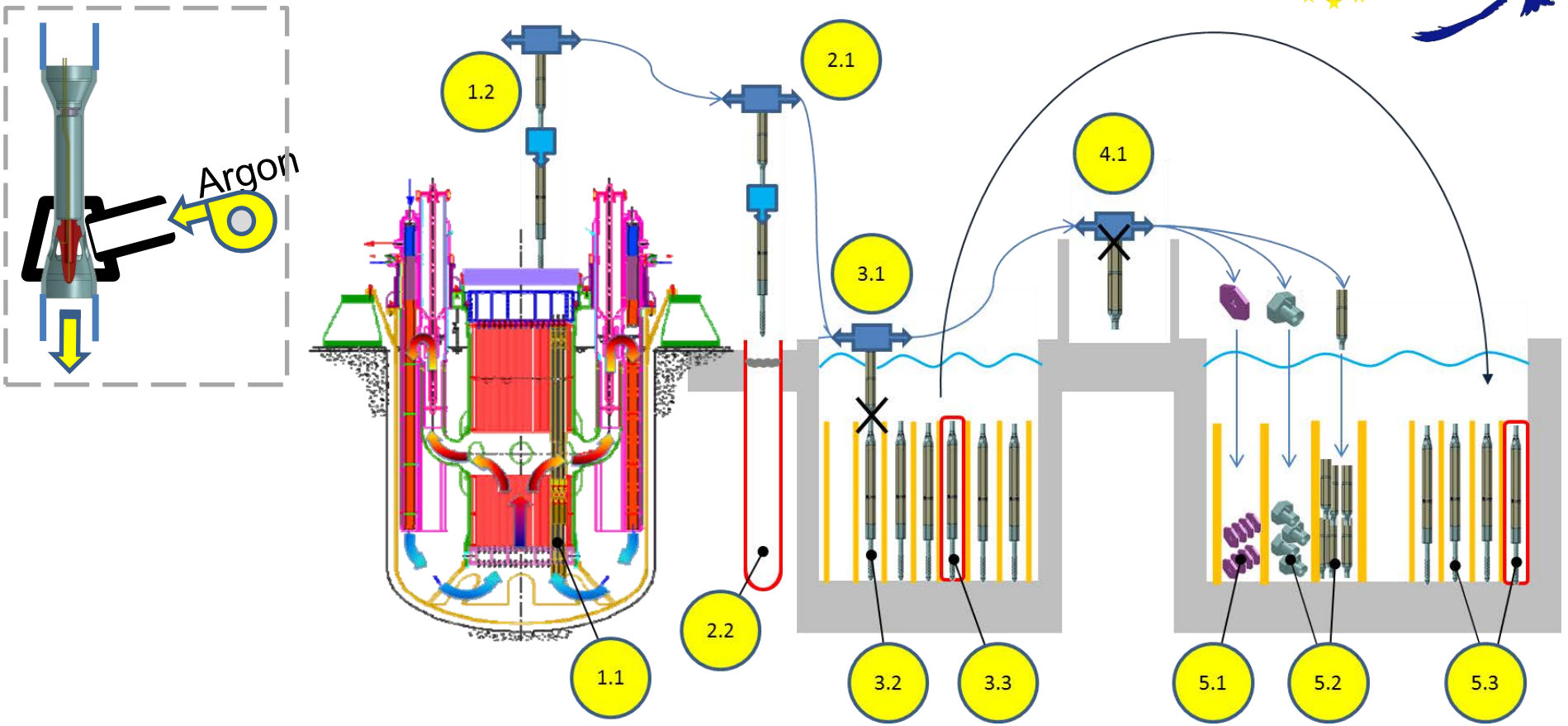




Modifiche e investigazioni sul Core

- Principali modifiche apportate
  - Aggiustata la termica delle barrette d'angolo
  - Irrobustita la monitorabilità del nocciolo
  - Migliorato lo schermaggio dell'Inner Vessel
  - Superate alcune approssimazioni di modello
  - Ingegnerizzata la configurazione
  - Definiti i cocktail per failed fuel detection con gas-tagging
  - Propagate le incertezze
- Approfondimenti necessari
  - Ricerca sperimentale sul fuel per ridurre ulteriormente le incertezze…
  - Programma di qualifica per fuel assembly e control/safety rods
  - Riduzione del gas plenum e ottimizzazione dello spike
  - Progettazione meccanica del fuel assembly
  - Riduzione del numero di dummies e ottimizzazione dello schermaggio
  - Effetti di core compaction
  - Terzo sistema di arresto (fail-safe e passivo)?

Fuel handling system



- Non pienamente compatibile con la filosofia di impianto passivo
- Da ripensare in modo integrato

Priorità e prospettive

Cosa è stato fatto per rendere più pratico un reattore accademico?

Su cosa occorre investire ancora nel breve e nel lungo termine?



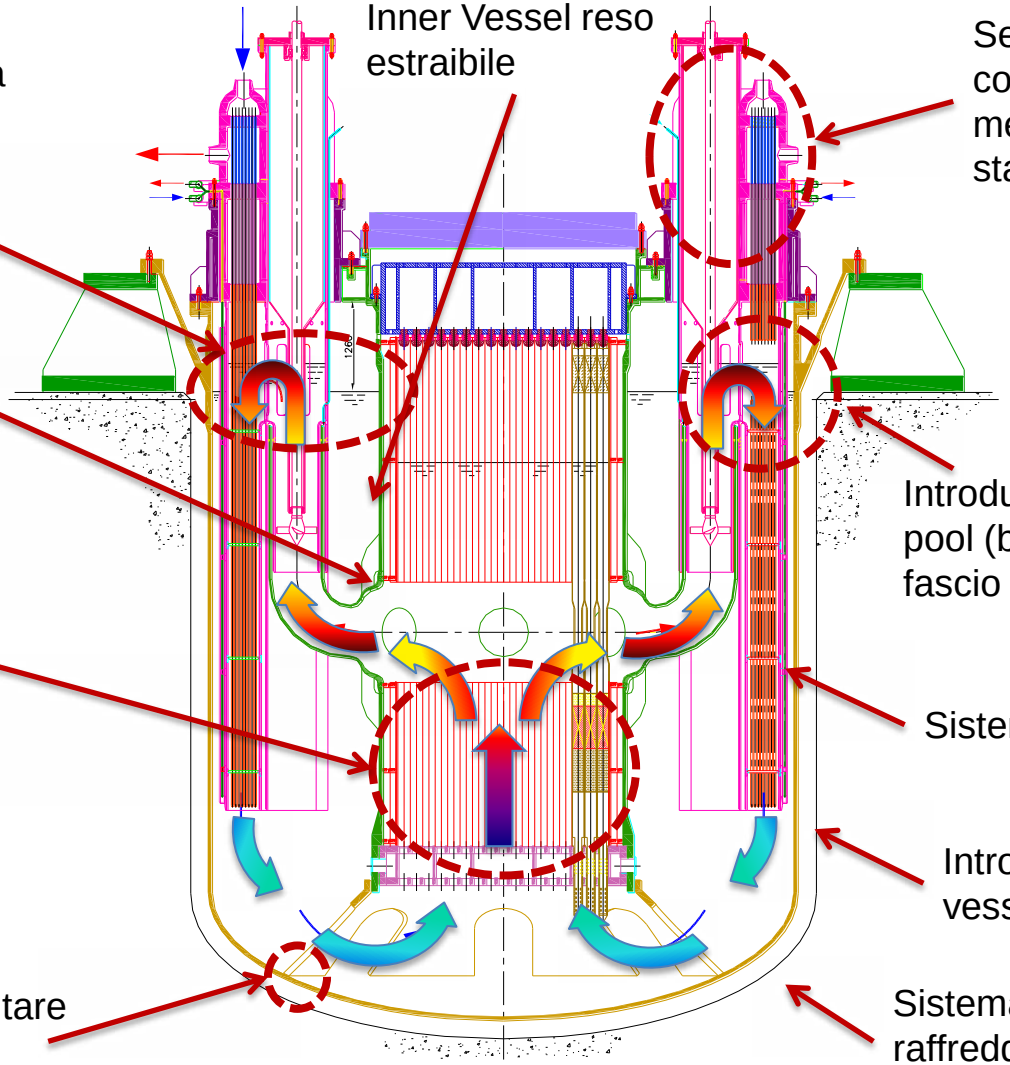
Aree migliorate

Stratificazione termica e gas entrainment eliminati con nuova configurazione termo-idraulica

Inner Vessel reso estraibile

Separazione dei componenti (qualifica meccanica, standardizzazione)

Funzioni di sicurezza delle strutture interne separate



Introduzione di una hot pool (bagnabilità del fascio tubiero)

Ottimizzazione ed ingegnerizzazione del core

Sistemi DHR diversificati

Introdotto un safety vessel

Radial restraint ripensato per evitare ispezioni

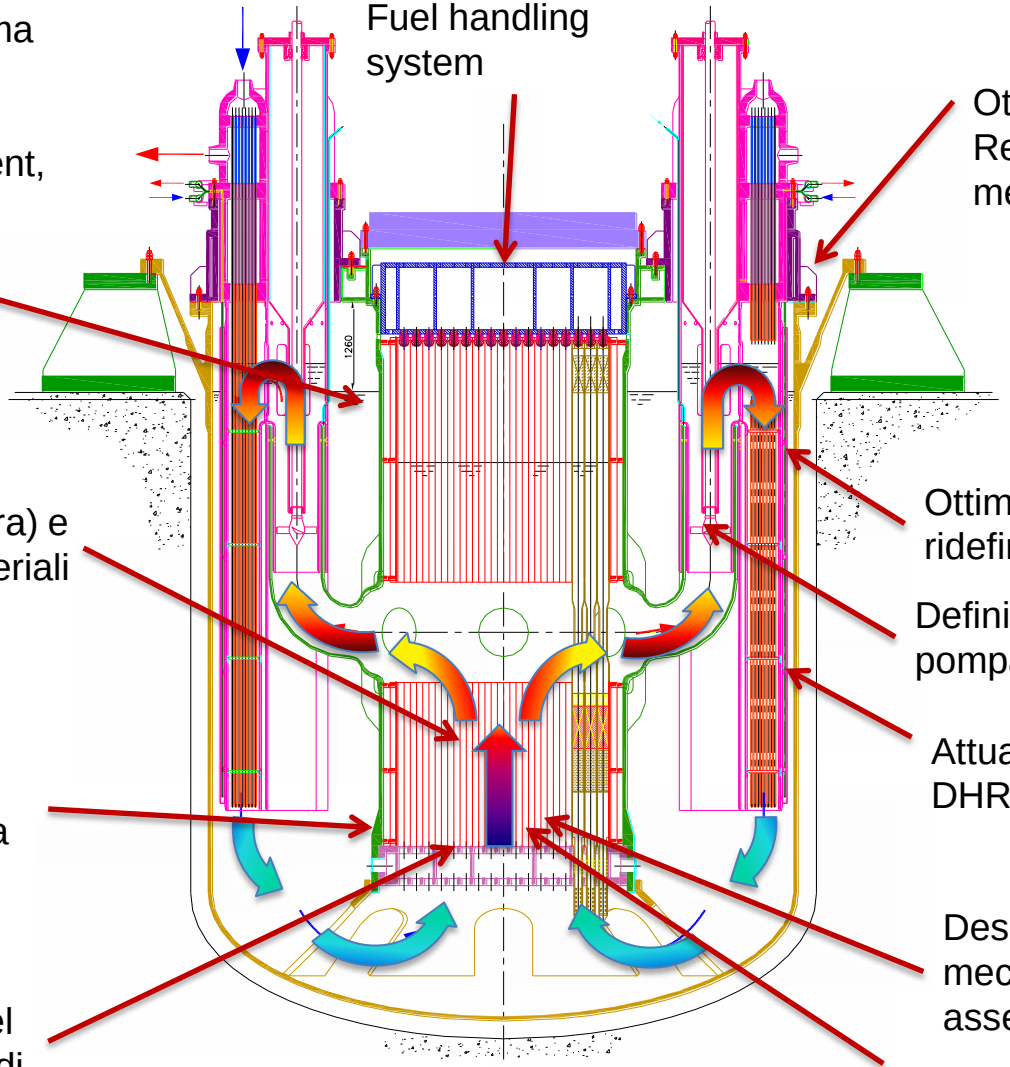
Sistema passivo di raffreddamento della cavity

Aree da migliorare

Analisi termoidrauliche di sistema (circolazione naturale)
Analisi CFD
(thermal striping, gas entrainment, free level fluctuation,…)

Fuel handling system

Ottimizzazione del Reactor cover (layout, mechanical design)



Condizioni operative (massima temperatura) e compatibilità coi materiali

Ottimizzazione o ridefinizione dello SG

Definizione della pompa primaria

Riduzione delle dimensioni del core (anche a discapito della vita dell'inner vessel)

Attuazione passiva del DHR2

Ottimizzazione della parte inferiore del fuel assembly (riduzione di altezza)

Design termo-meccanico del fuel assembly

Qualifica del fuel assembly (grid spaced)

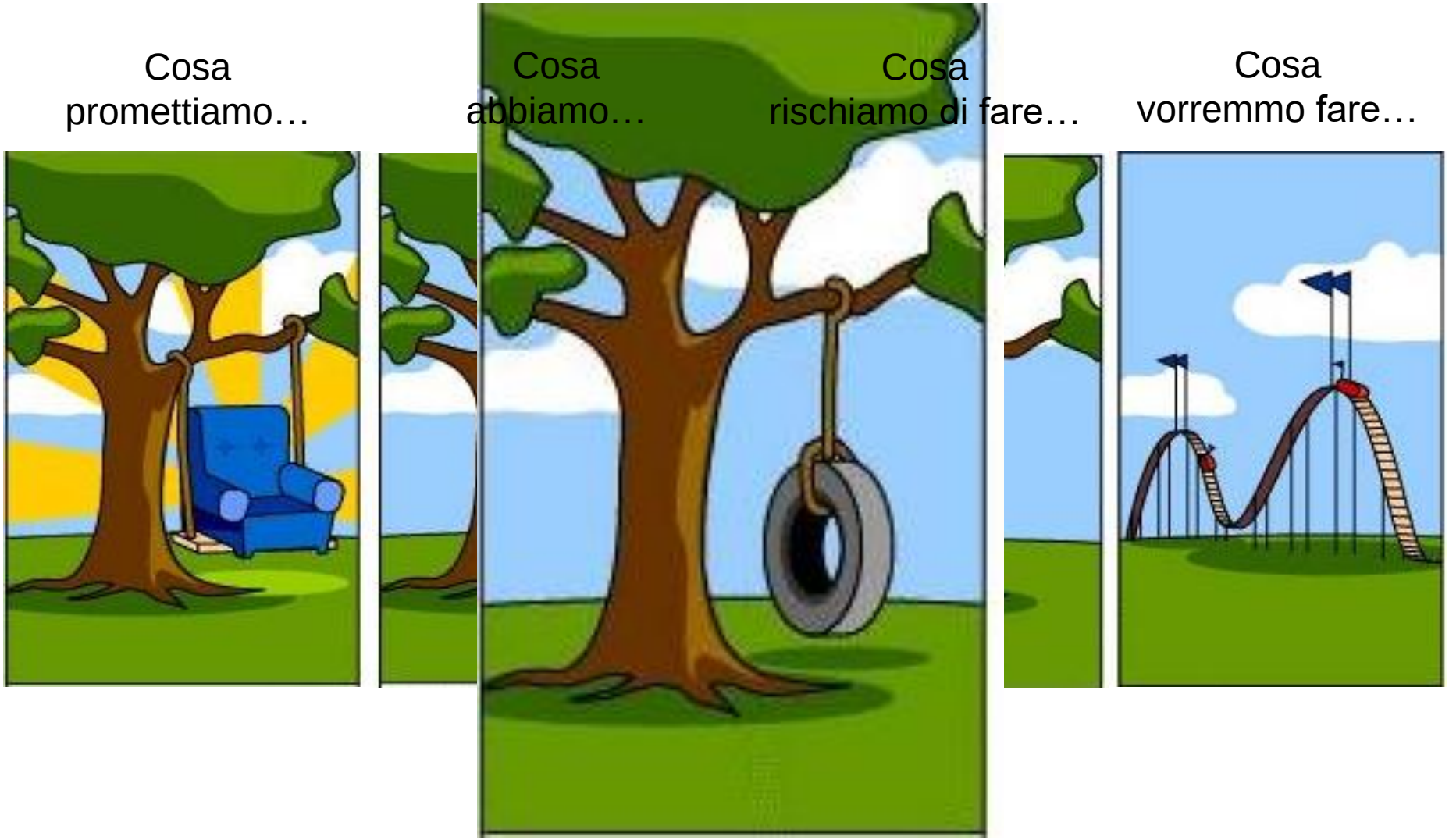
Cosa manca per arrivare ad avere un "Practical Reactor"?

- Altri temi di interesse trasversale
  - Strumentazione e logica di controllo
  - Strategia di confinamento
  - Gestione degli incidenti severi (difficili da escludere per un dimostratore)
  - Strategie di ispezione, manutenzione, refueling

- Strategia per lo short-term
  - Definire un design consistente ed un piano sistematico di R&D
  - Adeguare la potenza del reattore per mantenere ridotte dimensioni
  - Concentrarsi su materiali esistenti e colmare i gap
  - Esercire il dimostratore a bassa temperatura
  - Utilizzare il dimostratore stesso per qualificare nuovi materiali

- Strategia di lungo termine
  - Perseverare sulla qualifica di materiali innovativi e coating
  - Migliorare le prestazioni nel lungo termine
  - Integrare soluzioni ottimizzate grazie alla flessibilità del dimostratore

Colmare il divario tra aspettative, necessità e risultato



Agenzia nazionale per le nuove tecnologie,
l'energia e lo sviluppo economico sostenibile

Termomeccanica di nocciolo

Analisi vibrazionale della barretta

Aula Magna
Scuola di Ingegneria e Architettura, Università di Bologna
26-27 settembre, 2017

Alessandro Poggianti – ENEA

Contesto del lavoro

Riferimento

L'intera Linea Progettuale 2 è dedicata all'avanzamento della tecnologia del **LFR**, con attività tanto in campo tecnologico in senso stretto, quanto progettuale ed analitico. Le attività tutte vertono su **ALFRED**, assunto a riferimento nella sua qualità di **dimostratore** della tecnologia **LFR**.

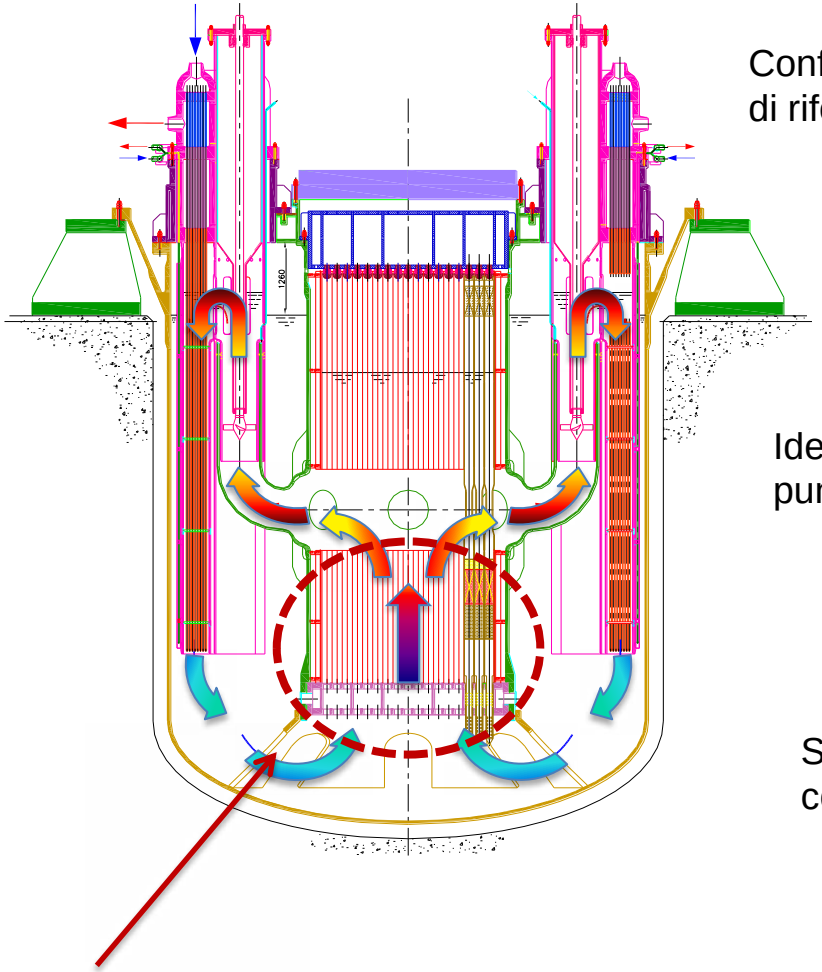
Fra le attività condotte nell'ambito dell'AdP, un blocco considerevole è dedicato al **progetto di nocciolo**, abbracciando in particolare:

- sviluppo, revisione e raffinamento del progetto;
- sviluppo, validazione ed applicazione di metodologie e strumenti di analisi a supporto della progettazione.

ALFRED core design: cosa è stato fatto

Nelle passate annualità è stata dettagliatamente analizzata la configurazione di riferimento del nocciolo, identificandone punti critici che sono stati quindi più dettagliatamente analizzati fino ad individuare soluzioni correttive.

Queste ultime sono infine state raccolte ed armonizzate, consentendo di proporre una configurazione ottimizzata ed ingegnerizzata del nocciolo.



Configurazione di riferimento

Identificazione punti critici

Soluzioni correttive

Raccolta e armonizzazione

Ottimizzazione ed ingegnerizzazione del core

Contesto del lavoro

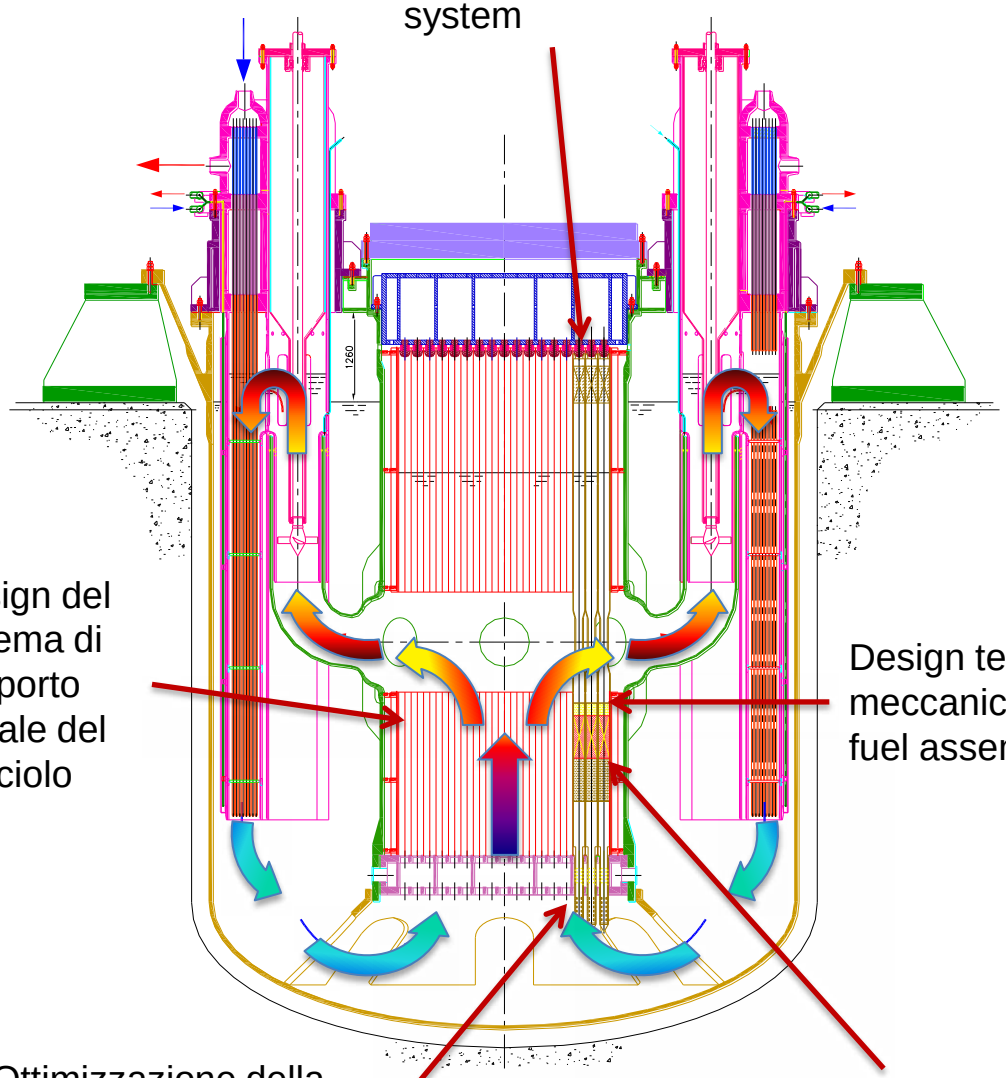
Razionale

Tanto in ambito progettuale, quanto a livello di capacità analitiche, si è rilevata un'**asimmetria** fra gli stati di avanzamento dei lavori nel campo della **termomeccanica** da un lato, e della **neutronica e termoidraulica** dall'altro.

Per questo motivo è stato deciso, a partire dal PAR2016, di avviare una pesante **azione di ricerca e sviluppo**, volta non solo ad una conoscenza più approfondita dello stato termomeccanico dei componenti di nocciolo di ALFRED, ma anche a disporre di strumenti appositamente concepiti per supportare la progettazione termomeccanica di questi.

ALFRED core design: cosa c'è da fare

La maggior parte dei punti aperti sul progetto di nocciolo riguardano il corretto dimensionamento (e, qualora richiesto, la rivisitazione) dei principali componenti del nocciolo, avendo come riferimento ultimo la qualifica dell'elemento di combustibile, del sistema di supporto del nocciolo e del sistema di movimentazione degli elementi freschi ed esausti per e da il nocciolo.



Analisi vibrazionale

Corner rod cooling and flow induced vibration in an ALFRED fuel assembly – FALCON doc. NRG-23591/16.140918

- Dati geometrici
- Proprietà fisiche di fluido e barretta
- Temperature del fluido
- Possibili risonanze a 400Hz e 10.2 Hz

Ipotesi

- Spacer posizionato fuori dalla zona attiva

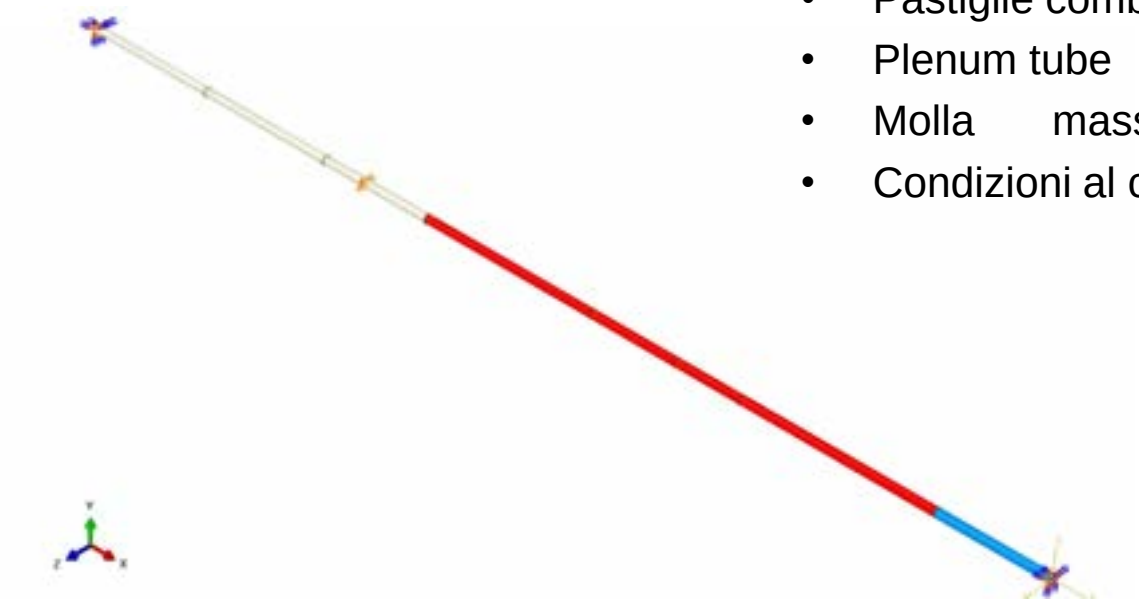
Aspetti da investigare

- Frequenze naturali della barretta
- Vibrazione della barretta immersa nel fluido
- Influenza delle barrette vicine
- Valutazione di possibili urti tra le barrette

Modello Elementi Finiti barretta

Barretta (componenti interni)

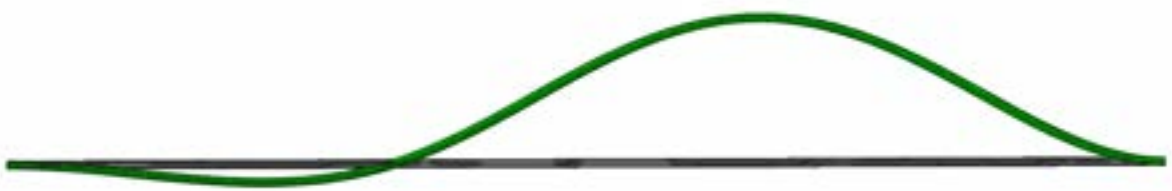




- Elementi ‘Shell’ per la guaina
- Pastiglie combustibile masse
- Plenum tube massa + rigidezza
- Molla massa
- Condizioni al contorno incastro

Analisi modale

Forme modali e frequenze



Mode	Hz
1	30.0
2	83.5
3	163
4	220
5	302
6	455

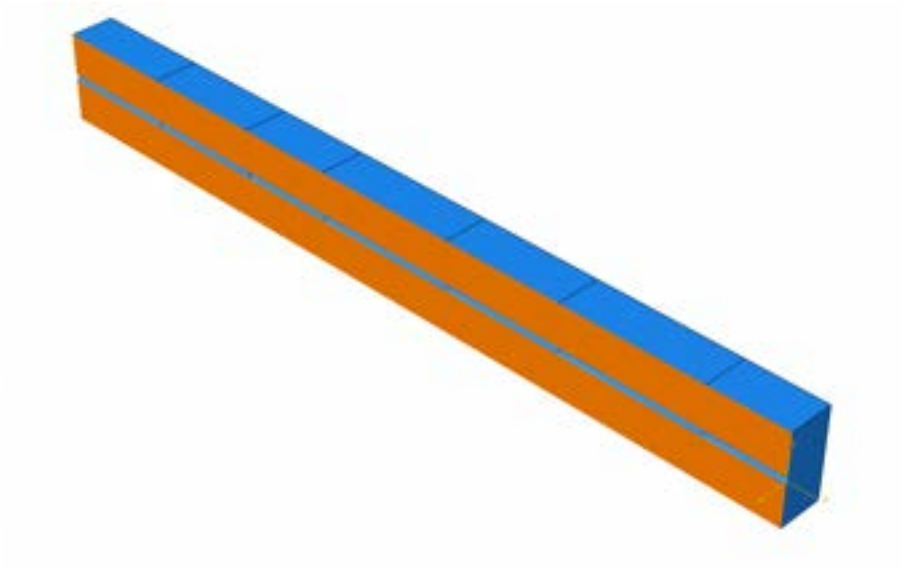




Analisi dinamica della barretta immersa nel fluido

- L’analisi modale non tiene in conto la presenza del fluido attorno alla barretta
- E’ stato costruito un nuovo modello che riproduce anche una parte del fluido attorno alla barretta.
- La zona di fluido modellata ha dimensioni 150x150mm





ABAQUS Co-esecuzione

- Tutte le analisi sono state fatte usando la tecnica di co-simulazione fornita dal codice Abaqus.
- La tecnica di co-simulazione di Abaqus consente di risolvere problemi complessi di interazione fluido-struttura (FSI) accoppiando il modulo Abaqus/Standard al modulo Abaqus che è un programma computazionale di analisi fluido dinamica (CFD).
- Abaqus/Standard risolve il problema strutturale e Abaqus CFD risolve il dominio del fluido.

Test della tecnica di co-esecuzione

- Il fluido attorno alla barretta è stato considerato “aria”
- E’ stato applicato un impulso di accelerazione all’intera barretta
- La barretta viene lasciata libera di vibrare sulla sua prima frequenza naturale

Risultati attesi:

- Frequenza molto simile a quella calcolata con l’analisi modale (30.0 Hz)
- Smorzamento trascurabile

Risultati ottenuti

- Frequenza 30.3 Hz
- Smorzamento trascurabile
- Gli spostamenti non sono realistici perché il carico imposto serve solo per valutare il modello



La tecnica di co-esecuzione sembra dare risultati affidabili

Vibrazione della barretta immersa in piombo

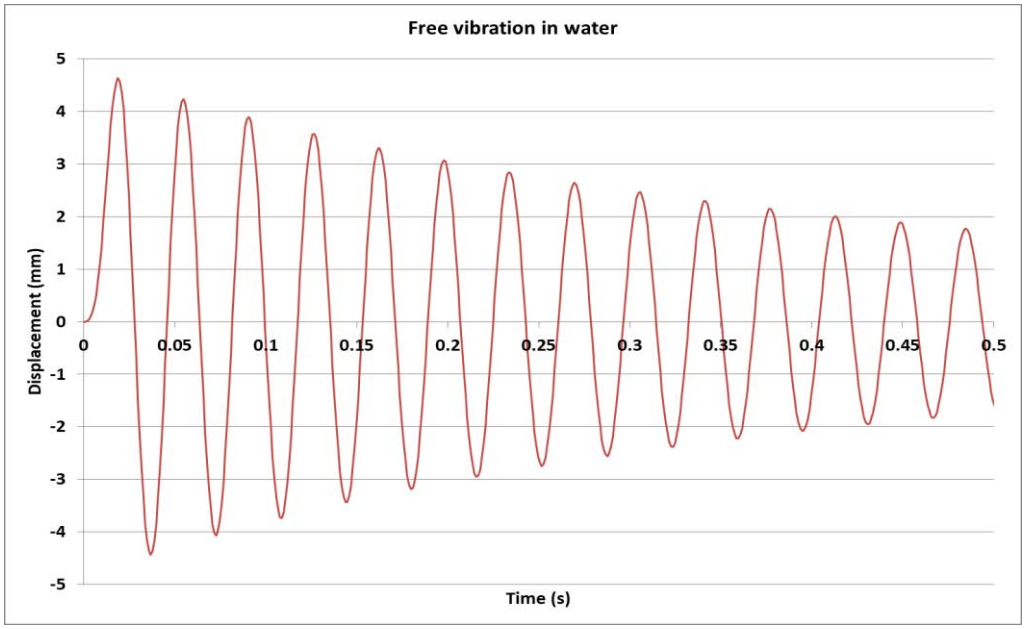
- Il fluido intorno alla barretta è modellato come piombo fuso
- E' stato applicato un impulso di accelerazione all'intera barretta
- La barretta viene lasciata libera di vibrare sulla sua prima frequenza naturale

Risultati attesi:

- Frequenza più bassa di quella calcolata in aria (30.3 Hz)
- Smorzamento non trascurabile

Risultati ottenuti

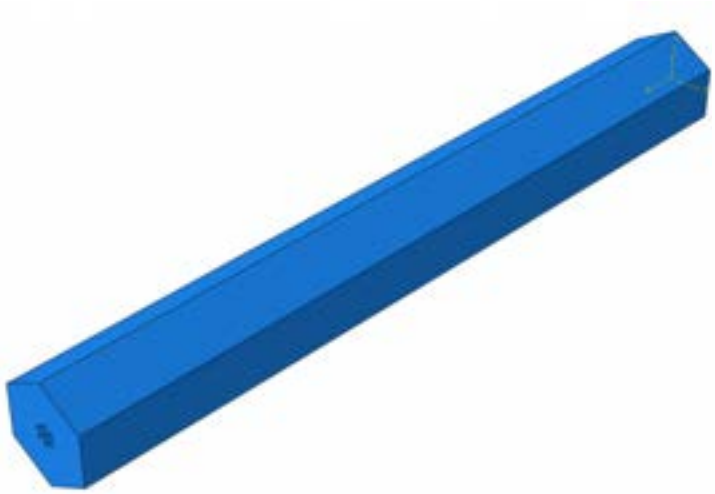
- Frequenza 18.5 Hz
- Smorzamento 2.8%
- Gli spostamenti non sono realistici perché il carico imposto serve solo per valutare il modello

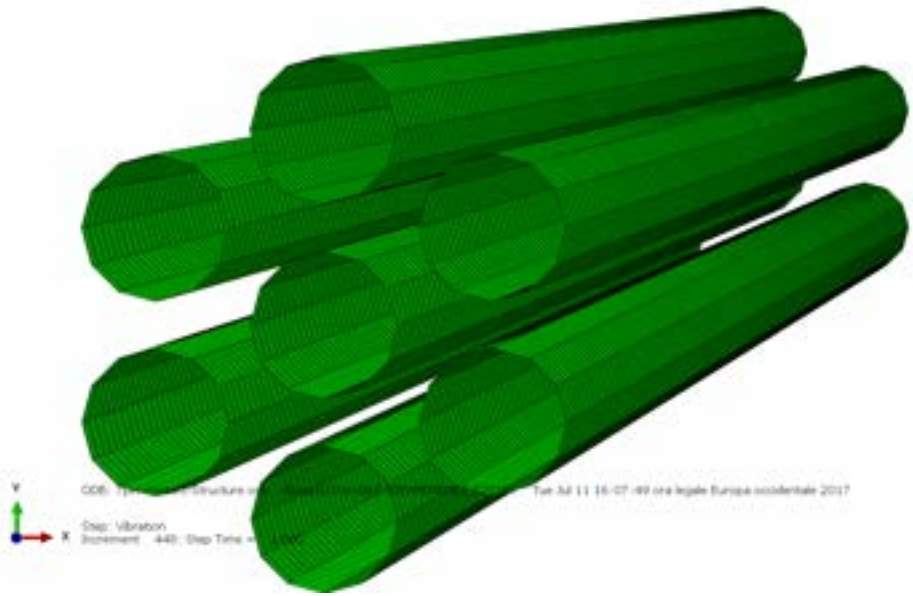


La prima frequenza della barretta immersa in piombo risulta abbastanza lontana dalla possibile risonanza a 10.2 Hz

Analisi dinamica di un gruppo di barrette immerse in piombo

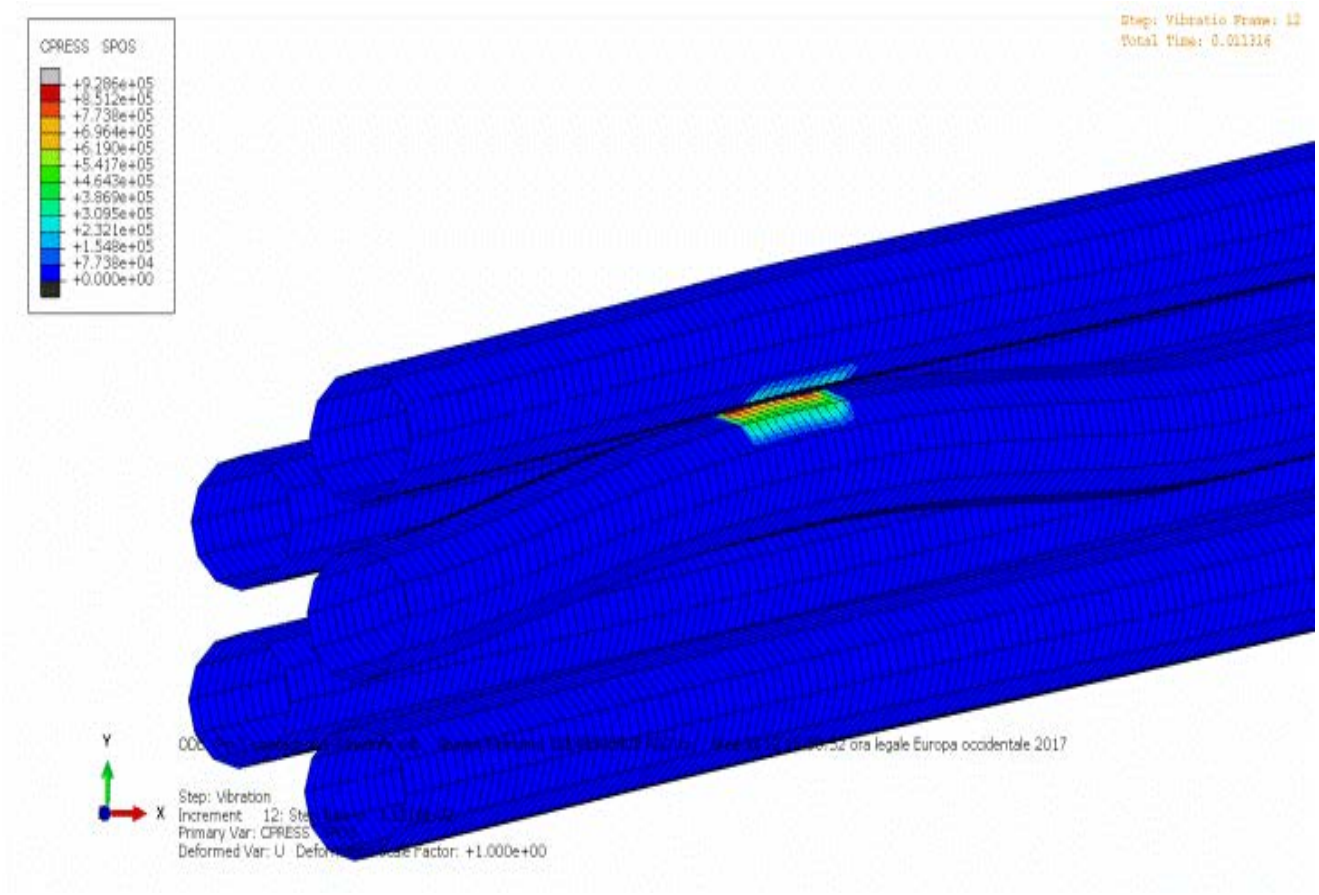
- Lo scopo è quello di studiare l'influenza delle prima fila di barrette attorno alla barretta centrale
- Per questo è stato modellato un gruppo di sette barrette
- La porzione di fluido considerata ha le stesse dimensioni della scatola dell'elemento
- Le condizioni al contorno imposte al fluido simulano una scatola rigida





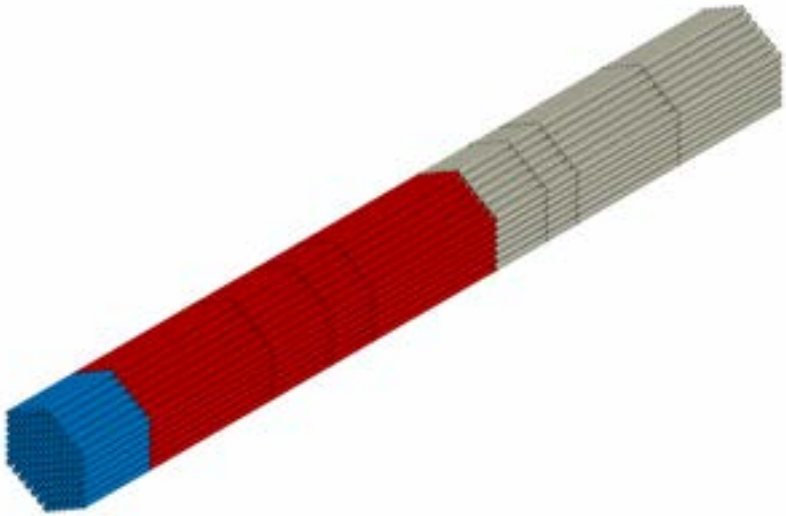
Analisi dinamica di un gruppo di barrette immerse in piombo

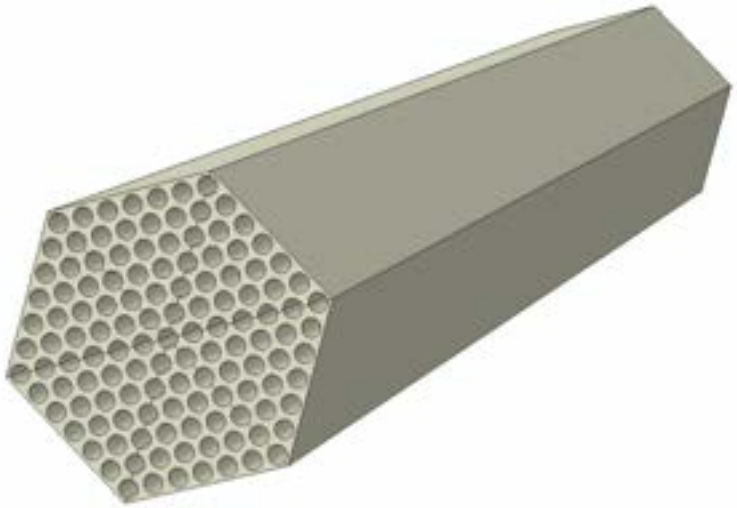
E’ possibile rilevare i possibili urti



Next steps

- Modellare tutte le barrette e il fuido per riprodurre una condizione più realistica
- Controllare la possibile risonanza sulle frequenze superiori alla prima





Next steps

GRAZIE PER L'ATTENZIONE

Italian National Agency for New Technologies,
Energy and Sustainable Economic Development

Results of the validation campaign of neutronic codes & recommendations for correct application to LFR systems

ADP PAR 2016 B.3.1 LP2

LFR-Gen.IV: Stato attuale della tecnologia e prospettive di sviluppo

UniBO, 26-27 September 2017

M. Sarotto, G. Grasso, P. Console Camprini (ENEA)

Contents

1) Main objectives
2) Neutronic codes: **ERANOS** and **MCNP**
3) The **VENUS-F** core layout for LFR systems (@ **SCK-CEN**, B)
4) ERANOS validation in the VENUS-F LFR mock-up
   (integral parameters: CR* worth, spectral indexes, k_{eff} → critical mass)
5) The **LR-0** core layout for LFR systems (@ **CV Řež**, CZ)
6) MCNP validation in the LR-0 LFR mock up
   (local parameters: fission and capture reaction rates)
7) Concluding remarks

* Control Rod

1. Main objectives

Validation of neutronic codes for the **LFR**:

→ **Experimental campaign** & **analysis of LFR representative experiences** through their **modelling with neutronic codes**, such as ERANOS (CEA) & MCNP (LANL);

→ **Validation of codes reliability** by comparison **with experimental measurements in VENUS-F** (Vulcan Experimental NUclear Study-Fast) & **LR-0 zero-power reactors**.

In ADP PAR2015-2016, the activity was focused on:

1) **Validation of ERANOS code by VENUS-F** experimental results obtained during the EURATOM FP7 project FREYA (Fast Reactor Experiments for hYbrid Applications)
   → PAR 2015 activity complementary with FREYA;

2) **Validation of MCNP code by LR-0** experimental results obtained in an (almost) LFR representative configuration → PAR 2015-2016 activity

2. Neutronic Codes

1) **ERANOS* v. 2.2N deterministic code**:

a) X-sections** of core regions by ECCO*** with energy-group-structures:

- 49 groups for “standard” calcs
- 33 groups for sensitivity analyses
- 15 groups for uncertainty analyses

b) JEFF3.1 and ENDF/B-VI.8 nuclear data libraries

c) Full core calcs with TGV module in 3D XYZ geometry (variational nodal method)

* European Reactor ANalysis Optimised System

** Macroscopic cross sections

*** European Cell COde

2) **MCNP**** v. 6.1 stochastic code**:

- Continuous treatment of energy dependence
- Exact heterogeneous geometry description
- ENDF/B-VII.1 nuclear data library

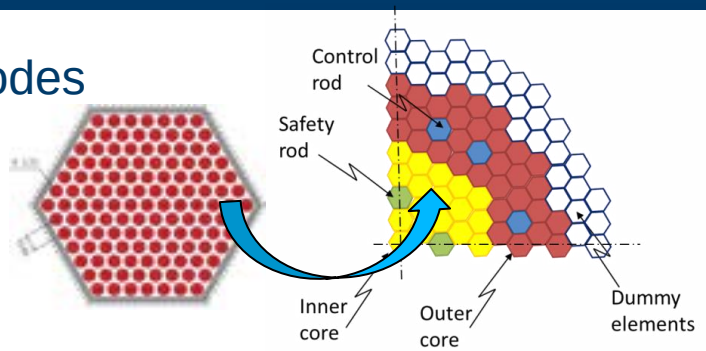
**** Monte Carlo N-Particle

3.1 VENUS-F core layout for LFR: rationale

Most aimed requirement for validation of neutronic codes is to achieve a “LFR representative spectrum”

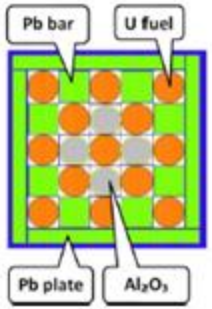
ALFRED* as LFR reference design

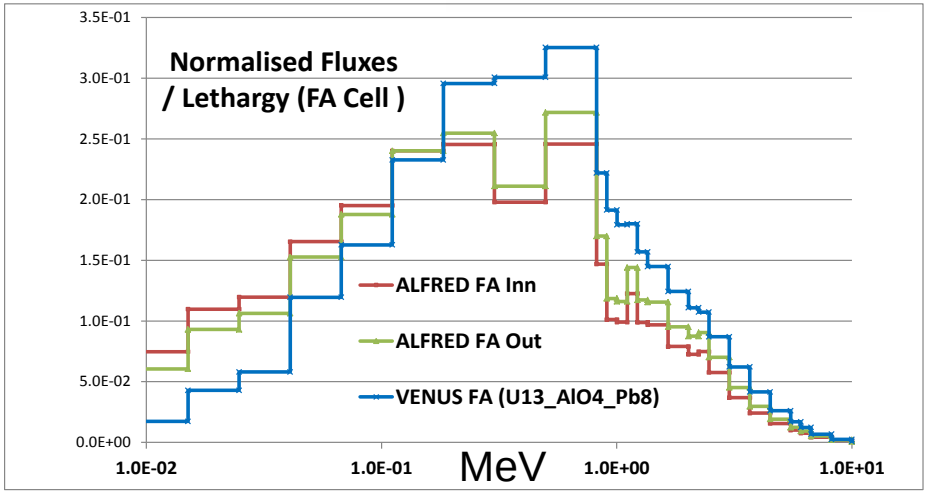
→ FA** with MOX fuel (22 / 27 wt.% Pu)



The VENUS-F FA is a 5x5 square matrix with U metal rods (# 13), Pb bars (# 8) and Al_2O_3 “moderating” rods (# 4) to simulate oxide fuel. But,

n spectrum is still too hard





* Advanced LFR European Demonstrator

** Fuel Assembly

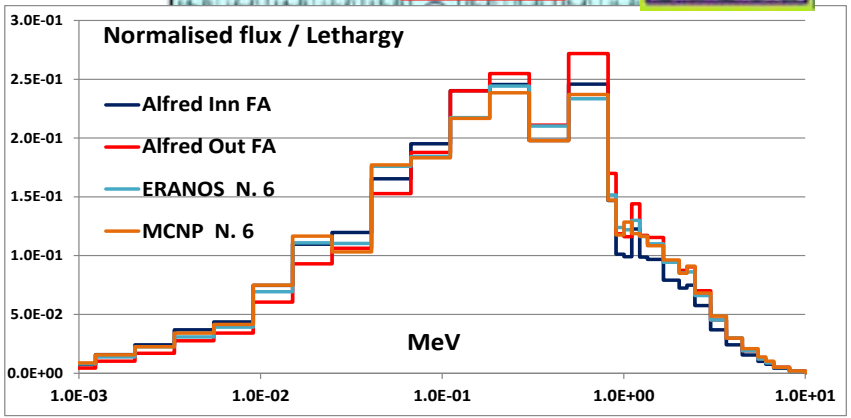
3.2 VENUS-F core layout for LFR: ALFRED island

To simulate MOX/LFR spectrum, a **3x3 ALFRED island** was designed by ENEA (& Ansaldo Nucleare) and assembled in VENUS-F at SCK-CEN.

4 "moderating" AlA (Alfred Inert Assembly: 25 Al_2O_3 rods) disposed as chess around an experimental FA (**EFA-2**) with SS tube for axial traverse meas.



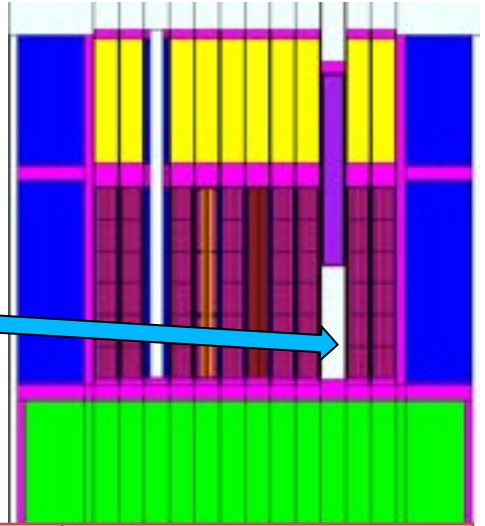
→ **Optimal spectral agreement with ALFRED FA in EFA-2**



4.1 ERANOS validation in VENUS-F: CR worth

In FREYA, most of measurements & code simulations done moving both CRs together. Some calibration measurements were done moving each CR separately. In PAR2015: C/E* **analyses for the reactivity worth** (ρ) due to **CR close to ALFRED island** (CR1).





* Calculated-to-Experimental

At insertion heights, **ERANOS accuracy:**

8 % with JEFF3.1 nuclear data

6% with ENDF/B-VI.8 data

(measurement uncertainty 3%; MCNP accuracy 11-12%)

z	C/E with ERANOS for CR1 worth	
[mm]	JEFF3.1	ENDF/B-VI.8
375	0.985	0.997
425	0.935	0.948
475	0.921	0.965
525	0.921	0.942
575	0.987	0.975

4.2 ERANOS validation in VENUS-F: spectral indexes

Spectral Indexes (SI, in EFA-2) measured in EFA-2: ratio of Fission Pu^{239} (F49), U^{238} (F28) and Np^{237}(F37) over U^{235} (F25).

$$SI^{r} = \frac{\sum_g \sigma_g^{r} \phi_g}{\sum_g \sigma_g^{F25} \phi_g}$$

where:

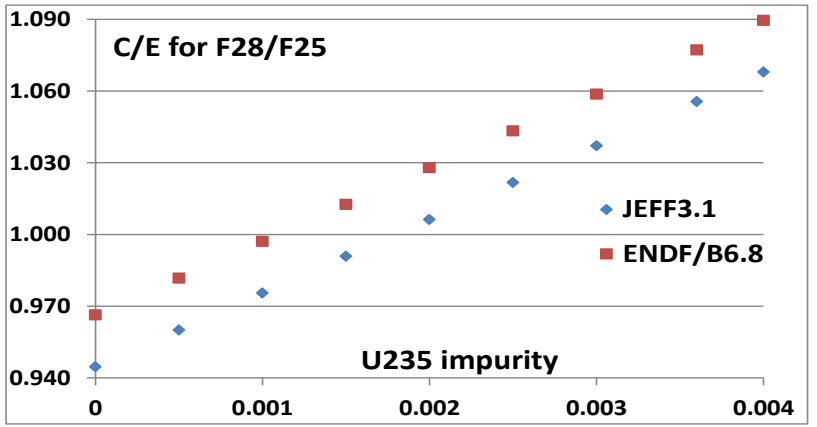
- "SI^r" is the spectral index value for F28/F25, F49/F25 and F37/F25;
- "ϕ_g" is the flux value in each energy group g
- "σ_g^{F25}" is the U235 fission microscopic cross section value in each energy group g (1-49);
- "σ_g^{r}" is the fission microscopic cross section value for the nuclide of interest (*i.e.*, F28, F49 and F37) in each energy group g (1-49).

Spectral index	ERANOS C/E	
	JEFF3.1	ENDF/B-VI.8
F28 / F25	0.945	0.966
F49 / F25	1.011	1.010
F37 / F25	0.964	0.951

With both libraries: **C/E 1.01 for F49/F25, C/E 0.95-0.97 for F28/F25 & F37/F25***.

Discrepancy for F28/F25 due to tiny U^{235} impurity in U^{238} fission chamber deposit (estimated 0.36%).

→ ERANOS accuracy simulating U^{235} impurity: 0.1-0.2% for optimal C/E in F28/F25.



* For U^{238} & Np^{237} threshold fission cross-sections

4.3.1 ERANOS validation in VENUS-F: k_{eff} sensitivity analysis

k_{eff} values evaluated (with codes & libraries) in VENUS-F critical LFR mock-up differ by 0.4-1% from 1 → Sensitivity and uncertainty analyses in ADP.

Using standard perturbation theory & adjoint approach,

the sensitivity coefficient S_k (k_{eff} with x-section *): $S_k = \frac{\partial k}{\partial \sigma}\frac{\sigma}{k}$

$$M\Phi = \left(A - \frac{1}{k}F\right)\Phi = 0$$
$$M^*\Phi^* = \left(A^* - \frac{1}{k}F^*\right)\Phi^* = 0$$

$$(*)\quad S_k = -\mathrm{k}\frac{\langle \Phi^*, \left(A - \frac{F}{k}\right)\Phi\rangle}{\langle \Phi^*, F\Phi\rangle}$$

* Microscopic cross section

Nuclides examined: U^{235}, U^{238}, Fe^{56}, Pb^{206}, Pb^{207}, Pb^{208}, Cr^{50}, Cr^{52}, Cr^{53}, Cr^{54}, Al^{27}, O^{16}

(*) Ratio calculated in diffusion approximation: integral « <,> » over space and E (33 groups). Scalar fluxes from (S8 discretisation) and with Legendre polinomials at P1 order.

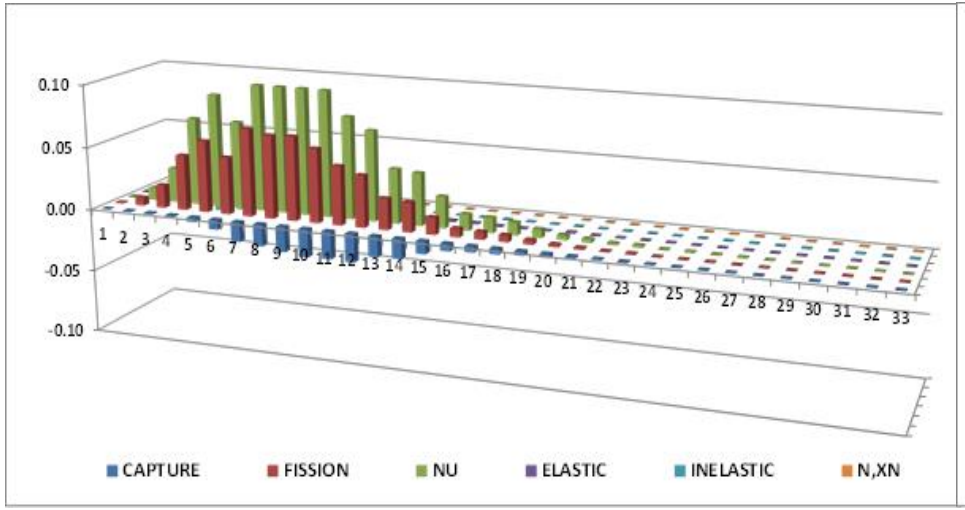
4.3.2 ERANOS validation in VENUS-F: some results of sensitivity analysis on k_{eff}

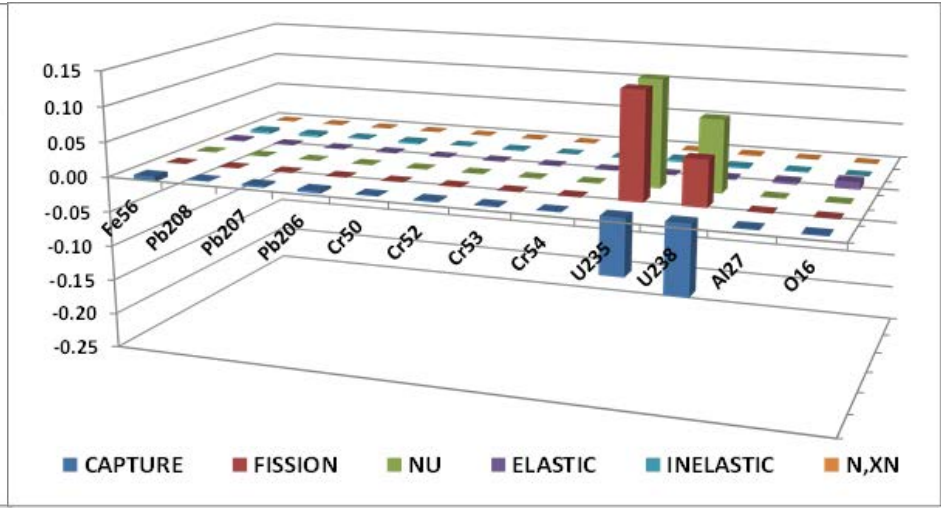
S_k (JEFF3.1) ∀ E group ∀ (sum over isotopes).

Dominant: , f, c in E [0.01, 3] MeV

S_k (ENDF/B-VI.8) ∀ isotope ∀ (sum over E groups).

Dominant: , f, c of U^{235} & U^{238}





All ERANOS JEFF3.1 & ENDF/B-VI.8 S_k results are very similar.

4.4.1 ERANOS Validation in VENUS-F: uncertainty analysis on k_{eff} (1/2)

Sensitivity coefficients relate uncertainties on nuclear data with uncertainty on k_{eff} value trough a **covariance matrix** (*B*):

$$\sigma_k^2 = S_k \, B \, S_k^t$$

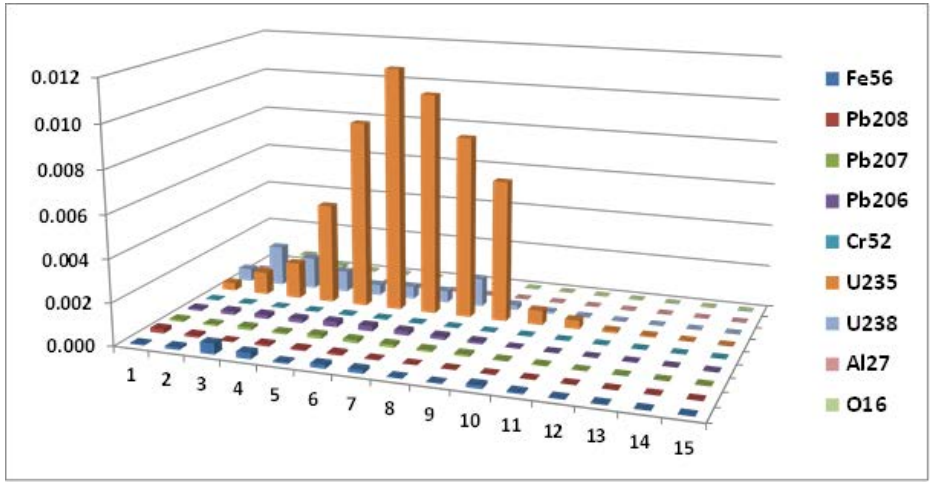
BOLNA* matrix (15 E groups) was used with **nuclides** U^{235}, U^{238}, Fe^{56}, Pb^{206}, Pb^{207}, Pb^{208}, Cr^{52}, Al^{27}, O^{16}

As for sensitivity coefficients, ERANOS/JEFF3.1 & ENDF/B-VI.8 $_k$ results are very similar

$_k$ **(JEFF3.1) ∀ isotope ∀ E groups** (sum over). Dominant:

U^{235} @ E [0.01, 1.5] MeV,

U^{238} @ E > 1.35 MeV (threshold fission)

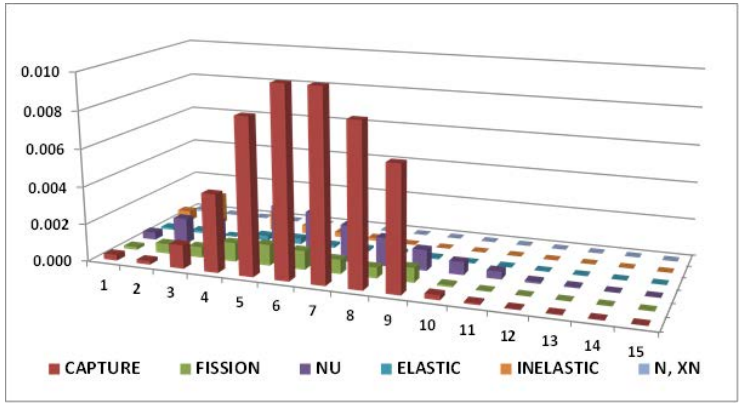


* Joint effort of **B**rookhaven, **O**ak Ridge, **L**os Alamos, **N**RG Petten & **A**rgonne

4.4.2 ERANOS Validation in VENUS-F: uncertainty analysis on k_{eff} (2/2)

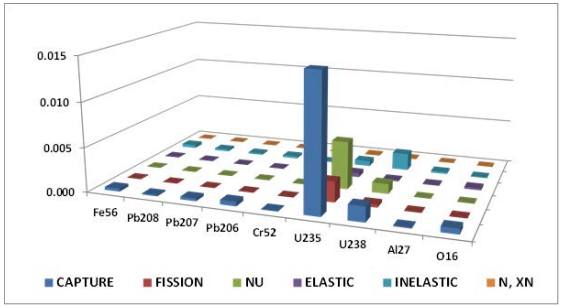
$_k$ **(ENDF/B-VI.8) ∀ E group ∀** (sum over isotopes). Dominant: $_c$

Group N.	CAPTURE	FISSION	NU	ELASTIC	INELASTIC	N, XN	TOTAL
1	3.05E-04	1.59E-04	4.03E-04	1.11E-04	5.66E-04	1.16E-04	**7.92E-04**
2	1.99E-04	5.26E-04	1.37E-03	1.33E-04	1.62E-03	2.84E-06	**2.20E-03**
3	1.26E-03	5.66E-04	1.40E-03	1.0185E-04	1.44E-03	0.00E+00	**2.43E-03**
4	4.14E-03	1.01E-03	2.22E-03	2.63E-04	1.03E-03	0.00E+00	**4.70E-03**
5	8.25E-03	1.12E-03	2.62E-03	3.16E-04	4.49E-04	0.00E+00	**8.75E-03**
6	1.10E-02	1.00E-03	2.47E-03	1.37E-04	2.61E-04	0.00E+00	**1.13E-02**
7	1.00E-02	7.56E-04	1.97E-03	1.27E-04	1.46E-04	0.00E+00	**1.03E-02**
8	8.50E-03	5.66E-04	1.52E-03	1.49E-04	4.38E-06	0.00E+00	**8.65E-03**
9	6.56E-03	7.81E-04	1.11E-03	6.54E-05	3.31E-09	0.00E+00	**6.70E-03**
10	2.55E-04	9.29E-05	6.83E-04	1.37E-05	0.00E+00	0.00E+00	**7.23E-04**
11	8.13E-05	2.22E-05	4.14E-04	1.28E-05	0.00E+00	0.00E+00	**4.22E-04**
12	3.22E-05	5.39E-06	1.03E-04	2.65E-06	0.00E+00	0.00E+00	**1.08E-04**
13	2.44E-05	1.24E-06	5.67E-05	9.77E-07	0.00E+00	0.00E+00	**6.17E-05**
14	9.11E-06	5.30E-07	1.53E-05	3.34E-07	0.00E+00	0.00E+00	**1.78E-05**
15	2.09E-06	1.23E-07	3.28E-06	0.00E+00	0.00E+00	0.00E+00	**3.[illegible]**
TOTAL	**2.06E-02**	**2.32E-03**	**5.47E-03**	**4.99E-04**	**2.06E-03**	**1.16E-04**	**0.0215**



TOTAL on $_k$ 2% (sum over E, & isotopes) **>** 0.4-1% accuracy of k_{eff} values by ERANOS (MCNP, SERPENT)

k_{eff} uncertainty due to uncertainty on nuclear data



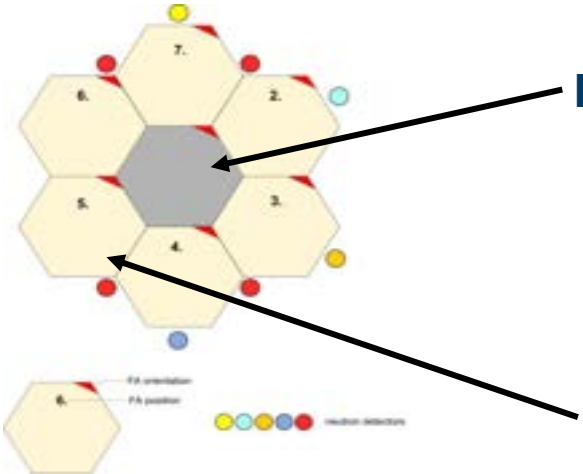
$_k$ **(JEFF3.1) ∀ isotope ∀** (sum over E groups).

Dominant: $_c$ (U^{235}), & $_f$ (U^{235}), & $_c$ & $_{in}$ (U^{238})

5.1 LR-0 core layout for LFR: main goal

LR-0 is a LWR (zero-power, pool-type) used for measuring neutron-physical characteristics of VVER (Water-Water Energetic Reactor) type reactors.

Main goal of PAR activity: Measurement of fissions and capture reaction rates in LFR representative conditions



Experiment: Dry test section in core centre designed to reproduce LFR conditions.

Actually, fission & capture reaction rates measured also in driver FA → 3D map of flux distribution

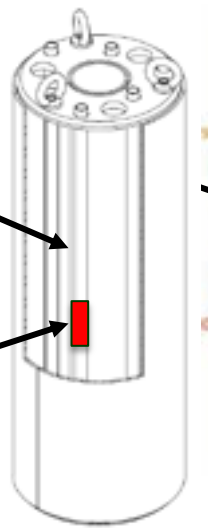
5.2 LR-0 core layout for LFR: experimental setup

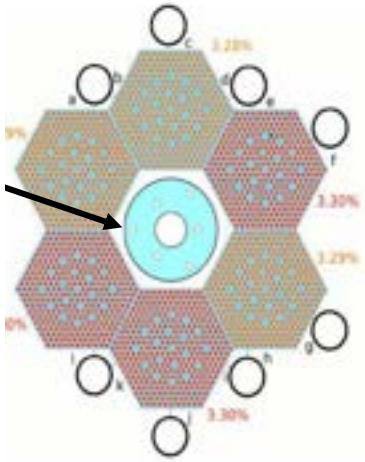
Six driver FAs with UO_2 fuel (3.28-3.3% wt.% U^{235}): criticality regulated by H_2O level.

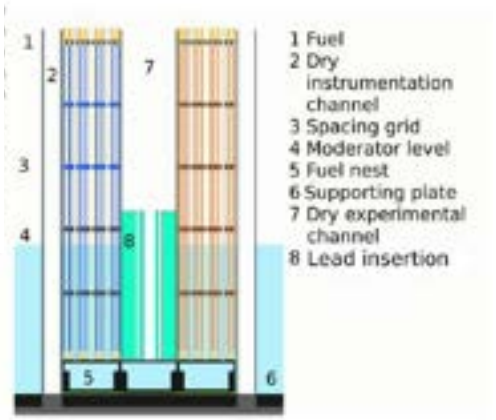
An optimised configuration for ALFRED was identified after extensive MCNP calcs & assembled: a SS cylindrical shell filled by lead inserted in central dry test section.

Six fuel pins (UO_2, 3.6 wt.% U^{235}) inserted in Pb part of test section.

Measurement of gamma ( ) emitted by driver & test pins in a 5 cm high piece at 30.5 cm from fuel beginning.







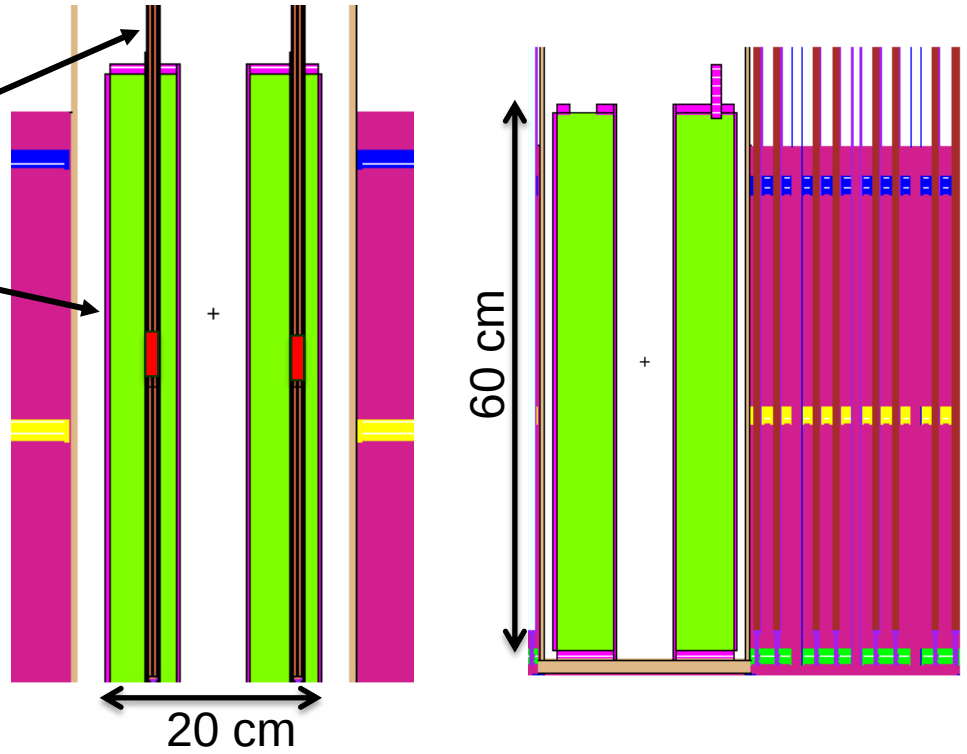
5.3 LR-0 core layout for LFR: MCNP model of experimental setup

The experimental set up was carefully simulated with MCNP6.1

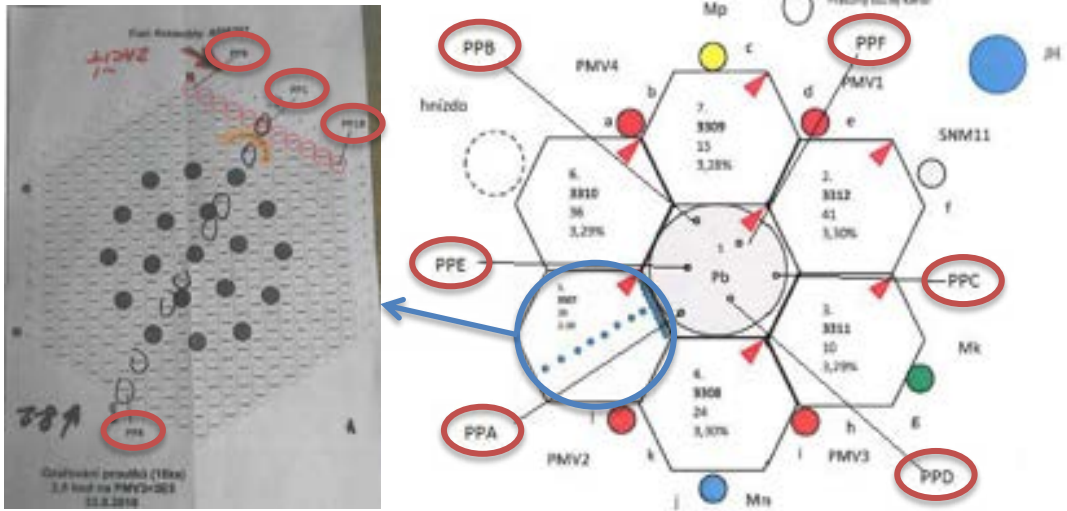
Fuel pin (125 cm active length) inserted in SS(pink)+Pb (green) cylindrical shell (20 x 60 cm).

.

By adopting ENDF/B-VII.1 library k_{eff} resulted 0.996 at moderator level yielding criticality.



5.4 LR-0 core layout for LFR: experimental data



Measured from pins **PPA – PPF** (in Pb test section) & **PP1 – PP18** (in driver FA)

emitted by: - Sr^{92} from U^{235} & U^{238} fission ($t_{1/2}$ = 2.7 h → 1384 keV)

- Np^{239} from U^{238} capture* ($t_{1/2}$ = 2.35 d → 277 keV)

* $t_{1/2}$ (U^{239}) = 23.5 min

6.1 MCNP validation: two steps approach

1) In **PP1** – **PP18**: # (NPA$_x$) → # Sr^{92}, Np^{239} (N_x) → Flux scaling factor ( )

PP1
…
PP18

$$NPA_x(t_{end_meas}) \rightarrow N_x(t_{end_irr}) \rightarrow \varphi$$

2) In **PPA** – **PPF**: Flux ( ) → # Sr^{92}, Np^{239} (N_x) → Calculated # (NPA$_x$)

$$\varphi \rightarrow N_x(t_{end_irr}) \rightarrow NPA_x(t_{end_meas}) \Longleftrightarrow$$

PPA
…
PPF

MCNP Validation

6.2 MCNP validation: methodology

Post-processing of MCNP results through **Bateman equations** for:

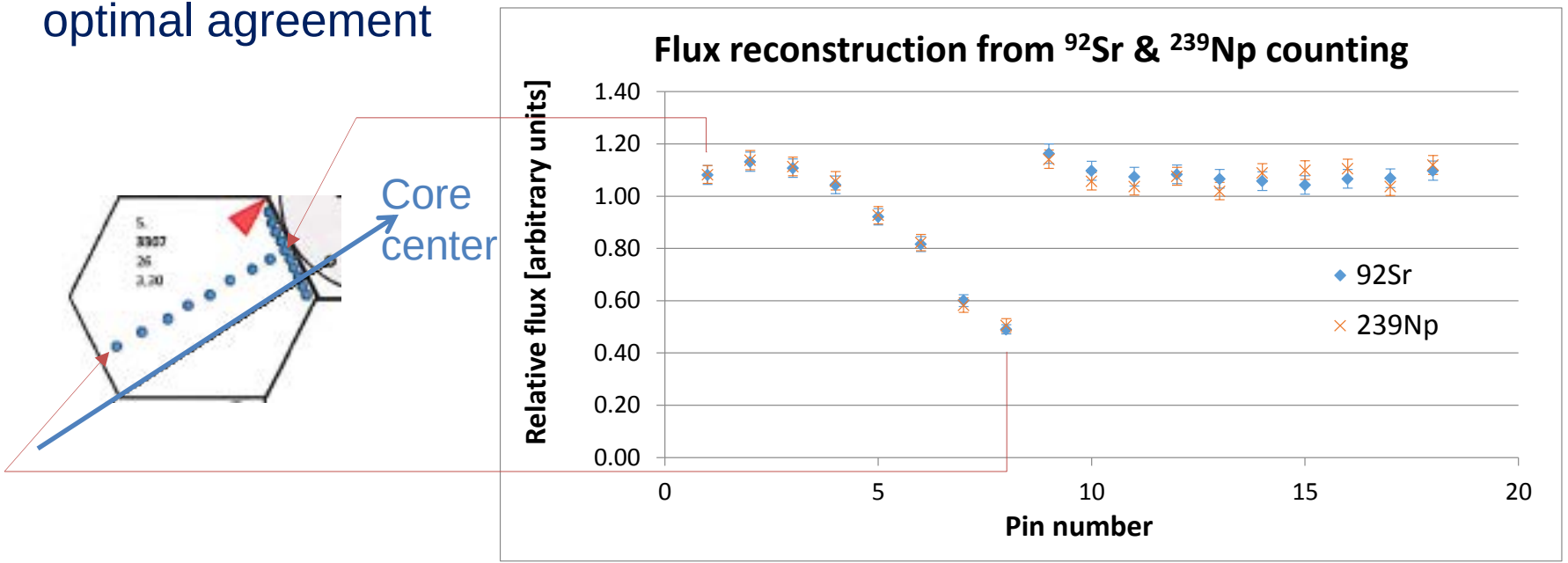
- **Irradiation** (2.5 h) $\frac{\partial N_x}{\partial t} = f_{y\to x} - \lambda_x N_x$ $\left(f_{y\to x}(t) = V\, N_y\, \sigma_{y\xrightarrow{f/c}x}\, \varphi\right)$

- **Decay in waiting + measurement time** (2 h (Sr^{92}), 2d (Np^{239}) + 250 s)

$$\frac{\partial N_x}{\partial t} = -\lambda_x N_x$$

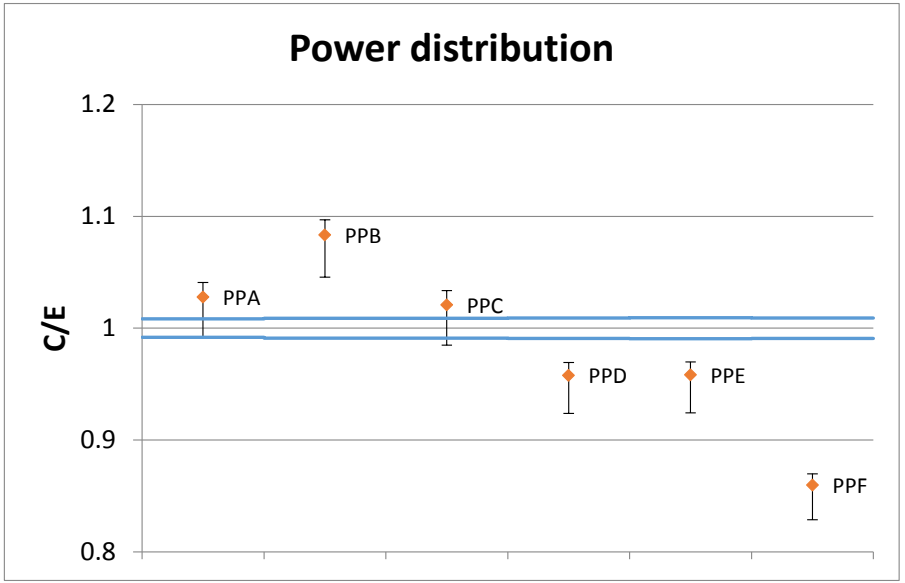
6.3 MCNP validation: first step results

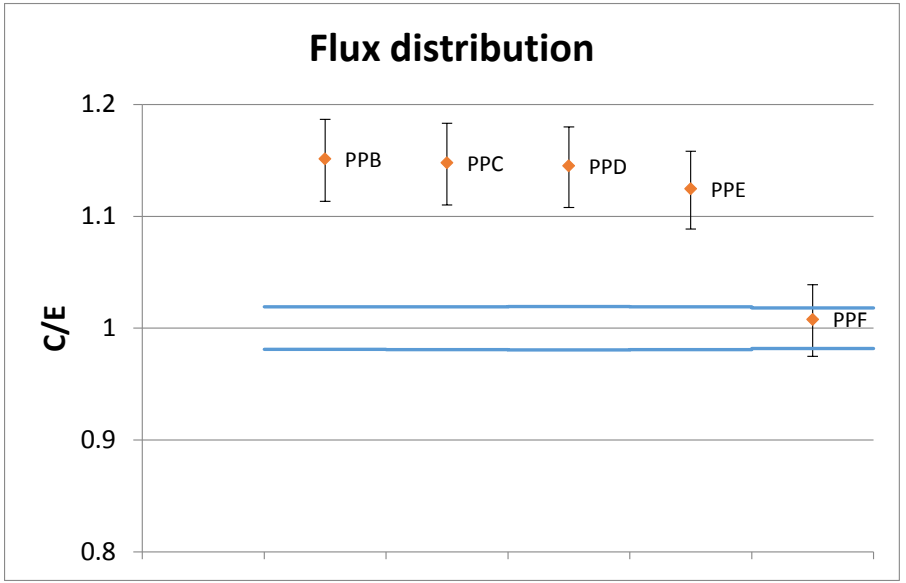
Flux shape reconstruction in driver pins: data from Sr^{92} & Np^{239} in optimal agreement



6.4 MCNP validation: second step results

C/E for counting from test pins in Pb due to Sr^{92} (power) & Np^{239} (flux)



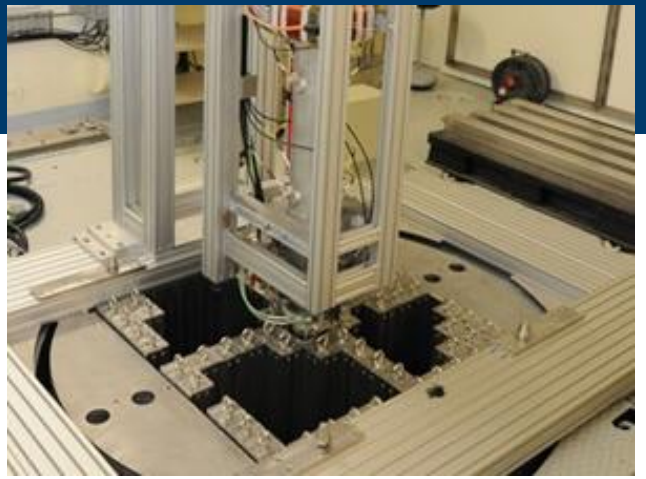


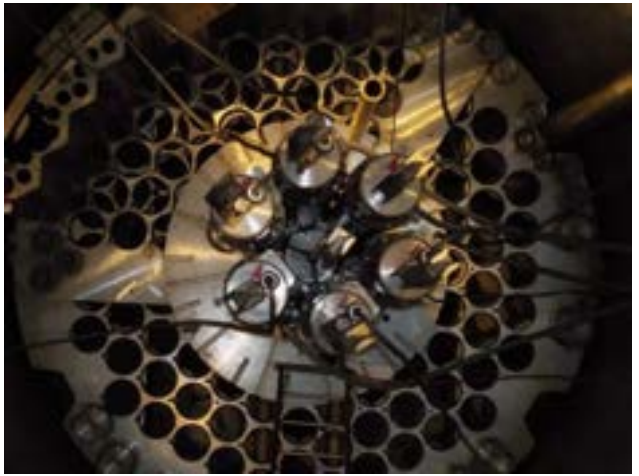
→ Confidence level of MCNP results was estimated (10-15%)

7 Concluding remarks

1) **VENUS-F** experiments in EU FP7 FREYA used to validate **ERANOS code** for calculations of LFR integral parameters. AdP PAR2015 (& FREYA) activity demonstrated the ERANOS (MCNP in FREYA) reliability to simulate LFR representative experiments.

2) **LR-0** experiments used to validate **MCNP code** for calculation of local parameters (power and flux distributions) in a Pb environment. PAR2015-16 activity provided an indication of the MCNP reliability although the configuration was not fully LFR representative.





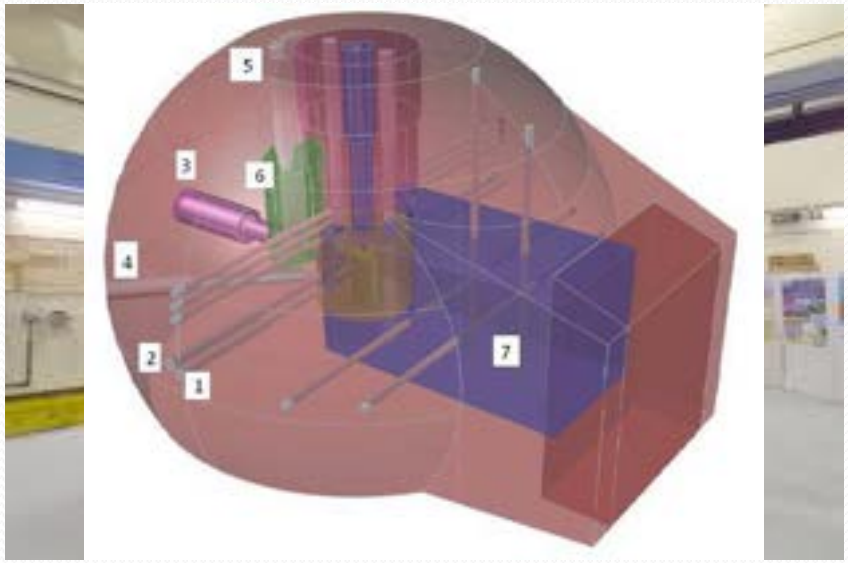
Thanks for your attention

massimo.sarotto@enea.it

Feasibility studies of an experimental campaign in TAPIRO devoted to the analysis of nuclear database for minor actinides

O. Dicuonzo[1], V. Fabrizio[2], D. Caron[1],
S. Dulla[1], M. Carta[2], K. W. Burn[3],
P. Console Camprini[3], P. Ravetto[1]
[1]*Politecnico di Torino, Italy*
[2]*ENEA Casaccia, Italy*
[3]*ENEA Bologna, Italy*

The TAPIRO reactor



- TAPIRO (TAratura PIla Rapida Potenza ZerO)
  - fast spectrum research reactor
  - Located in ENEA laboratories in Casaccia, Italy
  - In operation since 1971

- Square cylinder core (diameter about 12 cm)
- Fuel made of a uranium-molybdenum alloy (98.5 wt.% U–1.5 wt.% Mo, 93.5% enrichment)
- Maximum operating power 5 kW
- Multipurpose facilities
  - Well-characterized neutron spectrum
  - Allows irradiation in various conditions
  - Adopted for analysis of materials under irradiation

Activity performed

- Computational modelling of the TAPIRO reactor with deterministic and stochastic tools
  - SERPENT Monte Carlo code
  - ERANOS code system
- Reconstruction of experimental data performed in a previous campaign
- Preliminary sensitivity analysis on
  - Data library adopted
  - Characteristics of copper reflector
- Preparation of the AOSTA experimental campaign in TAPIRO
  - MCNP evaluation of reactivity insertion

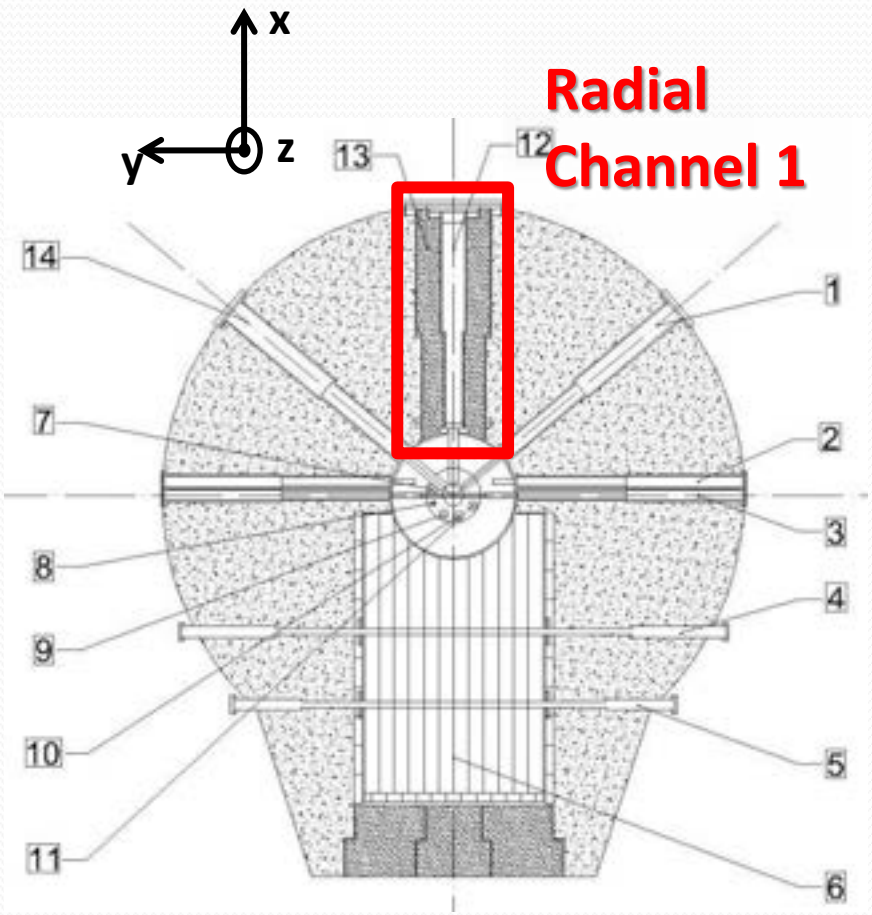
Paper/presentation @ M&C2017

Presentation @ OECD/NEA NSC EGIEMAM-II meeting

Experimental data available

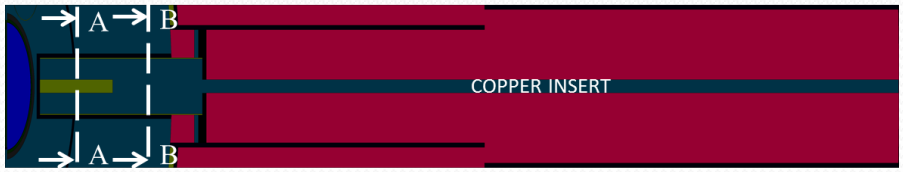
- SCK-CEN/ENEA experimental campaign carried out from 1980 to 1986
- Fission rates of Np-237, U-238 and U-235 measured in Radial Channel 1

x-y section of the reactor at z=1 m



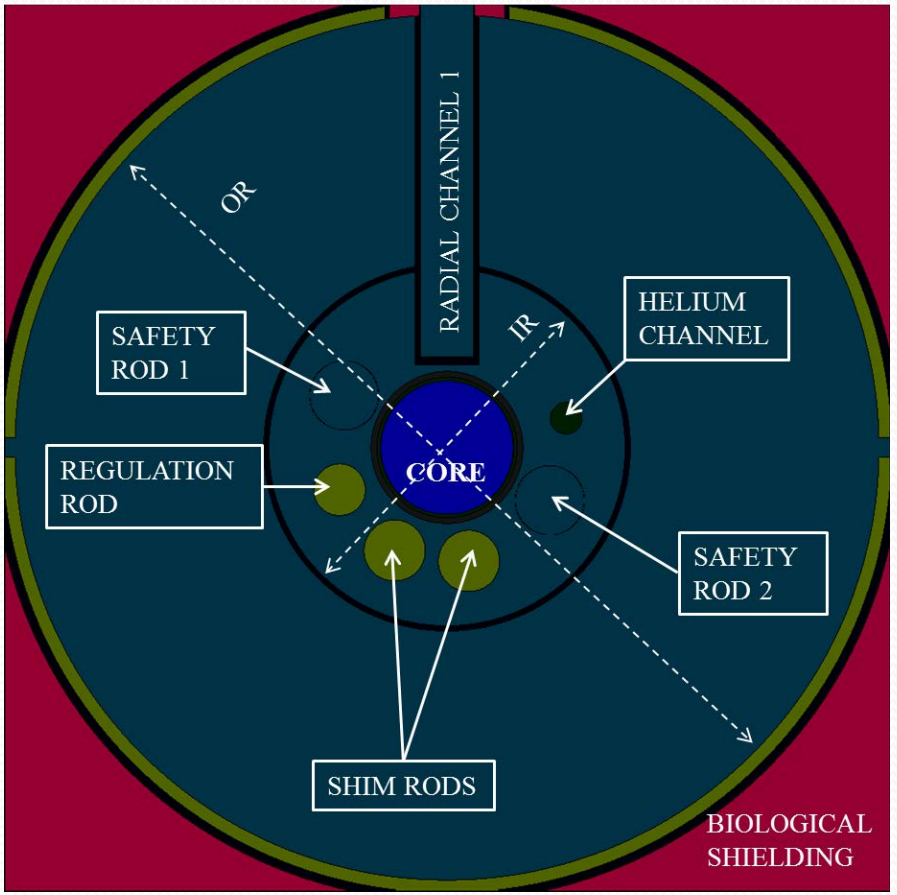
SERPENT model of TAPIRO

- SERPENT version 1.19 with data library JEFF 3.1.1
  - Model including the whole system (biological shield)
  - Focus on the modelling of Radial channel 1 (other channels not modelled)
  - Issue associated to the small dimension of the detectors



Radial channel geometry

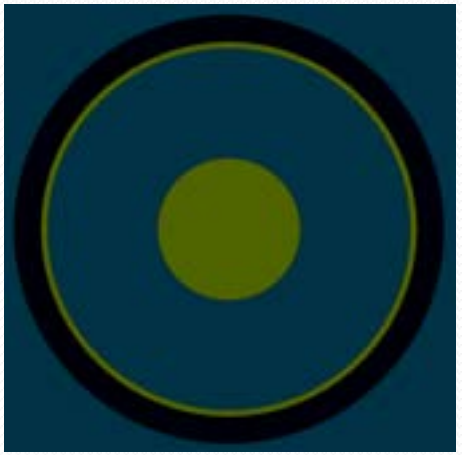
x-y section at z=1 m
IR= Inner Reflector OR= Outer Reflector



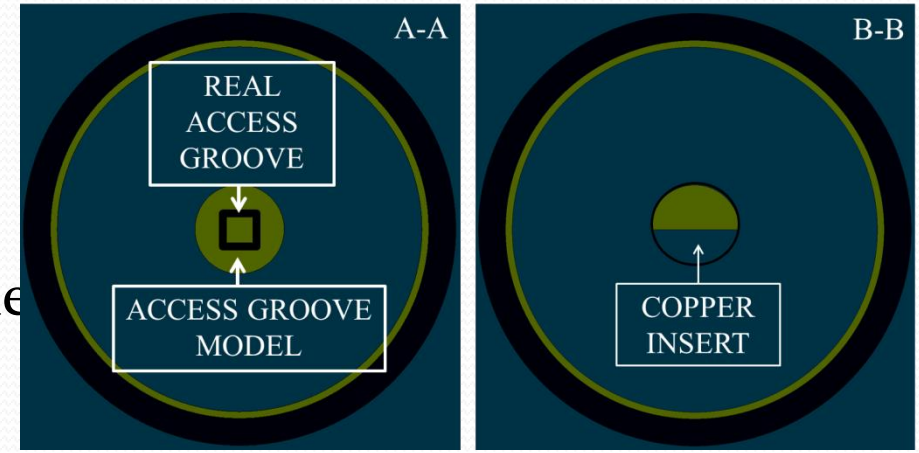
Model of the access groove

- The dimension of the channel has been modified to get better statistics
  - Large Access Groove (LAG): radius=1.065 cm, detector volume 0. 24 cm^3
  - Small Access Groove (SAG): radius=0.66 cm, detector volume 0.10 cm^3 (for verification)
  - Results show different performance depending on the fission rate observed

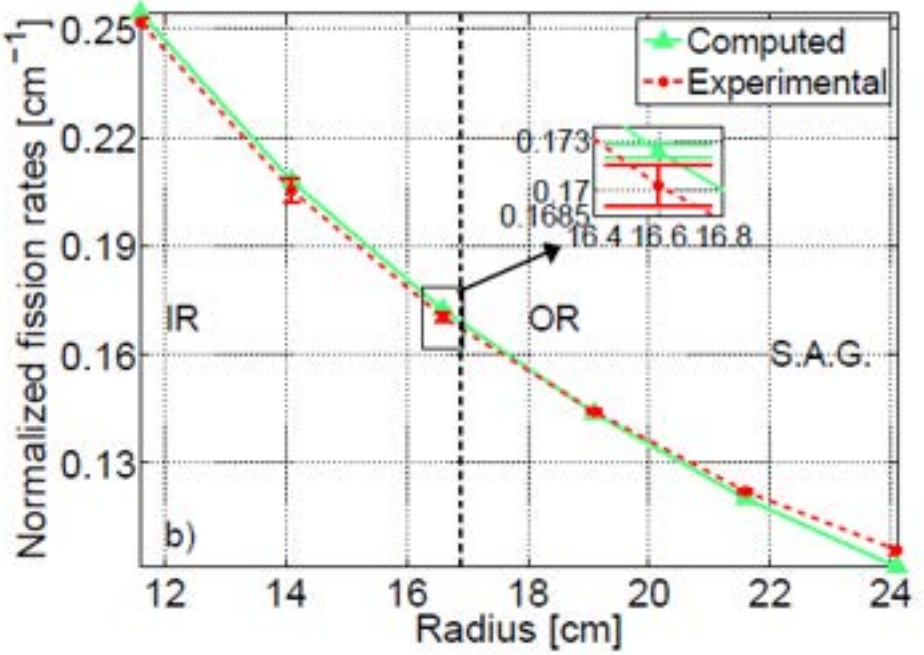
LAG

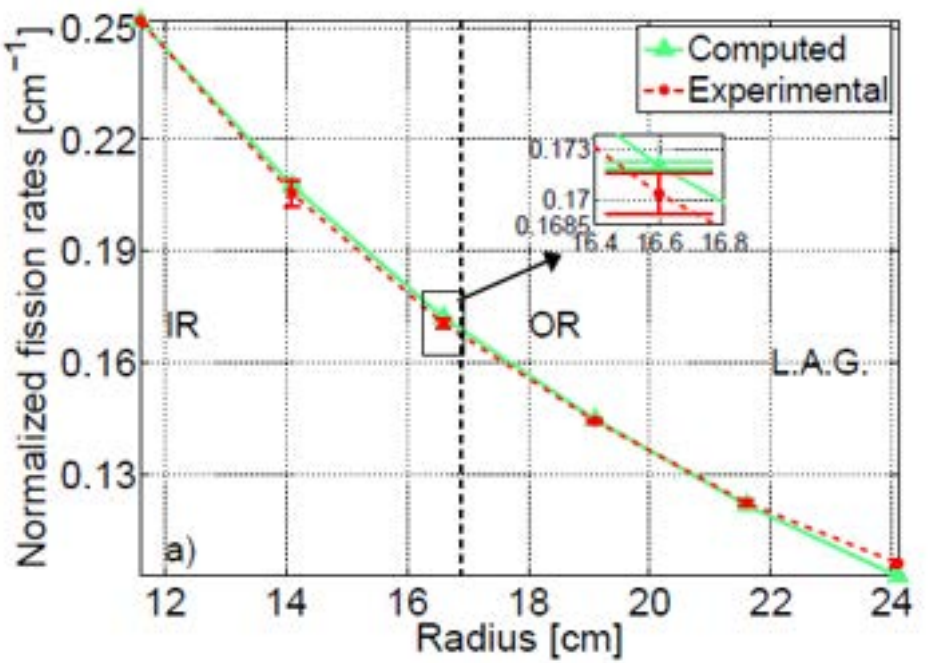


SAG



Comparison of groove models -I



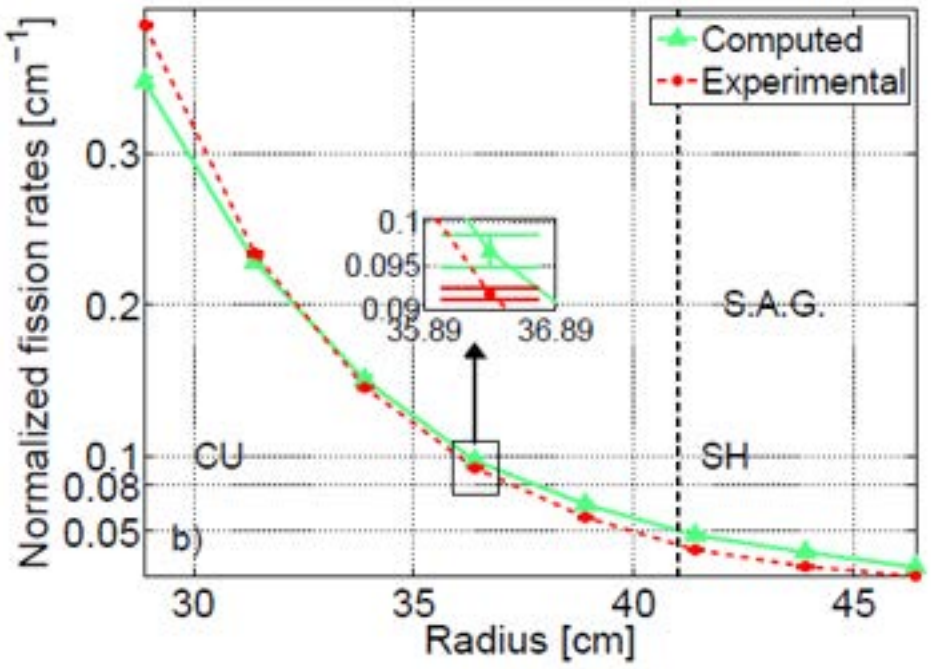


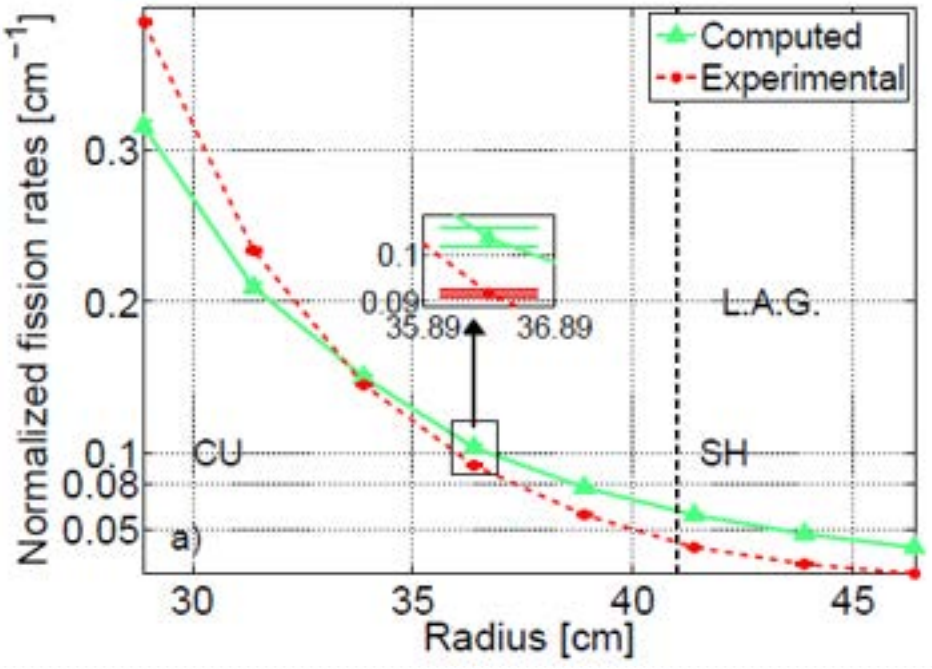
- Fission rate for U-235 shows small discrepancies
- Same results also for further detectors (r>24 cm)
- SAG simulations more computationally intensive

Localization of detectors



Comparison of groove models -II

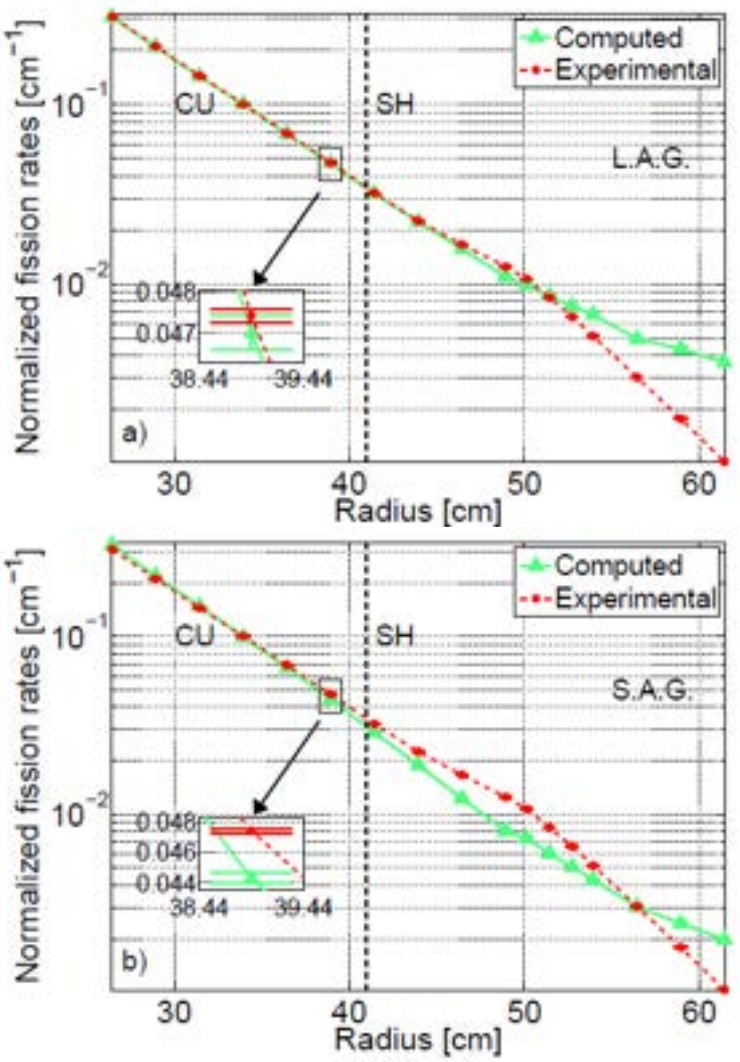




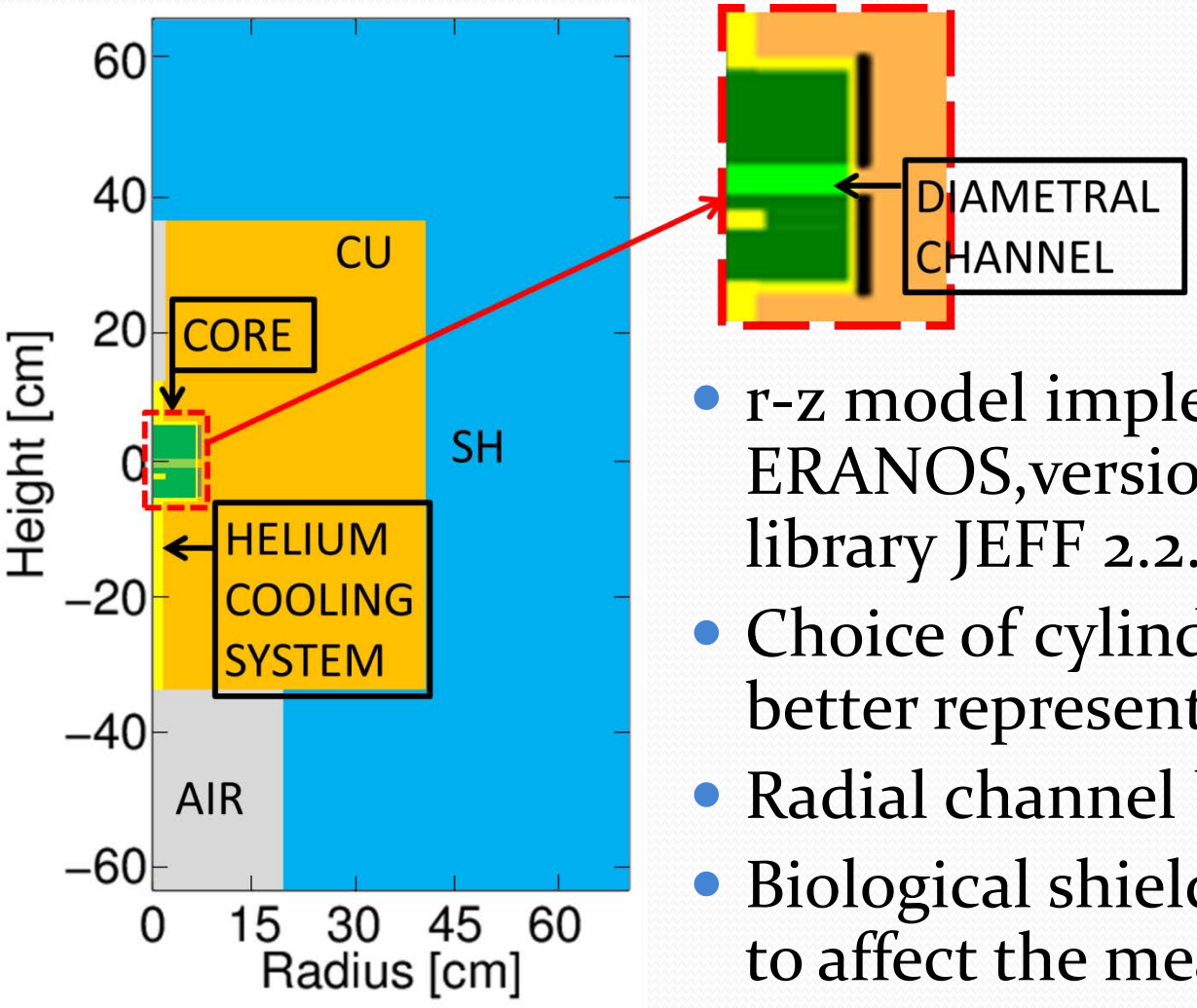
- Fission rate for U-238 shows relevant differences
- Comment on increased absorption by copper/concrete as in previous case is valid
- SAG simulations more computationally intensive

Comparison of groove models – III

- Fission rate for Np-237 with larger deviations
  - The dimension of the access groove modifies the material composition around the detector
  - SAG case:
    - more copper (r<41) or concrete (r>41)
    - Larger absorption in the energy range of fission of Np-237
    - Faster decay of fission rate
    - Still, open issues in the range 50-60 cm (current work on Cu X-sections)



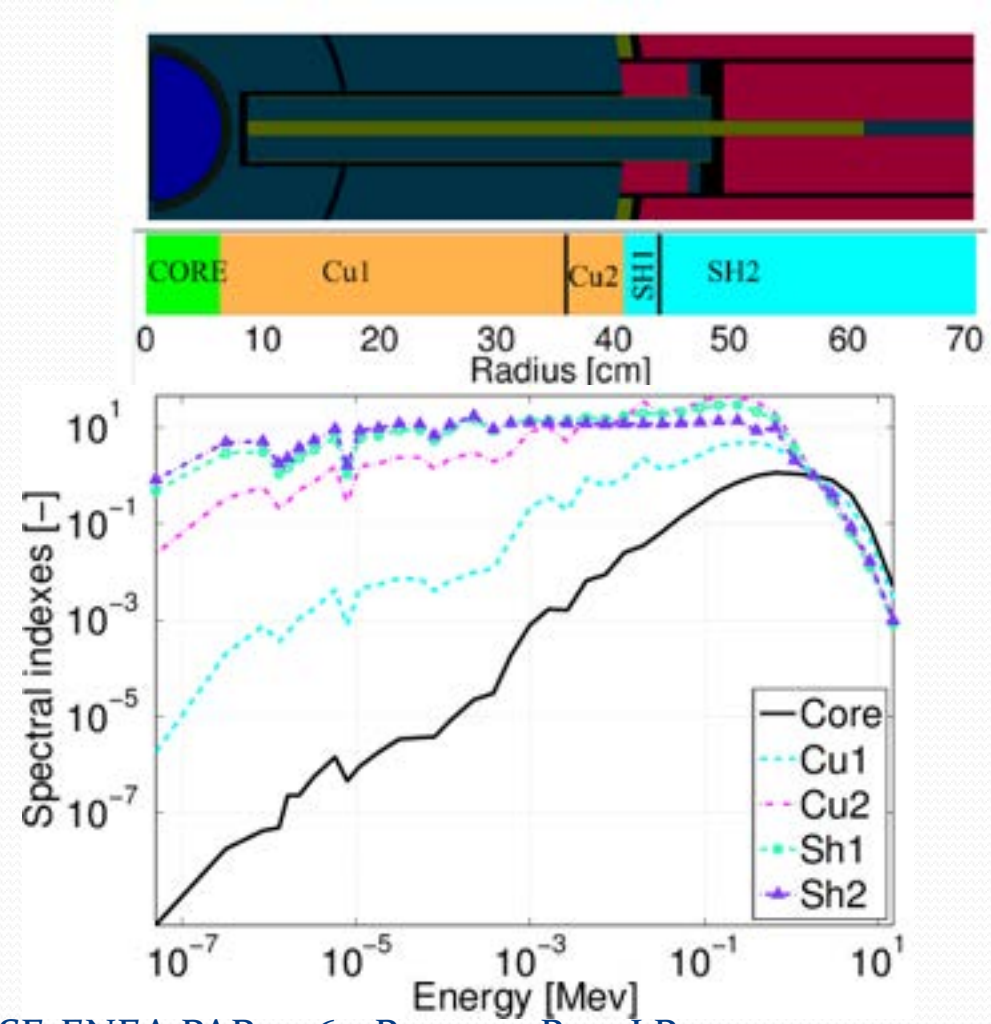
ERANOS model of TAPIRO



- r-z model implemented in ERANOS,version 2.0, with data library JEFF 2.2.
- Choice of cylindrical geometry to better represent core and reflector
- Radial channel becomes diametral
- Biological shield dimension set not to affect the measured fission rates

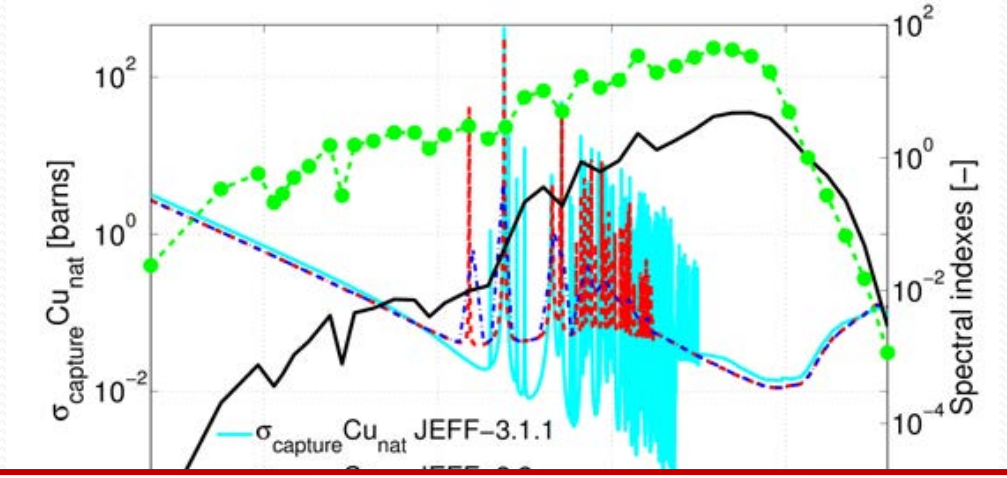
Spectrum calculation in ERANOS

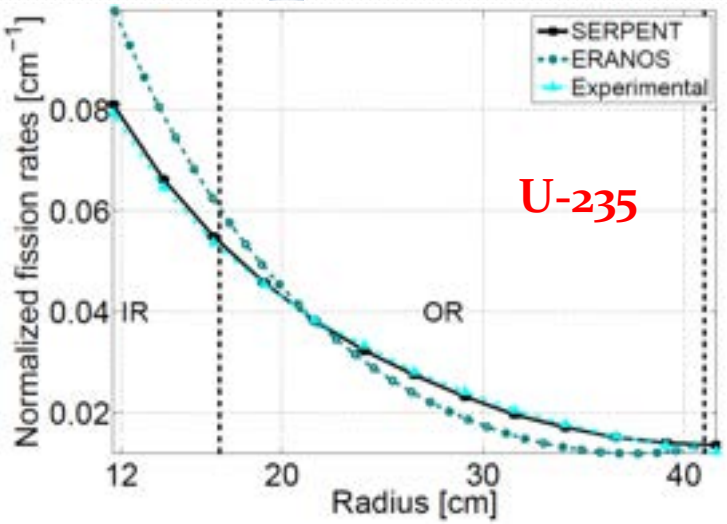
- ECCO module
- 38 groups structure (standard 33g + a finer resolution at low energies)
- Evaluation of spectral indexes (w.r.t. fission energy group) in the different regions
- Generation of cross-sections

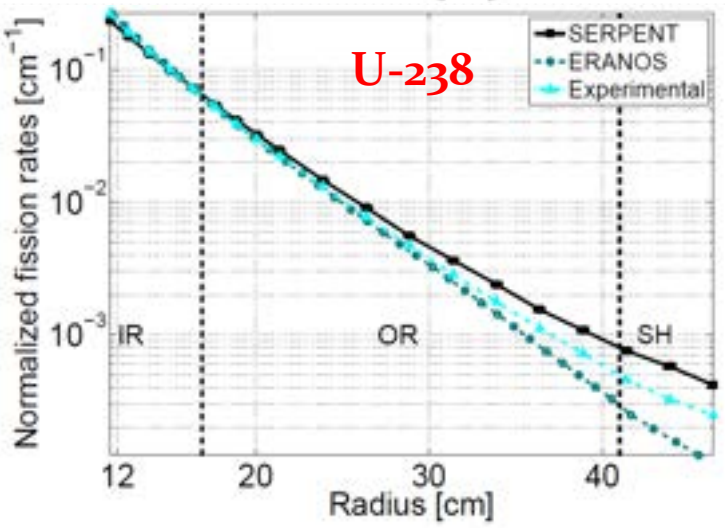


SERPENT to ERANOS comparison

- Different decay trends
  - Different libraries adopted
  - Role of capture in reflector → copper cross sections





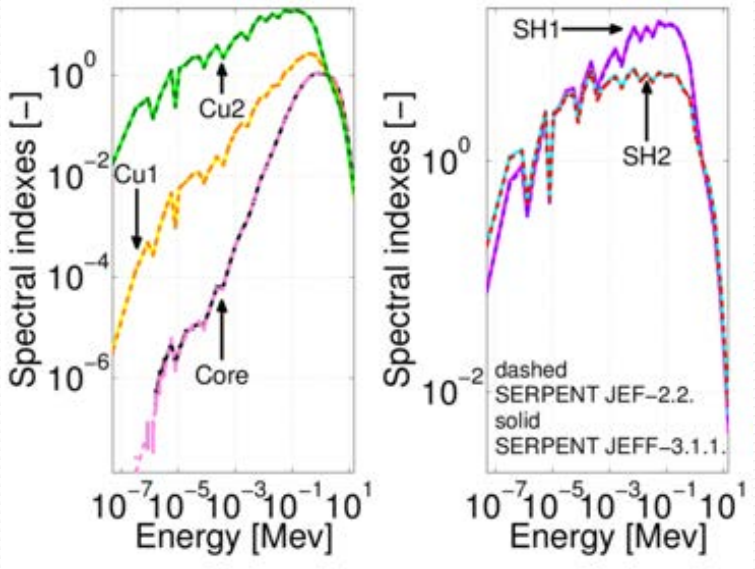


Interest in performing sensitivity analysis on the cross section data set

Preliminary sensitivity analysis - I

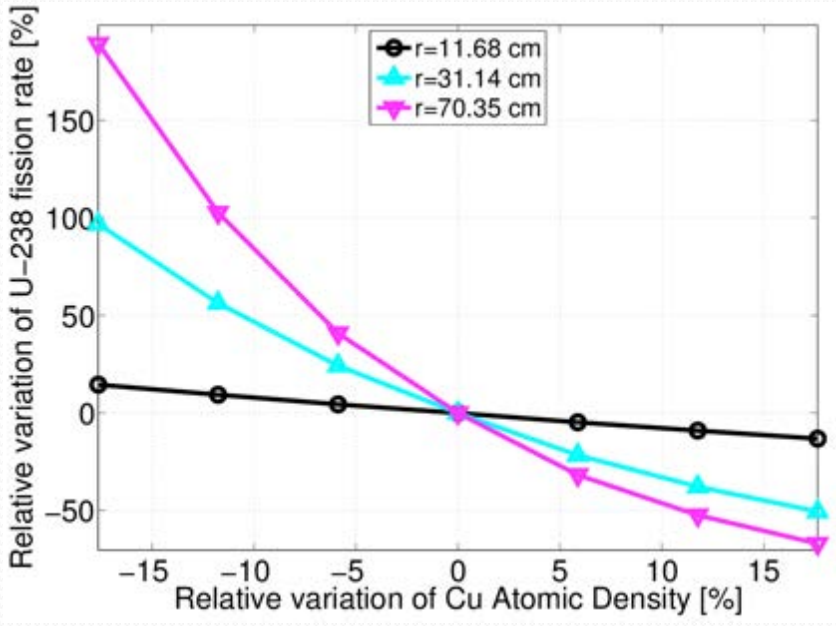
- The effect of the choice of the data library was assessed using SERPENT with both set available (JEFF 2.2 and JEFF 3.1.1).
- Effect on spectrum hardly visible
- Still, non negligible effect on k_{eff}

	JEFF-3.1.1	JEF-2.2
k_{eff}	1.00787	1.00874
Relative $\sigma_{k_{eff}}$	4.9E-06	4.9E-06
Relative variation [pcm]		-86.3



Preliminary sensitivity analysis - II

- Preliminary estimation of the effect of copper properties
  - Direct evaluation (no approx perturbation theory)
  - Modification of copper atomic density to address uncertainty on microscopic cross sections
- U-238 fission rate:
  - Monotonic behavior
  - Strongly non-linear behavior for higher r (reminder r>41 cm means measurements in shielding positions)



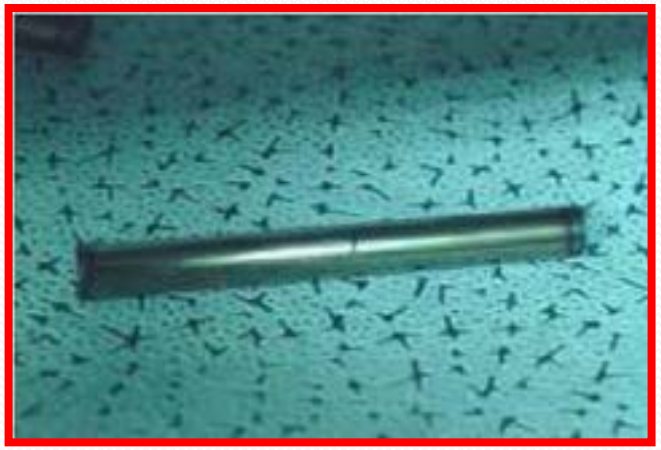
Preparation of the AOSTA experimental campaign

- Neutronic evaluations on on TAPIRO performed with SERPENT, ERANOS and MCNP (not shown here) provided positive indications on the capability to predict the system/sample behavior
- Interest (collaboration with CEA) in assessing the possibility to measure the reactivity effect of the sample insertion
  - ρ estimations performed with MCNP (comparison with different approaches)
  - Assessment of feasibility of "seeing" experimentally a difference in ρ

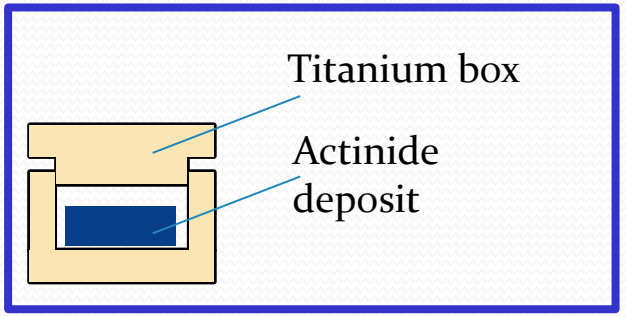
Sample characteristics - I

Name	Position	Penetration	Useful diameter
Diametral channel (D.C.)	Piercing. Horizontal. Diametral in the core.	Inner and outer fixed reflector. Core.	10 mm in core
Tangential channel	Piercing. Horizontal. 50 mm above core mid-plane. Parallel to D.C. 106 mm from core axis.	Inner and outer fixed reflector.	30 mm in reflector
Radial channel 1 (R.C.1)	Radial. Horizontal on core mid-plane, at 90° with respect to D.C.	Inner and outer fixed reflector, up to 93 mm from core axis.	56 mm in reflector
Radial channel 2	Radial. Horizontal on core mid-plane, at 50° with respect to R.C.1.	Outer fixed reflector, up to 228 mm from core axis.	80 mm in reflector
Grand Horizontal Channel (G.H.C.)	Radial. Concentric with R.C.1.	Up to reflector outer surface	400 mm near reflector
Grand Vertical Channel (G.V.C.)	Above core, on the same axis.	Outer fixed reflector, up to 100 mm from upper core base.	800÷900 mm in reflector
Thermal column	Horizontal.	Shield, up to outer reflector	110x116x160 cm³
Irradiation cavity	On safety plug upper base.	7.4 mm	33 mm

OSMOSE (used in previous campaign)



IRMM



Sample characteristics - II

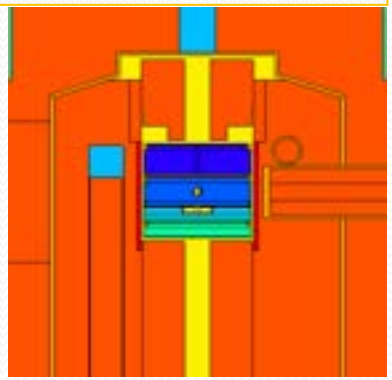
- OSMOSE: One Am-241 sample has been selected: Am241/2 containing 0.2 grams of Am241.
- IRMM: IRMM-1 sample has been selected containing 32 mg of Am241.

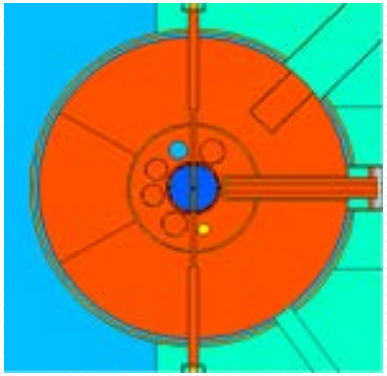
Series	Ref.	Dopant	Mass pellet (g)	^{241}Am Mass (mg)	Al_2O_3 Mass (g)
Americium	IRMM-1	$^{241}AmO_2$	0,342	32,23 ± 0,19	0,305
	IRMM-2	$^{241}AmO_2$	0,442	42,15 ± 0,25	0,394
	IRMM-3	$^{241}AmO_2$	0,428	40,32 ± 0,25	0,382
	IRMM-4	$^{241}AmO_2$	0,435	40,98 ± 0,25	0,388
	IRMM-5	$^{241}AmO_2$	0,448	41,21 ± 0,25	0,401
	IRMM-6	$^{241}AmO_2$	0,447	42,10 ± 0,25	0,399
	IRMM-7	$^{241}AmO_2$	0,444	41,84 ± 0,25	0,396
	IRMM-8	$^{241}AmO_2$	0,441	41,46 ± 0,25	0,394
	IRMM-9	$^{241}AmO_2$	0,447	42,09 ± 0,25	0,399
	IRMM-11	$^{241}AmO_2$	0,451	42,38 ± 0,25	0,408
	IRMM-13	-	0,395		0,395
	IRMM-14	-	0,407		0,407
	IRMM-15	-	0,385		0,385

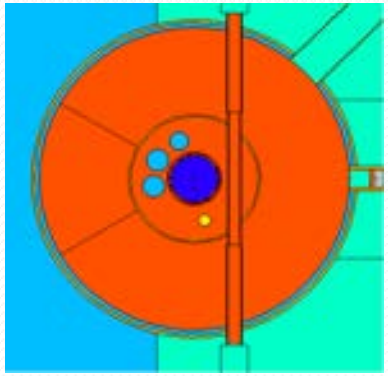
Calculation setup

- Code Used: MCNP – 6.1
- Nuclear x-section library: JEFF-3.1
- Tools available:
  - **Direct** calculations
  - Perturbation through method of differential operator: **PERT** card (assumes unaltered eigenfunction)
  - Perturbation through method of bilinear functional employing adjoint function: **KPERT** card (employs scattering approximation)

Reference case. TAPIRO standard configuration (Tangential and Radial-1 channels filled with Cu; Diametral channel filled with He)







Results

OSMOSE	ρ	Abs err	ρ	Abs err
Ref	-73	2	0	
Tang. Channel			-68	3
Rad. Channel 1			-33	2
IRMM	**ρ**	**Abs err**	**ρ**	**Abs err**
Ref	-73	2	0	
Diam. Channel			0.05	0.02
Tang. Channel			0.66	0.07
Rad. Channel 1			0.93	0.07

Non-negligible effect on reactivity, experimental measurement feasible

Small effect → relevant uncertainty and unfeasibility of experimental measurement

Conclusions and perspectives

- All computational tools adopted (ERANOS, SERPENT and MCNP) proved to be suitable tools for the neutronic characterization of TAPIRO and the analysis of experiments
- The geometry of TAPIRO has a large impact on the experimental setup, at times difficult to reproduce with computational tools
- The influence of copper properties on the experimental results is observed to be revelant, supporting the need for a re-assessment of the nuclear data for this material
- The feasibility to measure reactivity effect experimentally is strongly related to the sample choice



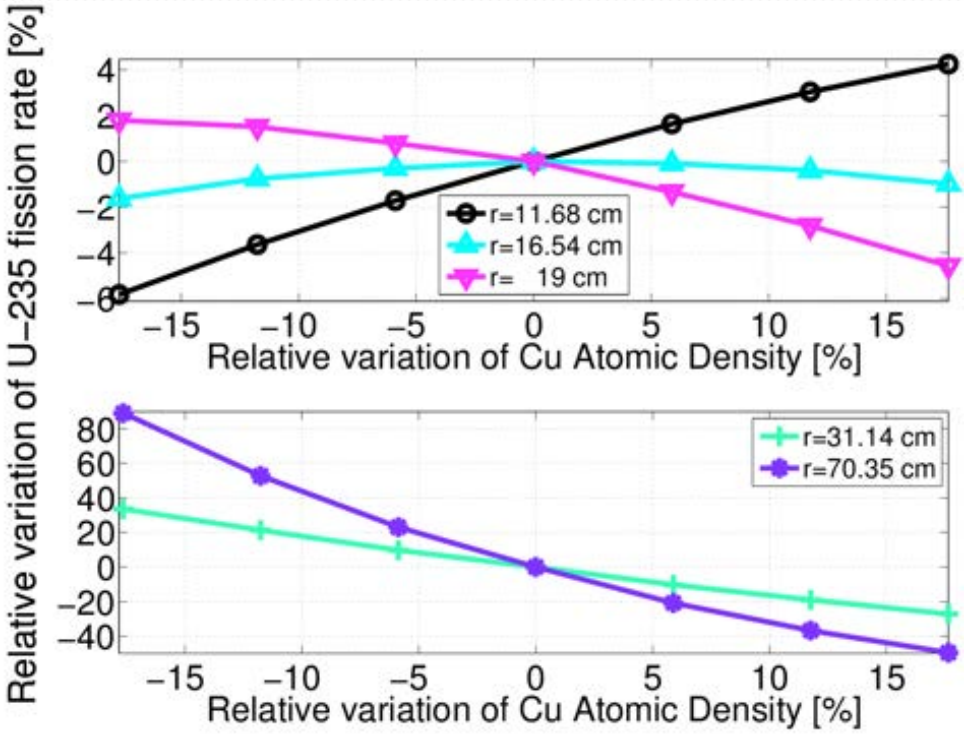
Thanks for your attention

CC BY-SA 3.0, https://commons.wikimedia.org/w/index.php?curid=531371
https://en.wikipedia.org/wiki/Tapir
https://it.wikipedia.org/wiki/Tapirus

Backup slides

Preliminary sensitivty analysis - III

- U-235 fission rate
  - Large r (outer reflector and shielding): relevant copper captures → lower neutron flux → fission rate decreases
  - Small r (inner reflector): higher energy neutrons → higher scattering-to-capture ratio in copper → small effect on fission rate





Calculation procedure for OSMOSE samples reactivity evaluation

Reactivity Variation for insertion of **OSMOSE** sample in TAPIRO Experimental Channels

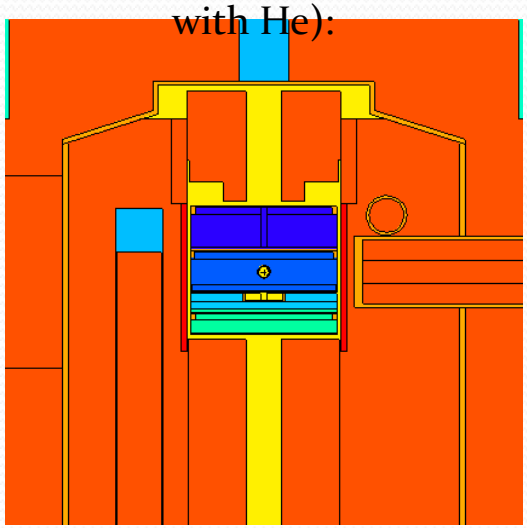
- ✓ Code Used: MCNP – 6.1
- ✓ Nuclear x-section library: JEFF-3.1

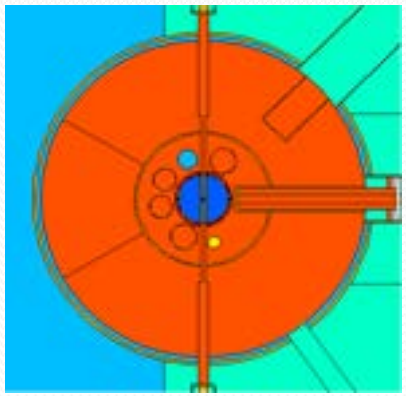
Tools available:

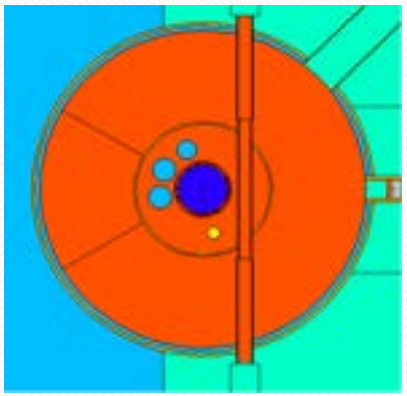
- ✓ Direct calculations
- ✓ Perturbation through method of differential operator: PERT card (assumes unaltered eigenfunction)
- ✓ Perturbation through method of bilinear functional employing adjoint function: KPERT card (employs scattering approximation)

Results with all 3 tools consistent.

Reference case. TAPIRO standard configuration (Tangential and Radial-1 channels filled with Cu; Diametrical channel filled with He):







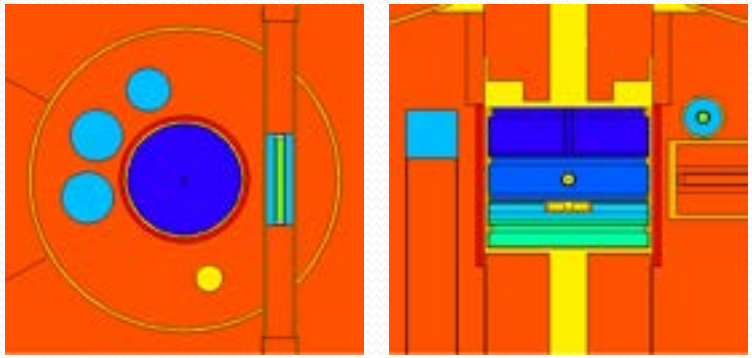


Results for OSMOSE samples reactivity evaluation

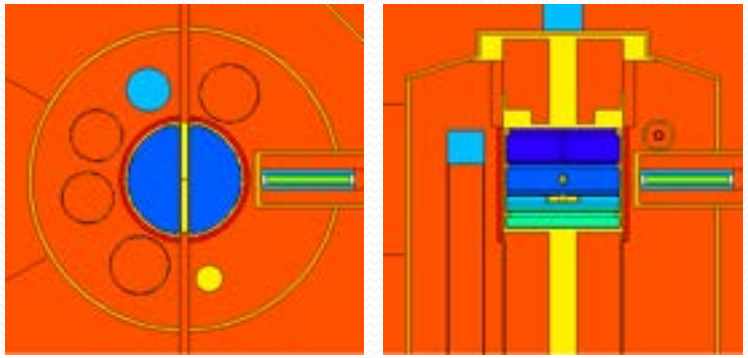
Reactivity Variation for insertion of **OSMOSE** sample in TAPIRO Experimental Channels

Results from direct calculations:

Tangential channel



Radial channel 1



Values in pcm				
OSMOSE	ρ	Abs Err	Δρ->common ref	Abs Err
Common Ref	-73	2	0	
Tg channel			-68	3
Rad channel 1			-33	2



Calculation procedure for IRMM samples reactivity evaluation

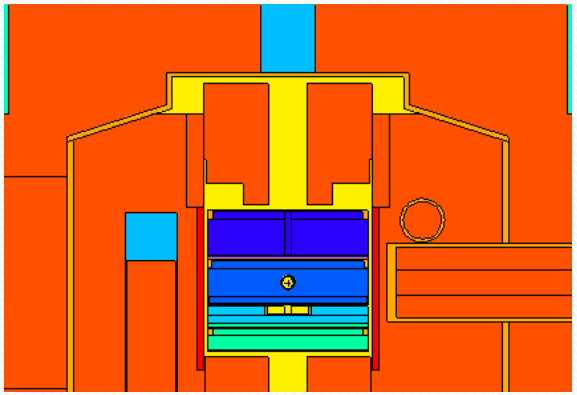
Reactivity Variation for insertion of **IRRM** sample in TAPIRO Experimental Channels

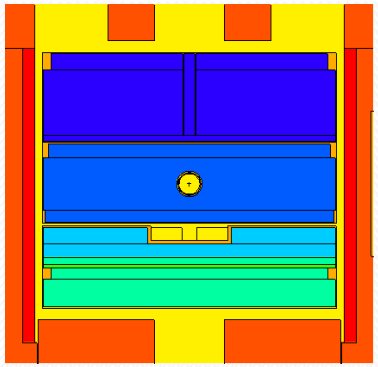
- ✓ Code Used: MCNP – 6.1
- ✓ Nuclear x-section library: JEFF-3.1

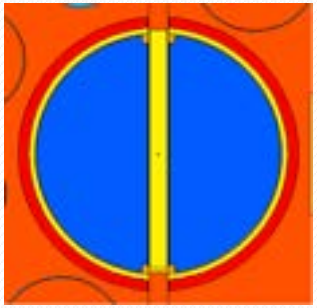
Tools available:

- ✓ Direct calculations (signal too small to detect through the noise)
- ✓ Perturbation through method of differential operator: PERT card (assumes unaltered eigenfunction). **Note that the quoted error estimates are almost certainly overestimates as standard MCNP6.1 does not allow a correct error evaluation on the final reactivity change. The code has now been patched in an *ad hoc* fashion and is being rerun so that correct error estimates will be posted in the final report.**
- ✓ Perturbation through method of bilinear functional employing adjoint function: KPERT card (employs scattering approximation) (results too noisy)

Reference case: TAPIRO standard configuration (Tangential and Radial-1 channels filled with Cu; Diametrical channel filled with He):







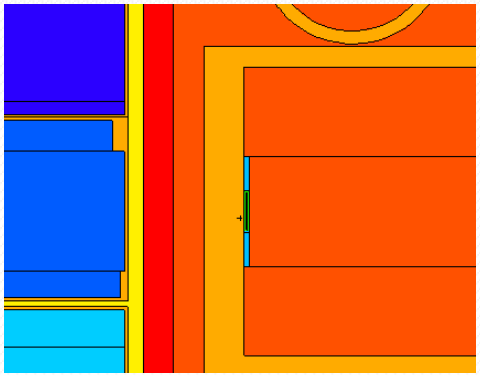


Results for IRMM samples reactivity evaluation

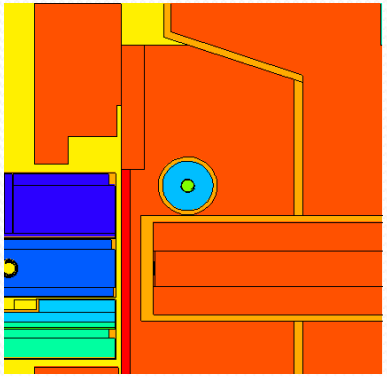
Reactivity Variation for insertion of **IRRM** sample in TAPIRO Experimental Channels

Results from PERT calculations:

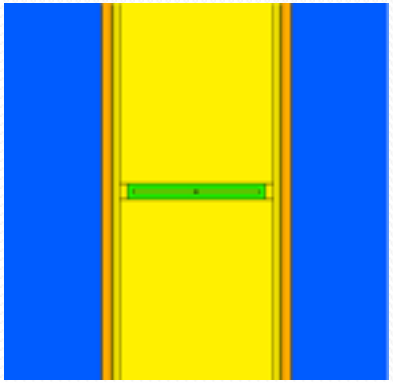
Radial channel 1



Tangential channel



Diametral channel



Values in pcm				
IRMM	ρ	Abs Err	Δρ->common ref	Abs Err
Common Ref	-73	2	0	
Diametral channel			0.05	0.02
Tg channel			0.66	0.07
Rad channel 1			0.93	0.07

Development of best estimate numerical tools for LFR design and safety analysis

A. Del Nevo, M. Tarantino [ENEA]

WORKSHOP TEMATICO: Gen. IV - LFR
ADP MiSE-ENEA (PAR2016-LP2)
Aula Magna - Scuola di Ingegneria e Architettura, Università di Bologna
26-27 Settembre, 2017

LIST OF CONTENTS

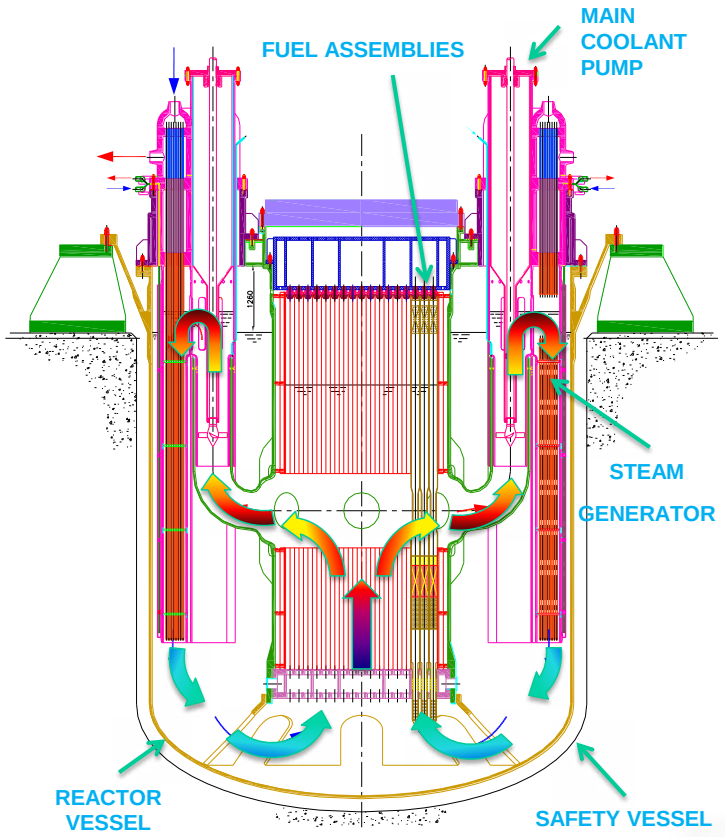
- INTRODUZIONE
- OBIETTIVI GENERALI
- DESCRIZIONE DELL'ATTIVITÀ
- RISULTATI ATTESI – INDICE DEL REPORT

INTRODUZIONE

AdP PAR LP2 (>2012)

Attività di collaborazione tra ENEA-CIRTEN condotte (anche) in sinergia con progetti EC e attività di ricerca internazionali (e.g. NEA, IAEA)

- A.2 Progettazione nocciolo
- A.3 Analisi di sicurezza
- C. Termoidraulica (parzialmente)



Sviluppo e validazione di codici e modelli multi-fisica per progetto e analisi di sicurezza di reattori veloci di IV generazione

- *Power*
  300 MWth (125 MWe)
- *Primary cycle*
  Molten Lead 400-480 °C
- *Secondary cycle*
  Water/superheated steam:335-450 °C

OBIETTIVI GENERALI

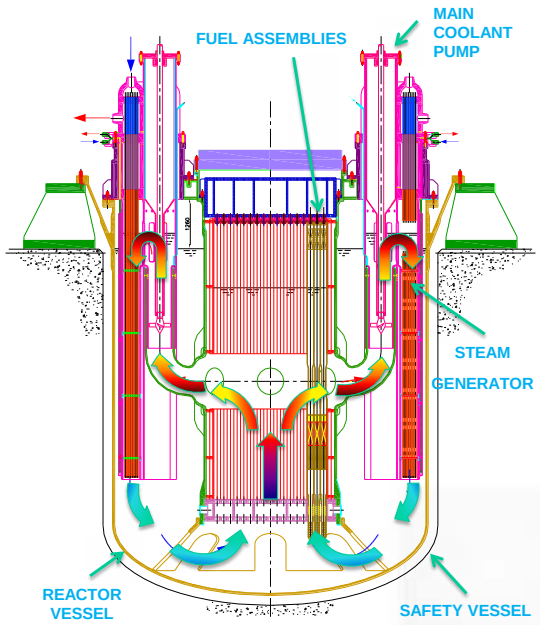
La Task ***sviluppo e convalida di codici e modelli multi-fisica per progetto e analisi di sicurezza di reattori veloci di IV generazione*** ha i seguenti obiettivi

1. **Collaborazione** tra ENEA-CIRTEN. Attività condotte (anche) in **sinergia con progetti EC e attività di ricerca internazionali (e.g. NEA, IAEA)**

2. **Continuità**. Le attività tecniche dovrebbero essere condotte in continuità con quanto svolto fino ad oggi
   → rendere gradualmente **l'attività coordinata e finalizzata**
   → **no brusche discontinuità** che possano penalizzare know-how acquisiti ed investimenti delle istituzioni coinvolte

3. **Coinvolgimento**. ENEA/Università CIRTEN coinvolte su un **progetto comune dove ognuno contribuisce per l'obiettivo comune**

Progetto di riferimento



OBIETTIVI GENERALI

4. **R&D e qualità**. Attività **orientata allo sviluppo di strumenti di calcolo, integrazione degli stessi, identificazione delle aree di utilizzo e documentazione, validazione ed applicazione**. **Risultati tangibili**.

5. **ENEA** stakeholder delle attività a supporto delle attività di R&D in corso e della progettazione ed implementazione delle campagne sperimentali al CR Brasimone

CIRTEN - CONSORZIO INTERUNIVERSITARIO PER LA RICERCA TECNOLOGICA NUCLEARE

POLITECNICO MILANO 1863

UNIVERSITÀ DI PISA

SAPIENZA UNIVERSITÀ DI ROMA

DESCRIZIONE DELL'ATTIVITÀ

- Strategia generale
  - definire le aree di simulazione e le interconnessioni rilevanti per la **progettazione e sicurezza di reattori Gen-IV**
  - definire i **codici e la piattaforma di accoppiamento e identificare le necessità di sviluppo e lo stato di convalida**
  - procedere con **l'attività di sviluppo, convalida e applicazione** in continuità con quanto fatto negli ultimi anni

DESCRIZIONE DELL'ATTIVITÀ

- Attività pianificate di sviluppo e convalida
  - termo-meccanica della barretta di combustibile
  - termo-idraulica di sistema
  - fluidodinamica tridimensionale e accoppiamento
  - dinamica accoppiata neutronica-termoidraulica tridimensionale
  - modello multifisico del reattore (neutronico – termoidraulico)
  - simulazione dell'interazione chimica refrigerante-combustibile

RISULTATI ATTESI – INDICE DEL REPORT

- Report comune che raccoglie le attività effettuate dai partner diviso in 2 parti

Part 1: General Aspects

1. Design and safety analysis areas in support of Lead-cooled Fast Reactor development (ANN)
2. Characterization of the **modelling needs** for the selected areas.(UNIBO)
   a. Core Design (ENEA-GG)
   b. Primary System Design (ENEA-MT)
   c. Auxiliary and Ancillary Systems Design (UNIROMA1)
   d. Instrumentation and Control Design (POLIMI)
   e. Probabilistic Safety Analysis (UNIROMA1)
   f. Deterministic Safety Analysis (ENEA-ADN)
   g.
   h. ……
   i. …….
3. Overview of the available modelling capabilities (ENEA→ draft, All!)
   a. Summary of the PART 2
   b. Capabilities and skills
   c. Future developments

RISULTATI ATTESI – INDICE DEL REPORT

Part 2: Ongoing activities on development, validation and application of computational tools

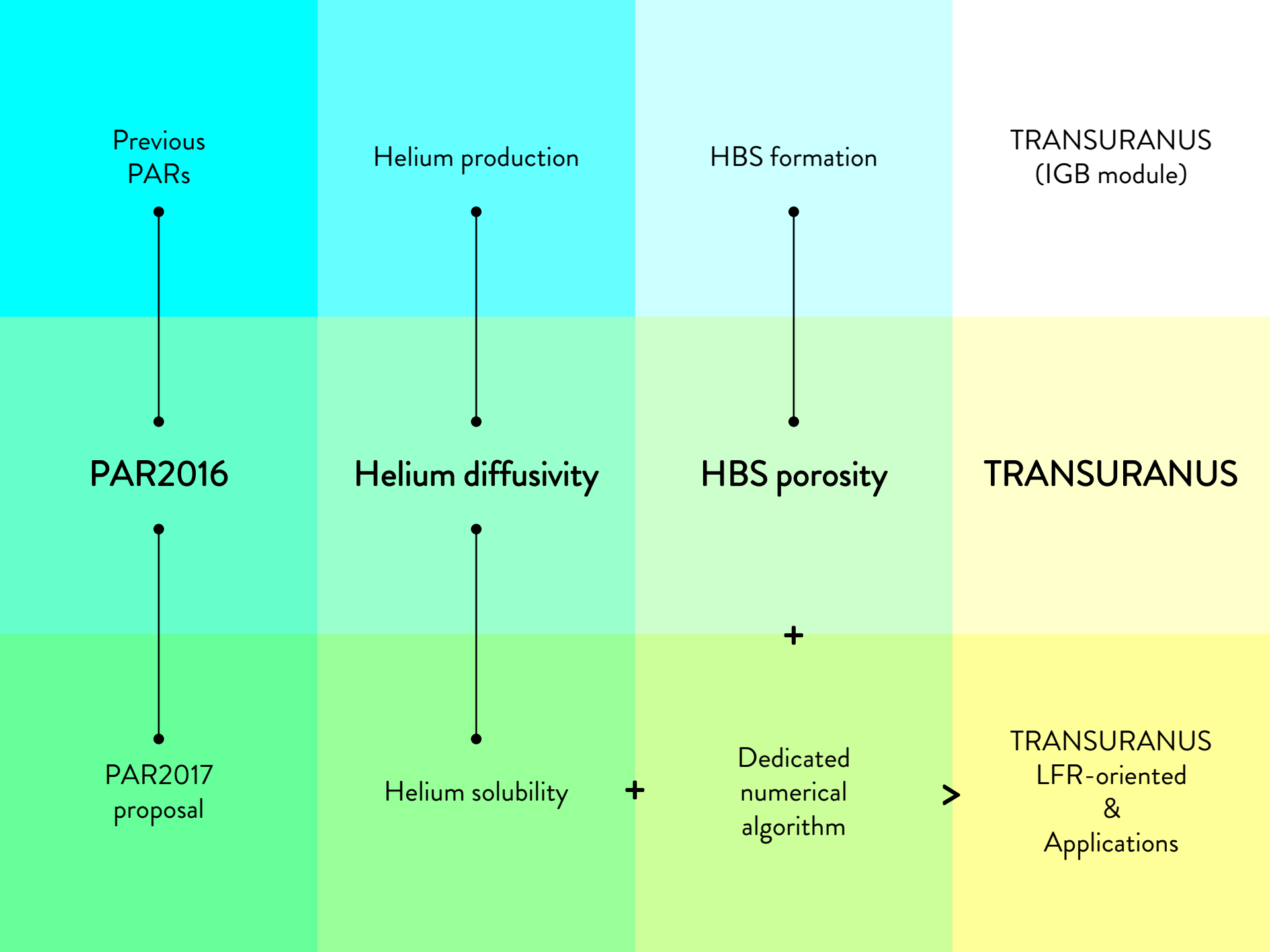
1. Development/assessment of models of inert gas behavior in the fuel for the application for the TRANSURANUS fuel pin mechanic code (POLIMI, max 30 pages)
   a. *Body of the report concerning the ongoing activities*
   b. *Role of the activity and general goals and future development*
   c. *Background and reference*
2. Validation of FEM-LCORE/CATHARE by TALL 3D experimental tests (UNIBO, max 30 pages).
3. Validation of RELAP53D by CIRCE-ICE experimental tests (UNIROMA1, max 30 pages).
4. Application of RELAP5/mod3.3 – Fluent coupling codes to CIRCE-HERO (UNIPI, max 30 pages).
5. Application of RELAP3D on Phenix Experimental Tests (UNIROMA1 + ENEA, max 30 pages).
6. Fuel-coolant chemical interaction (POLIMI, max 30 pages).
7. Development and validation of decay heat models into the FRENETIC code (POLITO, max 30 pages).
8. Development of multi-physic code for Lead-cooled Fast Reactor (POLIMI, max 30 pages).
9. Validation of SIMMER code against experimental data (UNIPI+ENEA, max 30 pages).

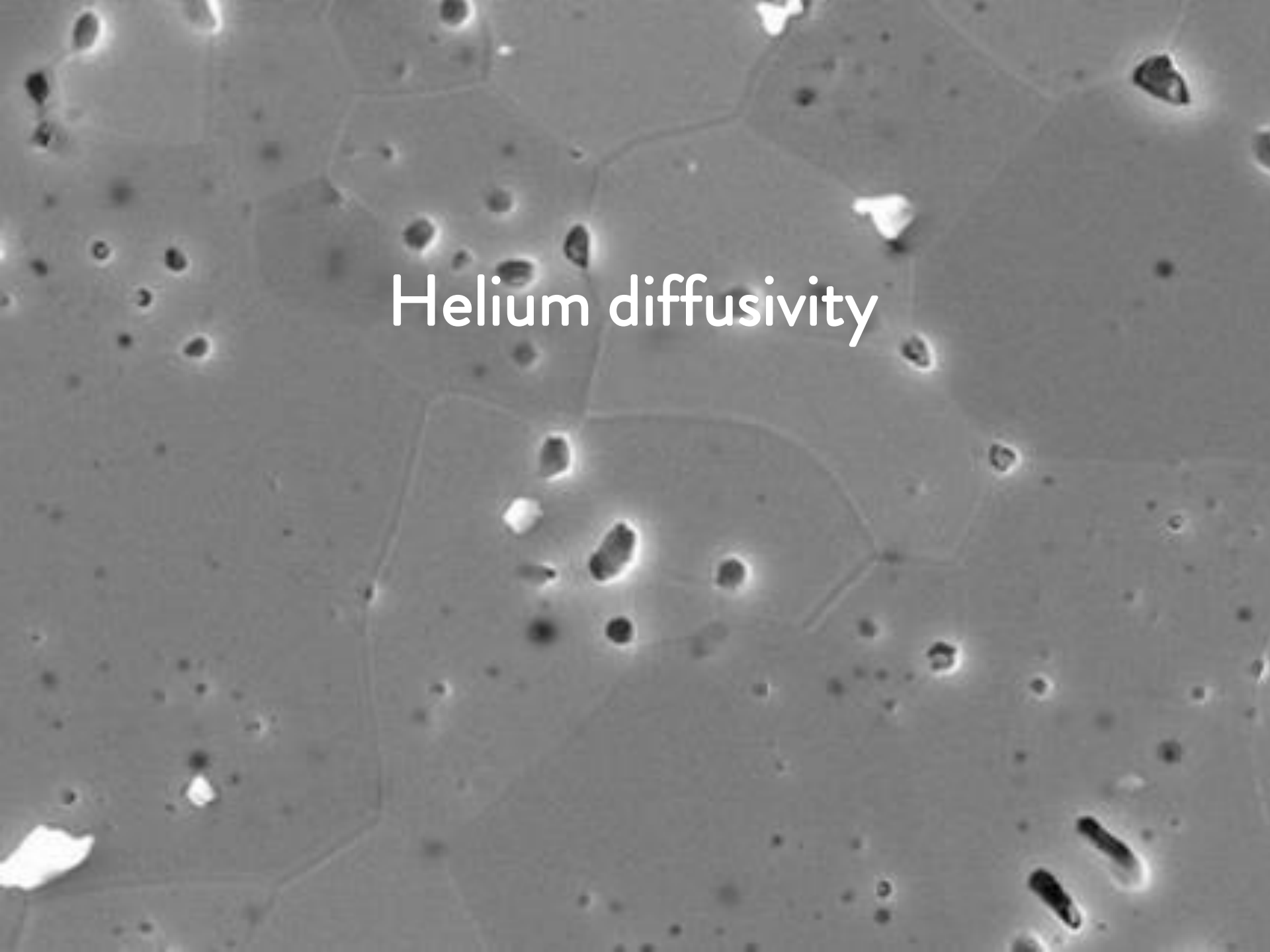


POLITECNICO
MILANO 1863

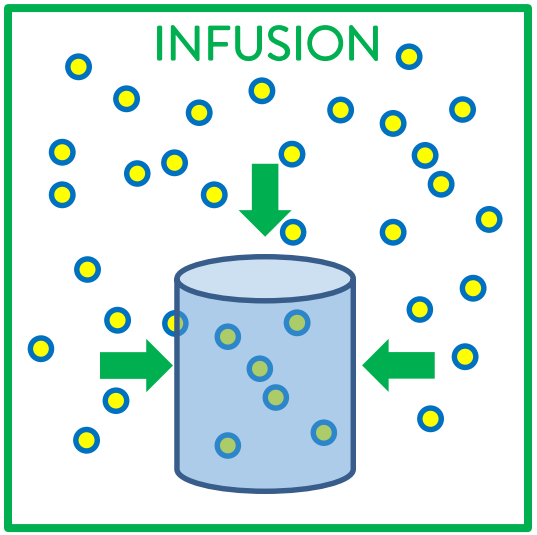
Development/assessment of models describing the inert gas behavior in the fuel for application to the TRANSURANUS fuel pin thermo-mechanical code

L. Luzzi, D. Pizzocri, T. Barani, L. Cognini
Politecnico di Milano, Nuclear Reactor Group
Workshop Tematico PAR2016-LP2, 26-27.09.2017

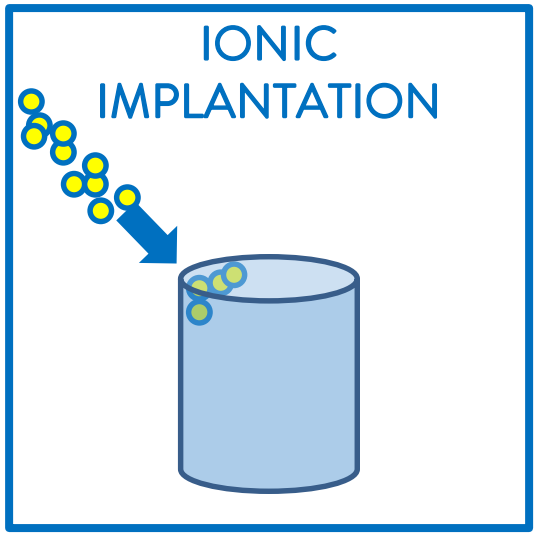

Previous PARs
Helium production
HBS formation
TRANSURANUS (IGB module)
PAR2016
Helium diffusivity
HBS porosity
TRANSURANUS
+
PAR2017 proposal
Helium solubility
+
Dedicated numerical algorithm
>
TRANSURANUS LFR-oriented & Applications


Helium diffusivity

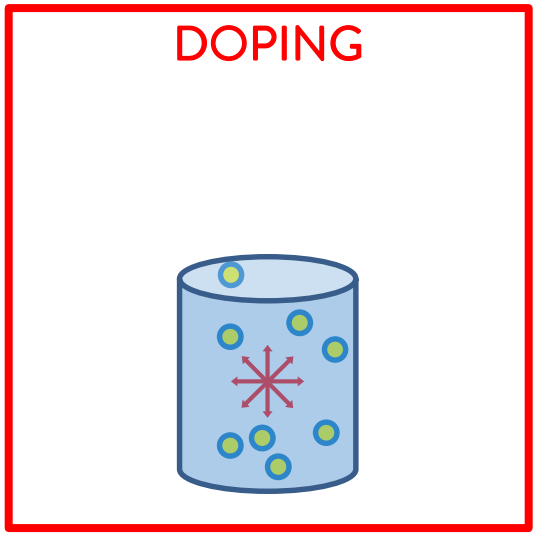
Literature review of experimental results: Diffusivity – Techniques overview



- Sample in a helium-pressurised capsule placed into a furnace
- The sample contains a concentration of He equal to the solubility limit at the imposed **p and T**

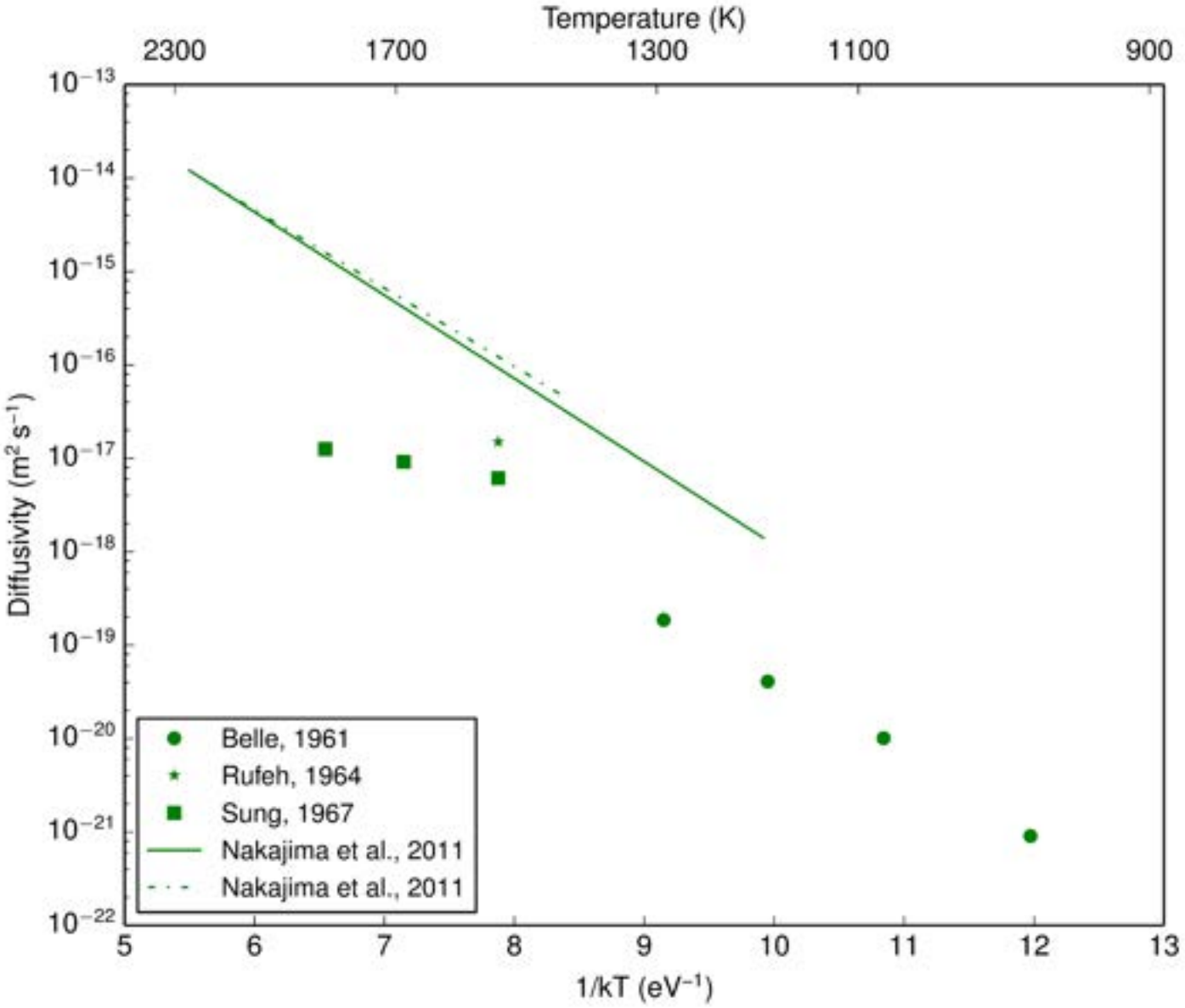


- Sample bombarded with a beam of ^{3}He ions (E ≈ MeV)
- Only the **surface layer** is affected
- Lattice is **damaged**

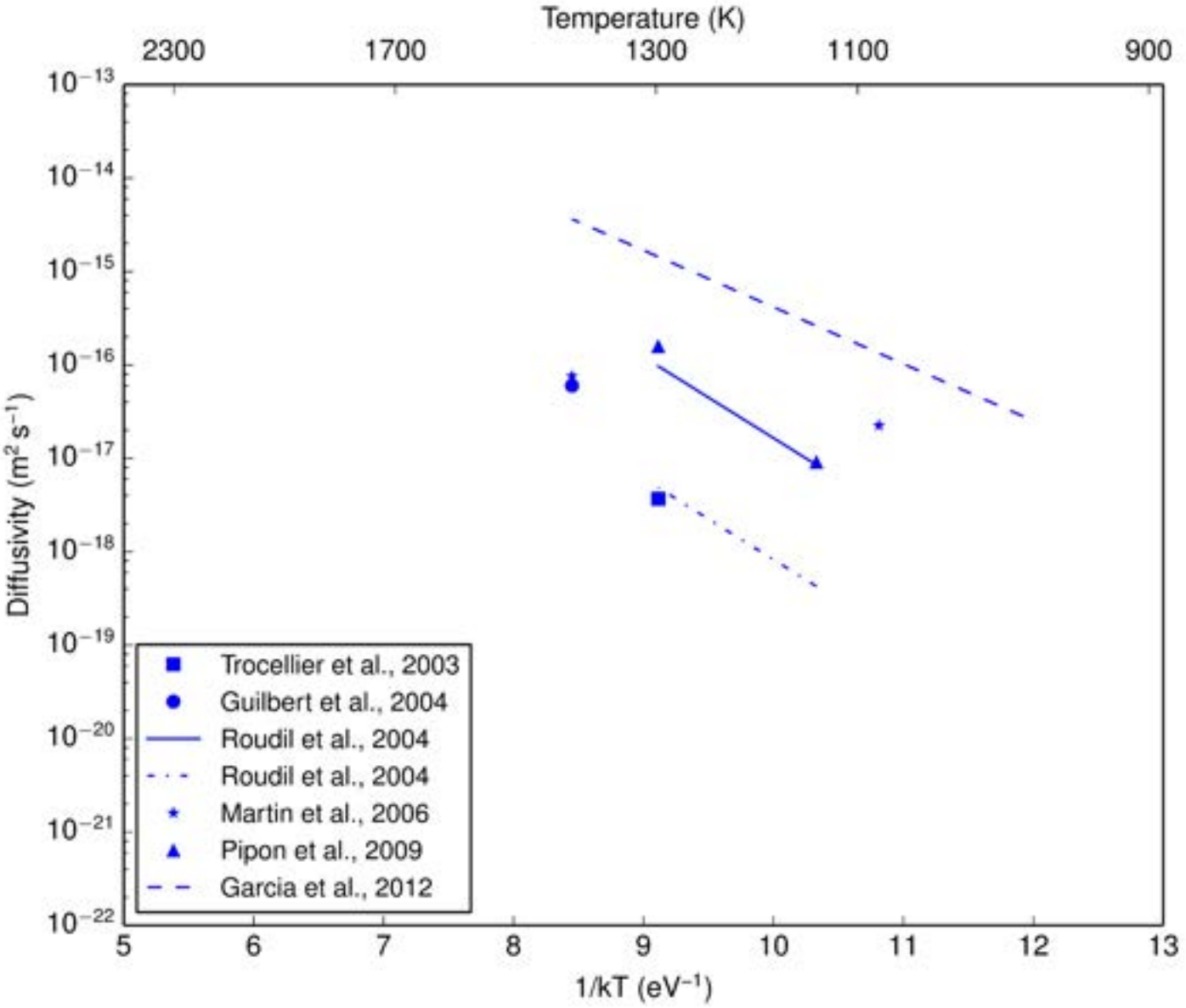


- α-emitters are introduced into the oxide matrix (e.g., ^{238}**Pu**)
- α particles interact with the lattice, **damaging** it

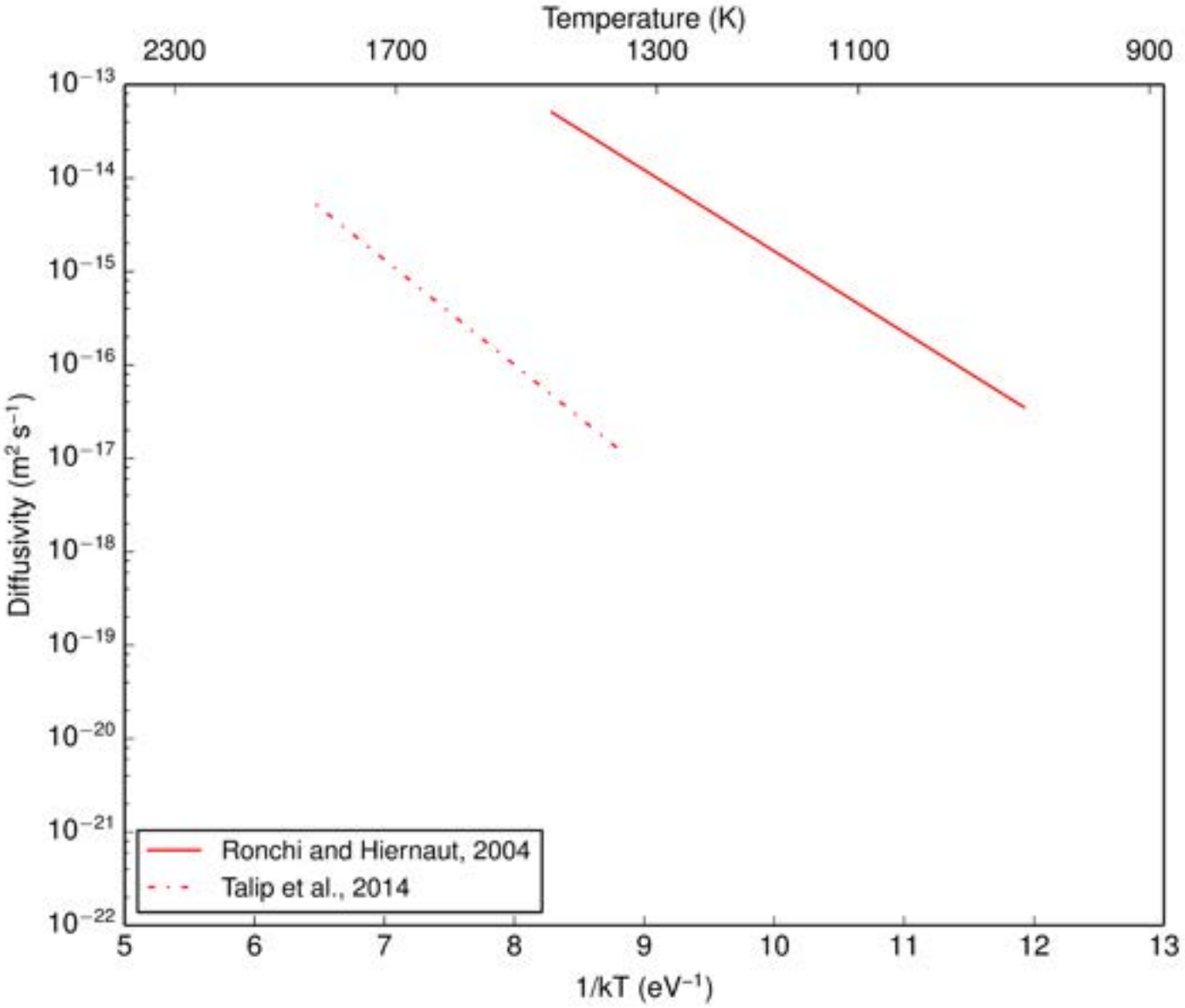
Literature review of experimental results: Diffusivity – Infusion technique



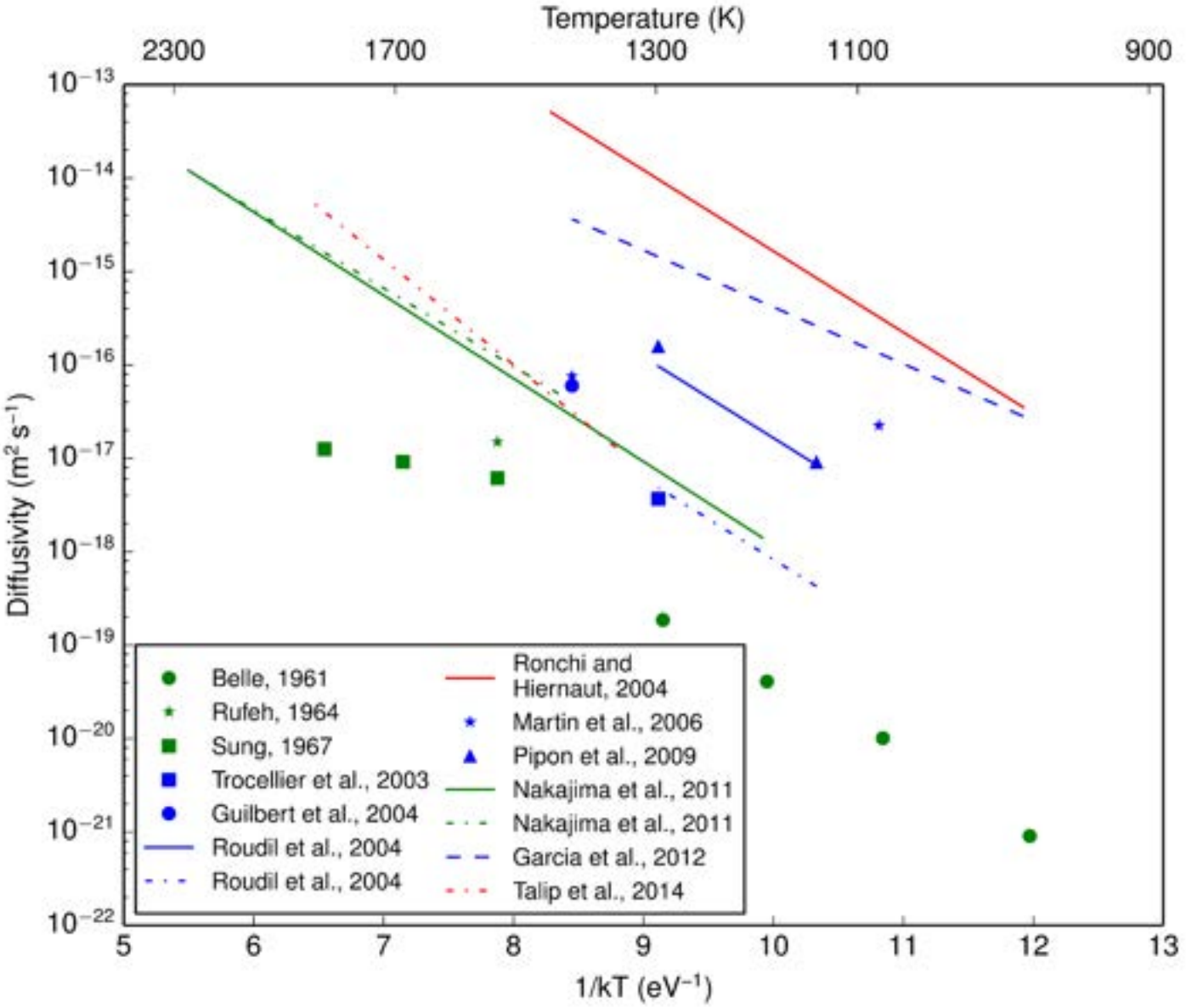
Literature review of experimental results: Diffusivity – Implantation technique



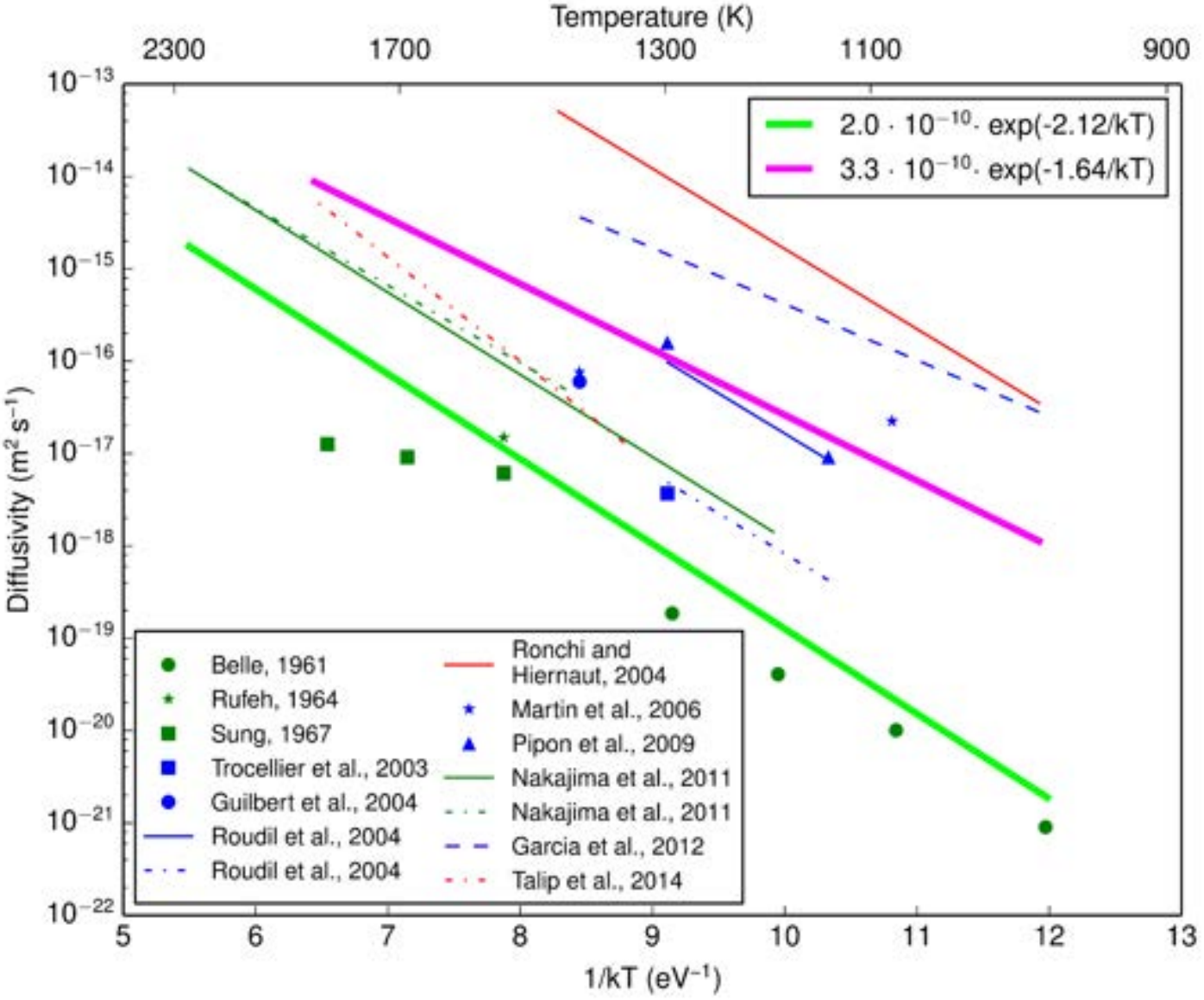
Literature review of experimental results: Diffusivity – Doping technique



Literature review of experimental results: Diffusivity – Summary



Literature review of experimental results: Diffusivity – New correlations



Literature review of experimental results: Diffusivity – New correlations

$$D_{\text{no damage}} = 2.0 \cdot 10^{-10} \exp\left(-\frac{2.12}{k_B T}\right)$$

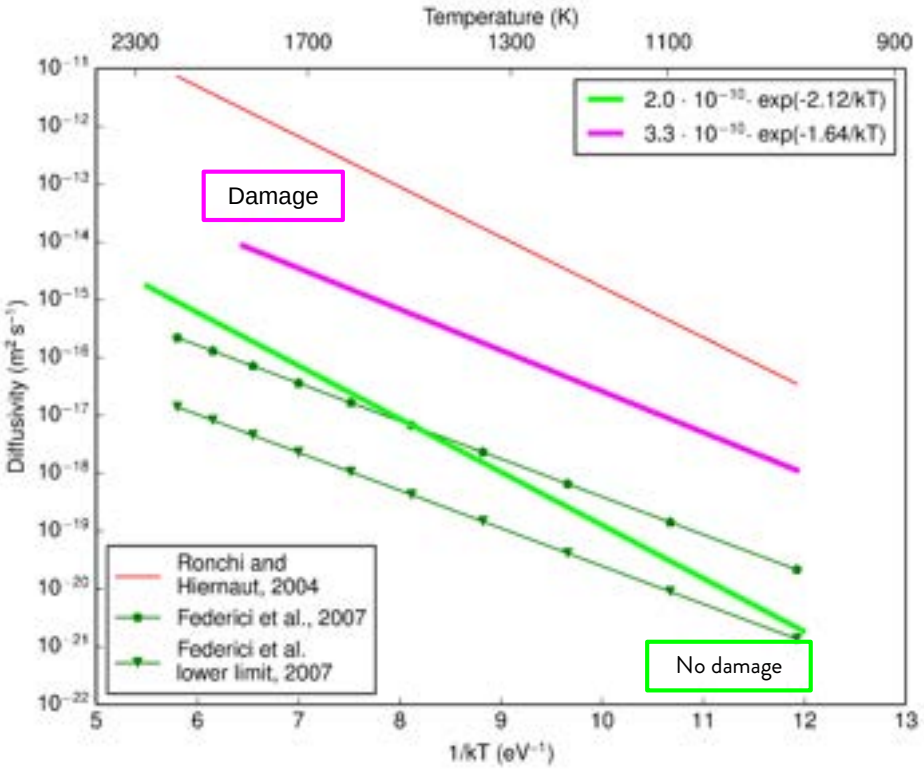
Validity range: 968 - 2110 K

$$D_{\text{damage}} = 3.3 \cdot 10^{-10} \exp\left(-\frac{1.64}{k_B T}\right)$$

Validity range: 973 - 1800 K

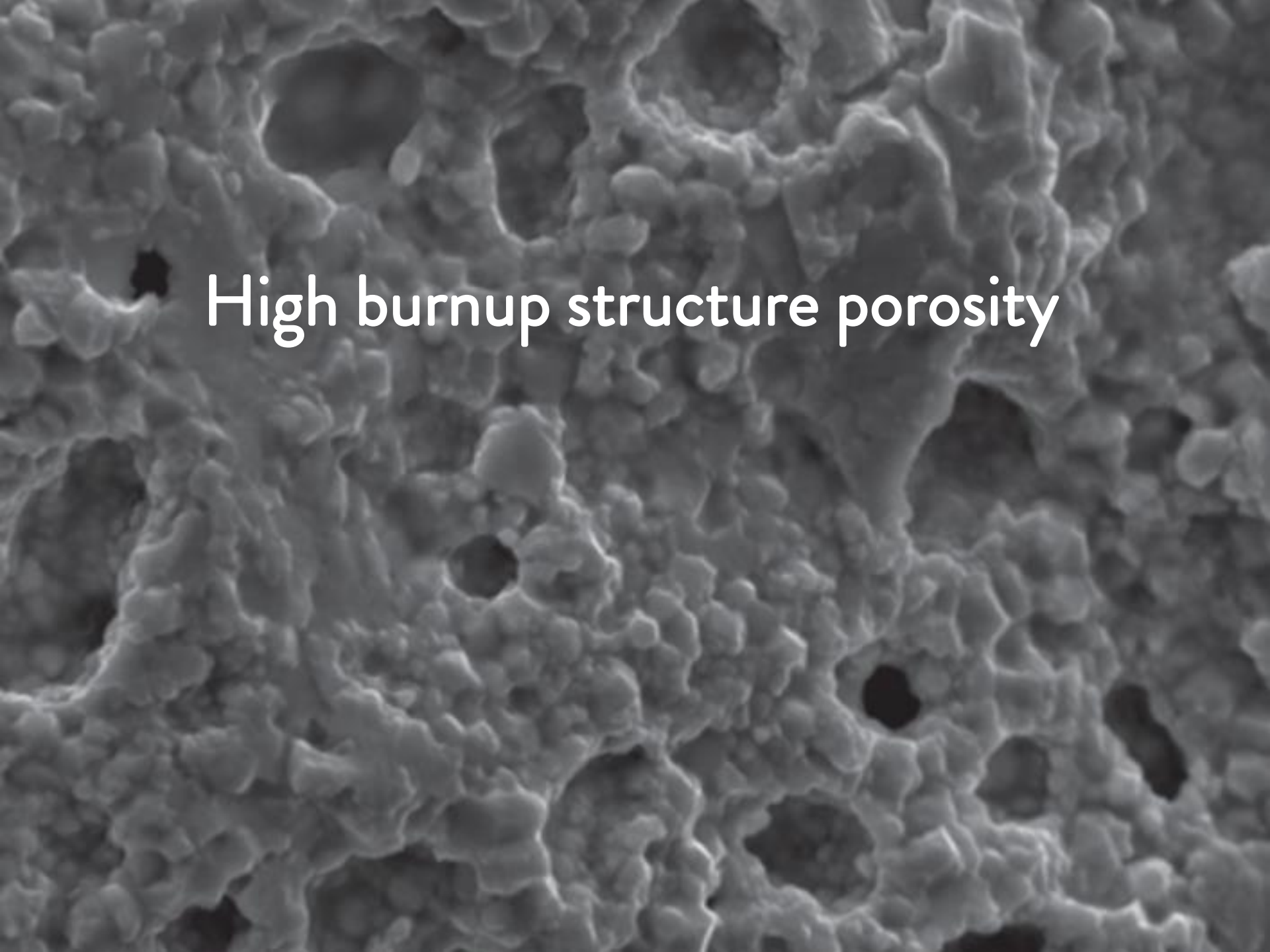
Each **correlation*** has **specific application** frame:

- For **in-pile conditions and storage conditions** it is recommended D_{damage} due to the similar lattice damage
- For **annealing experiment**, or experiments dealing with **fresh fuel** it is recommended $D_{no\ damage}$



Implementation and verification in Transuranus by Luana Cognini

*Manuscript submitted to NED

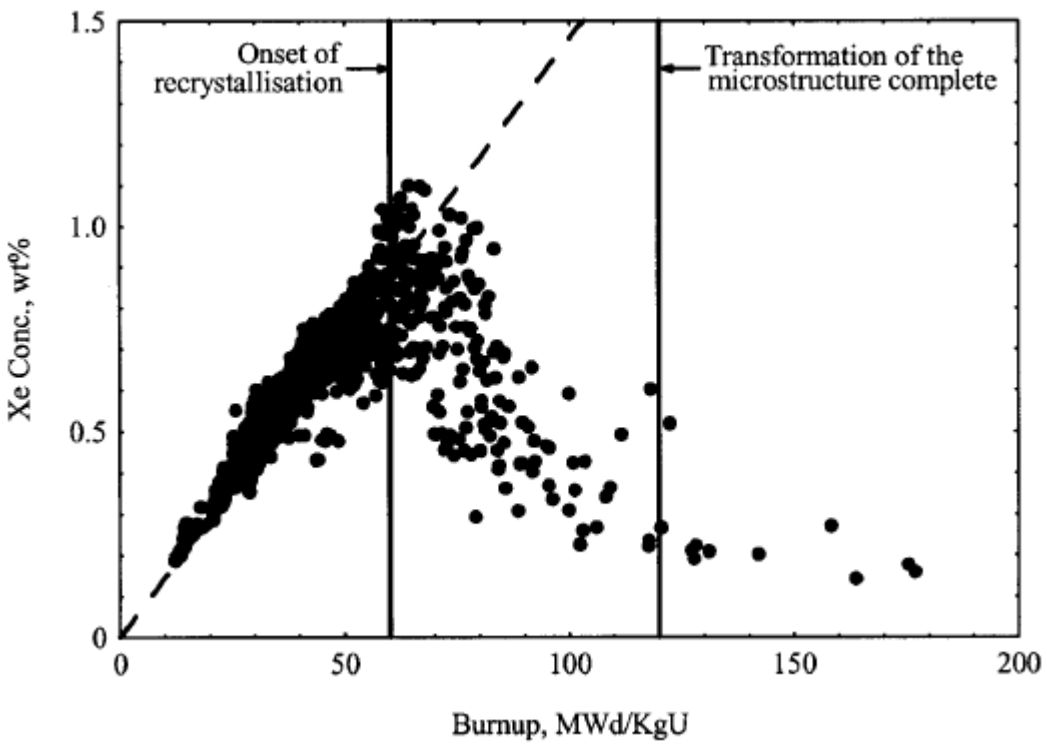

High burnup structure porosity

State of the art – HBS model in TRANSURANUS

HBS formation threshold	Empirical burnup/temperature threshold Holt et al., 2014. JNM, 452, 166–172.
Depletion of intra-granular fission gases	ODE with empirical coefficients Lassmann et al., 1995. JNM, 226, 1-8
Porosity evolution	Empirical correlation Porosity ~ Burnup

DECOUPLED !!!

HBS formation model
High burnup structure – Gas depletion



$$\frac{\mathrm{d}c}{\mathrm{d}bu_{\mathrm{eff}}} = \frac{\mathrm{D}}{a^2}\frac{1}{\rho^2}\frac{\partial}{\partial\rho}\rho^2\frac{\partial}{\partial\rho}c + y\mathrm{F}$$

IC $\quad c(\rho, bu_{\mathrm{eff},0}) = c_0(\rho)$

BC $\quad c(1, bu_{\mathrm{eff}}) = 0$

$[\partial c/\partial\rho]_0 = 0$

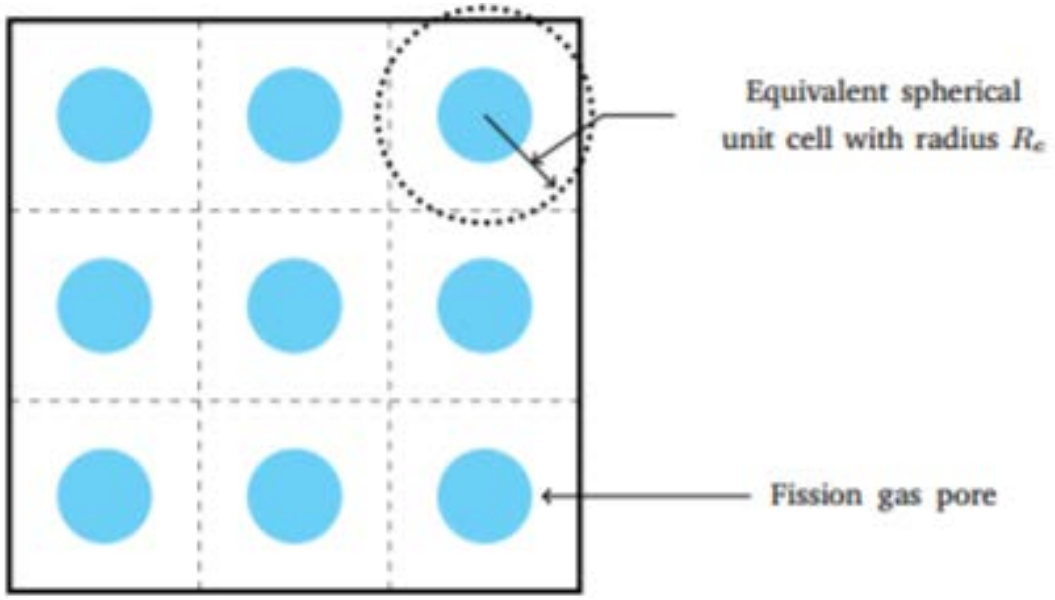
Diffusion of fission gas in spherical grains

Diffusion coefficient according to Brémier and Walker (2002), i.e., **based on asymptotic behaviour**

Pizzocri et al., 2017. Journal of Nuclear Materials, 487, 23-29.

Brémier and Walker, 2002., Radiation Effects and Defects in Solids, 157, 311–322.

HBS porosity evolution
Wigner-Size cells around pores



- Dislocation pile-up
- Grain recrystallization/ polygonization
- Depletion of intra-granular fission gas
- **Development of novel porosity**

Diffusion of fission gas in spherical grains

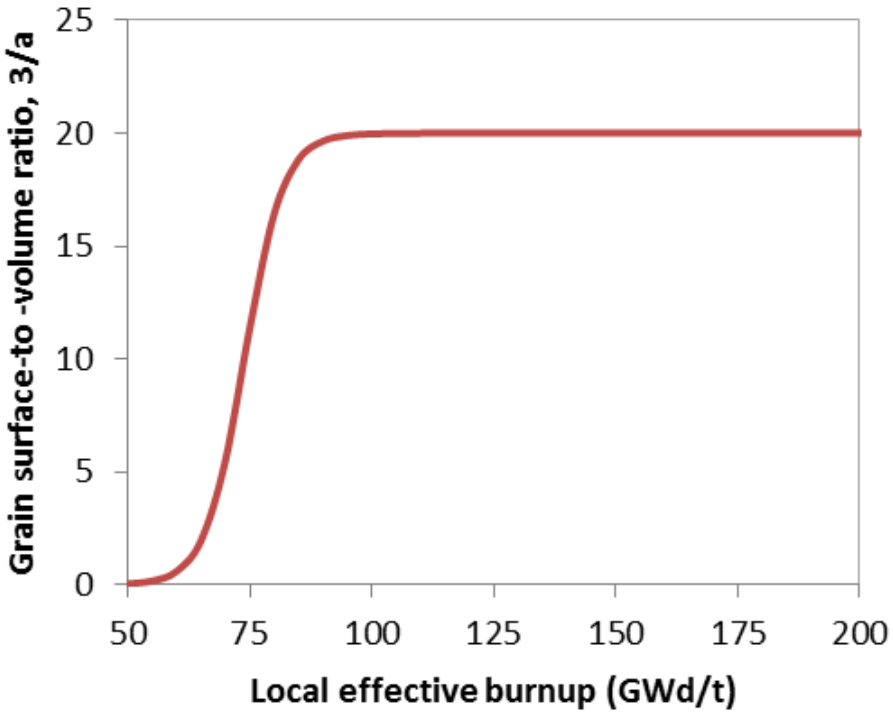
Precipitation in the pores of gas atoms **moving along grain boundaries**

Pore growth by vacancy absorption (pressure over equilibrium)

Cappia, PhD thesis, 2017

HBS porosity evolution
Pore nucleation

$$\frac{\mathrm{d}N}{\mathrm{d}bu_{\mathrm{eff}}} = -K\frac{3}{a^2}\frac{\mathrm{d}a}{\mathrm{d}bu_{\mathrm{eff}}}$$

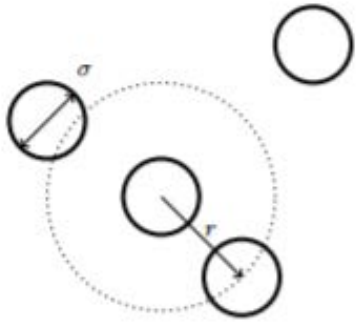


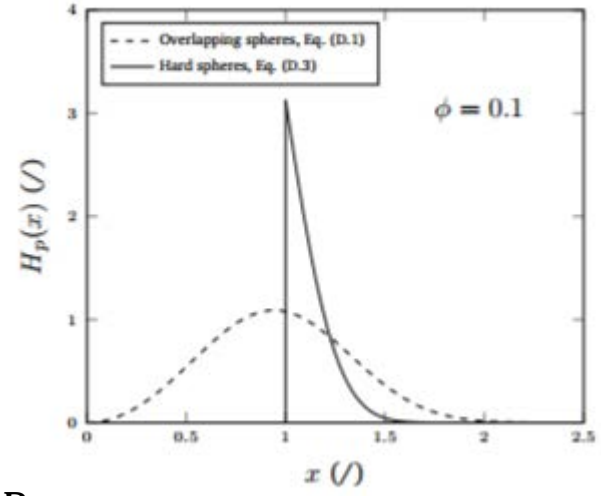
Assumed to be linked to grain-size reduction

Number of nucleated pores is proportional to grains surface-to-volume ratio

Intrinsically limited by grain reduction

HBS porosity evolution
Pore inter-connection





$$\frac{\mathrm{d}N}{N} = -\frac{1}{2}\int_{1}^{1+\frac{\mathrm{d}R}{R}} H(x)\,dx$$

Pores are considered as
non-overlapping
hard spheres

<u>Pore growth leads to pore inter-connection</u>

Similar to grain-boundary bubbles but in 3D-geometry

Pore are assumed as immobile

Summary of model equations (PAR2015, PAR2016)

EFFECTIVE BURNUP THRESHOLD

$$bu_{\text{eff}} = \int H(T_{\text{th}})\,\mathrm{d}bu$$

$$H(T_{\text{th}}) = \begin{cases} 1 & T \le T_{\text{th}} \\ 0 & T > T_{\text{th}} \end{cases}$$

GRAIN RECRYSTALLIZATION

$$\frac{\mathrm{d}a}{\mathrm{d}bu_{\text{eff}}} = -\frac{1}{\tau}(a - a_\infty)$$

IC $\quad a\left(bu_{\text{eff},0}\right) = a_0$

INTRA-GRANULAR DIFFUSION

$$\frac{\mathrm{d}c}{\mathrm{d}bu_{\text{eff}}} = \frac{\mathrm{D}}{a^2}\frac{1}{\rho^2}\frac{\partial}{\partial\rho}\rho^2\frac{\partial}{\partial\rho}c + y\mathrm{F}$$

IC $\quad c\left(\rho, bu_{\text{eff},0}\right) = c_0(\rho)$

BC $\quad c(1, bu_{\text{eff}}) = 0$

$\quad [\partial c/\partial\rho]_0 = 0$

PORE NUCLEATION

$$\frac{\mathrm{d}N}{\mathrm{d}bu_{\text{eff}}} = -K\frac{3}{a^2}\frac{\mathrm{d}a}{\mathrm{d}bu_{\text{eff}}}$$

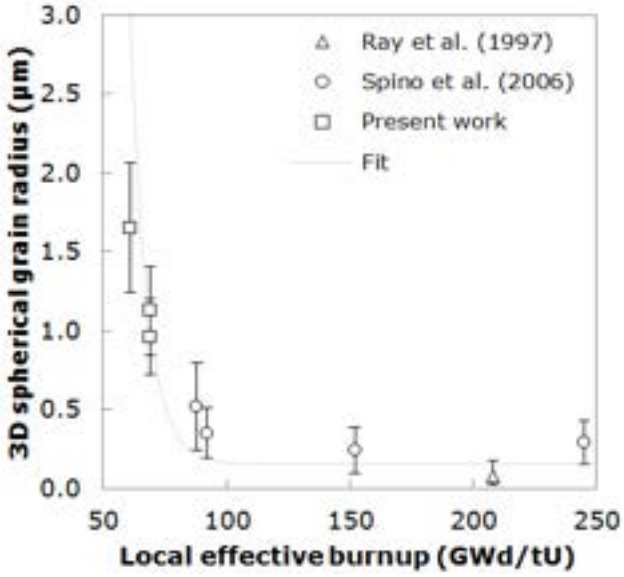
PORE INTERCONNECTION

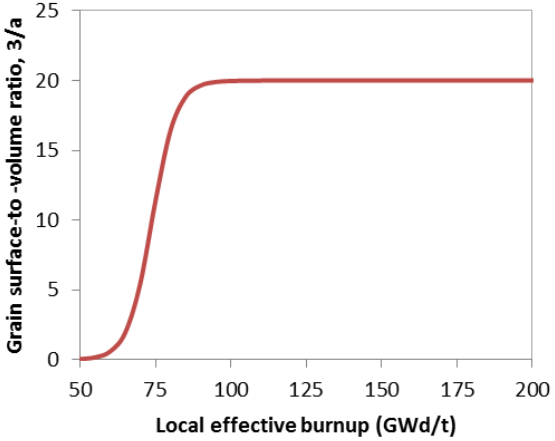
$$\frac{\mathrm{d}N}{N} = -\frac{1}{2}\int_1^{1+\frac{\mathrm{d}R}{R}} H(x)\,dx$$

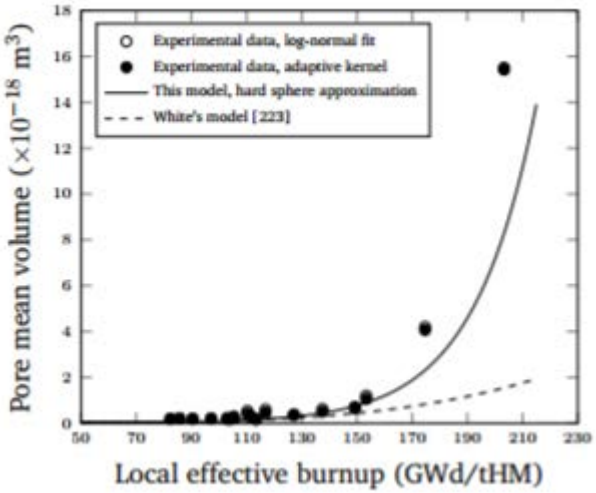
PORE GROWTH (VACANCY INFLOW)

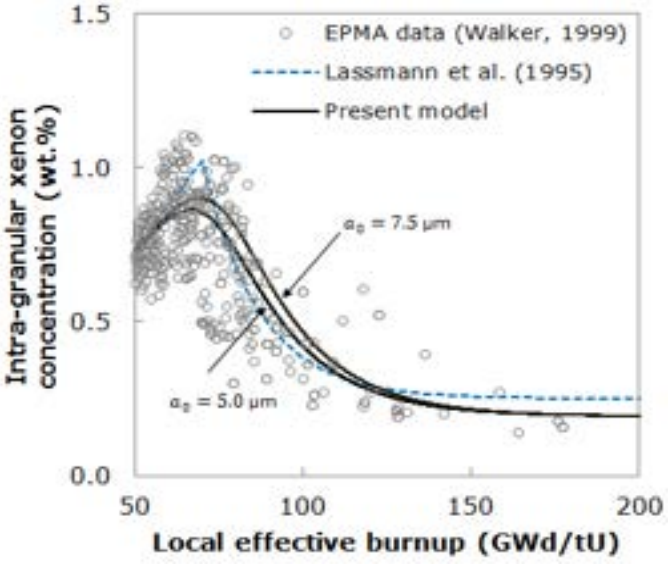
$$\frac{\mathrm{d}n_v}{\mathrm{d}bu_{\text{eff}}} = \frac{4\pi D}{kTS}\left(p - \frac{2\gamma}{R} - \sigma_h\right)$$

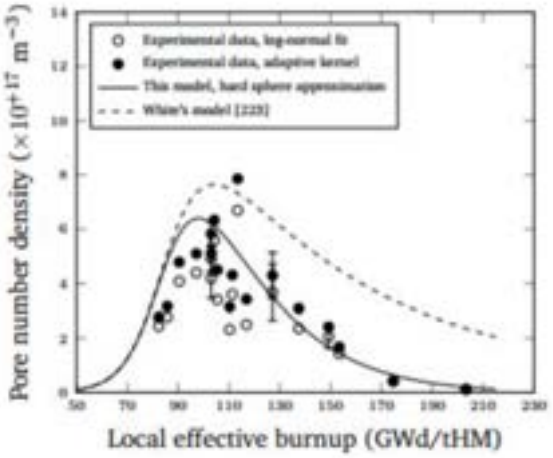
HBS formation & porosity evolution

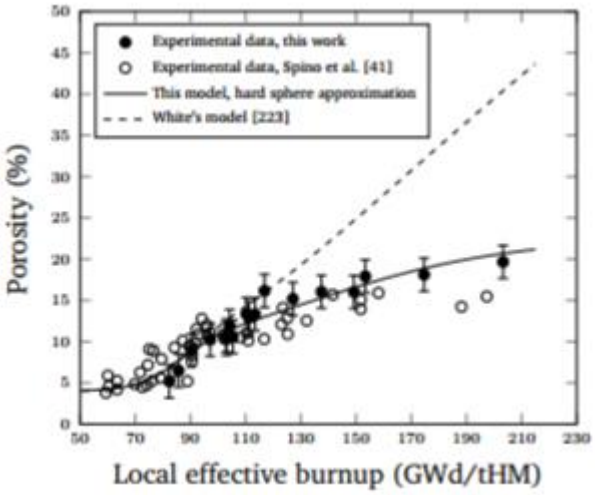












Conclusions and further developments

1. Development of new **correlations for Helium diffusivity**
   - Accounting for all available data
   - Greatly reducing in the calculation uncertainties
   - Clarified scope of application

2. Development of a new **model for HBS porosity evolution**
   - Semi-empirical pore nucleation
   - Pore growth by vacancy absorption
   - Pore inter-connection as hard spheres

- Development of new **correlations for Helium solubility**
- Development of **dedicated numerical algorithms**

- Fuel rod integral analysis in support of design of FRs using the improved version of TRANSURANUS

Thank you for your kind attention

1. Development of new **correlations for Helium diffusivity**
   - Accounting for all available data
   - Greatly reducing in the calculation uncertainties
   - Clarified scope of application

2. Development of a new **model for HBS porosity evolution**
   - Semi-empirical pore nucleation
   - Pore growth by vacancy absorption
   - Pore inter-connection as hard spheres

- Development of new **correlations for Helium solubility**
- Development of **dedicated numerical algorithms**

- Fuel rod integral analysis in support of design of FRs using the improved version of TRANSURANUS

PAR2016

Accordo di programma MiSE – ENEA

PAR2016 – Progetto B.3.1. LP2

GENERATION IV LEAD COOLED FAST REACTOR

UNIVERSITÀ DI PISA - DICI

"Validation of SIMMER code against experimental data "

Alessio Pesetti, Nicola Forgione

Scuola di Ingegneria e Architettura, Università di Bologna, 26-27 settembre 2017

List of contents

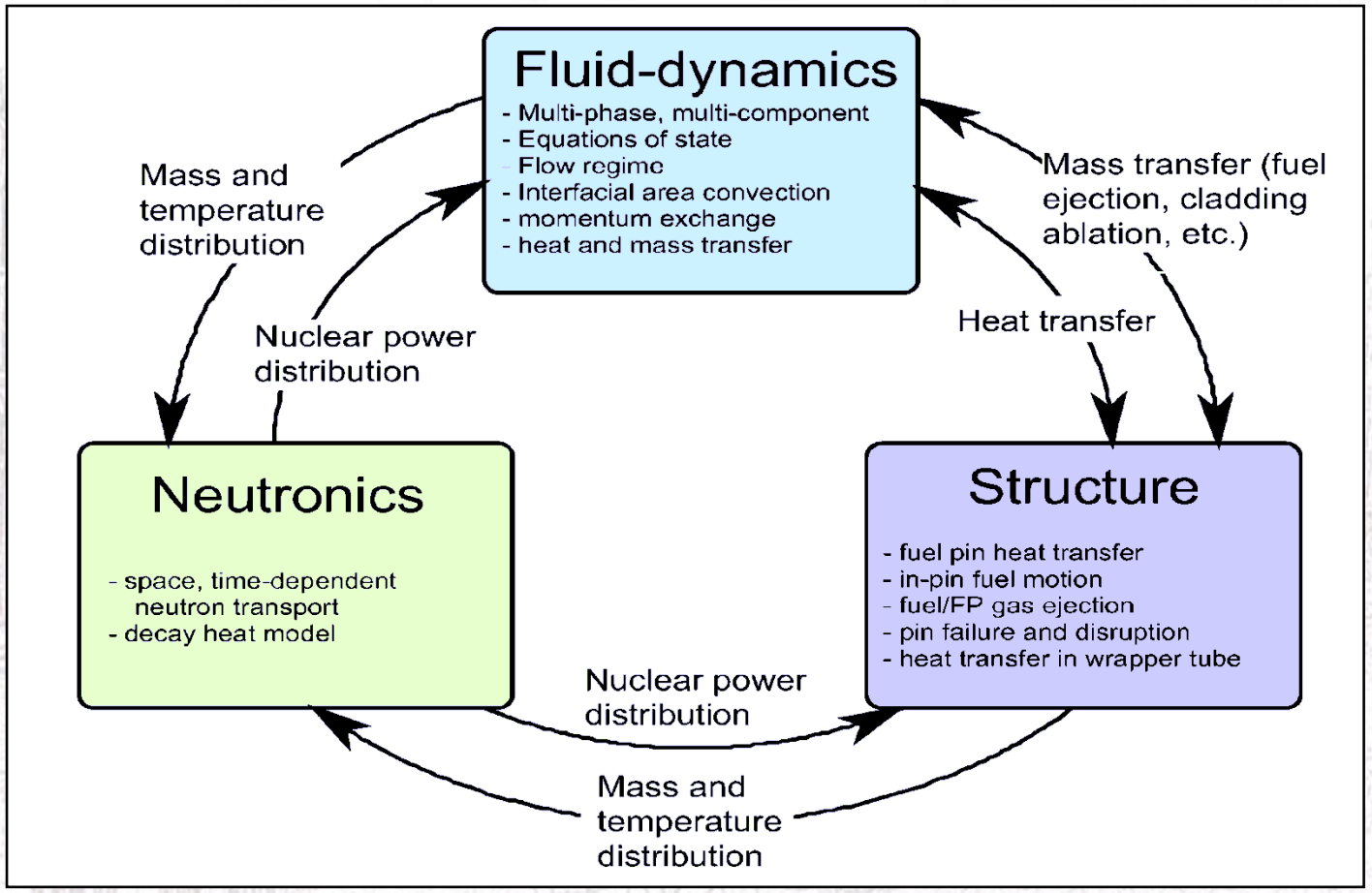
- Introductory remarks
- SIMMER generalities
- Phase 1 and 2 code assessment of SIMMER-III
- SIMMER applications for LFRs at UNIPI
  - LIFUS5 test n. 1 and 3 (ENEA C.R. Brasimone)
  - JAERI tests
  - FZK (KIT) SGI tests
  - LIFU5/Mod2 THINS tests (ENEA C.R. Brasimone)
  - LIFUS5/Mod2 LEADER tests (ENEA C.R. Brasimone)
  - CIRCE MAXSIMA tests (ENEA C.R. Brasimone)
- Conclusive remarks and future work

Introductory remarks

- A research activity at UNIPI was performed, in the framework of EU FP7 projects and ENEA collaboration, aiming to achieve knowledge improvement about water-heavy liquid metals interaction phenomena and postulated Steam Generator Tube Rupture (SGTR) event (H_2O-LBE interaction) in various SG configurations relevant for HLMFRs
- The SGTR scenario needs to be analysed in the integrated pool type HLMFR configurations, aiming to predict the hazardous consequences of the SG/PHX tube rupture taking place in the HLM pool (pressure wave propagation and cover gas pressurization, domino effect, steam dragged into the core, primary system pollution and slug formation)
- In the domain of UNIPI-ENEA collaboration pre- and post-tests were carried out by SIMMER-III and –IV code on the basis of experimental campaigns performed in LIFUS5 facility, implementing various test sections, investigating SGTR
- SIMMER code was also assessed on the basis of experimental data from literature, water impinging on LBE at JAERI and gas injection in water at FZK
- SIMMER code appears to be a suitable code in the simulation of the H_2O-LBE interaction scenario

SIMMER generalities

SIMMER-III is a 2D axisymmetric, up to eight velocity-field, multi-component, multiphase, Eulerian fluid-dynamics code coupled with neutron kinetics model. It can deals with safety analysis problems in advanced fast reactors. SIMMER-IV is a 3D polar or Cartesian code



Phase 1 and 2 code assessment of SIMMER-III

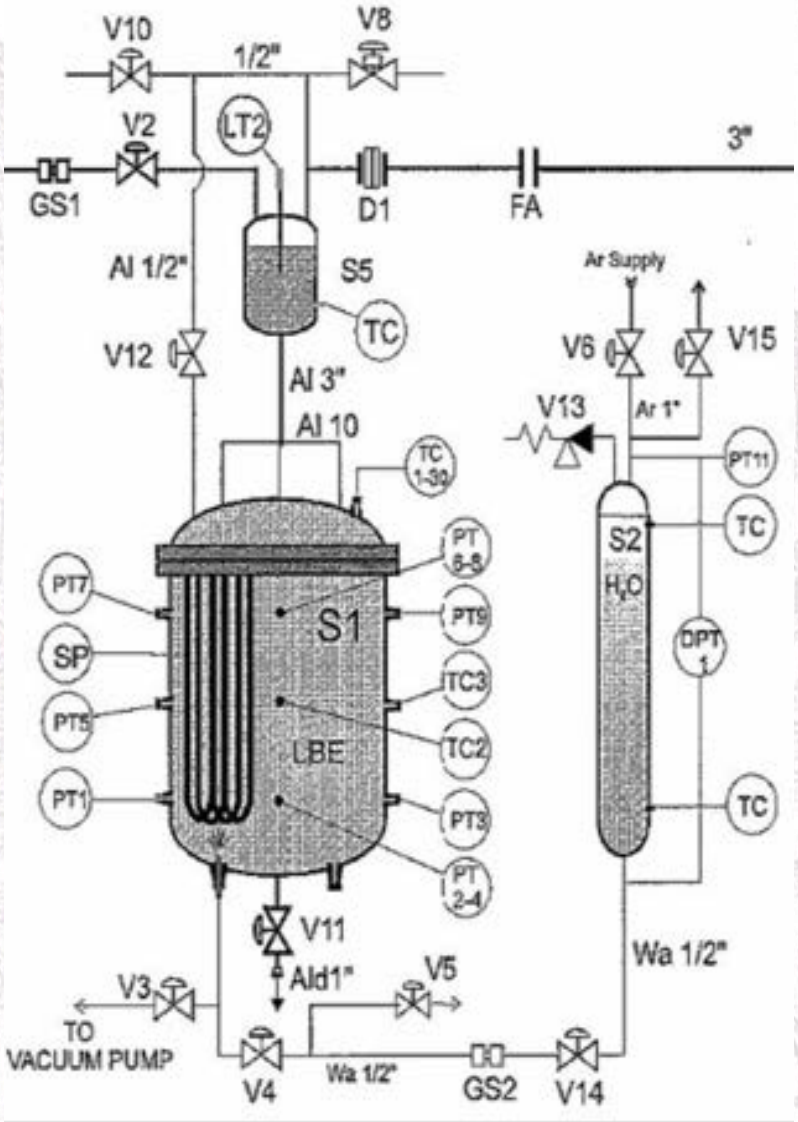
Phase 1 and 2 where carried out by PNC-JNC in collaboration with FZK and CEA

Phase 1 (1992-1996) for fundamental or separate-effect assessment of individual code models, in order to debug and verify its coding and validate individual models. Only the fluid-dynamics portion of the code was tested. Tests problems include: simple test calculations (code can simulate known physics plausibly); single and multi-phase flow benchmark problems to confirm the code is comparable with other state-of-the-art codes; and analyses of simple experiments with unambiguous data available. It consisted of 34 problems, which tested specific code models

Phase 2 (1996-2000) for integral assessment of key physical phenomena relevant to LMFR safety, in order to validate the code for integral accident phenomena and hence is relevant to the future application of SIMMER-III to reactor calculations. Applied the code to integral, complex multiphase situations. It consisted of 34 problems and it intended to cover key accident phenomena, which are directly relevant to the CDA analysis

SIMMER Applications for LFRs at ENEA/UNIPI

LIFUS5 test n.1



Facility components of main interest for simulations:

- Water tank S2
- Reaction tank S1
- Expansion tank S5
- Pipeline between S2 and S1

The main feature of the equipment in S1 is the asymmetry

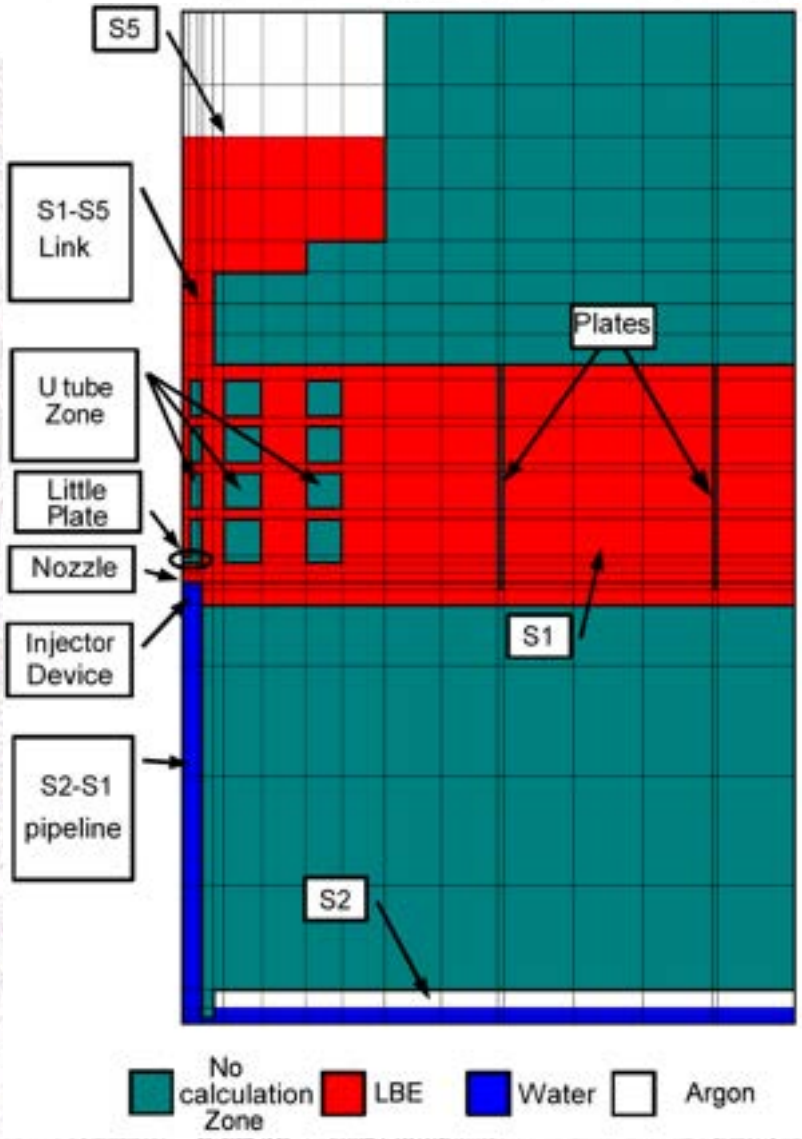
Test conditions:

LBE Temperature: 350°C
Water Temperature: 235°C
Water Pressure: 70 bar

Two different geometrical models have been developed: CM1 and CM2 Model

SIMMER Applications for LFRs at ENEA/UNIPI

LIFUS5 test n.1

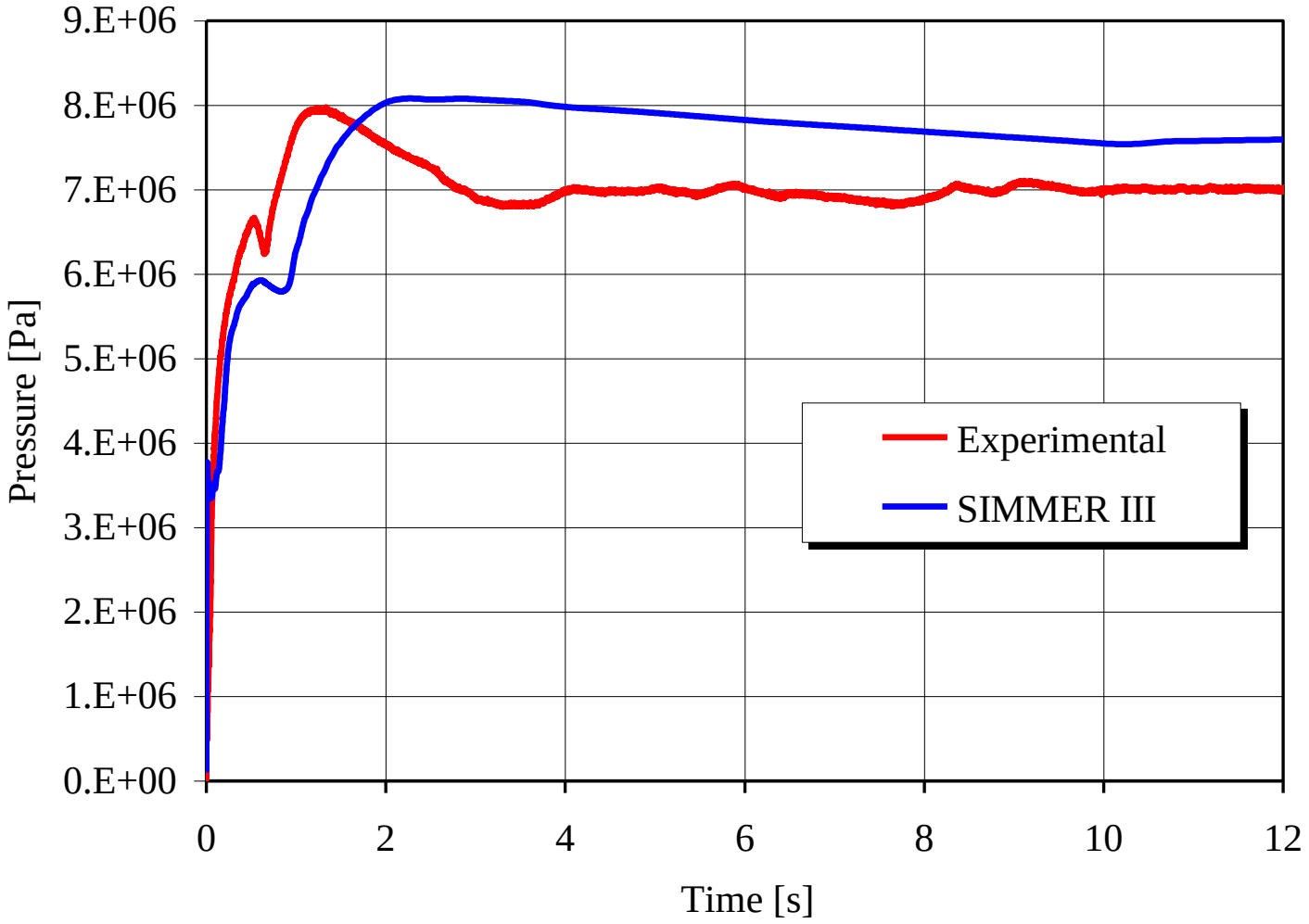


Main features of CM2 domain:

- subdivision into 20 radial and 32 axial meshes
- representation of the four connection tubes between S1 and S5 through only one central tube
- presence of two concentric annuli, representing the plates which divide S1 internal into four sectors
- detailed representation of the mock up U tubes zone (12 “no calculation regions”)
- presence of S2
- shape of S5 tank

SIMMER Applications for LFRs at ENEA/UNIPI

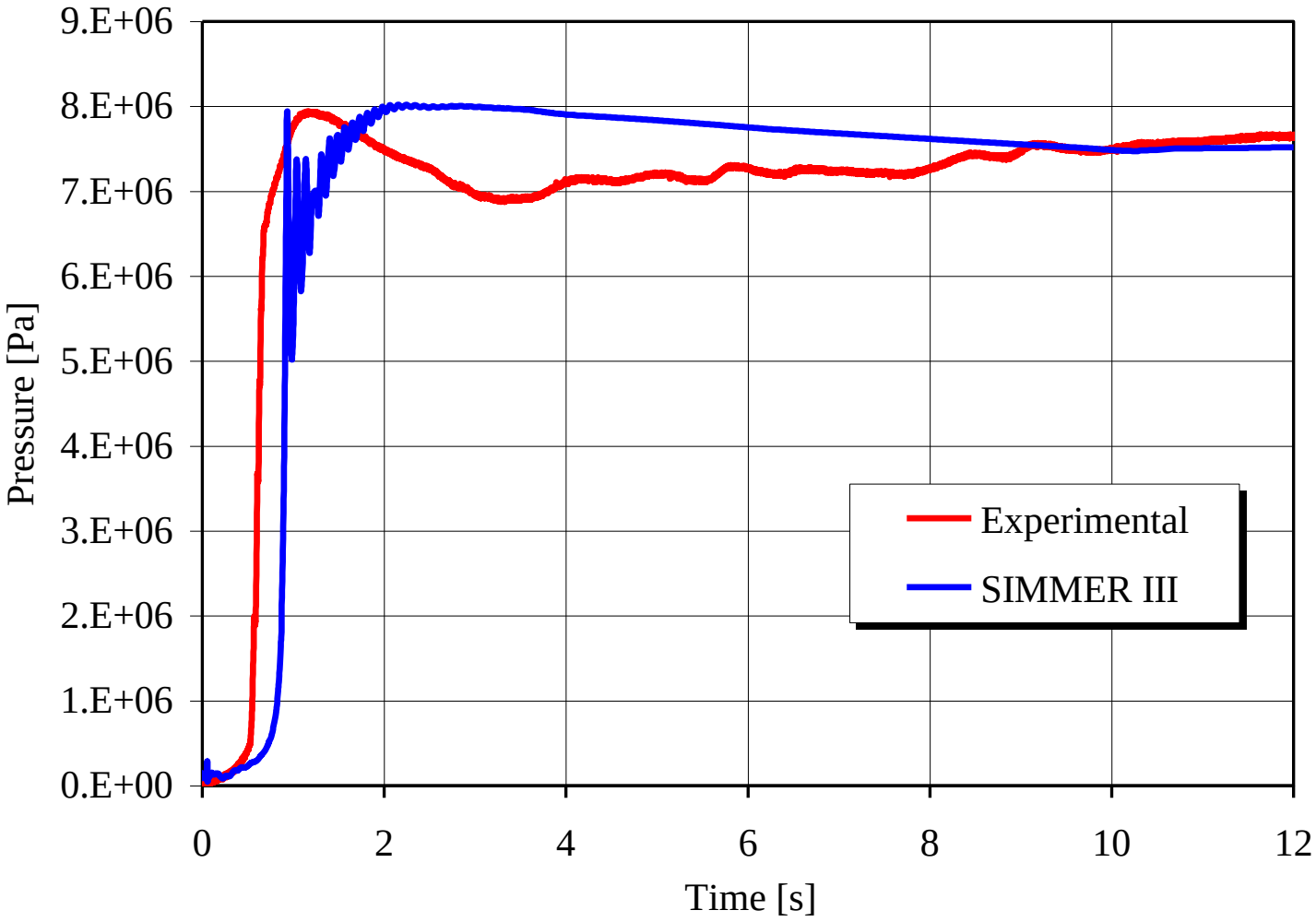
LIFUS5 test n.1



Comparison between calculated and experimental pressure in S1 tank

SIMMER Applications for LFRs at ENEA/UNIPI

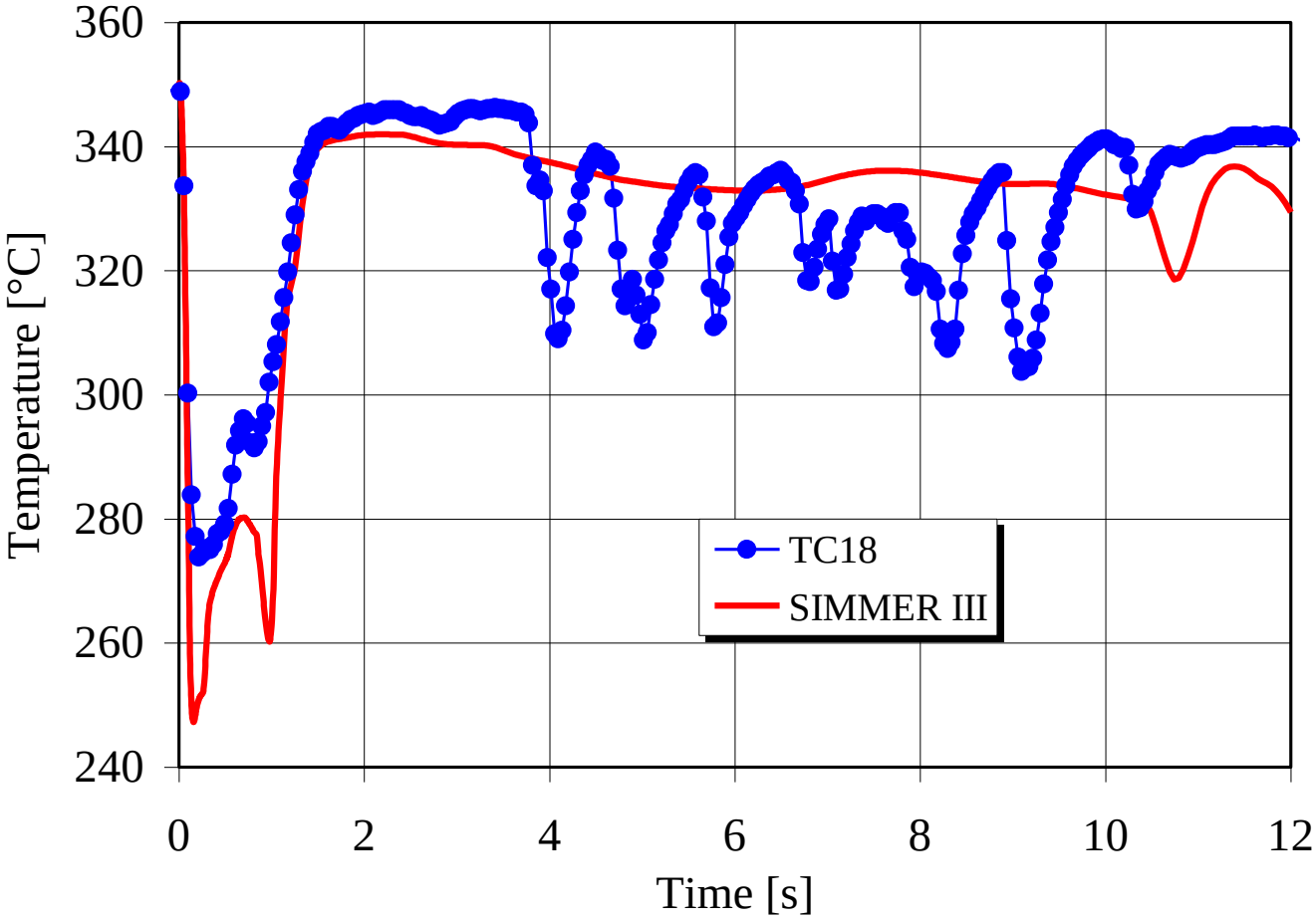
LIFUS5 test n.1

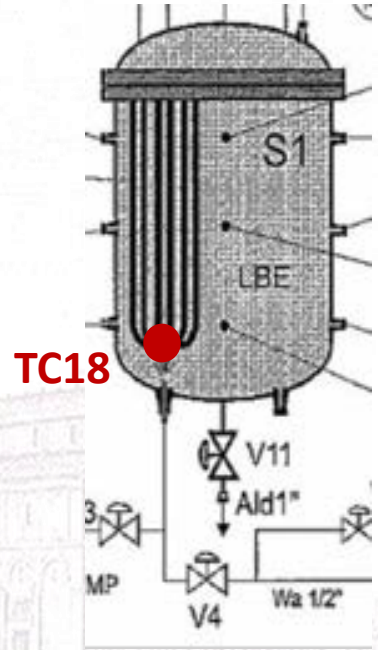


Comparison between calculated and experimental pressure in S5 tank

SIMMER Applications for LFRs at ENEA/UNIPI

LIFUS5 test n.1

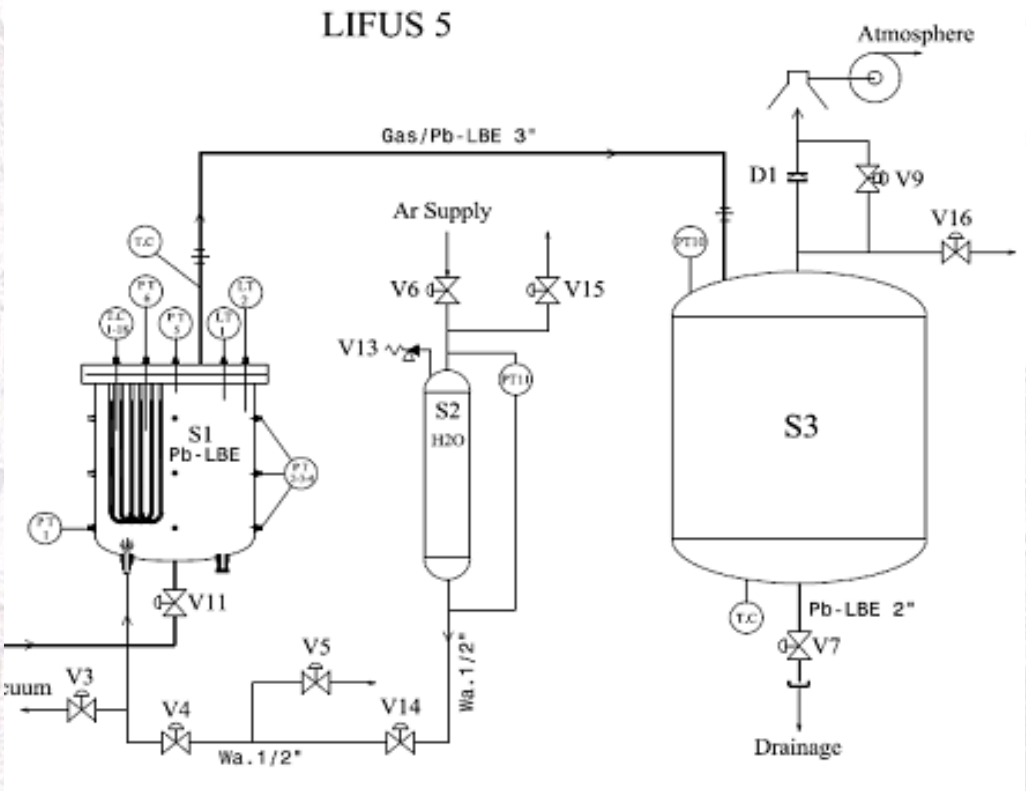




The temperatures measured with the axial thermocouple, placed close to the injector device, was compared with the corresponding one calculated by SIMMER-III code

SIMMER Applications for LFRs at ENEA/UNIPI

LIFUS5 test n.3



In this case the entire facility was simulated excluding the storage tank of LBE

Test conditions:

- LBE Temperature: 350°C
- Water Temp.: 235°C
- Water Pressure: 40 bar
- S1 completely filled with LBE

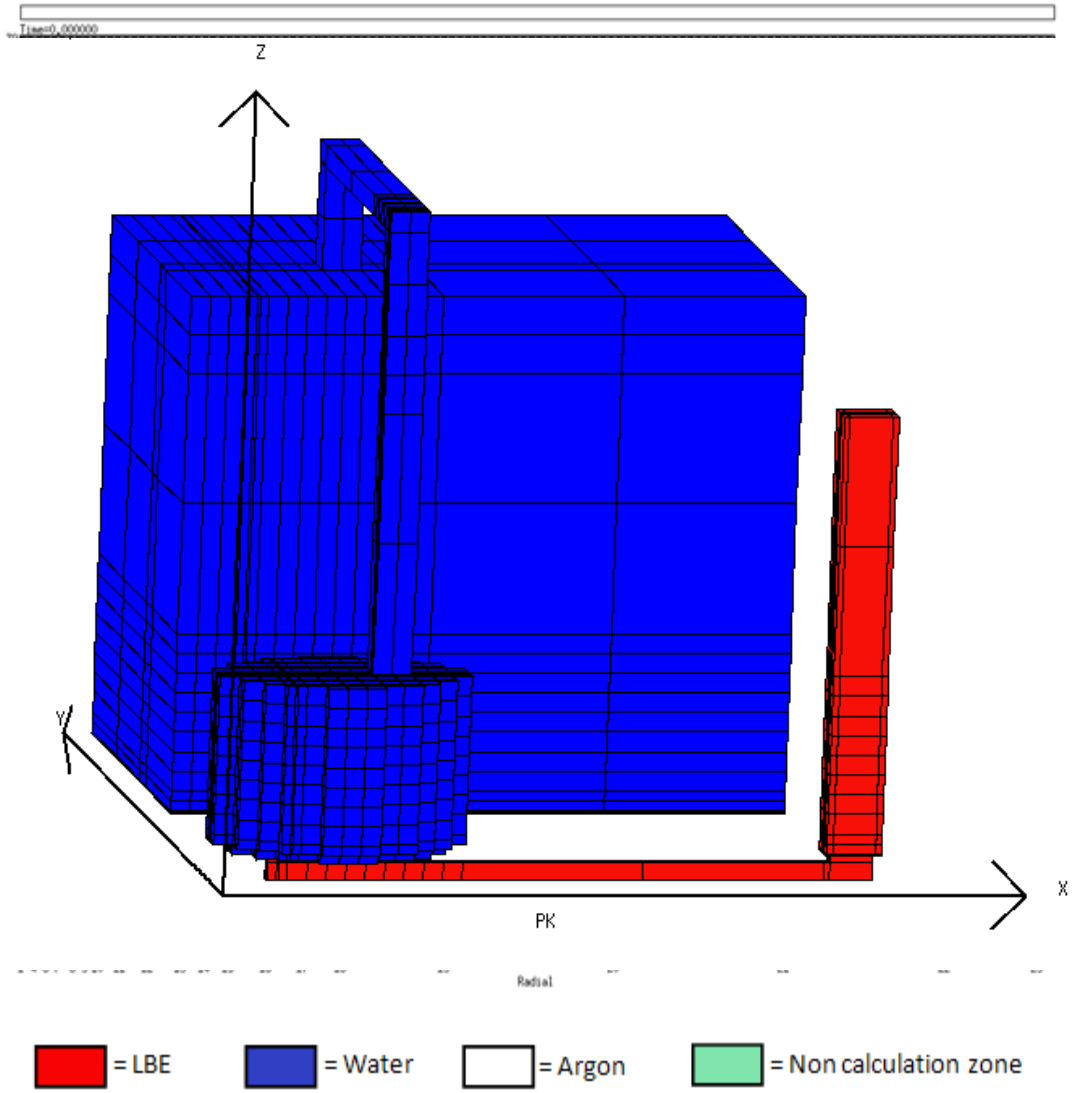
S5 was removed allowing a direct connection between S1 and the safety tank S3 through a vent pipe

The aerosol gases and the LBE expelled from S1 were collected in the safety tank S3

This test was simulated also by SIMMER-IV code

SIMMER Applications for LFRs at ENEA/UNIPI

LIFUS5 test n.3

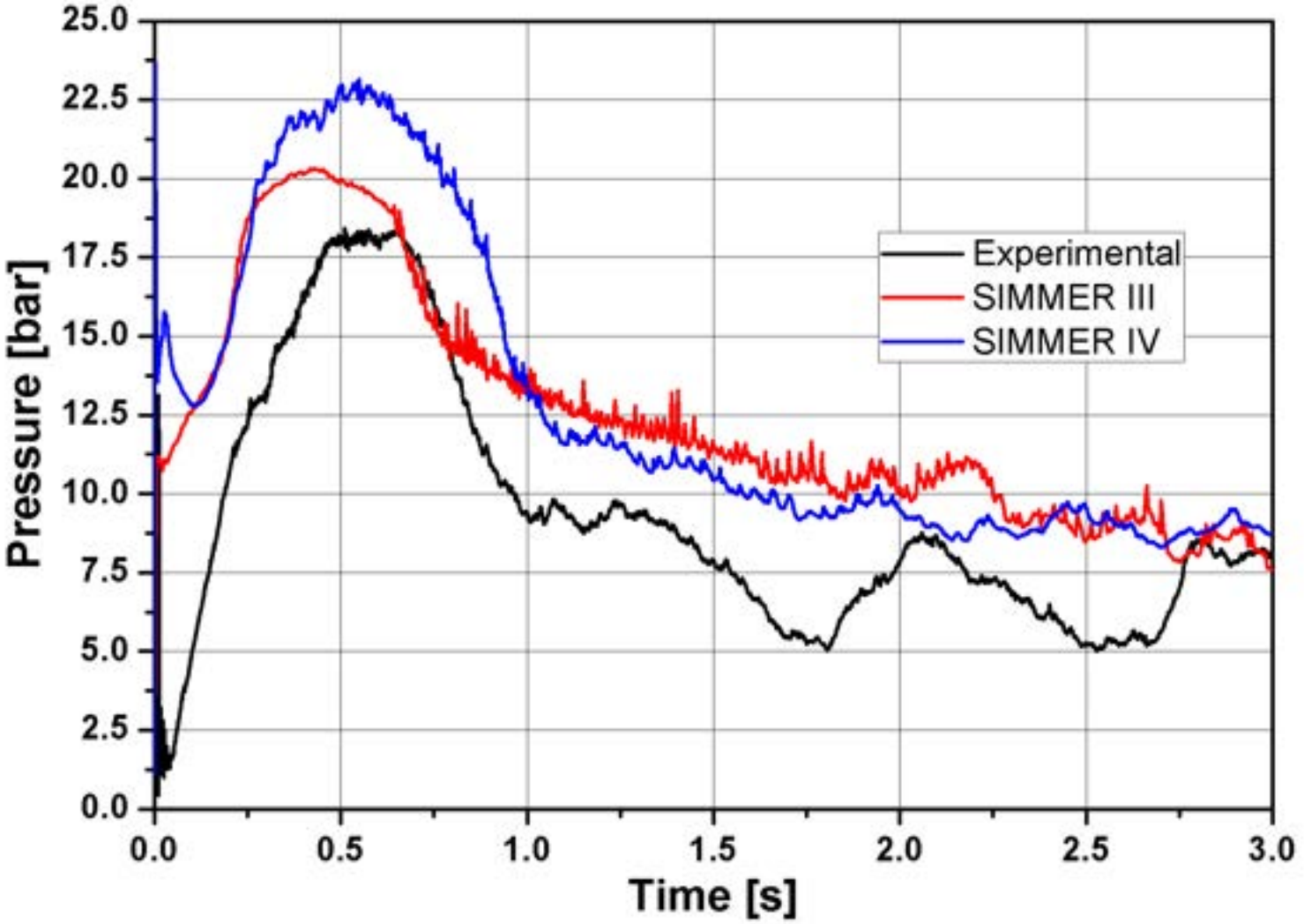


Main features of domain:

- subdivision into 23 radial and 39 axial meshes
- detailed representation of the mock up U tubes zone (12 “no calculation regions”)
- decentralization of the vent pipe
- volumes and surfaces of sections are maintained similar to the real values
- presence of S2 and S3

SIMMER Applications for LFRs at ENEA/UNIPI

LIFUS5 test n.3

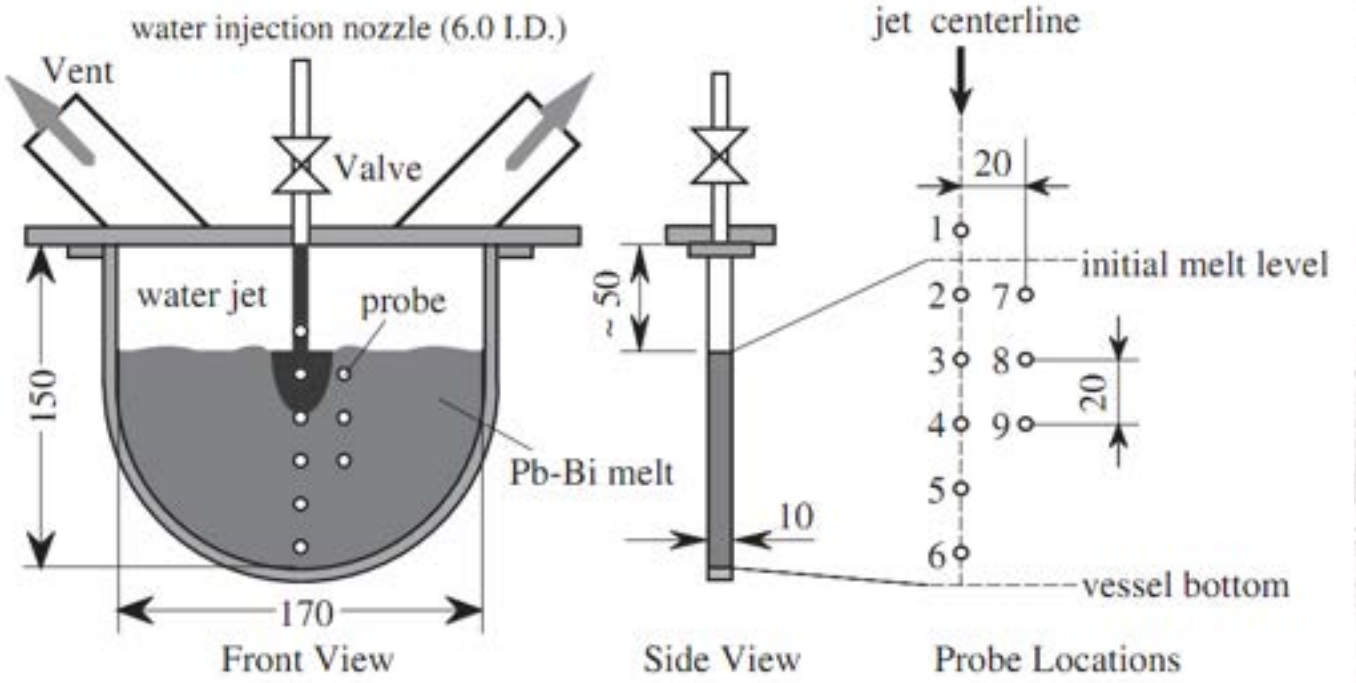


Comparison between calculated and experimental pressure in S1 tank

SIMMER Applications for LFRs at UNIPI

LBE-H_2O interaction tests at JAERI

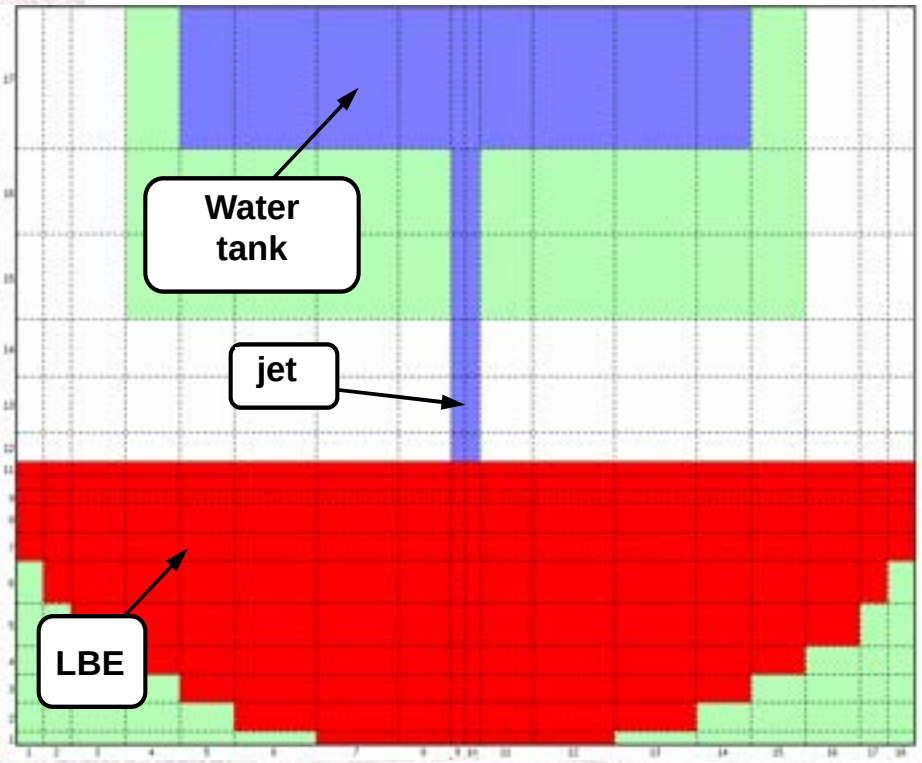
- For the qualification of SIMMER some experimental tests carried out at the JAERI on the interaction between molten LBE and water were simulated with the 3D version of the code (SIMMER-IV)
- The neutron radiography permits the visualization of the jet penetration effects and the consequent formation of the steam cavity in the region occupied by the molten LBE alloy



Schematic representation of the test section for small-scale experiment on subcooled water jet injection into molten alloy

SIMMER Applications for LFRs at UNIPI

LBE-H_2O interaction tests at JAERI



Calculation domain used for the simulation with SIMMER-IV code, frontal view

3D domain adopted due to asymmetric test section with small thickness

However, some simplifications were necessary:

- the openings that avoid the excessive pressurization of the test section have been simulated with two rectangular section pipes, where was imposed the boundary condition of atmospheric pressure;
- being not available any information about the water injection pressure, the initial condition of jet velocity was imposed as possible equal to that present at the initial time of each test;
- furthermore, to stabilize the values of the injection water flow, the top tank was simulated with greater dimensions respect to the real one, to permit at the cover gas to not undergoes big volume variations, in the characteristic time of the test

SIMMER Applications for LFRs at UNIPI

LBE-H_2O interaction tests at JAERI

The SIMMER-IV code allows to visualize the evolution of the cavity dimension during the transient. In the figure, referred to the test NRG4 (T_{LBE} = 500°C and T_w = 25°C)

It is possible to observe the various phases of the cavity formation:

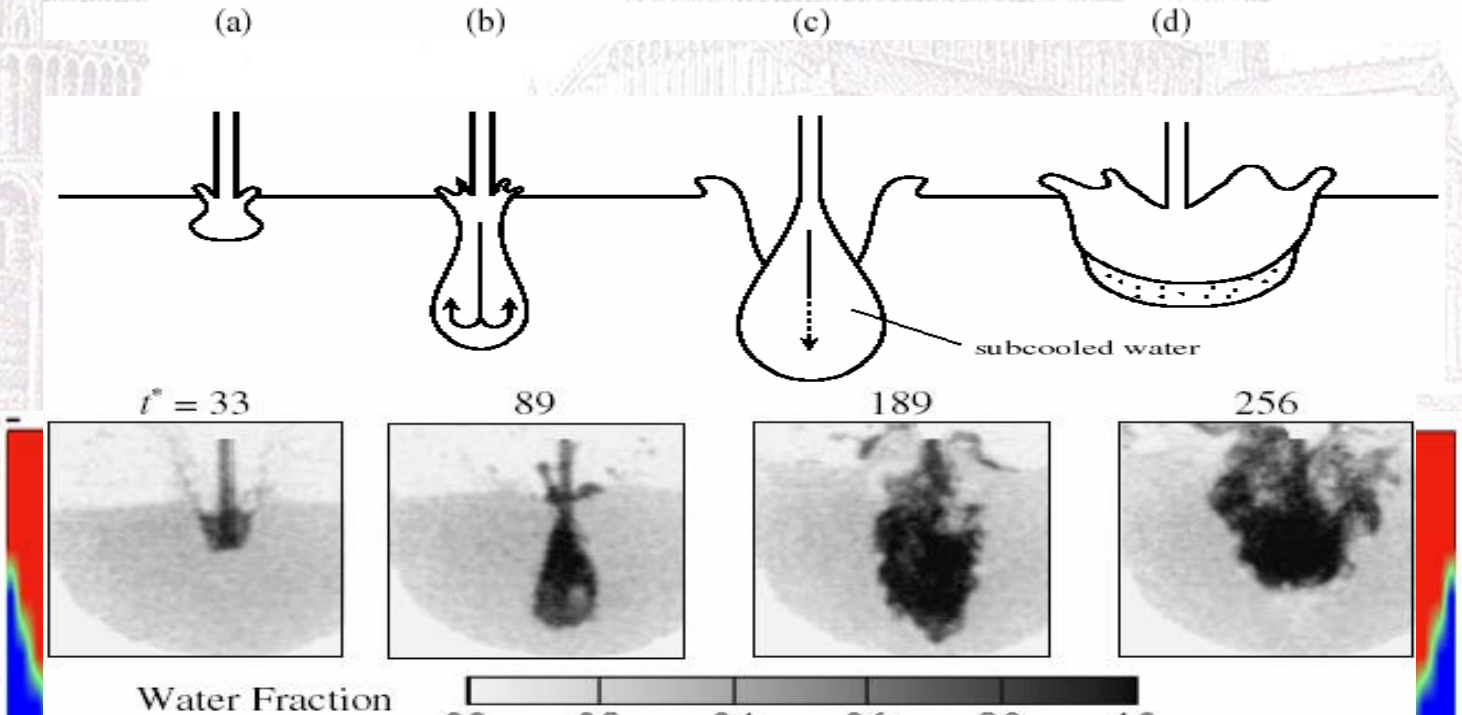
(a) beginning of the formation of the cavity,

(b) increasing of the jet penetration depth and the starting of the radial cavity collapse,

(c) cavity rapture that depends mainly on the jet velocity,

(d) reduction of the penetration caused by the steam production.

pensare che, per un certo intervallo di tempo, si instauri un regime di scambio termico in film boiling di tipo stazionario, sebbene la tecnica di radiografia neutronica, in questo caso, non permetta di visualizzare un film di vapore così sottile (c).La fine della penetrazione della cavità avviene in questo caso in maniera meno vigorosa rispetto al caso di getto iniettato a bassa velocità (d), con l'ebollizione di un sottile strato di acqua nella regione inferiore.



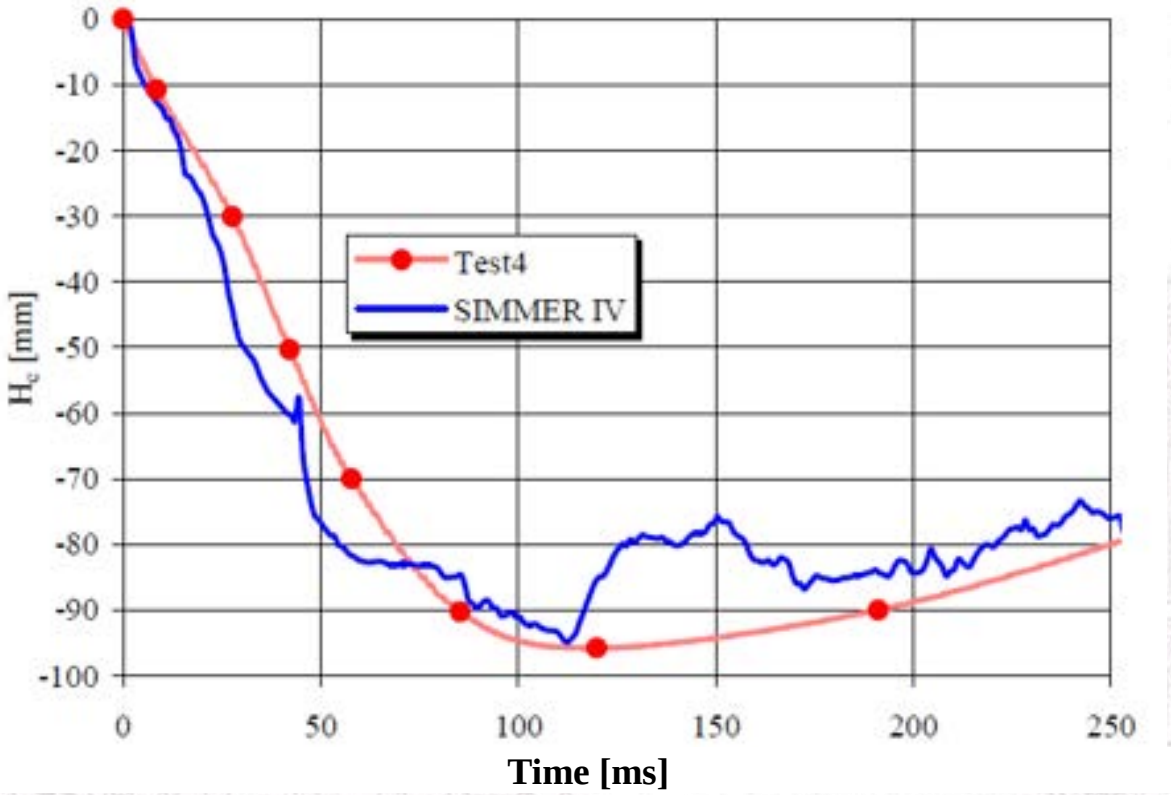
Expected phenomena

SIMMER-IV prediction

SIMMER Applications for LFRs at UNIPI

LBE-H_2O interaction tests at JAERI

There is a good agreement between calculated and experimental data, mainly in the first part of the interaction, characterized by the formation of the cavity and its expansion until the maximum penetration of the jet; this phase involves an interval of time between 100 and 130 ms, the code calculated a trend that reproduces in a good way the shape of the curve obtained from the experimental tests

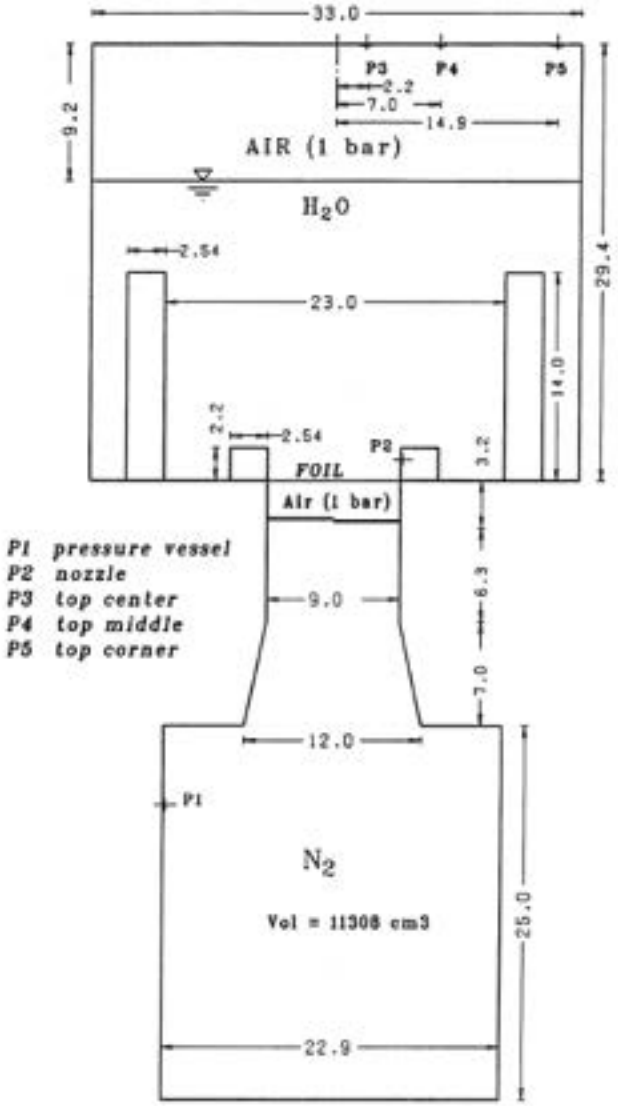


Evolution of the cavity depth obtained from the experimental test and from SIMMER-IV

(Test 4: T_{LBE} = 273°C, T_w = 25°C, w_{jet} = 5.8 m/s)

SIMMER Applications for LFRs at UNIPI

Gas-H_2O interaction tests at FZK (1994)



Scheme of the experimental facility for the SGI Campaign

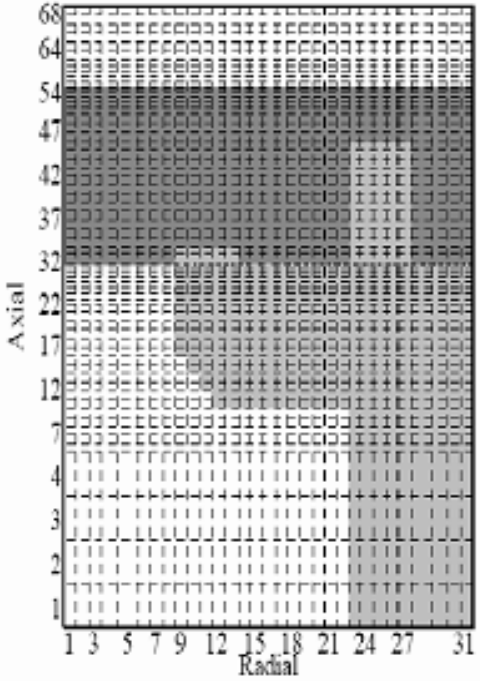
- An experimental campaign called SGI (Schnelle Gas Injection) was performed in 1994 in former Forschungszentrum Karlsruhe (KIT)
- The experiments dealing with the injection of a high pressure gas into a stagnant liquid pool
- Three tests (91, 93 and 95) were simulated by SIMMER -III and FLUENT codes

Test n.	Presence of inner structures	Inner structure diameter (cm)	Nozzle diameter (cm)	Initial pressure (MPa)
91	yes	23	9	1.1
93	yes	23	9	0.6
95	yes	23	9	0.3

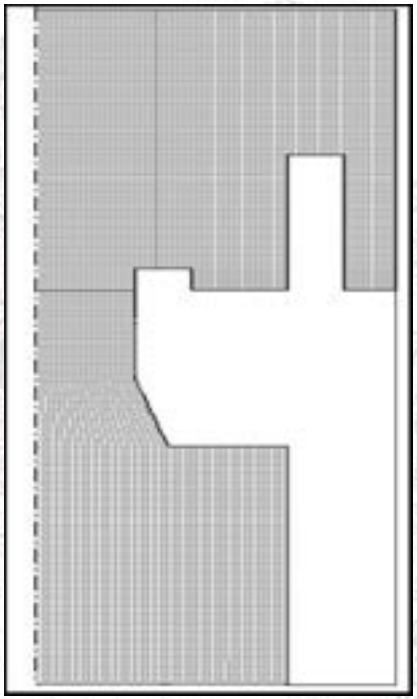
SIMMER Applications for LFRs at UNIPI

Gas-H_2O interaction tests at FZK (1994)

In order to perform a comparison between two different kinds of codes the tests 91, 93, 95 were chosen. These tests were arranged with the same geometrical features, an inner vessel wall with a diameter of 23 cm and nozzle diameter equal to 9 cm.
The only parameter changed was the nitrogen injection pressure which was respectively set equal to 1.1 MPa for test 91, 0.6 MPa for test 93 and 0.3 MPa for test 95.



A cylindrical domain was set up for representing the test section, it was subdivided into 31 radial and 68 axial cells The pressure vessel, the connection tube and the inner walls inside the main vessel were shaped through 'no calculation' regions



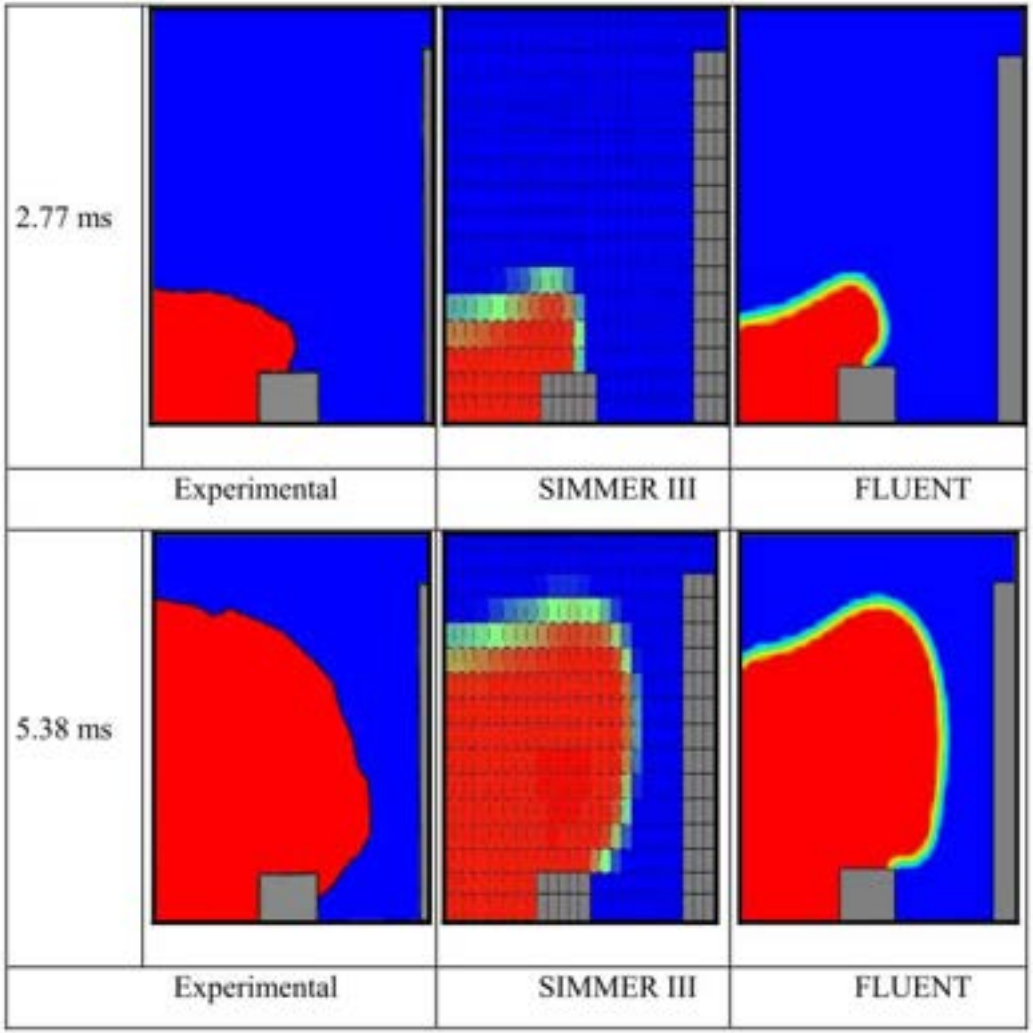
The simple geometry of the experimental facility allowed to set up a two dimensional axisymmetric computational domain, which was divided into about 10800 cells.
The time step chosen for the simulations was equal to 10^{-6} s

SIMMER-III geometrical domain

FLUENT geometrical domain

SIMMER Applications for LFRs at UNIPI

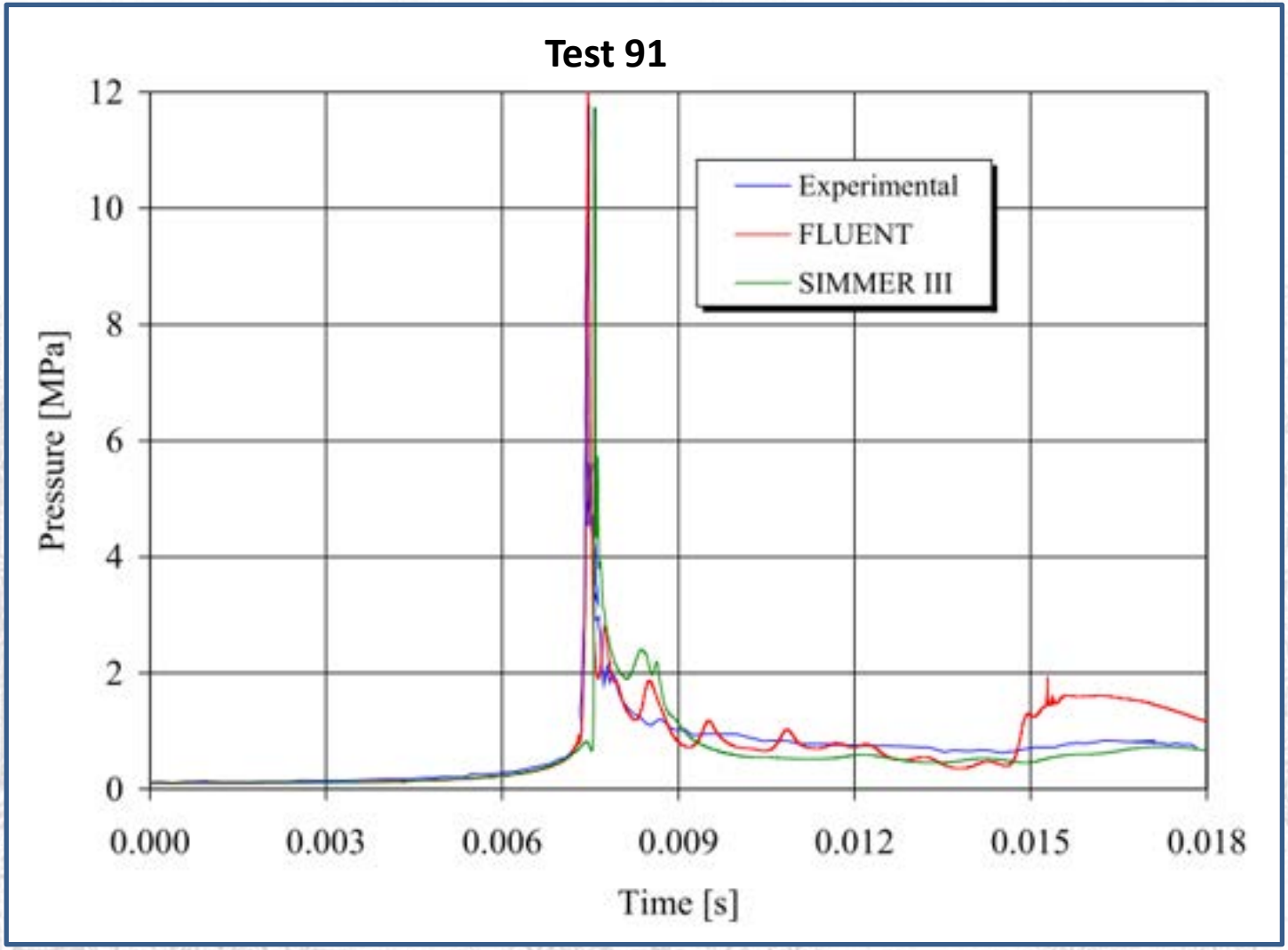
Gas-H_2O interaction tests at FZK (1994)



Experimental and numerical bubble's shape evaluation (Test 91)

SIMMER Applications for LFRs at UNIPI

Gas-H_2O interaction tests at FZK (1994)

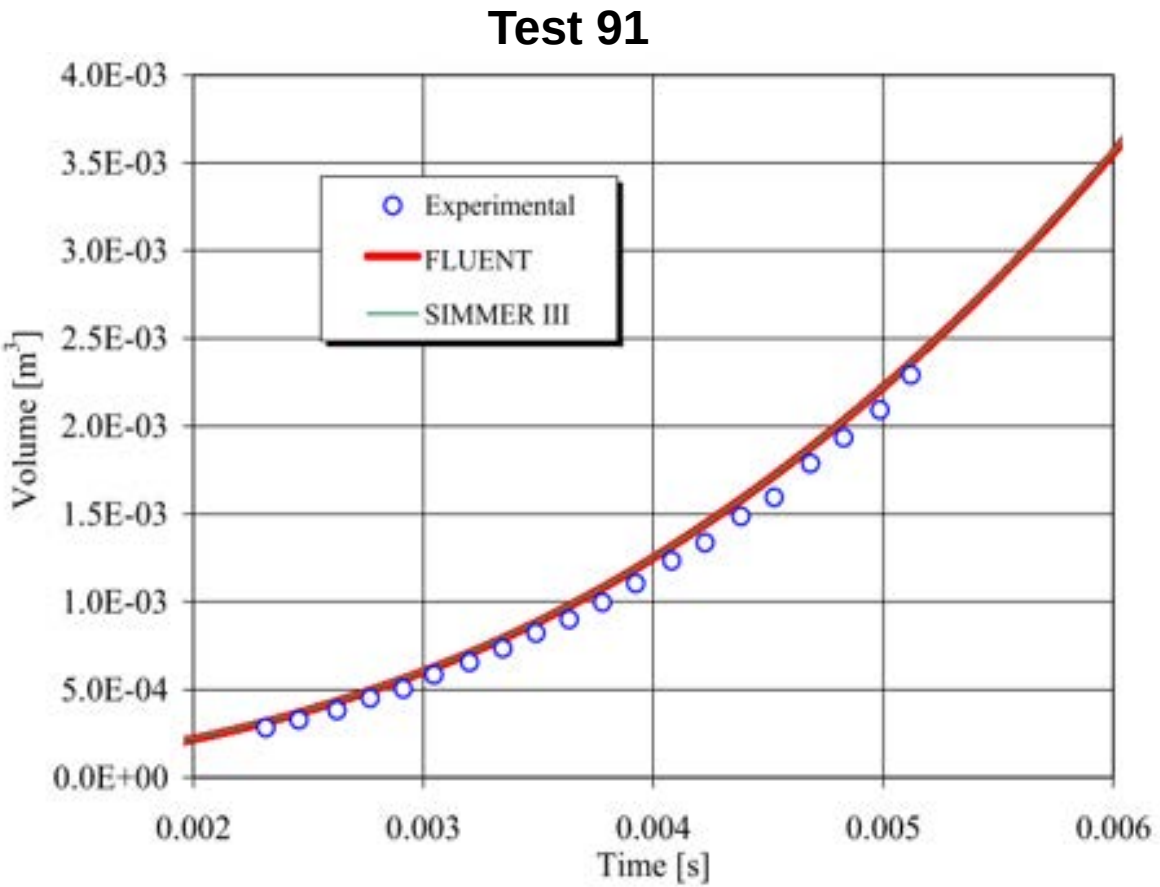


Pressure transient in cover gas region

SIMMER Applications for LFRs at UNIPI

Gas-H_2O interaction tests at FZK (1994)

As it can be seen the bubble volume time trends obtained from FLUENT and SIMMER-III match each other in the time range considered

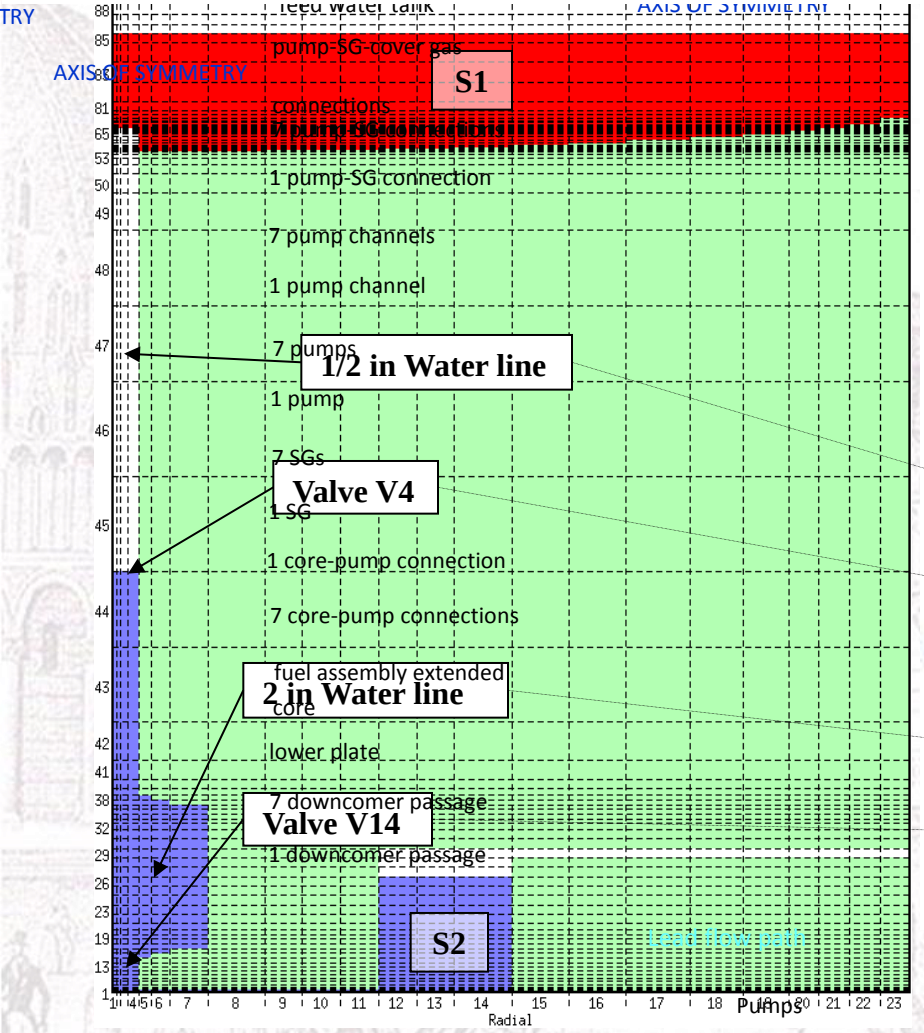


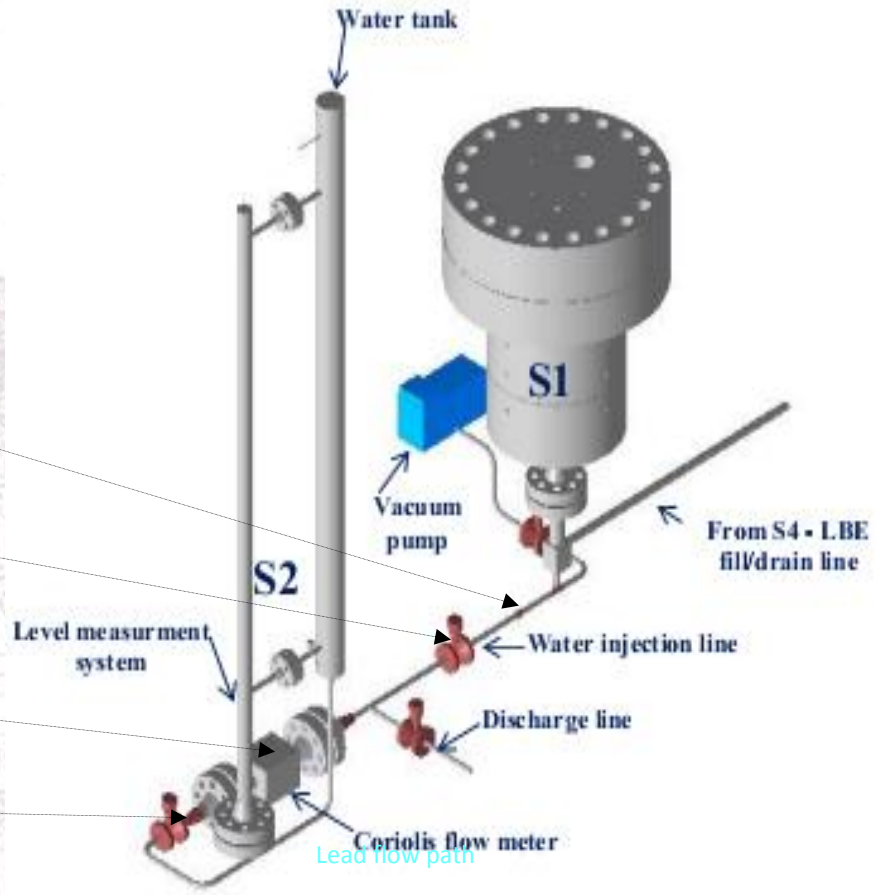
Gas bubble volume comparison

SIMMER Applications for LFRs at ENEA/UNIPI

THINS experiments in LIFUS5/Mod2

Computational 2D model, 23x88 cells, for series A2.x



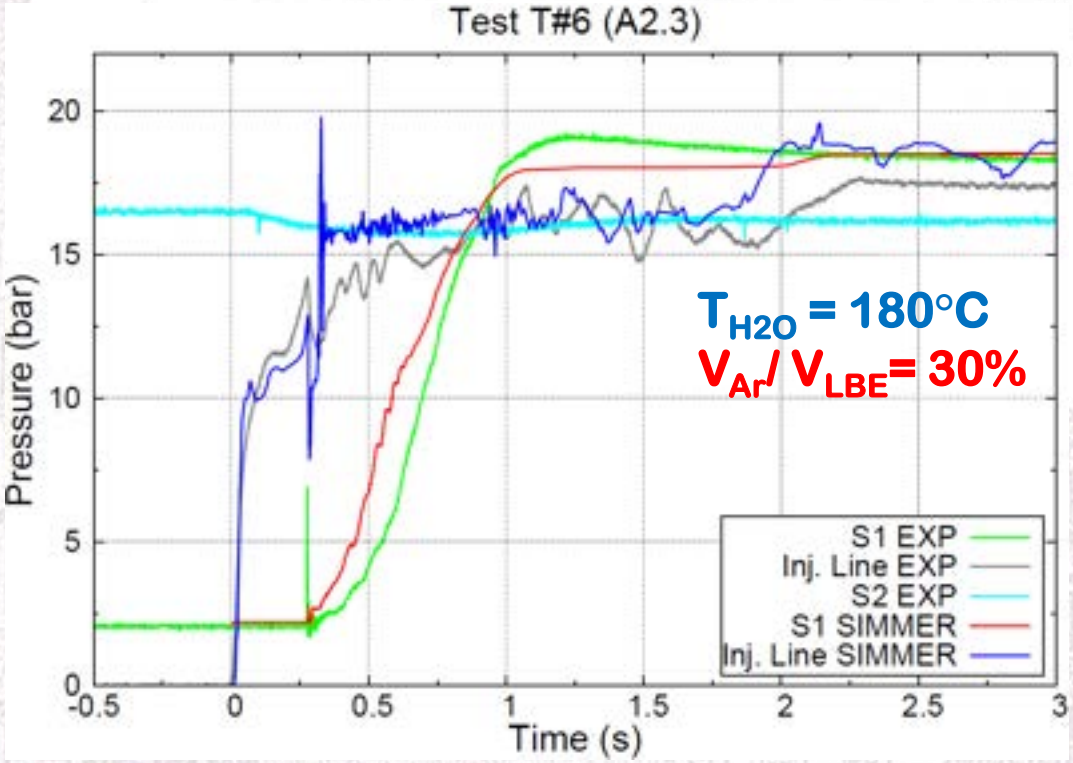


LIFUS5/Mod2: overall sketch

Argon-air | LBE | Water | Non calculation regions | Lead | Water | Argon | Tubes and grid

SIMMER Applications for LFRs at ENEA/UNIPI

THINS experiments in LIFUS5/Mod2



Test T#6 experimental and calculated by SIMMER-III code P(t) in S1 and water injection line

water mass injected 0.44 kg, exp = 0.25kg

C-BIC	Value
V4 opening	0 s
Orifice opening	0.28 s
V4 closure	1.868 s
S2 cover gas pressure	= experimental data

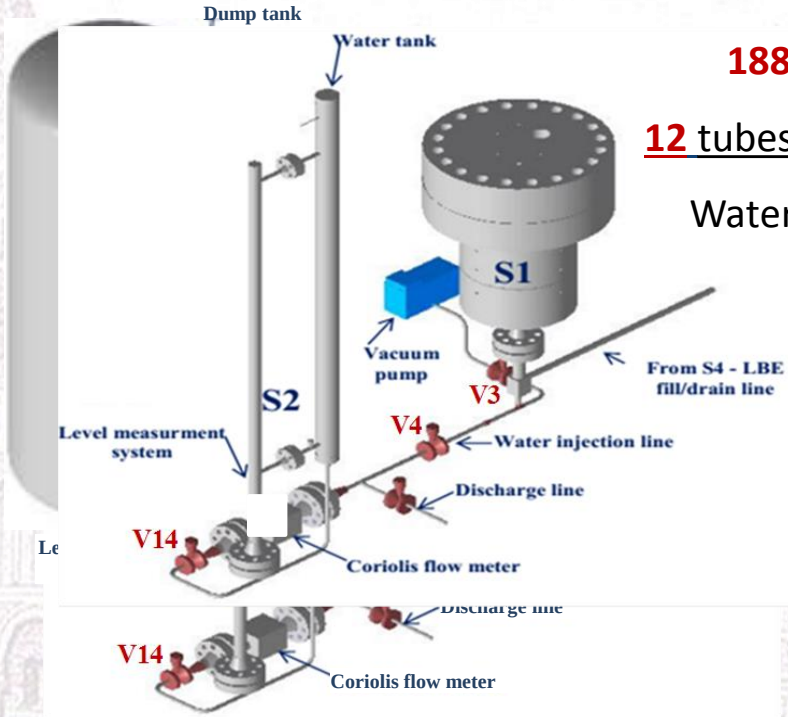
The SIMMER-III code computes a pressure gradient in S1 (red line) almost in agreement with the experimental data, due to the 1Ø pressure drops taken into account by the orifice coefficients set along the injection line

Constant orifice coefficients (K) along the tube during the whole transient

The 20°C water sub-cooled entails lower evaporation along the injection line and a better pressure prediction

SIMMER Applications for LFRs at ENEA/UNIPI

LEADER experiments in LIFUS5/Mod2



188 tubes (18x1 mm)

12 tubes filled by Ar at **180 bar**

Water injected at **180 bar**

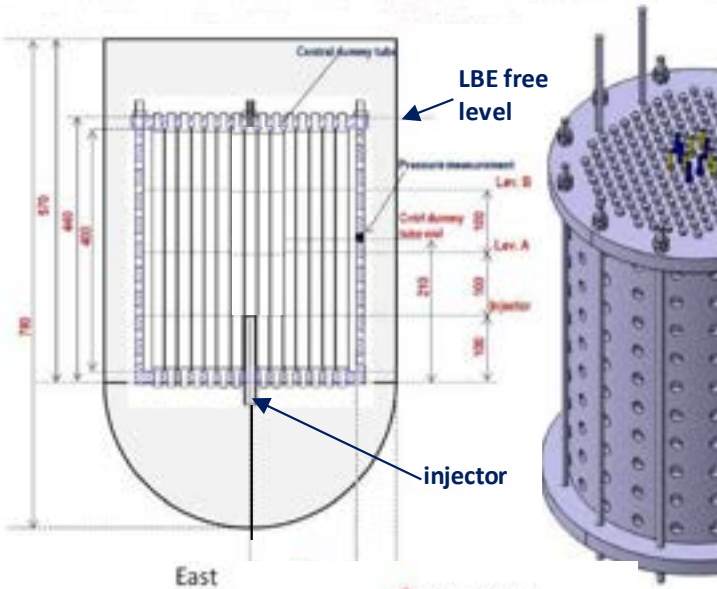
8 **PTs (10 kHz)**

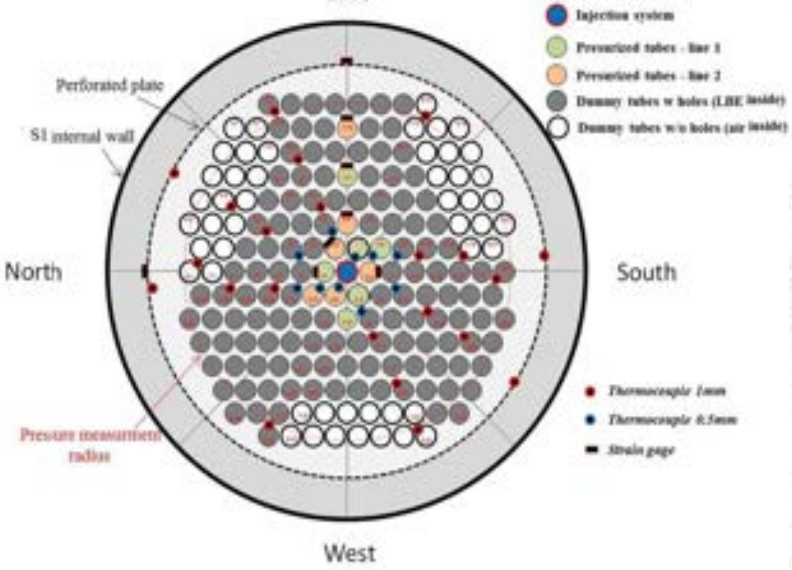
~ 70 **TCs** (level A and B)

5 **SGs** on tubes (level A)

2 **SGs** on perforated plate

6 **SGs** on S1 wall



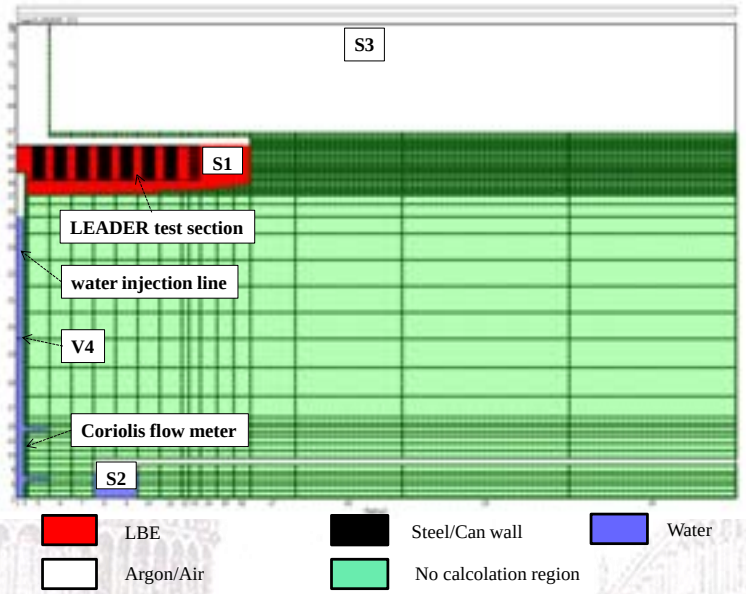


LEADER experimental campaign investigated in LIFUS5/Mod2 facility SGTR postulated event in a relevant configuration for Spiral Tube Steam Generator (STSG) implemented in ELFR conceptual design

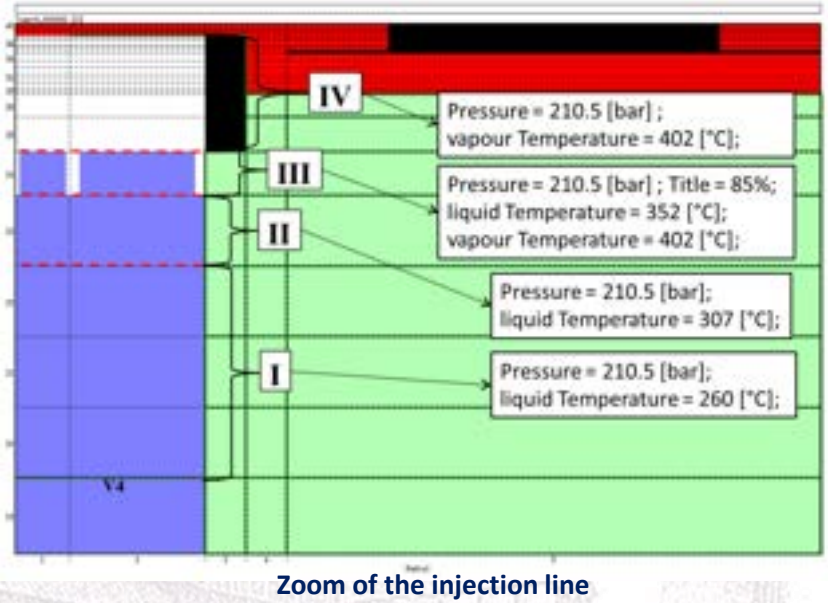
Test data were adopted to validate SIMMER-III code

SIMMER Applications for LFRs at ENEA/UNIPI

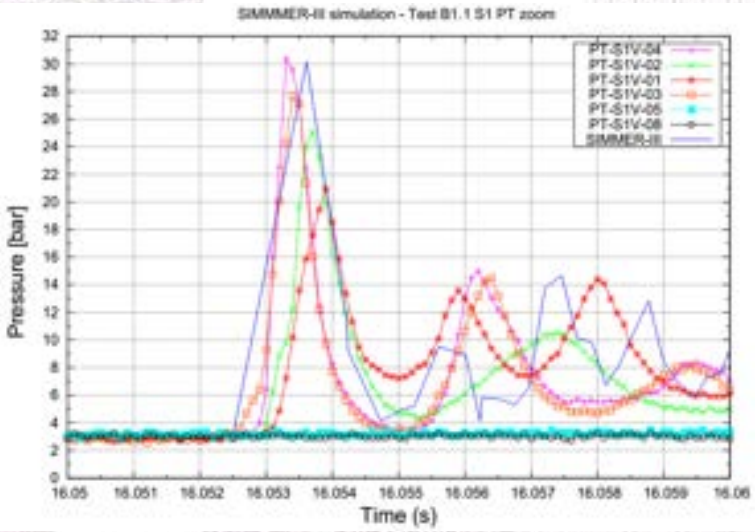
LEADER experiments in LIFUS5/Mod2



SIMMER-III model of LIFUS5/Mod2 facility



Zoom of the injection line

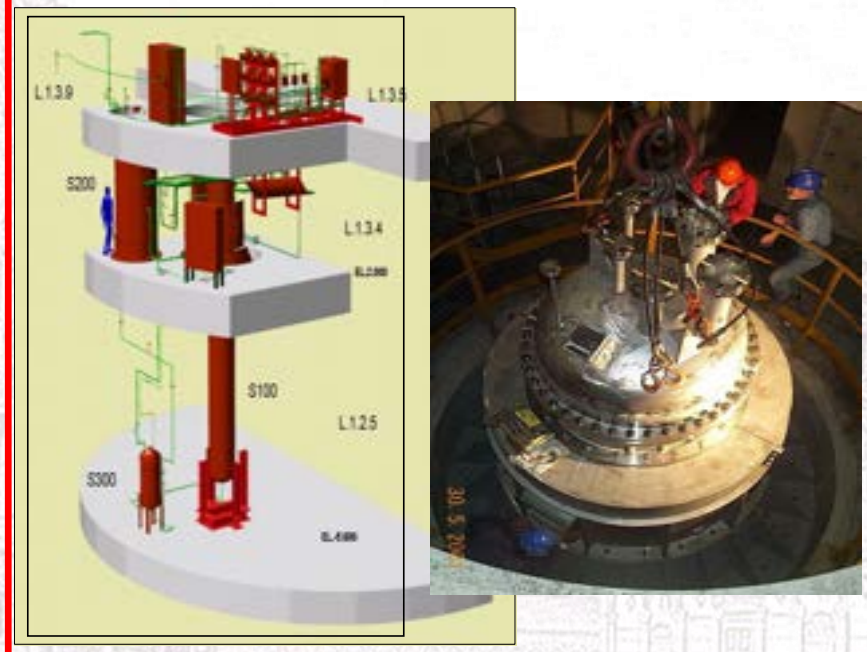


SIMMER-III model simulates all LIFUS5/Mod2 facility components (S2, S1, S3 and inj line)

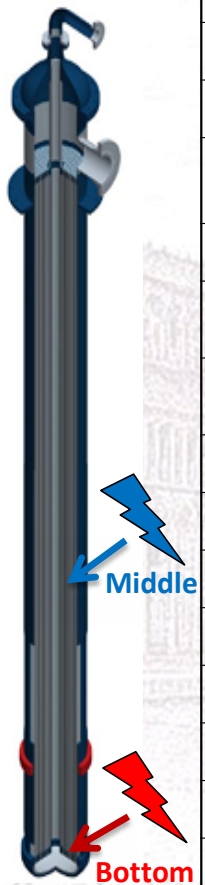
The initial conditions (at water injection start instant) were defined by RELAP5/MOD3.3 code

The first pressure peak computed by SIMMER-III code is in agreement with 10 kHz measured P(t)

SIMMER-IV application for SGTR in MYRRHA PHX



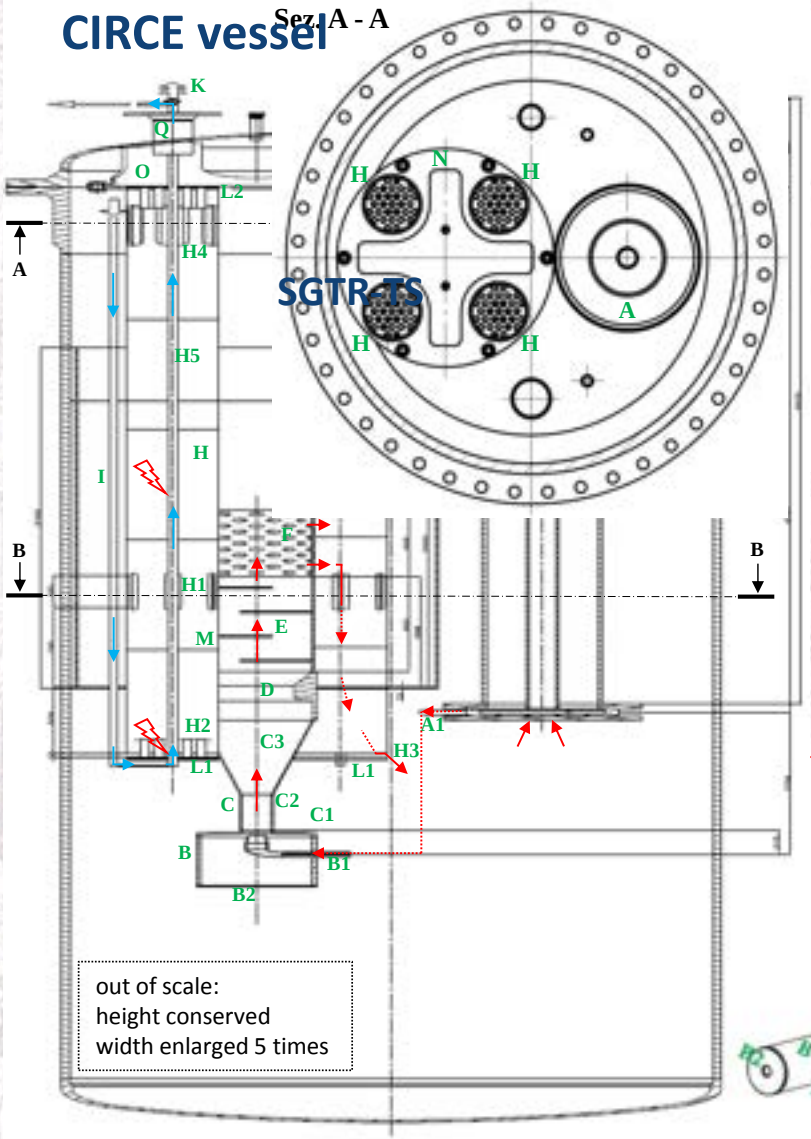
Main Vessel S100	
Outside Diameter	1200 mm
Wall Thickness	15 mm
Material	AISI 316L
LBE Inventory (max)	90 tons
Height	8-10 m
Design Pressure	**16 bar**
Design Temperature	450°C



Parameter	Unit	Value
Power of one HX	MW	27.5
Shroud external diameter	mm	~850
Shroud internal diameter	mm	~800
Feed water pipe external diameter	mm	~200
Number of water tubes	-	684
External diameter of water tubes	mm	16
Internal diameter of water tubes	mm	14
Thickness of water tubes	mm	1
Length of water tubes	mm	~8500
HX LBE inlet temperature	**° C**	**350**
HX LBE outlet temperature	° C	270
HX LBE mass flow rate	Kg/s	~2500
HX water inlet temperature	**° C**	**200**
HX water outlet temperature	° C	201.6
HX water mass flow rate	Kg/s	~47
HX water pressure	**bar**	**16**

SIMMER-IV application for SGTR in MYRRHA PHX

CIRCE vessel

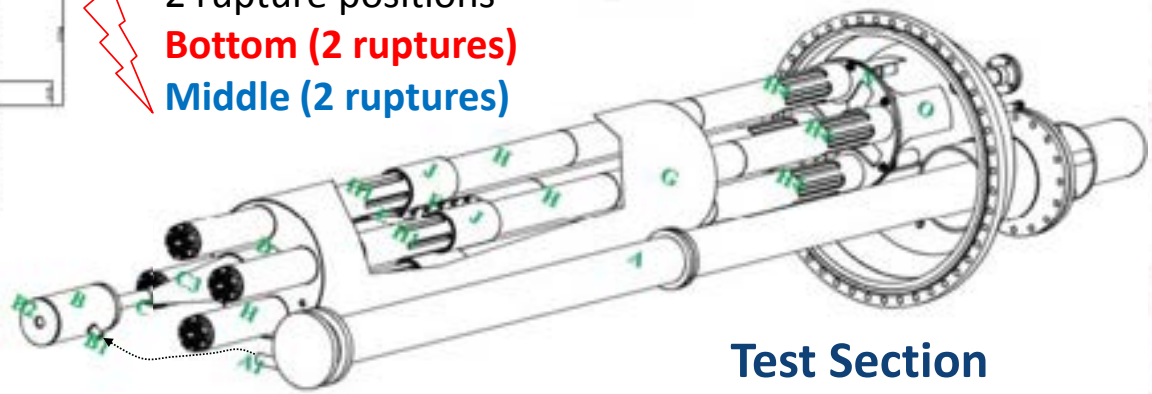


4 SGTR-TSs
one rupture
in each SGTR-TS
vertical scale 1:1

2 rupture positions
Bottom (2 ruptures)
Middle (2 ruptures)

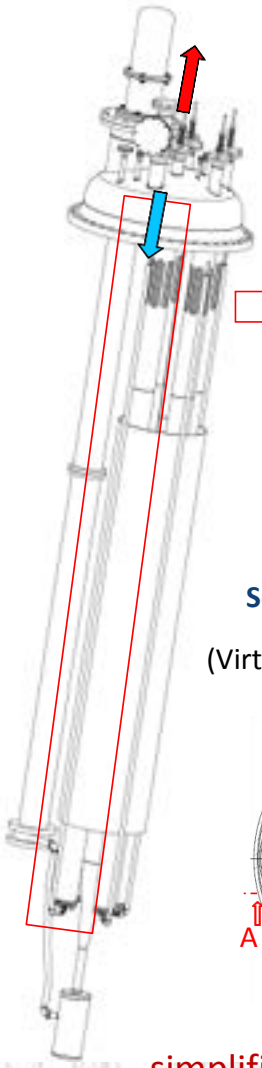
Operating conditions	Unit	Value
LBE temperature	°C	350
LBE mass flow rate (one SGTR-TS)	kg/s	~80
H_2O inlet temperature	°C	200
H_2O outlet temperature	°C	201.4
H_2O pressure	bar	16
H_2O mass flow rate (one SGTR-TS)	kg/s	~0.07
CIRCE cover gas pressure (abs)	bar	1.05
CIRCE Ar cover gas volume	m³	~2.2
CIRCE LBE pool volume	m³	~7
Ar monitoring tubes pressure	bar	16
Tubes length	mm	~5200

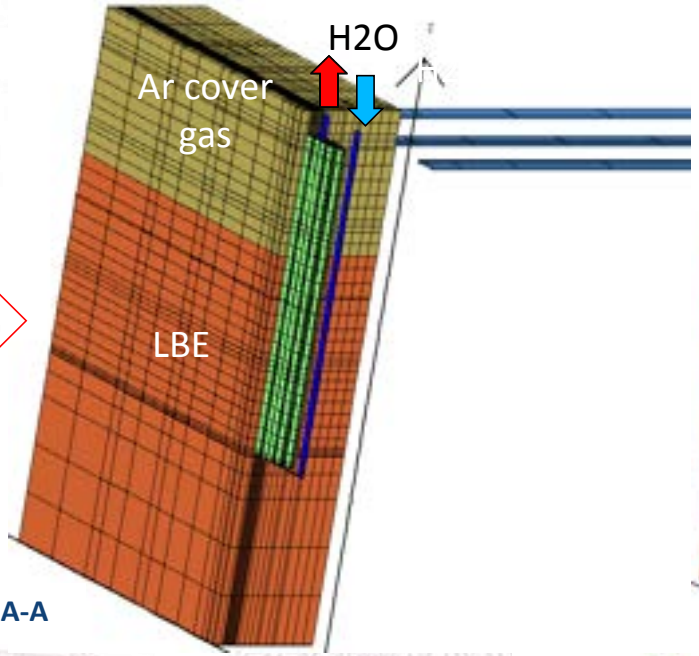
LBE flow path
Water flow path



Test Section

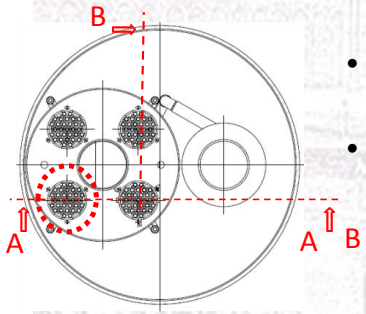
SIMMER-IV application for SGTR in MYRRHA PHX



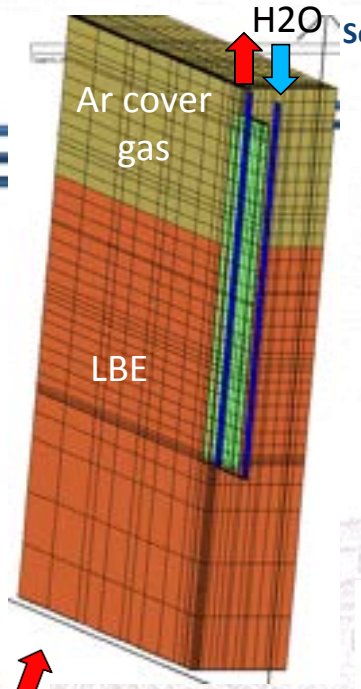


Section A-A

(Virtual walls are not shown in 3D views)

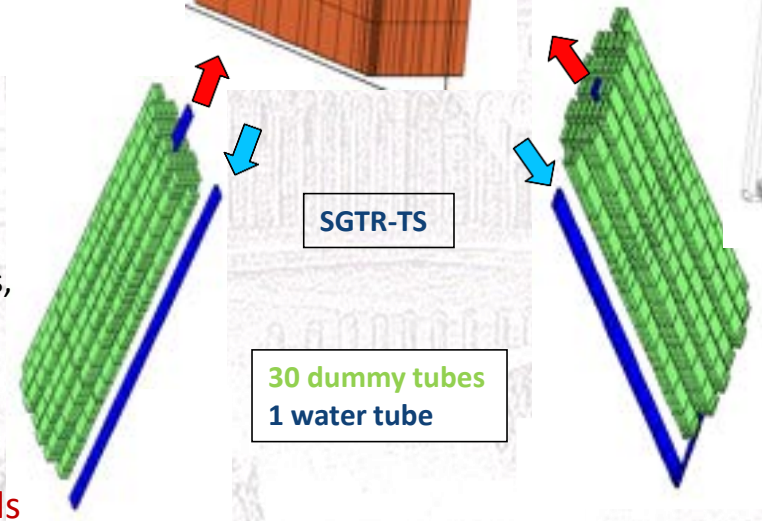


- Flowing areas conserved
- Mass flow rates, temperatures, conserved



Section B-B

SGTR-TS

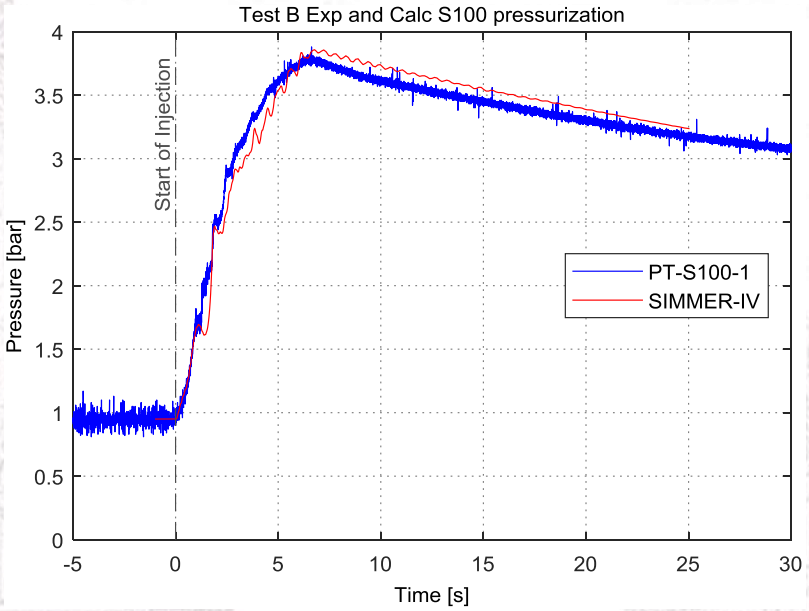


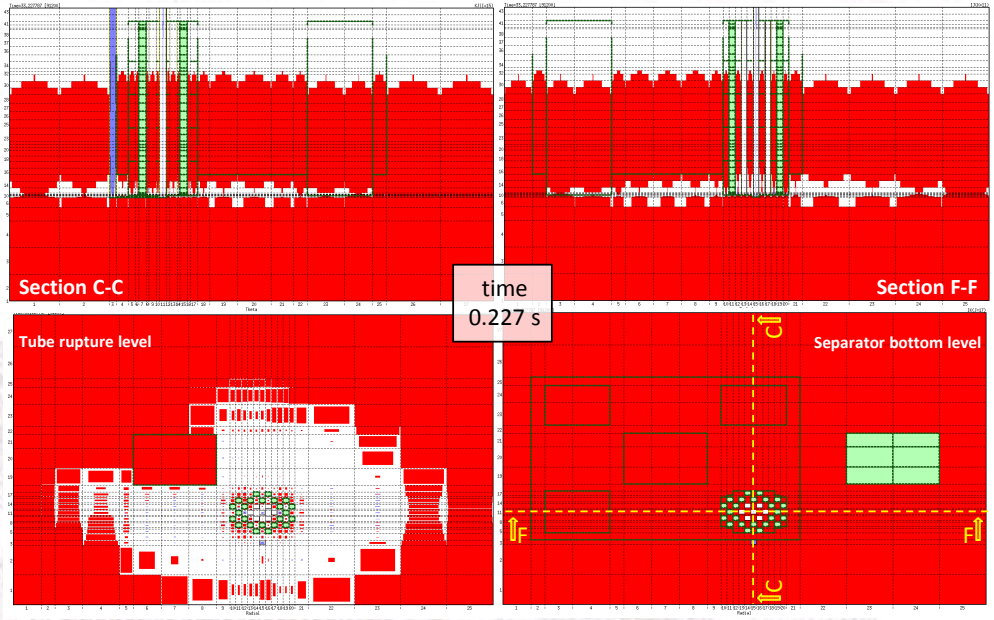
SGTR-TS

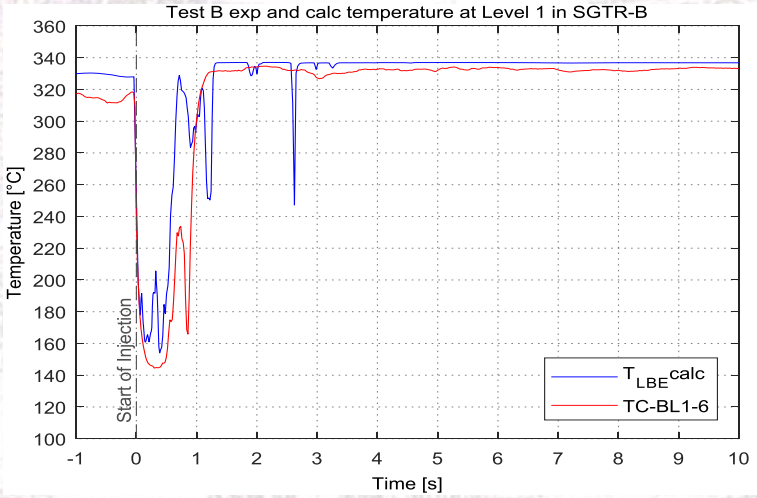
30 dummy tubes
1 water tube

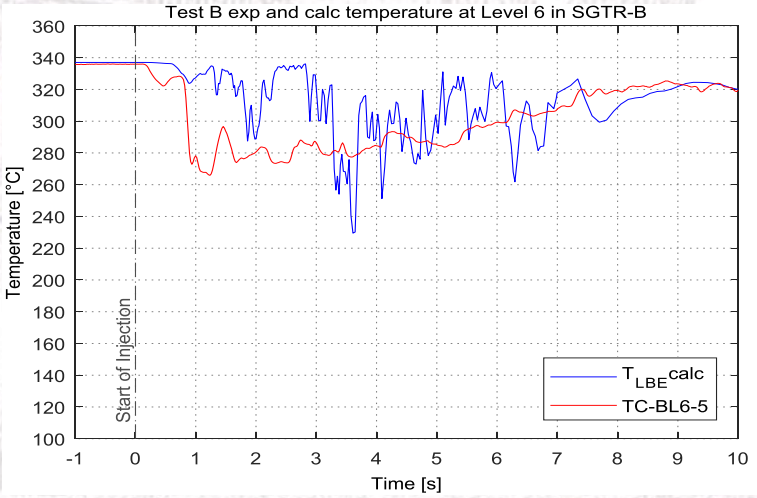
simplified model (30x27x42cells) 34020 cells

SIMMER-IV application for SGTR in MYRRHA PHX









Conclusive remarks and future work

- For what concerns the assessment and qualification of SIMMER code prediction capabilities, in addition to the analysis of the LIFUS5 experimental tests, the study of some relevant experimental tests coming from literature (JAERI-SIMMER-IV, FZK-SGI_SIMMER-III-FLUENT) was carried out
- The SIMMER-III -IV applications to LIFUS5 experimental campaigns highlighted the code suitability in the SGTR event simulation
- Validation activities of the SIMMMER-IV code was carried out in the framework of MAXSIMA project, on the basis of large scale experiments of LBE-H_2O interaction performed in CIRCE facilities at ENEA CR Brasimone



Thank you for your attention

GENERATION IV
Lead cooled Fast Reactor
Stato attuale della tecnologia e prospettive di sviluppo

Bologna, 26-27 Settembre 2017



SAPIENZA
UNIVERSITÀ DI ROMA

Thermal Stratification analysis in CIRCE-ICE pool facility with RELAP5-3D© model

V. Narcisi, F. Giannetti, G. Caruso

Outline

❖GOAL OF THE ACTIVITY

The activity aims to investigate the capability of **RELAP5-3D©** to reproduce thermal-hydraulic phenomena into the HLM pool type reactor

❖ OVERVIEW

- CIRCE-ICE Test Section
- CIRCE-ICE: Thermal-Hydraulic model
- Experimental Test Matrix
- Results
- Conclusions

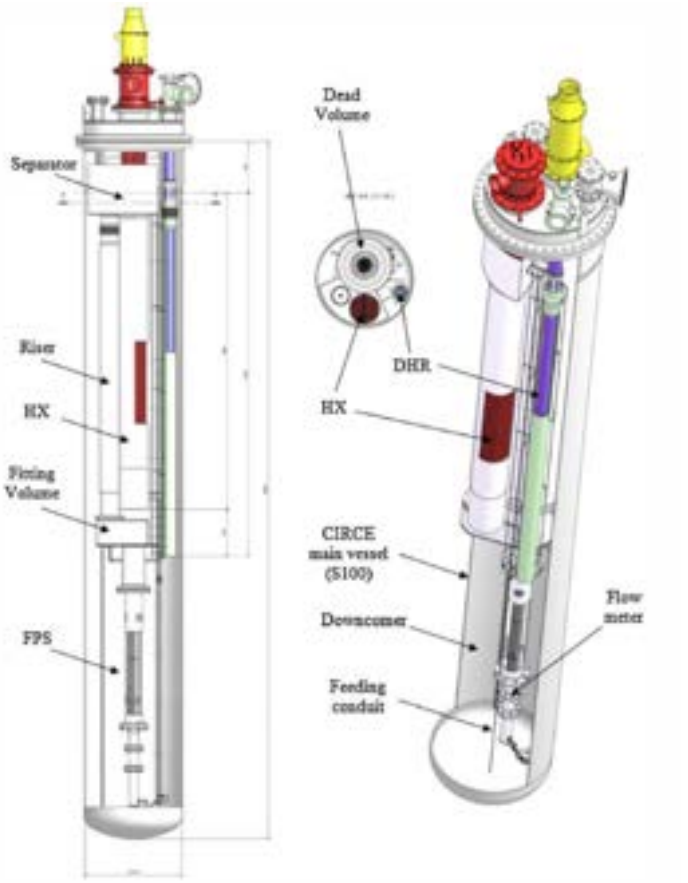
CIRCE-ICE Test Section

CIRColazione Eutettico – Integral Circulation Experiments

ICE test section aims to simulate the thermal-hydraulics of the primary system in a HLM cooled pool reactor.

The main goals of the experimental campaign are:

- To investigate **mixing convection** and **thermal stratification** phenomena in a pool type reactor
- To provide suitable experimental data to support the validation process of TH-Sys codes, CFD codes and coupled simulations

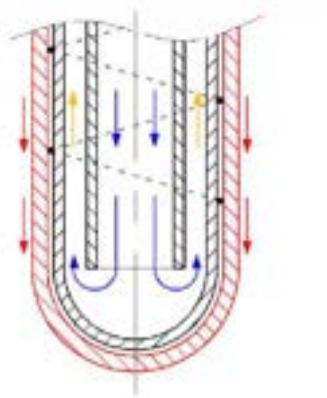


CIRCE-ICE: Test Section

CIRColazione Eutettico – Integral Circulation Experiments

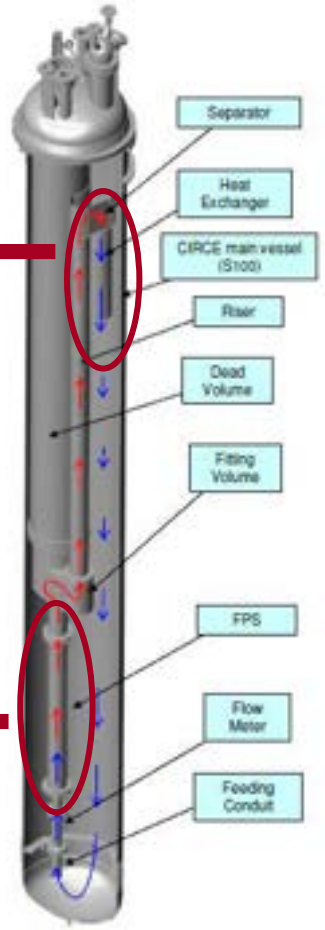
Primary circuit flow path

- **Feeding conduit**
- **Fuel Pin Simulator**: it corresponds to the h
  - 91 bayonet tubes
  - Active length of 3.5 m
  - Nominal power of 800 kW
- **Riser**: it is an insulated pipe connecting the separator. A nozzle is installed in the lower the argon injection inside this pipe
- **Separator**: it allows the separation of the LBE, flowing downward into the HX, and the argon, flowing upward in the gas plenum. It works as an expansion vesse
- **HX**: it corresponds to the heat sink of the s of 91 bayonet tubes
- **Pool**: It is the volume between the test se in vessel
- **DHR**: it consists of only one bayonet tube immersed into the pool



- 37 pins placed in a hexagonal lattice (p/d of 1.8)
- Nominal thermal power of 800 kW
- Active length of 1000 mm;
- Each pin has an outer diameter of 8.2 mm, a power of about 25 kW and a wall heat flux of 1 MW/m^2;
- 1 Lower Grid at the inlet section, 3 Spacer Grids along the active length





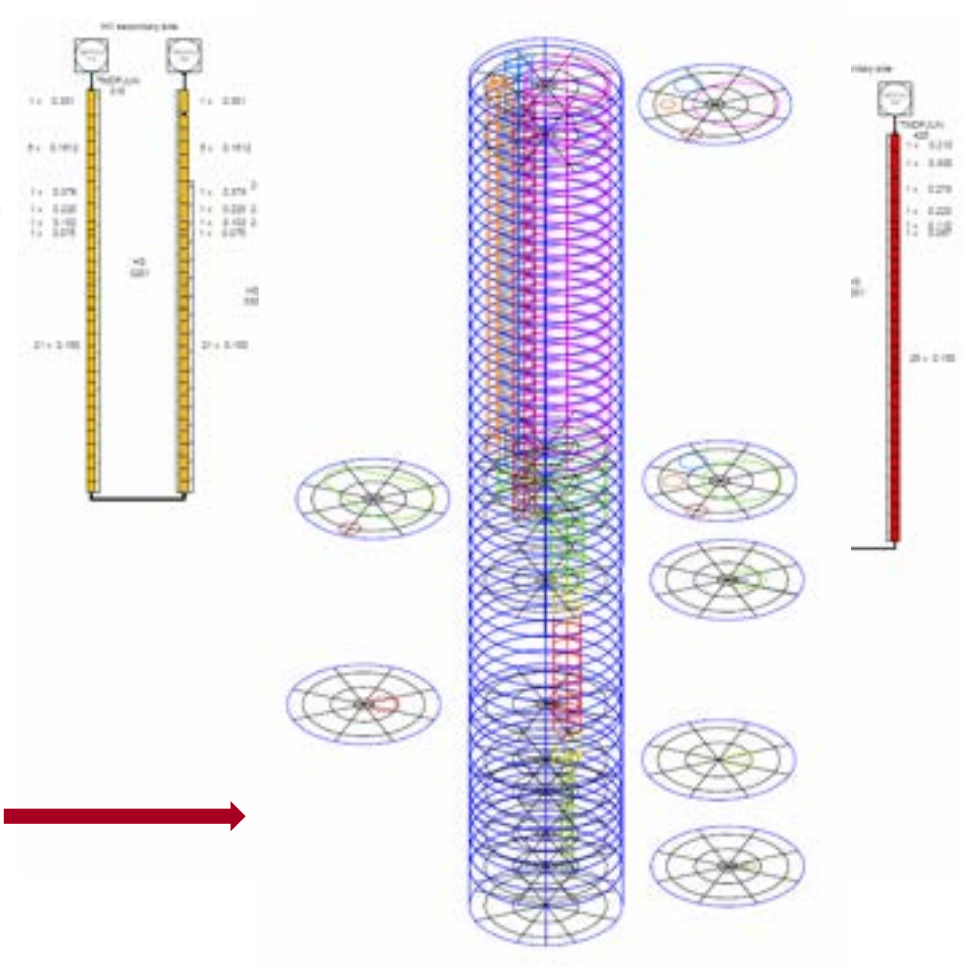
CIRCE-ICE: Thermal-Hydraulic Model

The hydraulic model of the facility has been developed using **RELAP5-3D© ver. 4.3.4**. The nodalization scheme can be divided into 2 macro-regions

- **Region #1**:
  - Primary main flow path: it is composed of the feeding conduit, FPS, fitting volume, riser, separator and the LBE side of the HX. At the bottom of the riser the Ar injection system is included
  - Secondary side of the HX and the DHR system
- **Region #2**: CIRCE pool. It consists of a **3D component** which reproduces the volume between the internals and the main vessel. The azimuthal discretization is combined with the arrangement of the TCs into the pool: 51 axial levels, 4 radial meshes and 8 azimuthal intervals

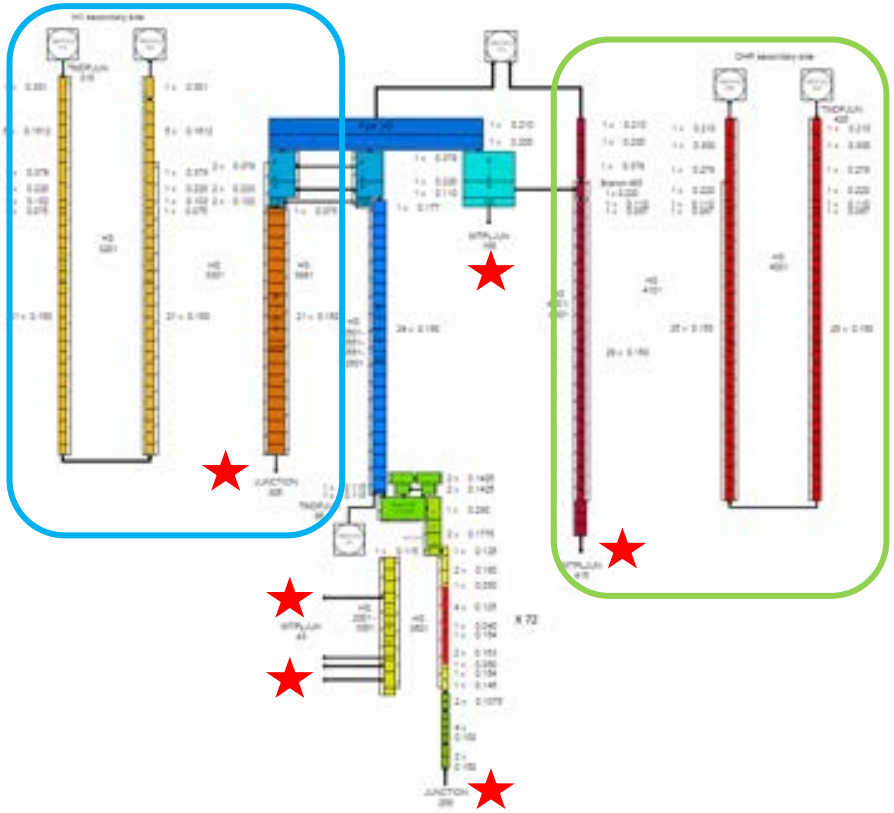
The full **CIRCE-ICE** model consists of:

- **2921** hydrodynamic volumes
- **7409** junctions
- **21033** heat transfer nodes



Thermal-Hydraulic Model: Region #1

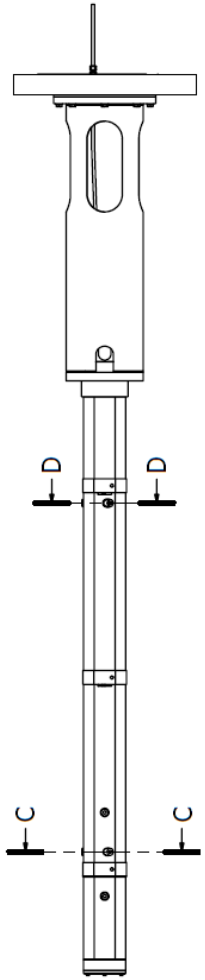
- **LBE side**: 22 volumes
- **Steam/water side**: 2 pipes for a total of 62 volumes
- 3 **heat structures** model thermal behavior of the unit:
  - HS 3201: 31 axial structures and 10 radial meshes
  - HS 3301: 24 axial structure and 31 radial meshes
  - HS 3981: 21 axial structure and 10 radial meshes.
- Calibrated **fouling factor** as the ratio between **Ushakov** and **Todreas&Kazimi** HTC correlation: 1.02



12 junctions couple the mono-dimensional model to the 3D component and several heat structure reproduce the **heat losses** between the LBE cold pool and the hot internal components

- **LBE side**: 34 volumes
- **Air side**: 2 pipes for a total of 66 volumes
- 3 **heat structures** model thermal behavior of the unit:
  - HS 4001 between the descending pipe and the annular riser: 33 axial structures and 7 radial meshes
  - HS 4101 between primary and secondary side: 28 axial structure and 7 radial meshes
  - HSs 4201 and 4301 reproduces the heat losses from the DHR to the pool: 118 axial structure and 24 radial meshes.

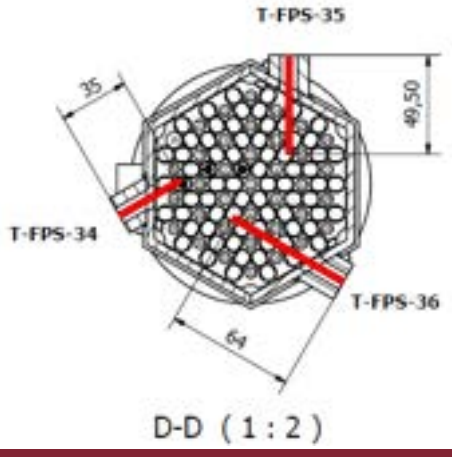
Thermal-Hydraulic Model: Region #1

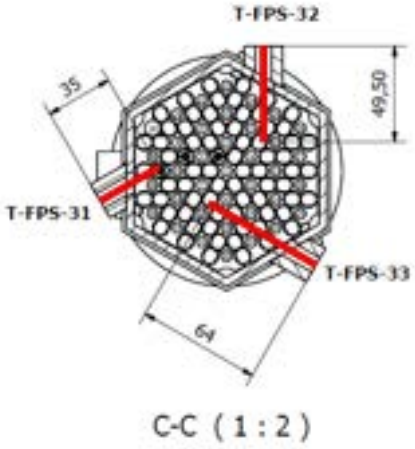


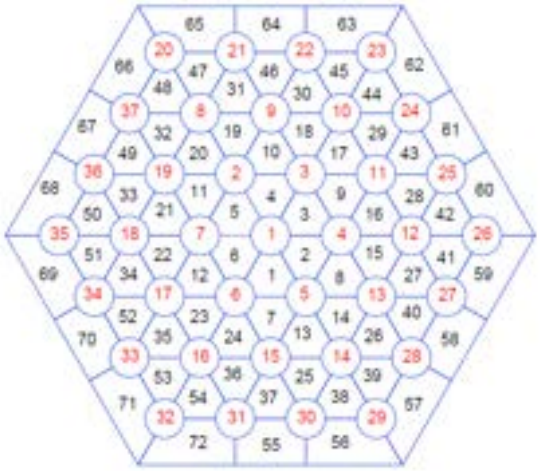
The **FPS** is analyzed subchannel by subchannel: the model consists of **72 parallel pipes** (15 control volumes for each pipe), which simulates the sub-channel, **5760 heat structure nodes** reproducing the thermal power supplied by the 37 pins and **1728 heat structure nodes** to models the heat dispersion through the hexagonal wrapper. **1536 cross junctions** link the 72 pipes.

The unit is equipped with several TCs to measured the LBE temperature across the HS. The model is obtained to compare the temperature in the **exact position of the TCs**. The grids are simulated with pressure loss coefficients, dependent on the flow conditions and evaluated with **Rheme correlation**.

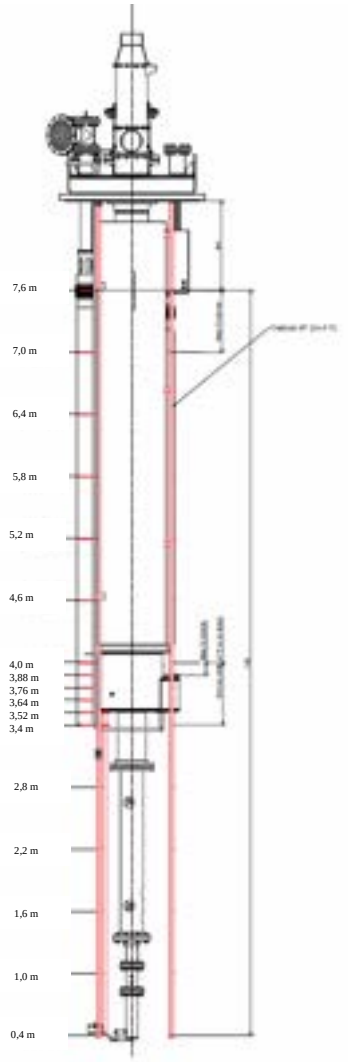
A calibrated fouling factor is evaluated as the ratio between **Ushakov (*p/d=1.8)*** and **Todreas&Kazimi (*p/d=1.6)*** equal to 0.86 in order to better reproduce the HTC







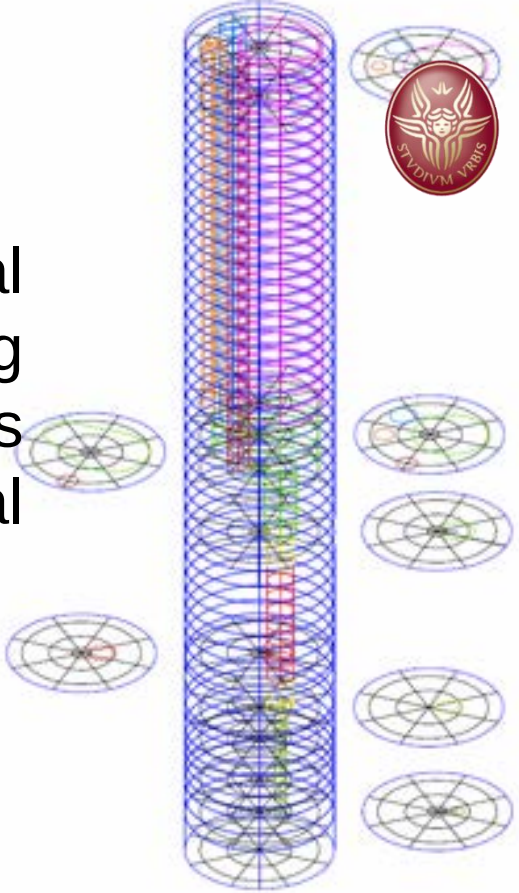
Thermal-Hydraulic Model: Region #2

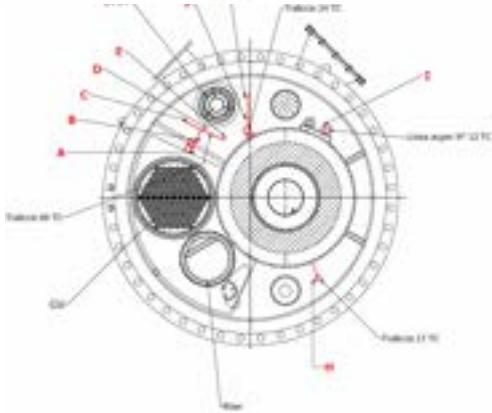


In order to investigate thermal stratification and mixing convection phenomena, **CIRCE** is equipped with several thermocouples (TCs):

- 17 axial levels
- 9 circumferential positions

The **3D component**, which reproduces the pool, is conceived to compare LBE temperature in the exact positions of the TCs

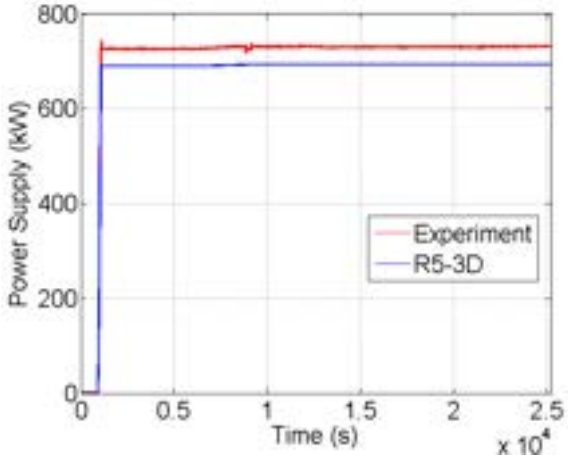


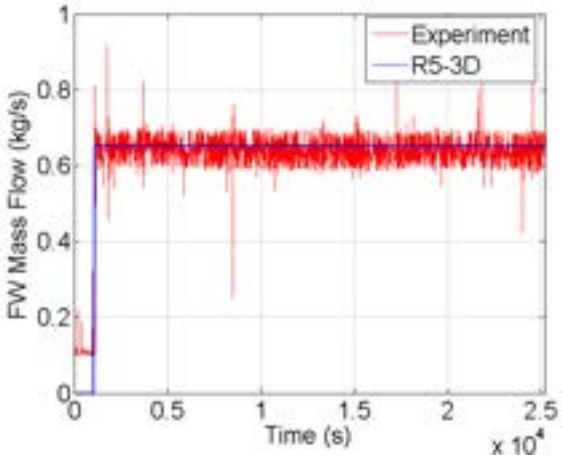


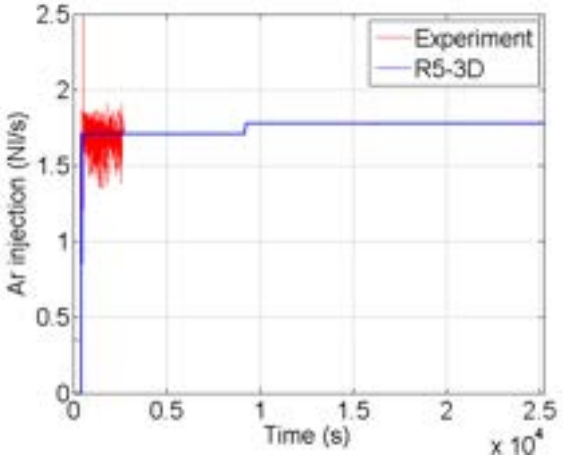
Experimental Test description

Duration	h	7
Electrical power supplied	kW	720
Average initial LBE temperature	K	600
LBE mass flow rate	kg/s	55
Feed-water mass flow rate	kg/s	0.65

The **electrical power supplied** to the FPS is reproduced with **RELAP5-3D©**: the experimental value is reduced by 5% to take into account the dissipations which occur in the cables and connectors of the outer circuits.

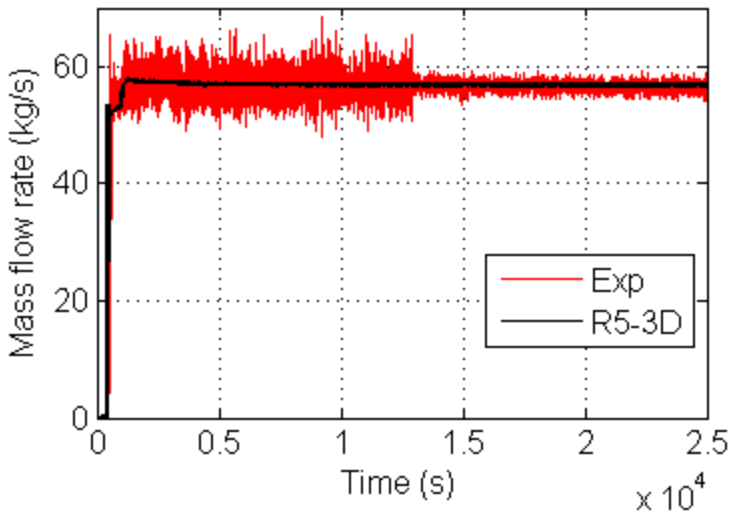


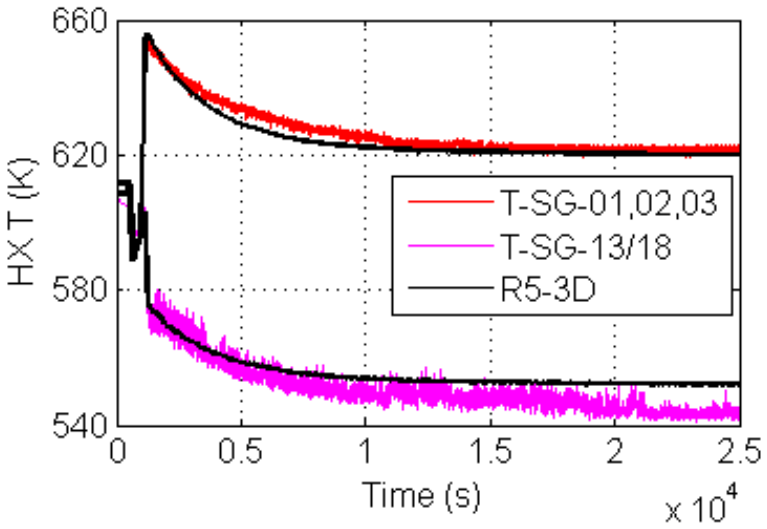




Results

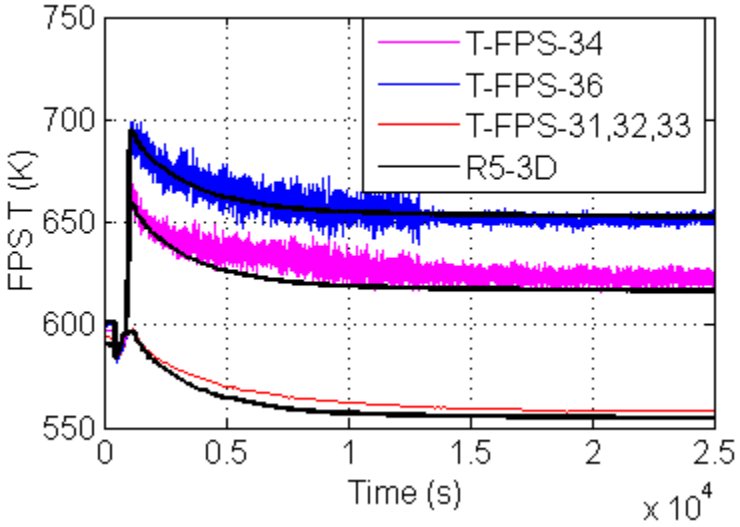
- The simulation analysis is conducted using the **most recent thermo-physical properties correlations for LBE**, recommended by NEA and implemented in R5-3D
- The **LBE mass flow rate**, measured by the Venturi-nozzle, is compared with the simulated value at the inlet section of the FPS.
- The LBE temperature at the inlet and outlet section of the HX are respectively obtained averaging the values of 3 (**T-SG 01, 02 and 03**) and 6 (**T-SG from 13 to 18**) TCs.
- The temperatures are compared with the simulated value at the first and the last control volume of the HX pipe

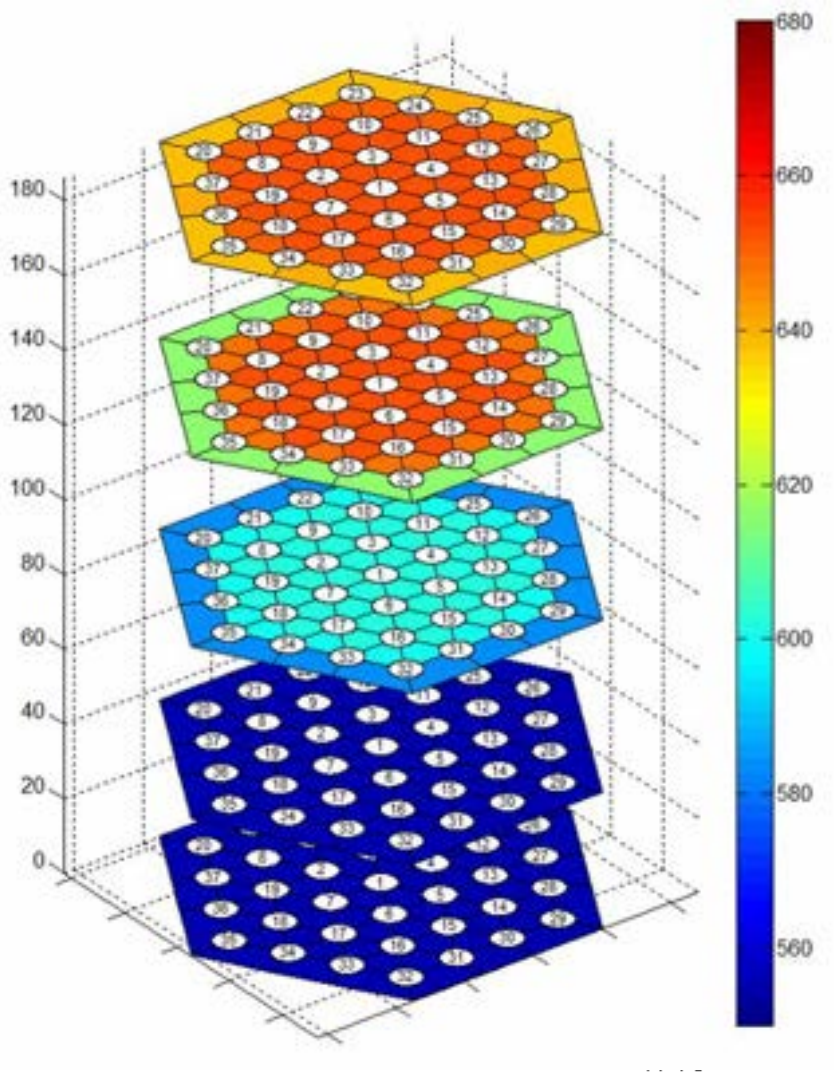




Results

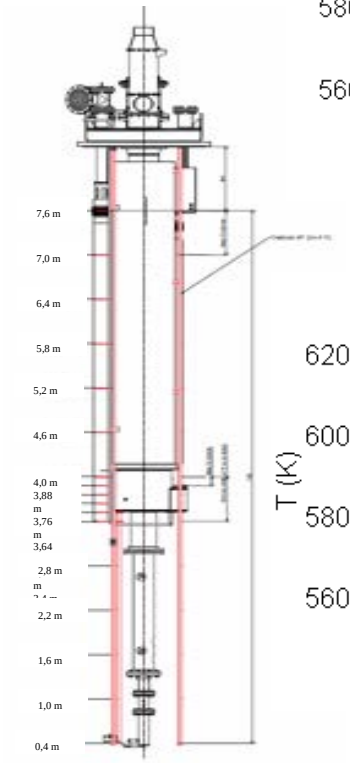
- The simulated temperature at the inlet section of the FPS is compared with the average temperature measured by T-FPS 31, 32 and 33, quickly uniform. At the outlet section of the HS the temperature is not uniform and the value measured by T-FPS 34 and 36 are compared with the temperature of the corresponding control volume

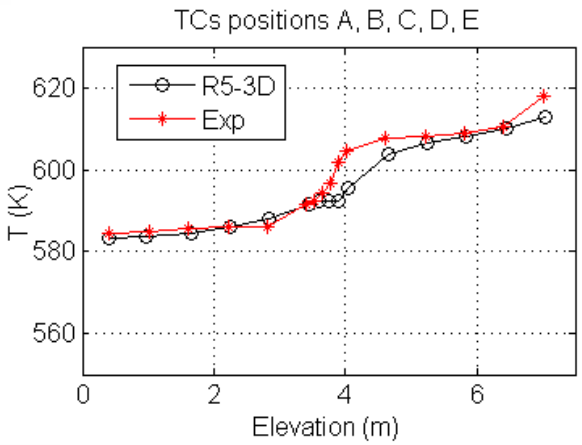


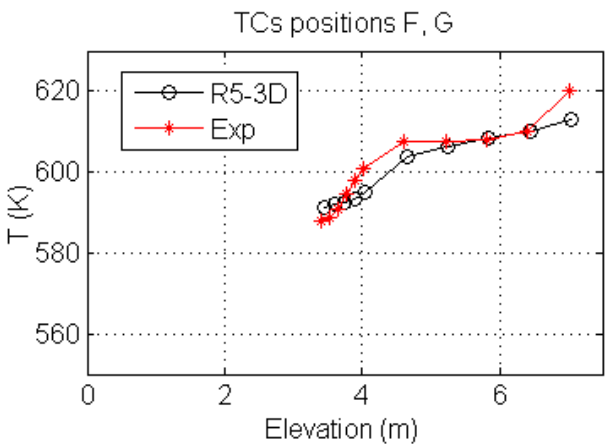


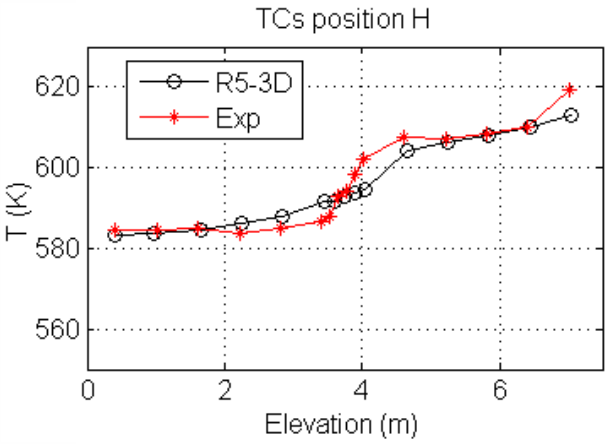
Results

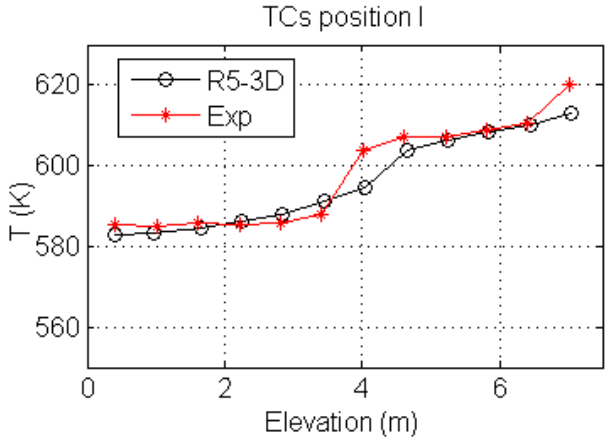




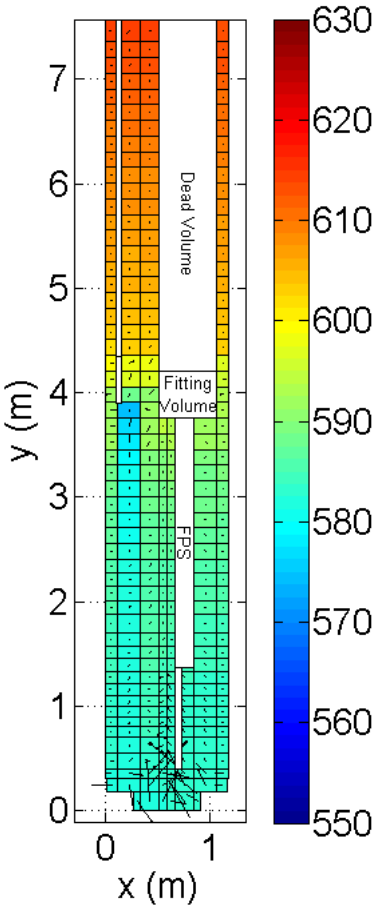






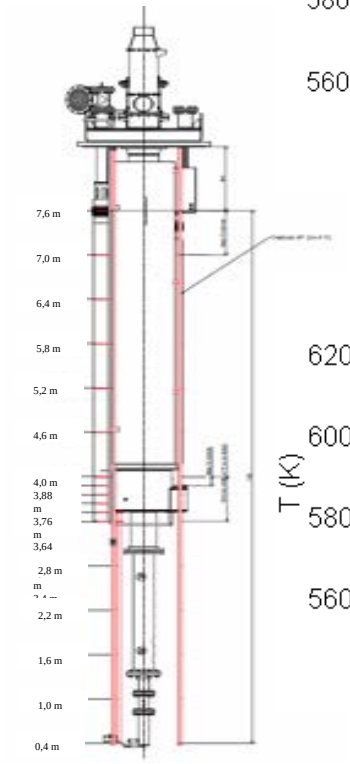


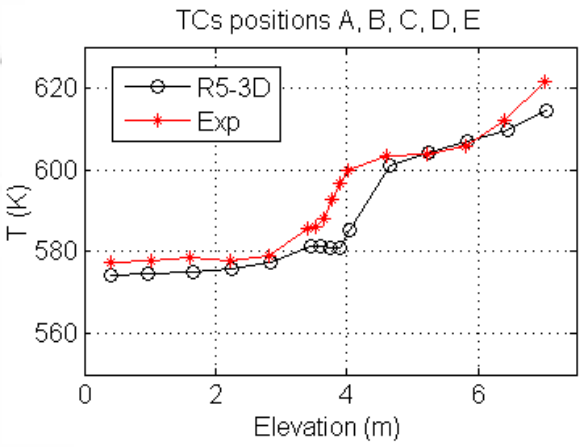
2000 s

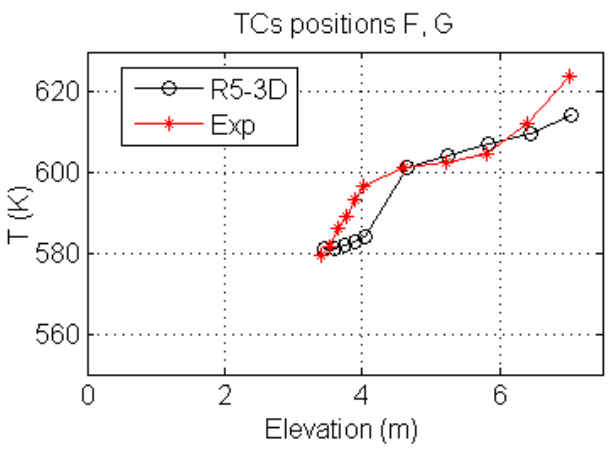


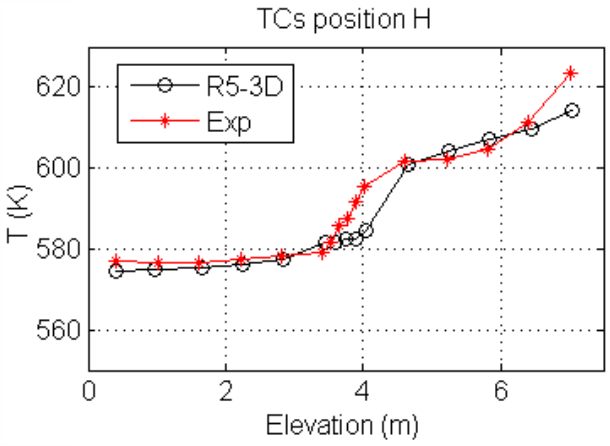
Results

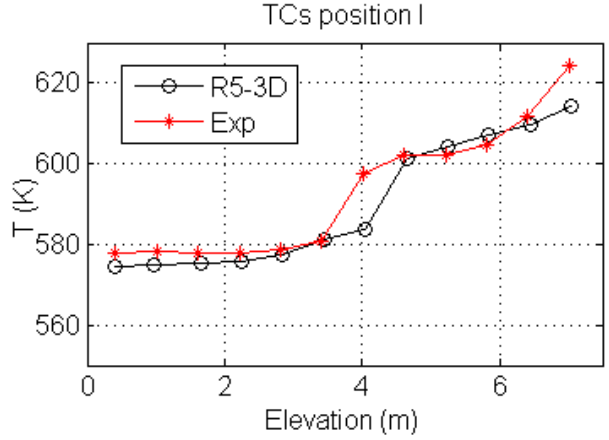




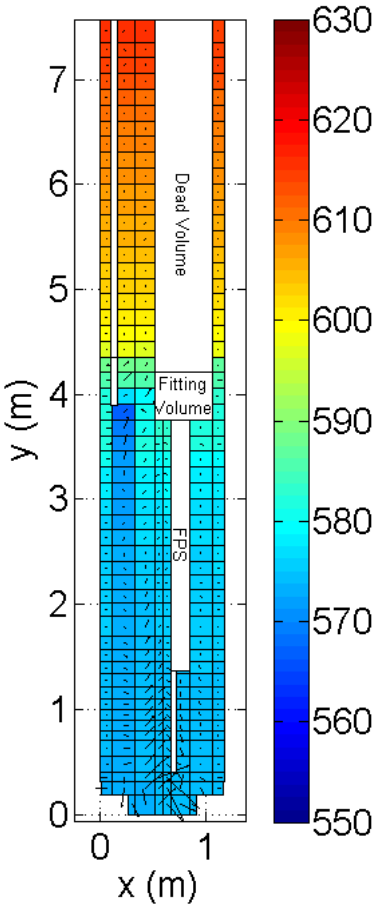






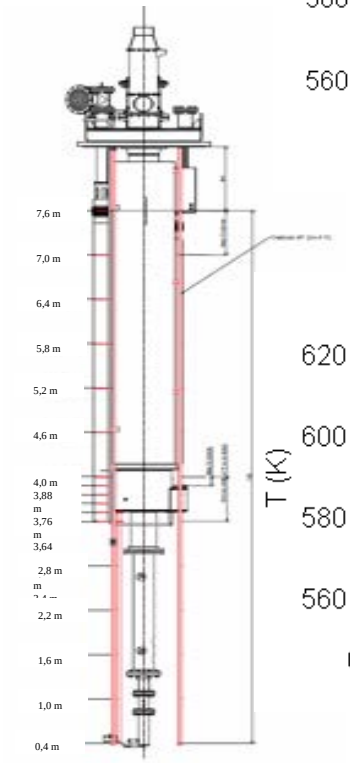


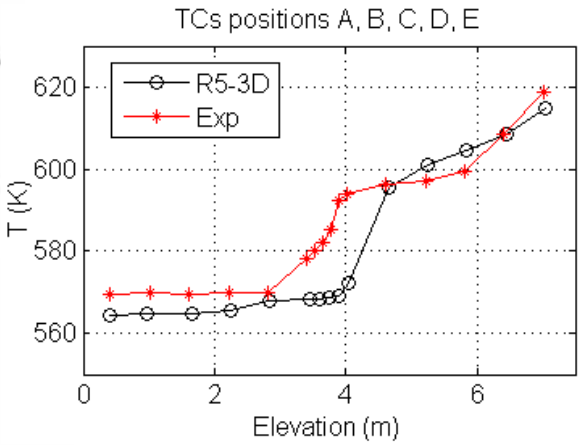
3000 s

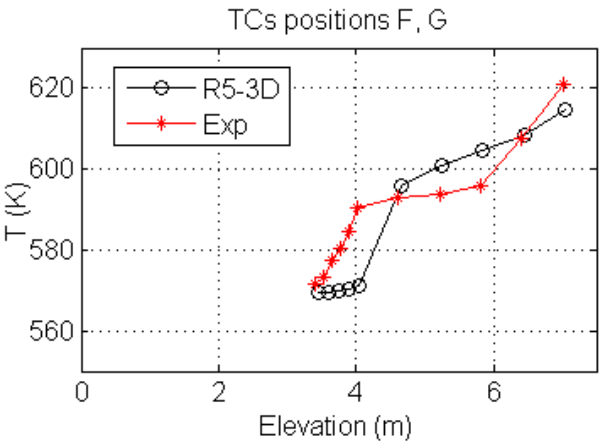


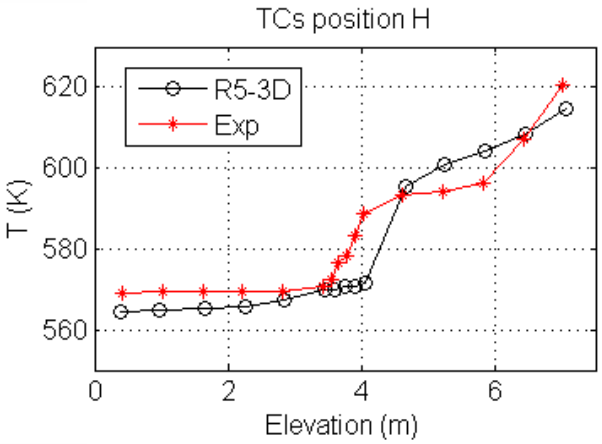
Results

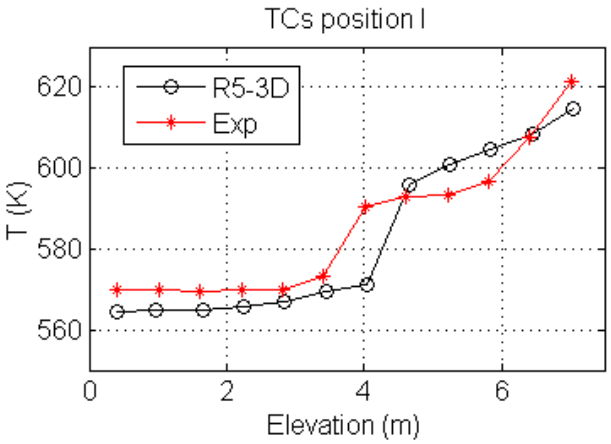




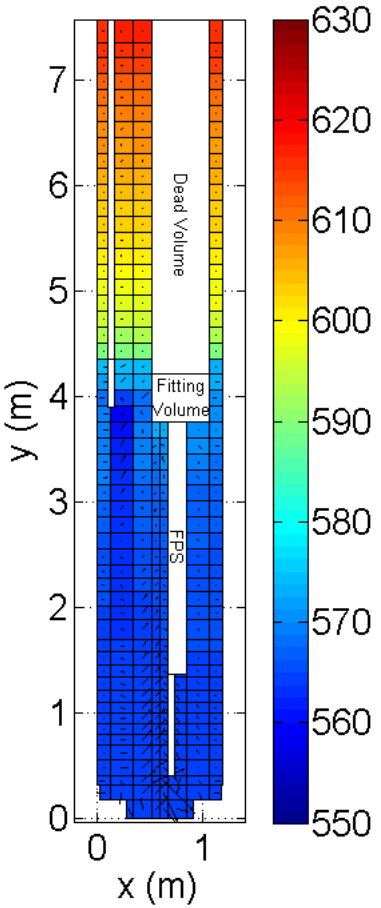






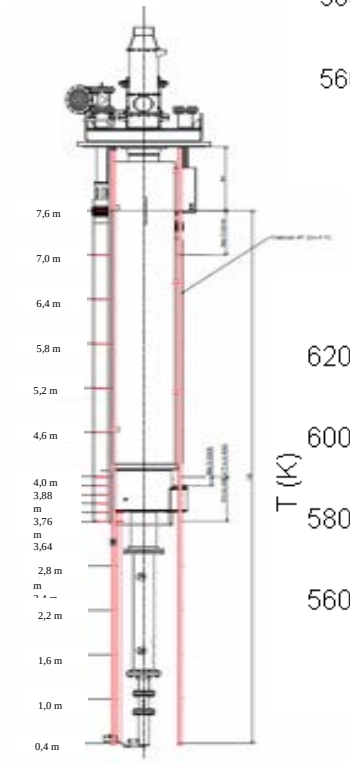


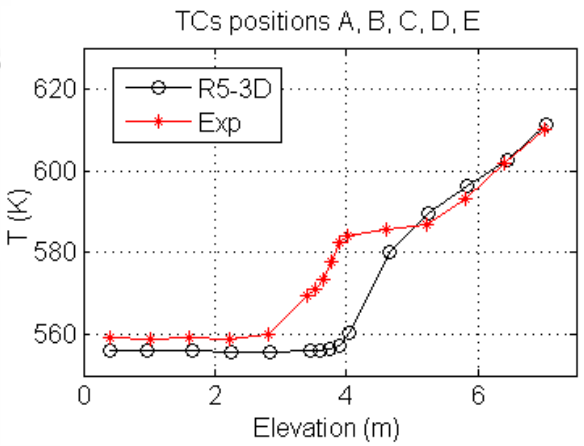
5000 s

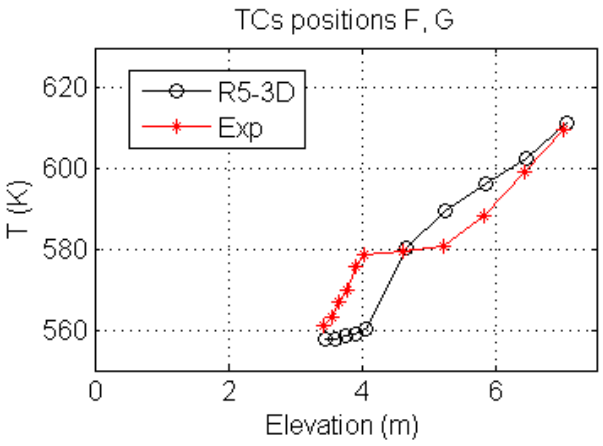


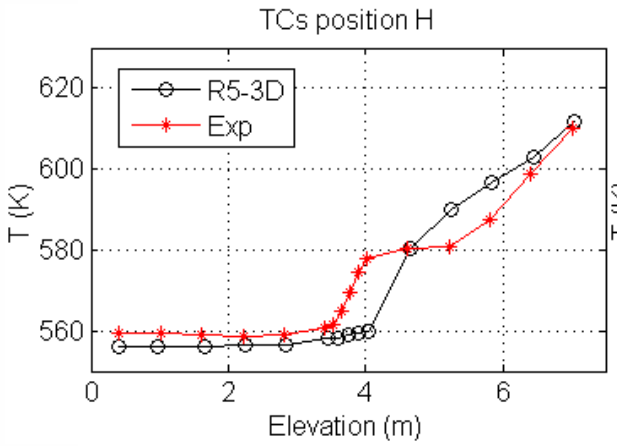
Results

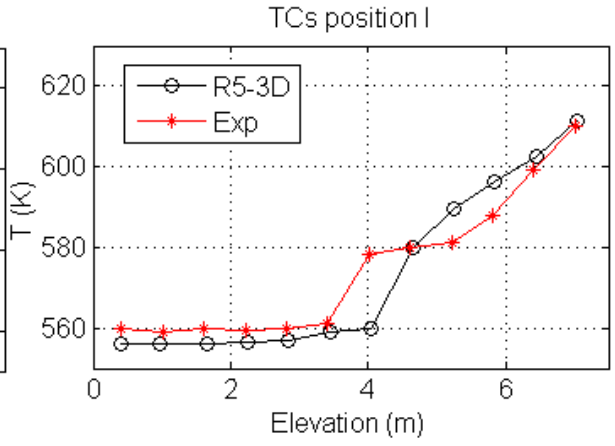




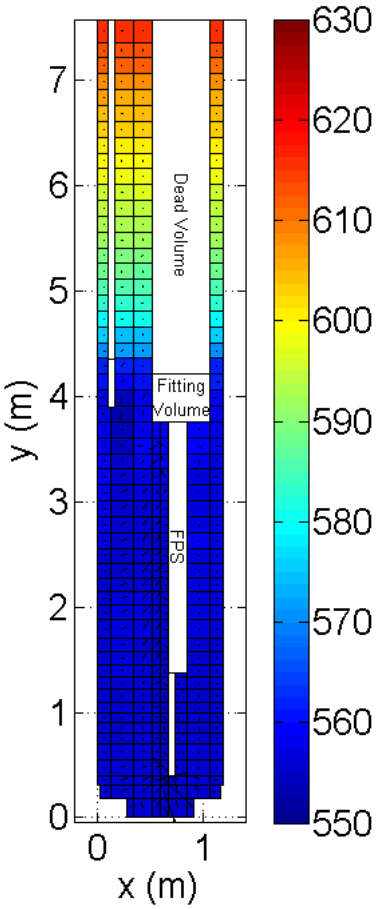






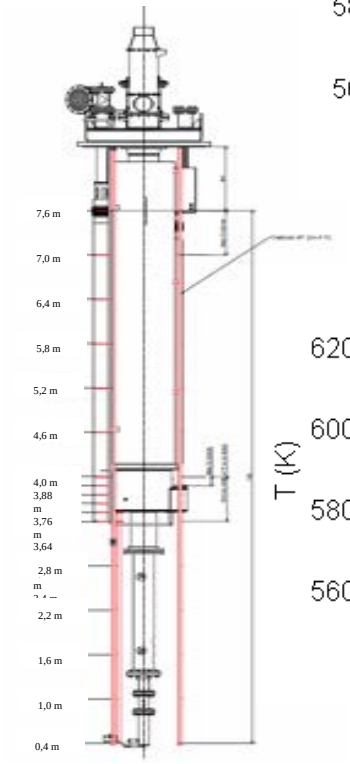


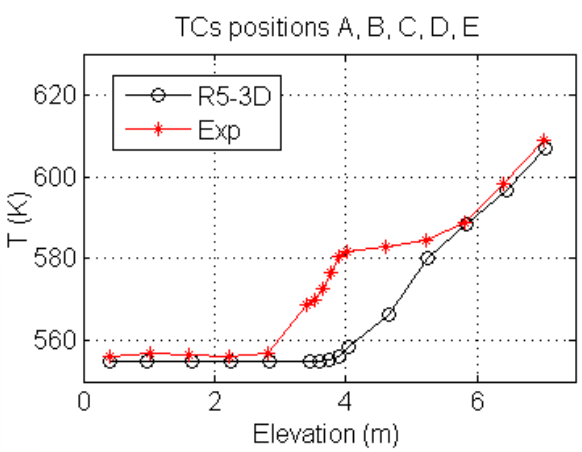
12000 s

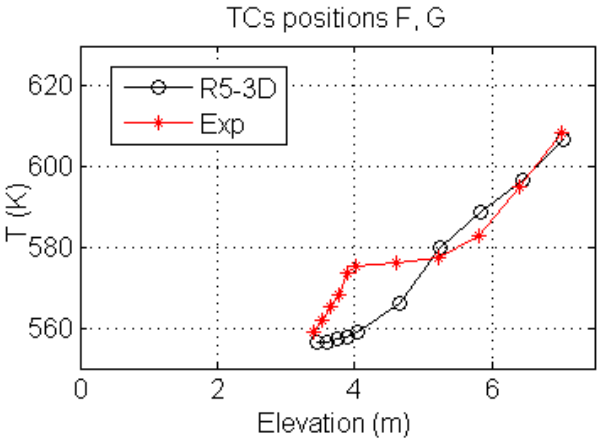


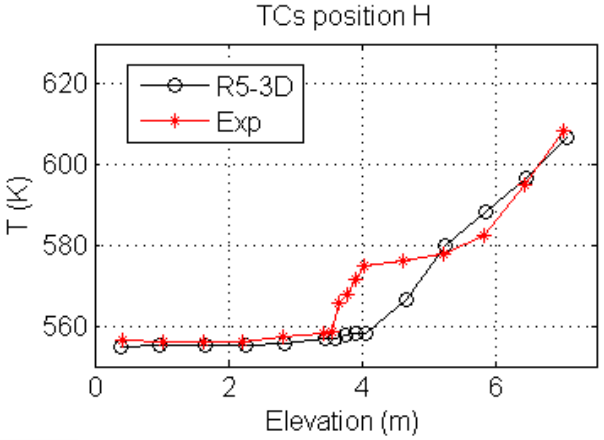
Results

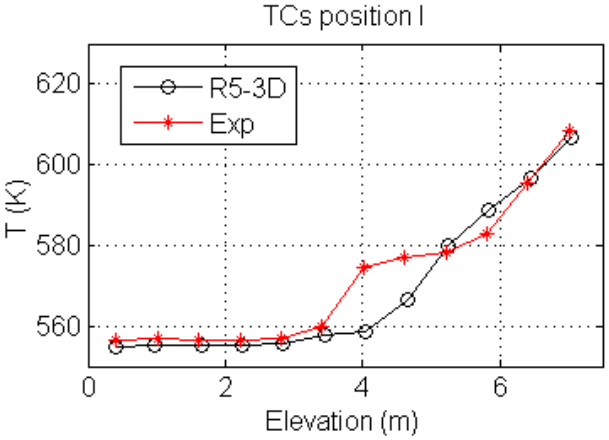



7,6 m
7,0 m
6,4 m
5,8 m
5,2 m
4,6 m
4,0 m
3,88 m
3,76 m
3,64
2,8 m
2,2 m
1,6 m
1,0 m
0,4 m

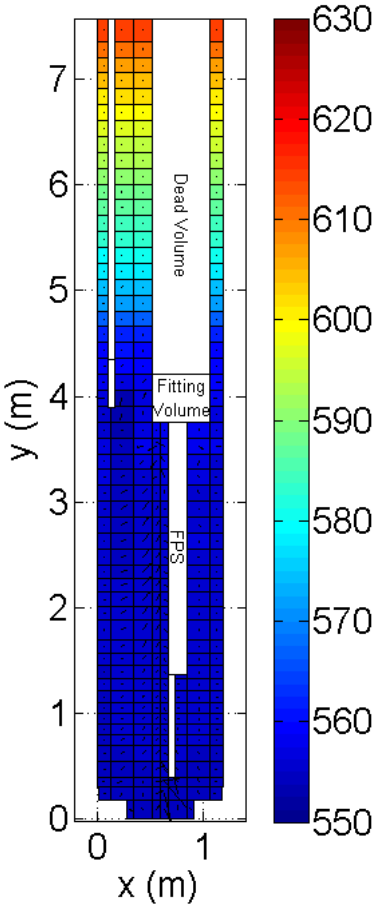

TCs positions A, B, C, D, E
R5-3D
Exp
T (K)
Elevation (m)


TCs positions F, G
R5-3D
Exp
T (K)
Elevation (m)


TCs position H
R5-3D
Exp
T (K)
Elevation (m)


TCs position I
R5-3D
Exp
T (K)
Elevation (m)

END


Dead Volume
Fitting Volume
FPS
y (m)
x (m)

Conclusions

- The geometrical nodalization scheme of **CIRCE-ICE** has been developed using **RELAP5-3D©**
- The code well reproduces thermal-hydraulics of the primary main flow path. The implementation of the **most recent thermophysical properties correlations** allows a better estimation of the LBE temperature variation along the flow path
- The code is in good agreement with experimental data for **thermal stratification phenomena** into the pool, except between 5 and 3 m
- Further investigations for the thermal stratification are needed, with a heat losses detailed characterization which could be carried out with **CIRCE-HERO** experimental data contribution

THANKS FOR YOUR ATTENTION

Research and development of the FRENETIC code: development of time step adaptivity for the quasistatic method

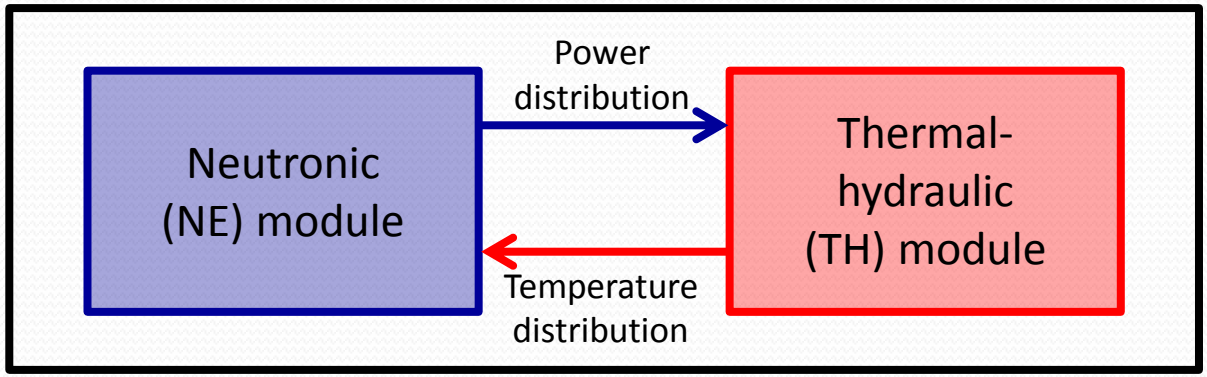
R. Bonifetto, D. Caron, S. Dulla,
P. Ravetto, L. Savoldi, R. Zanino
Politecnico di Torino, Italy

Table of contents

- Description of the FRENETIC code
- Verification and validation
- Latest activities
  - Coupled photon-neutron transport
  - Quasi-static time step adaptiveness
- Future work and perspectives

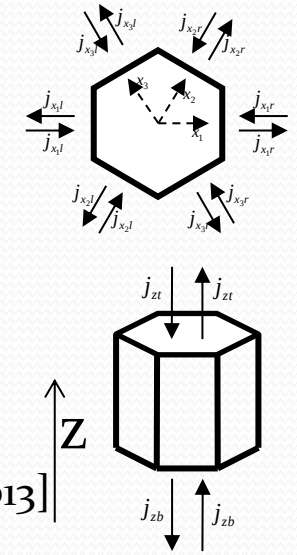
The FRENETIC code

- Fast **RE**actor **NE**utronics/Thermal-hydraul**IC**s (**FRENETIC**) code for full-core coupled analyses of fast reactors with liquid-metal coolant [R. Bonifetto et al., *Nucl. Eng. Des.*, 2013]



- **Principal objective**: computationally efficient, multiphysics analyses suitable for design and safety studies
- **Preliminary validation** of coupled code on EBR-II experimental data [D. Caron et al., Int. J. Energy Res., 2016]

FRENETIC: NE module (1)



- Physical model
  - multigroup neutron diffusion theory with delayed neutron precursors
- Mathematical models
  - space: polynomial nodal method [D. Caron et al., ICENES, 2013]
  - time: point-kinetic, direct and quasi-static methods [D. Caron et al., Ann. Nuc. Energy, 2015]
- Additional physics models
  - decay and photon heat (with photon transport) [D. Caron et al., PHYSOR, 2016]

FRENETIC: NE module (2)

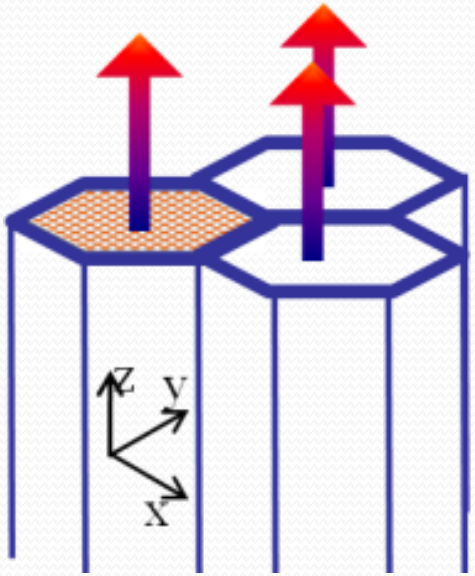
- Time-dependent multigroup neutron diffusion equations with delayed neutron precursors and (possible) independent source

$$\begin{cases} \dfrac{1}{v_g}\dfrac{\partial}{\partial t}\phi_g(\mathbf{r},t) = \nabla\cdot D_g(\mathbf{r},t)\nabla\phi_g(\mathbf{r},t) - \Sigma_g(\mathbf{r},t)\phi_g(\mathbf{r},t) + \displaystyle\sum_{g'=1}^{G}\Sigma_{gg'}(\mathbf{r},t)\phi_{g'}(\mathbf{r},t) \\ \quad + (1-\beta)\chi_g(\mathbf{r})\displaystyle\sum_{g'=1}^{G}\nu\Sigma_{fg'}(\mathbf{r},t)\phi_{g'}(\mathbf{r},t) + \sum_{i=1}^{R}\chi_{gi}(\mathbf{r})\lambda_i c_i(\mathbf{r},t) + S_g(\mathbf{r},t), \qquad g=1,\ldots,G, \\ \dfrac{\partial}{\partial t}c_i(\mathbf{r},t) = \beta_i\displaystyle\sum_{g'=1}^{G}\nu\Sigma_{fg'}(\mathbf{r},t)\phi_{g'}(\mathbf{r},t) - \lambda_i c_i(\mathbf{r},t), \qquad i=1,\ldots,R, \end{cases}$$

Temperature-dependent cross sections

- subject to appropriate initial and boundary conditions.
- Additionally: steady-state multigroup neutron diffusion equations with (possible) independent source, both for direct and adjoint problems.
- Cross sections: input data, produced through auxiliary codes; potential for on-the-fly generation.

FRENETIC: TH module (1)



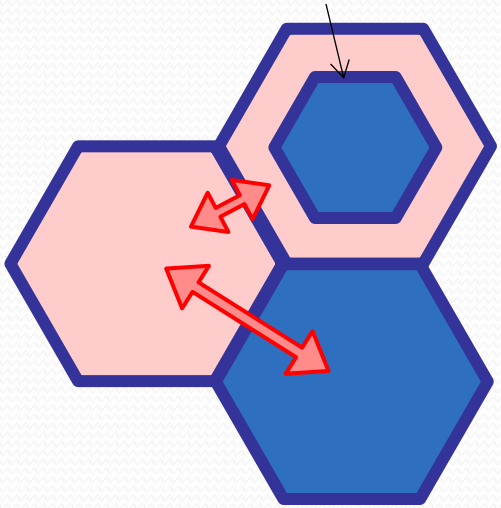
IN EACH HA:
Coolant: 1D axial model (mass, momentum, and energy eqs.) along each closed assembly (**z**), for 1+ regions in each hexagonal assembly (HA)

- **Single HA** (1D) **validation** against experimental data from CIRCE facility @ ENEA Brasimone (**Pb-Bi eutectic**) [R. Zanino et al., Trans. Am. Nucl. Soc., 2012]

Pins: **1D** radial model, locally coupled to coolant

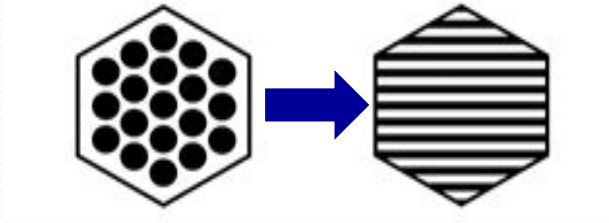
BETWEEN HAs: (weak) **2D** inter-assembly thermal coupling (**xy**)

- Steady-state **benchmark** against RELAP5-3D© in a simplified EBR-II geometry (**Na**) [R. Zanino et al., Trans. Am. Nucl. Soc., 2013]
- Preliminary **validation** against EBR-II data (**Na**) [R. Zanino et al., Proc. ATH, 2014]

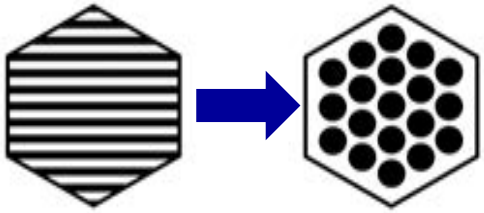


FRENETIC: coupling algorithm

- Spatial coupling procedure:
  - TH→NE: fuel and coolant average temperatures attributed to entire node

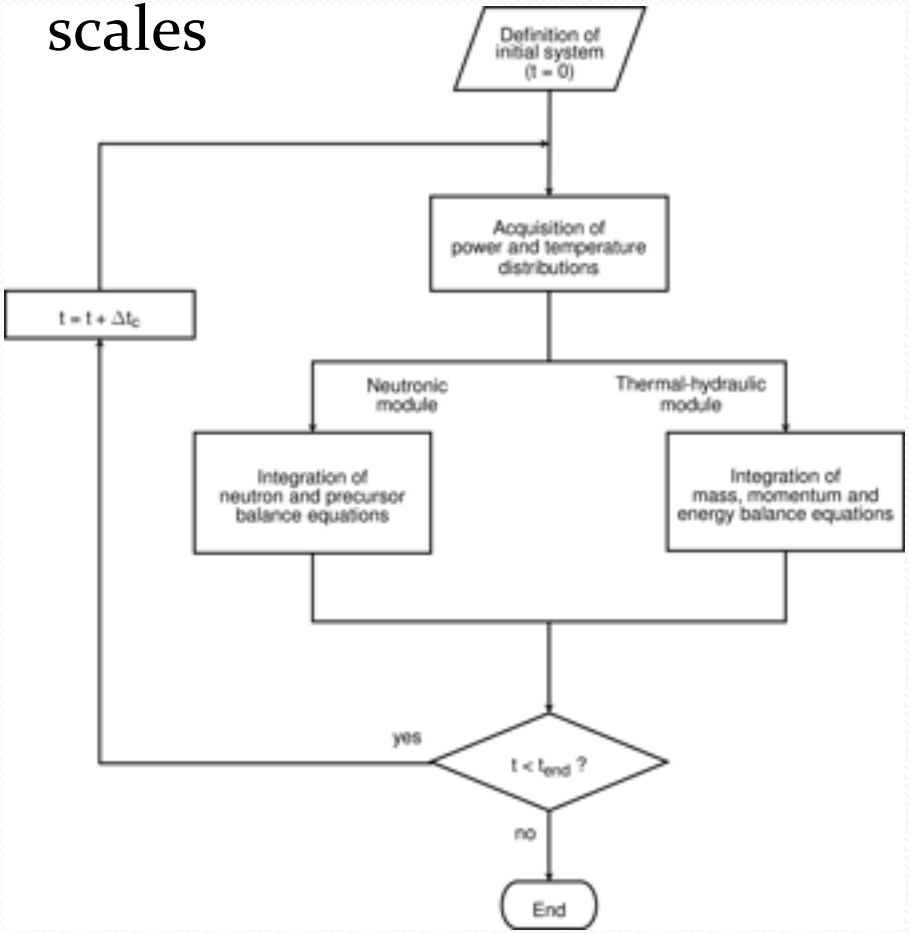


  - NE→TH: node-averaged power localised in appropriate region



  - Averaging or interpolation on mesh as necessary

- Temporal coupling algorithm accounts for different time scales



FRENETIC: feedback coupling

- Thermal-hydraulic module
  - neutronic effects accounted for directly by time- and position-dependent heat source term
- Neutronic module
  - thermal effects accounted for indirectly by dependence of macroscopic cross sections on fuel and coolant temperatures
  - 1.) linear feedback model:

$$\Sigma(T_f, T_c) = \Sigma(T_{f0}, T_{c0}) + \left(\frac{\partial \Sigma}{\partial T_f}\right)_{T_c} (T_f - T_{f0}) + \left(\frac{\partial \Sigma}{\partial T_c}\right)_{T_f} (T_c - T_{c0})$$

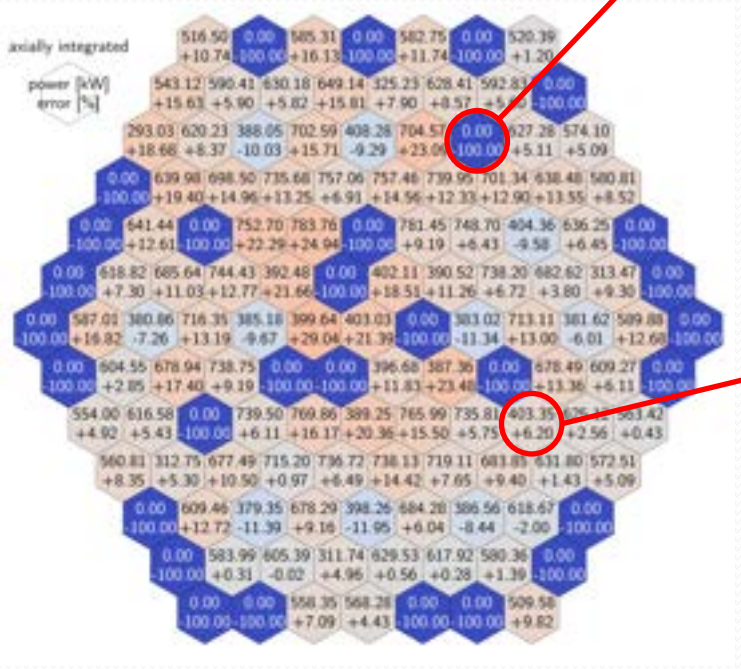
  - 2.) tabular lookup model: bivariate linear interpolation.

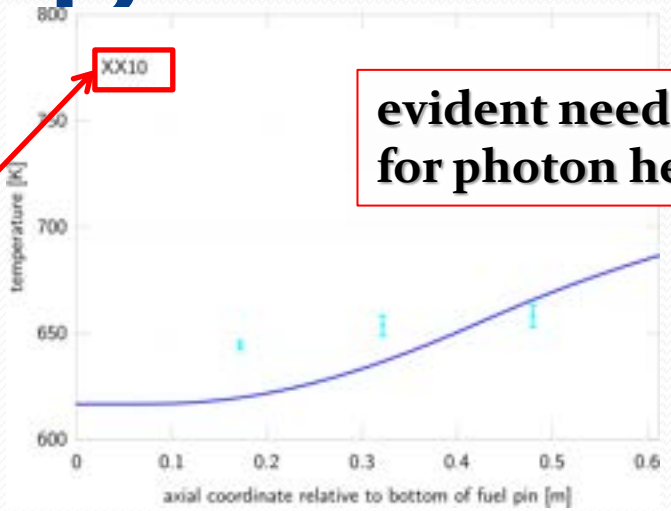
Validation activities

- Neutronic module
  - reference numerical test problems, steady-state and transient
- Thermal-hydraulic module
  - reference numerical test problems, steady-state and transient
  - ICE test section of CIRCE facility, transient
  - EBR-II SHRT-17 steady-state and transient
- **Coupled code**
  - **EBR-II SHRT-45R steady-state and transient**

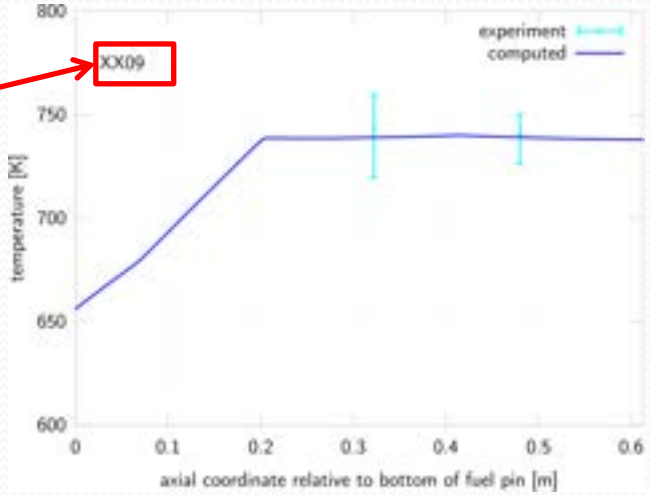
EBR-II SHRT-45R benchmark

- transient: ULOF in the EBR-II fast reactor
- reactor returns to stable conditions thanks to intrinsic safety of the design

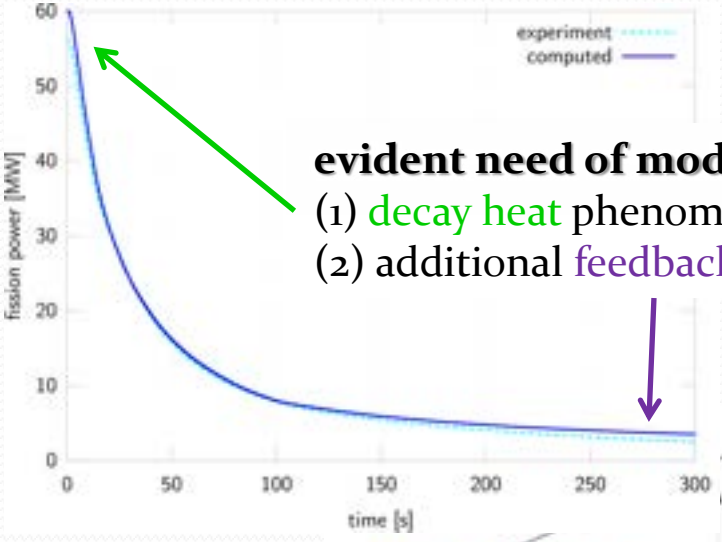




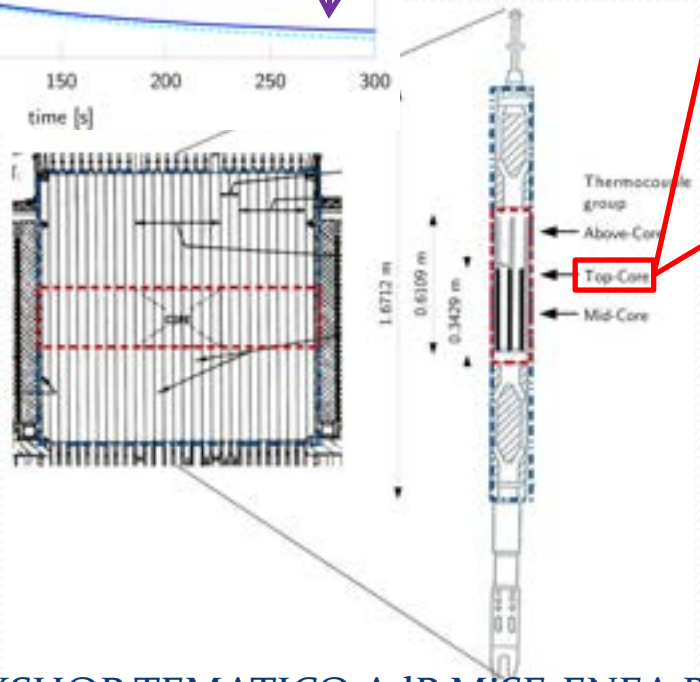
evident need of a model for photon heat

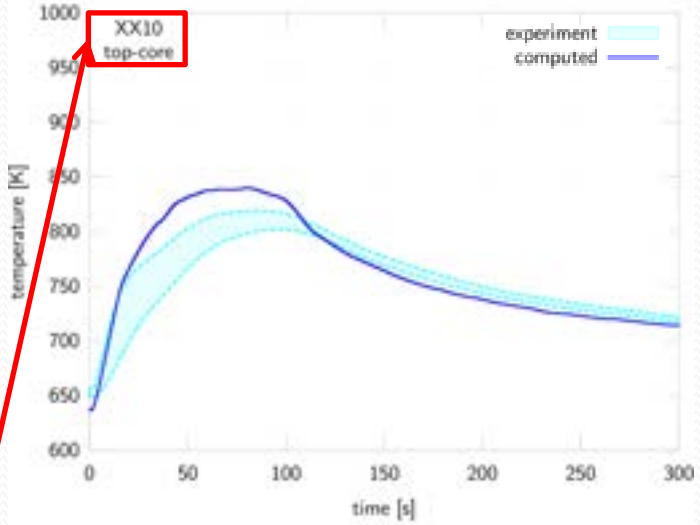


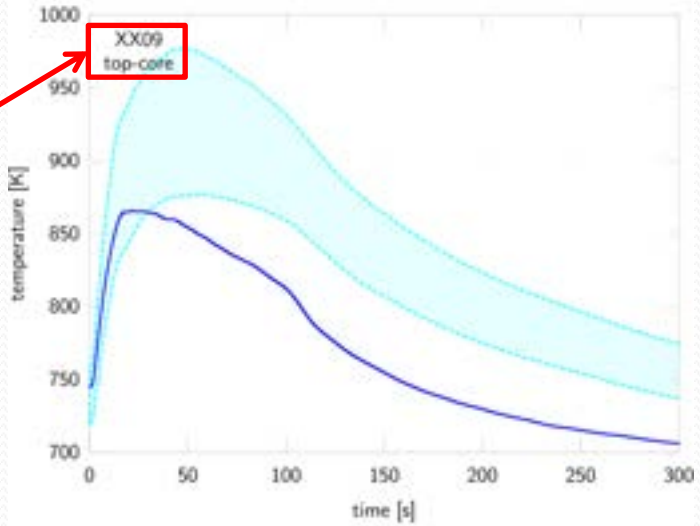
EBR-II SHRT-45R benchmark



evident need of models for:
(1) decay heat phenomenon
(2) additional feedback mechanisms







Coupled neutron-photon dynamics (1)

- Approach: to represent photon production (prompt and delayed) in neutron-nuclear interactions, as well as photon transport
- Time-dependent photon and delayed photon precursor balance equations

Neutron coupling

$$
\begin{cases}
\dfrac{1}{v_\gamma}\dfrac{\partial}{\partial t}\phi_\gamma(\mathbf{r},E_\gamma,\boldsymbol{\Omega}_\gamma,t) = [\mathcal{L}_\gamma\phi_\gamma](\mathbf{r},E_\gamma,\boldsymbol{\Omega}_\gamma,t) + [\mathcal{P}_{\gamma n}\phi](\mathbf{r},E_\gamma,\boldsymbol{\Omega}_\gamma,t) \\
\qquad + \displaystyle\sum_{i=1}^{R_\gamma} \frac{\zeta_i(\mathbf{r},E)}{4\pi}\lambda_i g_i(\mathbf{r},t) + S_\gamma(\mathbf{r},E_\gamma,\boldsymbol{\Omega}_\gamma,t), \\
\dfrac{\zeta_i(\mathbf{r},E_\gamma)}{4\pi}\dfrac{\partial}{\partial t}g_i(\mathbf{r},t) = [\mathcal{P}_{\gamma i}\phi](\mathbf{r},E_\gamma,\boldsymbol{\Omega}_\gamma,t) - \dfrac{\zeta_i(\mathbf{r},E_\gamma)}{4\pi}\lambda_{\gamma i} g_i(\mathbf{r},t), \\
\qquad i=1,\ldots,R_\gamma,
\end{cases}
$$

Coupled neutron-photon dynamics (2)

- Photon and delayed photon precursor balance equations analogous to neutron and delayed neutron precursor balance equations.
- Photon and delayed photon precursor balance equations solved simultaneously with neutron and delayed neutron precursor balance equations.
- Total power density

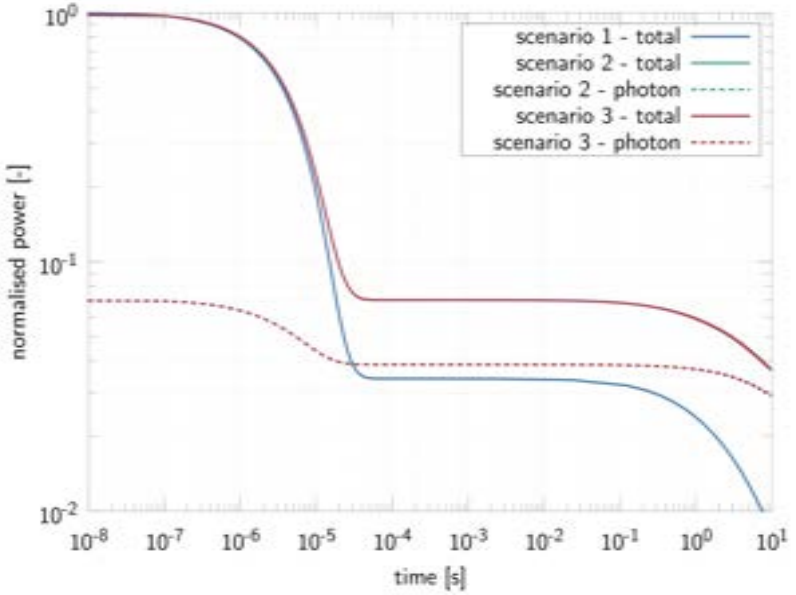
$$p(\mathbf{r},t) = [(\mathcal{E}+\mathcal{K})\phi](\mathbf{r},t) + [\mathcal{K}_\gamma \phi_\gamma](\mathbf{r},t),$$

- Accounts implicitly for delayed effects both of neutrons and of photons.

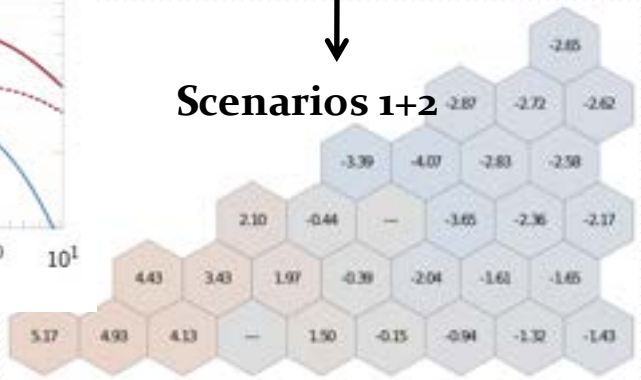
Coupled neutron-photon dynamics (3)

- SCRAM-type transient in a fast reactor
- «follower»→«absorber» (-8685 pcm of reactivity)

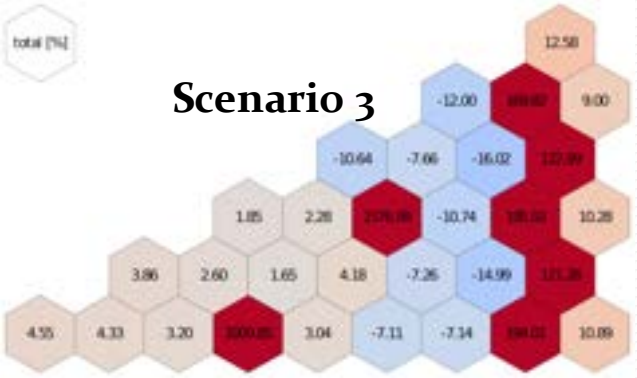




- distortion of the total power distribution with respect to the initial conditions after 10 s

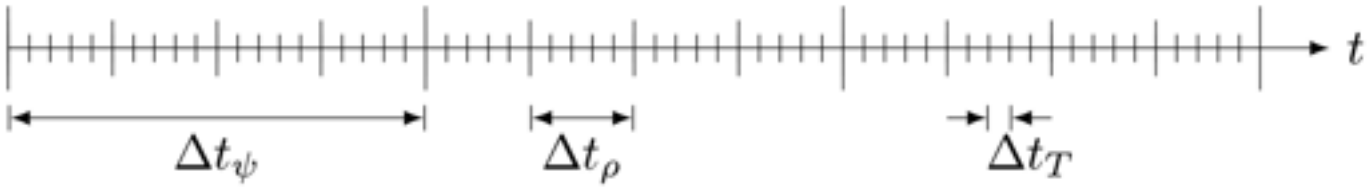


Scenario	Delay	Transport
1	No	No
2	Yes	No
3	Yes	Yes



Adaptive time-step selection

- Correct application of the quasi-static method requires the appropriate selection of the time steps employed in the algorithm.



- shape time steps (Δt_ψ)
  - representability of the shape function by a set of discrete values and interpolation rules
- reactivity time steps ($\Delta t_\rho < \Delta t_\psi$)
  - coupling of the operators of the shape equations to the coefficients of the amplitude equations
- amplitude time steps ($\Delta t_T < \Delta t_\rho$)
  - accuracy of the solution of the amplitude equations

Reactivity time-step adaptiveness

- Approach: to limit the allowed variation of each integral kinetic parameter on a reactivity time step.
- Evolution of an arbitrary integral kinetic parameter

$$h(\tau) = H_0 + H_1\tau + H_2\tau^2 \quad \text{with} \quad \tau \equiv (t - t_n)/\Delta t_{\psi,n} \in [0;1]$$

- Require

$$\frac{\left(\overline{\delta h^2}\right)^{1/2}}{|\bar{h}|} < \varepsilon_\rho \quad \text{for} \quad \tau \in [\tau_\rho; \tau_\rho + \delta] \quad \text{with} \quad \delta \equiv \Delta t_\rho/\Delta t_{\psi,n}$$

- with $\bar{h}$ the mean value and $\overline{\delta h^2}$ the quadratic mean.
- Leads to a fourth-order polynomial in δ whose zeros are the intervals of time for which the criterion is verified.

Reactivity time-step adaptiveness

- infinite medium reactor
- one group of neutrons, one delayed neutron precursor family
- initial condition: steady-state, critical
- transient: linear perturbation of the multiplication eigenvalue

$$k(t) = 1 + at \qquad t \in [0; \infty)$$

	reference	$\varepsilon_\rho = 10^{-5}$	$\varepsilon_\rho = 10^{-6}$	$\varepsilon_\rho = 10^{-7}$	$\varepsilon_\rho = 10^{-8}$
t [s]	$T(t)/T(0)$ [-]	$T(t)/T(0)$ [-]	$T(t)/T(0)$ [-]	$T(t)/T(0)$ [-]	$T(t)/T(0)$ [-]
0.000	1.00000	1.00000	1.00000	1.00000	1.00000
0.001	1.00028	1.00029	1.00028	1.00028	1.00028
0.010	1.00858	1.00858	1.00858	1.00858	1.00858
0.100	1.10887	1.10888	1.10887	1.10887	1.10887
0.200	1.24786	1.24787	1.24786	1.24786	1.24786
0.300	1.42806	1.42809	1.42807	1.42806	1.42806
0.400	1.67042	1.67046	1.67042	1.67042	1.67042
0.500	2.01254	2.01261	2.01255	2.01255	2.01254
0.600	2.52922	2.52935	2.52923	2.52922	2.52922
0.700	3.39159	3.39186	3.39162	3.39160	3.39159
0.800	5.08633	5.08700	5.08639	5.08633	5.08633
0.900	9.62994	9.63240	9.63018	9.62996	9.62994
1.000	35.8596	35.8844	35.8621	35.8598	35.8596

	$\varepsilon_\rho = 10^{-5}$		$\varepsilon_\rho = 10^{-6}$		$\varepsilon_\rho = 10^{-7}$		$\varepsilon_\rho = 10^{-8}$	
time [s]	N_ρ	(ΔN_ρ)	N_ρ	(ΔN_ρ)	N_ρ	(ΔN_ρ)	N_ρ	(ΔN_ρ)
0.000	0	(0)	0	(0)	0	(0)	0	(0)
0.001	67	(67)	640	(640)	6367	(6367)	63640	(63640)
0.010	6368	(6301)	63641	(63001)	636367	(630000)	6363641	(6300001)
0.100	72838	(66470)	728341	(664700)	7283358	(6646991)	72833548	(66469907)
0.200	92848	(20010)	928436	(200095)	9284302	(2000944)	92842984	(20009436)
0.300	104553	(11705)	1045484	(117048)	10454779	(1170477)	104547754	(11704770)
0.400	112858	(8305)	1128531	(83047)	11285246	(830467)	112852421	(8304667)
0.500	119300	(6442)	1192947	(64416)	11929406	(644160)	119294021	(6441600)
0.600	124564	(5264)	1245579	(52632)	12455723	(526317)	124557191	(5263170)
0.700	129014	(4450)	1290079	(44500)	12900718	(444995)	129007138	(4449947)
0.800	132869	(3855)	1328627	(38548)	13286190	(385472)	132861858	(3854720)
0.900	136270	(3401)	1362629	(34002)	13626201	(340011)	136261962	(3400104)
1.000	139312	(3042)	1393044	(30415)	13930351	(304150)	139303459	(3041497)

- convergence to reference solution as $\varepsilon_\rho \to 0$
- asymptotically, number of reactivity time steps behaves as $N_\rho \propto \varepsilon_\rho^{-1}$

Shape time-step adaptiveness

- Approach: to monitor and to control the variation of the local error of the shape during the integration algorithm.
- Step size relation

$$\frac{\Delta t_{\psi,n}}{\Delta t_{\psi,n-1}} = \left(\frac{1}{\hat{r}_n}\right)^{1/(q+1)}$$

- Excess local error estimated according to an appropriate definition
  - mathematical (q=1): regulate the local error of the shape

$$\hat{r}_n = \frac{\left\| -\frac{1}{2}\left[\frac{\partial^2}{\partial t^2}\psi(\mathbf{r},E,\mathbf{\Omega},t)\right]_{t=t_{n-1}} \Delta t^2_{\psi,n-1} \right\|_{L^p}}{\varepsilon^{abs}_{\psi} + \varepsilon^{rel}_{\psi} \left\| \widetilde{\psi}(\mathbf{r},E,\mathbf{\Omega},\widetilde{t}) \right\|_{L^p}}$$

  - physical (q=0): regulate the (weighted) variation of the shape

$$\hat{r}_n = \frac{\left\| -\phi^{\dagger}_0(\mathbf{r},E,\mathbf{\Omega})\left[\frac{\partial}{\partial t}\psi(\mathbf{r},E,\mathbf{\Omega},t)\right]_{t=t_{n-1}} \Delta t_{\psi,n-1} \right\|_{L^p}}{\varepsilon^{abs}_{\psi} + \varepsilon^{rel}_{\psi} \left\| \phi^{\dagger}_0(\mathbf{r},E,\mathbf{\Omega})\widetilde{\psi}(\mathbf{r},E,\mathbf{\Omega},\widetilde{t}) \right\|_{L^p}}$$

Shape time-step adaptiveness

- slab reactor, three regions, symmetric
- two materials, two energy groups, six delayed precursor families
- boundary conditions: zero flux
- initial condition: steady-state, critical
- transient: piecewise linear variation of removal cross section

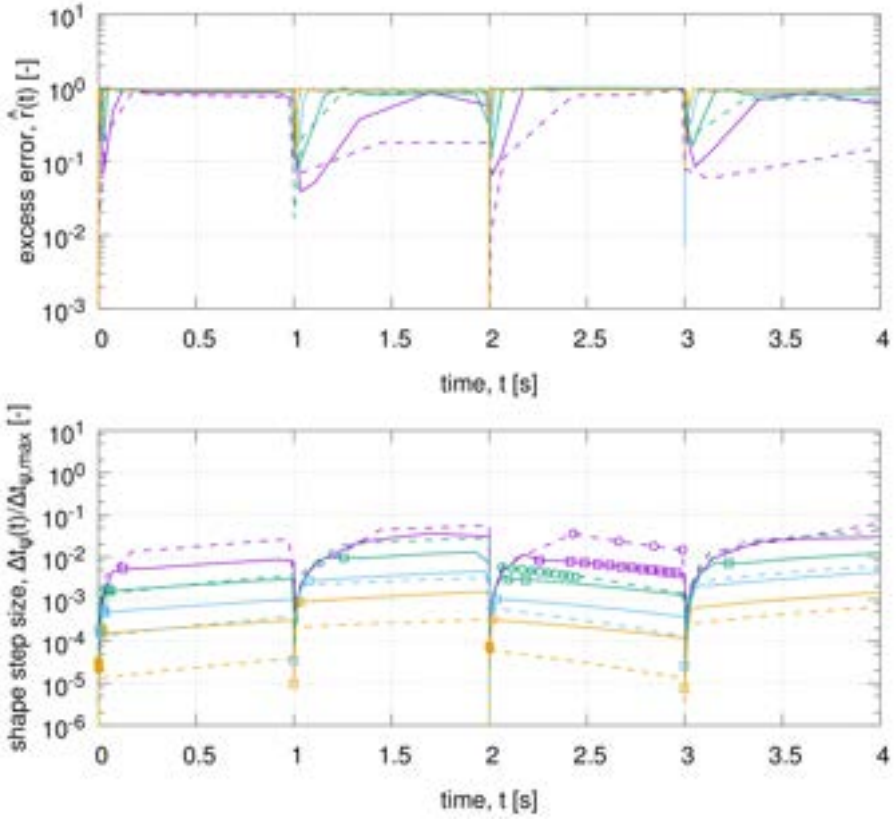
mathematical	$\Delta t_\psi = 10^{-5}$ s	$\varepsilon_\psi = 10^{-3}$	$\varepsilon_\psi = 10^{-4}$	$\varepsilon_\psi = 10^{-5}$	$\varepsilon_\psi = 10^{-6}$
t [s]	$p(t)/p(0)$ [-]	$p(t)/p(0)$ [-]	$p(t)/p(0)$ [-]	$p(t)/p(0)$ [-]	$p(t)/p(0)$ [-]
0.0	1.00000	1.00000	1.00000	1.00000	1.00000
1.0	0.65904	0.65902	0.65904	0.65904	0.65904
2.0	0.63088	0.63085	0.63088	0.63088	0.63088
3.0	0.86221	0.86218	0.86221	0.86221	0.86221
4.0	0.88634	0.88628	0.88633	0.88634	0.88634
10.0	NA	0.92096	0.92098	0.92099	0.92099
100.0	NA	0.95077	0.95078	0.95079	0.95079
1000.0	NA	0.95192	0.95193	0.95193	0.95193
physical	$\Delta t_\psi = 10^{-5}$ s	$\varepsilon_\psi = 10^{-1}$	$\varepsilon_\psi = 10^{-2}$	$\varepsilon_\psi = 10^{-3}$	$\varepsilon_\psi = 10^{-4}$
t [s]	$p(t)/p(0)$ [-]	$p(t)/p(0)$ [-]	$p(t)/p(0)$ [-]	$p(t)/p(0)$ [-]	$p(t)/p(0)$ [-]
0.0	1.00000	1.00000	1.00000	1.00000	1.00000
1.0	0.65904	0.65887	0.65903	0.65904	0.65904
2.0	0.63088	0.63072	0.63087	0.63088	0.63088
3.0	0.86221	0.86193	0.86220	0.86221	0.86221
4.0	0.88634	0.88471	0.88626	0.88634	0.88634
10.0	NA	0.92052	0.92094	0.92098	0.92099
100.0	NA	0.95067	0.95077	0.95078	0.95079
1000.0	NA	0.95182	0.95192	0.95193	0.95193

mathematical ($q = 1$)	$\varepsilon_\psi = 10^{-3}$		$\varepsilon_\psi = 10^{-4}$		$\varepsilon_\psi = 10^{-5}$		ε_ψ
time [s]	N_ψ	(N_ψ^R)	N_ψ	(N_ψ^R)	N_ψ	(N_ψ^R)	N_ψ
0.0	0	(0)	0	(0)	0	(0)	
1.0	22	(4)	57	(3)	167	(3)	51
2.0	29	(4)	72	(6)	206	(7)	62
3.0	50	(20)	129	(9)	377	(9)	115
4.0	58	(21)	150	(12)	434	(11)	132
10.0	65	(21)	168	(12)	489	(11)	149
100.0	79	(21)	198	(12)	574	(11)	175
1000.0	170	(21)	289	(12)	674	(11)	192
physical ($q = 0$)	$\varepsilon_\psi = 10^{-1}$		$\varepsilon_\psi = 10^{-2}$		$\varepsilon_\psi = 10^{-3}$		$\varepsilon_\psi = 10^{-4}$
time [s]	N_ψ	(N_ψ^R)	N_ψ	(N_ψ^R)	N_ψ	(N_ψ^R)	N_ψ (N_ψ^R)
0.0	0	(0)	0	(0)	0	(0)	0 (0)
1.0	9	(0)	50	(1)	456	(4)	4523 (7)
2.0	11	(0)	55	(1)	496	(4)	4903 (7)
3.0	19	(4)	95	(11)	875	(5)	8674 (11)
4.0	20	(4)	99	(11)	904	(5)	8940 (11)
10.0	22	(4)	105	(11)	944	(5)	9329 (11)
100.0	31	(4)	116	(11)	987	(5)	9723 (11)
1000.0	122	(4)	207	(11)	1078	(5)	9866 (11)

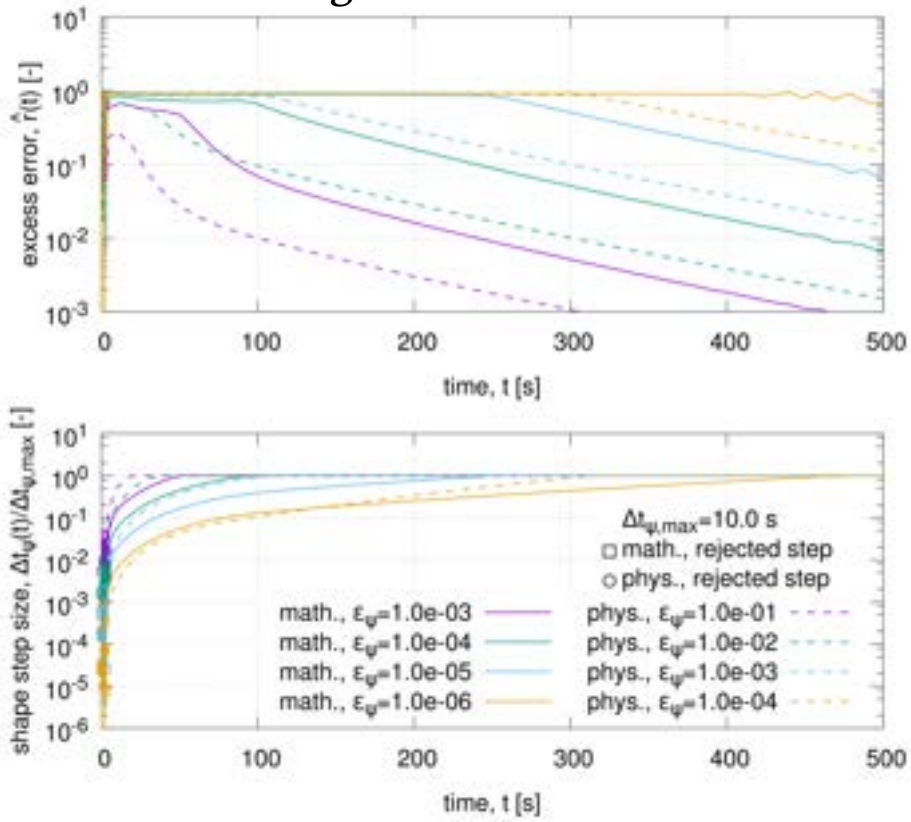
- convergence to reference solution as $\varepsilon_\rho \to 0$, regardless of error metric
- asymptotically, number of shape time steps behaves as $N_\rho \propto \varepsilon_\rho^{-1/(q+1)}$

Shape time-step adaptiveness

Short-term evolution



Long-term evolution



- Excess error: in absence of artificial limitations, maintained close to unity
- Time step: expansion or contraction as appropriate for the current conditions of the transient

Ongoing and future development

- Neutronic module
  - quasi-static coupled neutron-photon dynamics model
- Thermal-hydraulic module
  - By-pass flow modelling
- Feedback models
  - thermal expansion model
- Multiphysics
  - advanced coupling algorithms
  - additional physics models
  - advanced cross section update techniques
- Application
  - EBR-II, ALFRED, MYRRHA, …

Thanks for your attention

Frenetic

Da Wikipedia, l'enciclopedia libera.

Questa voce sull'argomento sparatutto è solo un abbozzo.
Contribuisci a migliorarla secondo le convenzioni di Wikipedia.

Frenetic è un videogioco per Amiga e Atari ST di tipo shoot'em up a scorrimento verticale. Sviluppato da Core Design nel 1991. All'epoca il game riscosse un medio successo, difficoltà elevata e poche novità per il genere. Ottima la musica curata da Martin Walker. Il videogame ricorda molto Xenon 2 Megablast.

Indice [nascondi]
1 Storia
2 Modalità di gioco
3 Armi
4 Collegamenti esterni



https://it.wikipedia.org/wiki/Frenetic

Backup slides

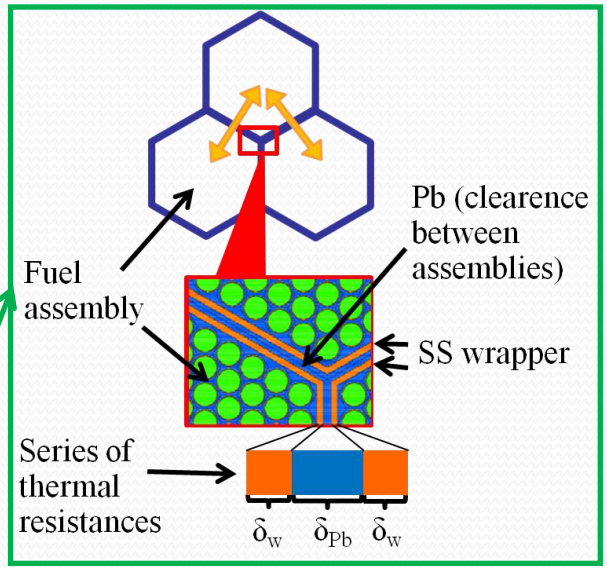
FRENETIC: TH module (2)

Coolant: compressible flow with buoyancy (1D, axial)

$$\begin{cases} \dfrac{v}{t} \quad v\dfrac{v}{z} \quad \dfrac{1}{\rho}\dfrac{p}{z} \quad Fv \quad g\cos \\ \dfrac{p}{t} \quad \rho c_s^2 \dfrac{v}{z} \quad v\dfrac{p}{z} \quad \dfrac{}{z}\left(k\dfrac{T}{z}\right) \quad \dfrac{{}_{fuel}H}{A}T_{fuel,s} \quad T \quad v\rho F \\ \rho c_v \dfrac{T}{t} \quad \rho c_v v\dfrac{T}{z} \quad \rho c_v T\dfrac{v}{z} \quad \dfrac{}{z}\left(k\dfrac{T}{z}\right) \quad \dfrac{{}_{fuel}H}{A}T_{fuel,s} \quad T \quad v\rho F \quad \sum_{i=1}^{6}\dfrac{{}_{hex}h_i}{A}T_i \quad T \end{cases}$$

Used to compute coolant-pin heat transfer

Inter-channel coupling (2D, planar)



Pin: thermal conduction (1D, axial)

$$\rho_{fuel}c_{fuel}\frac{T_{fuel}}{t} \quad \frac{}{z}\left(k_{fuel}\frac{T_{fuel}}{z}\right) \quad \frac{{}_{fuel}H}{A_{fuel}}T \quad T_{fuel,s} \quad \frac{q^{lin}_{fuel}}{A_{fuel}}$$

Neutronics-dependent heat source term

Friction term $F \quad 2f\dfrac{|v_x|}{D_h}$

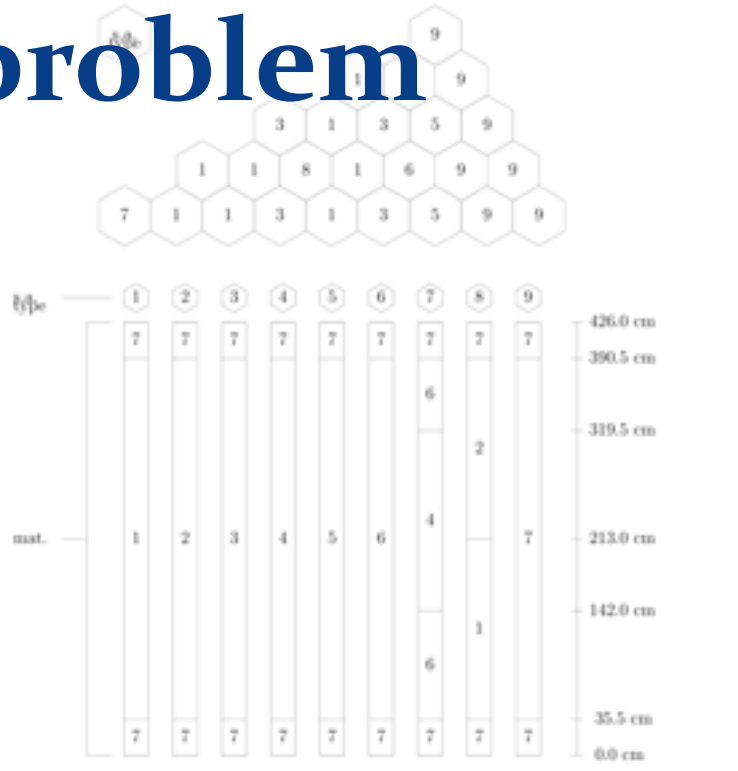
Gruneisen parameter $\dfrac{\rho}{T}\dfrac{T}{\rho}_s$

2D+1D heat exchange model

- ***1D:*** *advection + diffusion in each HA*
- ***2D:*** *simplified «slab» inter-HA heat exchange*

verification and validation (1) - steady-state reference problem

- Performance of the nodal method
  - three dimensional benchmark of a prototype VVER-1000 core in one twelfth symmetry;
  - fuel elements of four different compositions, burnable absorber, partially inserted control elements and axial and radial reflectors;
  - diffusion theory parameters for two neutron energy groups;
  - reference solutions based on fine triangular-z mesh calculations with finite element methods.



method	Δz (cm)	k_{eff}	e_k
FRENETIC	3.5500e+01	1.050600	1.02e-03
FRENETIC	1.7750e+01	1.050478	9.08e-04
FRENETIC	8.8750e+00	1.050467	8.97e-04
FRENETIC	4.4375e+00	1.050469	8.98e-04
reference	–	1.049526	–

Neutronic module: verification and validation (2) - transient reference problem

- three-dimensional system comprised of two materials;
- two energy groups, one precursor family (characteristic of light water reactor);
- compensated transient initiated by instantaneous interchange of materials;

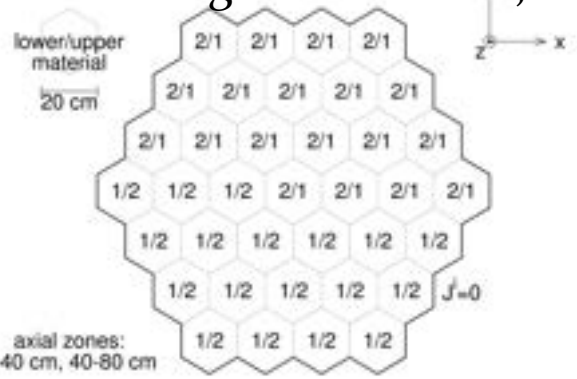
Improved quasi-static method — IQM

Δt_φ [s]	NI	NO	e^2_ϕ [-]	e^2_p [-]	e^∞_p [-]
1.00e-05	10065	19146	1.83e-05	1.83e-05	1.83e-05
2.00e-05	5050	17207	2.49e-05	2.51e-05	2.50e-05
1.00e-04	1116	12166	7.21e-05	7.25e-05	7.22e-05
2.00e-04	607	9474	1.17e-04	1.18e-04	1.17e-04
1.00e-03	221	6800	2.68e-04	2.70e-04	2.69e-04

Predictor-corrector quasi-static method — PCQM

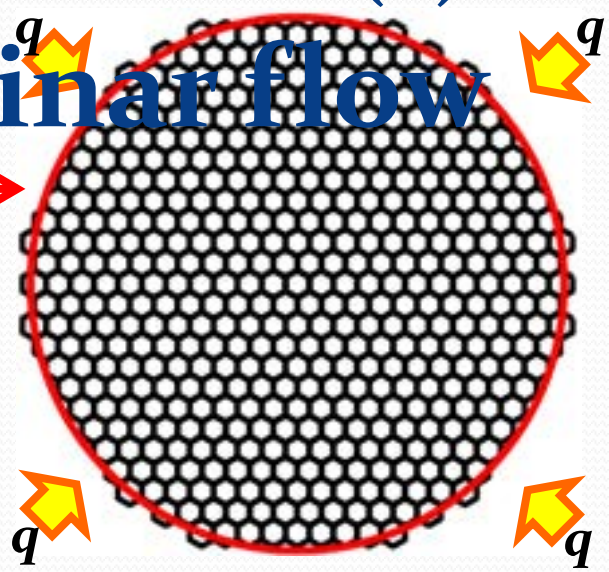
Δt_φ [s]	NI	NO	e^2_ϕ [-]	e^2_p [-]	e^∞_p [-]
1.00e-05	10001	27095	4.11e-07	4.18e-07	4.13e-07
2.00e-05	5001	20967	3.96e-06	3.99e-06	3.97e-06
1.00e-04	1001	6960	3.12e-05	3.13e-05	3.12e-05
2.00e-04	501	5793	5.98e-05	6.01e-05	5.99e-05
1.00e-03	101	2420	1.86e-04	1.87e-04	1.86e-04

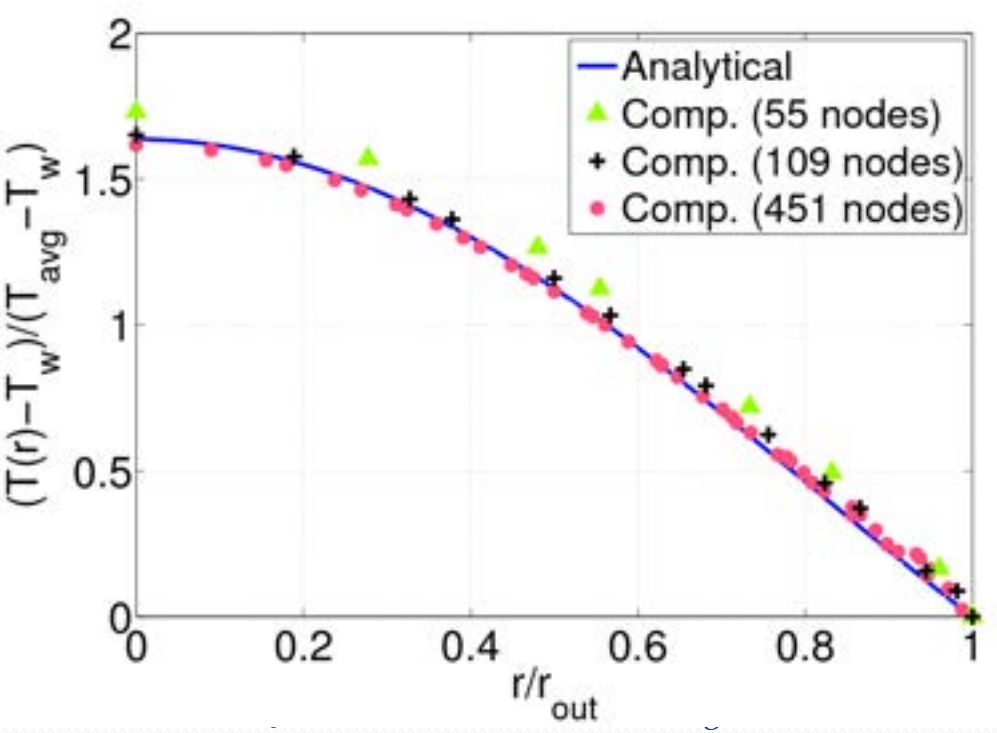
NI: total number of inversions of the flux or shape equations performed up to the point of evaluation; NO: total number of outer iterations performed up to the point of evaluation; e^2_ϕ: L_2 norm of the flux distribution; e^2_p: L_2 norm of the power distribution; e^∞_p: L_∞ norm of the total power.



Thermal-hydraulic module: verification and validation (1) - fully developed laminar flow

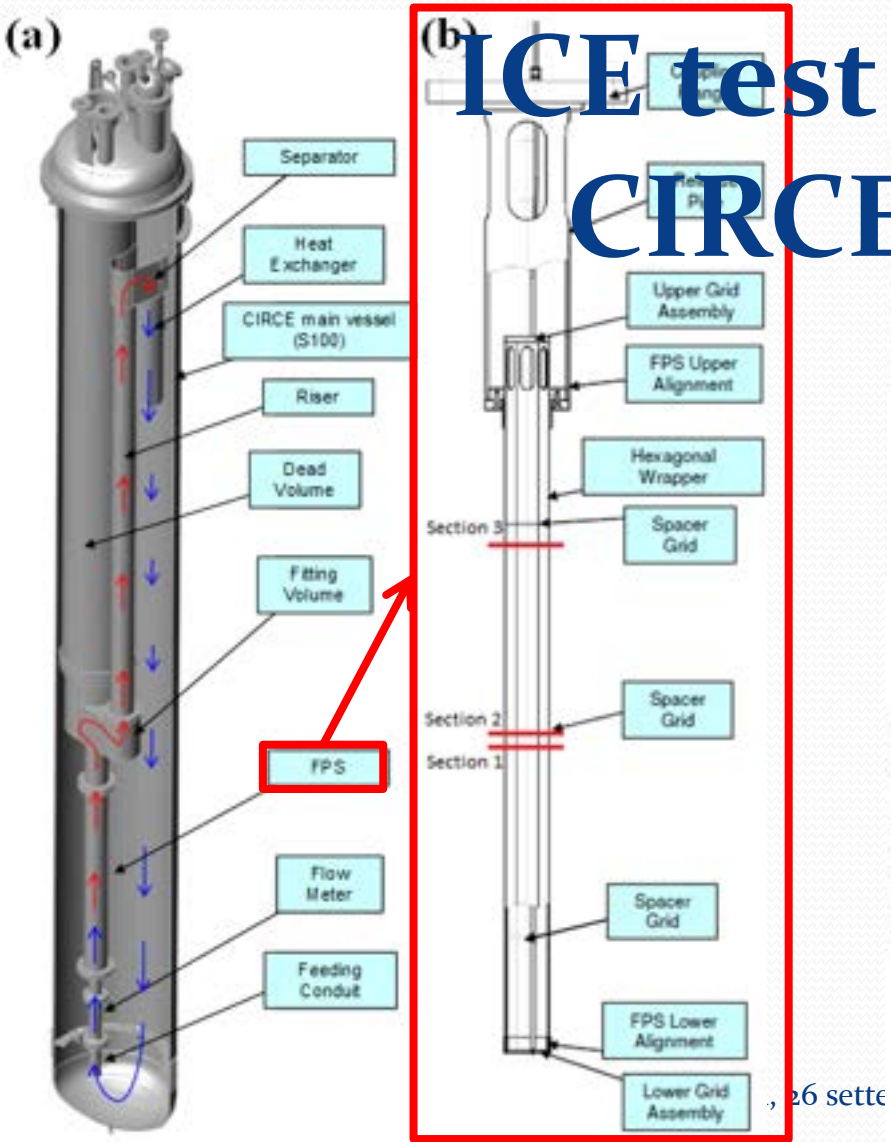
- T_{in} = 673 K
- $V_{in} = V(r)$ of a fully developed laminar flow in a circular pipe ($d \sim d_{reactor}$)
- "Perfect" thermal coupling among channels
- Prescribed heat flux q on the side wrappers



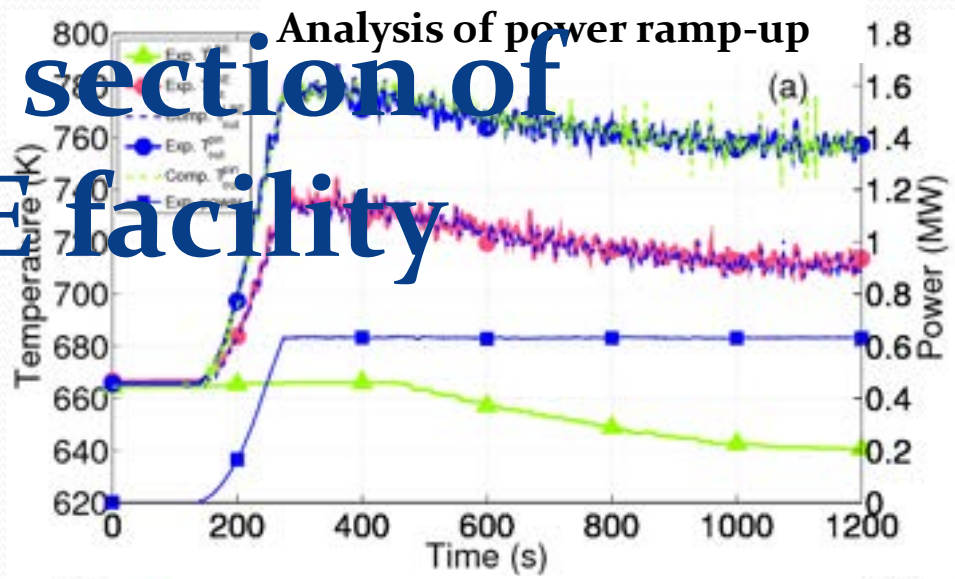


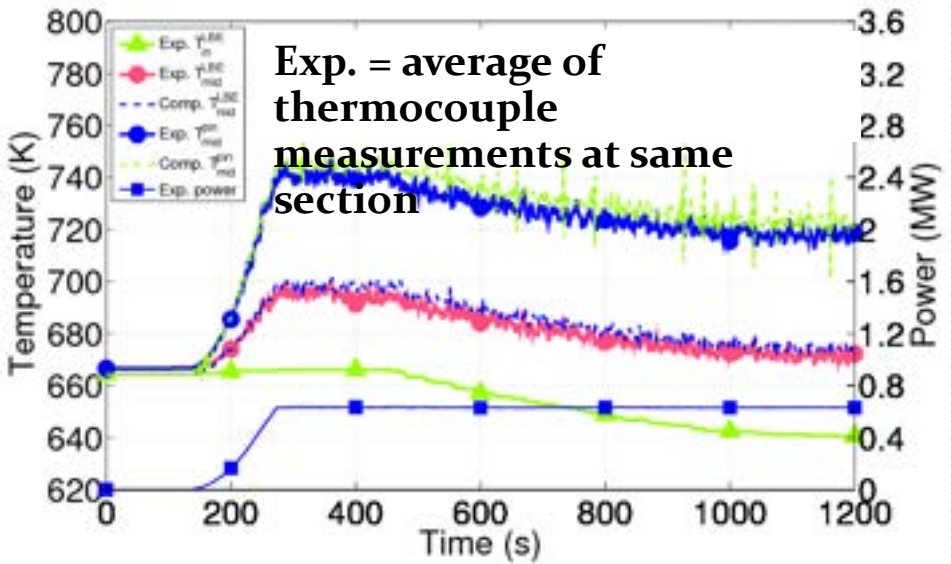
- Steady state $T_{out}(r)$ converges to analytical profile from fully developed region of a circular pipe, as number of hexagons increases
- Laminar flow assumption justified by the absence of inter-HA mixing

verification and validation (2) - ICE test section of CIRCE facility



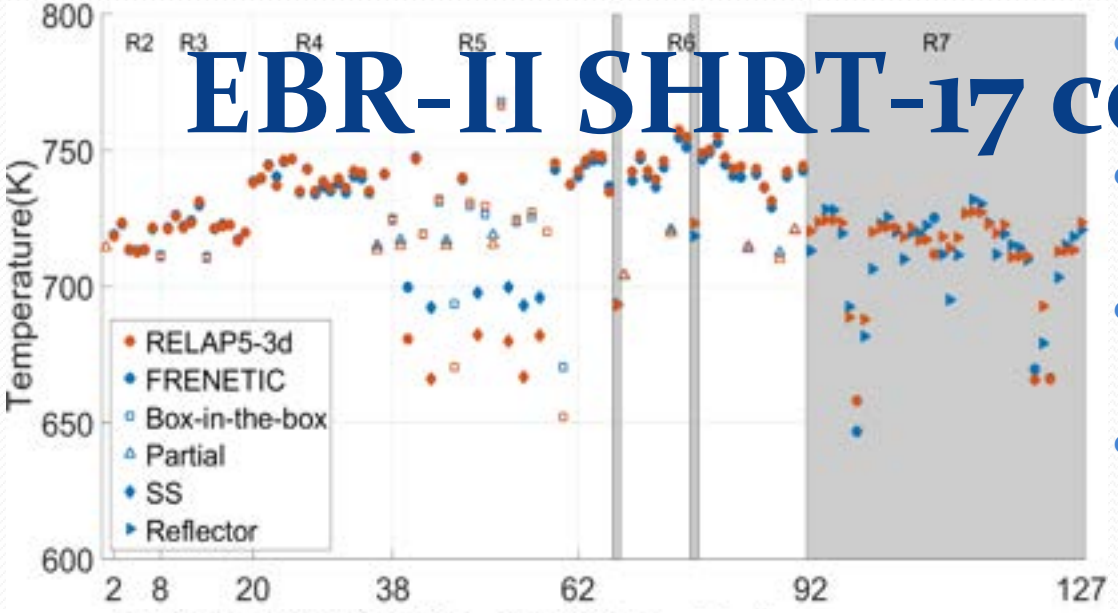
Analysis of power ramp-up



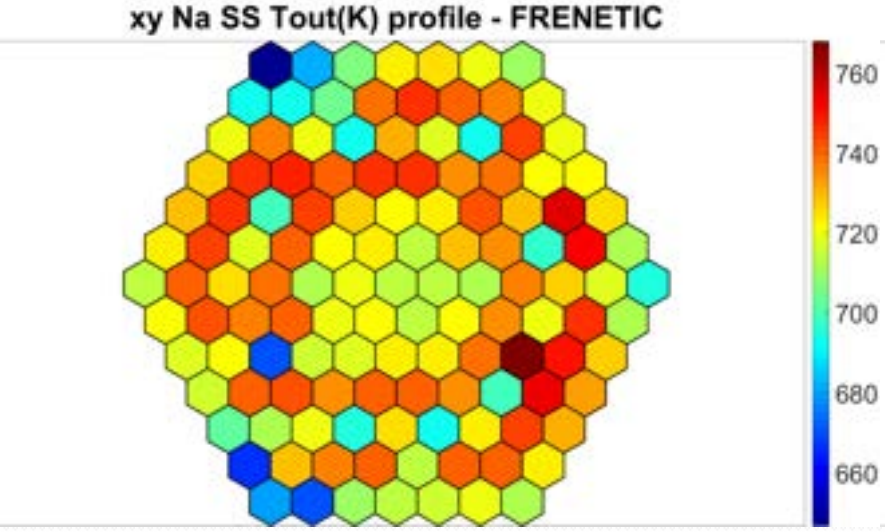


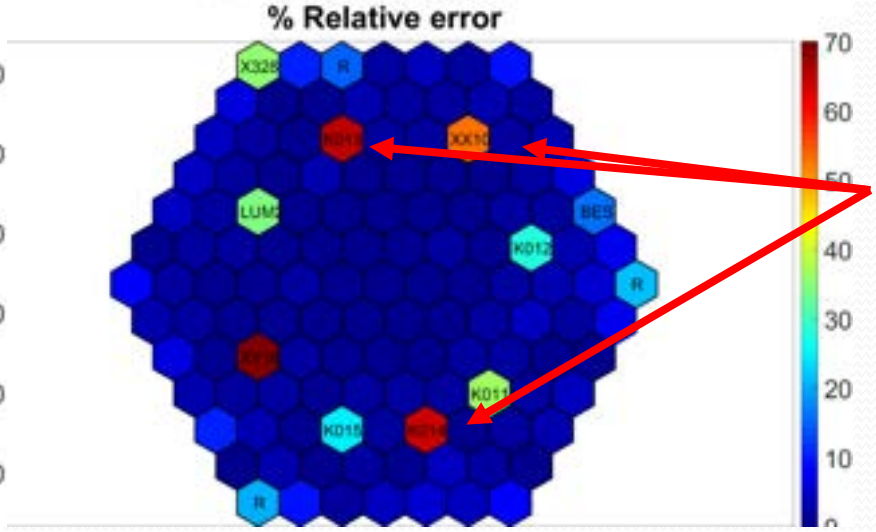
Exp. = average of thermocouple measurements at same section

Thermal-hydraulic module: verification and validation (3) - EBR-II SHRT-17 comparison

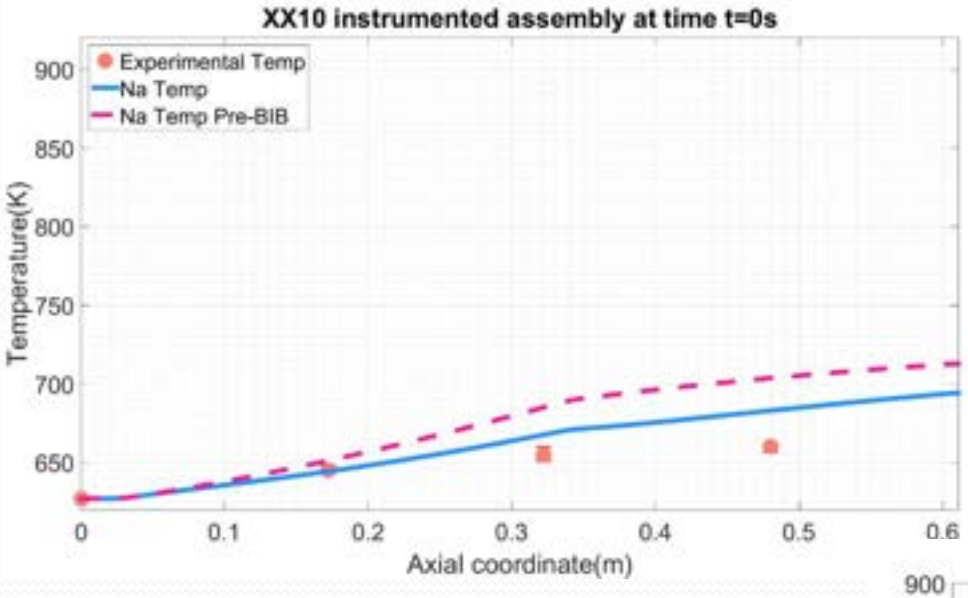


- EBR-II in SHRT-17 configuration at steady-state
- Code-to-code comparison with RELAP5-3D results of ENEA
- Relative error within 10% for hot (fuel) HA
- Highest error for cold (SS) HAs (overestimation of inter-HA exchange)

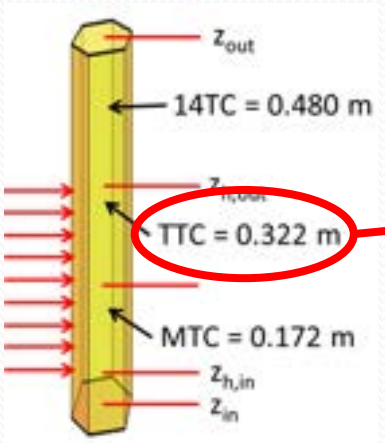


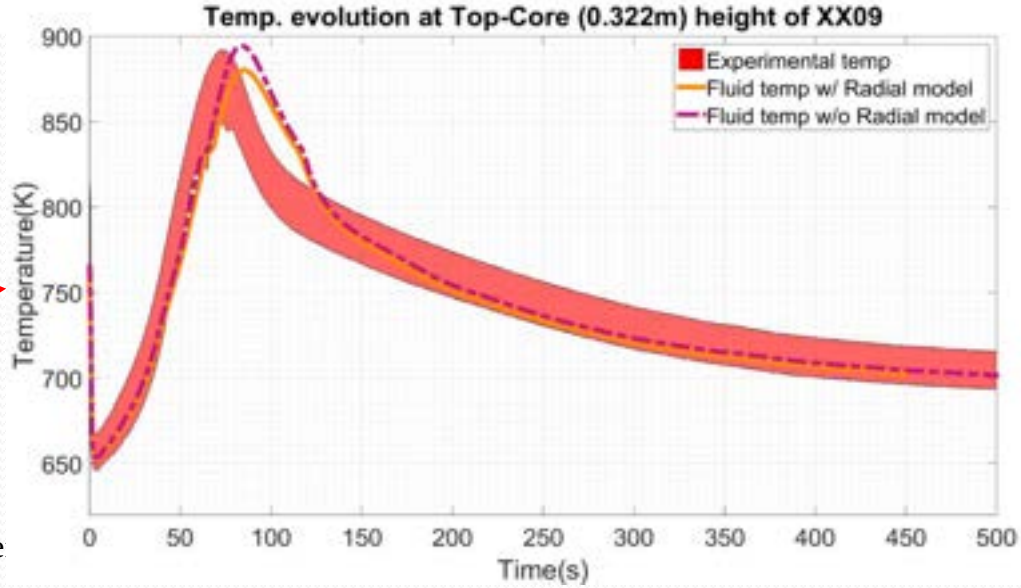


Thermal-hydraulic module: verification and validation (4) - 7 benchmark



- Improvement achieved through implementation of new models:
  - box-in-box (BIB) in steady-state
  - radial heat diffusion model in transient





Academic involvement

- Advisory group (professors and researchers)
  - R. Bonifetto, L. Savoldi, R. Zanino: thermal-hydraulics
  - S. Dulla, P. Ravetto: neutronics
- Doctoral students
  - R. Bonifetto (2011-2014): initial version of code and validation of thermal-hydraulics models
  - D. Caron (2014-2017): development of adjoint and quasi-static capabilities, photon dynamics models and validation of coupled models
  - G.F. Nallo (2017-2020): R&D on FRENETIC (thermal expansion model, QS applied to photon transport, modelling of bypass flow)
- Master students
  - D. Caron (2013): development of three-dimensional neutronics capabilities and spatial kinetics solver
  - V. Mascolino (2015): development of box-in-box channel model and radial heat conduction model

Related publications

- D. Caron, S. Dulla, and P. Ravetto. "Adaptive time step selection in the quasi-static methods of nuclear reactor dynamics," *Annals of Nuclear Energy*, **105**, pp. 266–281, 2017.
- D. Caron, R. Bonifetto, S. Dulla, V. Mascolino, P. Ravetto, L. Savoldi, D. Valerio and R. Zanino. "Full-core coupled neutronic/thermal-hydraulic modelling of the EBR-II SHRT-45R transient," *International Journal of Energy Research*, **In press (Available online)**, 2016.
- D. Caron, S. Dulla, P. Ravetto, L. Savoldi and R. Zanino. "Models and methods for the representation of decay and photon heat in spatial kinetics calculations," Proceedings of *Physics of Reactors 2016: Unifying theory and experiments in the 21st century (PHYSOR 2016)*, Sun Valley ID (USA), 1–5 May 2016, pp. 2416–2425, 2016.
- D. Caron, S. Dulla and P. Ravetto. "New aspects in the implementation of the quasi-static method for the solution of neutron diffusion problems in the framework of a nodal method," *Annals of Nuclear Energy*, **87**, pp. 34–48, 2016.
- R. Zanino, R. Bonifetto, A. Del Nevo and L. Savoldi Richard. "Benchmark and preliminary validation of the thermal-hydraulic module of the FRENETIC code against EBR-II data," *Transactions of the International Topical Meeting on Advances in Thermal Hydraulics*, Reno NV (USA), 15–19 June 2014.
- R. Bonifetto, D. Caron, S. Dulla, P. Ravetto, L. Savoldi Richard and R. Zanino. "Extension of the FRENETIC code capabilities to the three-dimensional coupled dynamic simulation of LFR," Madrid (Spain): Presentation at *16th International Conference on Emerging Nuclear Energy Systems (ICENES)*, 26–30 May 2013.
- R. Bonifetto, S. Dulla, P. Ravetto, L. Savoldi Richard and R. Zanino. "A full-core coupled neutronic/thermal-hydraulic code for the modeling of lead-cooled nuclear fast reactors," *Nuclear Engineering and Design*, **261**, pp. 85–94, 2013.
- R. Zanino, R. Bonifetto, A. Ciampichetti, I. Di Piazza, L. Savoldi Richard and M. Tarantino. "Validation of the thermal-hydraulic model in the FRENETIC code against data from the ENEA-CIRCE experiment," *Transactions of the American Nuclear Society*, **107**, pp. 1395–1398, 2012.
- R. Bonifetto, S. Dulla, P. Ravetto, L. Savoldi Richard and R. Zanino. "Progress in multi-physics modeling of innovative lead-cooled fast reactors," *Transactions of Fusion Science and Technology*, **61**, pp. 293–297, 2012.

WORKSHOP TEMATICO

LFR-GEN IV: STATO ATTUALE DELLA TECNOLOGIA E PROSPETTIVE DI SVILUPPO

ADP ENEA-MSE (PAR2016-LP2)



Contributo di POLIMI al PAR-2016

E. Macerata, M. Mariani, M. Cerini, S. Cervino, L. De Luca, M. Giola
Laboratorio di Radiochimica e Chimica delle Radiazioni

26 Settembre 2017, Bologna

LP2.A3_a Fuel-coolant chemical interactions in LFR systems

Ongoing implementation of a
Database of thermochemical data
of interest for LFR



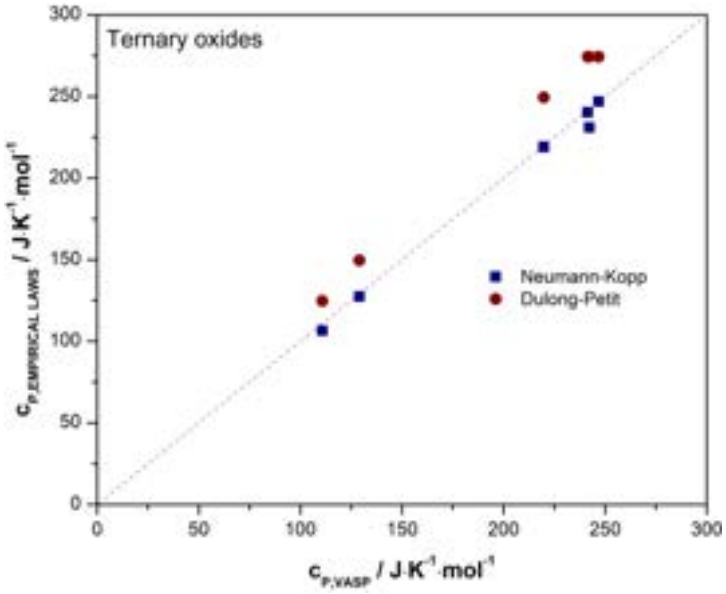
- ✓ **Literature Update:** New experimental data from databases, handbooks and scientific literature
- ✓ **Computational *approach*:**
  thermochemical data estimation by DFT-GGA simulations applied to binary and ternary oxides and intermetallic compounds containing U, FPs, Pb and O
- ✓ **Experimental *approach*:**
  measurements of heat capacity as function of T
  Investigations of reactivity of some oxides in liquid lead

LP2.A3_a Fuel-coolant chemical interactions in LFR systems

Computational activities:

Thermodynamic properties for ternary oxides: An/FPs – O – Pb

- Negative formation enthalpy for all the investigated compounds
- No experimental data → hard to evaluate the accuracy of the computational approach
- Comparison of the heat capacity values obtained by DFT-GGA simulations with the data calculated by Neumann-Kopp and Dulong-Petit laws



✓ Good agreement with heat capacity values obtained with Dulong-Petit law

✓ Excellent agreement with heat capacity values obtained with Neumann-Kopp law

M.Cerini et al., ***NuFuel2017 - Second Workshop on Research into Nuclear Fuel and cladding in Europe***, 4-6 September 2017, Lecco, Italy. Oral presentation

LP2.A3_a Fuel-coolant chemical interactions in LFR systems

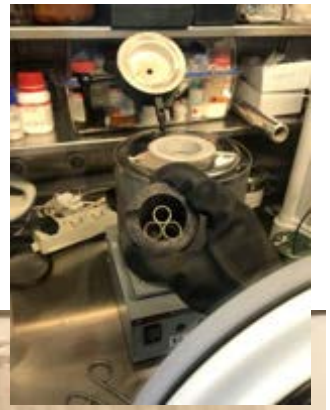
Computational activities:

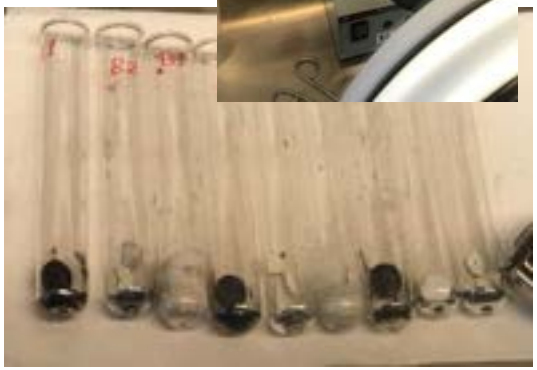
- Investigations on computational thermodynamics
  - Increasingly important for scientists and materials producers
- CALPHAD method
  - based on minimization of the Gibbs free energy of the system
  - enable the modeling of thermochemical properties and phase diagrams
  - originally developed for metallic systems, thereafter adopted for inorganic systems
  - enable to study multi-phase and multi-component systems by extrapolation of the description of the lower component subsystems
  - Successfully used for describing diffusion mobilities, molar volumes, elastic properties and thermal conductivity
  - Software: old free source codes, a number of commercial software packages (FactSage, Thermo-Calc), recent development of free CALPHAD software (OpenCalphad)
  - Database: specific commercial databases in continuous developemnt in order to improve accuracy and reliability

Hickel et al., *Phys. Status Solidi B* **251**, 1, 9-13 (2014)
Kattern et al., Tecnol. Metal. Mater. Miner., 13, 3-15 (2016)
Kattern et al., *Calphad*, 24, 55-94 (2000)

LP2.A3_a Fuel-coolant chemical interactions in LFR systems

Experimental activities





- Interaction studies on different **oxide-Pb** systems:
  - Preliminary characterization of reagents by XRD, DSC and EDX
  - Preparation of pellets of SrO, ZrO_2, La_2O_3 and CeO_2
  - Thermal treatment at 500-550°C under argon atmosphere
  - Reaction time of 3-7 hours

- Post-treatment characterization:
  - New phase identification by XRD on powder or pellet
  - Thermal analyses by DSC on powder
  - ICP-MS measurements of Pb
  - Investigations on pellet cross section by SEM-EDS
    - Sample preparation under evaluation

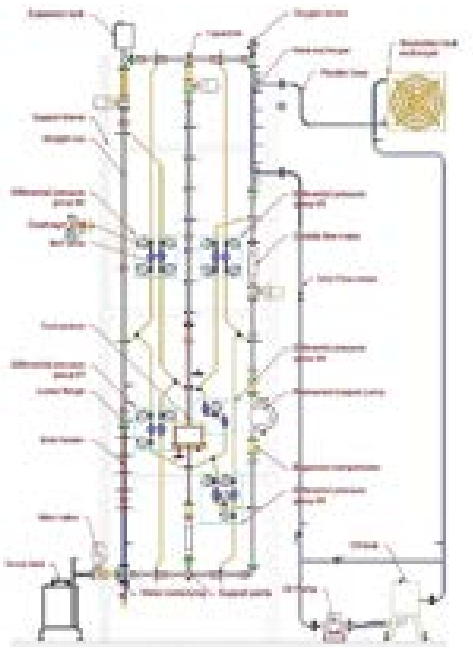


Vigier et al., *Journal of Nuclear Materials,* 467 (2015), 840-847.

Validation of FEM-LCORE/CATHARE by TALL-3D experimental tests

A. Cervone[2], **L. Chirco**[1]
R. Da Vià[1], **S. Manservisi**[1]

Alma Mater Studiorum - Bologna[1]
Centro Ricerche ENEA - Bologna[2]



Summary

SALOME platform development for LFR

TALL-3D Facility and computational test

1D-CATHARE simulation and experimental results.

3D-test section

3D-1D coupling simulation

Conclusions



Sommario

SALOME platform development for LFR

TALL-3D Facility and computational test

1D-CATHARE simulation and experimental results.

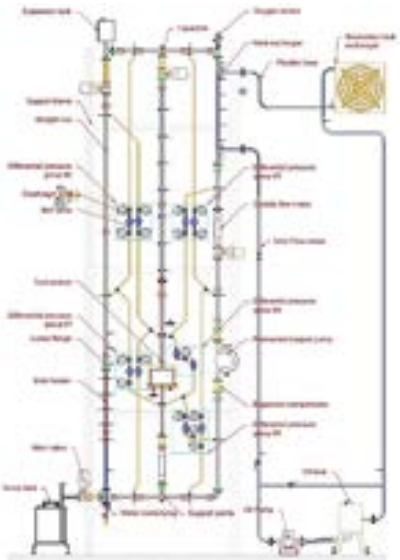
3D-test section

3D-1D coupling simulation

Conclusions

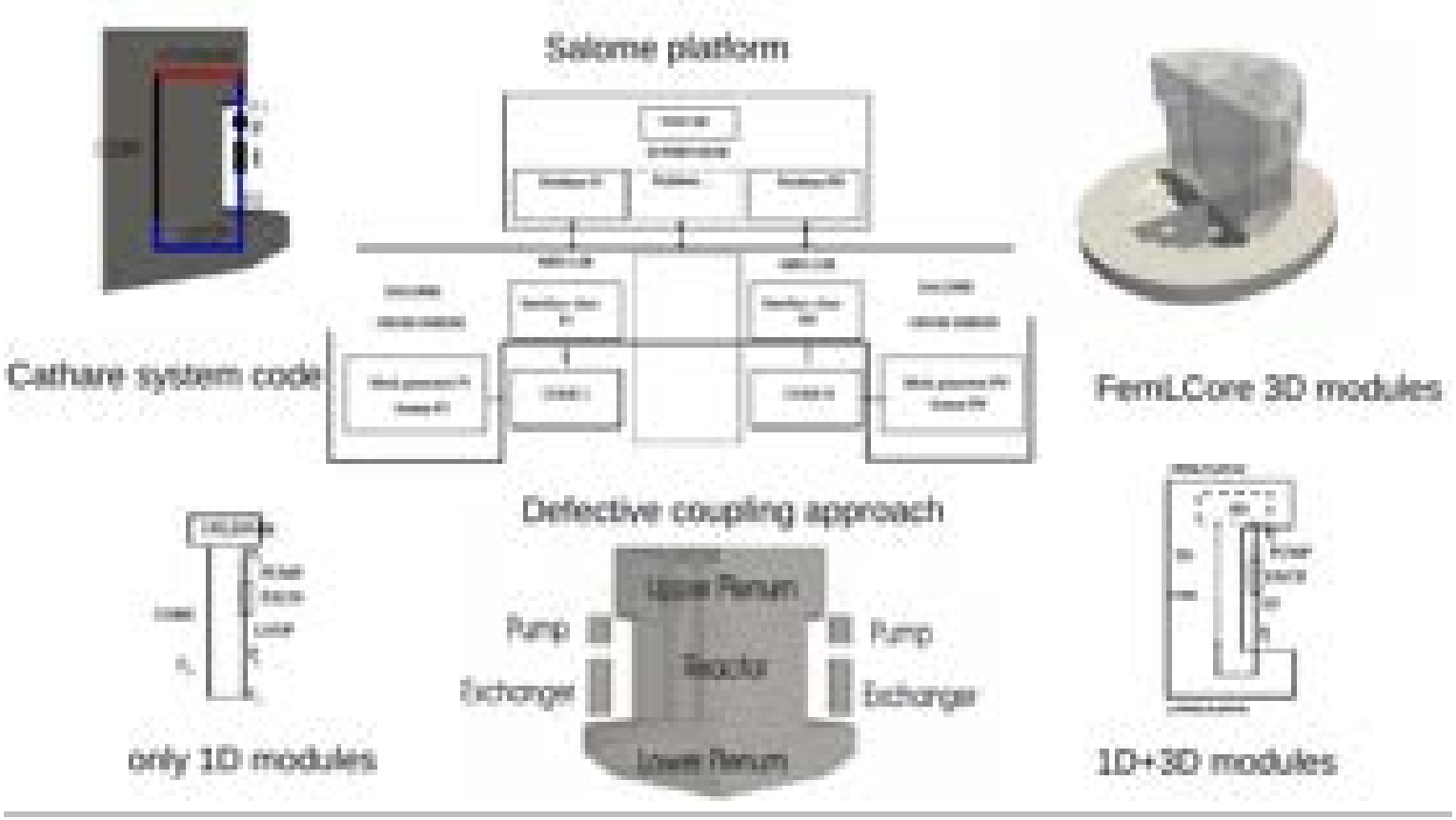


Computational platform ENEA-UNIBO (LFR)



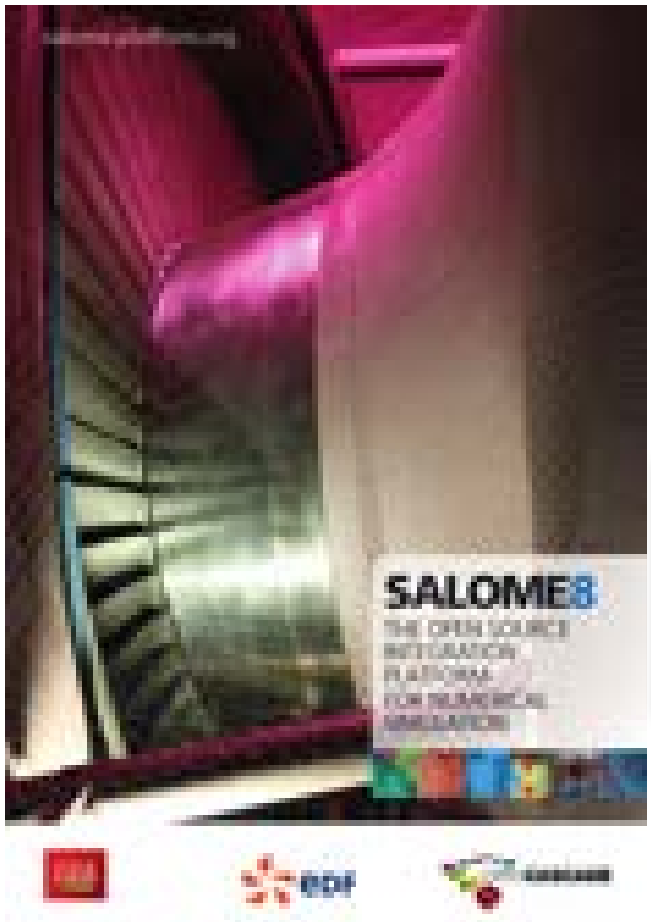
fisica	scala 1	scala 2
Thermalhydraulics	CFD-porous 3D	system 1D
open-src CEA-EDF open-src	FEMLCORE (FEM) MC/TRIOCFD OPENFOAM (FV) ?	FEMuS (FEM) CATHARE OPENFOAM (FV) ?
Neutronics	Trasport	2-5 group diffusion
open-src CEA-EDF	DRAGON (assembly)	DONJON (bundle) APOLLO
Structural	3D structural	1D beam
open-src CEA-EDF open-src	FEMuS (FEM) Code_Aster OPENFOAM (FV)	FEMuS (FEM) Code_Aster OPENFOAM (FV) ?
Two-phase	interface	two-fluid model
open-src CEA-EDF open-src	FEMuS (FEM) TRIOU NEPTUNE OPENFOAM (FV) ?	FEMuS (FEM) CATHARE

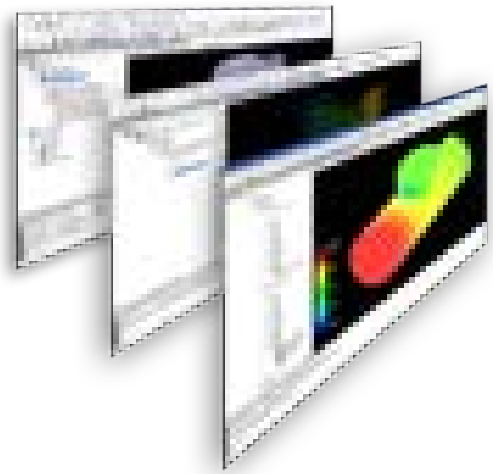
FEMLCORE-SALOME-CATHARE platform (LFR)

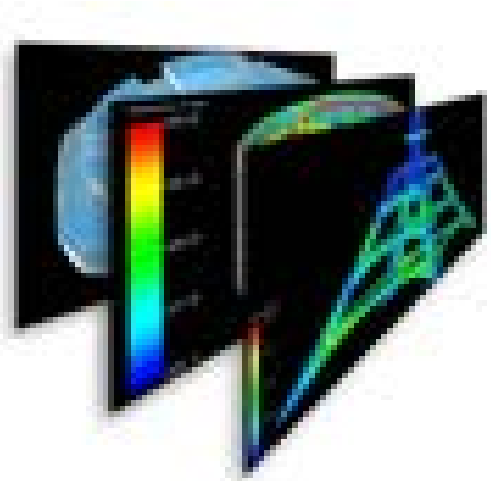


SALOME development

SALOME opensource $\longleftrightarrow$ CAD-MESH-VISUALIZATION





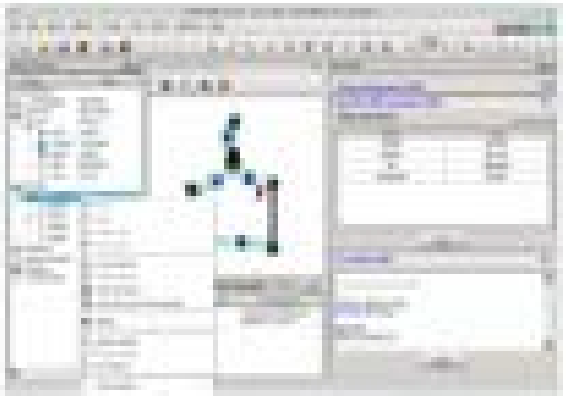


VISUALIZATION(PARAVIEW) CAD(GEOM) MES GEN(SMESH)

CATHARE development

CATHARE interface $\longleftrightarrow$ SALOME





CATHARE Mesh generator (GUI)



Class interface CATHARE-MED

FEMLCORE development:

FEMLCORE interface $\longleftrightarrow$ SALOME



void	[illegible]	[illegible]
void void	[illegible] [illegible]	[illegible] [illegible]
void void	[illegible] [illegible]	[illegible] [illegible]
void void	[illegible] [illegible]	[illegible] [illegible]
double MEDCouplingFieldDouble *	[illegible] [illegible]	[illegible] [illegible]

Commandi per modificare i dati in/out FemLCore

Reattore LF



Generatore di mesh per CATHARE sulla Piattaforma SALOME

MEDCouplingUMesh * MEDCouplingUMesh * MEDCouplingFieldDouble *	[illegible] [illegible] [illegible]	[illegible] [illegible] [illegible]
int int * int *	[illegible] [illegible] [illegible]	[illegible] [illegible] [illegible]

Mesh e connectivita' per le interfacce 3D/1D 2D/1D 3D/2D

Core

Upper Plenum



Sommario

SALOME platform development for LFR

TALL-3D Facility and computational test

1D-CATHARE simulation and experimental results.

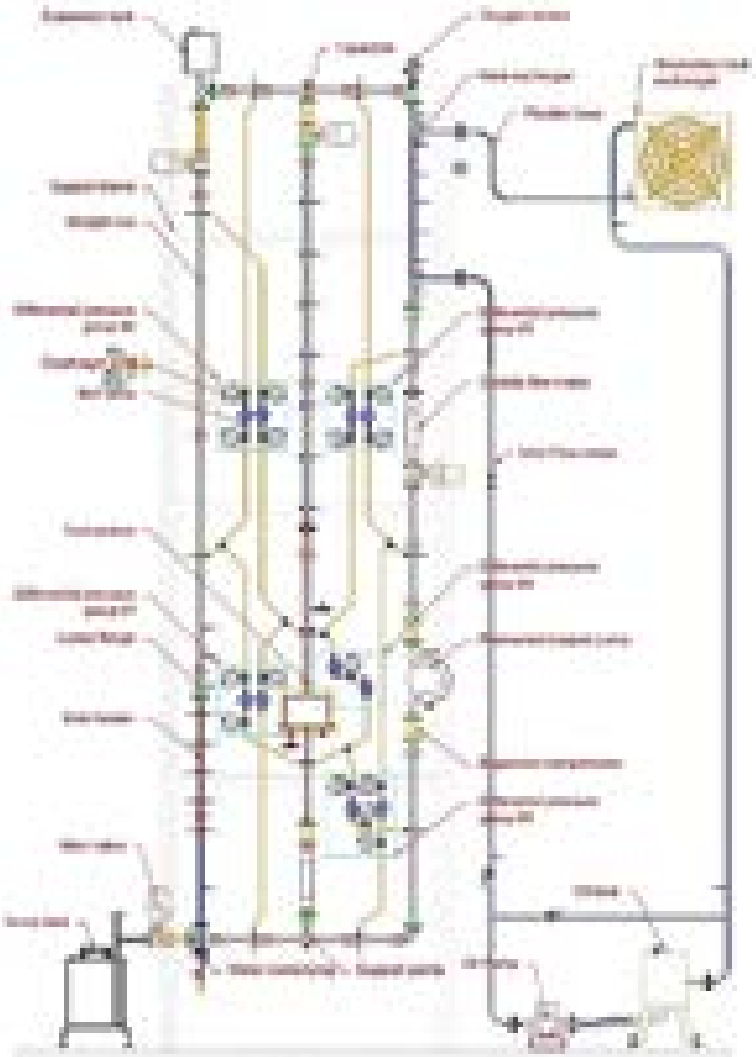
3D-test section

3D-1D coupling simulation

Conclusions



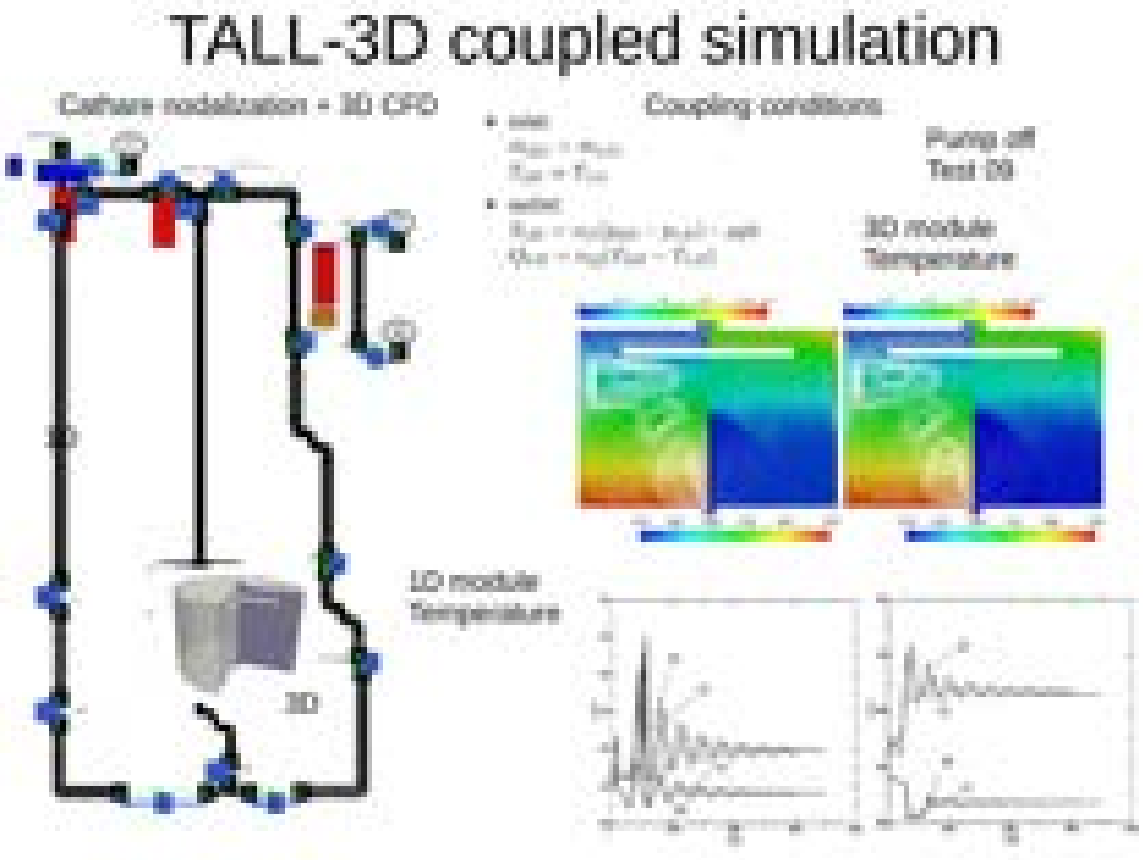
TALL-3D Facility



Primary loop (LBE):
1D loops (3)
3d- Test section (1)
(MH) main heater (2)
(EPM) Electromagnetic Pump
(HX) Heat exchanger
Secondary loop (oil):
Pump-Tank
Secondary HX
Working conditions:
Pressure: 0.7MPa
Temperature: 400-500^oC
flow rate (LBE)= 5Kg/s; vel 1.7m/s
heat removal=40 kW (10kw)
flow rate (oil)= 50 l/min;

Defective coupling FEMLCORE 3D + CATHARE 1D

Defective coupling: overlapping mesh

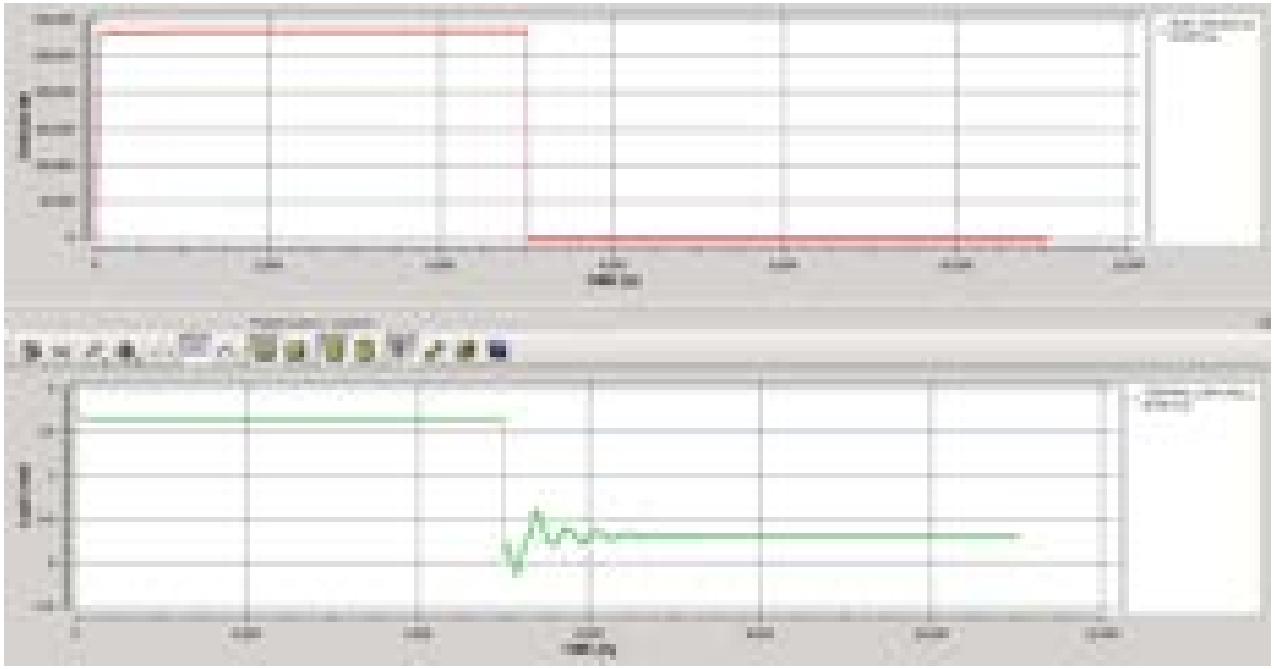


- inlet:
  $\dot{m}_{3D} = \dot{m}_{1D}$,
  $T_{3D} = T_{1D}$
- outlet:
  $S_{1D} =$
  $\alpha_S(p_{3D} - p_{1D})$
  $Q_{1D} =$
  $\alpha_Q(T_{3D} - T_{1D})$

COUPLING FEMLCORE 3D + CATHARE 1D

Test 9: flowrate at the 3D section

Test 9: pump failure -> Natural convection



Sommario

SALOME platform development for LFR

TALL-3D Facility and computational test

1D-CATHARE simulation and experimental results.

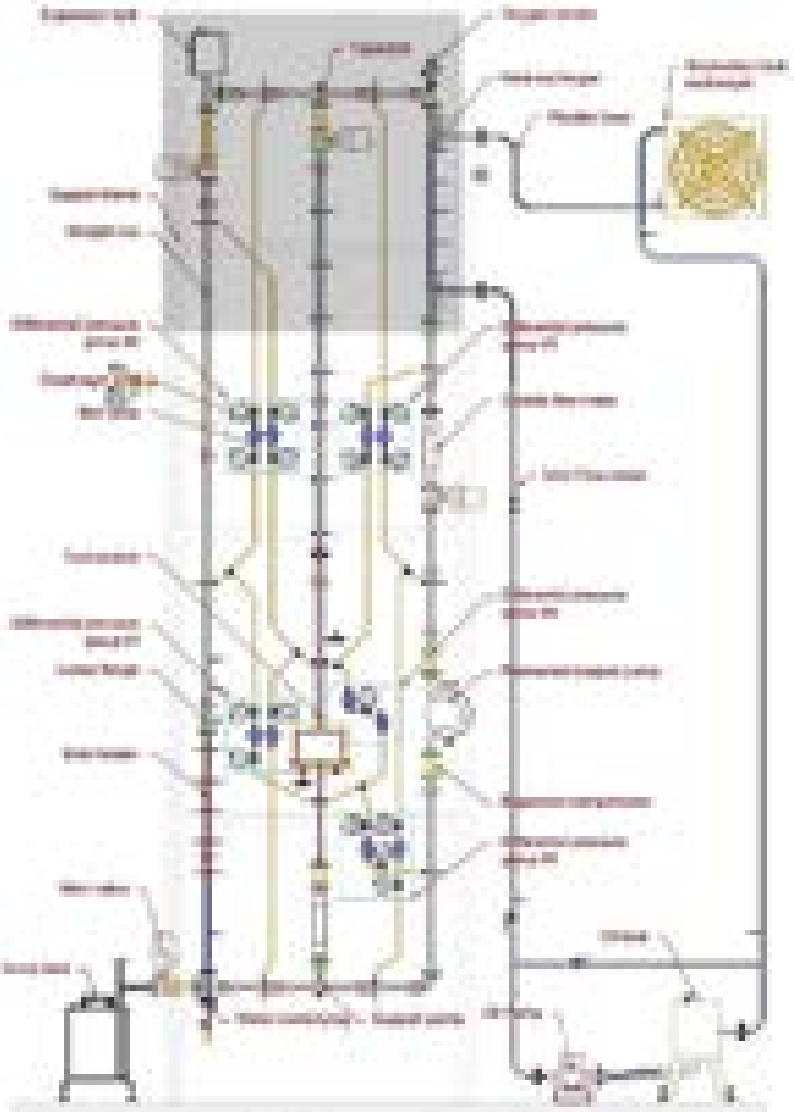
3D-test section

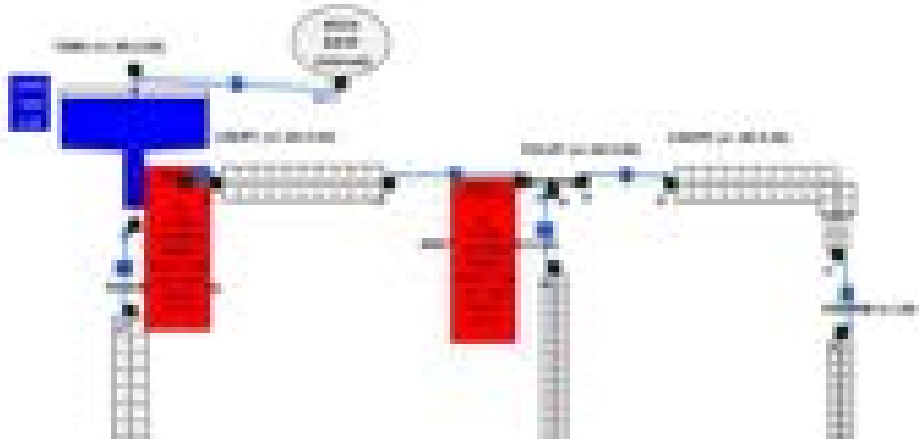
3D-1D coupling simulation

Conclusions

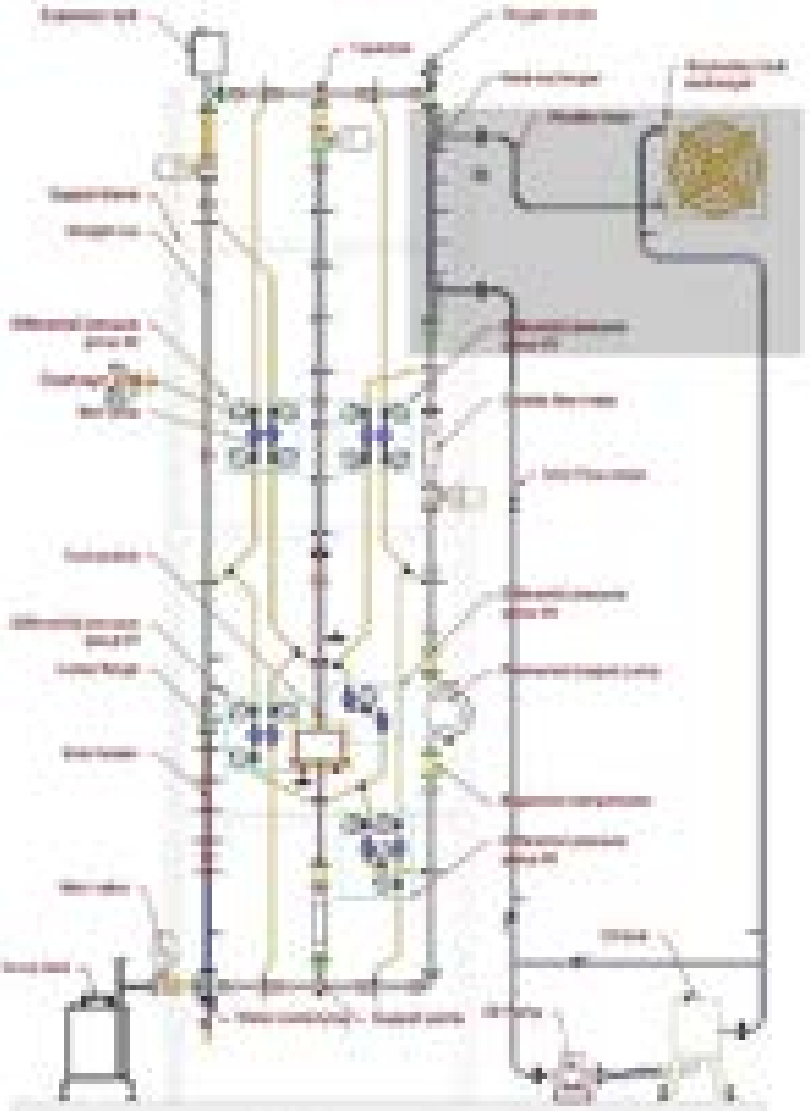


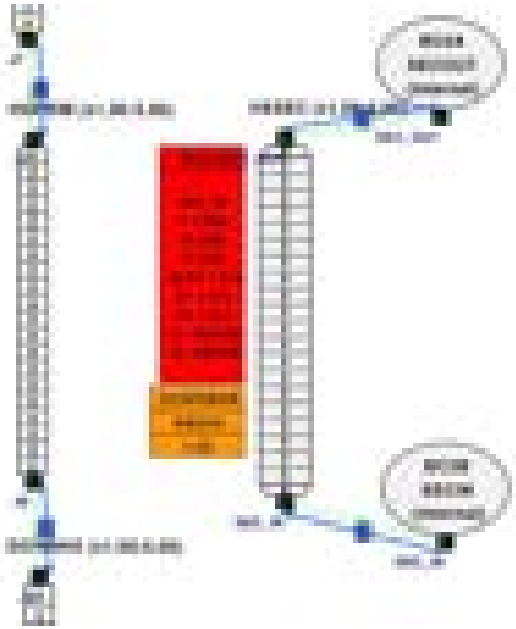
Cathare nodalization



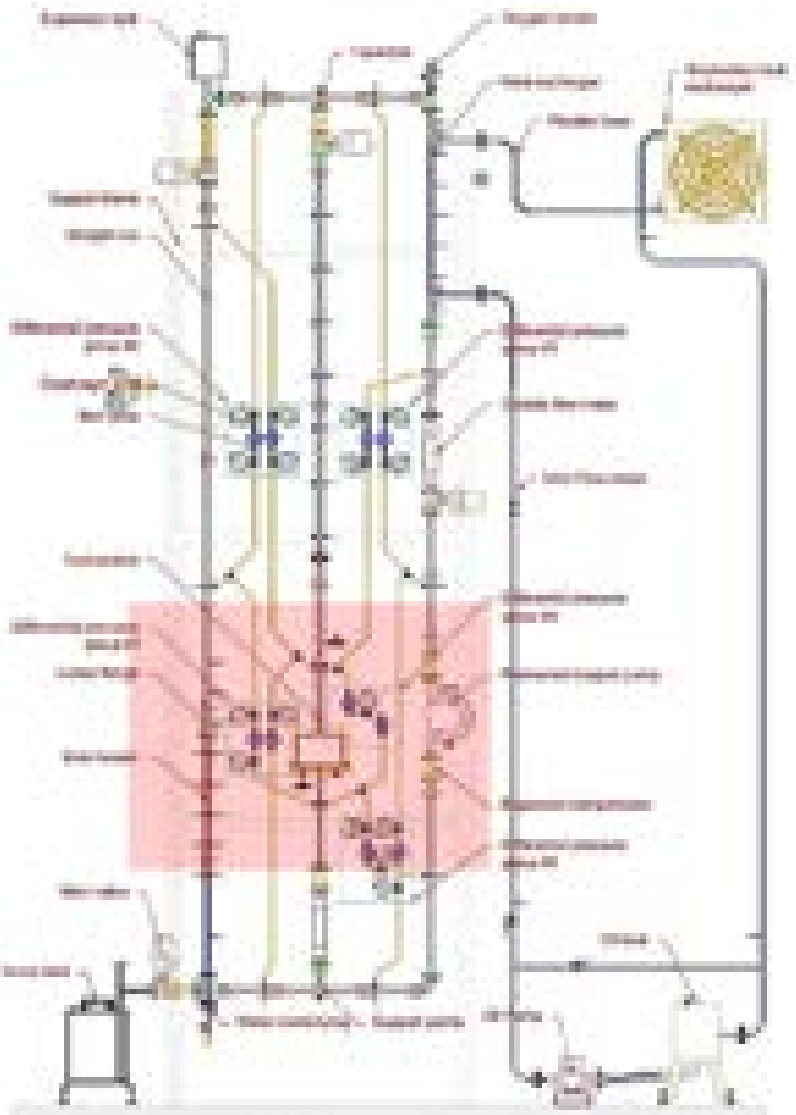


Cathare nodalization (heat exchanger)

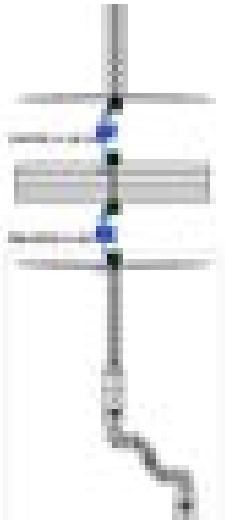




Cathare nodalization (test section and pump)

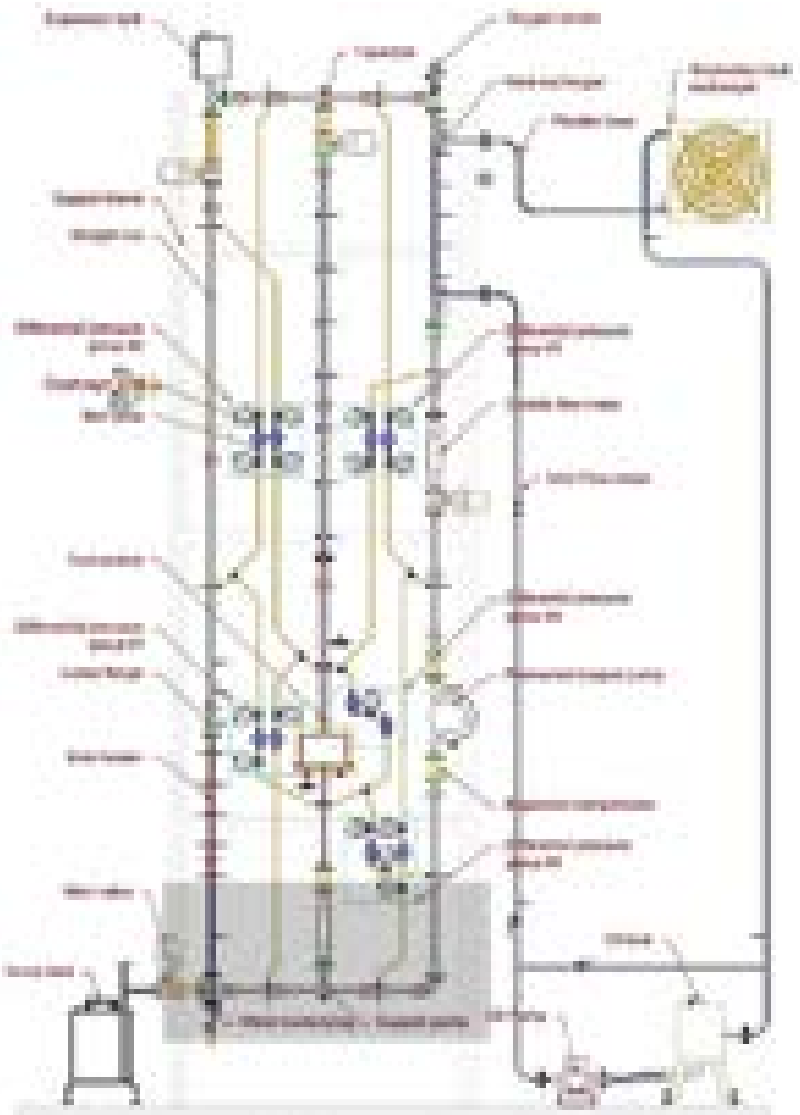


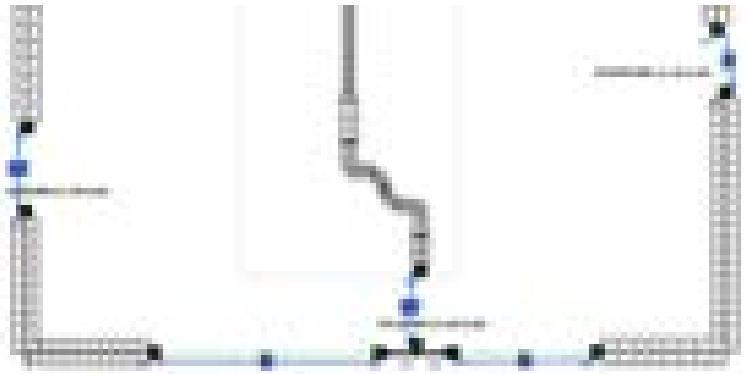




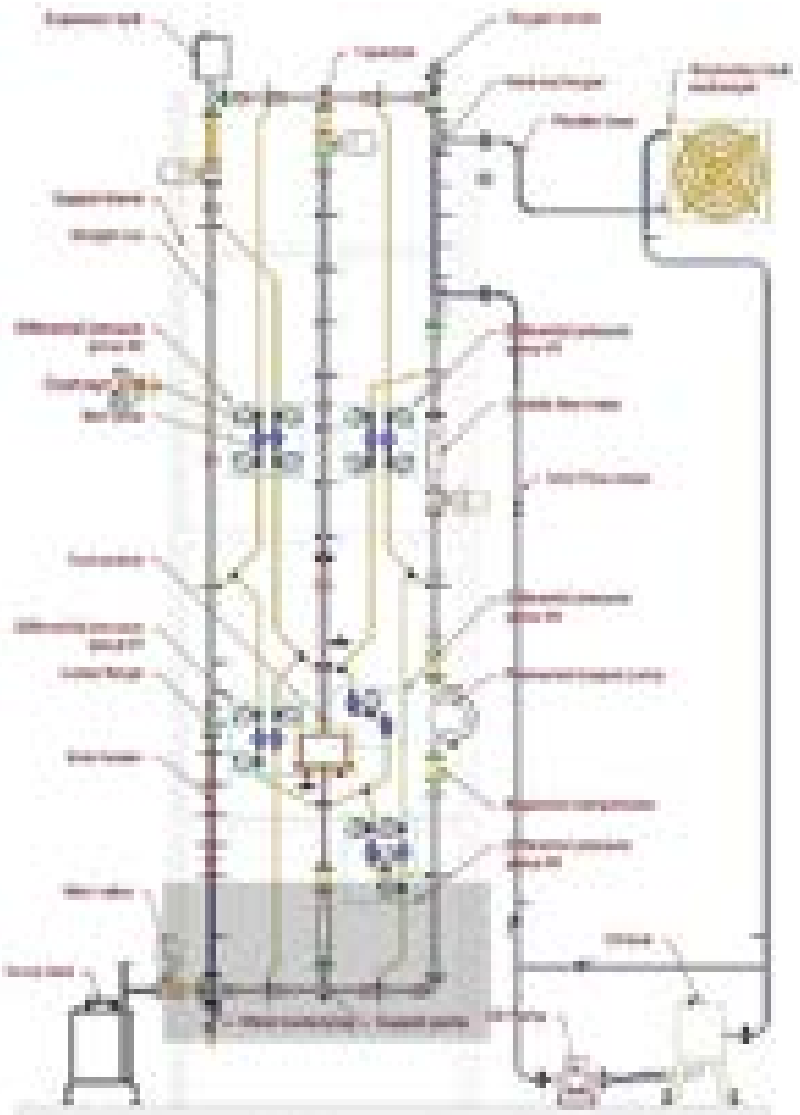


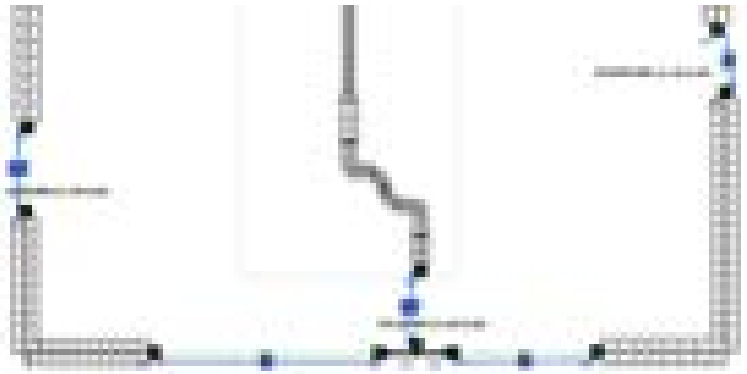
Cathare nodalization (bottom)



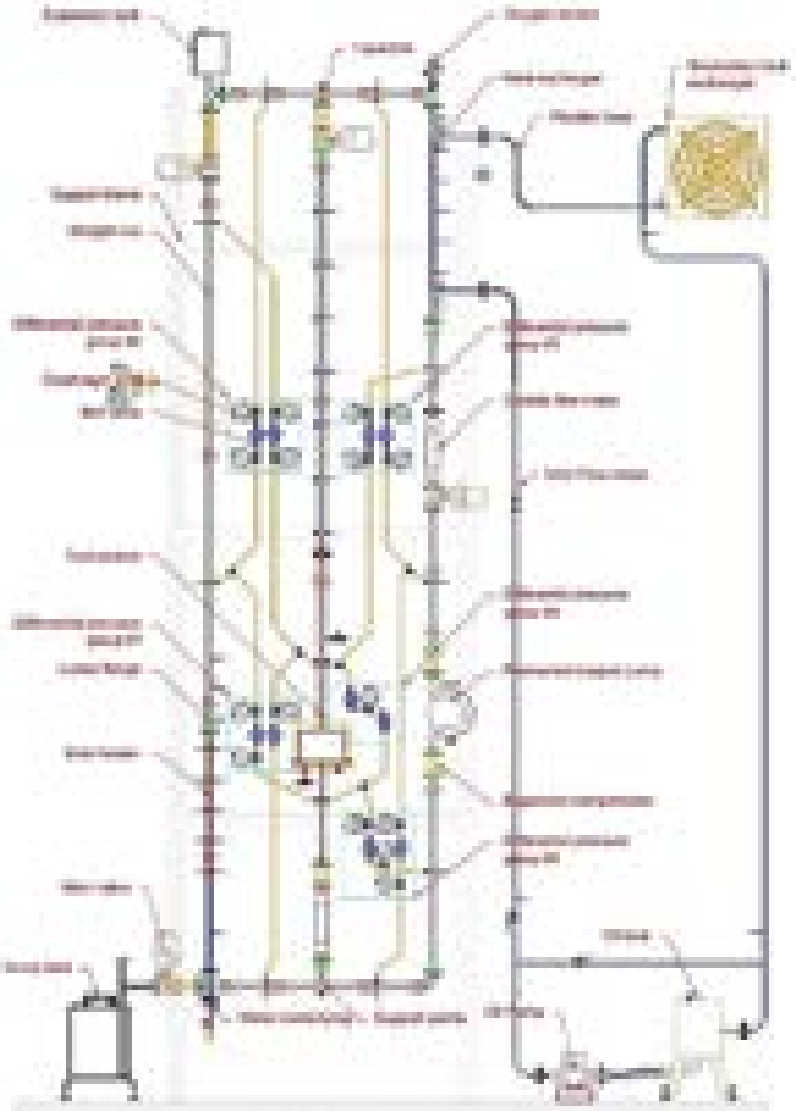


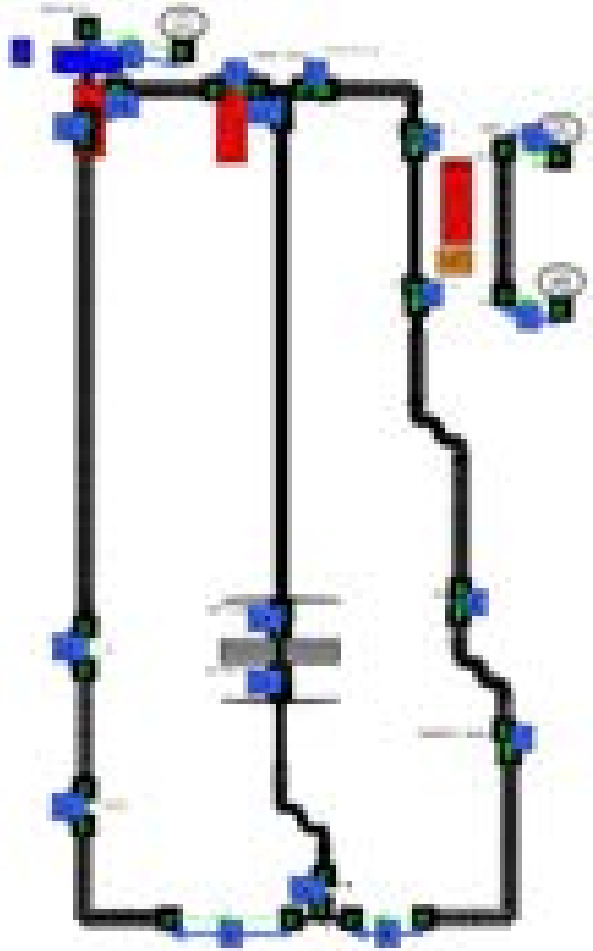
Cathare nodalization (bottom)



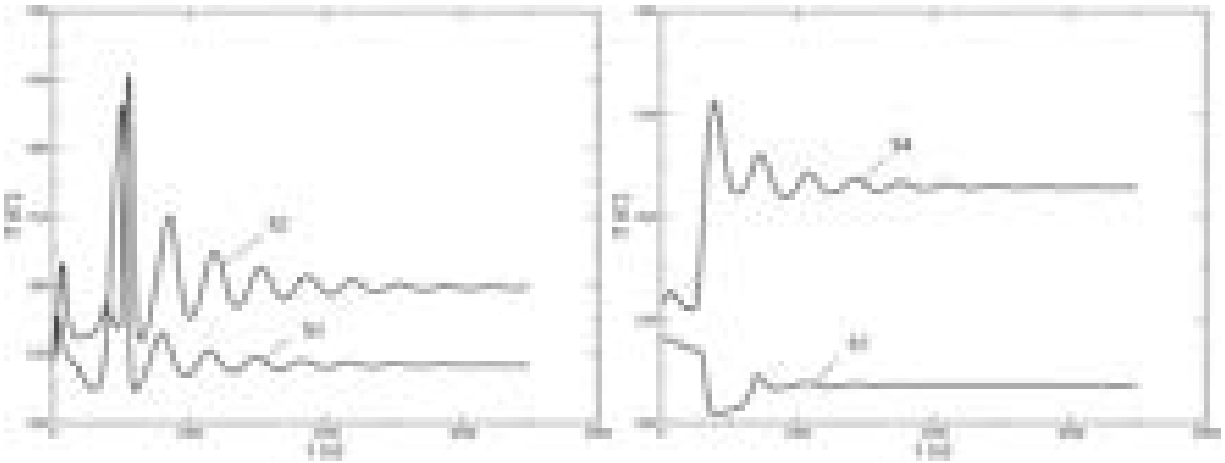


Cathare nodalization

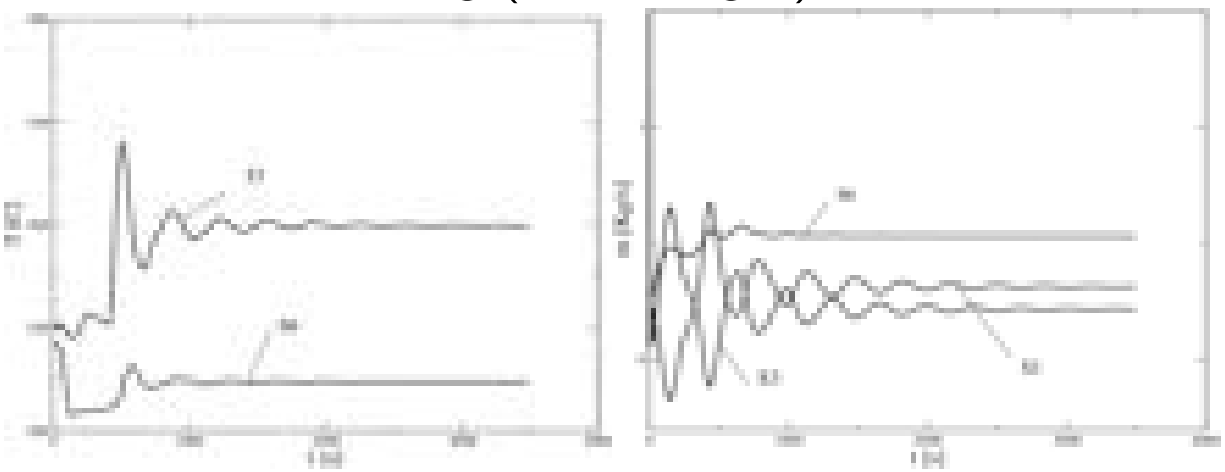




Initial conditions for 1D-CATHARE simulation



Computed temperature at points $S1$-$S2$ of the left leg (on the left) and at $S3$-$S4$ of the central leg (on the right) as a function of time t.



Computed temperature at the points $S5$-$S6$ of the right leg (on the left) and fluid flow rate at $S1$ (left), $S3$ (central) and $S6$ (right leg) (on the right) as a function of time t.

1D-CATHARE initial state condition

	Initial Condition	Unit
T BELOW3D	241.45	$^{\circ}C$
T ABOVE3D	259.81	$^{\circ}C$
T LINUP2	251.76	$^{\circ}C$
T PUMP	242.38	$^{\circ}C$
T COR	244.16	$^{\circ}C$
T RESERVE	248.33	$^{\circ}C$
MH rod power	2578	W
3D vessel power	4833	W
LBE mass flowrate	4.2750	kg/s
Oil inlet temperature	61.1	$^{\circ}C$
Oil outlet temperature	82.6	$^{\circ}C$
Oil mass flowrate	0.1435	$[kg/s]$

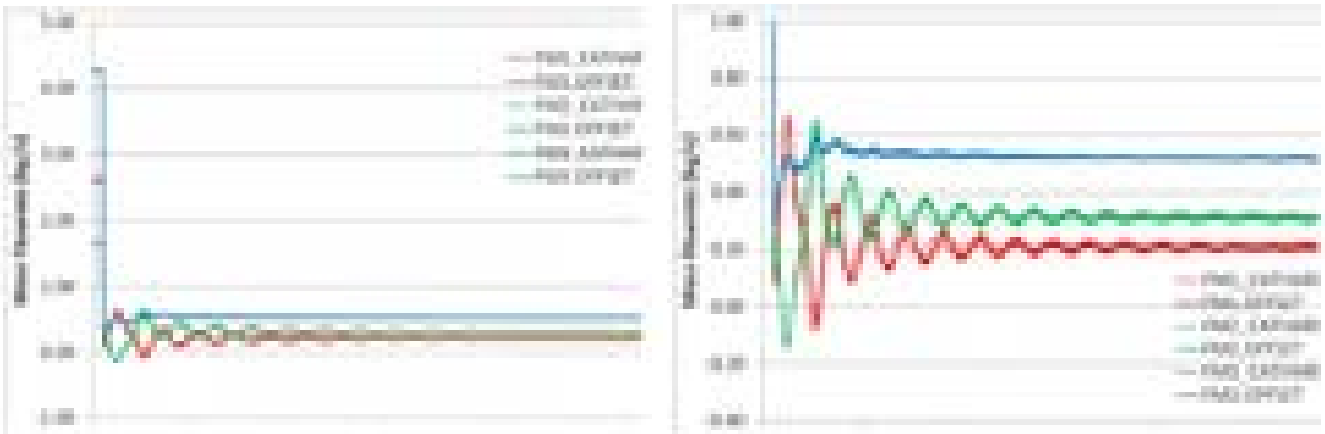
	Final Condition	Unit
T BELOW3D	218.01	$^{\circ}C$
T ABOVE3D	314.93	$^{\circ}C$
T LINUP2	299.41	$^{\circ}C$
T PUMP	223.53	$^{\circ}C$
T COR	241.89	$^{\circ}C$
T RESERVE	298.58	$^{\circ}C$
MH rod power	2578	W
3D vessel power	4833	W
LBE mass flowrate	0.53054	kg/s
Oil inlet temperature	61.2	$^{\circ}C$
Oil outlet temperature	80.6	$^{\circ}C$
Oil mass flowrate	0.1404	kg/s

Initial state condition for the one-dimensional Problem C. The initial condition satisfies the steady state equation. Final state condition for the one-dimensional code (CATHARE) solved without coupling.



1D-uncoupled CATHARE simulation

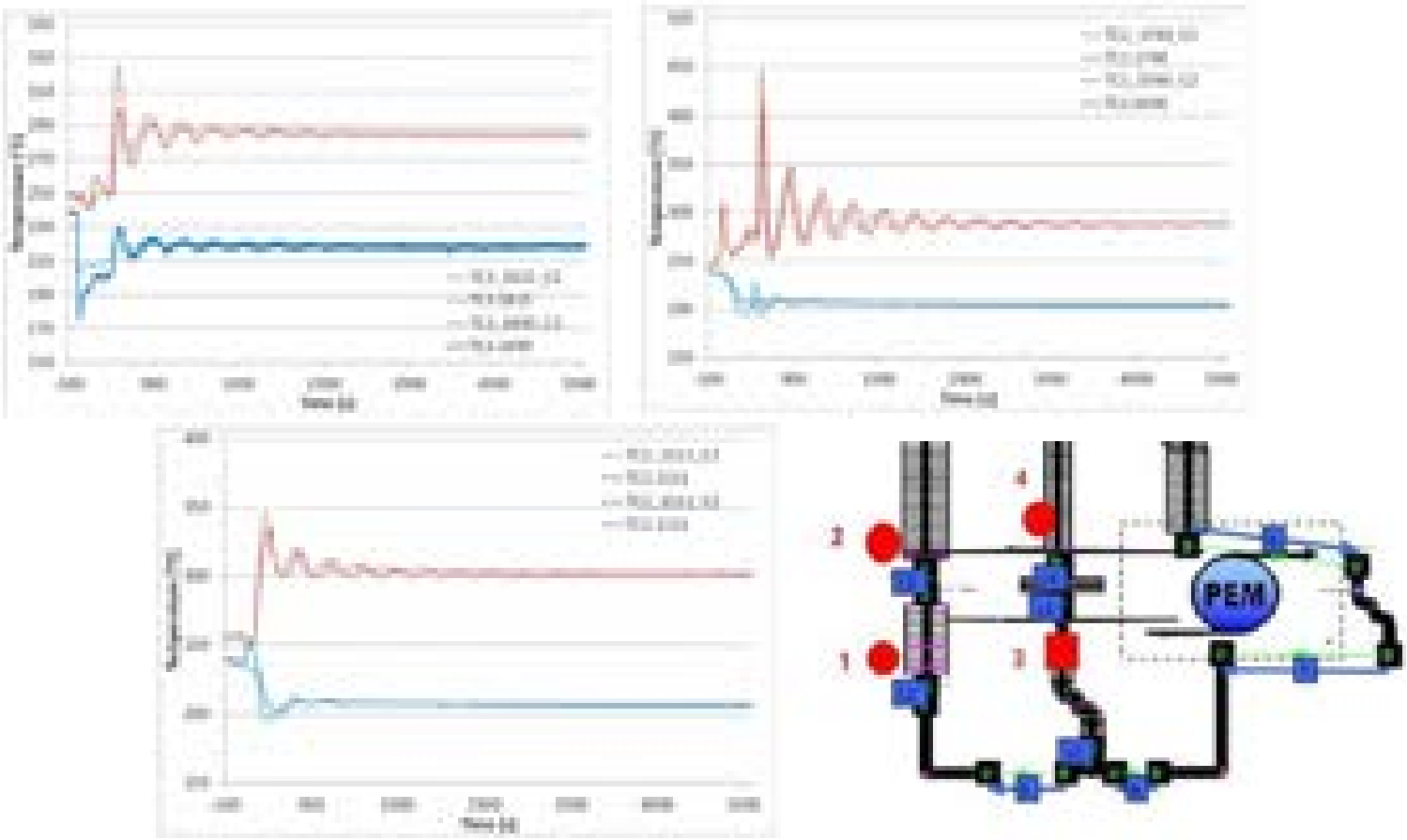
Experimental and computed mass flow rate on different legs



Experimental and computational mass flow rate for the left (FM3), right (FM1) and central leg (FM2).

1D-uncoupled CATHARE simulation

Experimental and computed temperature on different legs



Experimental and computed temperature at the thermocouple points TC34490, TC35615 (left leg), at TC10346, TC11740 (right leg) and at the thermocouple points TC1211, TC22111 (central).

Sommario

SALOME platform development for LFR

TALL-3D Facility and computational test

1D-CATHARE simulation and experimental results.

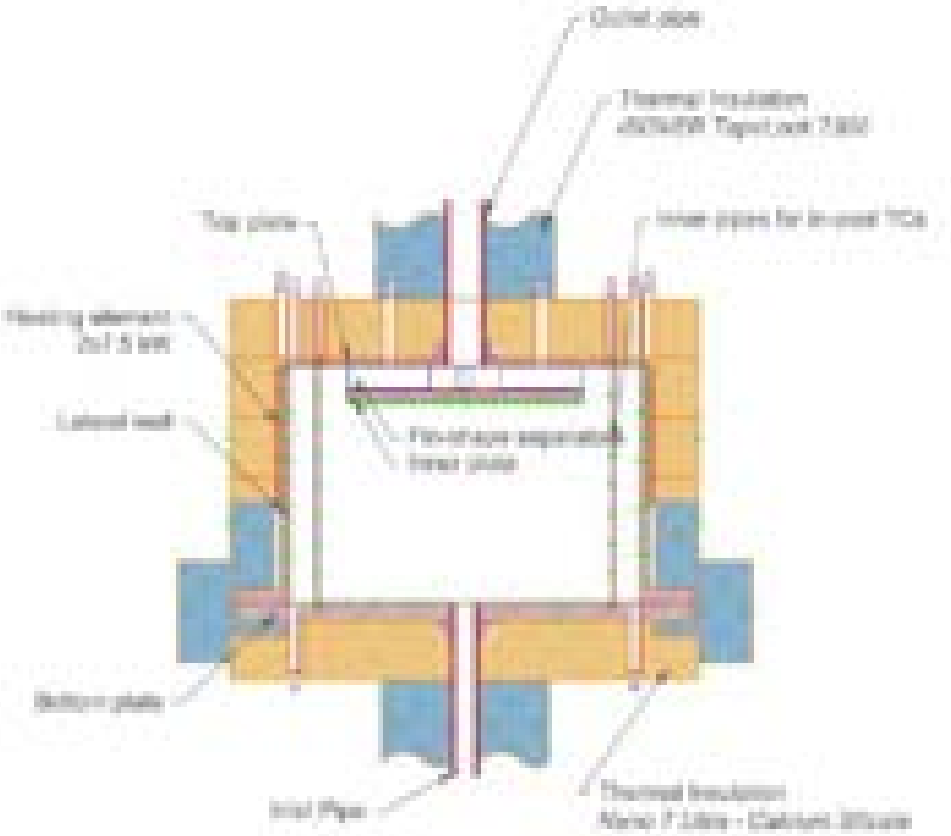
3D-test section

3D-1D coupling simulation

Conclusions



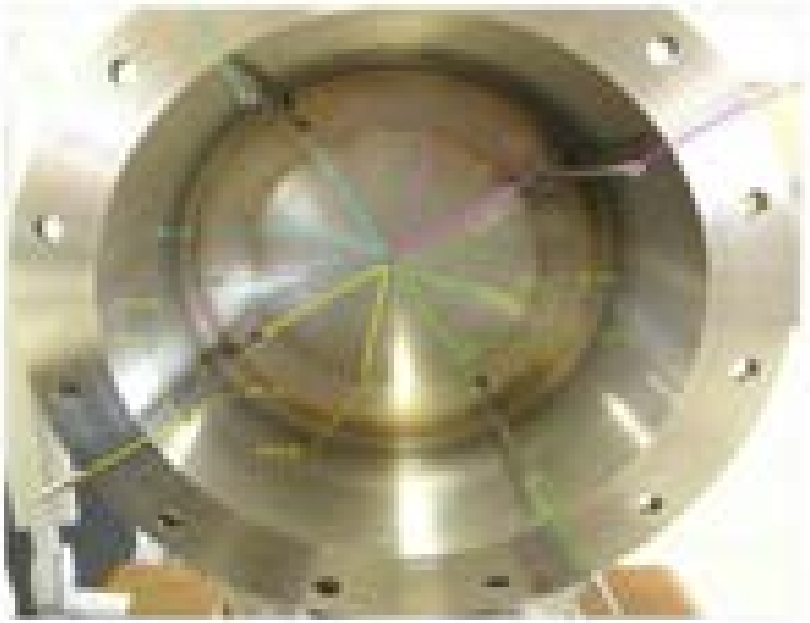
3D test section



Components:
(green) Thermocouples
(red) Heating coil
(yellow) insulator 1
(blue) insulator 2

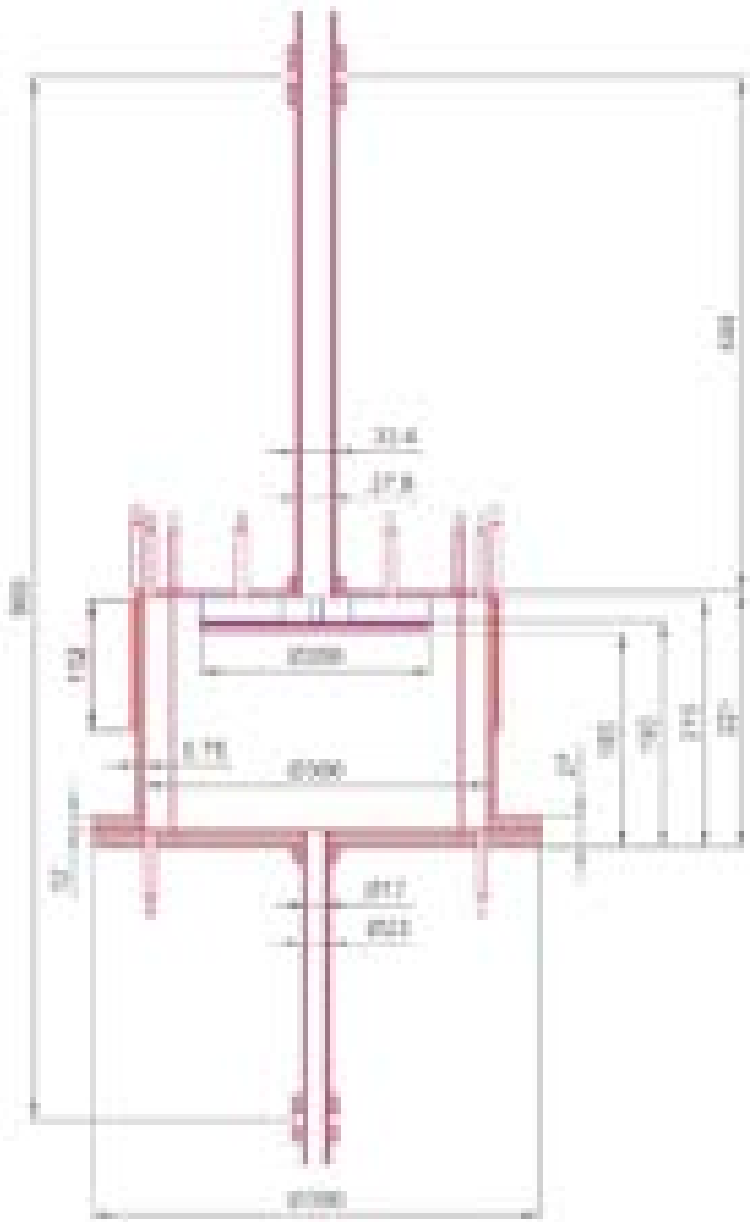
Flow:
inlet pipe (bottom)
around inner plate
oulet pipe (top)

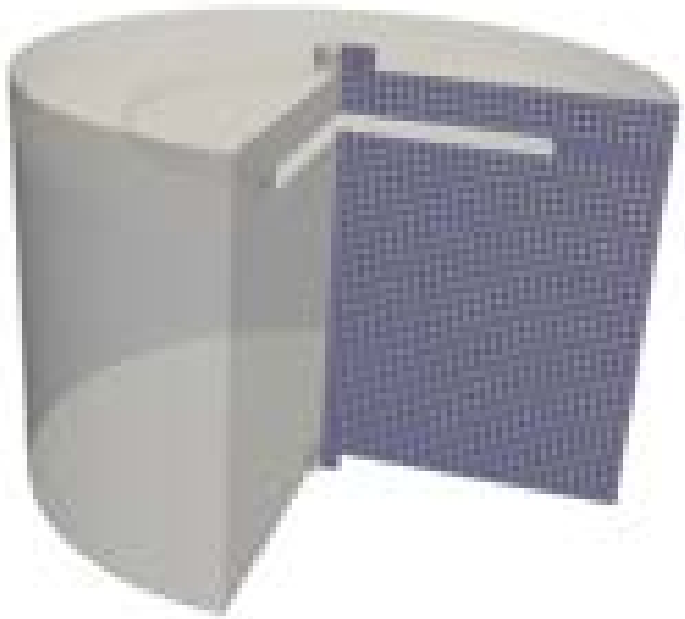
Thermocouple location



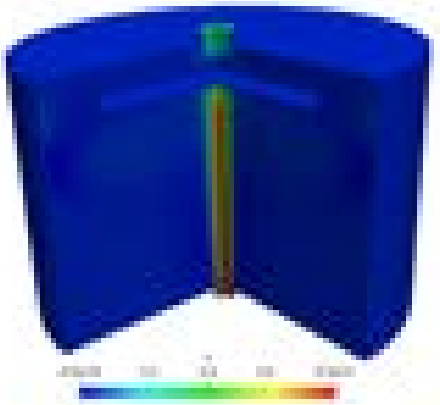


Mesh of the 3D section

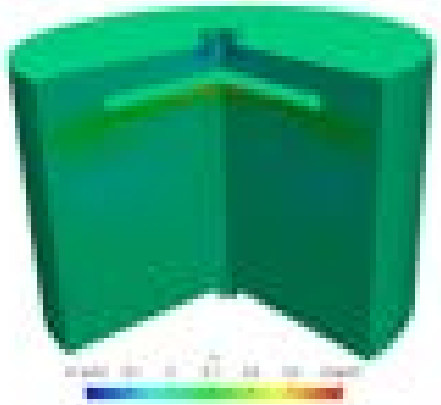




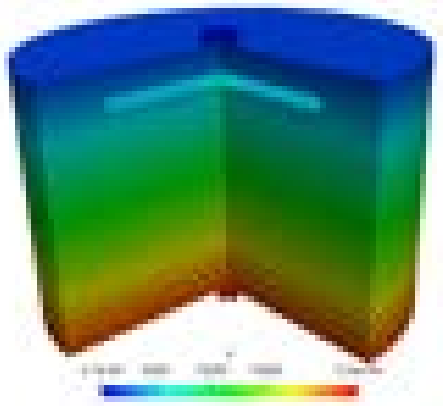
Initial conditions for 3D-FEMLCORE simulation



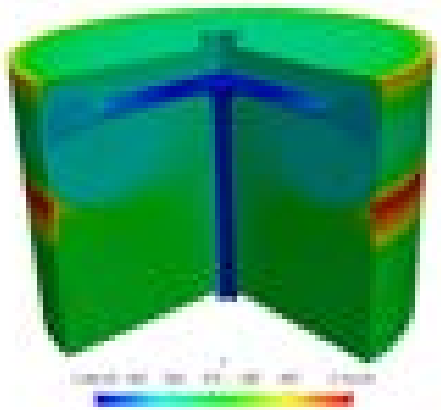
Velocity v



Velocity u



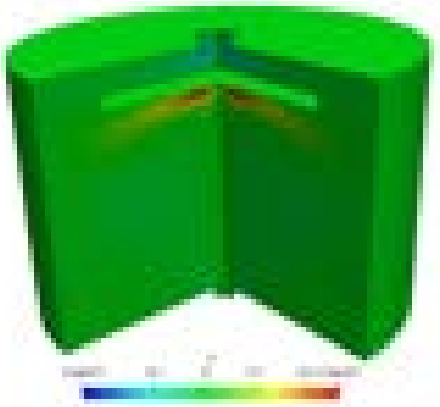
Pressure



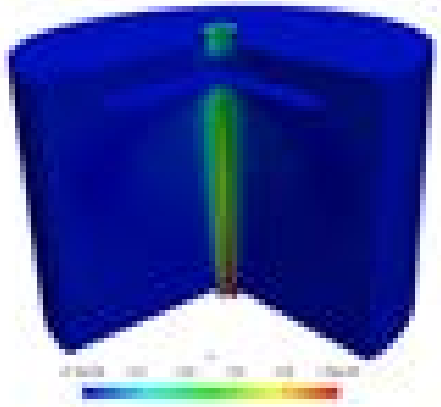
Temperature

Figura : Initial steady state for non-turbulent flow.

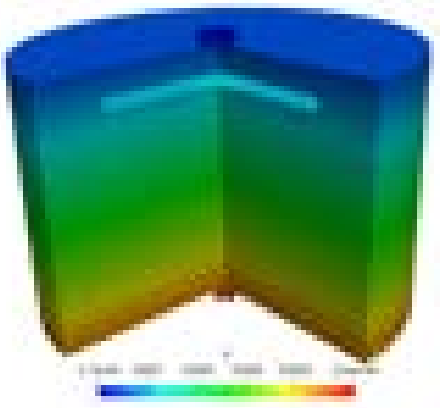
Initial conditions for 3D-FEMLCORE simulation



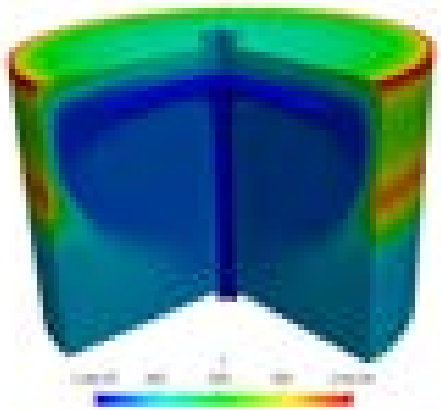
Velocity v



Velocity u



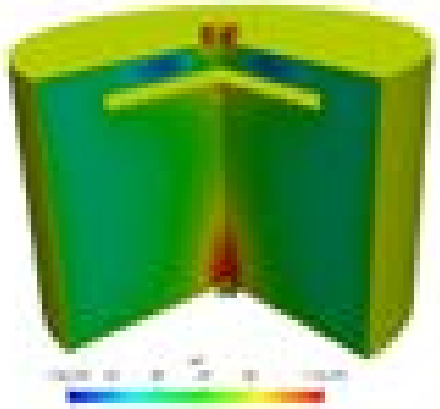
Pressure



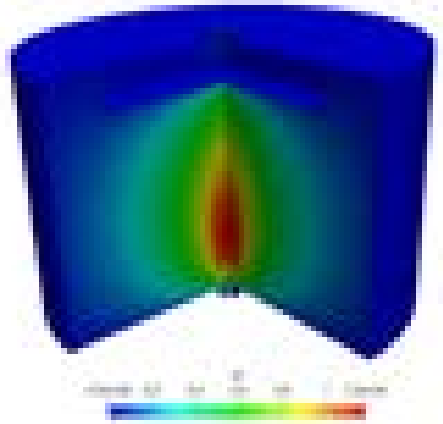
Temperature

Figura : Initial steady state for turbulent flow model case ($\kappa - \omega$).

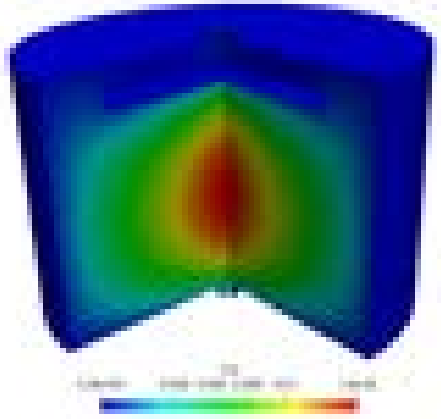
Initial conditions for 3D-FEMLCORE simulation



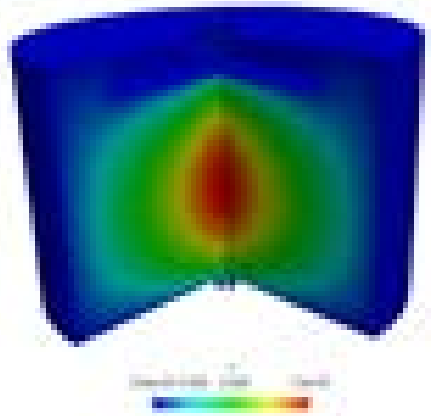
Turbulent kinetic energy rate ω



Turbulent kinetic energy k



Turbulent viscosity ν_t



Turbulent thermal conductivity α_t

Figura : Initial steady state for turbulent flow model case ($\kappa - \omega$).

Sommario

SALOME platform development for LFR

TALL-3D Facility and computational test

1D-CATHARE simulation and experimental results.

3D-test section

3D-1D coupling simulation

Conclusions



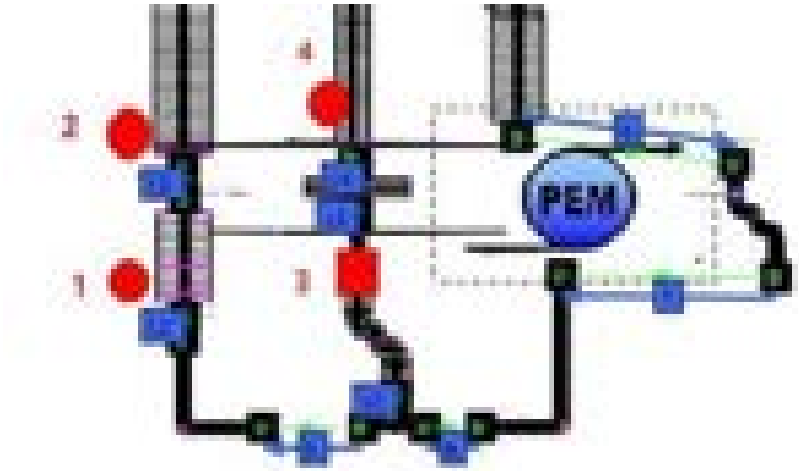
3D-1D coupling simulation

Test numerical stabilization and turbulence models

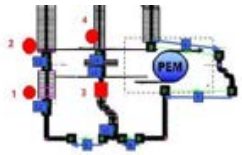
	A	B	C	D	E	F
Stabilization	-	SUPG	SUPG	Upwind	Upwind	SUPG
Dynamical Turb	-	-	κ-ω	κ-ω	κ-ω	κ-ω
Thermal Turb	-	-	Const Pr_t	Const Pr_t	Kays Pr_t	Kays Pr_t

Case A refers to Cathare standalone.

Points of interest in the 1D overlapping mesh

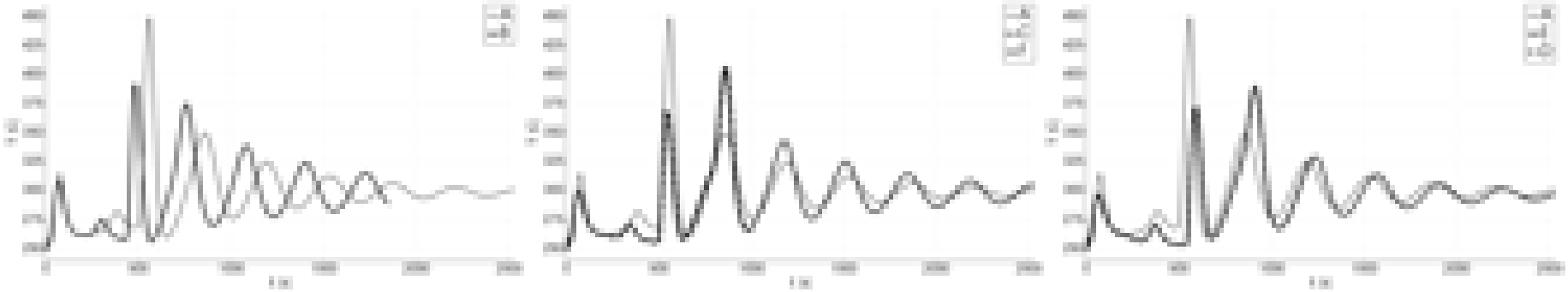


Reference point 2 (RESERVE4, leg 1)

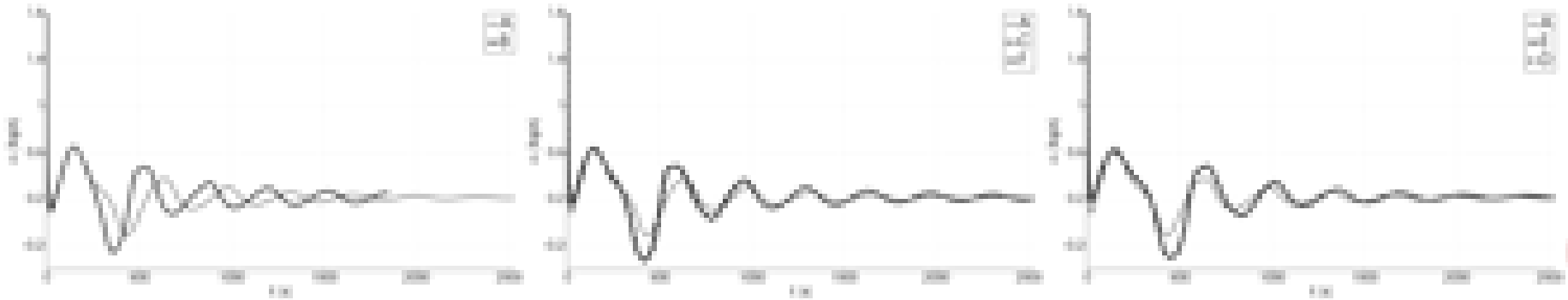


	A	B	C	D	E	F
Stabilization	-	**SUPG**	**SUPG**	**Upwind**	**Upwind**	**SUPG**
Dynamical Turb	-	-	κ-ω	κ-ω	κ-ω	κ-ω
Thermal Turb	-	-	**Const** Pr_t	**Const** Pr_t	**Kays** Pr_t	**Kays** Pr_t

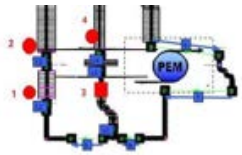
Temperature. Reference point 2 (RESERVE4, leg 1)



Mass flow . Reference point 2 (RESERVE4, leg 1)

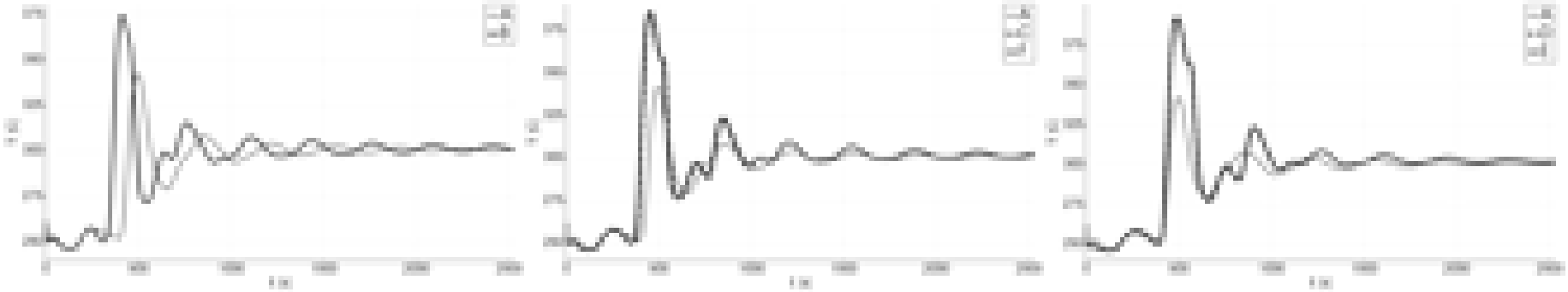


Reference point 5 (LINUP2, leg 3)



	A	B	C	D	E	F
Stabilization	-	**SUPG**	**SUPG**	**Upwind**	**Upwind**	**SUPG**
Dynamical Turb	-	-	κ-ω	κ-ω	κ-ω	κ-ω
Thermal Turb	-	-	**Const** Pr_t	**Const** Pr_t	**Kays** Pr_t	**Kays** Pr_t

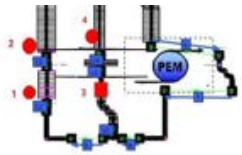
Temperature. Reference point 5 (LINUP2, leg 3)



Mass flow . Reference point 5 (LINUP2, leg 3)

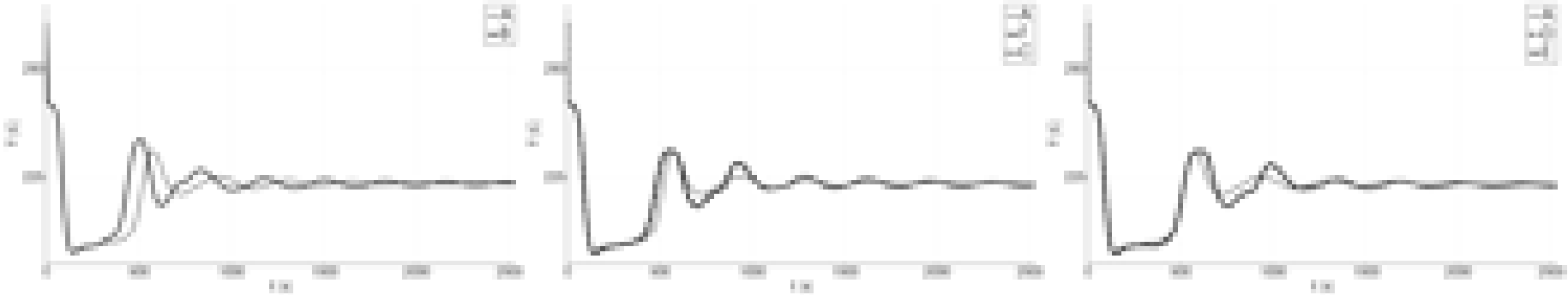


Reference point 6 (PUMP0, leg 3)



	A	B	C	D	E	F
Stabilization	-	**SUPG**	**SUPG**	**Upwind**	**Upwind**	**SUPG**
Dynamical Turb	-	-	κ-ω	κ-ω	κ-ω	κ-ω
Thermal Turb	-	-	**Const** Pr_t	**Const** Pr_t	**Kays** Pr_t	**Kays** Pr_t

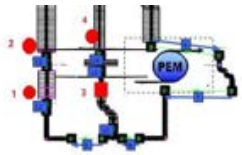
Temperature. Reference point 6 (PUMP0, leg 3)



Mass flow . Reference point 6 (PUMP0, leg 3)

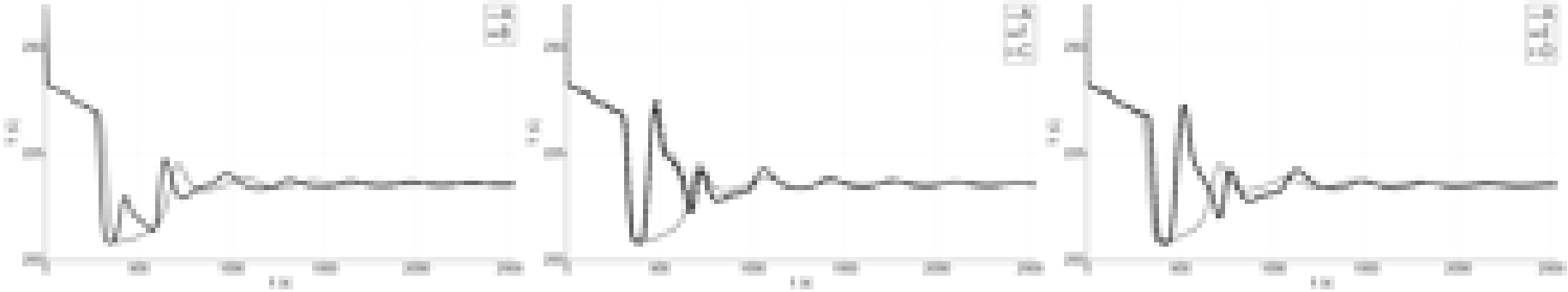


Reference point 3 (BELOW3D25, central leg)

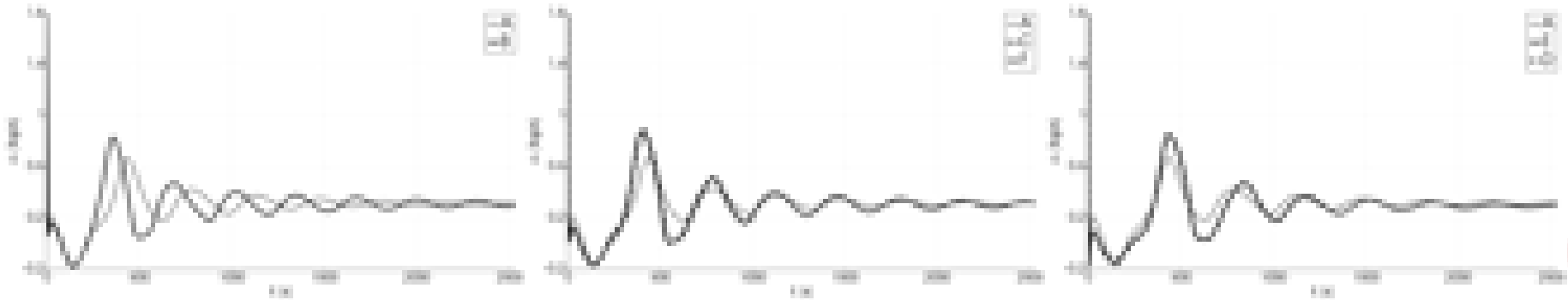


	A	B	C	D	E	F
Stabilization	-	**SUPG**	**SUPG**	**Upwind**	**Upwind**	**SUPG**
Dynamical Turb	-	-	κ-ω	κ-ω	κ-ω	κ-ω
Thermal Turb	-	-	**Const** Pr_t	**Const** Pr_t	**Kays** Pr_t	**Kays** Pr_t

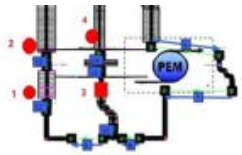
Temperature. Reference point 3 (BELOW3D25, central leg)



Mass flow . Reference point 3 (BELOW3D25, central leg)

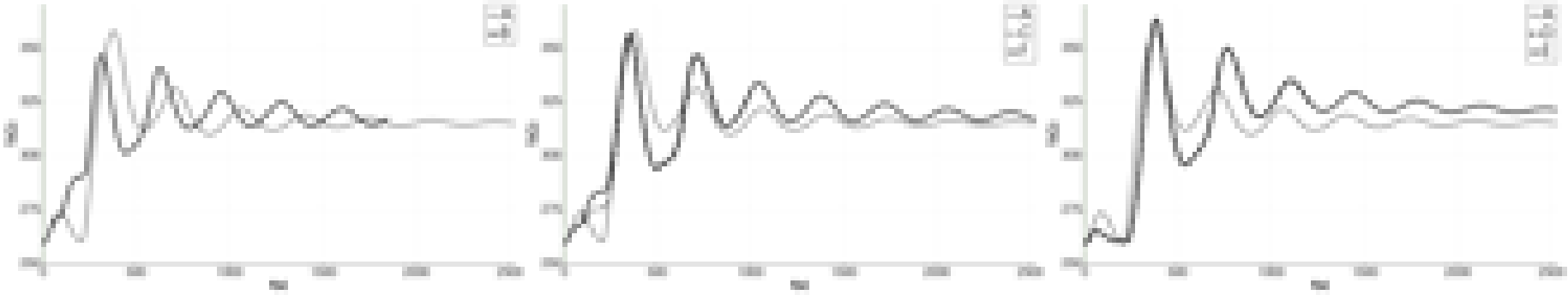


Reference point 4 (ABOVE3D3, central leg)

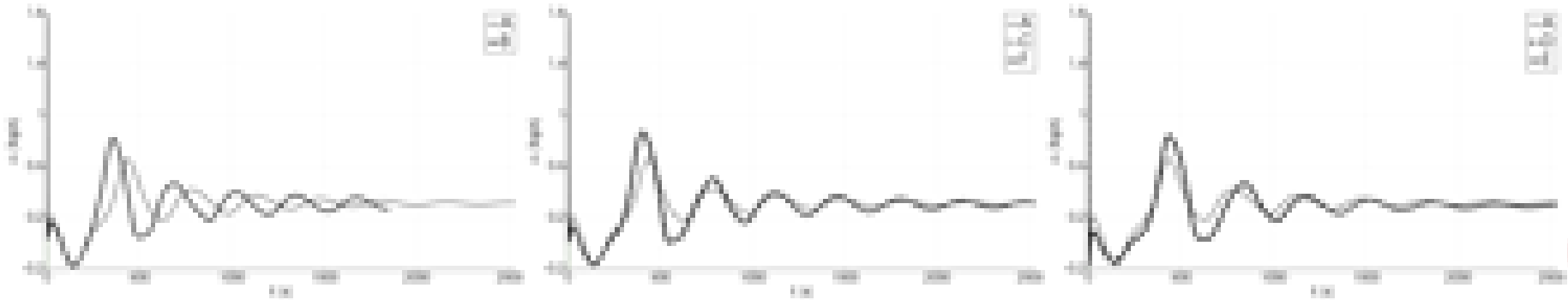


	A	B	C	D	E	F
Stabilization	-	**SUPG**	**SUPG**	**Upwind**	**Upwind**	**SUPG**
Dynamical Turb	-	-	κ-ω	κ-ω	κ-ω	κ-ω
Thermal Turb	-	-	**Const** Pr_t	**Const** Pr_t	**Kays** Pr_t	**Kays** Pr_t

Temperature. Reference point 4 (ABOVE3D3, central leg)



Mass flow . Reference point 4 (ABOVE3D3, central leg)



3D coupling solution

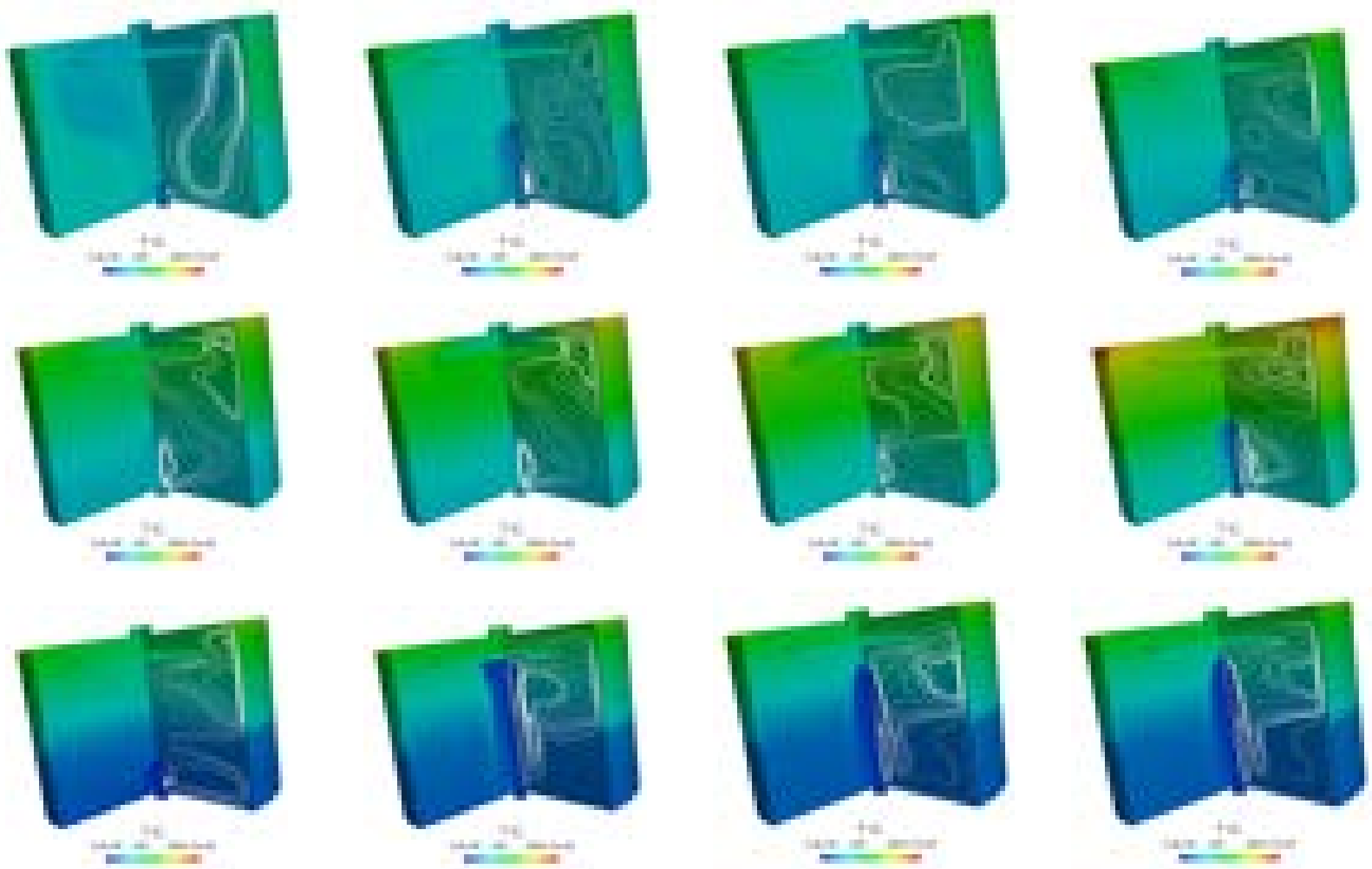
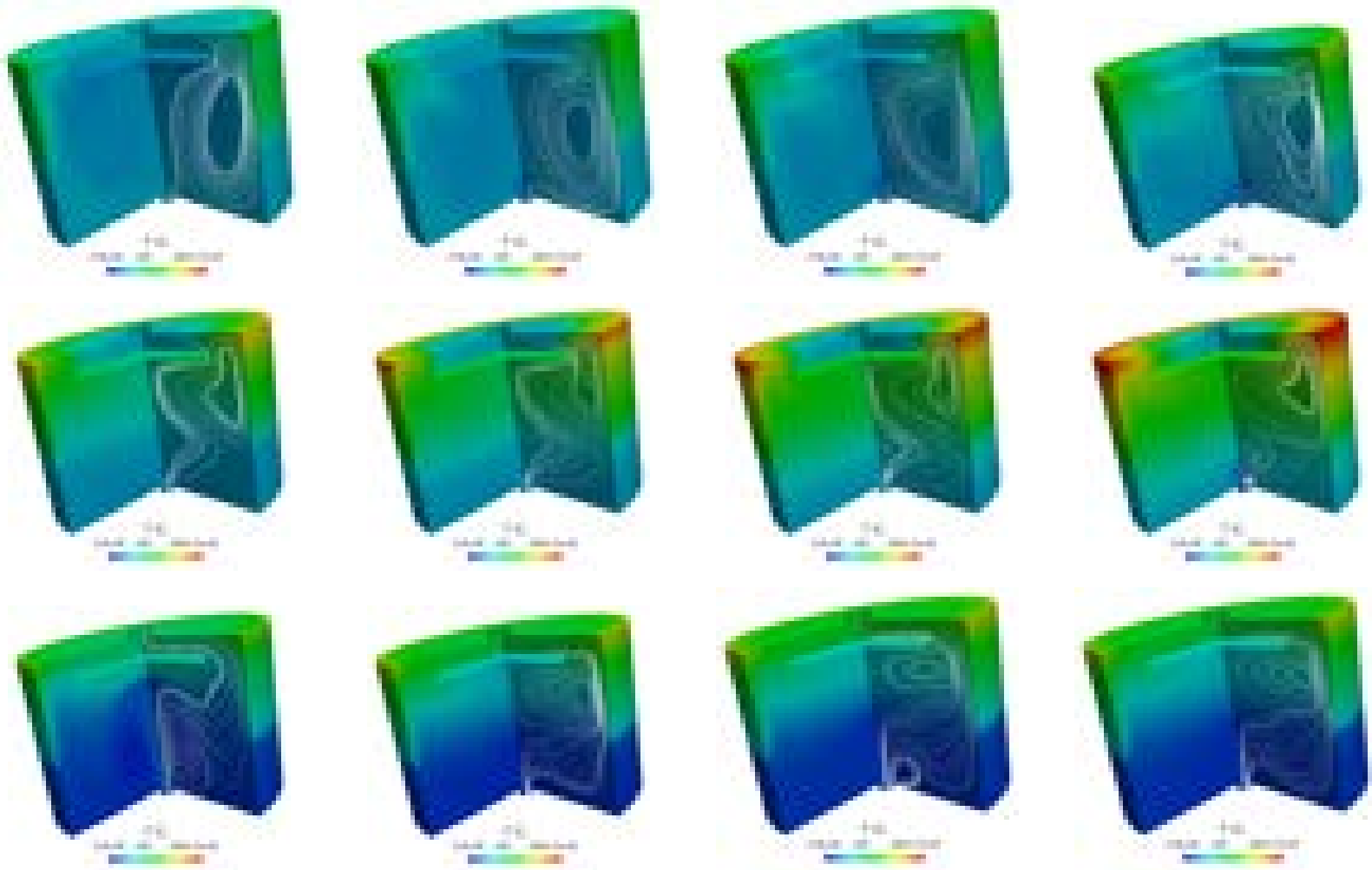


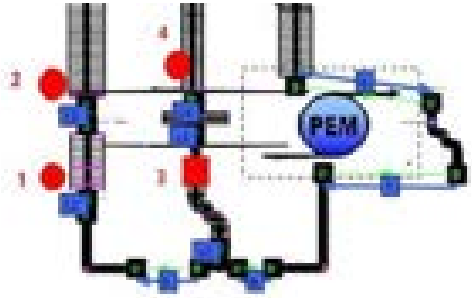
Figura : Temperature and streamline profiles over the 3D test component for $t = 10 - 2000$ for case B (non turbulent natural convection) and constant turbulent Prandtl number.

3D coupling solution. Temperature

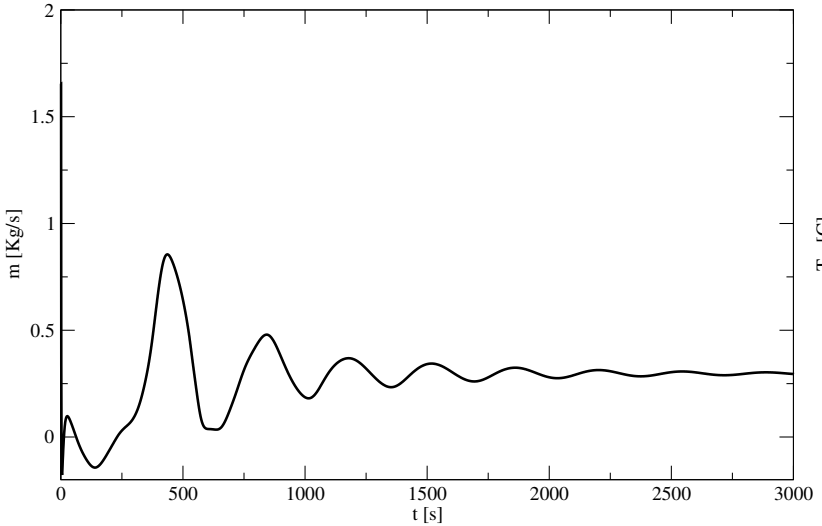


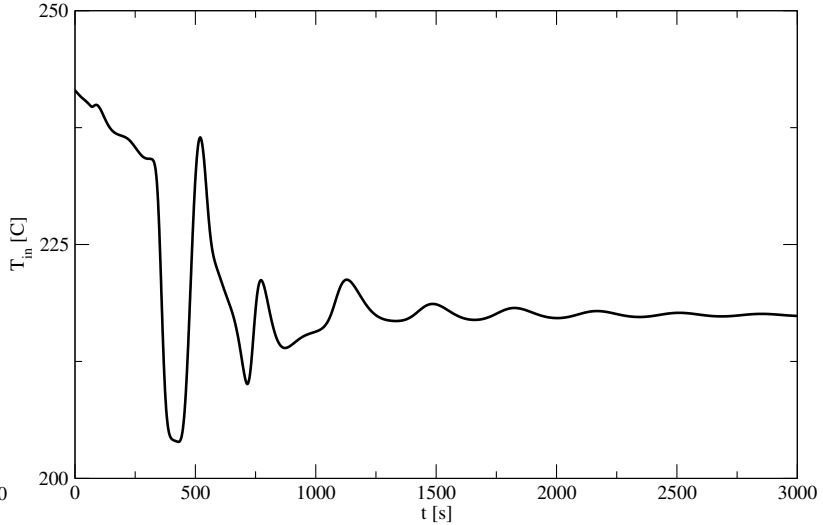
Temperature and streamline profiles over the 3D test component for $t = 10 - 2000$ for κ-ω turbulence case and Kays turbulent Prandtl number model for heat exchange

Result

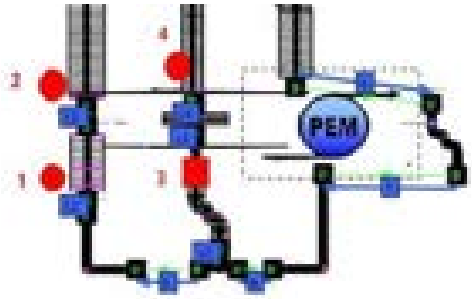


Mass flow rate (right) and temperature (left) as boundary conditions from CATHARE to FEMLCORE as a function of time.

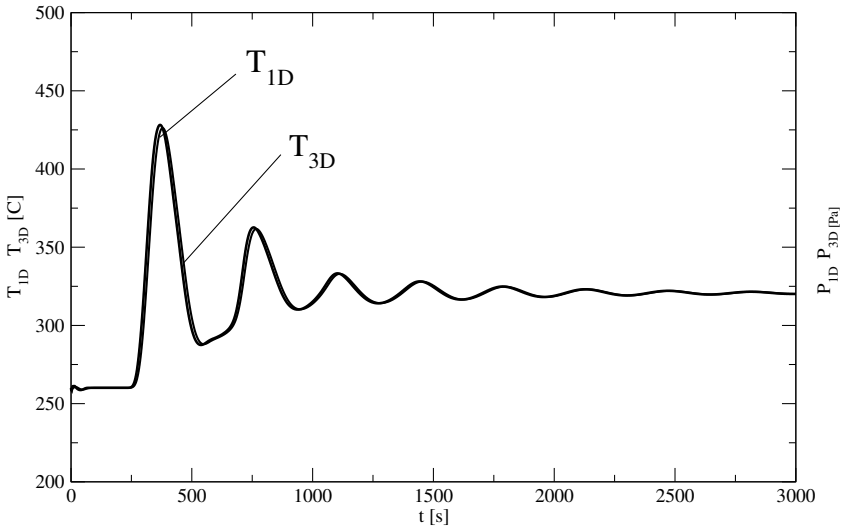


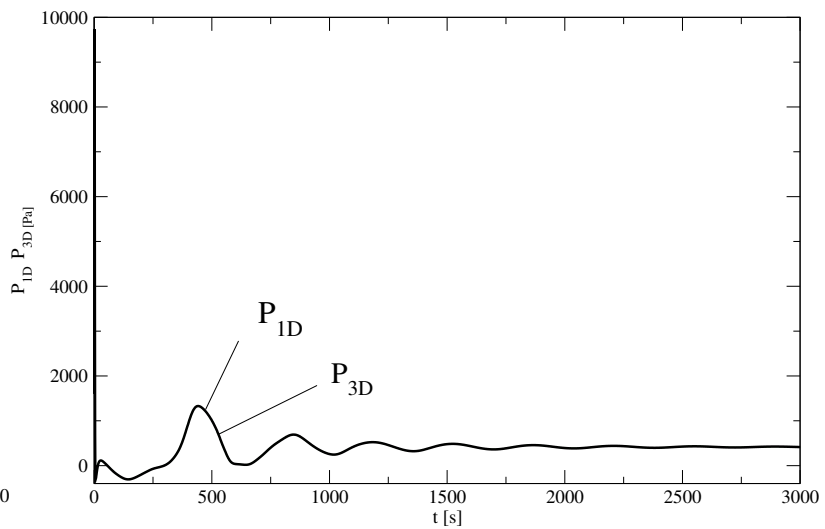


Result



Temperature and pressure imposed to CATHARE by FEMLCORE at point 4 as a function of time





Sommario

SALOME platform development for LFR

TALL-3D Facility and computational test

1D-CATHARE simulation and experimental results.

3D-test section

3D-1D coupling simulation

Conclusions



Conclusions

Conclusion: platform development

- Defective algorithm ->stability
- Evaluation for need of 3D computations -> 3D correction of 1D

Conclusion: TALL-3D experiment

- With tuning everything is possible
- Easy tuning: improve 1D (add or subtract of 1d sources)
- Understanding physics $\rightarrow$ 3D model correction
- Understanding physics $\rightarrow$ 1D-3D interfacecorrection (κ-ω, mass)

Planning

- Enlarge the platform with OPENFOAM $\leftarrow$ wide range of models
- Enlarge the platform with OPENFOAM $\leftarrow$ open source codes
- OPENFOAM interface $\leftarrow$ MED, SALOME mesh generator





Bologna, 27th June, 2017

Development of multi-physic code for Lead-cooled Fast Reactor

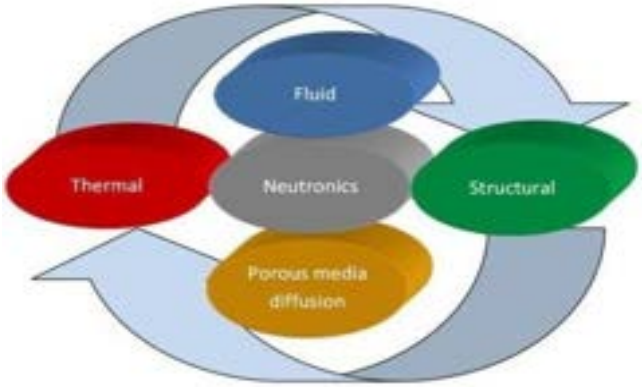
Davide Pizzocri, Antonio Cammi, Stefano Lorenzi

Nuclear Reactors Group

Motivation and background

Multiphysics: the study of the mutual interaction of different physical phenomena

. Fluid dynamics
. Neutronics
. Mechanics
. Heat Transfer
. Chemistry
. BoP



Purpose of multi-physics code:

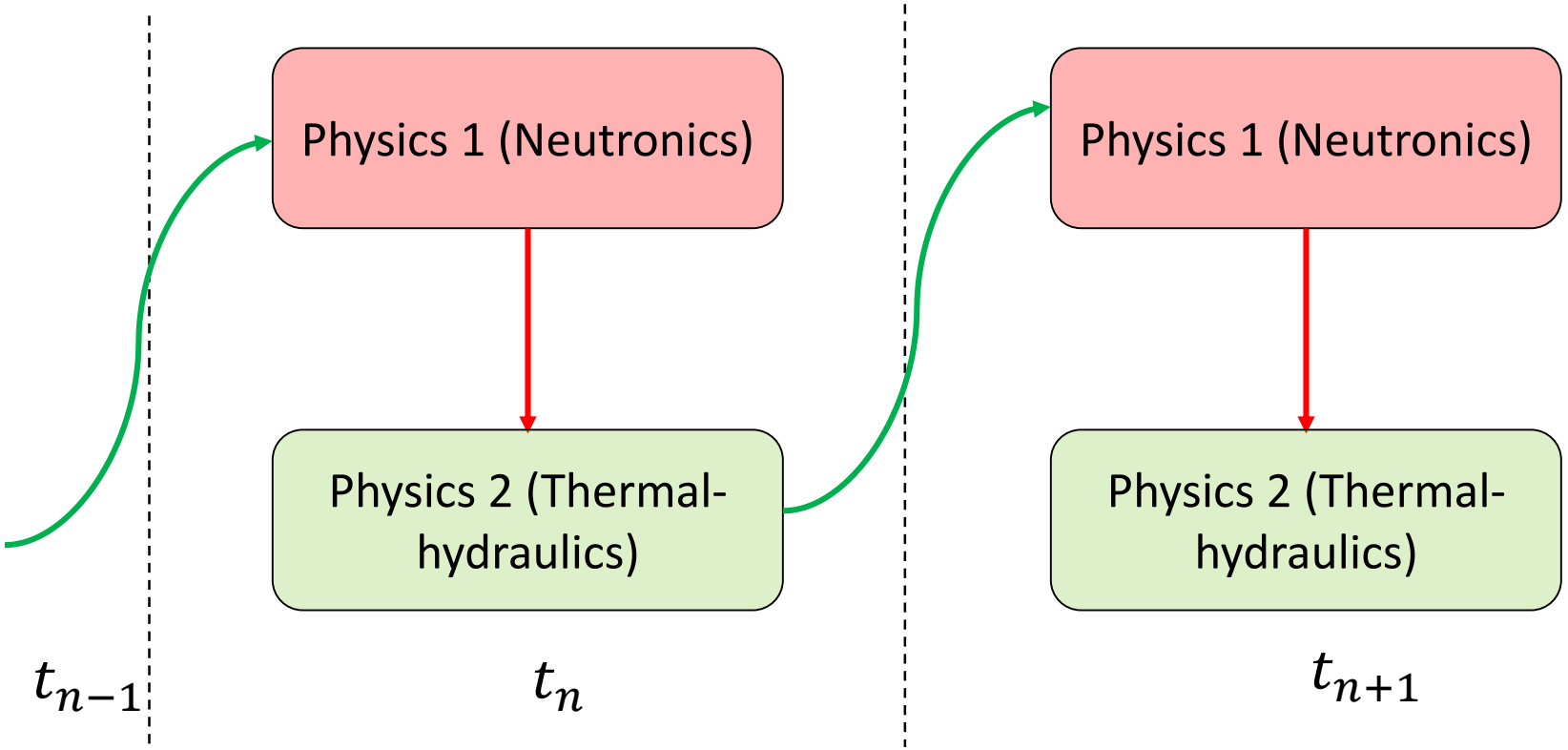
. **deeper insight** about the complex physical phenomena occurring in the reactor system (and their mutual interactions)

. allows **evaluating** a wide set of core parameters (e.g., temperature field, velocity field, and neutron fluxes) with a unique simulation tool

. valuable for core designing, when **verifying** the satisfaction of the operational constraints

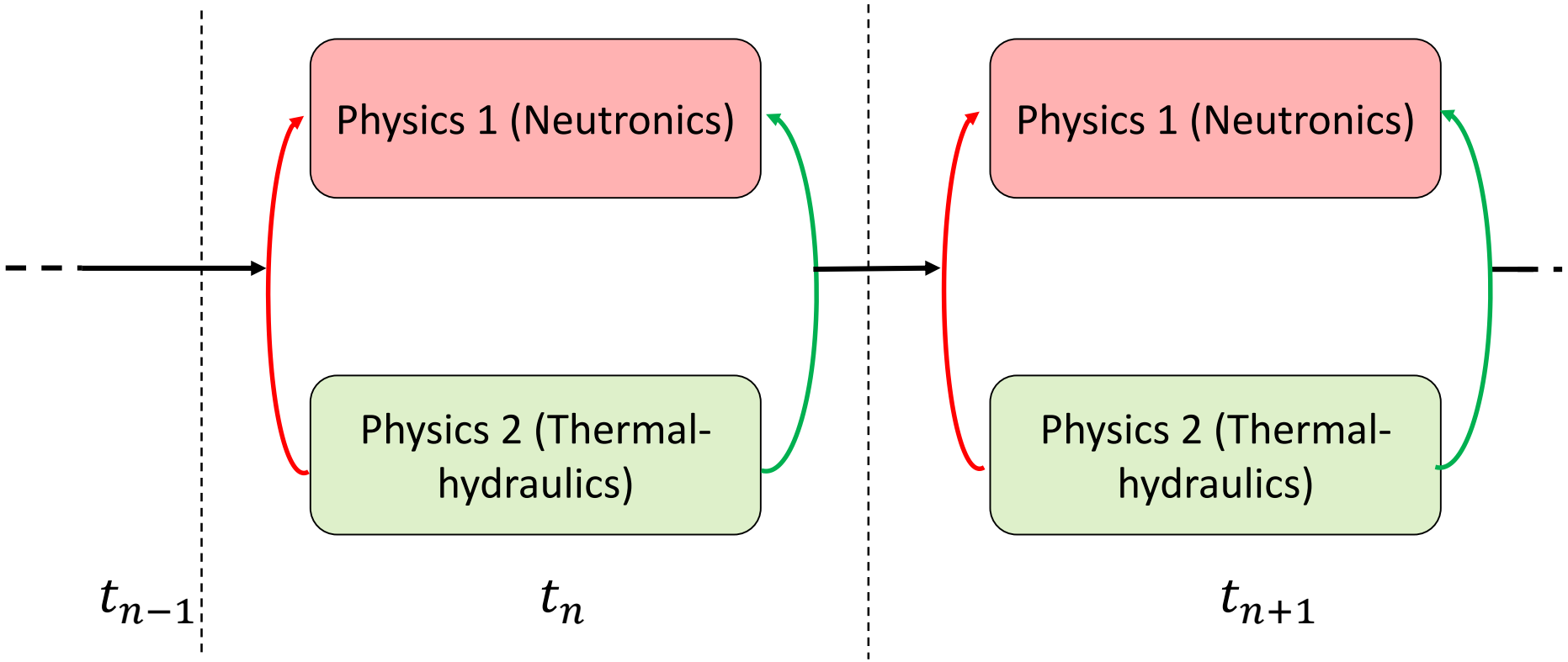
. **combined analysis** with system codes (not replacing)

Explicit/one way coupling



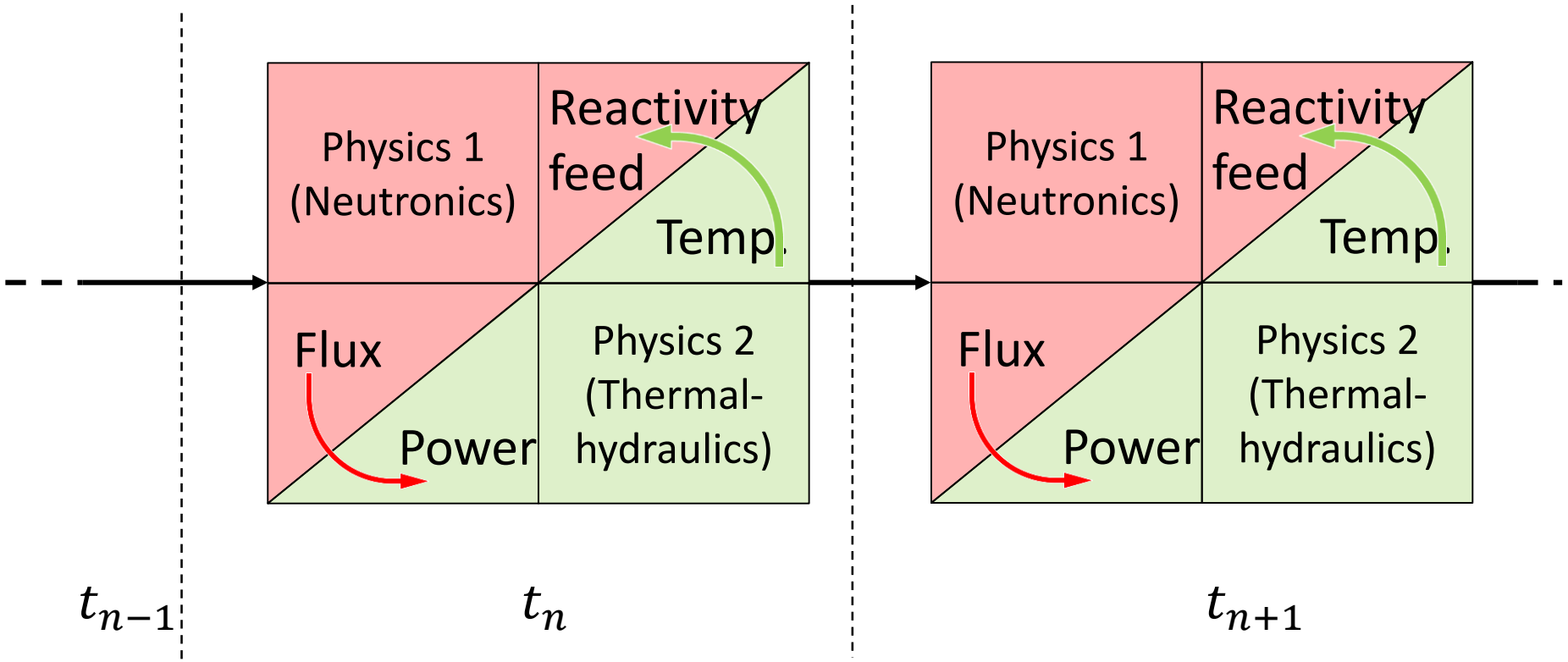
. Operator-split coupling strategies
. Explicit (weak) coupling
. Existing specialized mono-disciplinary codes
. Often non-iterative, multiphysics nonlinearities not resolved over a time step
. Reduced accuracy

Implicit coupling



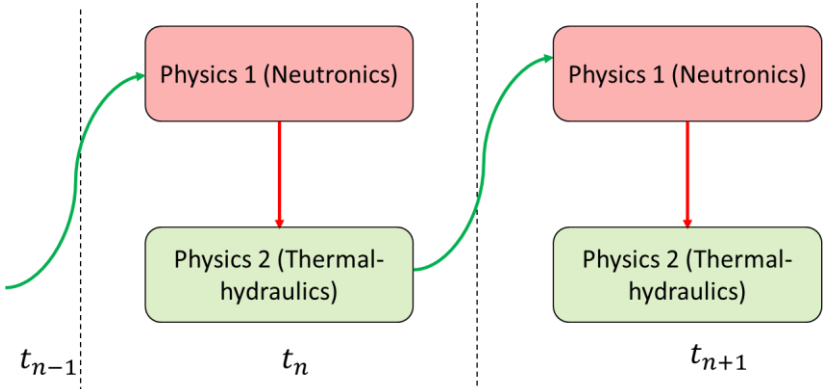
. Iterative (Picard iteration)
. Implicit coupling
. Reuse of existing specialized mono-disciplinary codes
. Avoid solving large monolithic system
. Convergence of iteration can take time (acceleration technique needed)

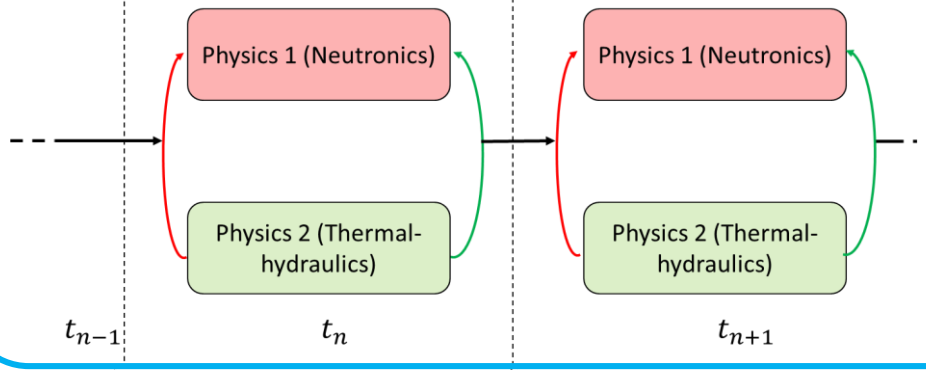
Implicit coupling



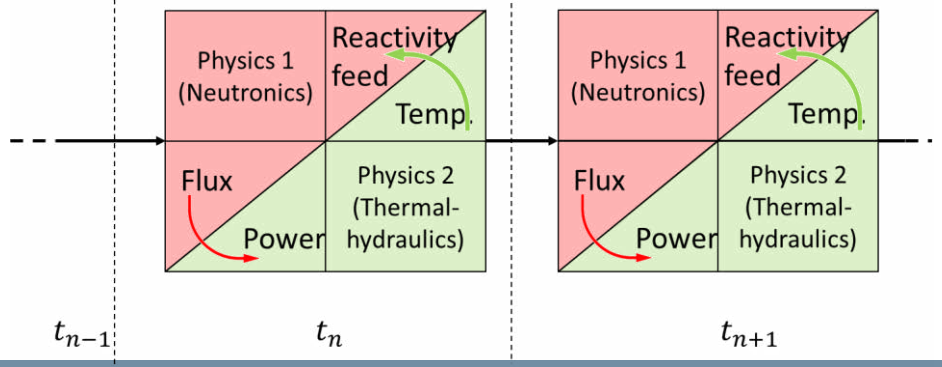
. Monolithic approach (Jacobian-Free Newton Krylov)
. Implicit coupling
. Need of creating codes from scratch
. Numerical issues due to the high non-linearity
. Highest level of accuracy

Multiphysics modelling





Approach used in the activity of this year (PAR 2016)

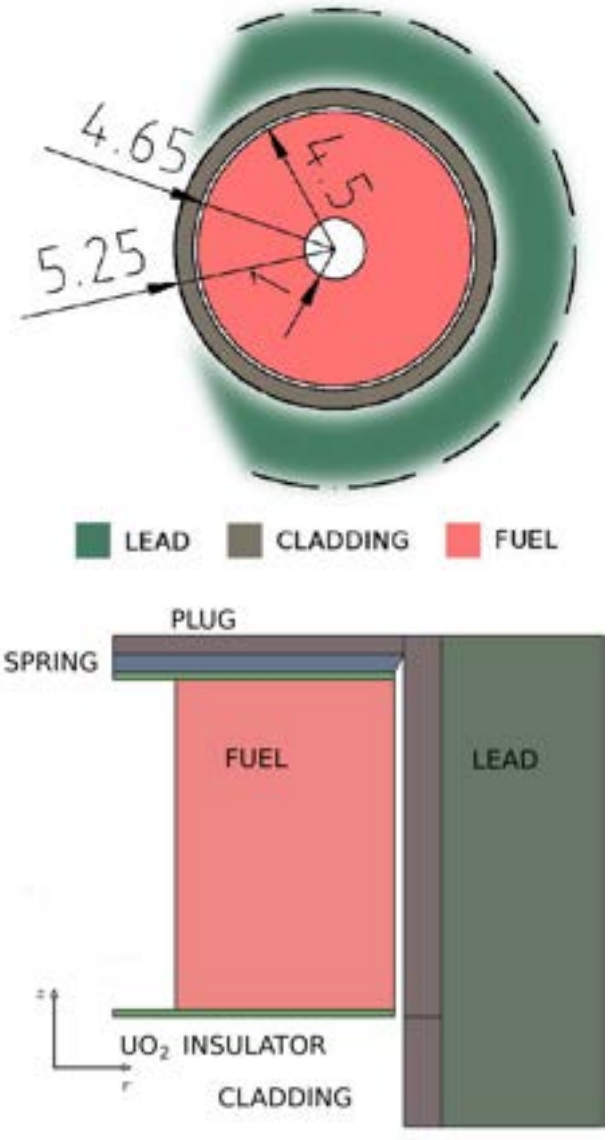


Test case

The implicit multi-physics approach is adopted to study the behaviour of an **LFR single-channel** representative of the active-core average conditions

Physics	Modelling approach
Neutornics	Multi-group neutron diffusion
Thermal-hydraulics	CFD
Mechanics	Linear elasticity

Average linear power	23.5 kW m^{-1}
Inlet lead temperature	400 °C
Outlet lead temperature	480 °C
Inlet lead velocity	1.6 m s^{-1}
Pu enrichment	17 vol:%
Fuel density	95 %TD
Fuel pin active height	900 mm
Pin-pitch	13.9 mm
UO2 thermal insulator height	20 mm
Spring height	50 mm
Upper plug height	50 mm
Inactive channel length	300 mm



Neutronics modelling

. Neutron diffusion approximation, 6 neutron energy groups and 8 neutron precursors groups

$$\frac{1}{v_g}\frac{\partial \phi_g}{\partial t} = \nabla \cdot D_g \nabla \phi_g - \Sigma_{a,g}\phi_g - \sum_{g' \neq g} \Sigma_{s,gg'}\phi_g + \sum_{g' \neq g} \Sigma_{s,g'g}\phi_{g'} + (1-\beta)\chi_{p,g}\sum_{g'}\left(\nu\Sigma_f\right)_{g'}\phi_{g'} + \sum_i \chi_{d,g}\lambda_i c$$

$$\frac{\partial c_j}{\partial t} = -\lambda_i C_i + \beta_i \sum_g \left(\nu\Sigma_f\right)_g \phi_g$$

. Group constants by SERPENT – pointwise T and density dependence

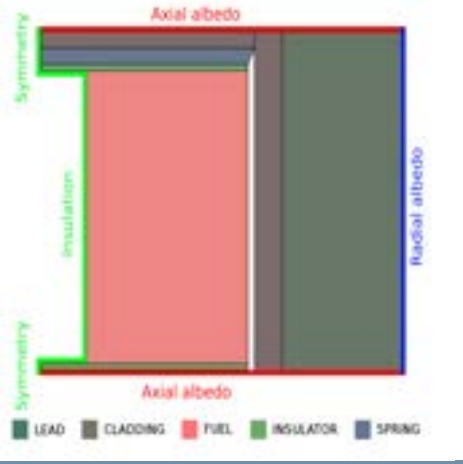
$$\Sigma(T,\rho) = \left(\frac{\rho}{\rho_0}\right)\left[\Sigma_0 + \alpha \cdot log\left(\frac{T}{T_0}\right)\right] \qquad \Sigma(T,\rho) = \left(\frac{\rho}{\rho_0}\right)\Sigma_0$$

Group number	Upper boundary		Lower boundary	
1	20	MeV	2.23	MeV
2	2.23	MeV	0.82	MeV
3	0.82	MeV	67.38	keV
4	67.38	keV	16.03	keV
5	16.03	keV	0.75	keV
6	0.75	keV	0	keV

. Albedo boundary conditions

$$\boldsymbol{n} \cdot \left(D_g \nabla \phi_g\right) = -\gamma_z \phi_g$$

$$\boldsymbol{n} \cdot \left(D_g \nabla \phi_g\right) = -\gamma_r \phi_g$$



Fluid dynamics and heat transfer

. **Fluid dynamics** incompressible k-ε turbulence model, prescribed inlet lead velocity and temperature

$$\nabla \cdot \mathbf{v} = 0$$

$$\rho \frac{\partial \mathbf{v}}{\partial t} + \rho(\mathbf{v} \cdot \nabla)\mathbf{v} = \nabla \cdot \left[-p\boldsymbol{I} + (\eta + \eta_t)\left(\nabla \mathbf{v} + (\nabla \mathbf{v})^T - \frac{2}{3} k \boldsymbol{I} \right) \right]$$

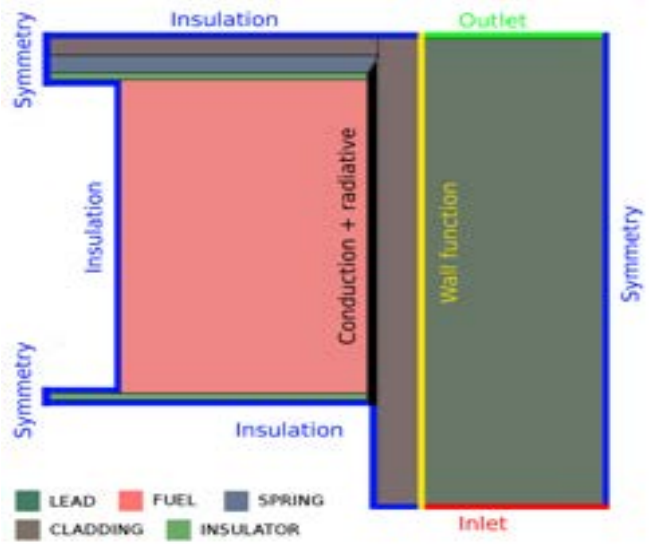
$$\rho \frac{\partial k}{\partial t} + \rho(\mathbf{v} \cdot \nabla)k = \nabla \cdot \left[\left(\eta + \frac{\eta_t}{\sigma_k} \right) \nabla k \right] - \rho\varepsilon + \eta_t [\nabla \mathbf{v} \ : \ (\nabla \mathbf{v} + (\nabla \mathbf{v})^T)]$$

$$\frac{\partial \varepsilon}{\partial t} + \rho(\boldsymbol{v} \cdot \nabla)\varepsilon = \nabla \cdot \left[\left(\eta + \frac{\eta_t}{\sigma_\varepsilon} \right) \nabla \varepsilon \right] - \frac{C_{\varepsilon 2} \rho \varepsilon^2}{k} + \frac{C_{\varepsilon 1} \eta_t \varepsilon}{k} [\nabla \boldsymbol{v} \ : \ (\nabla \boldsymbol{v} + (\nabla \boldsymbol{v})^T)]$$

Heat transfer

$$\begin{cases} \rho C_p \dfrac{\partial T}{\partial t} + \nabla \cdot [-(K + K_t)\nabla T] = \rho C_p \mathbf{v} \cdot \nabla T & coolant \\ \rho C_p \dfrac{\partial T}{\partial t} = \nabla \cdot (K \nabla T) & gap, cladding \\ \rho C_p \dfrac{\partial T}{\partial t} + \nabla \cdot (-K \nabla T) = Q & fuel \end{cases}$$

$$Q_f = \sum_g E_{f,g} \cdot \Sigma_{f,g} \cdot \phi_g$$



Mechanics

Linear elasticity + thermal expansion

$$\rho \frac{\partial^2 \mathbf{u}}{\partial t^2} = \nabla \cdot \boldsymbol{\sigma}$$

$$\epsilon = \frac{1}{2}[\nabla \mathbf{u} + (\nabla \mathbf{u})^T]$$

$$\boldsymbol{\sigma} = \mathbf{C} : \left(\epsilon - \alpha_{th}\left(T - T_{ref}\right)\right)$$

. The column of fuel pellets is modelled as a unique continuous structure. Cracking, irradiation induced and other mechanical (e.g., creep) effects are neglected.

. “moving mesh” technique allows deforming the mesh of the simulated domain. the different physics are influenced by the displacement field of the fuel and the cladding.

. PDEs of neutronics, heat transfers and fluid dynamics are solved in deformed mesh

Numerical solution

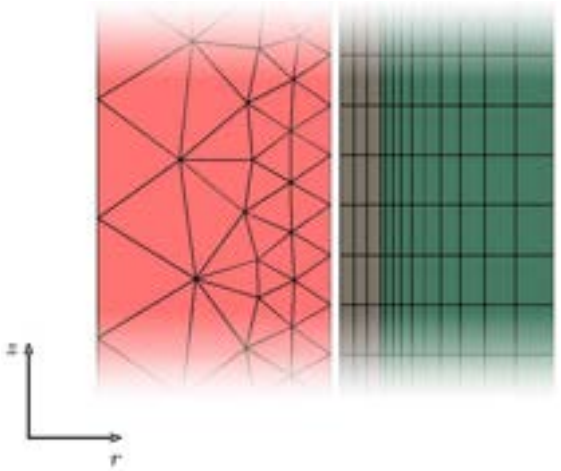




X 2 X 4 Core



X 64 GB



Group		Variables	Solvers
1	$\phi_1 \ldots \phi_6$	Neutron fluxes	MUMPS
2	$c_1 \ldots c_6$	Precursors density	MUMPS
3	T,u	Temperature and displacements	MUMPS
4	p, v	Pressure and velocity	MUMPS
5	k-ε	Turbolence variables	Pardiso

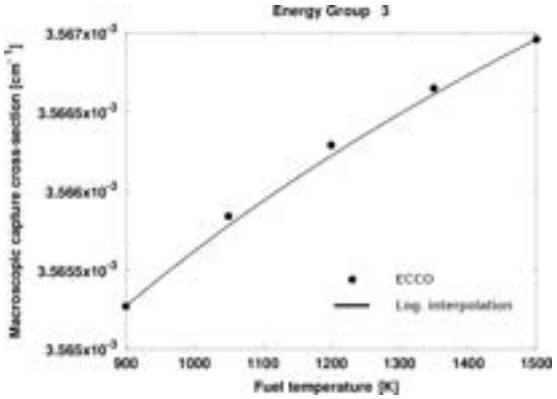
Segregated solver – Lagrangian elements (Quadratic order)

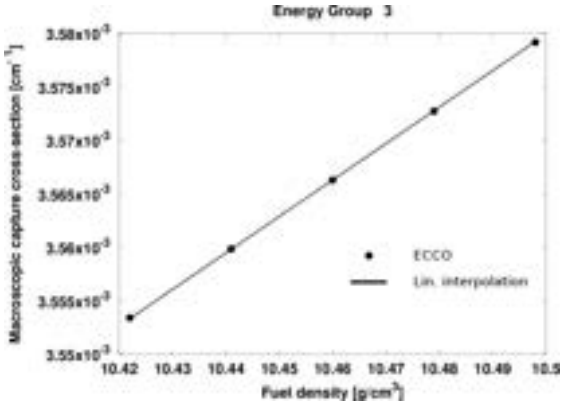
SERPENT model

$D_g, \nu_g, \beta_i, \nu\Sigma_{f,g}, \Sigma_{a,g}, \Sigma_{s,gg'}, \chi_{p,g}, \chi_{d,g}$

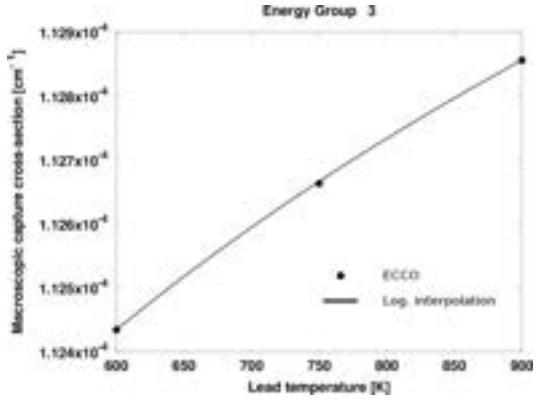
Neutronics parameters of six energy groups calculated by means of the MC transport code SERPENT

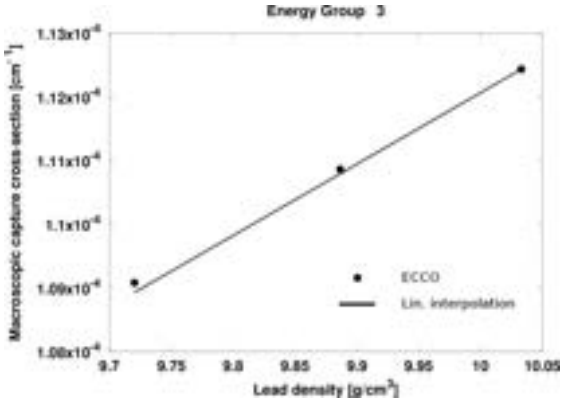
Verification of the macroscopic cross-sections functional form





Fuel

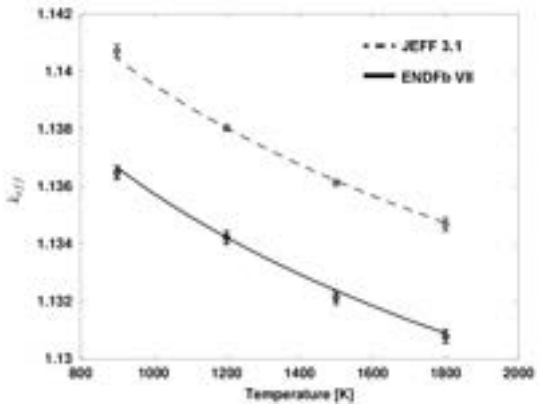




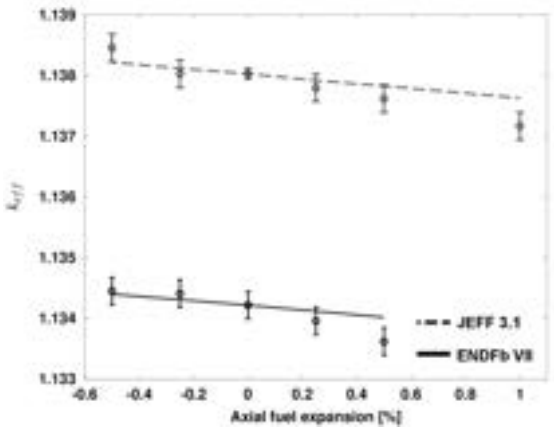
Lead

SERPENT model

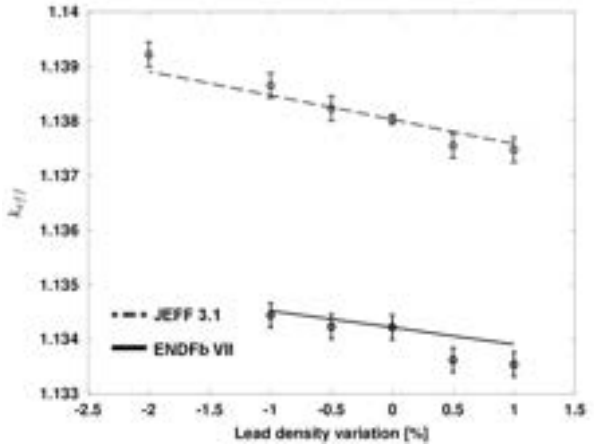
Verification of the adopted neutron diffusion model



k_{eff} vs fuel Temp.



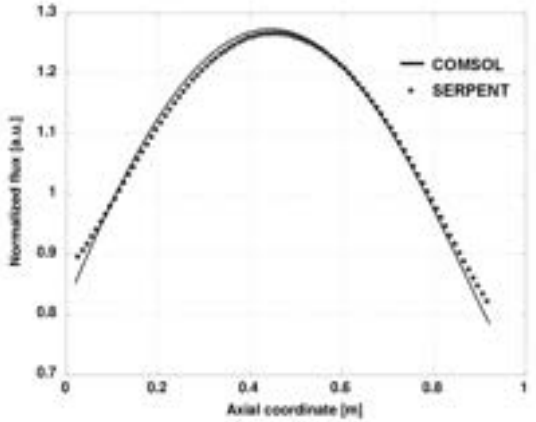
k_{eff} vs fuel axial exp.



k_{eff} vs lead density

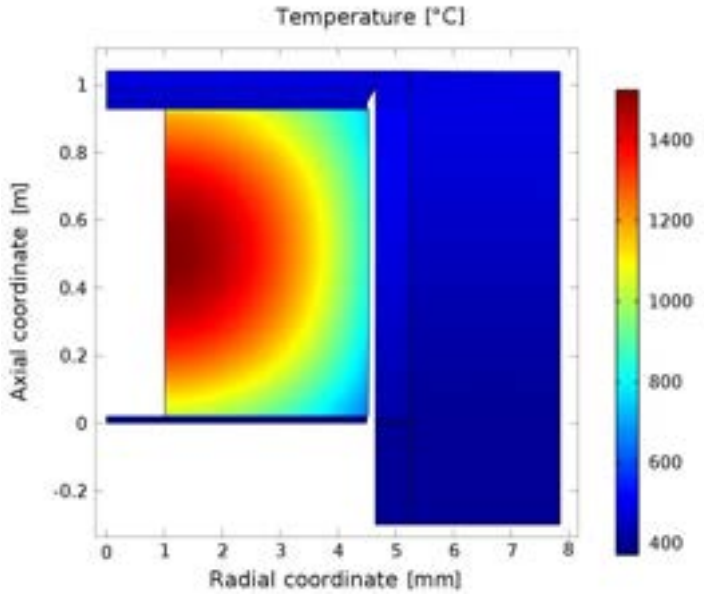
. Good agreement between Comsol and SERPENT

. Similar trend for JEFF3.1 and ENDFb VII

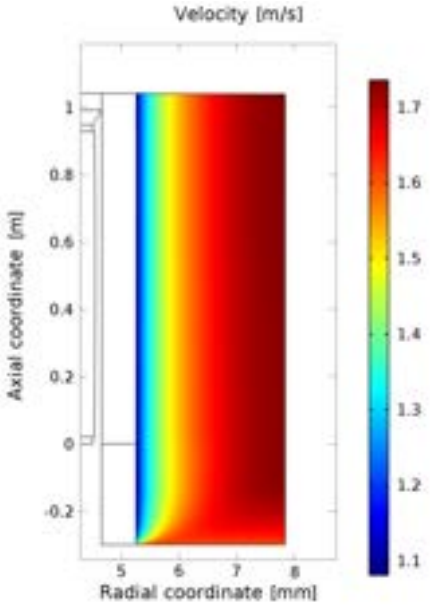


Results

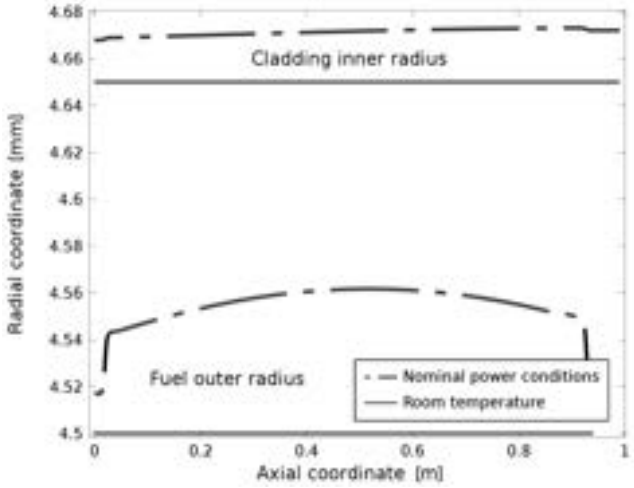
Transient analysis:



Temperature



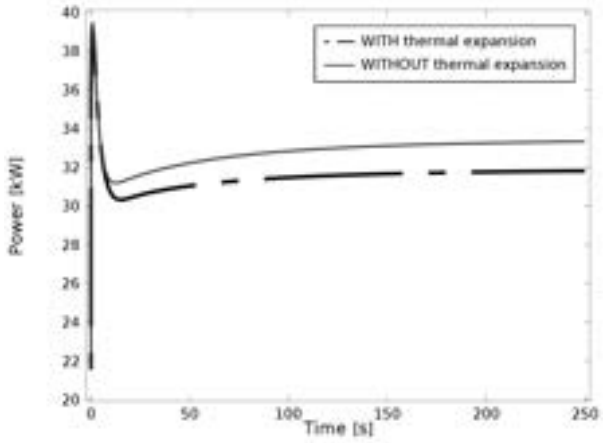
Fluid dynamics



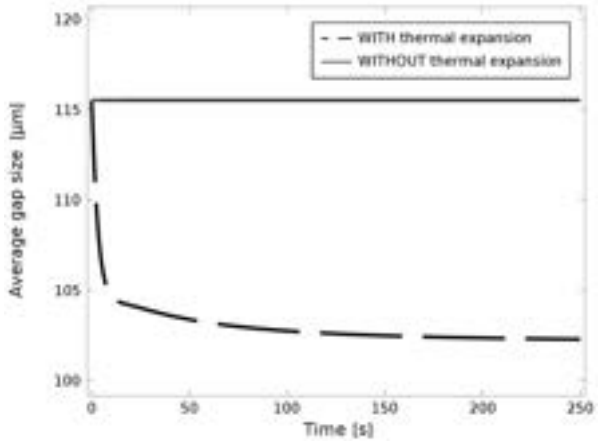
Mechanics

Results

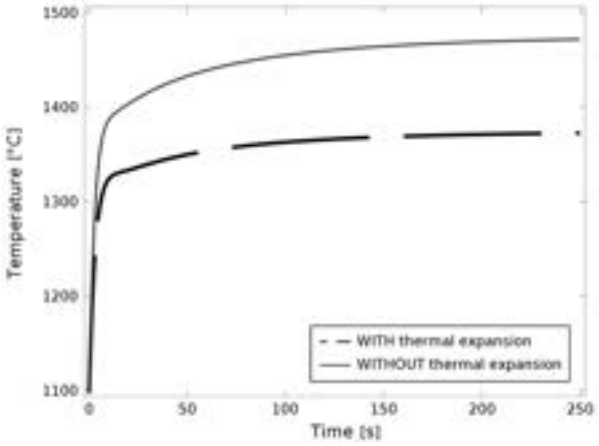
Steady-state analysis: step-wise insertion of 150 pcm



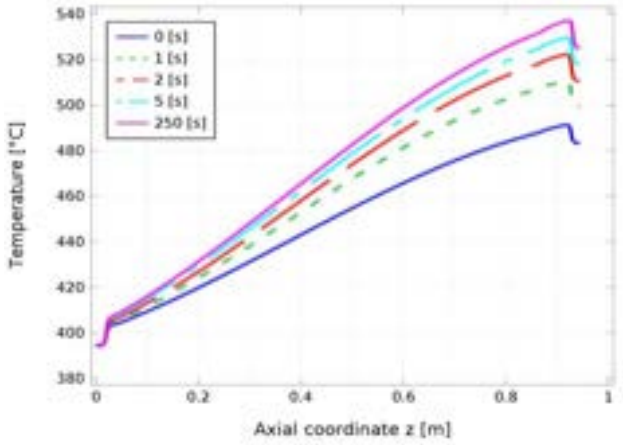
Power



Gap size



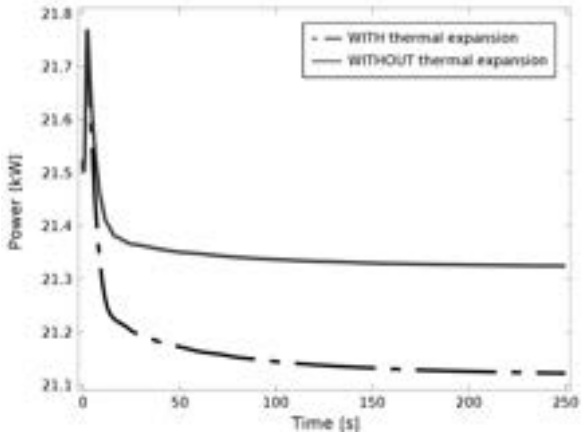
Average fuel temperature



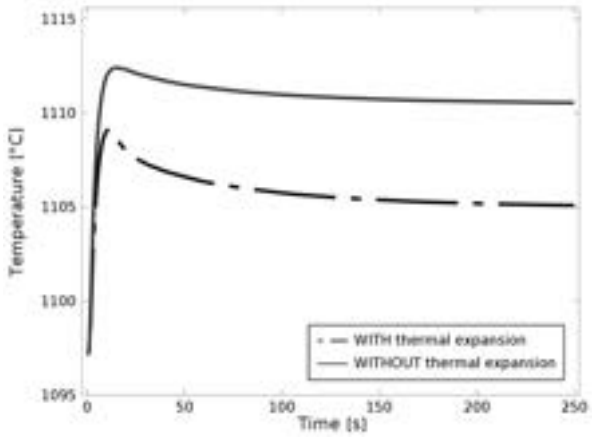
Outer cladding temperature

Results

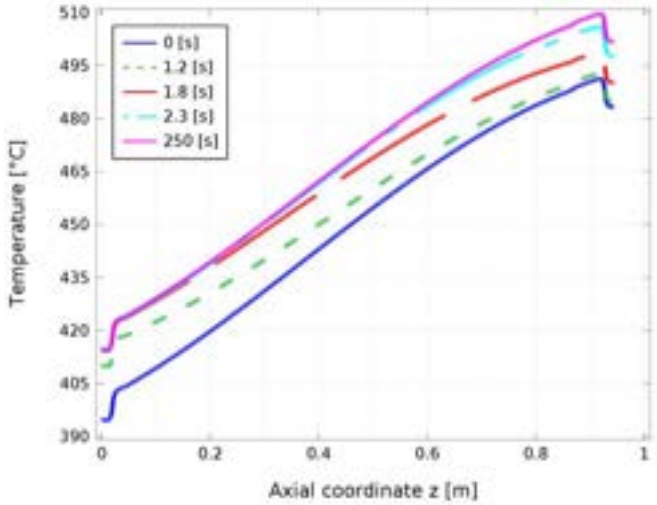
Steady-state analysis: increase of inlet lead temperature



Power



Average fuel temperature



Outer cladding temperature

Conclusions and future developments

.When considering multiple phenomena, the coupling between single-physics code is not the optimal way to solve the phenomena due to the explicit exchange of data (lower accuracy due to non-linearity) and to the difficulties in parallel computation.

. The activity is the first step for the development of a multi-physics code for lead-cooled fast reactor aimed at supporting both the design choice and the verification of other numerical tools

. Even if the model simulates a single-channel a LFR, it takes into account the main physical phenomena – and their couplings – occurring within the reactor

. The work has been useful also in order to evaluate the modelling approach of the different physics and how to couple the different phenomena (e.g., the neutronics and the thermal elasticity).

Conclusions and future developments

. Near-term efforts focus on efficient use of the available computational resources (i.e., parallelization) and easy modification of the modelling description (in order to be adjusted on the specific modelling needs and for a multi-user development) – possible option OpenFOAM

. OpenFOAM is an open source library for numerical simulation in continuum mechanics using Finite Volume Method. Very flexible (object-oriented programming), allowing users to customize, extend and implement complex physical model.

. Future developments will be devoted to develop a multi-physics platform in OpenFOAM, starting with simple geometry but aiming at representing more complex geometry.

Thank you for your attention

METODOLOGIA HGPT-BU PER L'ANALISI PERTURBATIVA NEL CAMPO NEUTRONI/NUCLIDI. IMPLEMENTAZIONE E VALIDAZIONE NEL CODICE ERANOS

Augusto Gandini
Università Sapienza di Roma

Vincenzo Peluso
ENEA/Bologna

METODOLOGIA HGPT-BU PER L'ANALISI PERTURBATIVA NEL CAMPO NEUTRONI/NUCLIDI. IMPLEMENTAZIONE E VALIDAZIONE NEL CODICE ERANOS

Metodologia GPT-BU

La metodologia per il calcolo perturbativo di funzionali della densità neutronica e di quella dei nuclidi che evolvono durante l'evoluzione (burn-up) del nocciolo è stata sviluppata secondo la teoria delle perturbazioni generalizzate su base euristica (HGPT). Essa viene quindi definita HGPT-BU e può essere applicata a studi relativi all'evoluzione temporale del campo nonlineare neutroni/nuclidi in sistemi critici, o sottocritici. I funzionali di interesse possono riguardare, in particolare:

- Gli isotopi del combustibile a fine ciclo. In questo caso il metodo potrebbe essere utilizzato per l'analisi della vita del nocciolo durante il burn-up ed essere quindi ricercati valori ottimali di parametri di progetto oppure strategie ottimali di caricamento e shuffling del combustibile,
- La fluenza ad un tempo e punto stabiliti. In questo caso il metodo potrebbe essere usato per analizzare il danneggiamento sui materiali con la vita del reattore.
- La radiotossicità delle scorie a lungo termine.
- Il controllo residuale (riserva di reattività) a fine ciclo. L'analisi di questa quantità può essere di particolare interesse in studi volti ad estendere il ciclo di vita del reattore.

METODOLOGIA HGPT-BU PER L'ANALISI PERTURBATIVA NEL CAMPO NEUTRONI/NUCLIDI. IMPLEMENTAZIONE E VALIDAZIONE NEL CODICE ERANOS

La metodologia HGPT per l'analisi dell'evoluzione dei nuclidi

Equazioni non-lineari governanti il flusso neutronico (vettore , la densità dei nuclidi (vettore **c)** e la funzione di controllo $\rho(t)$ durante l'evoluzione (burn-up) del nocciolo:

$$\mathbf{m}_{(\ )} \quad \frac{}{t} \quad B \quad \mathbf{0} \qquad (reattore\ critico)$$

$$\mathbf{m}_{(\ )} \quad \frac{}{t} \quad B \quad \rho\mathbf{s} \quad \mathbf{0} \qquad (reattore\ sottocr.)$$

$$\mathbf{m}_{(\mathbf{c})} \quad \frac{\mathbf{c}}{t} \quad E\mathbf{c} \quad 0$$

$$m_{(\rho)} \quad \mathbf{c}, S \quad -W \quad 0$$

- Equazione relativa a (in condizioni quasi statiche / t 0)
- Equazione di evoluzione dei nuclidi
- Condizione di conservazione della potenza (W)

L'operatore *B* dipende dalla densità del combustibile (vettore **c**) e dalla funzione di controllo (ρ), mentre la matrice *E* dipende dal flusso neutronico neutroni (vettore).

La funzione ρ è una variabile di controllo intensiva, dipendente solo dal tempo. Essa, ad esempio, può agire, come coefficiente, sulla concentrazione di boro solubile in un reattore PWR o sulla sorgente esterna in un reattore sottocritico.

METODOLOGIA HGPT-BU PER L'ANALISI PERTURBATIVA NEL CAMPO NEUTRONI/NUCLIDI. IMPLEMENTAZIONE E VALIDAZIONE NEL CODICE ERANOS

Le equazioni su indicate possono essere rappresentate sinteticamente con l'equazione

$$\mathbf{m}(f) = 0 \qquad \mathbf{f} \equiv \begin{vmatrix} \mathbf{c} \\ \rho \end{vmatrix}$$

che governa la funzione (vettore)

L'espressione del tutto generale di una risposta, o funzionale, Q (lineare, o linearizzata) può essere scritta nella forma sintetica

$$Q \equiv \int_o^{t_F} dt \quad \mathbf{s}_{syst}(\mathbf{f}) \equiv \mathbf{h}(\mathbf{f})$$

con $\mathbf{h}^+$ un vettore assegnato.

Attraverso un procedimento di tipo euristico la metodologia HGPT consente di determinare in un campo lineare, o linearizzato, la variazione δQ del funzionale a seguito della perturbazione δp_j di un parametro p_j , o il relativo coefficiente di sensitività dQ/dp_j. Questa metodologia è basata essenzialmente sul *'principio di conservazione dell'importanza'*, che si può esprimere nel seguente modo:

METODOLOGIA HGPT-BU PER L'ANALISI PERTURBATIVA NEL CAMPO NEUTRONI/NUCLIDI. IMPLEMENTAZIONE E VALIDAZIONE NEL CODICE ERANOS

"Il contributo ad una determinata risposta (misura) fissata nel tempo e nello spazio da parte di una particella (per esempio, un neutrone o un nuclide) posta ad un certo tempo in un determinato punto dello spazio delle fasi del sistema, si conserva, direttamente o attraverso la progenie cui essa può dar luogo, fino al momento della misura stessa."

Tale contributo viene per l'appunto definito come *'importanza'* associata alla particella ed alle coordinate che ne definiscono la posizione ed il tempo.

Per come è stata definito, il principio di conservazione dell'importanza, e le formulazioni perturbative che da esso traggono origine, sono applicabili a campi lineari, o linearizzati, di densità di particelle.

In una formulazione più generale esso è stato generalizzato a ogni altro campo di funzioni lineari, purchè aventi caratteristiche di derivabilità sufficienti. In altre parole, per questi campi si è stabilito un principio, che chiamiamo di 'rappresentazione euristica', per cui essi possono essere trattati come campi di densità.

METODOLOGIA HGPT-BU PER L'ANALISI PERTURBATIVA NEL CAMPO NEUTRONI/NUCLIDI. IMPLEMENTAZIONE E VALIDAZIONE NEL CODICE ERANOS

Implementazione della metodologia HGPT-BU nel codice ERANOS

Scopo del lavoro è l'implementazione nel codice neutronico ERANOS della metodologia HGPT-BU, di cui in recenti rapporti PAR si è ampiamente dimostrata la validità. A questo scopo nel codice sono state costruite delle prime nuove procedure di calcolo partendo da casi semplici, in cui possono essere fatte delle verifiche con metodi di risoluzione analitica come riferimento, a casi via via più complessi. Assieme ad ERANOS è stato utilizzato in molti casi il programma Excel per una più veloce verifica dei risultati.

Il codice ERANOS nella sua forma corrente, consente infatti solamente l'utilizzo della metodologia GPT per il calcolo perturbativo di funzionali del flusso e del flusso aggiunto, quali i rapporti di tassi di reazione e i coefficienti di reattività.

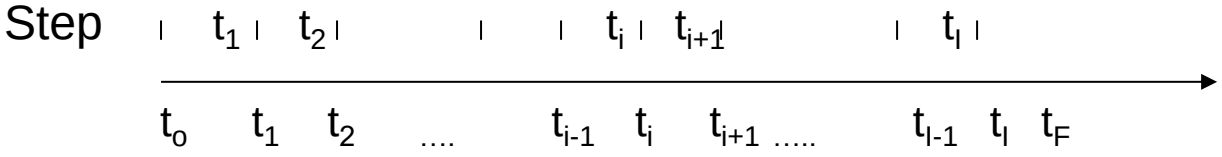
L'implementazione della metodologia HGPT-BU nel codice ERANOS consiste nello sviluppo di una nuova procedura per consentire calcoli multistep delle funzioni importanza ($\mathbf{c}^*$ e ρ^*) associate, rispettivamente, al campo dei nuclidi ($\mathbf{c}$) ed alla variabile di controllo (ρ). Il calcolo ad ogni step della funzione importanza associata ai neutroni (*) viene fatto attraverso la procedura già esistente nel codice stesso.

METODOLOGIA HGPT-BU PER L'ANALISI PERTURBATIVA NEL CAMPO NEUTRONI/NUCLIDI. IMPLEMENTAZIONE E VALIDAZIONE NEL CODICE ERANOS

Procedura del calcolo

Il nocciolo viene suddiviso in macrozone z (z=1,2,…,Z) in cui nel calcolo d'evoluzione vengono considerati i valori medi del flusso neutronico e dei nuclidi che evolvono. Nell'equazione che regge il flusso, la densità dei nuclidi evolventi che compaiono nell'operatore del trasporto, o della diffusione, sarà quindi data dai valori medi di ciascuna macrozona.

Consideriamo ora l'intervallo di tempo considerato suddiviso in step t_i come mostrato di seguito:



Come già accennato, con il metodo quasi-statico la densità di neutroni viene ricalcolata a tempi t_i specifici (i = 0,1,2, ..., I). A tali tempi t_i essa viene rinormalizzata alla potenza assegnata.

Con questa procedura non si tiene conto quindi della variazione della potenza con il burn-up durante lo step temporale. Si introduce pertanto un'incertezza nei valori finali delle concentrazioni dei nuclidi, incertezza che può essere ridotta aumentando il numero degli step.

L’espressione del tutto generale di una risposta Q (lineare, o linearizzata) può essere scritta nella forma (discretizzata nel tempo)

$$Q \quad \mathbf{h}_{,i}^{T} \quad {}_{i} \quad {}_{sys} \quad V_z \mathbf{h}_{c,i}^{T} \mathbf{c}_{z,i} \quad h_{\rho,i} \rho_i$$

$$i \;\; 0 \qquad\qquad z \;\; 1$$

con $\mathbf{h}_{\,i}, \mathbf{h}_{ci}, h_{\rho,i}$ quantità assegnate.

Seguendo la metodologia HGPT, per le funzioni importanza, può essere ottenuto uno schema di calcolo ricorrente, procedendo all'indietro a partire dal tempo finale t_F .

Le equazioni che reggono le funzioni importanza $\boldsymbol{\psi}_i^*, \mathbf{c}^*$, associate alle funzioni reali $_{i}, \mathbf{c}$ rispettivamente, risultano, all’interno di ciascuno step:

$$B_i^* \boldsymbol{\psi}_i^* \quad {}_{c,i}^{*} \int_{t_{i\;1}}^{t_i} \mathbf{c}^* dt \quad S_i^T \mathbf{c}_i \rho_i^* \quad {}_{i} \quad \mathbf{h}_{\,,i} \quad 0$$

$$\frac{\mathbf{c}^*}{t} \quad E_i^T \mathbf{c}^* \quad \delta(t \quad t_i) \quad {}_{,i}^{*} \boldsymbol{\psi}_{z,i}^{*} \quad S_i \quad {}_{z,i} \rho_i^* \quad {}_{i} \quad \mathbf{h}_{c,z,i}$$

Ω^* e Ω_c^* sono gli aggiunti degli operatori di accoppiamento $\Omega \quad \frac{\bar{}(B\ )}{\mathbf{c}}$ e $\Omega_c \quad \bar{}(E\mathbf{c})$

METODOLOGIA HGPT-BU PER L'ANALISI PERTURBATIVA NEL CAMPO NEUTRONI/NUCLIDI. IMPLEMENTAZIONE E VALIDAZIONE NEL CODICE ERANOS

L'equazione relativa alla funzione importanza ρ^*, associata al parametro di controllo ρ, risulta:

$$\boldsymbol{\psi}_i^{*T} \quad \frac{B(\rho)}{\rho} \quad {}_i \quad (1 \quad)\mathbf{s} \quad {}_{syst} \quad h_{\rho,i} \quad 0 \qquad \begin{matrix} 1 & per\ sistemi\ critici \\ 0 & per\ sistemi\ sottocritici \end{matrix}$$

Nel caso in cui h_ρ=0, questa equazione rappresenta, nel caso di sistemi critici, una condizione di ortogonalità della funzione importanza $\boldsymbol{\psi}_i^*$ rispetto al modo fondamentale $_i$, mentre nel caso di sistemi sottocritici essa risulta ortogonale alla sorgente **s**.

Questa condizione consente di ricavare l'espressione della funzione importanza relativa al controllo. Essa risulta:

$$\rho_i^* \quad \frac{1}{i} \quad \frac{(\quad 1)\ \boldsymbol{\psi}_i^{*T}\mathbf{s}_i \quad {}_{sys} \quad {}_{z\ 1}^{Z} V_z \quad {}_{z,i}^{T}\Omega_{c,z,i}^* \quad {}_{t_i\ 1}^{t_i} \mathbf{c}^* dt \quad {}_i^T\mathbf{h}_{,i} \quad {}_{sys}}{W}$$

dove $\begin{matrix} 1 & \text{per sistemi critici} \\ 0 & \text{per sistemi sottocrit.} \end{matrix}$

La funzione ρ^* riveste un ruolo fondamentale nella metodologia in quanto è attraverso di essa che l'effetto di una perturbazione su un dato funzionale tiene conto della variazione del controllo tale da mantenere la potenza prefissata. In particolare, è attraverso questa funzione che la perturbazione della densità di uno di due nuclidi tra loro indipendenti modifica la densità dell'altro per la variazione del flusso neutronico conseguente all'alterazione del controllo.

METODOLOGIA HGPT-BU PER L'ANALISI PERTURBATIVA NEL CAMPO NEUTRONI/NUCLIDI. IMPLEMENTAZIONE E VALIDAZIONE NEL CODICE ERANOS

Il significato fisico di $\rho^*(t)$ è l'effetto sul funzionale considerato dall'introduzione al tempo t di una unità di energia (un burst simulato da una delta di Dirac).
Nel nostro caso avrebbe effetto nullo per via del controllo imposto sulla potenza.

Espressione perturbativa discretizzata per step temporali ($_i$) assegnati e macrozone (z) in cui vengono utilizzati i valori ad inizio step delle densità neutroniche ($_i$) e dei nuclidi ($\mathbf{c}_i$):

$$\delta Q \quad \sum_{i\ 1}^{I}\sum_{j\ 1}^{J} \delta p_j \sum_{z\ 1}^{Z} \boldsymbol{\psi}_i^{*T} \frac{\mathbf{B}_{i\ 1}}{p_j}\ _z \sum_{z\ 1}^{Z} V_z\ _i d\mathbf{t}\mathbf{c}_z^{*T} \frac{E_{(c),z}}{p_j} dt \quad \rho_i^* \frac{\mathbf{c}, S\ _{t_{i\ 1}}}{p_j}\ _i$$

dove B e E rappresentano gli operatori/matrice che reggono le funzioni flusso neutronico (vettore) e densità nuclidi (vettore **c)**. S è una matrice con le sezioni d'urto macroscopiche di fissione.
L'integrale $\mathbf{c}, S\ _{t_{i\ 1}}$ rappresenta quindi il tasso di fissione totale.

METODOLOGIA HGPT-BU PER L'ANALISI PERTURBATIVA NEL CAMPO NEUTRONI/NUCLIDI. IMPLEMENTAZIONE E VALIDAZIONE NEL CODICE ERANOS

Per specifici casi di interesse si devono individuare le condizioni 'finali' che sono specifiche per ogni singolo problema. Ad esempio:

- Risposta della sorgente aggiunta del tipo $\mathbf{h}_{c,z,i}\ \delta(t - t_F)\begin{vmatrix}\mathbf{0}\\ \mathbf{h}_c\\ 0\end{vmatrix}$

  corrisponde, per esempio, all'accumulo di uno o più materiali al tempo t_F.

- Risposta della sorgente aggiunta del tipo: $\mathbf{h}_{,z,i}\ \delta(t - t_F)\begin{vmatrix}\mathbf{h}\\ \mathbf{0}\\ 0\end{vmatrix}$

  corrisponde, per esempio, ad un tasso di reazione al tempo t_F

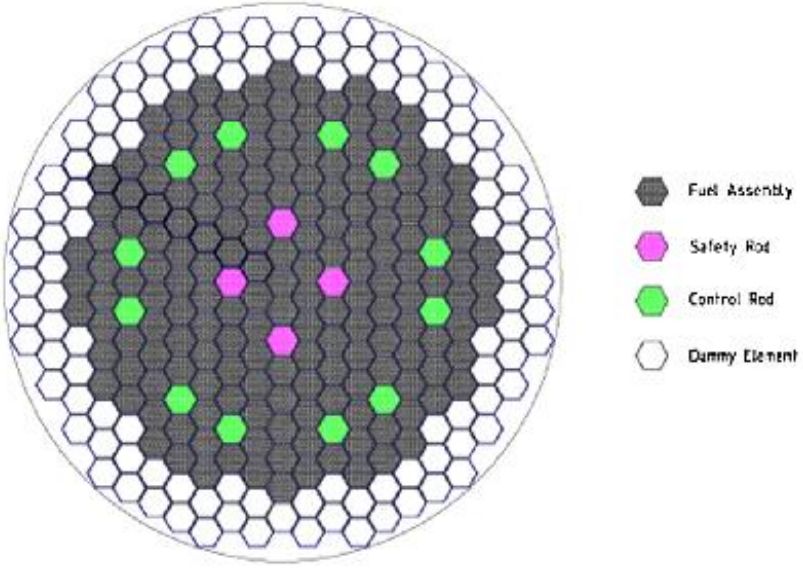
- Risposta della sorgente aggiunta del tipo: $h_{\rho,i}\ \delta(t - t_F)\begin{vmatrix}\mathbf{0}\\ \mathbf{0}\\ 1\end{vmatrix}$

  corrisponde al controllo residuo al tempo finale t_F

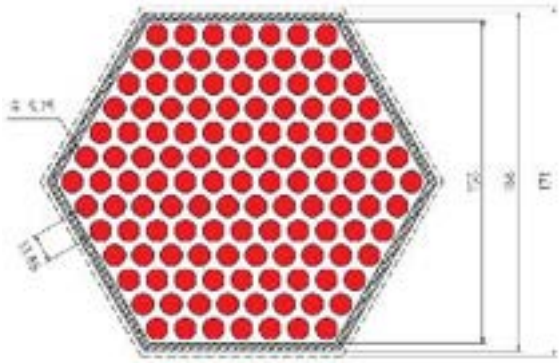
METODOLOGIA HGPT-BU PER L'ANALISI PERTURBATIVA NEL CAMPO NEUTRONI/NUCLIDI. IMPLEMENTAZIONE E VALIDAZIONE NEL CODICE ERANOS

Sistema di riferimento

Il modello matematico, opportunamente semplificato nei vari vari casi considerati, fa riferimento, con qualche variante, al progetto di reattore veloce ALFRED. Esso consiste in un sistema cilindrico con due zone di nocciolo circondate da un riflettore, con dimensioni dei raggi esterni, rispettivamente di 70, 110 e 160 cm. In ciascuna delle due zone di nocciolo viene definita una cella di combustibile per il necessario calcolo dei valori medi delle densità dei nuclidi fissili e fertili evolventi (in questo studio, per semplicità, limitati al Pu-239 e Pu-240). Per semplicità con flussi neutronici ottenuti dai calcoli di cella le sezioni d'urto sono state mediate ad un gruppo.



Core layout



Fuel assembly cross-section

[1]G.Grasso et al., "The core design of ALFRED,a demonstrator for the European lead-cooled reactors", Nuclear Engineering and. Design 278, 287 (2014)

METODOLOGIA HGPT-BU PER L'ANALISI PERTURBATIVA NEL CAMPO NEUTRONI/NUCLIDI. IMPLEMENTAZIONE E VALIDAZIONE NEL CODICE ERANOS

Caso 1. Sistema di due zone attive senza leakage. Un solo nuclide fissile (Pu239)

Questo caso semplicissimo è inteso per avviare una rigorosa prima impostazione delle procedure di calcolo necessarie all'implementazione della metodologia GHTP-BU nel codice ERANOS. La semplicità del sistema scelto consente soluzioni analitiche che rendono possibili verifiche rigorose dei risultati dei calcoli, oltre a consentire di procedere in parallelo con calcoli indipendenti (con il programma EXCEL) per un utile confronto e aiuto a meglio definire alcune modalità di programmazione.

In questo e nei prossimi casi trattati si è ritenuto di poter trascurare nel calcolo dei coefficienti di sensitività il contributo ai funzionali considerati da parte dei termini contenenti la ψ_i^* . Questa funzione serve a tenere conto degli scostamenti della distribuzione del flusso neutronico a causa della perturbazione. Il tenerne conto certamente renderebbe i risultati ancora più precisi.

Per questo caso sono stati scelti:

Geometria: radiale con due zone di volume eguale e corrente nulla al confine esterno;
Ciclo: 180 giorni con step di 5 giorni per un burnup del 9% circa;
Funzionali: densità del Pu239 al tempo di fine ciclo (t_F) in ciascuna delle due zone interna ed esterna (rispettivamente, Z1 e Z2) che formano il nocciolo;

Parametro (p) perturbato: +1% della concentrazione iniziale del Pu239 nella zona 1.

I valori dei coefficienti di sensitività dQ/Q sono riportati nella Tabella che segue

METODOLOGIA HGPT-BU PER L'ANALISI PERTURBATIVA NEL CAMPO NEUTRONI/NUCLIDI. IMPLEMENTAZIONE E VALIDAZIONE NEL CODICE ERANOS

Coefficienti di sensitività dQ/dp
[parametro perturbato p=$Pu^{239}(t_0)$_z1]

		Calcoli EXCEL	
Funzionale (Q)	dQ/dp Soluz. analitica	dQ/dp Calc.diretto (36step)	dQ/dp Calc.GPT-BU
Densità Pu239 a t_F in Z1	0.955	0.956	0.955
Scarto vs. soluz. analit.	-	**0.10%**	**0%**
Densità Pu239 a t_F in Z2	0.0460	0.0438	0.0449
Scarto vs. soluz. analit.	-	**-4.76%**	**-2.22%**
		Calcoli ERANOS	
Dens. Pu239 a t_F in Z1	-	1.00	0.955
Scarto vs. soluz. analit.	-	**4.71%**	**0%**
Dens. Pu239 a t_F in Z2	-	0.0503	0.0452
Scarto vs soluz. analit.	-	**9.29%**	**-2.46%**

Come si vede, i risultati ottenuti utilizzando la metodologia HGPT-BU si confrontano molto bene con la soluzione analitica. I risultati meno soddisfacenti, anche se accettabili, ottenuti con il metodo diretto sono dovuti al fatto che essi, a differenza della metodologia HGPT che richiede solo processi di integrazione, sono ottenuti dalla differenza di numeri molto grandi, dell'ordine di 1E+20, e quindi facilmente affetti da errori numerici.

Caso 2. Sistema di due zone attive senza leakage. Due nuclidi fissili (Pu239 e Pu240)

Per questo caso sono stati scelti:

Geometria: radiale con due zone di volume eguale e corrente nulla al confine esterno;
Ciclo: 180 giorni per un burnup del 9% circa;
Funzionali: densità del Pu239 e del Pu240 al tempo di fine ciclo (t_F) in ciascuna delle due zone interna ed esterna (rispettivamente, Z1 e Z2) che formano il nocciolo;

Parametro (p) perturbato: +1% della concentrazione iniziale del Pu239 nella zona 1.

I valori dei coefficienti di sensitività dQ/Q sono riportati nella Tabella che segue.

METODOLOGIA HGPT-BU PER L'ANALISI PERTURBATIVA NEL CAMPO NEUTRONI/NUCLIDI. IMPLEMENTAZIONE E VALIDAZIONE NEL CODICE ERANOS

Coefficienti di sensitività dQ/dp
[parametro perturbato p=$Pu^{239}(t_0)$_z1]

	Calcoli EXCEL		
Funzionale (Q)	dQ/dp Calc.diretto (36step)	dQ/dp Calc. HGPT-BU	Scarto
Densità Pu239 a t_F in Z1	9.54E-01	9.55E-01	**0.10 %**
Densità Pu239 a t_F in Z2	2.43E-02	2.38E-02	**-1.99%**
Densità Pu240 a t_F in Z1	3.96E-02	3.88E-02	**-2.04%**
Densità Pu240 a t_F in Z2	4.91E-03	4.81E-03	**-2.08%**
	Calcoli ERANOS		
Densità Pu239 a t_F in Z1	9.08E-01	9.10E-01	**-0.46%**
Densità Pu239 a t_F in Z2	7.68E-02	7.69E-02	**-0.22%**
Densità Pu240 a t_F in Z1	5.31E-02	5.51E-02	**-3.61%**
Densità Pu240 a t_F in Z2	1.38E-03	1.39E-03	**-2.29%**

Come si vede, anche in questo caso i risultati ottenuti utilizzando la metodologia HGPT-BU si confrontano molto bene con i valori ottenuti con il calcolo diretto, sia usando il programma EXCEL che il codice ERANOS.

METODOLOGIA HGPT-BU PER L'ANALISI PERTURBATIVA NEL CAMPO NEUTRONI/NUCLIDI. IMPLEMENTAZIONE E VALIDAZIONE NEL CODICE ERANOS

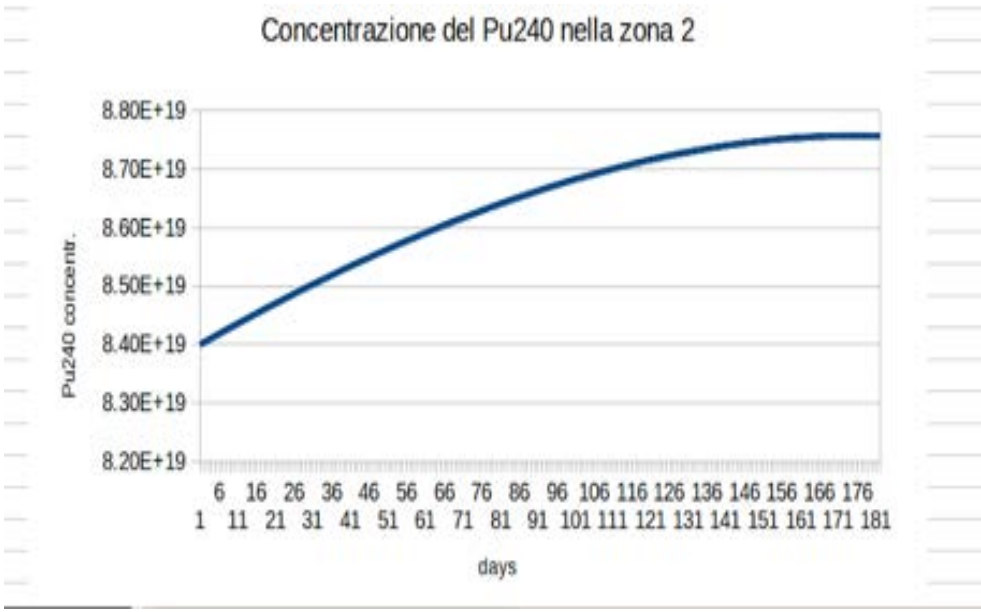
Caso critico

Considerando il caso particolare di un ciclo di 180 giorni con burn-up di circa il 40% si sono ottenuti i risultati riportati in tabella

Come si vede, gli scarti a vari tempi di burn up sono contenuti e soddisfacenti, salvo per il caso Q=Pu_{240}_z2 a 180 gg. Tale scarto è spiegabile osservando il grafico a fianco. Si osserva il raggiungimento di un massimo attorno ai 180 gg. E' chiaro che a quel punto una perturbazione qualsiasi modifica di pochissimo la concentrazione del nuclide in esame. Da qui lo scarto elevato tra calcolo diretto e HGPT per i conseguenti errori numerici.

Scarti HGPT/Calcolo diretto a vari tempi di burn-up (Calcoli Excel)
[parametro perturbato p=$Pu^{239}(t_0)$_z1]

Q	36gg	72gg	108 gg	144gg	180gg
$Pu^{240}(t_F)$_z2	1.61%	2.15%	0.74%	-5.34%	168.12%
$Pu^{240}(t_F)$_z2					4.55%
$Pu^{239}(t_F)$_z2					5.17%
$Pu^{239}(t_F)$_z2					-1.33%



METODOLOGIA HGPT-BU PER L'ANALISI PERTURBATIVA NEL CAMPO NEUTRONI/NUCLIDI. IMPLEMENTAZIONE E VALIDAZIONE NEL CODICE ERANOS

Caso 3. Sistema di due zone attive e riflettore. Due nuclidi fissili (Pu239 e Pu240)

.

Per questo caso sono stati scelti:

Geometria: radiale con nocciolo formato da due zone seguite da riflettore;
Ciclo: 180 giorni per un burnup del 9% circa;
Funzionali: densità del Pu239 e del Pu240 al tempo di fine ciclo (t_F)in ciascuna delle due zone interna ed esterna (rispettivamente, Z1 e Z2);

Parametro (p) perturbato: +1% della concentrazione iniziale del Pu239 nella zona 1.

I valori dei coefficienti di sensitività dQ/Q sono riportati nella Tabella che segue.

METODOLOGIA HGPT-BU PER L'ANALISI PERTURBATIVA NEL CAMPO NEUTRONI/NUCLIDI. IMPLEMENTAZIONE E VALIDAZIONE NEL CODICE ERANOS

Coefficienti di sensitività dQ/dp
[parametro perturbato $p=Pu^{239}(t_0)_z1$]

	Calcoli EXCEL		
Funzionale (Q)	dQ/dp Calc.diretto (36step)	dQ/dp Calc. HGPT-BU	Scarto
Densità Pu239 a t_F in Z1	9.20E-01	9.38E-01	**-1.90%**
Densità Pu239 a t_F in Z2	5.05E-02	5.43E-02	**-6.97%**
Densità Pu240 a t_F in Z1	2.96E-02	2.84E-02	**4.28%**
Densità Pu240 a t_F in Z2	-6.91E-03	6.51E-03	**6.14 %**

Anche in questo caso i risultati ottenuti utilizzando la metodologia HGPT-BU si confrontano bene con i valori ottenuti con il calcolo diretto, usando il programma EXCEL. Prove sullo stesso test sono in corso con il codice ERANOS.

METODOLOGIA HGPT-BU PER L'ANALISI PERTURBATIVA NEL CAMPO NEUTRONI/NUCLIDI. IMPLEMENTAZIONE E VALIDAZIONE NEL CODICE ERANOS

Risultati raggiunti:

• Prima implementazione in ERANOS di procedure per il calcolo perturbativo nel campo non lineare neutroni/nuclidi.

• Dimostrazione della validità della metodologia HGPT-BU attraverso test dimostrativi su primi casi di evoluzione, rappresentativi un reattore veloce refrigerato a piombo. La precisione dei calcoli eseguiti secondo la procedura risulta in tutti i casi considerati inferiore al 6-7%

Dopo questa prima implementazione si proseguirà aumentando il numero di nuclidi che compongono l'elemento di combustibile ed eventualmente il numero di zone in cui calcolare i valori medi delle loro concentrazioni ai vari step di burn-up.

THERMAL-HYDRAULIC ANALYSIS OF PHENIX NPP DISSYMMETRIC TRANSIENTS USING RELAP5-3D COMPUTER PROGRAM

Andrea Subioli [UNIROMA1]
Fabio Giannetti [UNIROMA1]
Alessandro Del Nevo [ENEA]

WORKSHOP TEMATICO: Gen. IV - LFR
ADP MiSE-ENEA (PAR2016-LP2)
Aula Magna - Scuola di Ingegneria e Architettura, Università di Bologna
26-27 Settembre, 2017

CONTENTS

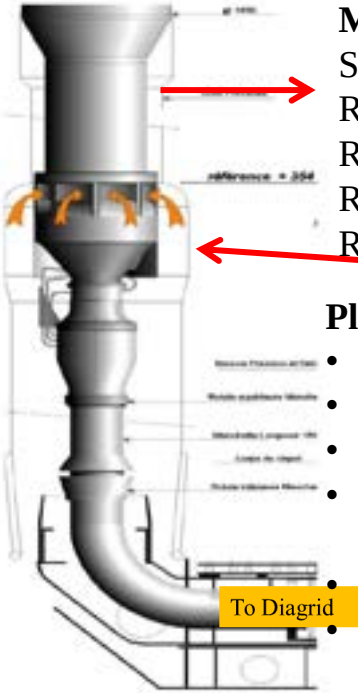
- Introduction
- Objectives of the activity
- Outline of PHENIX reactor
- “Dissymmetric test” description
- RELAP5-3D© nodalization
- Preliminary steady state
- Summary and follow-up

INTRODUCTION

- PHENIX End Of Life Tests performed in 2009 after the 56th irradiation cycle
- 2 tests were performed in thermal-hydraulics area
  - *a natural convection test* and
  - a dissymmetrical configuration test
    → this has been selected as a benchmark transient
    → synergy with H2020 SESAME project

OBJECTIVES OF THE ACTIVITY

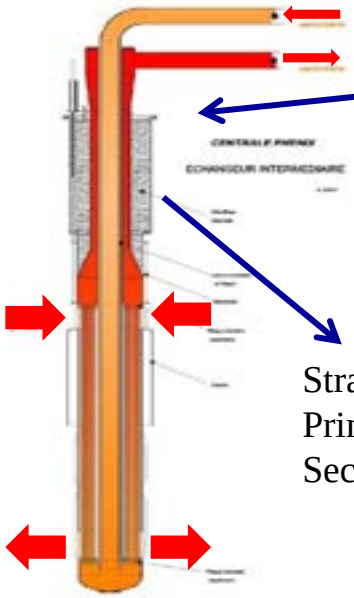
- to increase knowledge about FR thermal-hydraulics
- to compare best-estimate TH-SYS code calculations to experimental data, thus to validate RELAP5-3D© system code in simulating FR designs
- to assess the reliability of SYS-TH multiD components in modeling transient in LM pool FR
- to identify and, as far as possible, to quantify the code limitations and the source of uncertainties in simulating postulated accidents occurring in liquid metal FR designs
- to improve the understanding of the TH processes and phenomena observed in dissymmetrical test
- to improve the understanding of FR neutronics, TH and SYS analysis (beyond PAR and SESAME objectives)



MCP data:
Speed : 540 rpm
Rated speed : 800 rpm
Rated flow : 1.0312 m^3/s
Rated head : 63.2 m
Rated torque : 8.795 m^5/s^2

Plant operating features:

- Power: 350 MWth
- 3 Main Coolant Pumps running
- 2 IHX x MCP
- 2 out of 3 secondary circuits in operation
- 4 IHX in service
- 2 plugged IHX - secondary circuit #2 (DOTE)

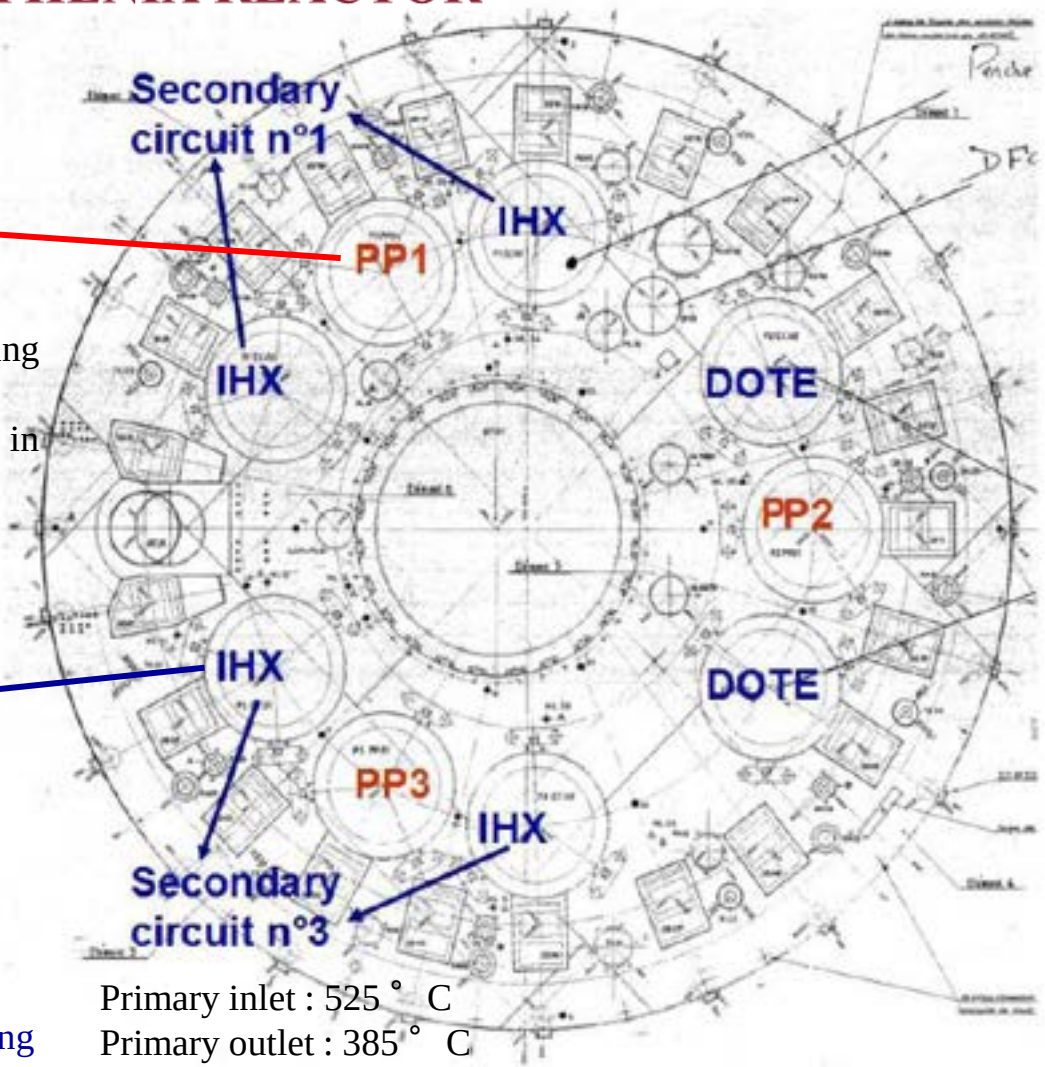


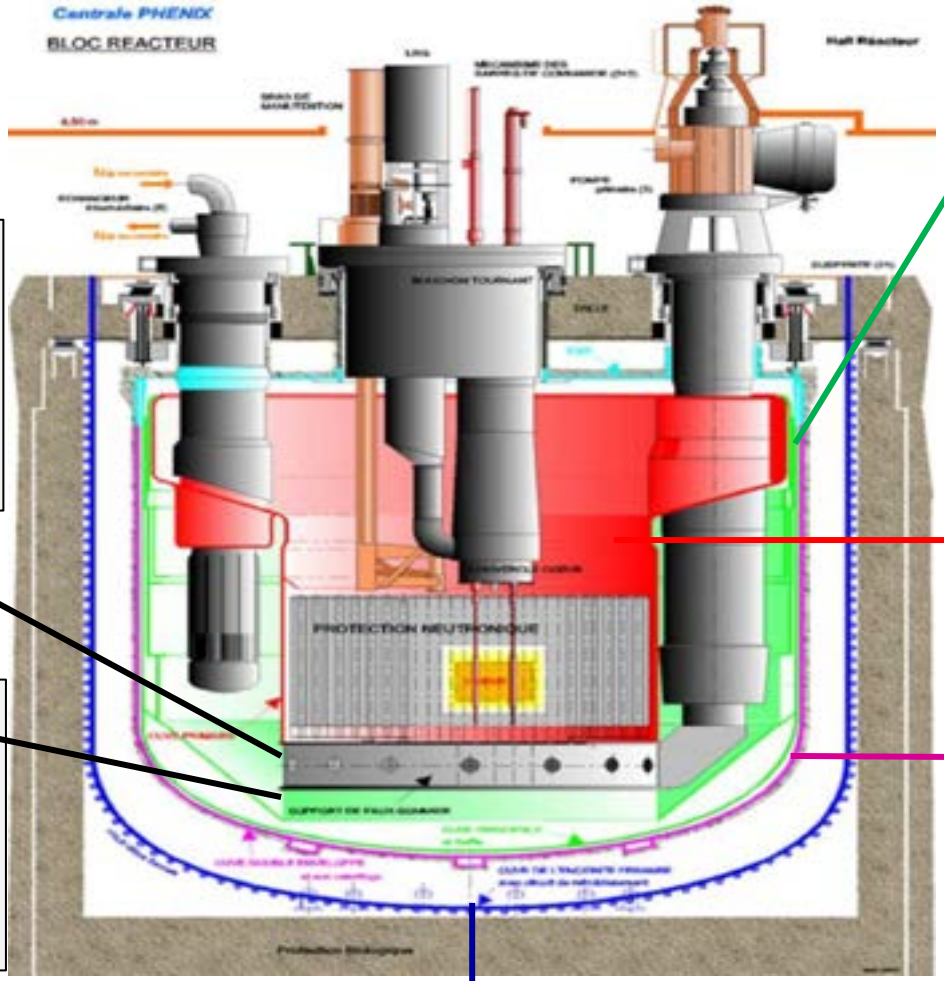
Straight-tube HEX
Prim coolant shell side
Sec coolant tube side

Operating conditions

Primary inlet : 525 ° C
Primary outlet : 385 ° C
Secondary inlet : 320° C
Secondary outlet : 525 ° C
Primary flow rate : 497 kg/s
Secondary flow rate in IHX : 345 kg/s

PHENIX REACTOR





Diagrid is connected to primary pumps.
It has the function of positioning, supporting and supplying sodium to core SA

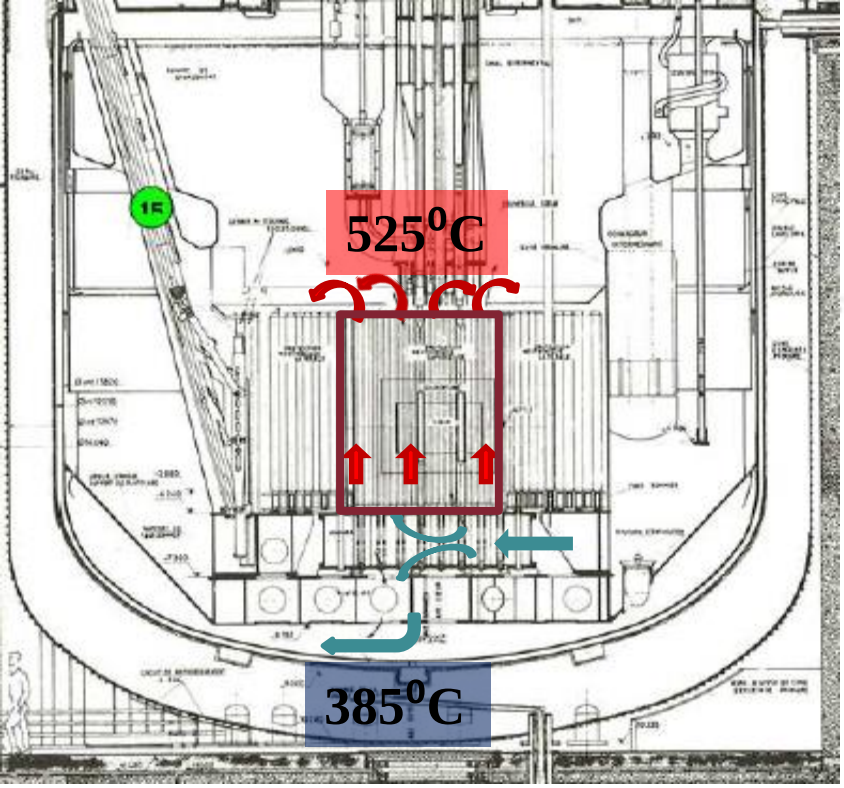
Strongback has the function of supporting the core and it carries about the 10% of operating flow to the vessel cooling system.

Main vessel
Diameter = 11.8 m
Na inventory = 800 tons
Attached to the upper slab by 21 suspension hangers
Cooled in the upper zone by a vessel cooling system

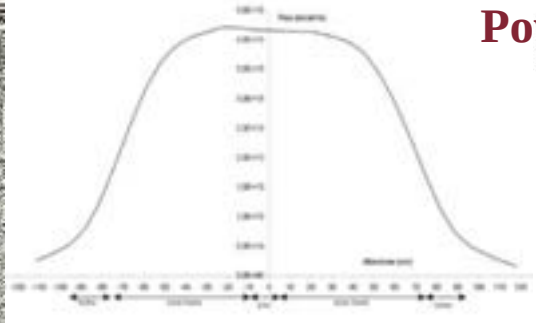
Inner vessel separates the pool in two regions: hot and cold.

Double- envelope vessel is welded to the upper region of the main vessel and it has the function of containing any possible sodium leaks.

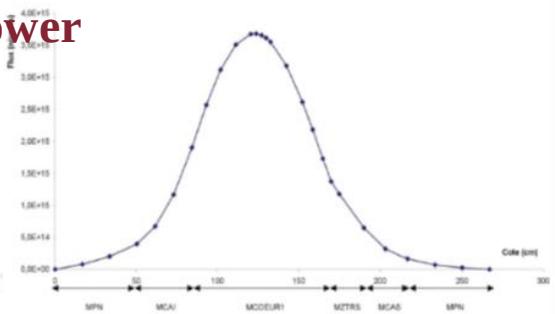
Primary containment vessel is welded to the slab's underside, and attached to the reactor pit. It has to retain radioactive release of postulated severe accident. It carries the final emergency cooling system which is designed to keeping the reactor concrete at ambient temperature, and to ensure the decay heat removal



Power

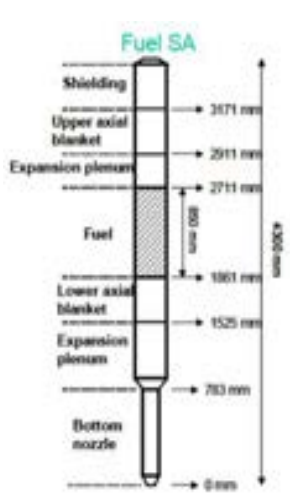


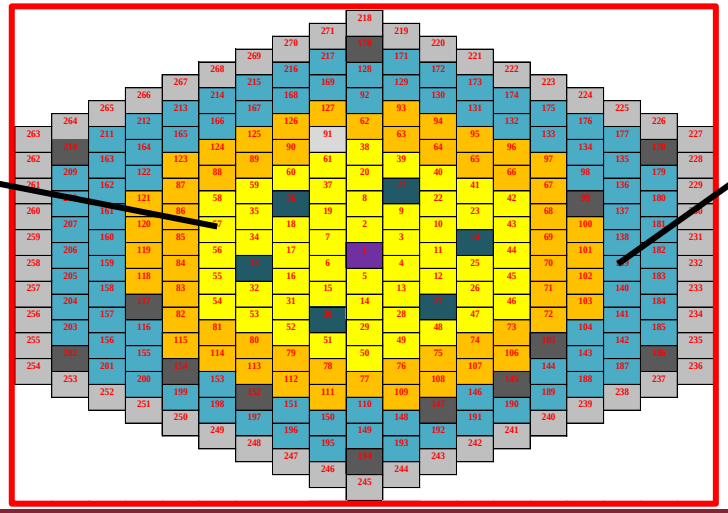
Radial distribution

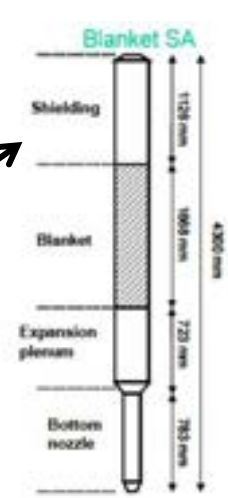


Axial distribution

	Power [MWth]	Flow rate [kg/s]
Inner core	180.9	861
Outer core	143.1	779
Blanket zone	24.1	226
Control rods zone	0.7	14
Steel zone	1.2	62
Storage zone	1.7	46
Total	351.7	1988



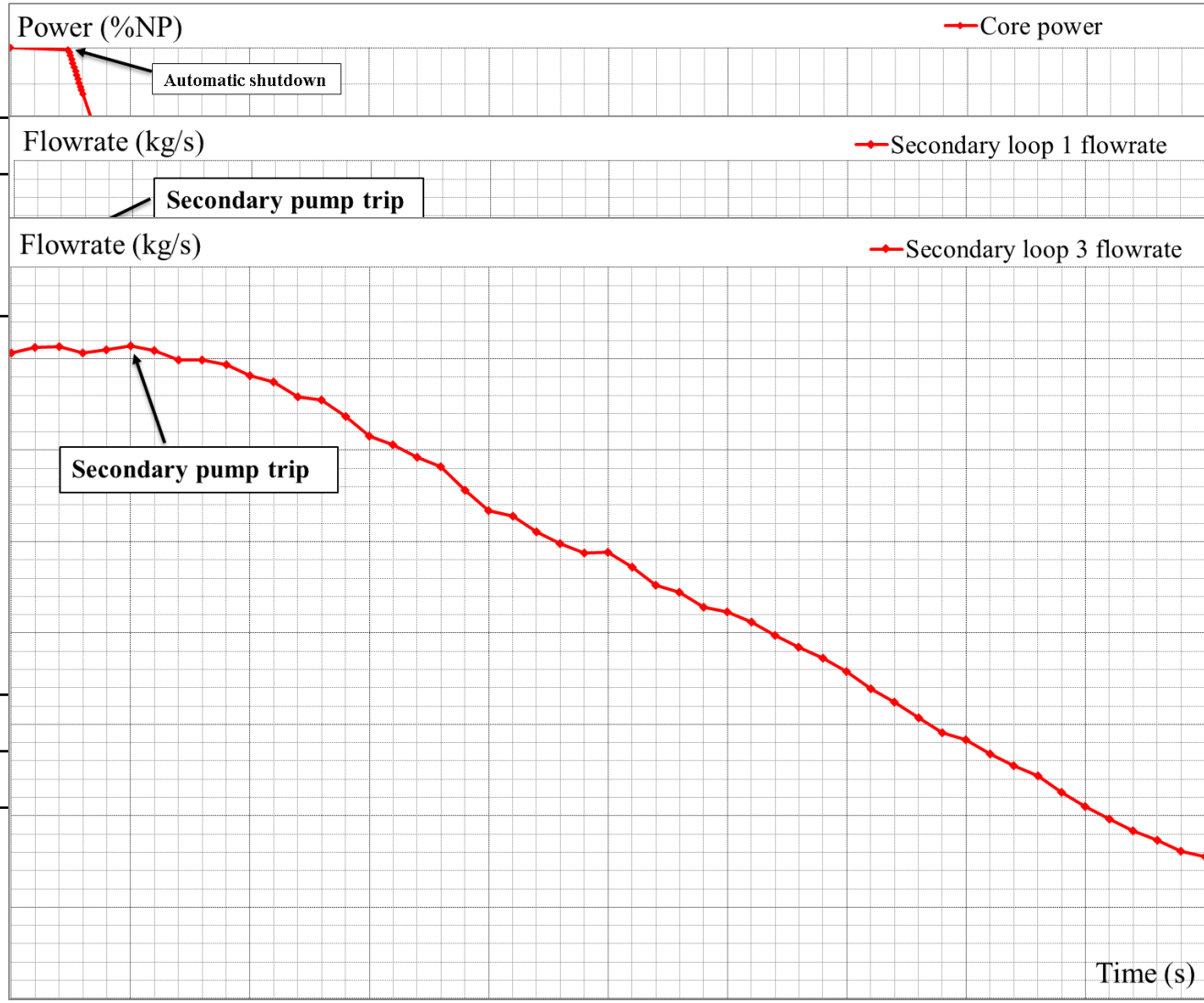




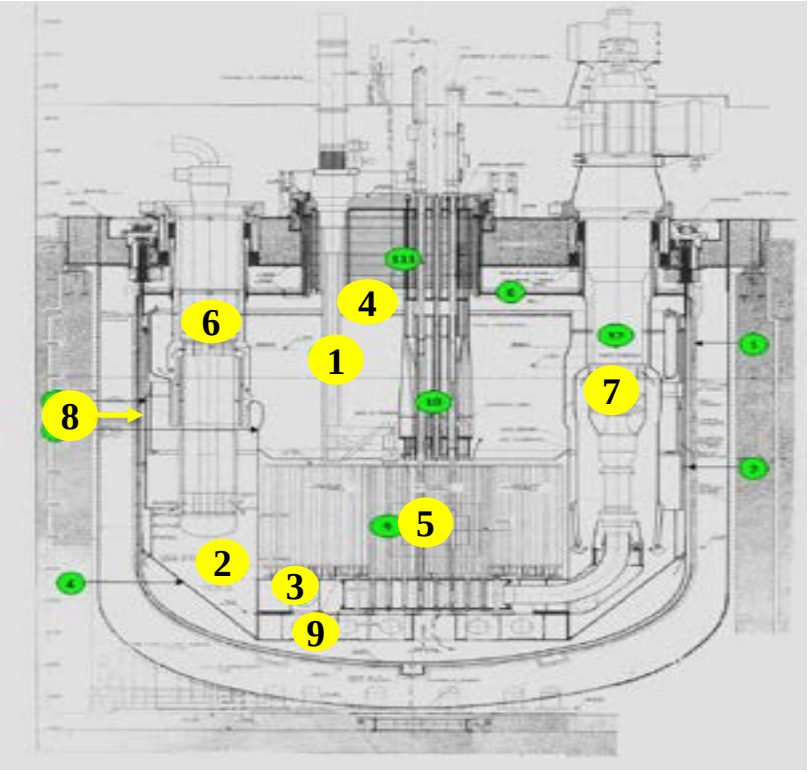
- Inner core (54 SA)
- Outer core (56)
- Steel neutron reflector (212 SA)
- Control rod (6 SA)
- Safety rod (1 SA)
- Experimental SA (1)
- Blanket (86 SA)
- Neutronic steel shielding (297 SA)
- Neutronic B4C shielding (765 SA)

TEST DESCRIPTION

Time (s)
0
5
48
1800



PHENIX NODALIZATION



Nodalization is composed by

- a MULTID component (CV 900) modelling large part of the primary system (2520 volumes)
- 1D components (i.e. PIPES and BRANCH) in charge of representing the zones where a predominant 1D flow is expected (i.e. hexagonal fuel assembly; heat exchangers; pump suction and feeding conduit, etc.)

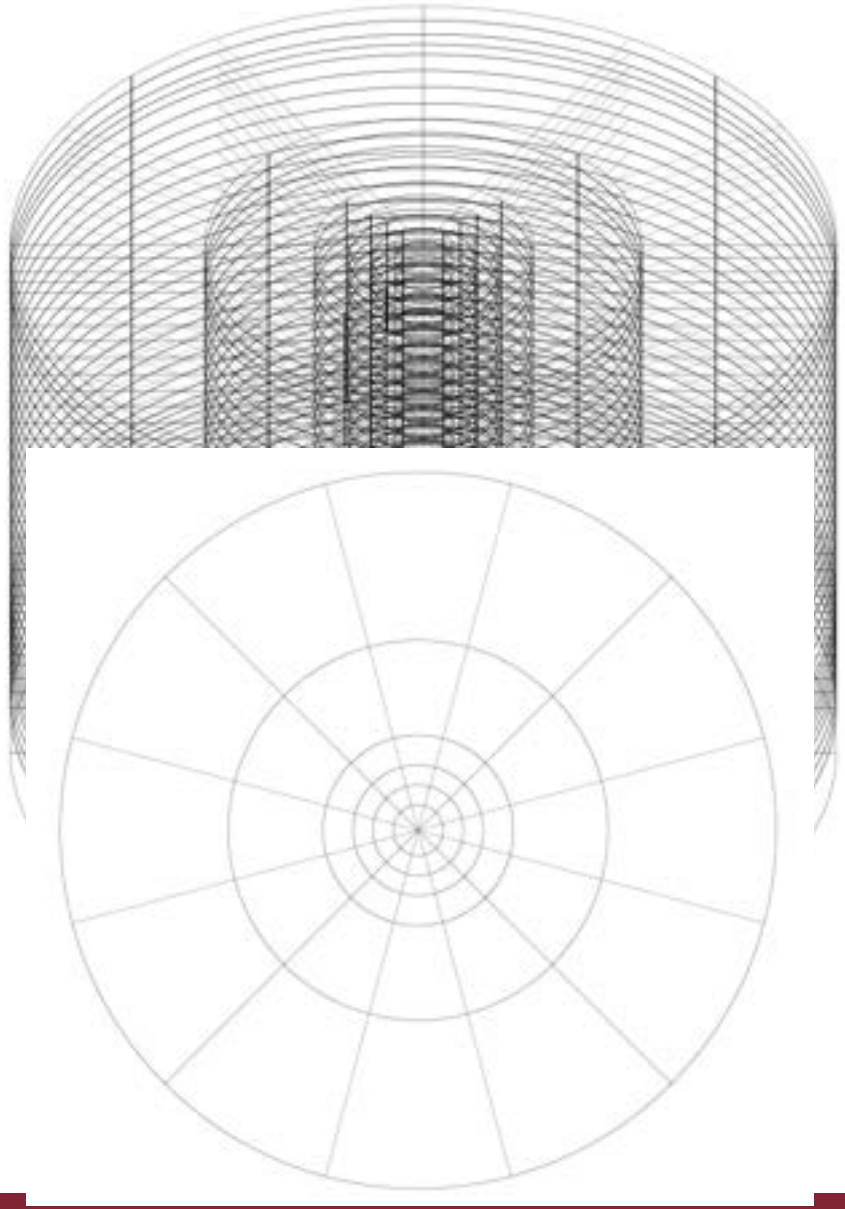
Nodalization features:

- ❑ "Sliced approach" is applied in all systems
- ❑ Relevant elevations of PHENIX are maintained in the nodalization, with minor exceptions due to modeling constraints (e.g. IHX bottom)
- ❑ 1 MULTID and1D components
- ❑ The ratio between the length of adjacent nodes is limited to 1.2 with few exception
- ❑ Westinghouse heat transfer correlation in bundle region
- ❑ Wire wrapped fuel bundle friction losses are modeled with Cheng and Todreas
- ❑ K-loss coeff. in junct. evaluated or estimated on the basis of geometries
- ❑ FA orifice setup on the basis of mass flow rates and overall DP
- ❑ Roughness is set 3.2e-5m with the exception of the core region where is set 1.e-6

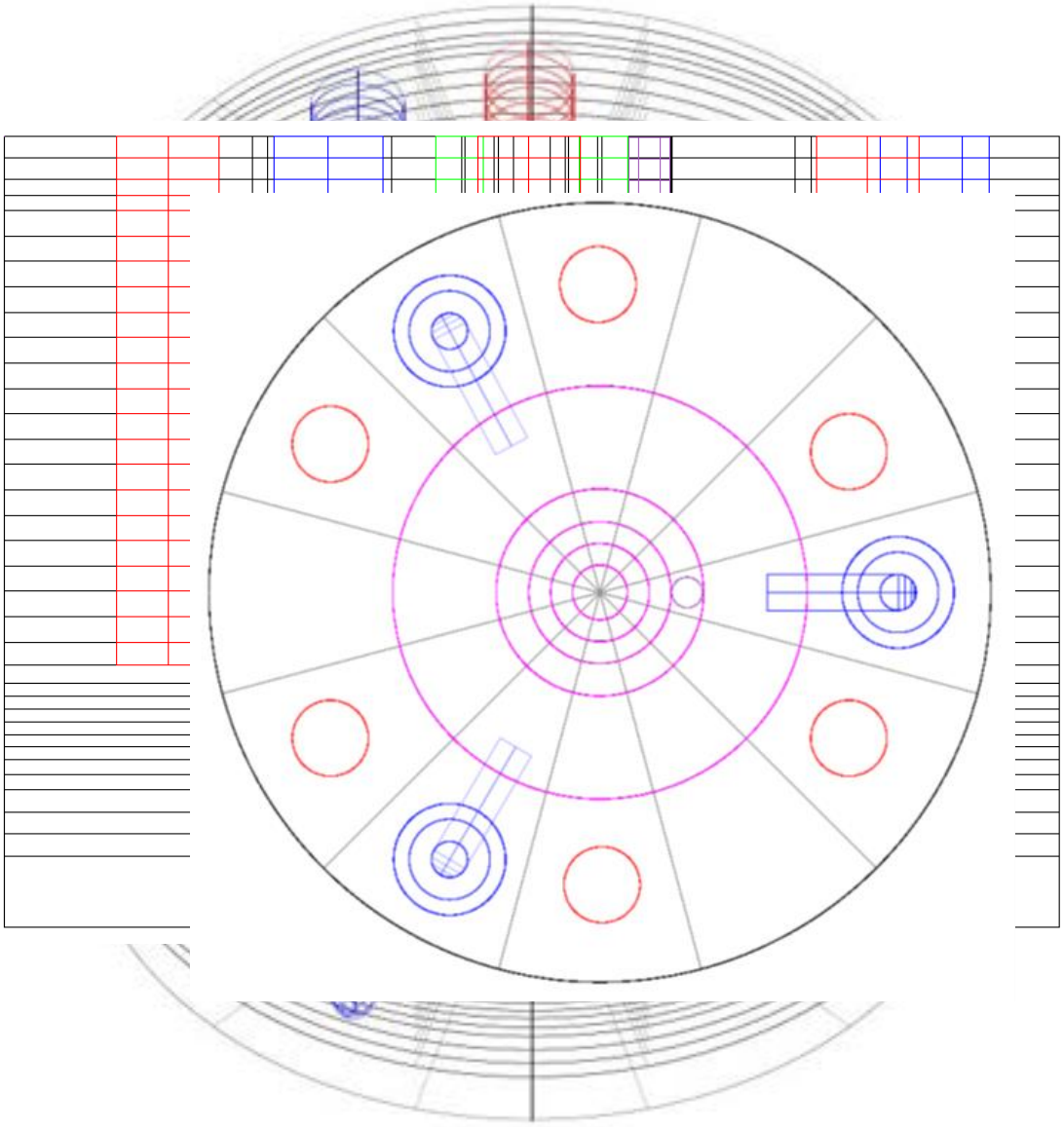
#	QUANTITY	Value
1	Tot. No. of HYDR vol.	7258
2	Tot. No. of HYDR junct.	12034
3	Tot. No. of heat structures	TBC
4	Tot. No. of mesh points in the heat structures	TBC
5	Tot. No.of core active structures (radial x axial)	21716

3D MODEL OF PRIMARY TANK

- MULTID features → 6x12x35
- MULTID models:
  - Diagrid
  - Core bypass
  - Hot pool
  - Cold pool



- Layout of MCP conduits and IHXs modeled according with the real configuration (θ, z)
- Porosity factors are used to model the geometry and the flow paths

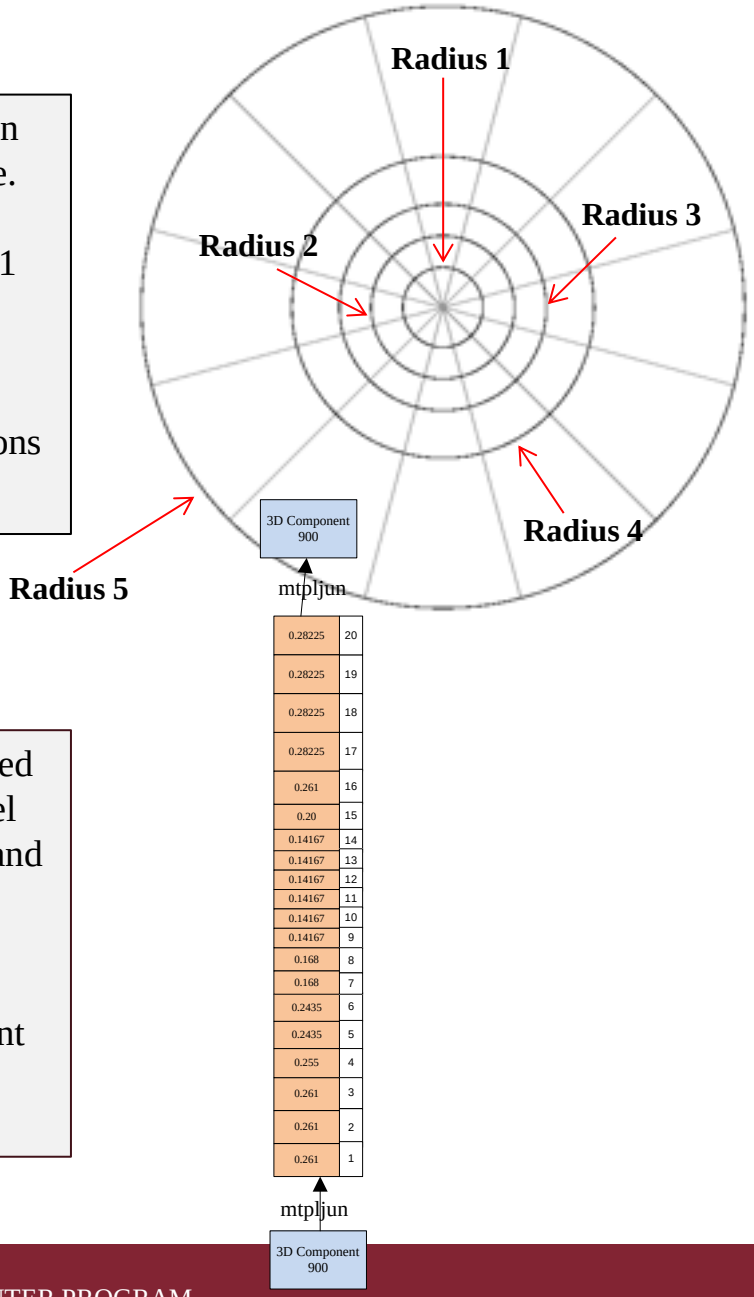


5) THE REACTOR CORE

- Radius 1 models PHENIX core ranks 1 to 3
- Radius 2 models PHENIX core ranks 4 and 5
- Radius 3 models PHENIX core ranks 6 and 7

Full core SA representation of first seven ranks of core.

The SA are modeled 1 by 1 with PIPE components according with the geometrical description reported in the specifications



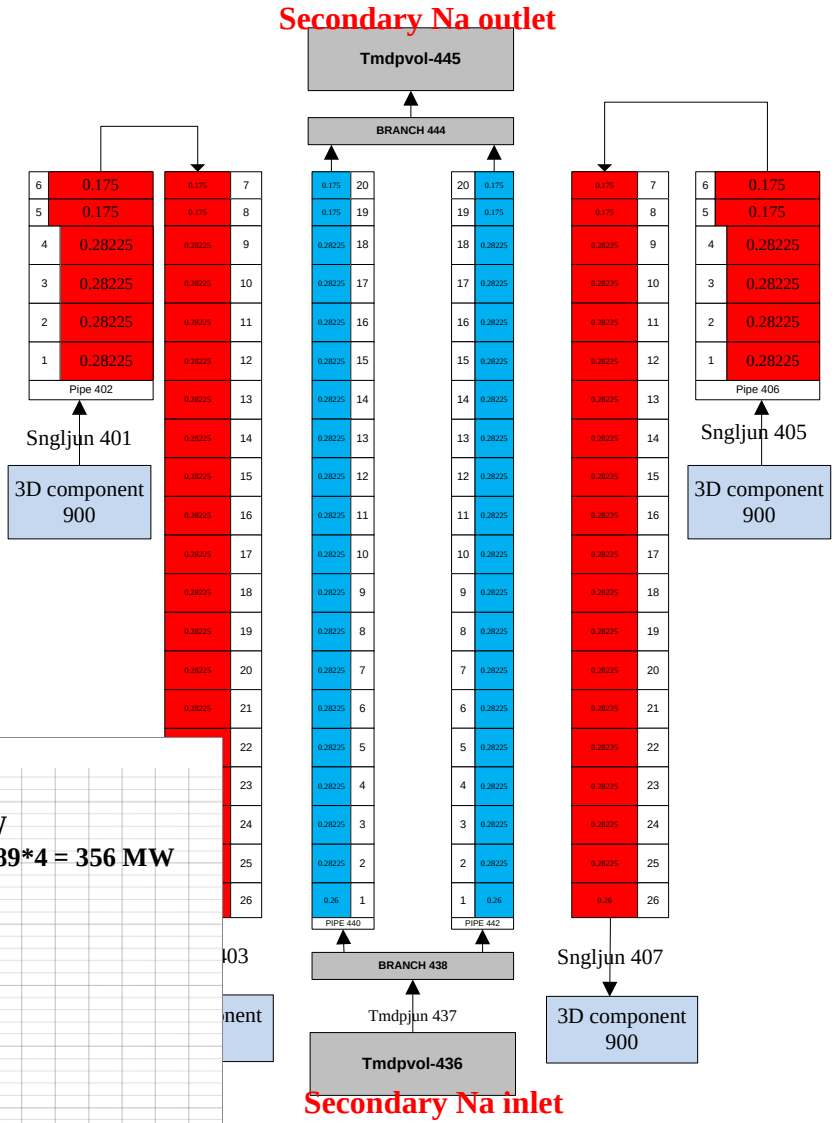
- Radius 4 models PHENIX core ranks 8 to 10
- Radius 5 models PHENIX core ranks > 10

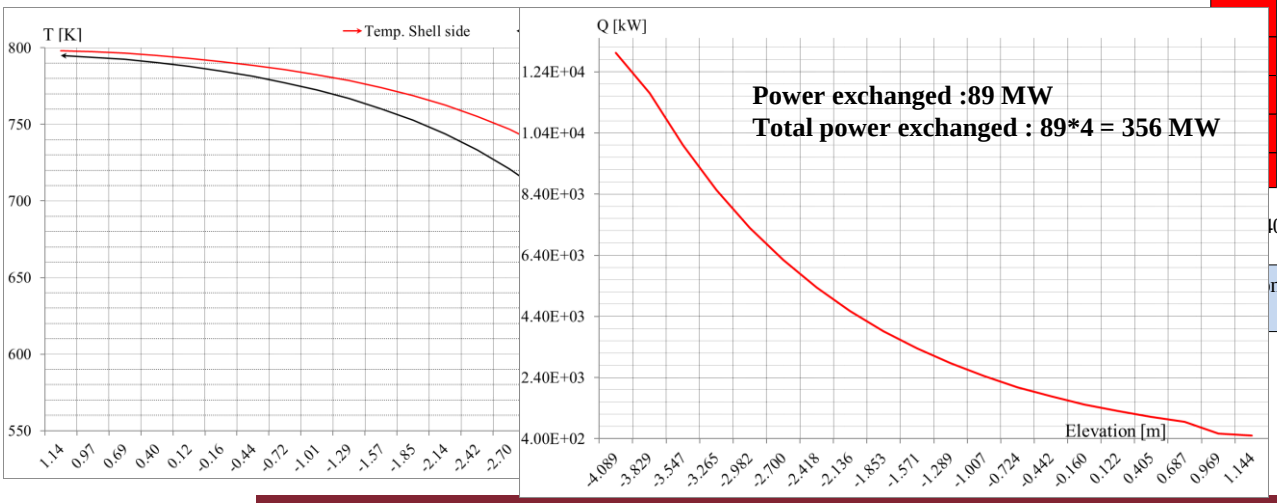
SA of each type are grouped (i.e. blanket, reflector, steel shielding, B4C shielding and storage, separately)

They are modeled with an equivalent PIPE component per sector (12 equivalent PIPEs - 1 per sector)

6 INTERMEDIATE HEAT EXCHANGERs

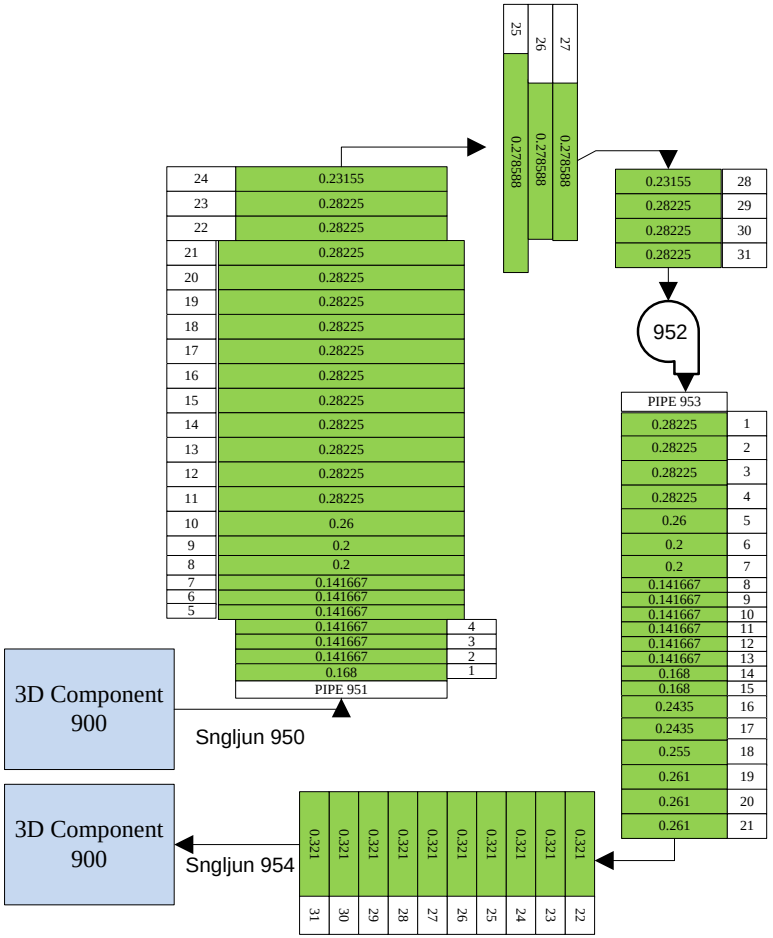
- 4 IHX primary sides are modeled separately with PIPE components (CV 402, CV406,CV 412 , CV 416) connected upstream and downstream with the MULTID component
- The 4 IHX secondary sides a modeled separately with PIPE components (CV 440, CV 442, CV 450, CV 452) and connected with proper boundary conditions imposing the pressure, temperature and the mass flow rate of secondary fluid
- Primary and secondary sides of DOTE components are modeled and idle. The connections between the IHXs #2 are closed to prevent the primary mass flow rate passing through
- Heat structures of IHX are modeled with EM10 (T91) material





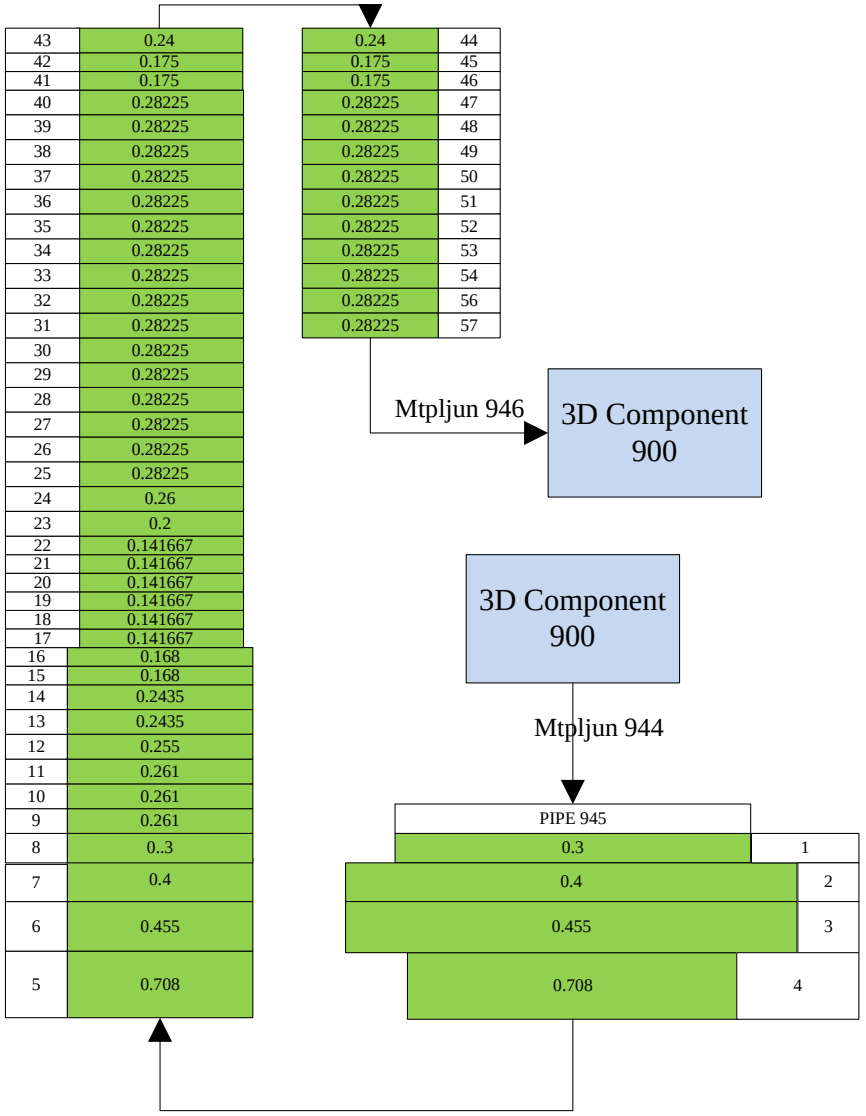
7) PRIMARY PUMP

- 3 MCP are modelled separately with proper PUMP components
- Homologous curves have set-up using PHENIX reference data
- PIPE components model the ‘pump skirt’ and the feeding conduits
- These are connected upstream and downstream with the MULTID component accounting for the real 3D representation



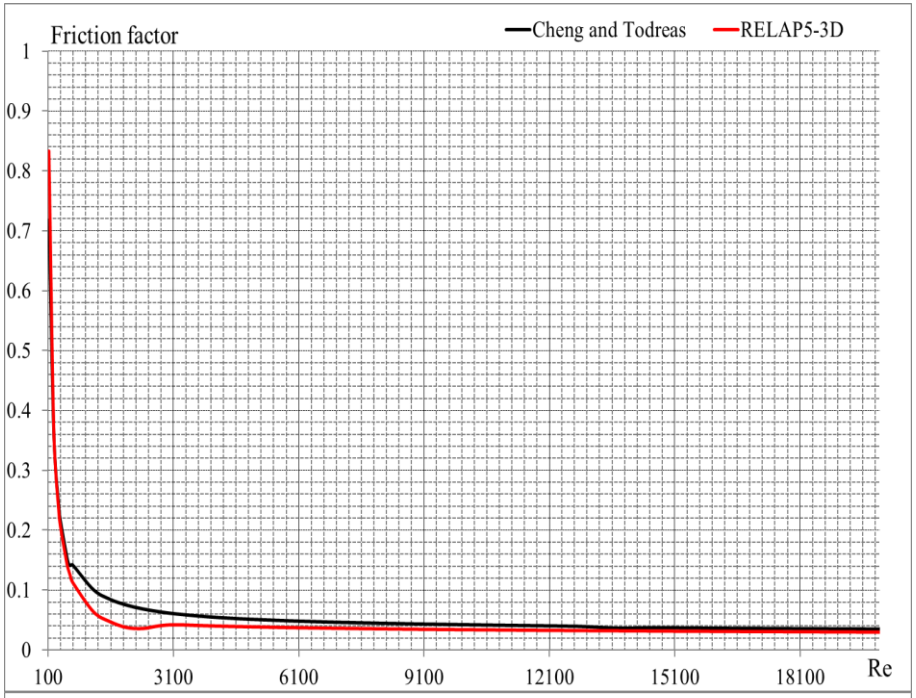
8) VESSEL COOLING SYSTEM; 9) STRONGBACK

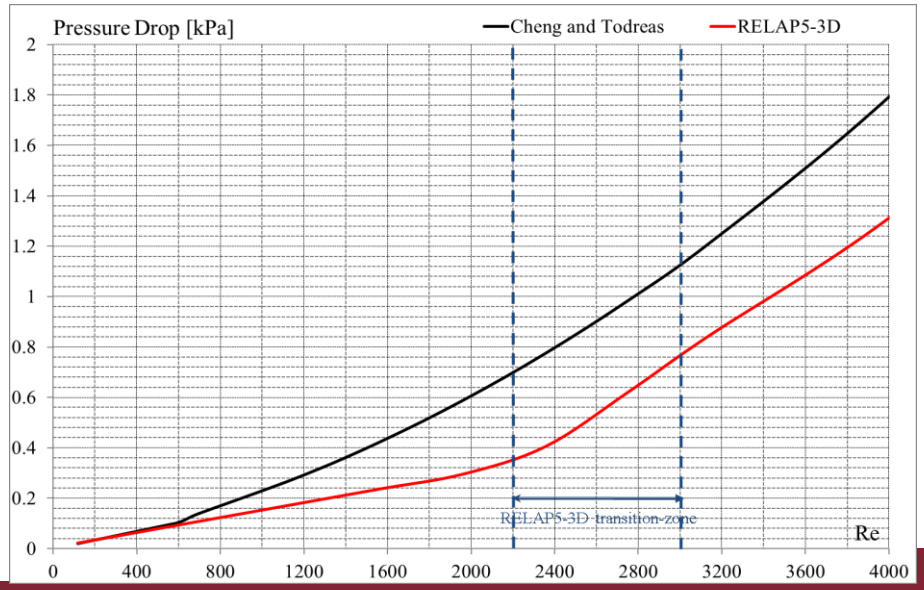
The vessel cooling system and the strongback are modeled with an only PIPE component (CV 945). The inlet and outlet are connected to the correspondent regions of 3D component (CV 900) with two MTPLJUN components .

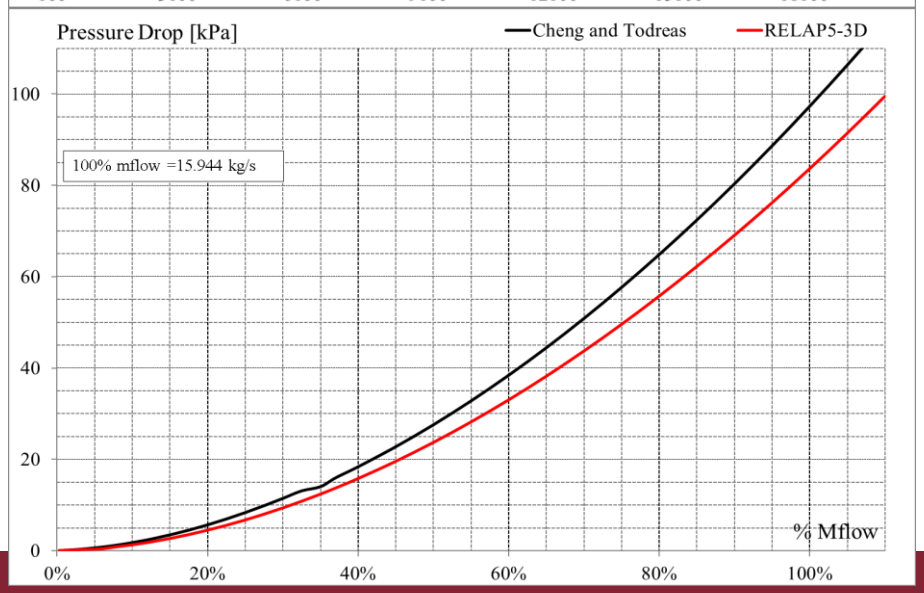


Testing FA performances: pressure drops

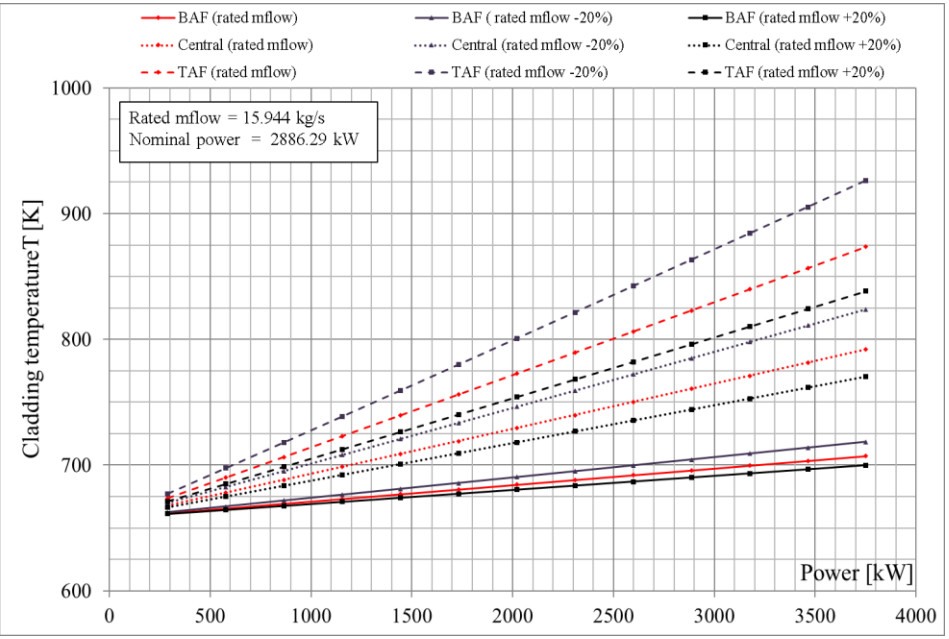
- Dynamic pressure drop in wire wrapped fuel bundle
  - Comparison between laminar-turbulent transition with RELAP5-3D code and Cheng and Todreas correlation
  - Quantification of pressure drop in the wire wrapped zone in the range of mass flow of interest
  - "100% Mflow" corresponds with average nominal mass flow rate in the inner core

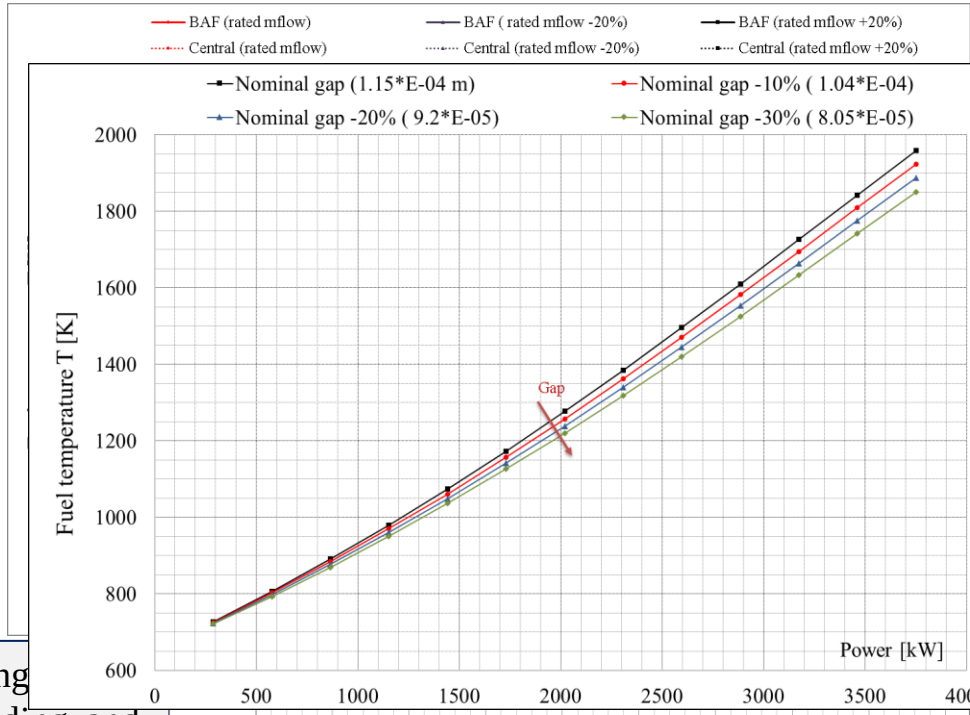






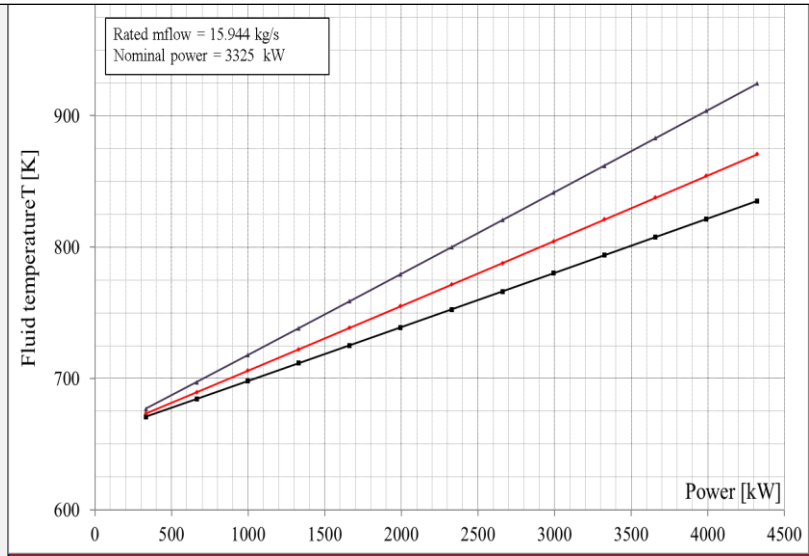
Testing FA performances: heat exchange





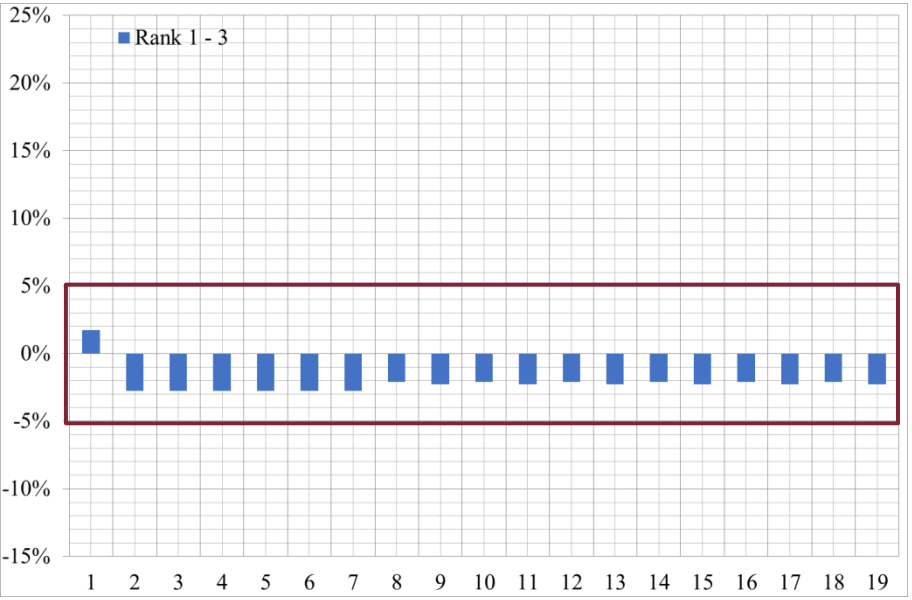
- Evaluation of heat transfer in the inner core FA considering parameters of benchmark specifications (i.e. coolant, cladding, and fuel centerline Ts)
  - Fuel temperature and cladding temperature are evaluated in the zone of the assembly with MAX power (fuel zone)
  - The value of gap conductibility refers to the conditions of thermal exchange at the end of life
  - Fluid temperature is evaluated at the outlet of FA

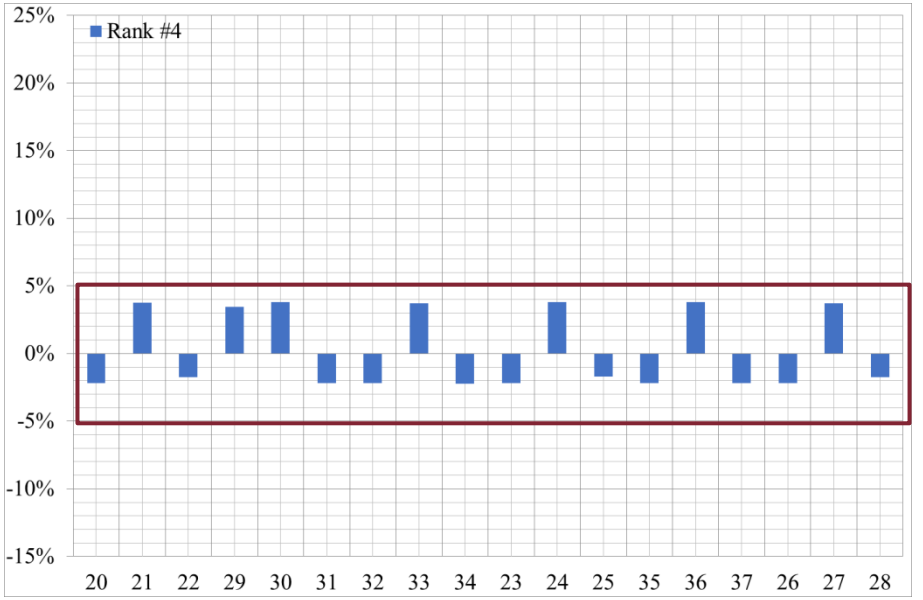
Fuel centerline temperature cannot be evaluated w/o considering modifications in hot conditions and occurring during irradiation

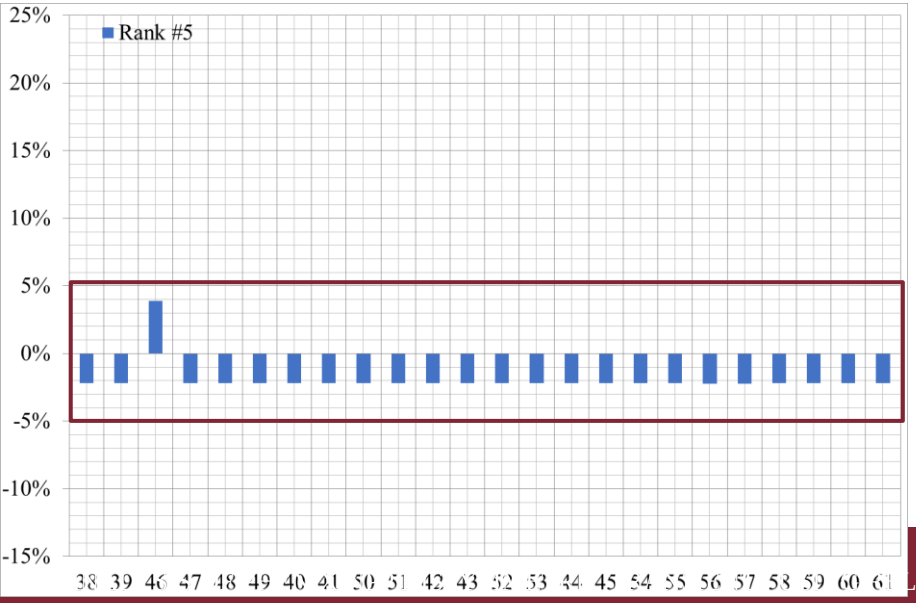


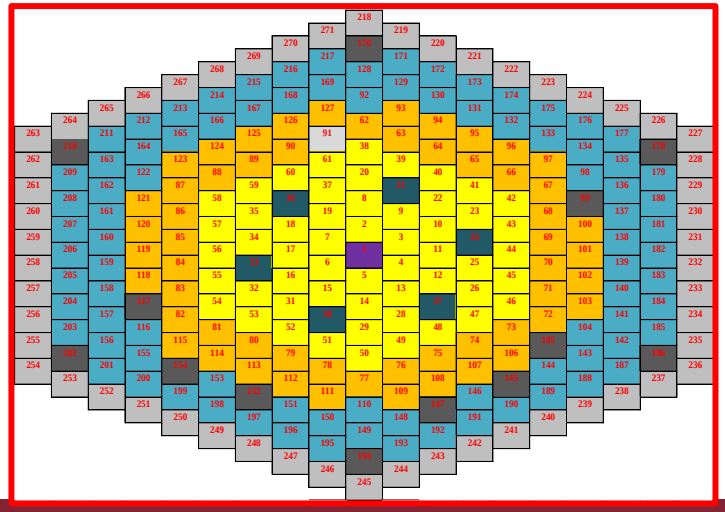
Mass flow distribution in the core

- Mass flow distribution in core SA is compared with reference benchmark data



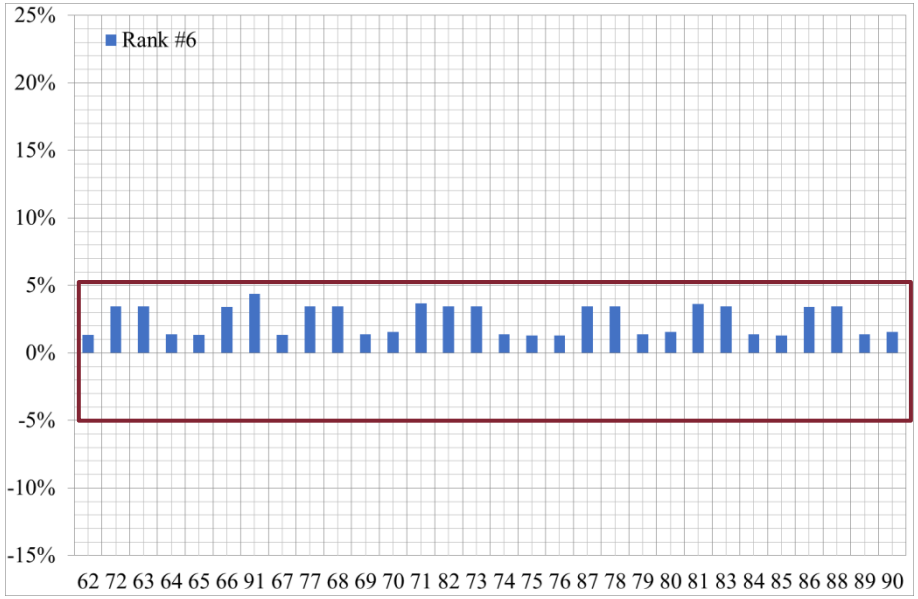


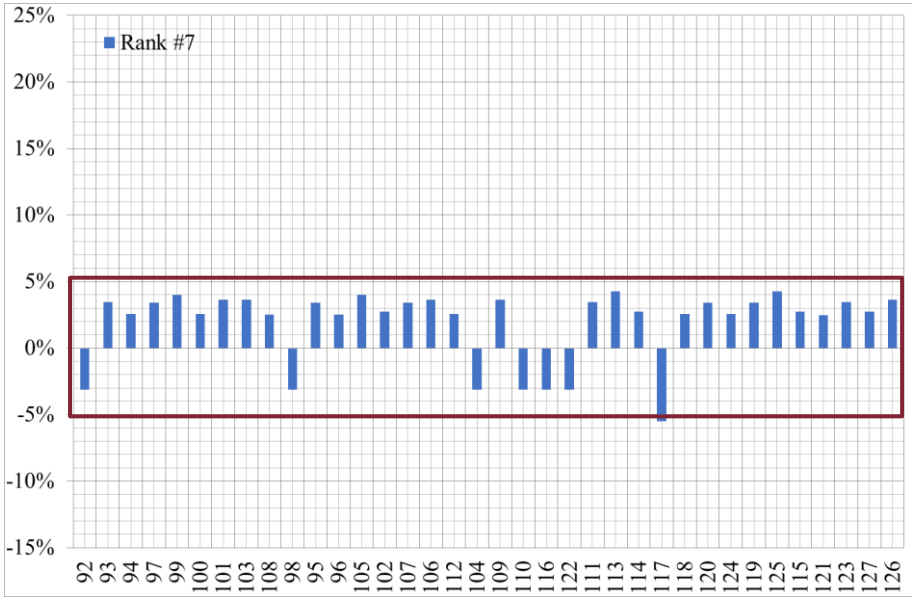


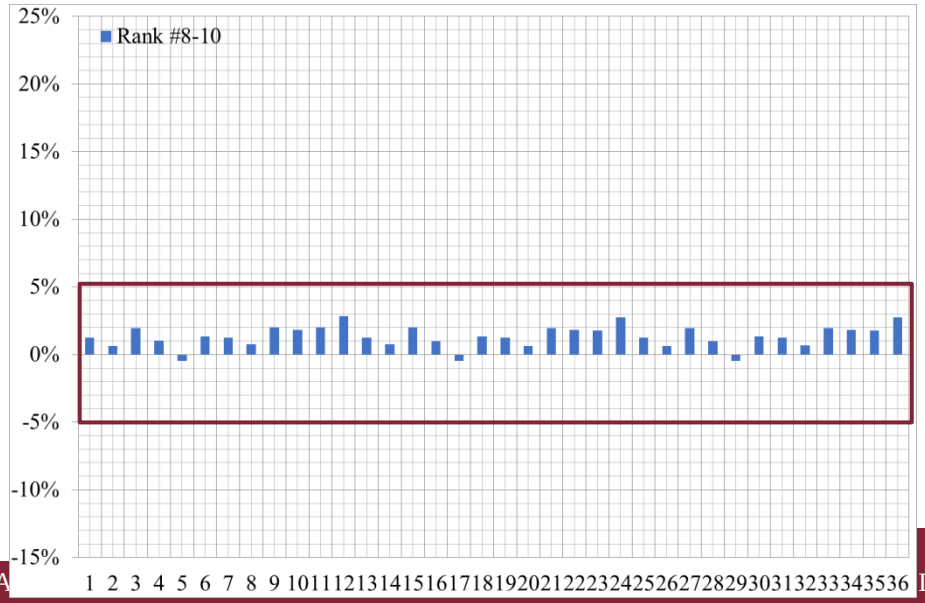


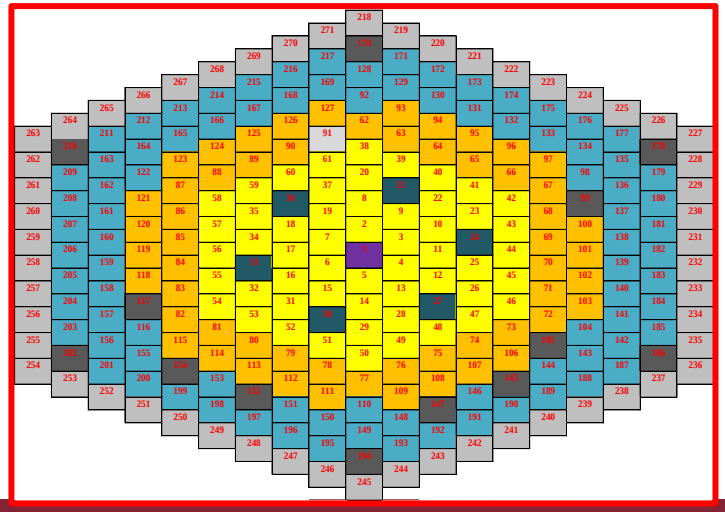
Mass flow distribution in the core

- Mass flow distribution in core SA is compared with reference benchmark data









Conclusive remarks and follow up

- Nodalization of PHENIX by REALP5-3D© available
  - TH model for dissymmetrical test is going to be completed
  - Nodalization is highly detailed and suitable for 3D NK coupling
  - Mass flow distribution in SA achieved
- Following activities are in progress and will be completed and documented in the PAR deliverable
  1. Achievement of the steady state
  2. Blind calculation of the dissymmetrical configuration test
- Following activities are planned in PAR-2017
  - Comparison of the blind results with the experimental data
  - Post-test calculation and sensitivity study





UNIVERSITÀ DI PISA

Dipartimento di Ingegneria Civile e Industriale

"Application of RELAP5/mod3.3 – Fluent coupling codes to CIRCE-HERO"

Scuola di Ingegneria e Architettura
Università di Bologna 26-27/09/2017

Morena Angelucci
Gianluca Barone
Nicola Forgione
Cristina Ulissi

morena.angelucci@for.unipi.it

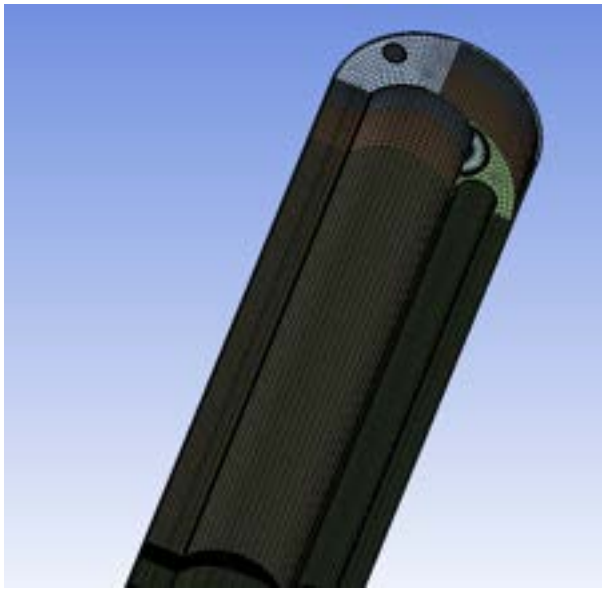
Workshop tematico ADP MiSE-ENEA (PAR2016-LP2)
Generation IV Lead Cooled Fast Reactor: Stato Attuale Della Tecnologia E Prospettive Di Sviluppo

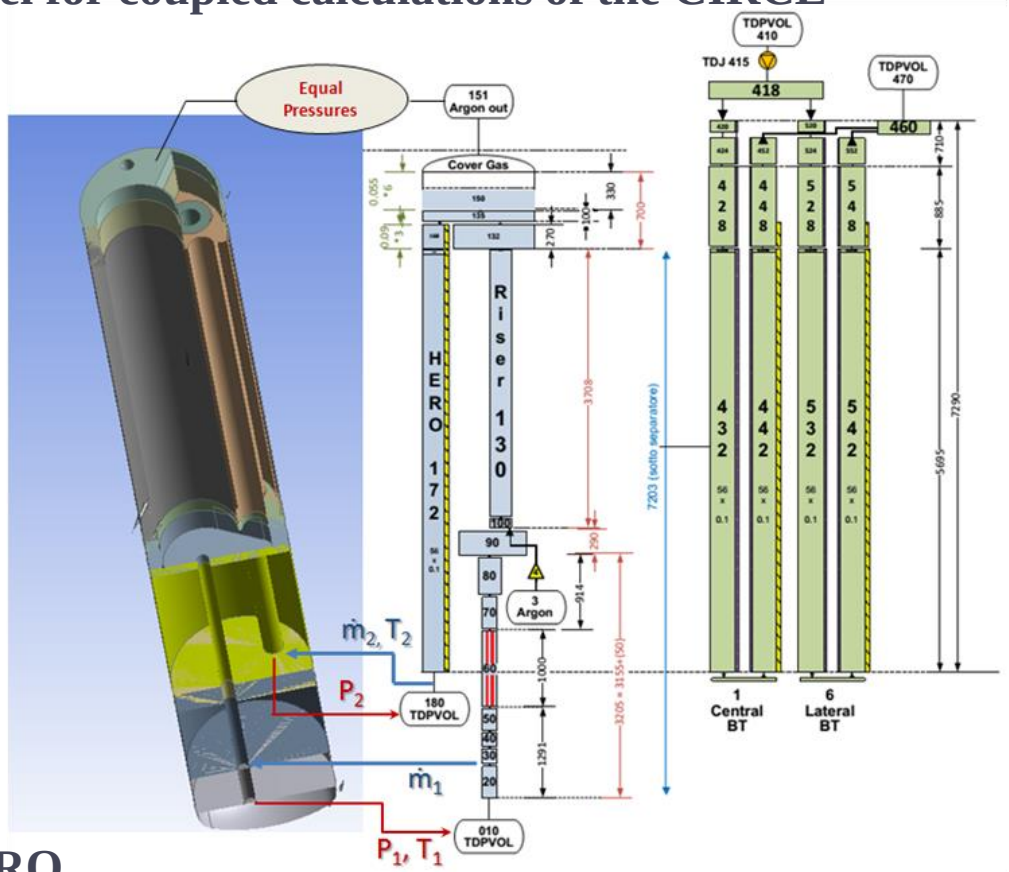
Summary

- **Objectives**
- **Coupling method**
- **HERO model for coupled calculation**
  - **CFD model of LBE domain**
  - **RELAP5 nodalization of H_2O domain**
- **Obtained results (comparison with RELAP5 standalone simulation)**
  - **Temperatures, HTC, Heat Flux**
- **Conclusions**

Objective

- **Improvement & optimization of the developed coupling procedure**
- **Development of a 3D CFD model of the CIRCE pool for coupled calculations**
- **Development of a CFD-Fluent model for coupled calculations of the CIRCE-HERO configuration**

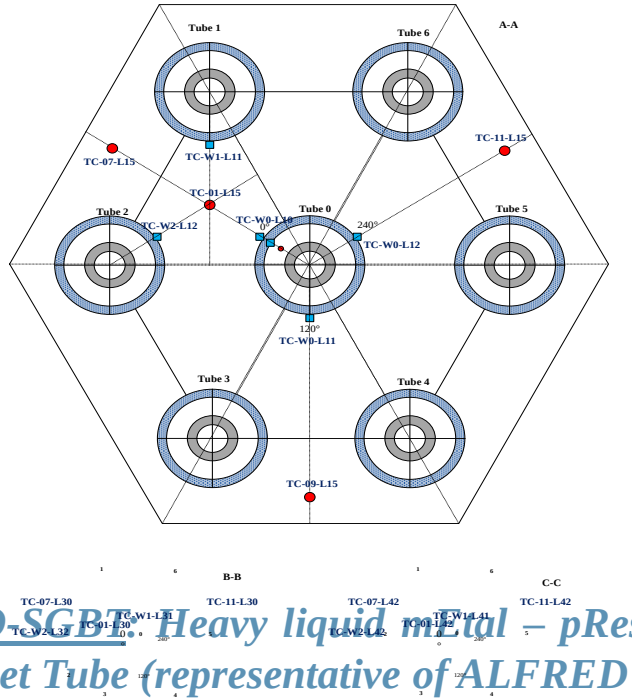


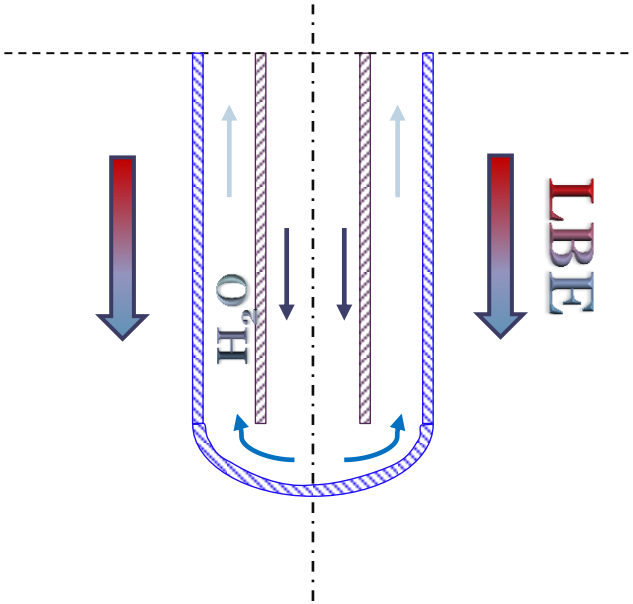


- **Application of the coupling methodology to the component HERO**

CIRCE-HERO test section



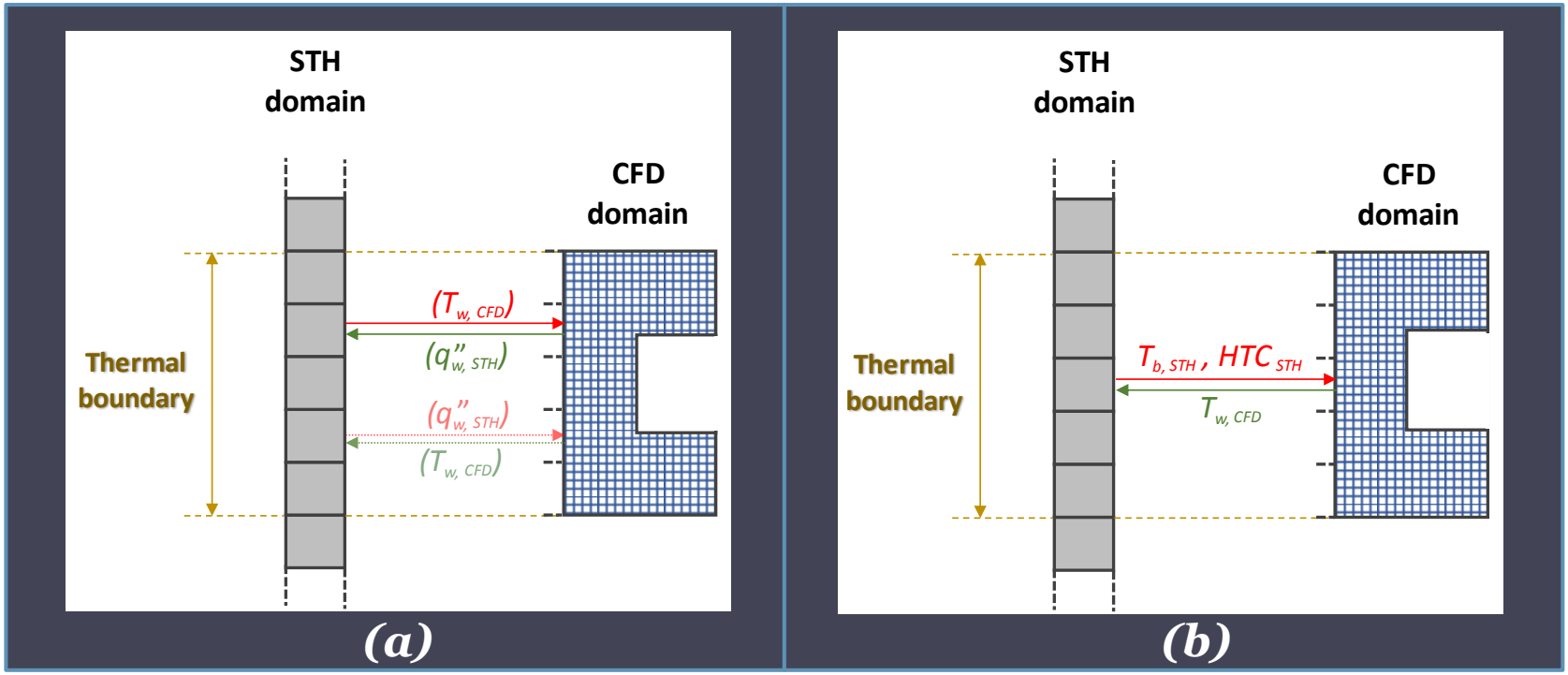




HERO-SGBT: Heavy liquid mEtal – pRessurized water cOoled Steam Generator Bayonet Tube (representative of ALFRED SG)

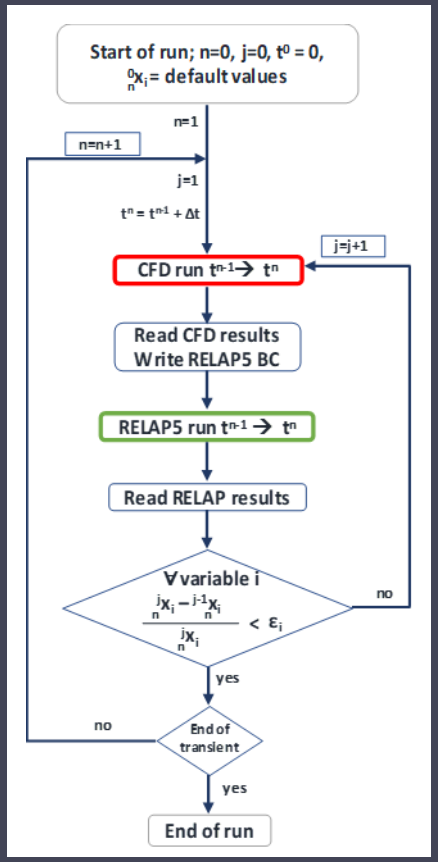
- **7 double-walls bayonet tubes inside hexagonal shroud**
- Tubes active length is 6 m, side of hexagonal shroud 72.6 mm
- Thermal duty of about **500 kW**
- Stainless steel powder (AISI316) + He filling the gap
- Secondary side with water-steam at 180 bar
- Cylindrical shell, concentric to the hexagonal shroud, filled with air to insulate the HX from the main pool

Coupling method (1/2)

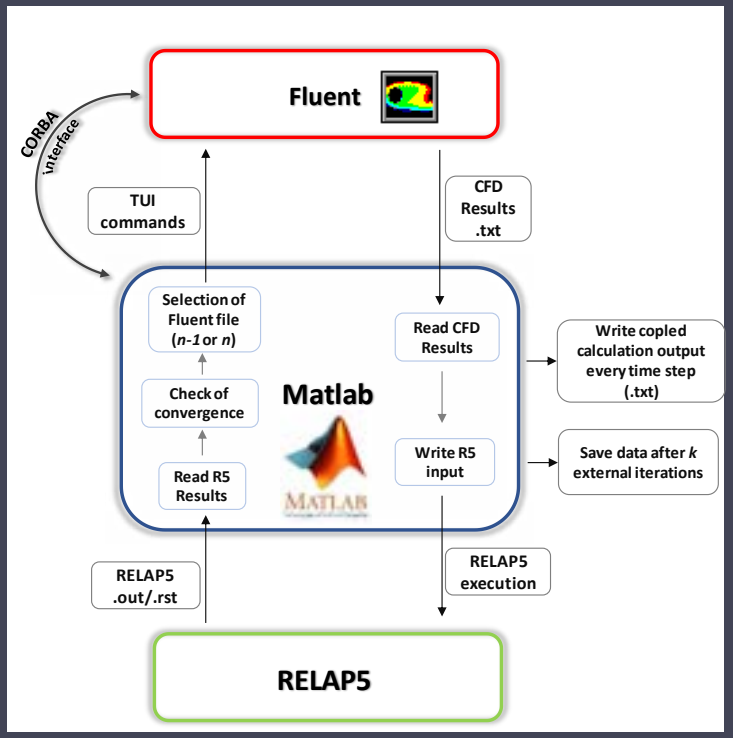


- **No hydraulic interaction between the two codes**
- **One code (STH) gives to the other (CFD) the wall temperature, which passes back to the first code the wall heat flux (Figure *a*)**
- **In cases where the boiling heat transfer occurs, the imposition of the wall heat flux as BC can lead to unphysical results**
- **<u>New strategy</u>: the wall temperature (calculated by the CFD code) is given to the STH code as BC, the STH code gives to the CFD code the bulk temperature and the heat transfer coefficient (calculated in the STH side)**
- **This condition is analogous to impose an equivalent average wall heat flux, but the <u>heat flux distribution is not forced to be uniform over the boundary surface</u>**

Coupling method (2/2)

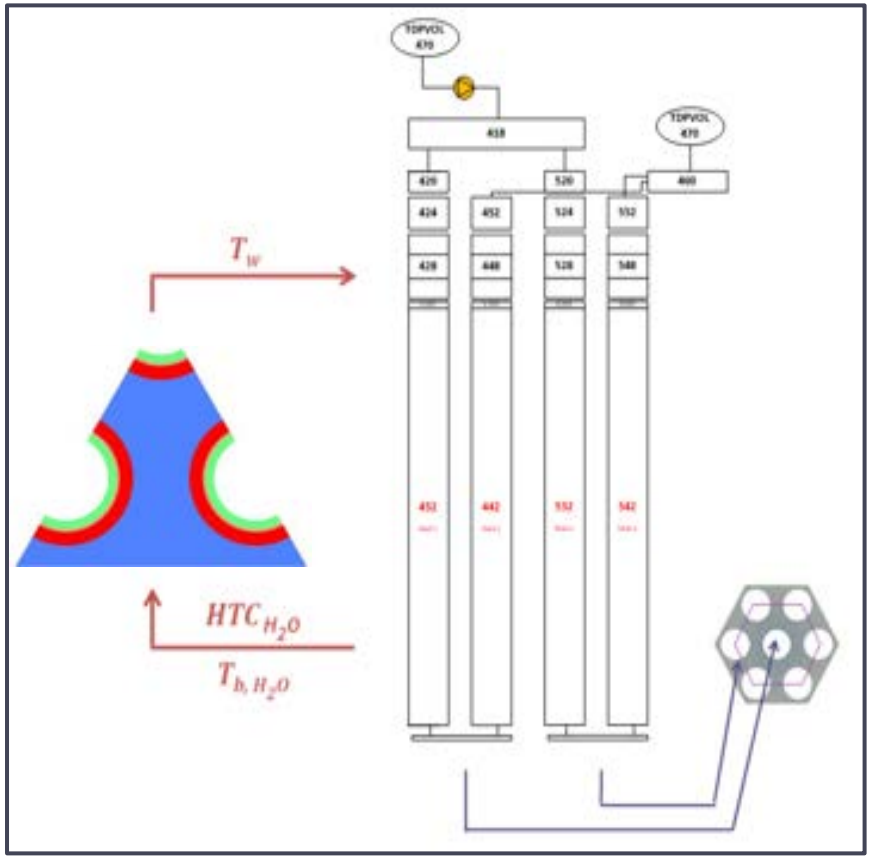


Coupling numerical scheme



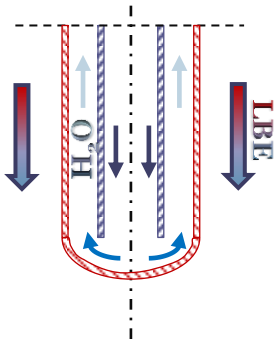
Coupling logic managed by the Matlab software

Coupling method for HERO



RELAP5 domain: 2 pipes for water side + inner tube solid structure

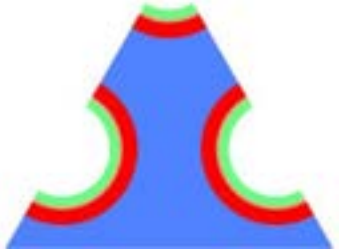
- one representative of central tube
- one representative of 6 external tubes



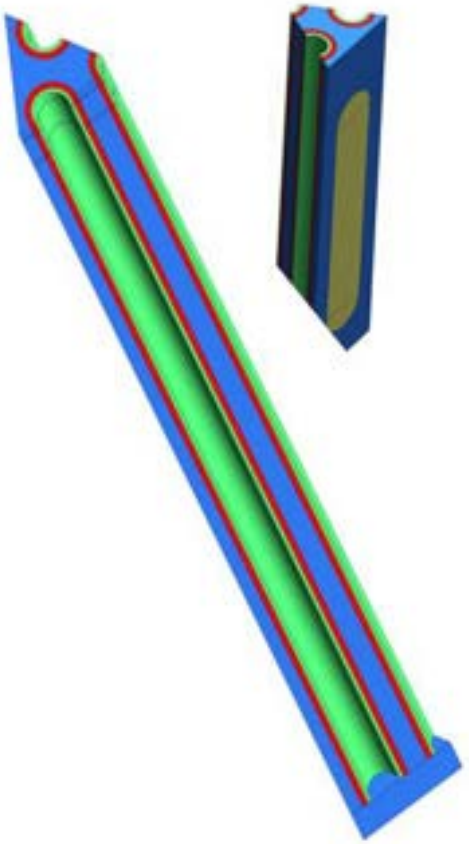
CFD domain: LBE side + annulus solid structures (1/6 of the transversal section)

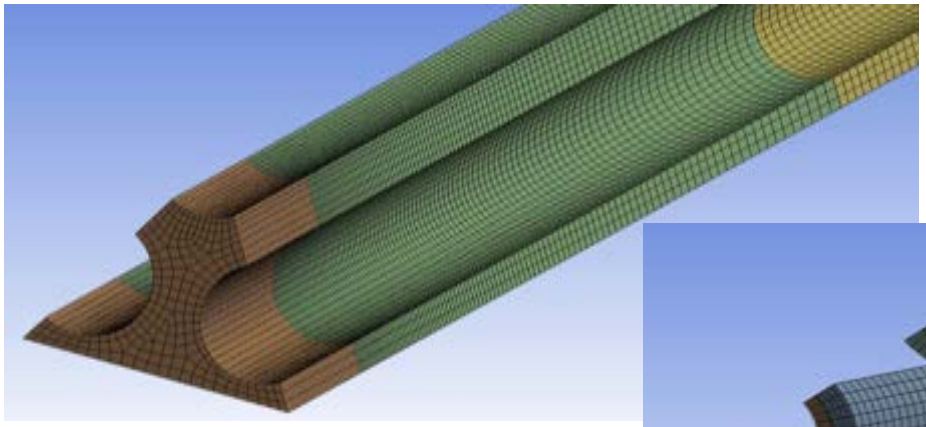
- In **blue** the LBE domain
- In **red** the AISI304 tube in contact with LBE
- In **green** the AISI304 tube in contact with H_2O
- In **orange** the AISI316 powder in between the tubes

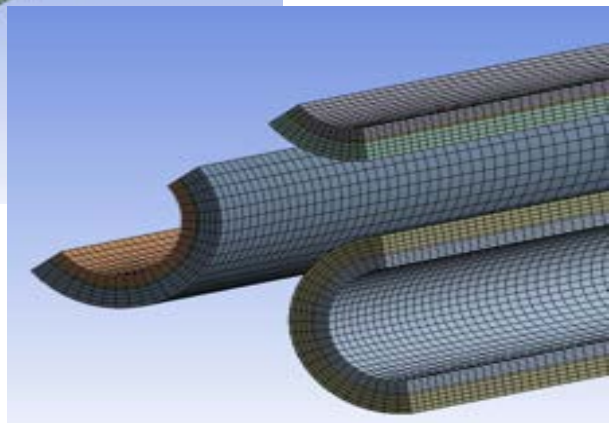
Data are exchanged at the interface of water tubes



CFD model





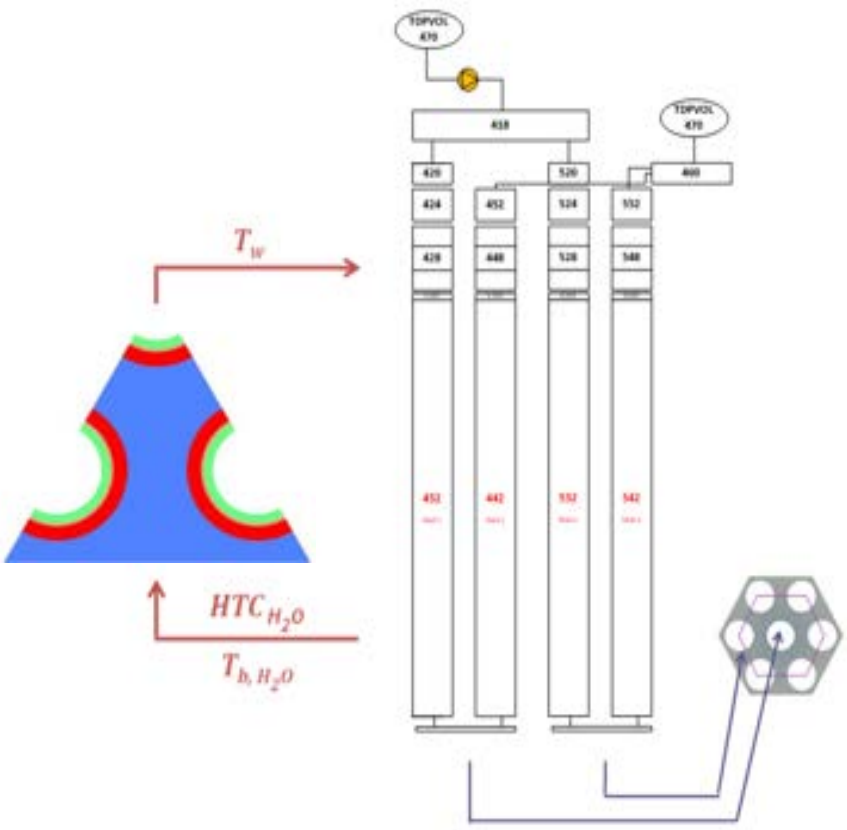


Nodes	731454
Elements	688213
Max Aspect Ratio	38.94
Max Skewness	0.79
Min Orthogonal Quality	0.999
Avg Orthogonal Quality	0.983

Models and methods

- Multi-body, mainly structured hexahedral blocks
- 1/6 of the domain with symmetry boundary conditions at the lateral walls
- Solid Structures in the CFD model (Steel pipes + steel powder in between)
- 730000 nodes and 690000 elements
- k-epsilon realizable with standard wall function ($y^+>30$), $Pr_t = 1.5$

Coupled calculation

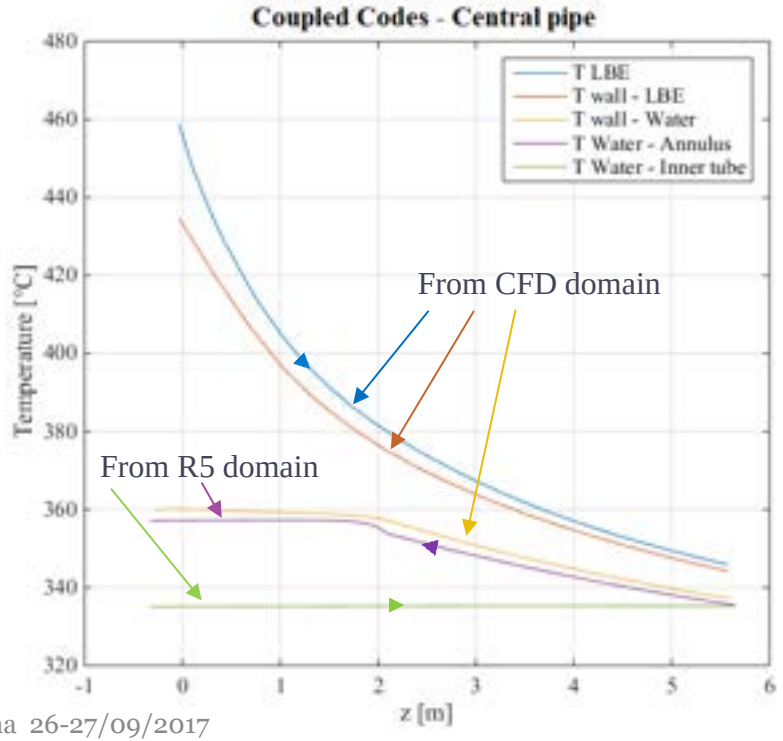


BC of the Fluent calculation

LBE inlet mass flow rate [kg/s]	1.5
Outlet gauge pressure [Pa]	0
LBE inlet temperature [°C]	480

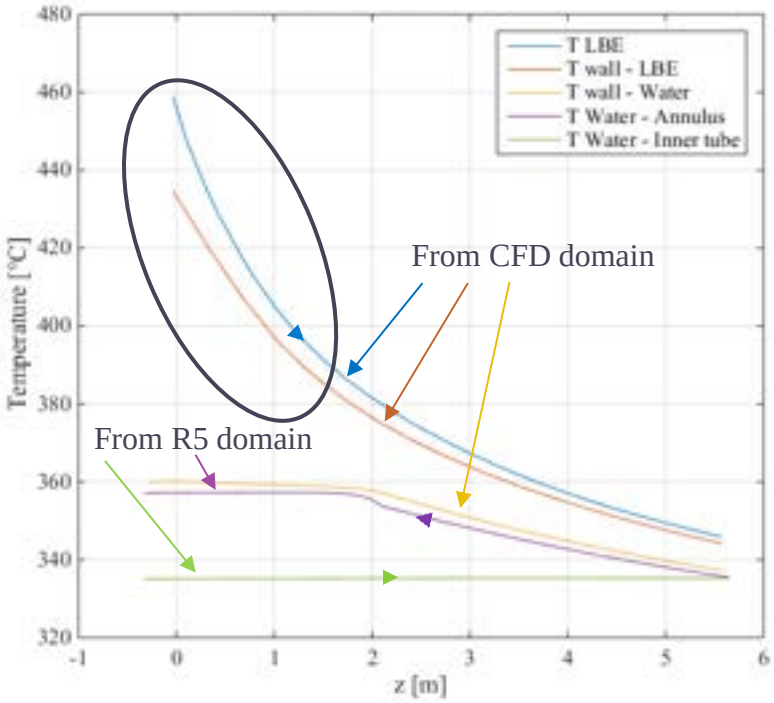
BC of the RELAP5 calculation

Water mass flow rate [kg/s]	0.33
HERO outlet pressure [bar]	180
Water inlet temperature [°C]	335

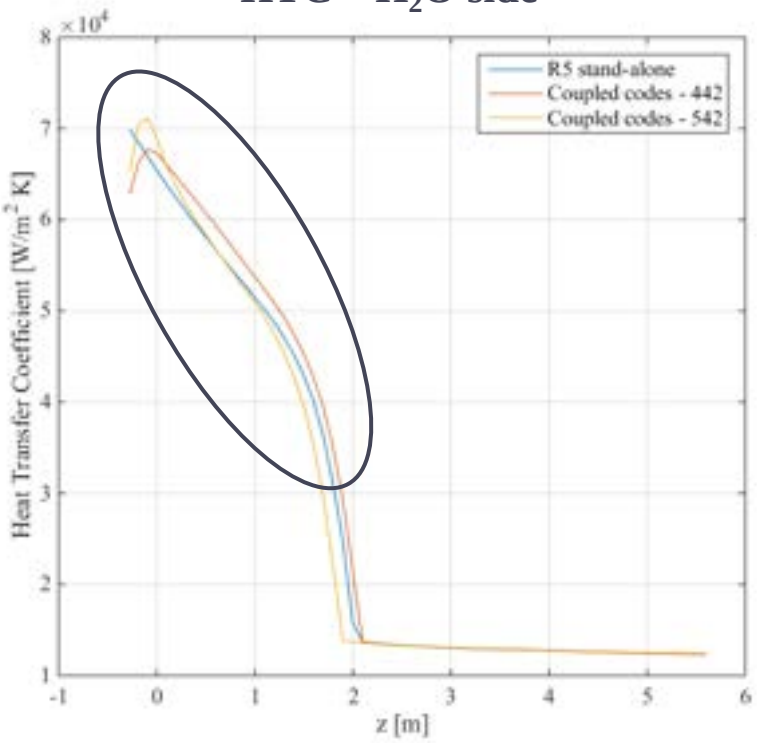


Coupled calculation: obtained results (1/4)

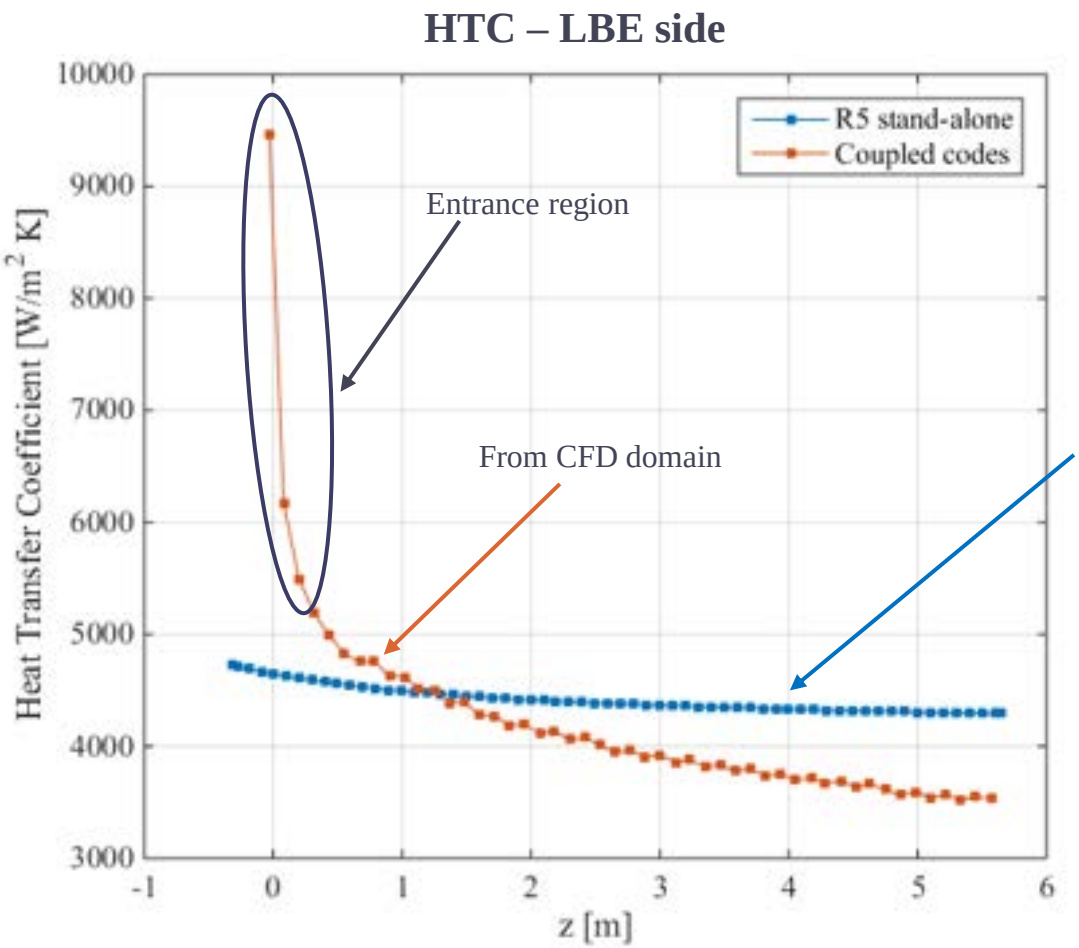
Central pipe



HTC – H_2O side

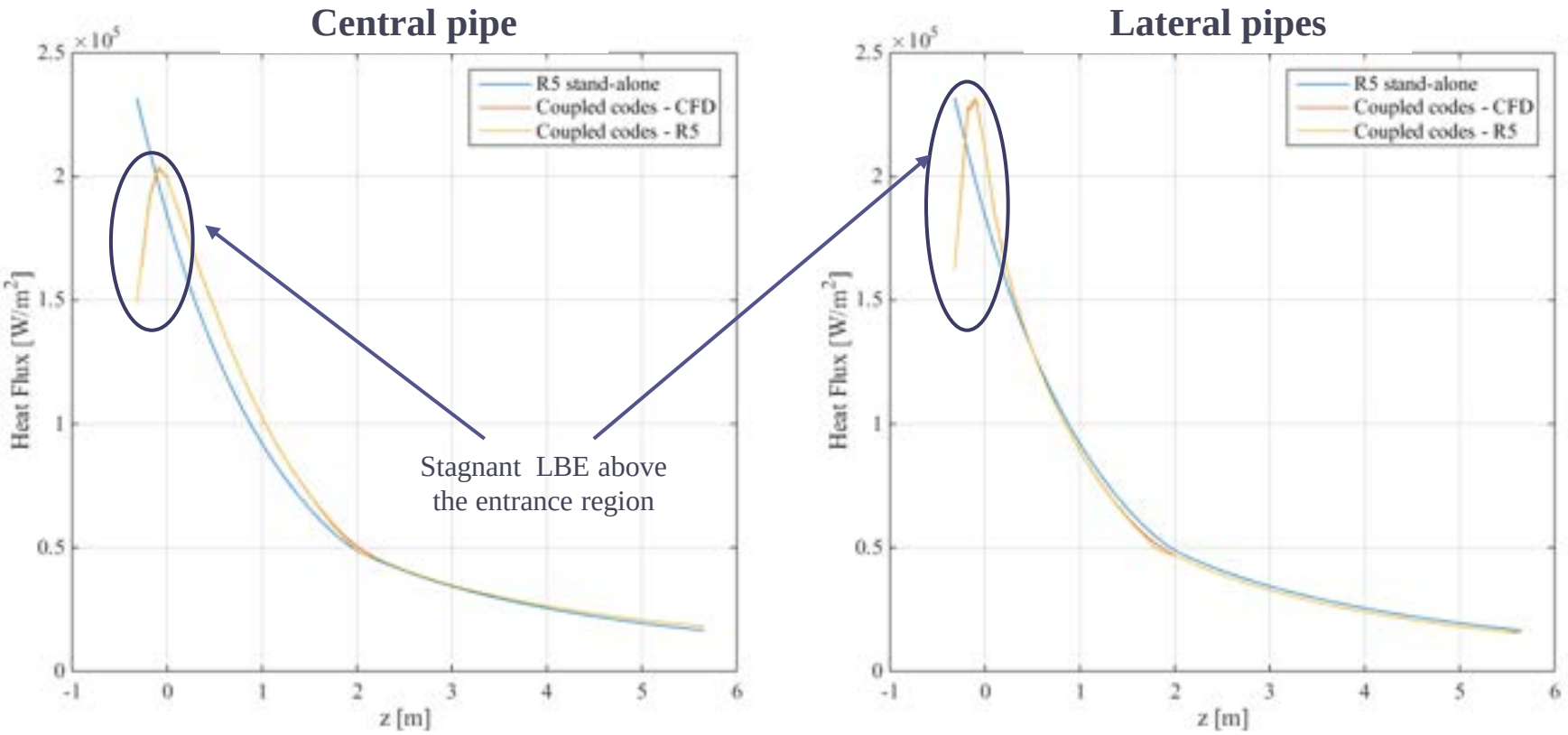


Coupled calculation: obtained results (2/4)



$$HTC_{LBE}(z) = \frac{q''_{wall}(z)}{\bar{T}_{wall}(z) - T_b(z)}$$

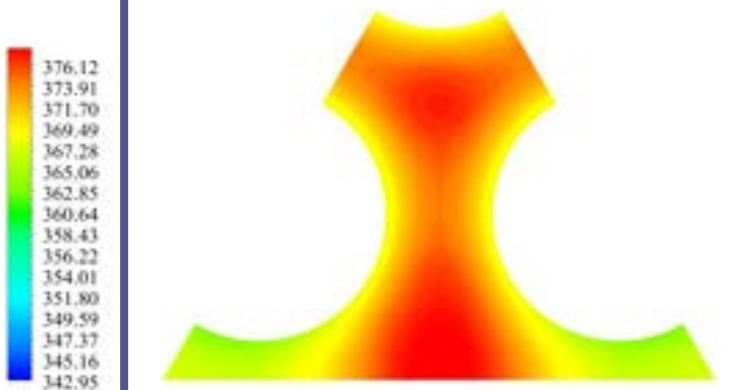
Coupled calculation: obtained results (3/4)



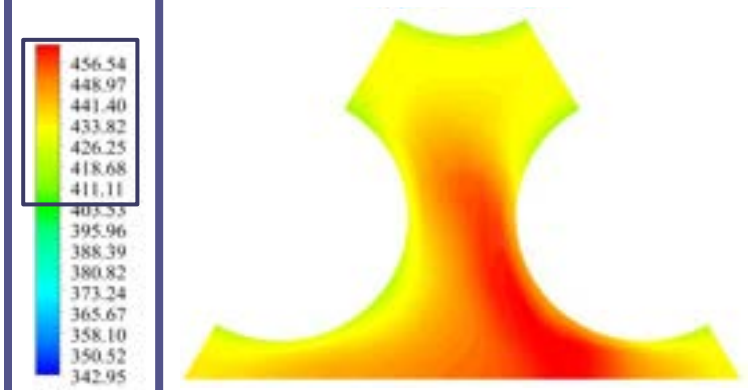
Wall heat flux comparison

Coupled calculation: obtained results (4/4)

LBE temperature

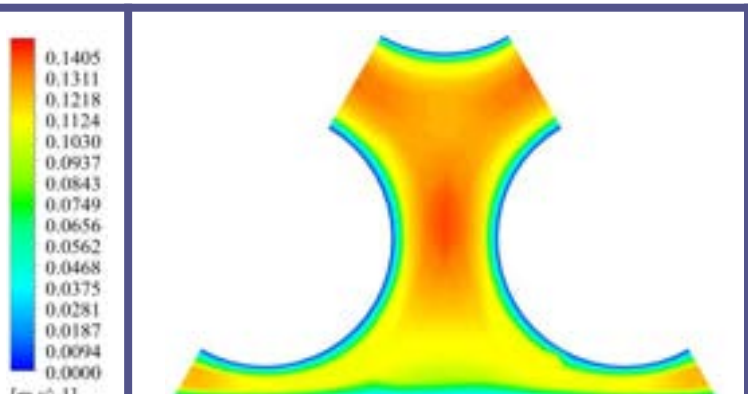


z = 1.6m

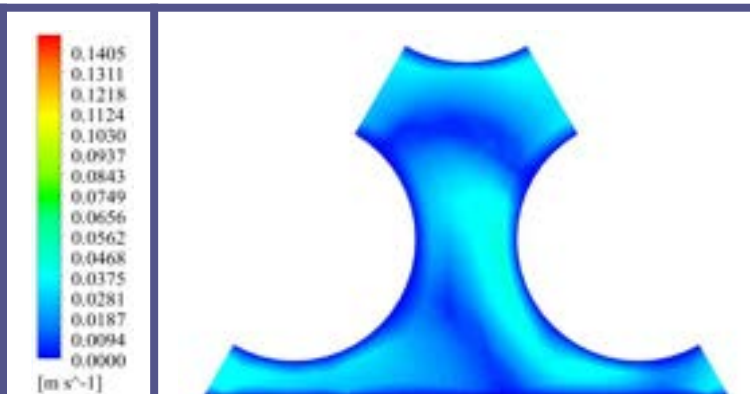


z = -0.3 m

LBE velocity magnitude



z = 1.6m



z = -0.3 m

Conclusions

- **A RELAP5 + CFD coupled calculation for HERO test section was setup**
  - Water side modelled with 2 tubes to take into account the differences between the central and the external pipes
  - LBE side + solid structures modelled with the CFD to obtain more details about LBE flow (HTC of LBE calculated by CFD code)
- A **new coupling procedure** was developed for HERO application
  - Coupling at the thermal boundaries: Tw, Tb and HTC as exchanged data
- The coupling procedure was verified by **comparing** the obtained **results with** the analogous ones by **RELAP5 standalone calculation**
- No big differences between central and external tubes in this reference case
- As next step, **further test cases will be analysed** to evaluate the efficiency of HERO in several operating condition (varying water side pressure, LBE and/or water inlet mass flow rates and temperatures)
- In the future, verification of the coupled simulation with experimental tests

ISTITUTO ITALIANO DI TECNOLOGIA
CENTER FOR NANOSCIENCE AND TECHNOLOGY

Nanoceramic Coatings for Advanced Nuclear Systems

M. Vanazzi, D. Iadicicco, F. Garcia. Ferré,
F. Di Fonzo

fabio.difonzo@iit.it

Acknowledgements & ongoing collaborations

Corrosion tests + financial support

Serena Bassini
Marco Utili
Mariano Tarantino
Pietro Agostini

heavy ion irradiations

Patrick Trocellier
Yves Serruys
Lucile Beck
Cédric Baumier
Odile Kaitasov

TEM + XRD

Alexander Mairov
Kumar Sridharan

POLITECNICO DI MILANO

Brillouin & CTE/Res Stress

Edoardo Besozzi
Marco Beghi

ISTITUTO ITALIANO DI TECNOLOGIA

Nanoindentation + nanoimpact

Luca Ceseracciu

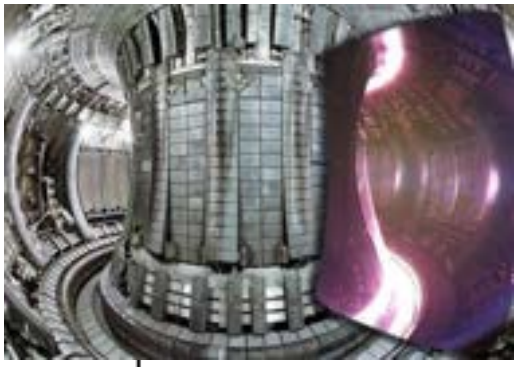
EUROfusion

CIRTEN - Consorzio Interuniversitario per la Ricerca Tecnologica Nucleare

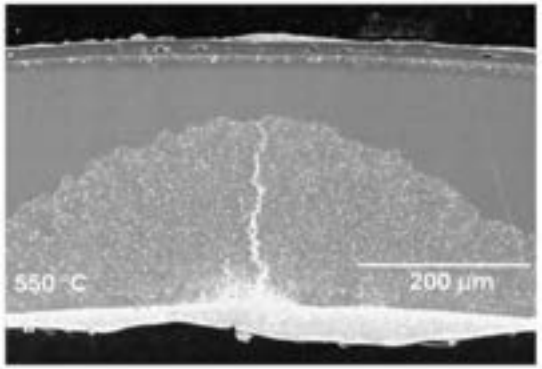
Introduction

Future generation nuclear systems (GIV)

Tritium management

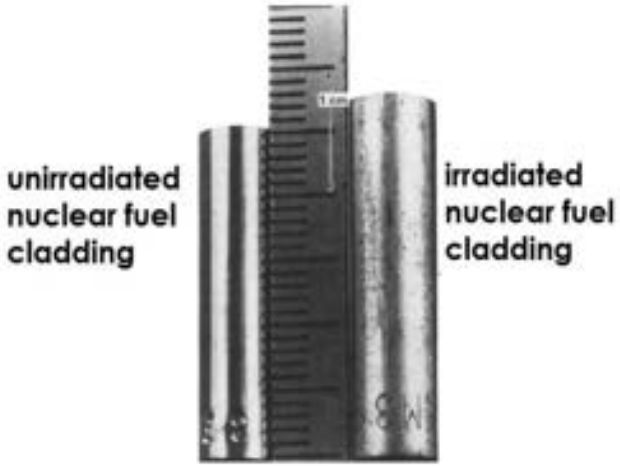


Corrosion

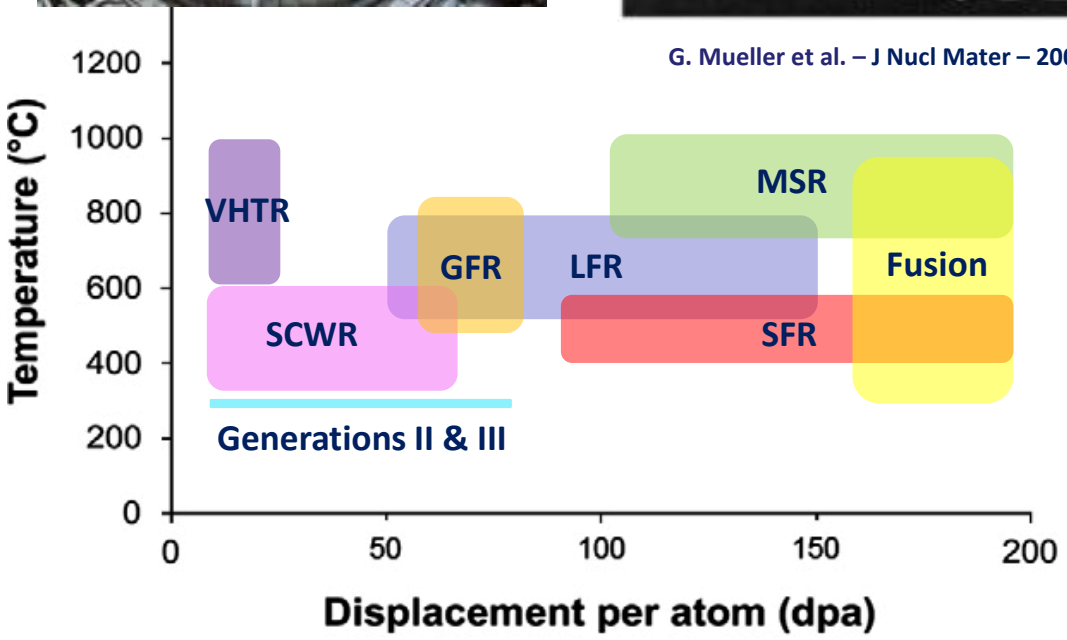


G. Mueller et al. – J Nucl Mater – 2004

Radiation damage



J.L. Straalsund – Westinghouse Hanford



S.J. Zinkle and G.S. Was – Acta Materialia - 2013

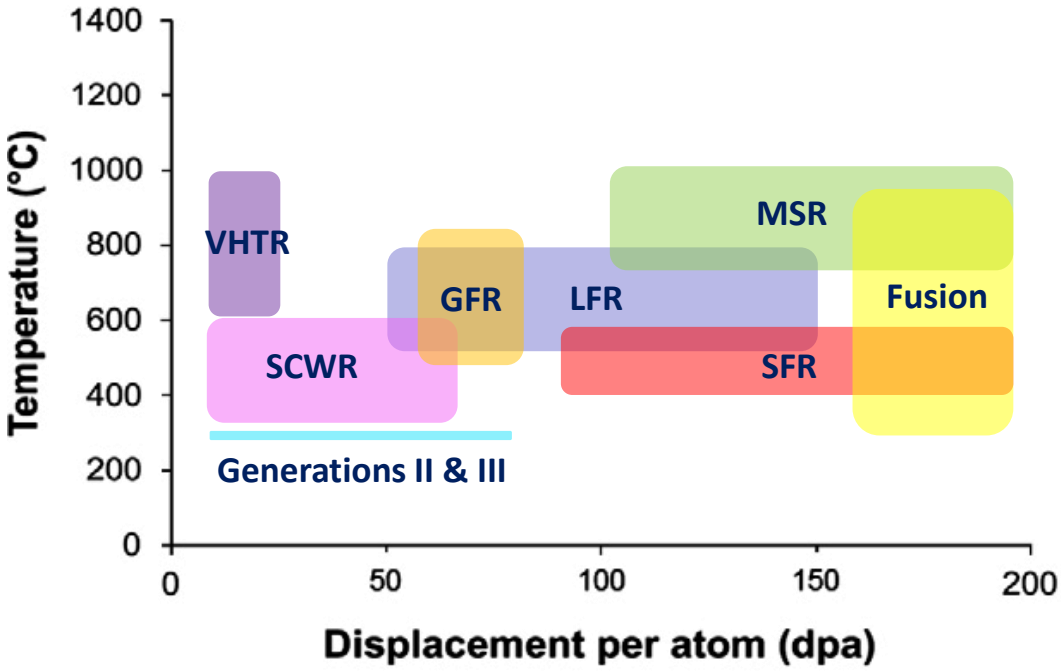
MAJOR BOTTLENECKS FOR ALL SYSTEMS

↓

NEED FOR COATINGS

Future generation nuclear systems aim at:

- Increase efficiency
- Reduce waste generation
- Enhance safety
- Promote non-proliferation



S.J. Zinkle and G.S. Was – Acta Materialia - 2013

Ultimate goal for LFRs:

- 800 °C
- 150 dpa

Advantages:

safety
transmutation of minor actinides / fuel breeding

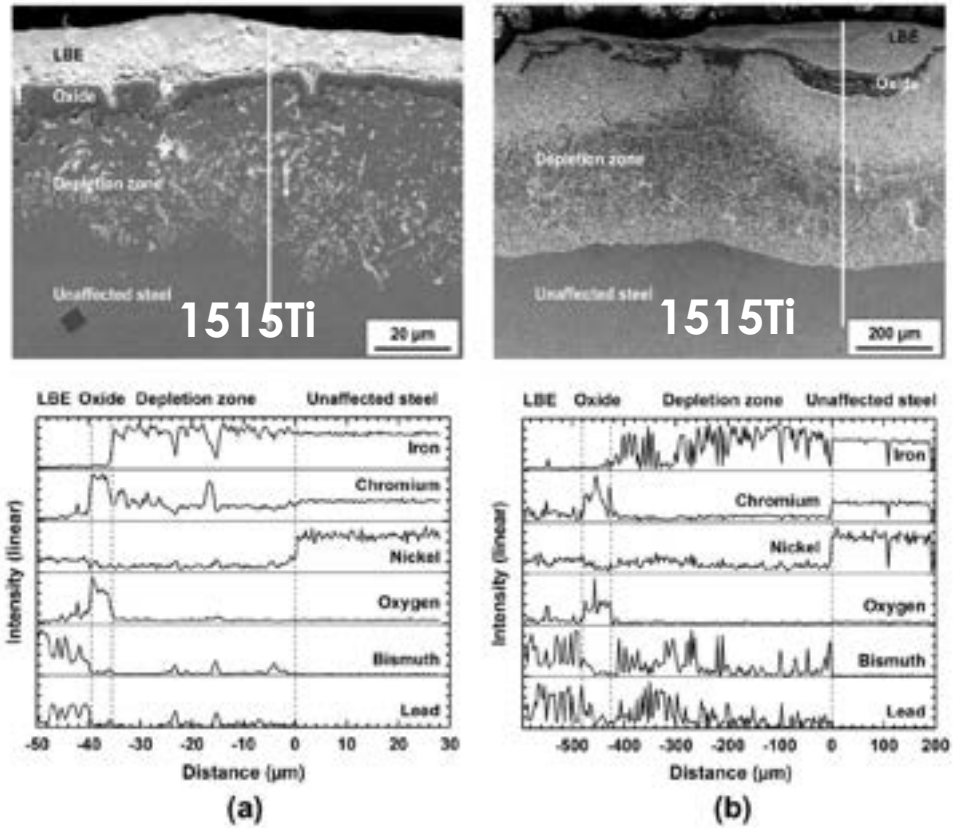
Major issues:

- corrosion
- radiation damage

S.J. Zinkle and G.S. Was – Acta Materialia - 2013

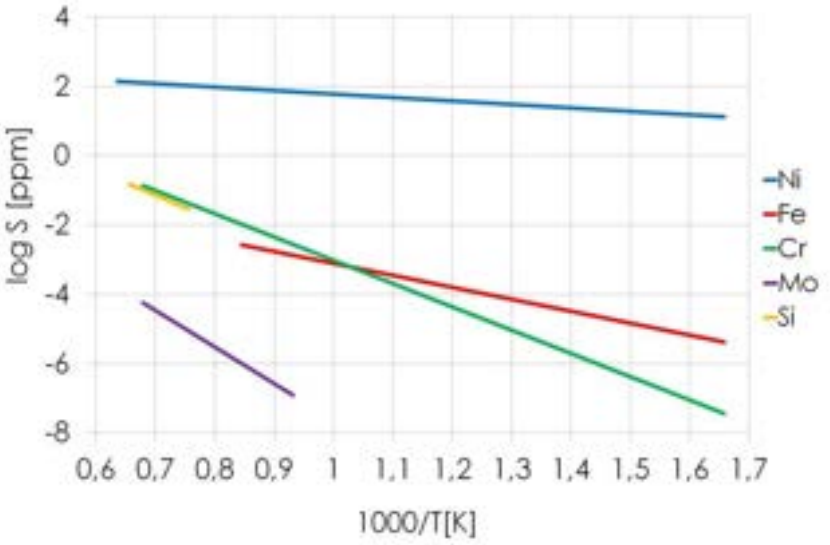
Heavy liquid metal corrosion

Ni leaching in austenitics (23000 h @ 550°C, 10^{-6} wt.% O)



C. Schroer et al. - Corros. Sci. - 2014

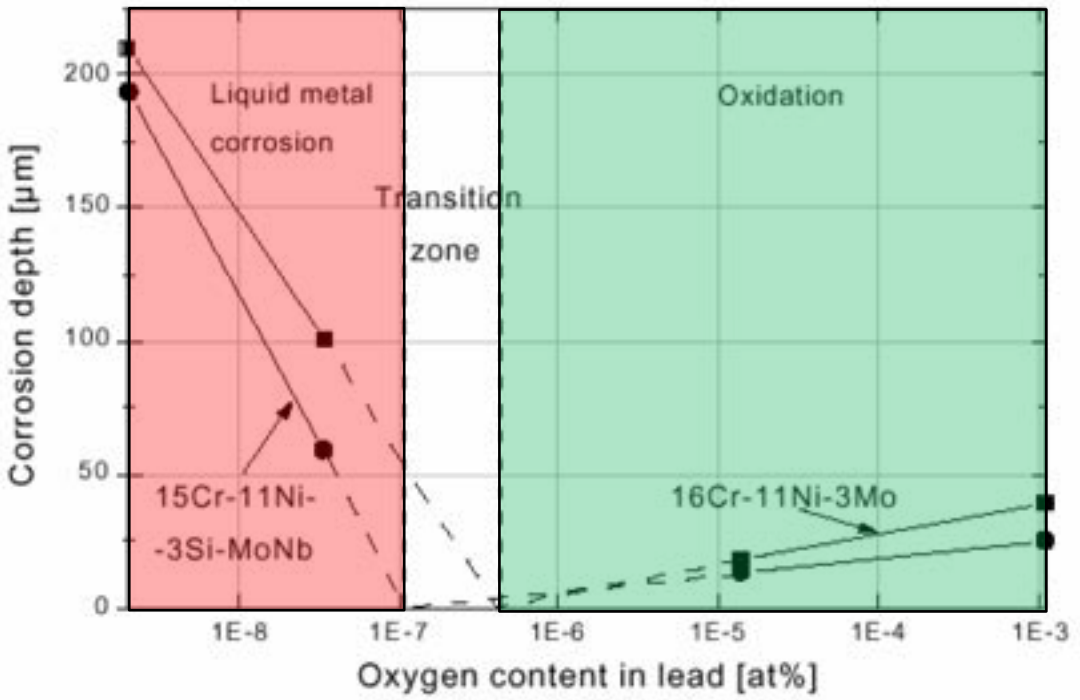
Solubility of Ni in lead is very high



In-situ passivation is not viable for T > 500°C-550°C

(will be exceeded by fuel cladding)

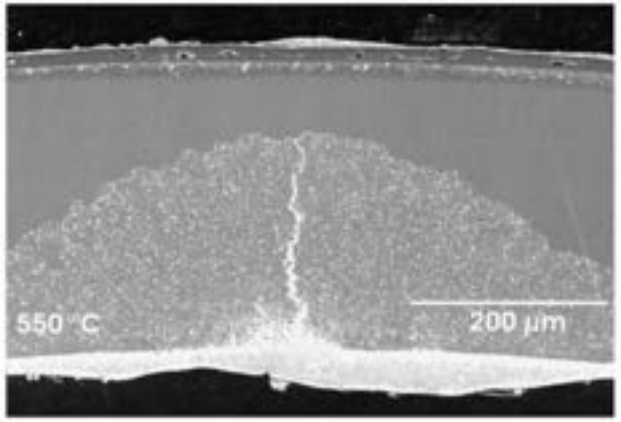
Heavy liquid metal corrosion



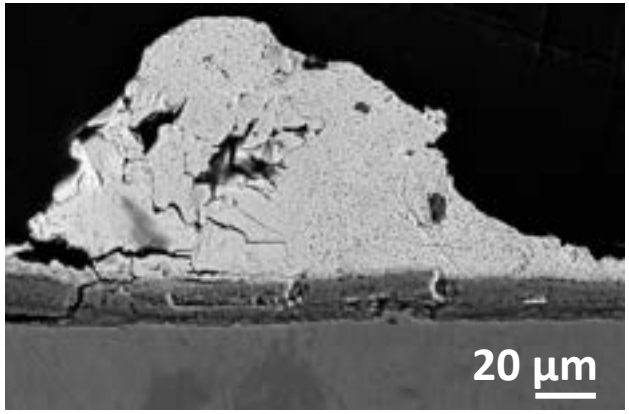
Austenitic steels exposed to HLM for 3000 hours at 550°C

V. Gorynin et al. – Metal Science and Heat Treatment - 1999

G. Mueller et al. – J Nucl Mater – 2004



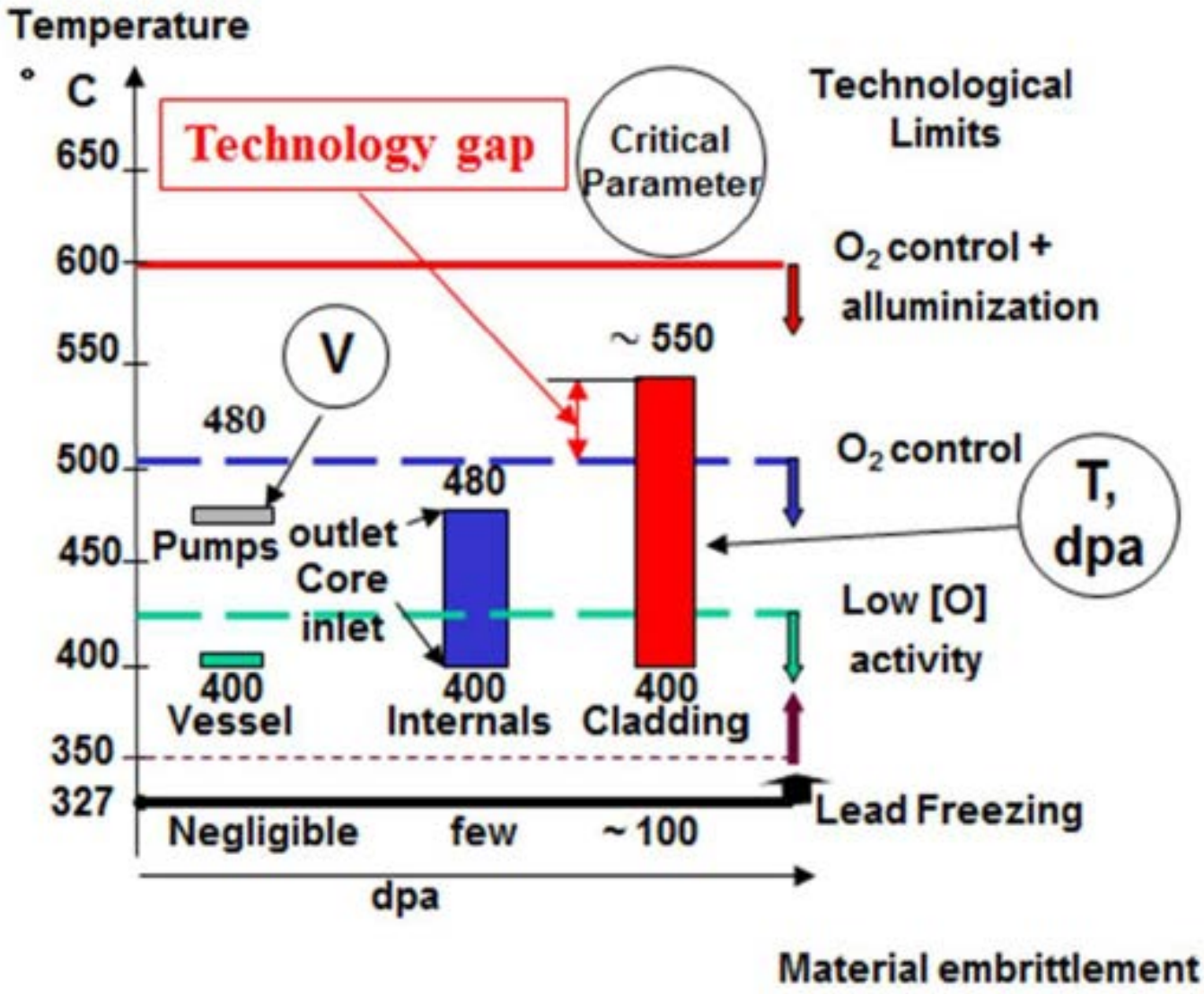
Dissolution



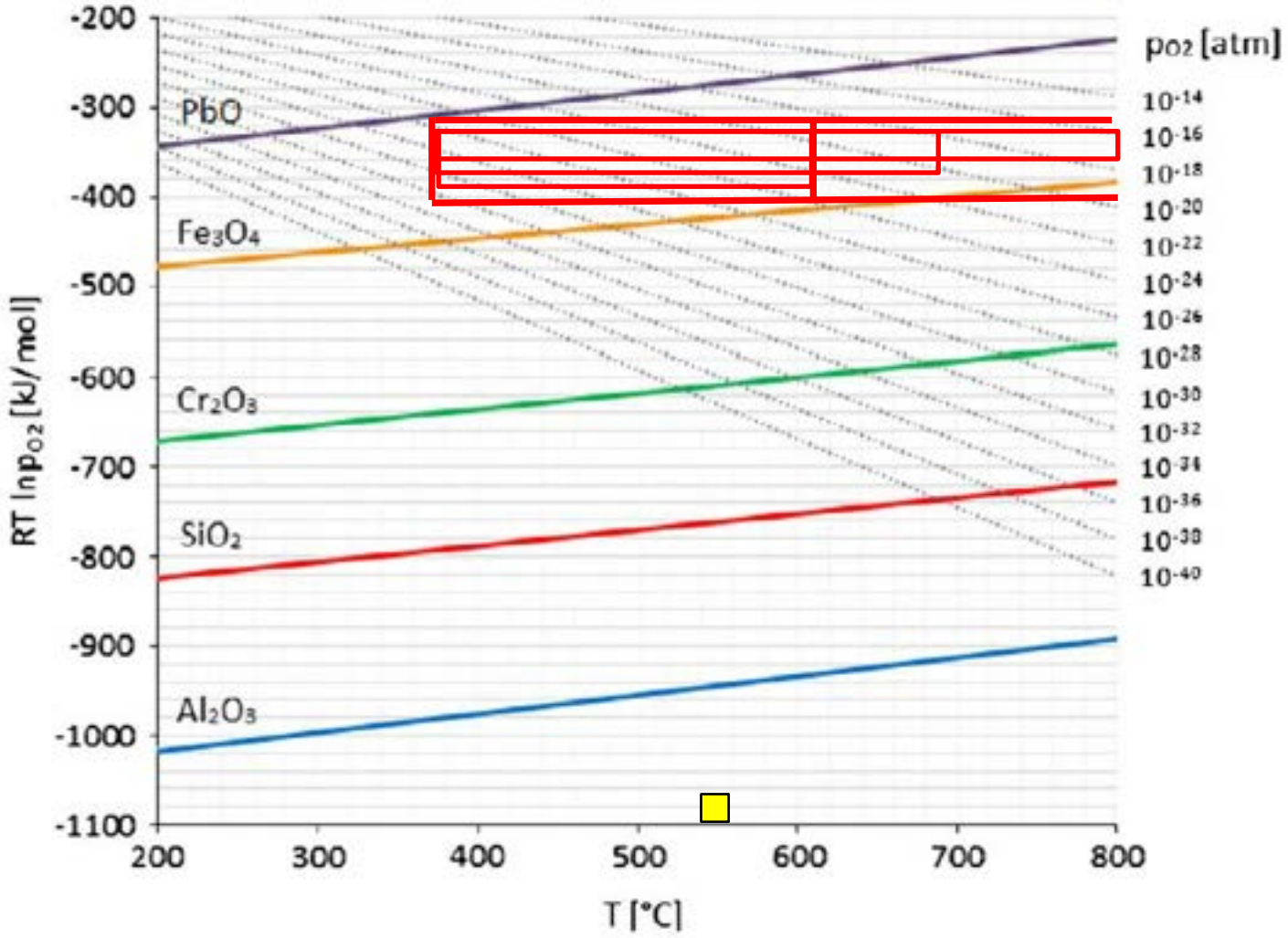
Oxidation

In-situ passivation is not viable for T > 500°C
(will be exceeded by fuel cladding)

Technology Constraints for ALFRED



Oxygen Control, fighting with ever narrow operational window!



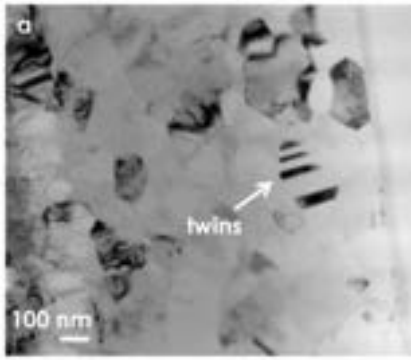
NANOCERAMICS

enhanced

enhanced

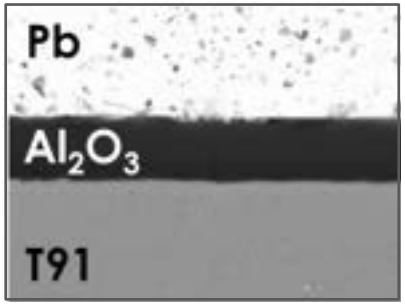
Mechanical performance

Coble creep, twinning, etc.



F. Garcia Ferré et al. – SCI REP – 2016

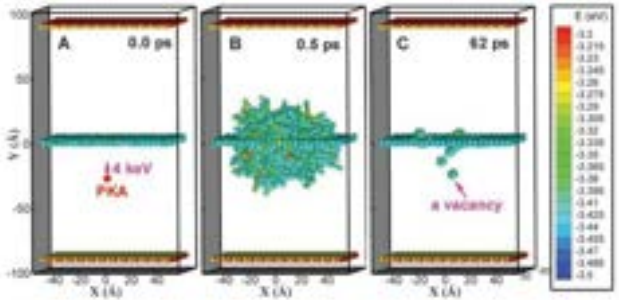
Corrosion resistance



F. Garcia Ferré et al. – CORROS SCI – 2013

Radiation tolerance

Interstitial emission from GBs



X.M. Bai et al. – Science - 2010

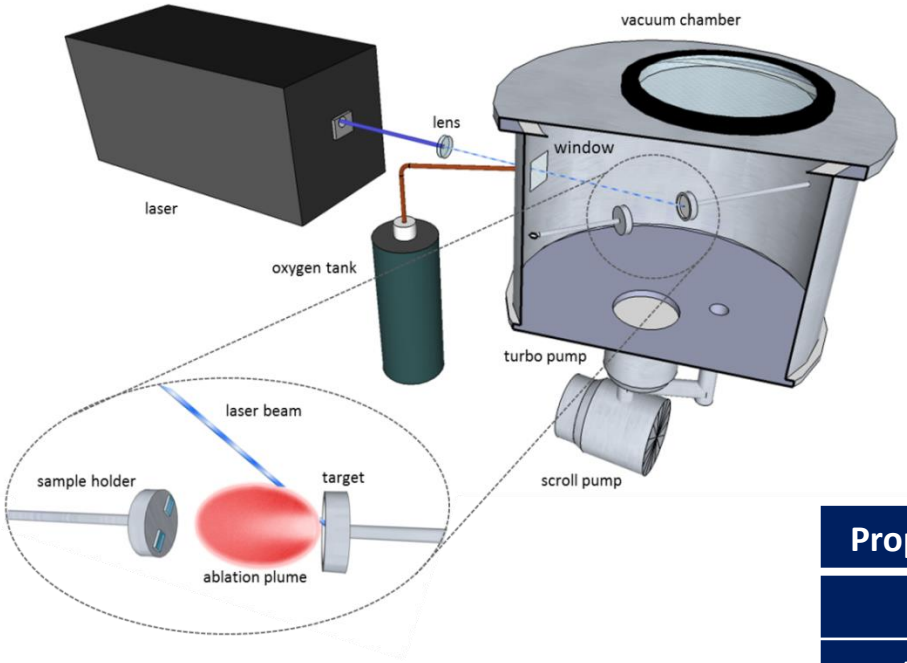
ISTITUTO ITALIANO
DI TECNOLOGIA

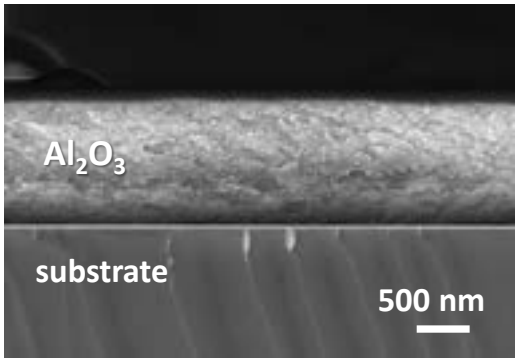
Aluminium Oxides - Al_2O_3 films deposited by Pulsed Laser Deposition (PLD)

Acta Materialia 61 (7), 2662-2670, 2013
Corrosion Science 77, 375-378, 2013
Scientific Reports 6, 33478, 2016
Corrosion Science on line, 2017
Acta Materialia on line, 2017

fabio.difonzo@iit.it

PLD-grown Al_2O_3 nanoceramic coatings





- ✓ **high quality coatings**
- ✓ custom process: bottom-up approach
- ✓ process at **room temperature**
- ✓ amorphous films with **nanodispersed crystalline domains**

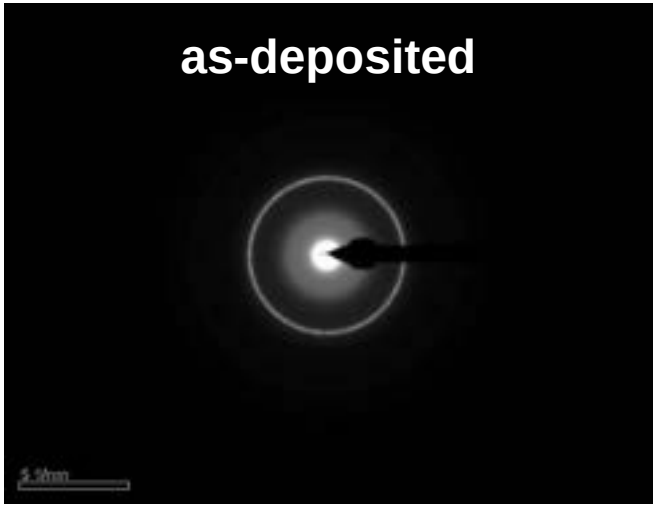
F. Garcia Ferré et al. – ACTA MATER – 2013

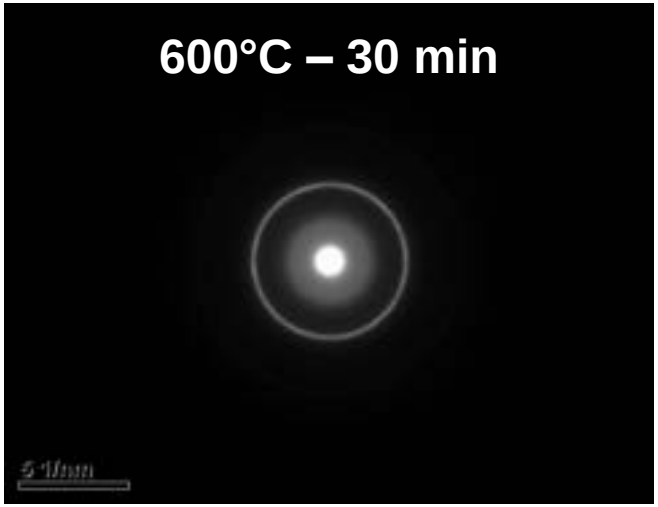
Property @RT	Sapphire	PLD Al_2O_3	AISI 316L
ν	0,24	0,295 0,025	0,3
E [GPa]	345	193,8 9,9	200
G [GPa]	175	75,5 ± 3,8	80
B [GPa]	240	159,2 ± 11,8	140
H [GPa]	27,8	10,3 1	4
H/E	0,059	0,049 0,007	0,025

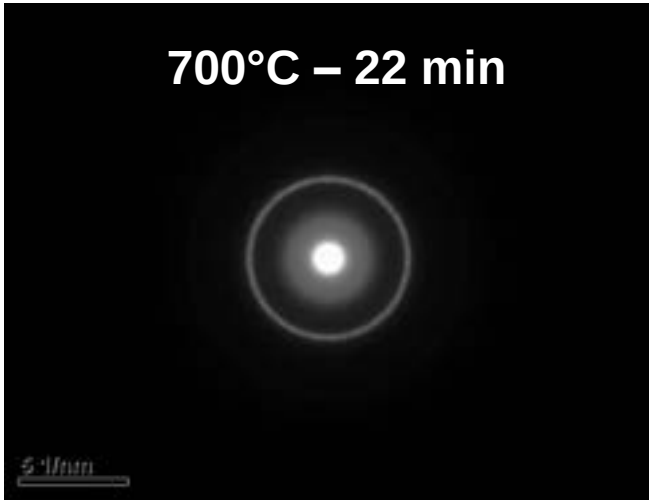
H/E parameter index of wear resistance and fracture toughness

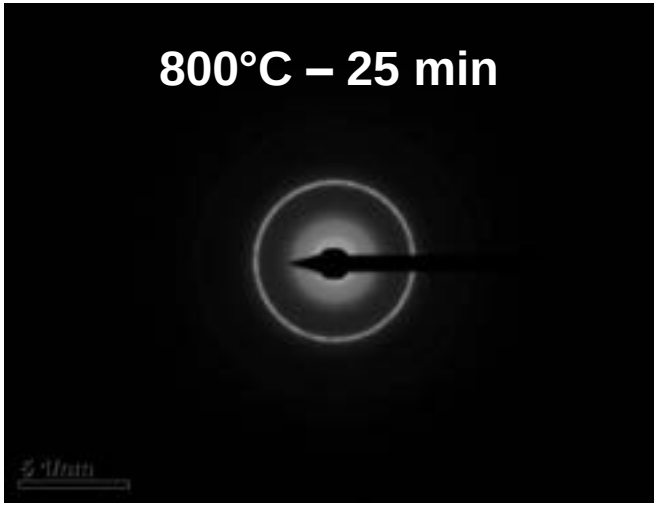
Thermal stability

Thermal stability: in-situ TEM

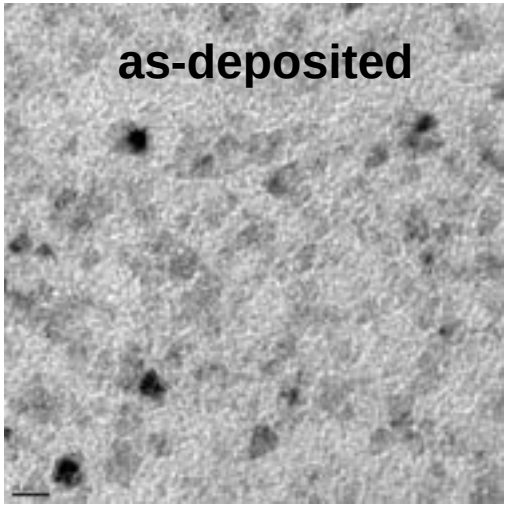


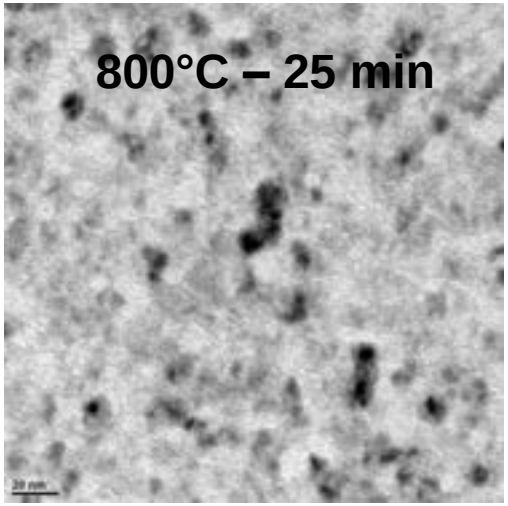






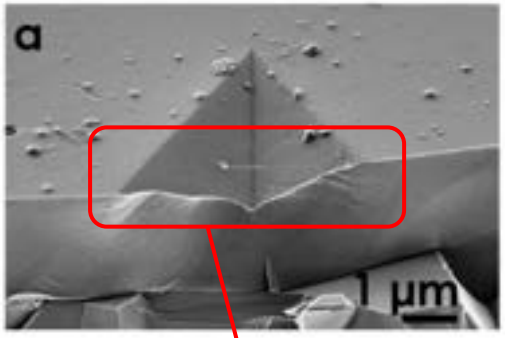
BF-HRTEM

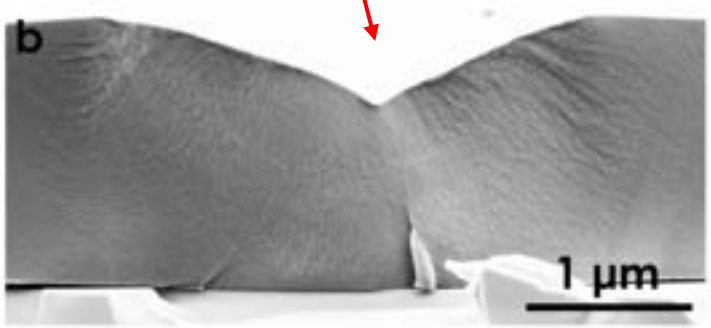




Mechanical behaviour of PLD-grown Al_2O_3

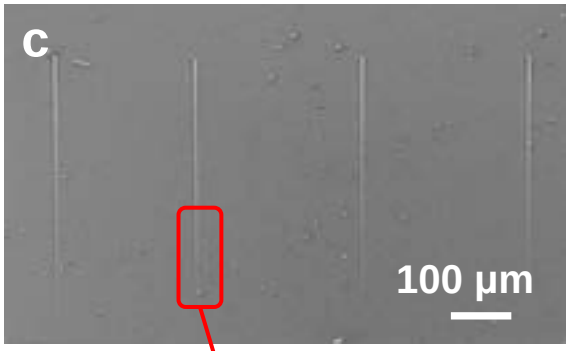
- **Nanoindentation Tests**



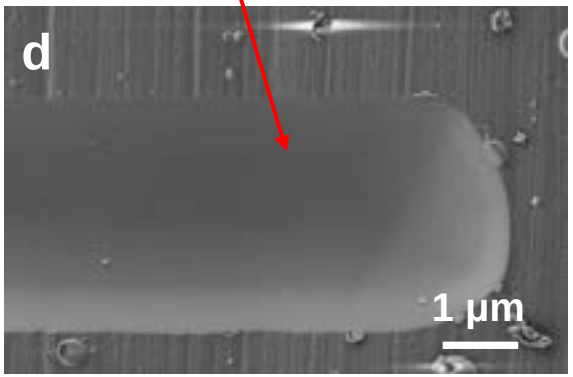


metal-like behavior under plastic strain

- **Nanoscratch Tests**



F. Garcia Ferré et al. – ACTA MATER – 2013

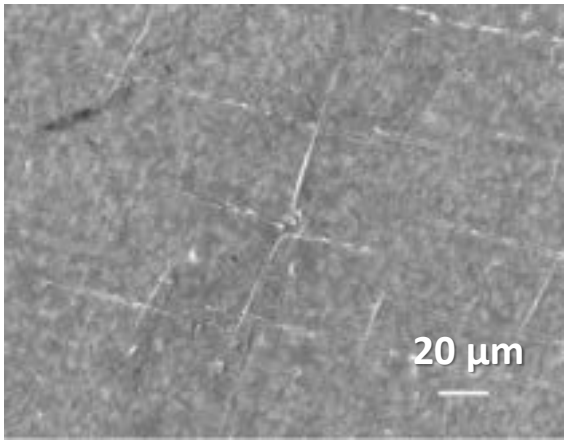


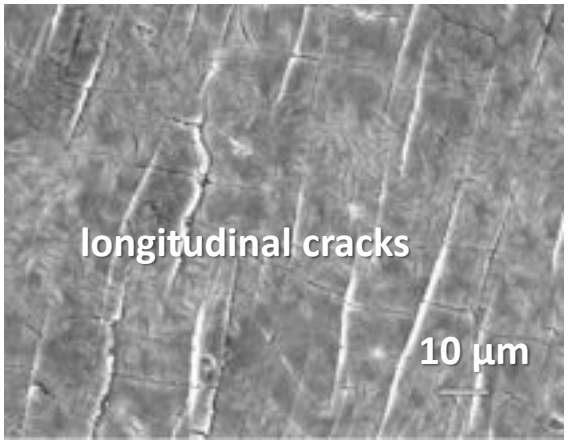
strong interfacial bonding

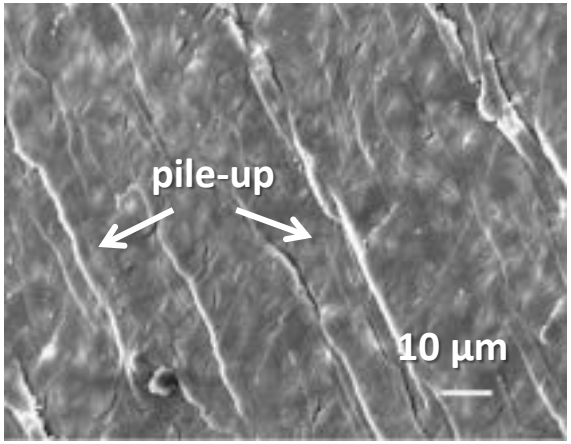
Burst test

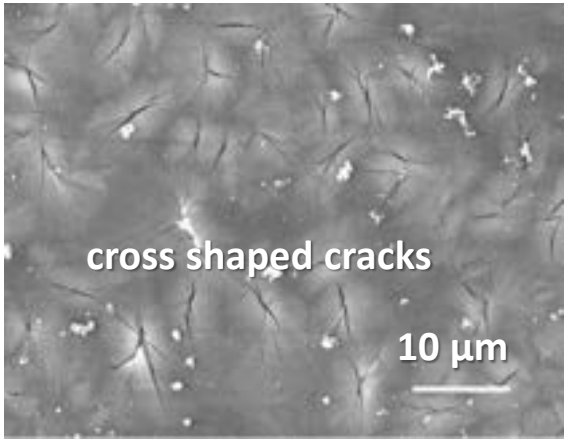


BEFORE











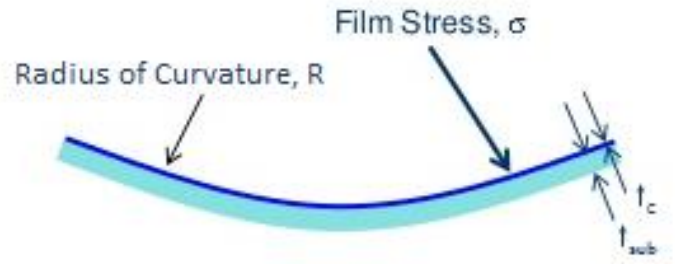
AFTER

Residual Stress Measurements

➢ Curvature Method

- **Stress relief** through mechanical deformation (bending)
- Evaluation of **substrate curvature** before and after deposition
- Laser techniques (i.e. cantilever beam), contact measures or video
- **Stoney Equation**

$$\sigma_{res} = \frac{E_{sub}t_{sub}^3 + E_c t_c^3}{6\mathrm{R}(t_{sub} + t_c)^2}$$

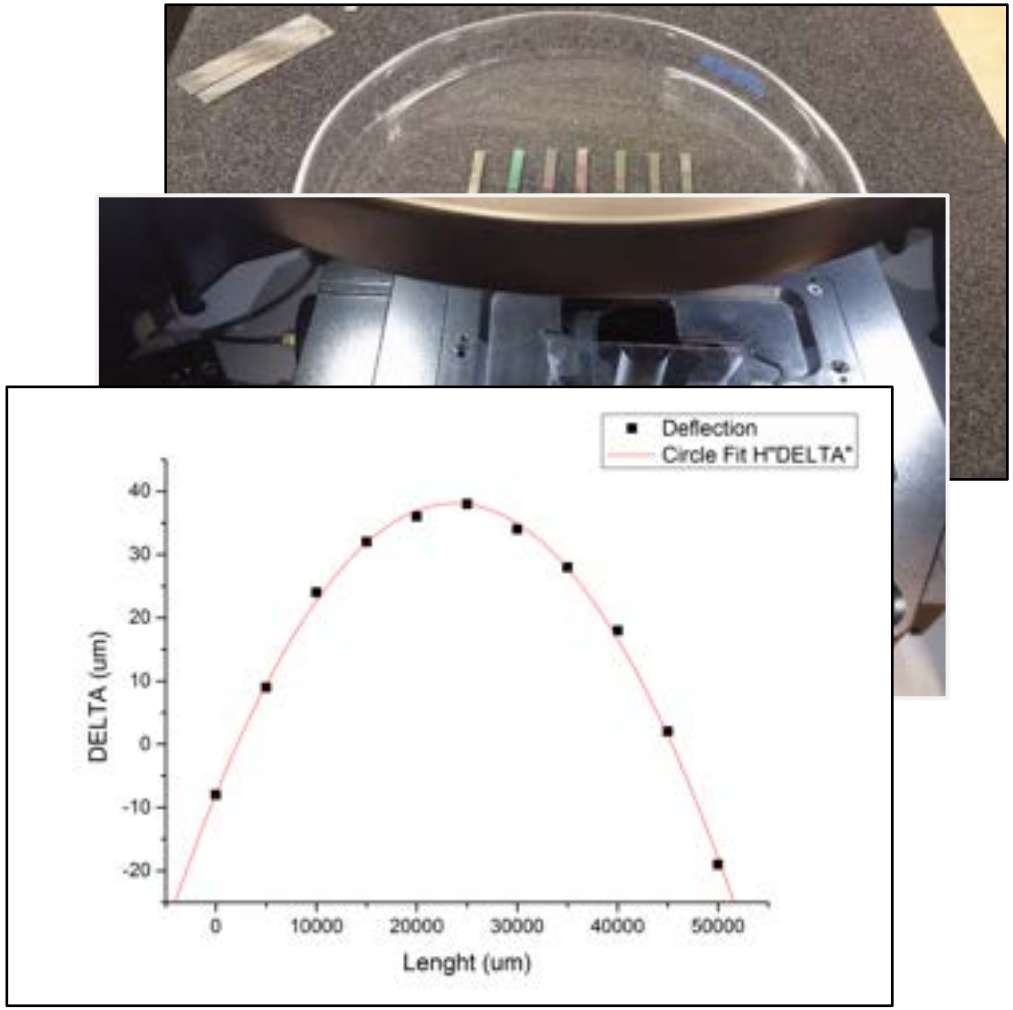


Residual Stress Measurements

1 – Samples fabrication

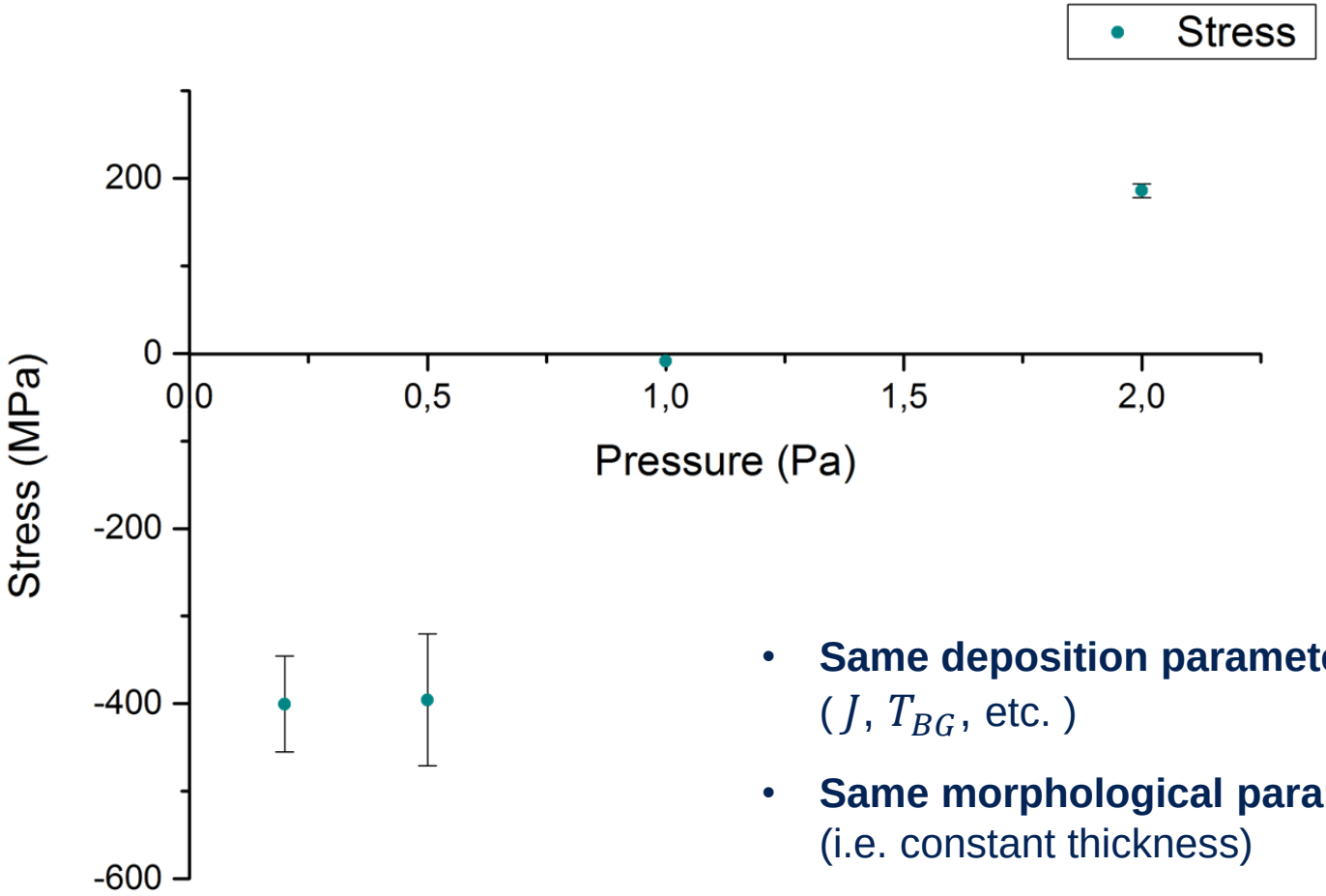
2 – Optical Prolimometry

3 – Data Fitting



Residual Stress Measurements

Residual Stress VS Backgroud Pressure



- **Same deposition parameters** (J, T_{BG}, etc.)
- **Same morphological parameters** (i.e. constant thickness)

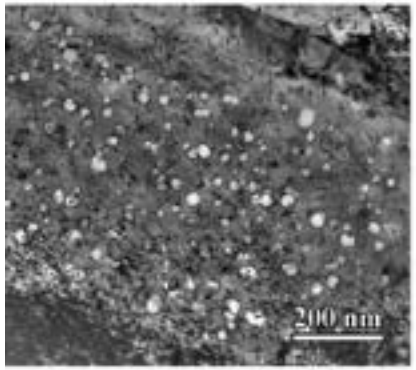
ISTITUTO ITALIANO
DI TECNOLOGIA

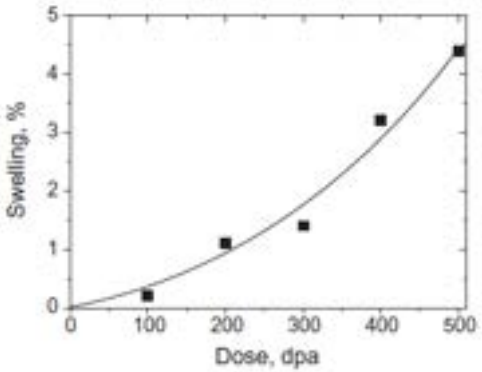
Heavy Ion Irradiation of Al_2O_3 barrier coatings

fabio.difonzo@iit.it

Radiation tolerant materials

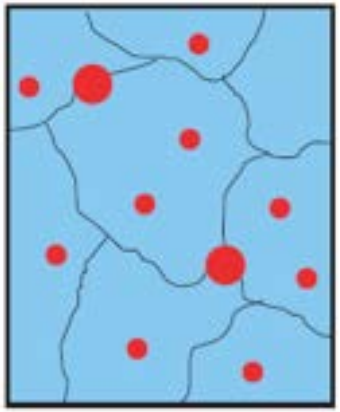
Low-swelling ferritic martensitic steels

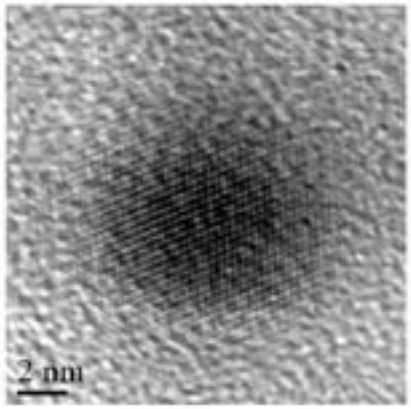




M.B. Toloczko et al. - J. Nucl. Mater. - 2014

Oxide-dispersion strengthened steels & alloys

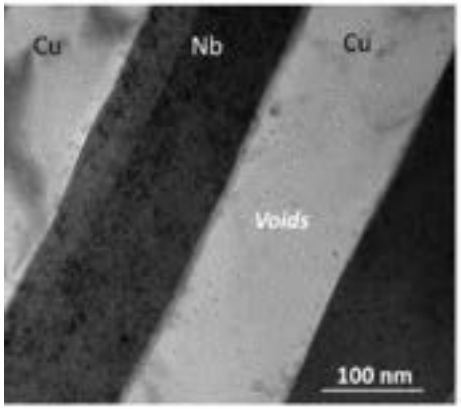


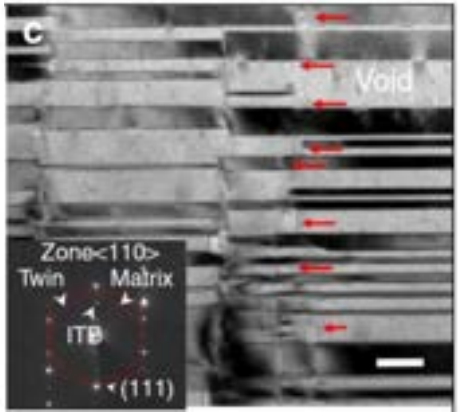


G. Liu et al. – Nature Mater. – 2013

M.L. Lescoat et al. – J. Nucl. Mater. – 2012

Nanolaminates & nanotwinned metals

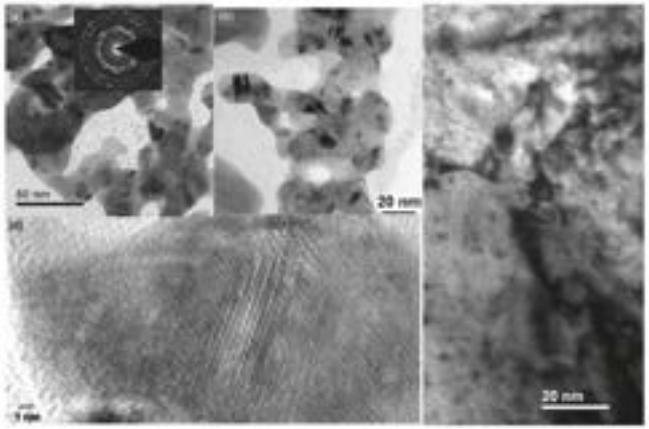




D. Rollet et al. – Adv. Mater. – 2013

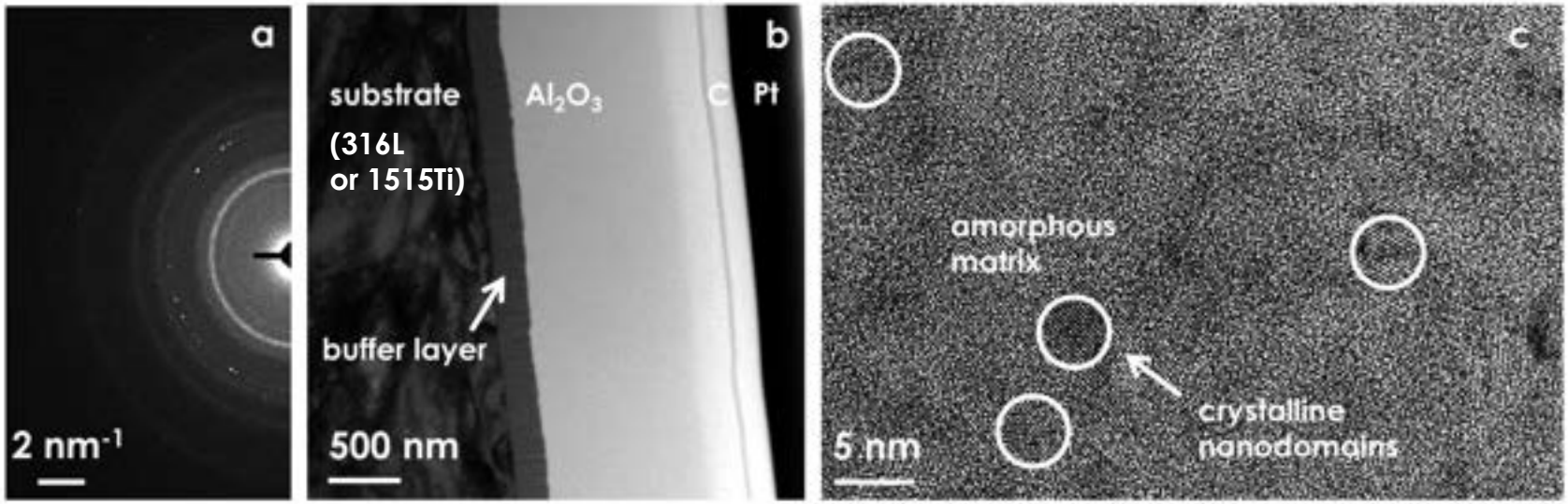
Y. Chen et al. – Nature Commun. – 2015

Nanoporous materials



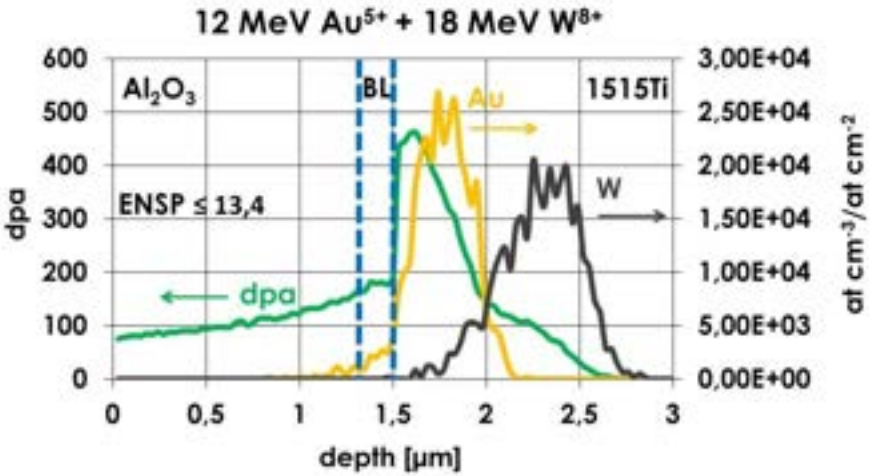
Y. Chen et al. – Nature Commun. – 2015

Heavy ion irradiation (Au + W) of Al_2O_3



Main criteria

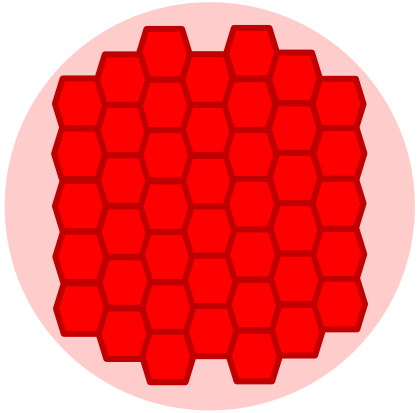
- Minimum coating thickness for nanoindentation: 1 µm
- Implantation beyond coating → negligible chemical effects
- Low ENSP ratio to simulate effect of neutrons
- Low enough absolute electronic stopping power to avoid single swift ion track formation (7 keV/nm vs ≈ 9,5 keV/nm threshold @RT)
- Different doses, corresponding to **20, 40, 150, 250 and 450 dpa** at the interface between Al_2O_3 and BL
- dpa calculated using SRIM (Kinchin-Pease)

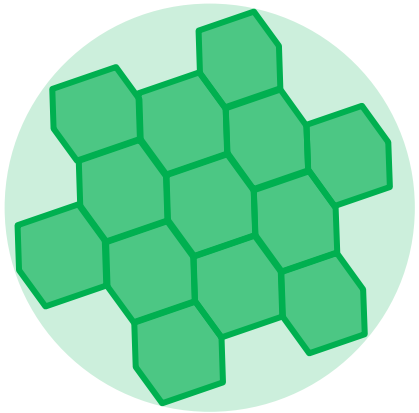


Model of evolution

moderate dpa

ultra-fine nanoceramic
GB-driven deformation
highest fracture toughness

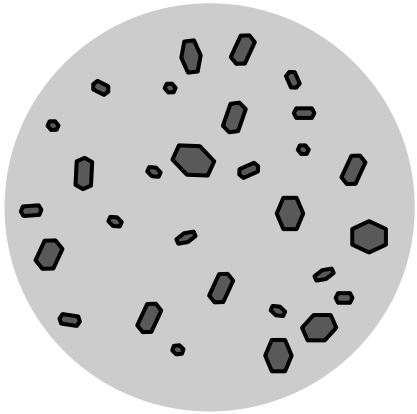




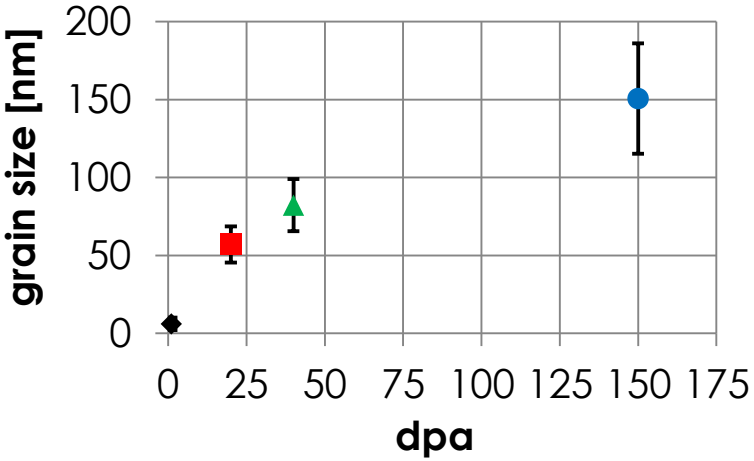
high dpa

fine nanoceramic
GB-driven deformation
sub-linear grain growth

pristine

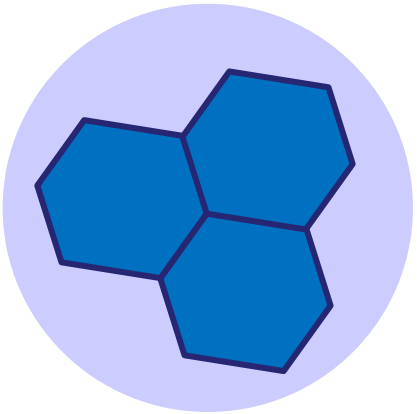


bi-phase nanocomposite
shear banding
highest fracture strength



Sublinear grain growth

end-of-life dpa



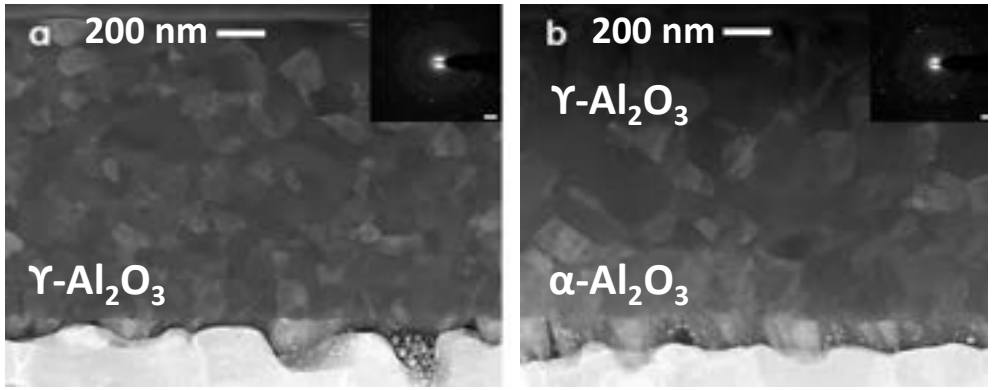
nanoceramic
GB-driven deformation
highest stiffness

fabio.difonzo@iit.it

Model of evolution

moderate dpa

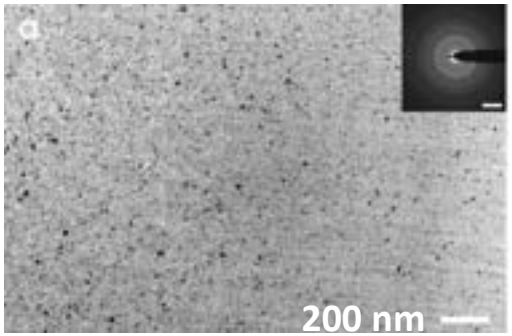
ultra-fine nanoceramic
GB-driven deformation
highest fracture toughness



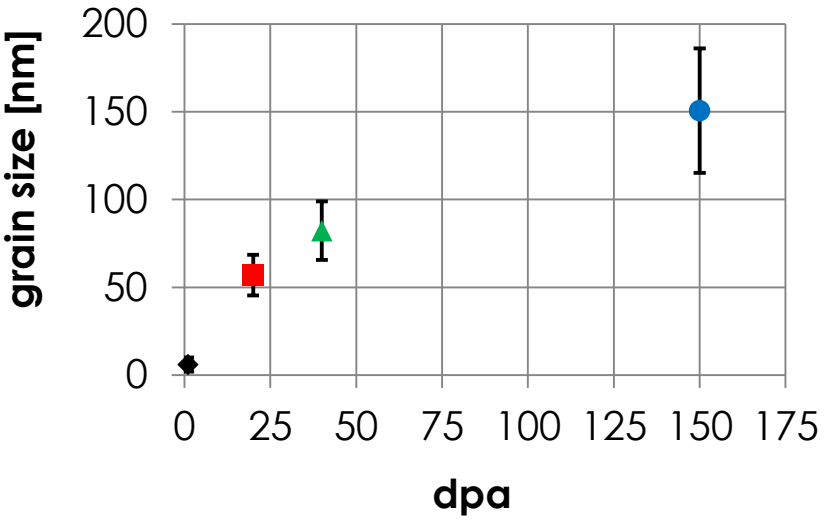
high dpa

fine nanoceramic
GB-driven deformation
sub-linear grain growth

pristine

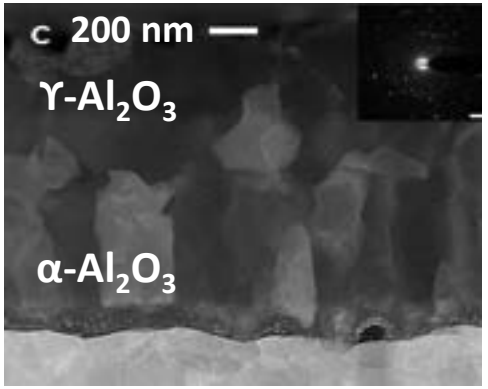


bi-phase nanocomposite
shear banding
highest fracture strength



Sublinear grain growth

end-of-life dpa



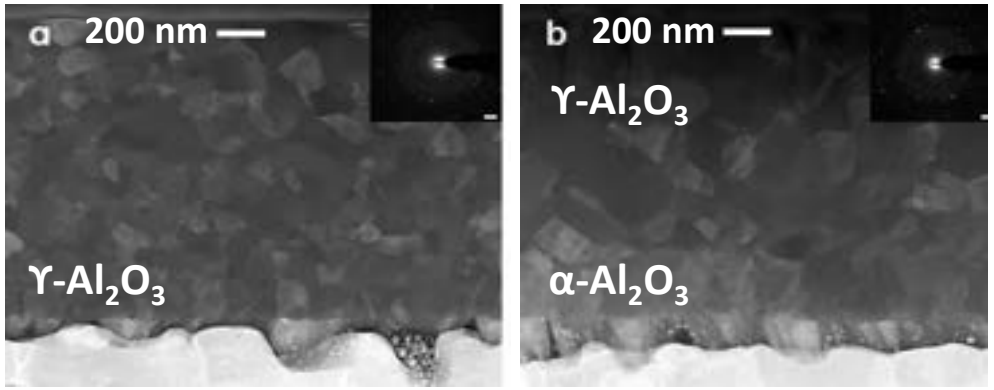
nanoceramic
GB-driven deformation
highest stiffness

fabio.difonzo@iit.it

Model of evolution

moderate dpa

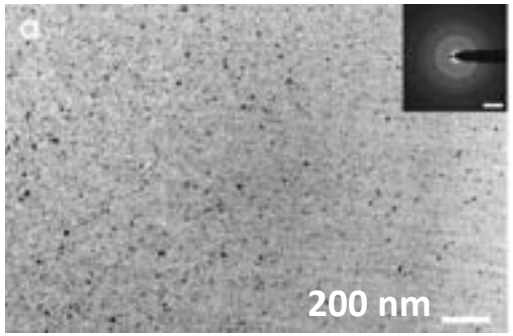
ultra-fine nanoceramic
GB-driven deformation
highest fracture toughness



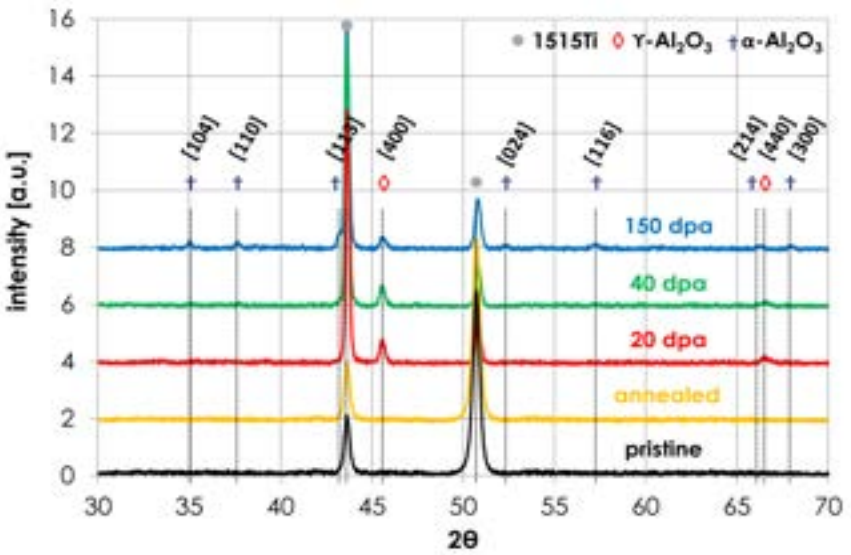
high dpa

fine nanoceramic
GB-driven deformation
sub-linear grain growth

pristine

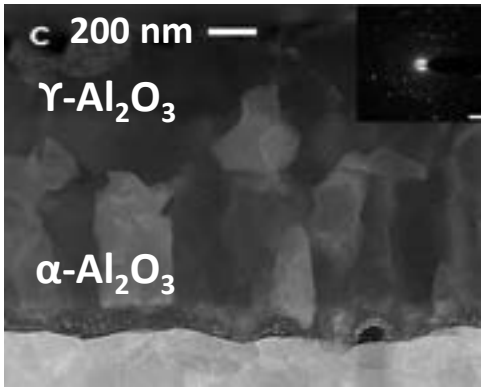


bi-phase nanocomposite
shear banding
highest fracture strength



Phase Transition

end-of-life dpa



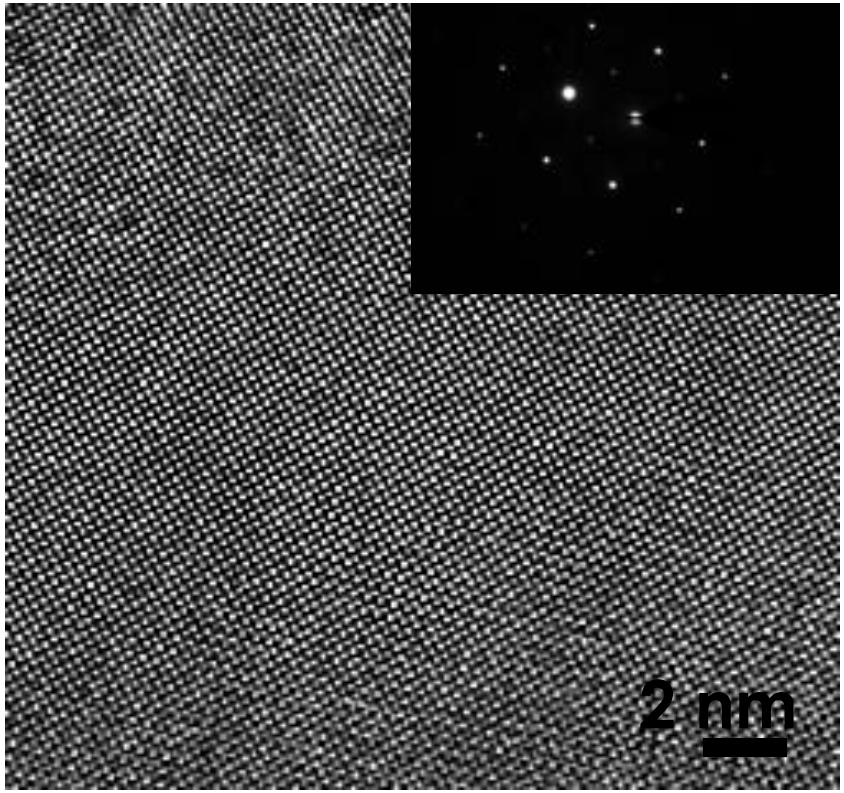
nanoceramic
GB-driven deformation
highest stiffness

fabio.difonzo@iit.it

Heavy ion irradiation (Au + W): structural features

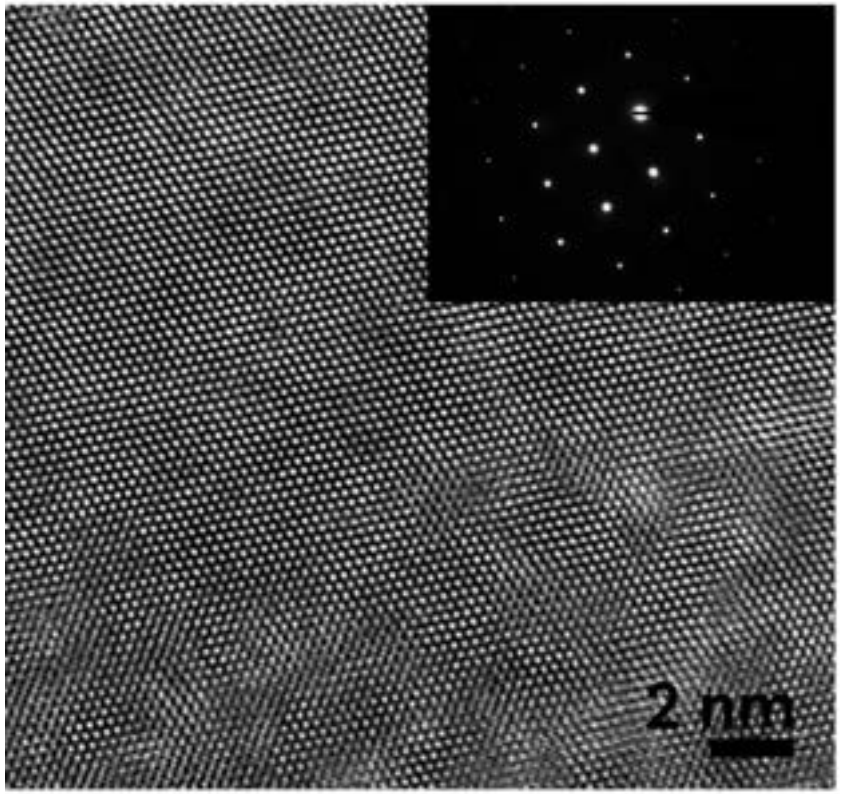
HR-TEM @ 150 dpa

External grains



ϒ-series Al_2O_3

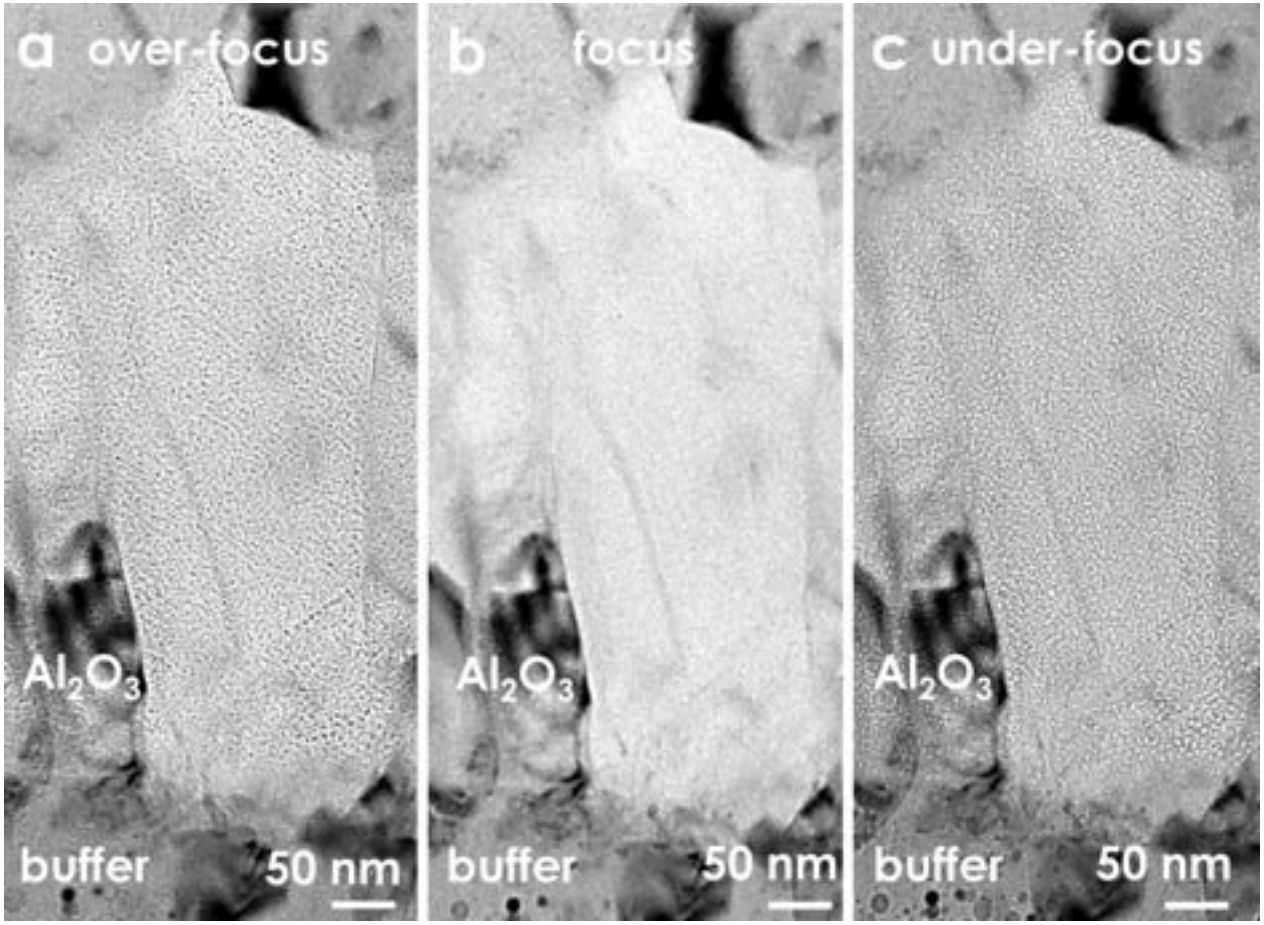
Internal grains



α-series Al_2O_3

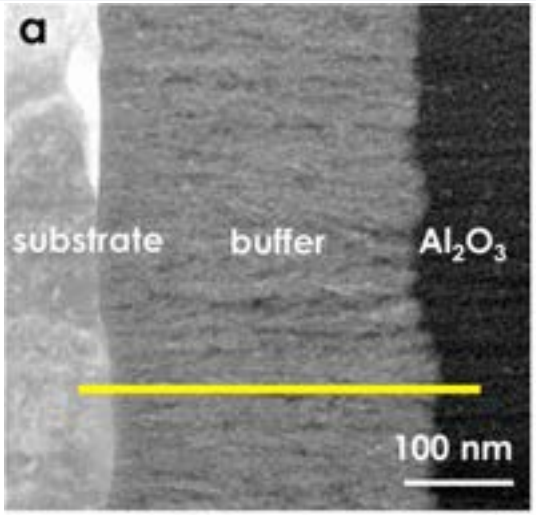
fabio.difonzo@iit.it

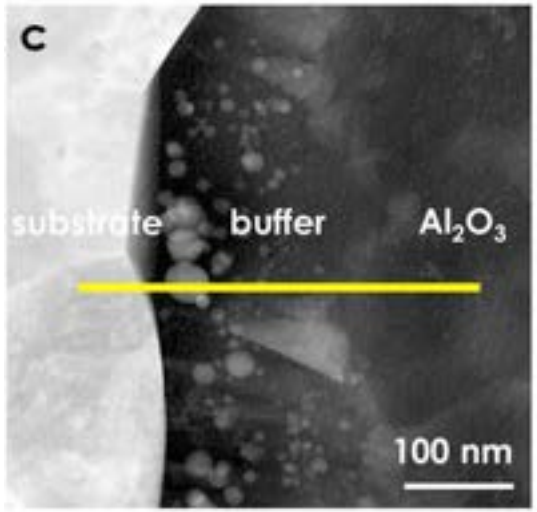
Heavy ion irradiation (Au + W): structural features

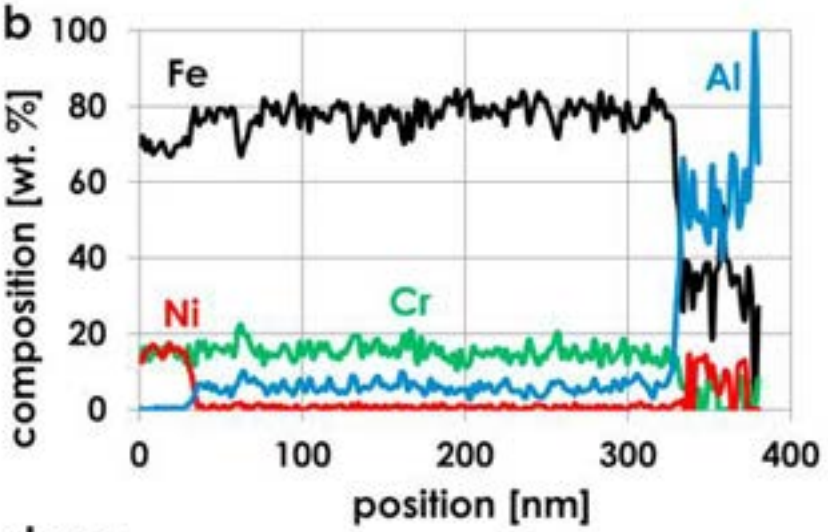


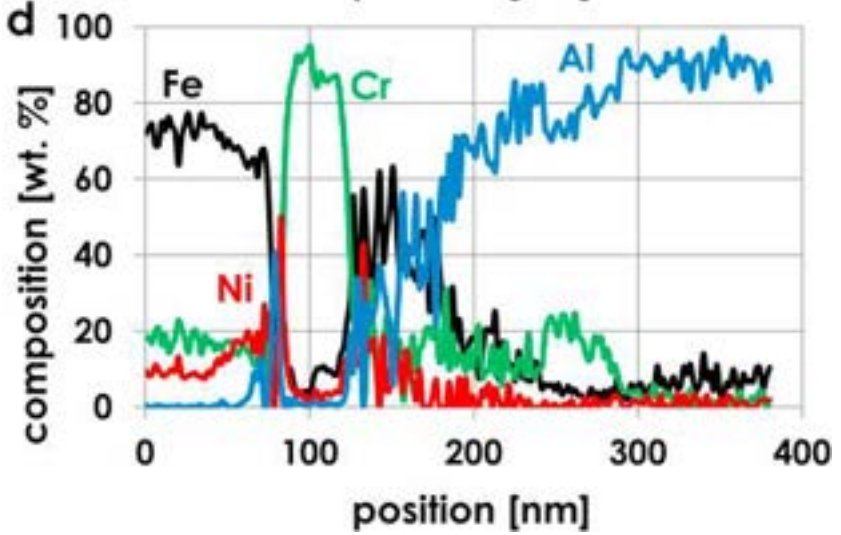
- Large number of small voids, only in a monolayer of grains, at the interface with the buffer layer
- These grains are alpha-alumina. All the other grains are gamma-alumina

Heavy ion irradiation (Au + W): buffer layer



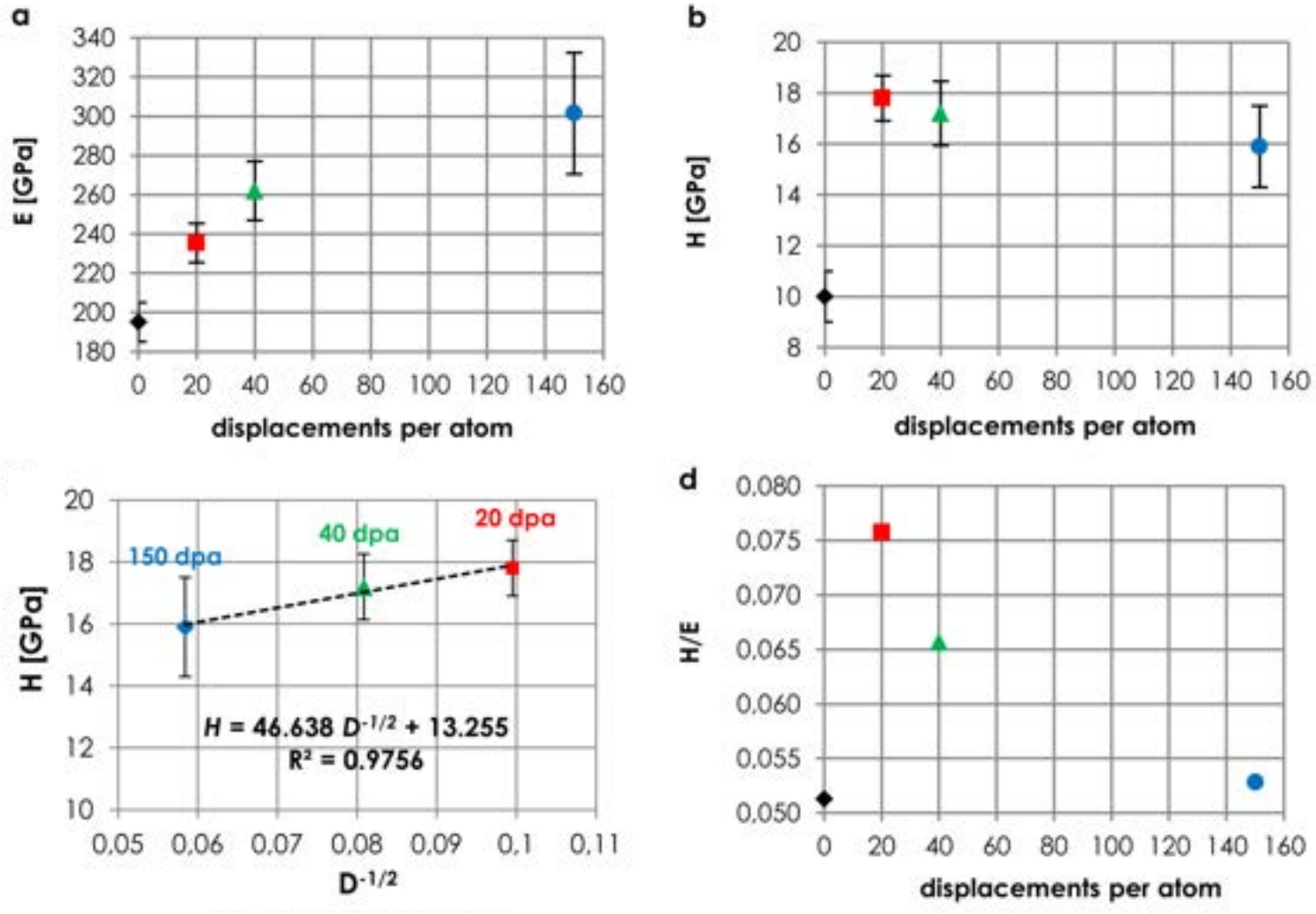






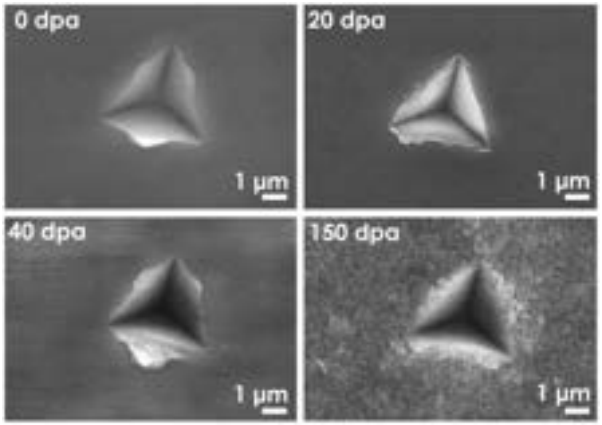
Densification & radiation induced segregation

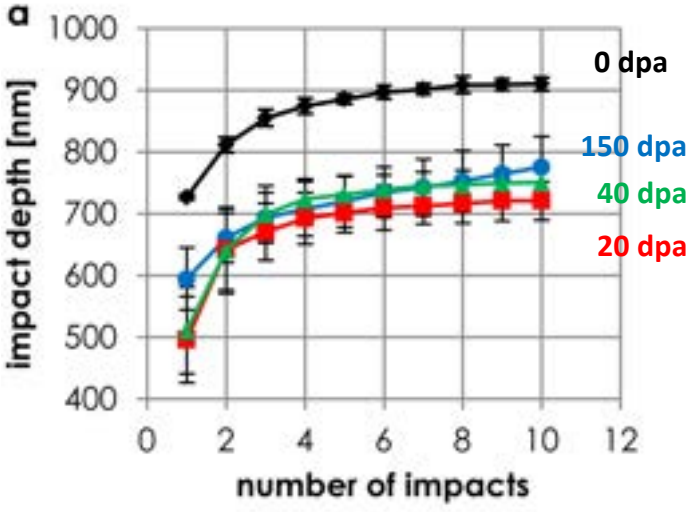
Heavy ion irradiation (Au + W): mechanical properties

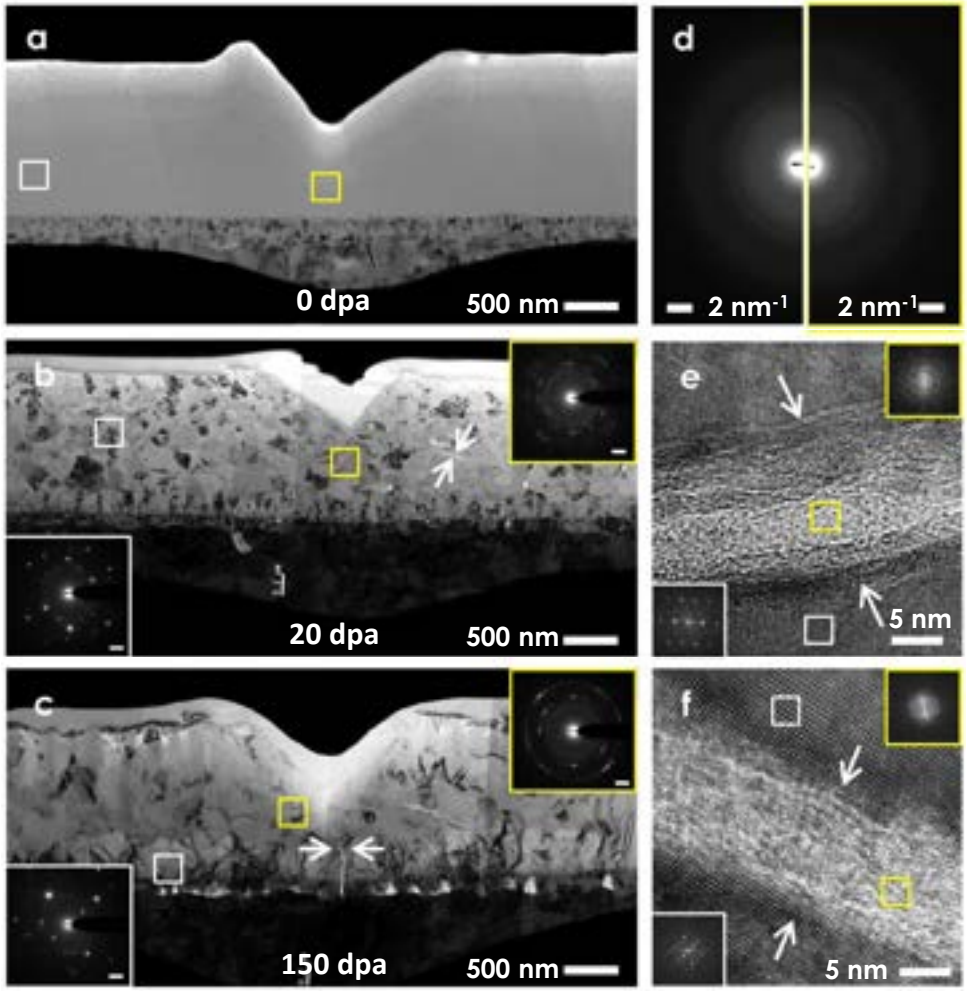


- The evolution of the mechanical properties is well fitted by the Hall-Petch relationship
- The structural rearrangements lead to an increase of the H/E ratio in-service (index of fracture toughness)

Heavy ion irradiation (Au + W): nanoimpact







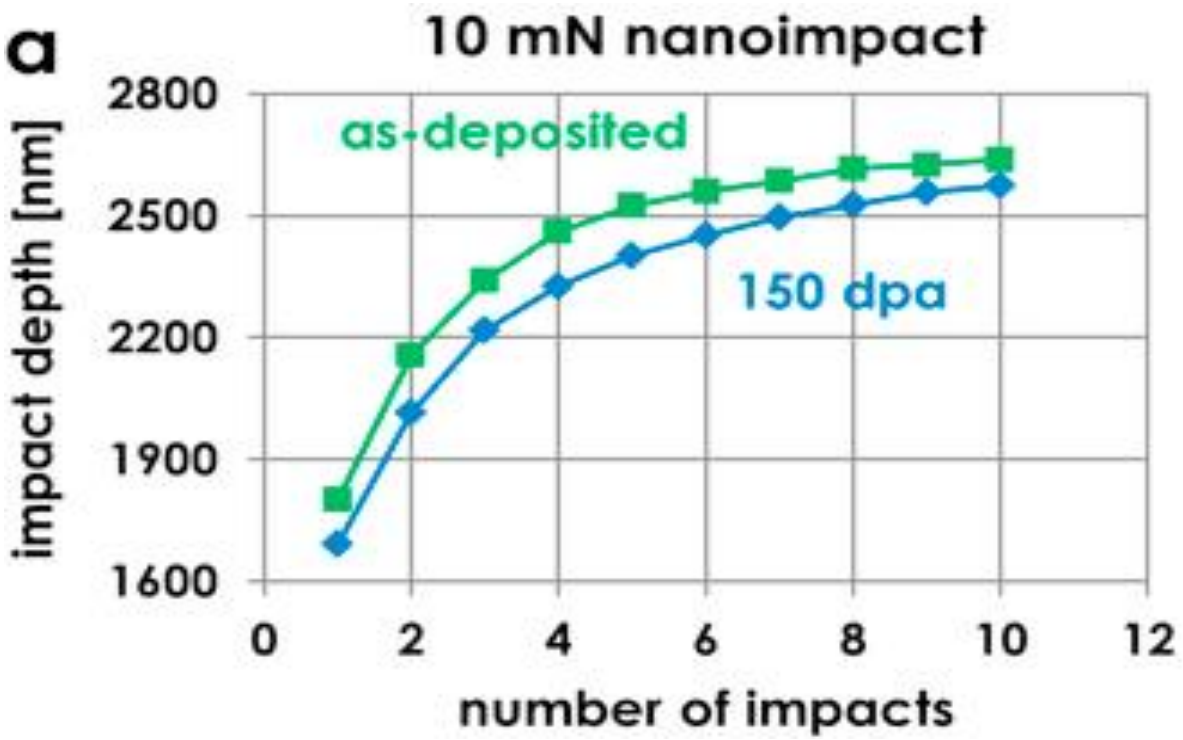
Shear banding

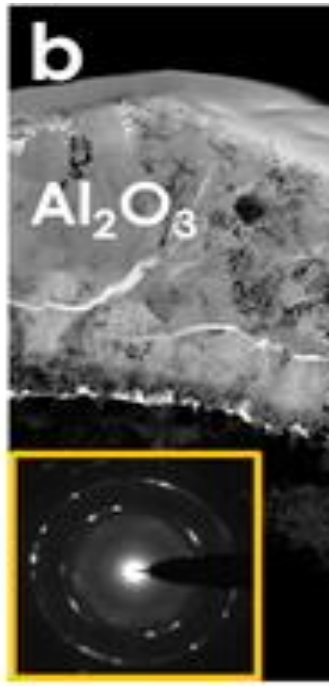
Lattice bending & localized shear amorphization

Lattice bending & localized shear amorphization

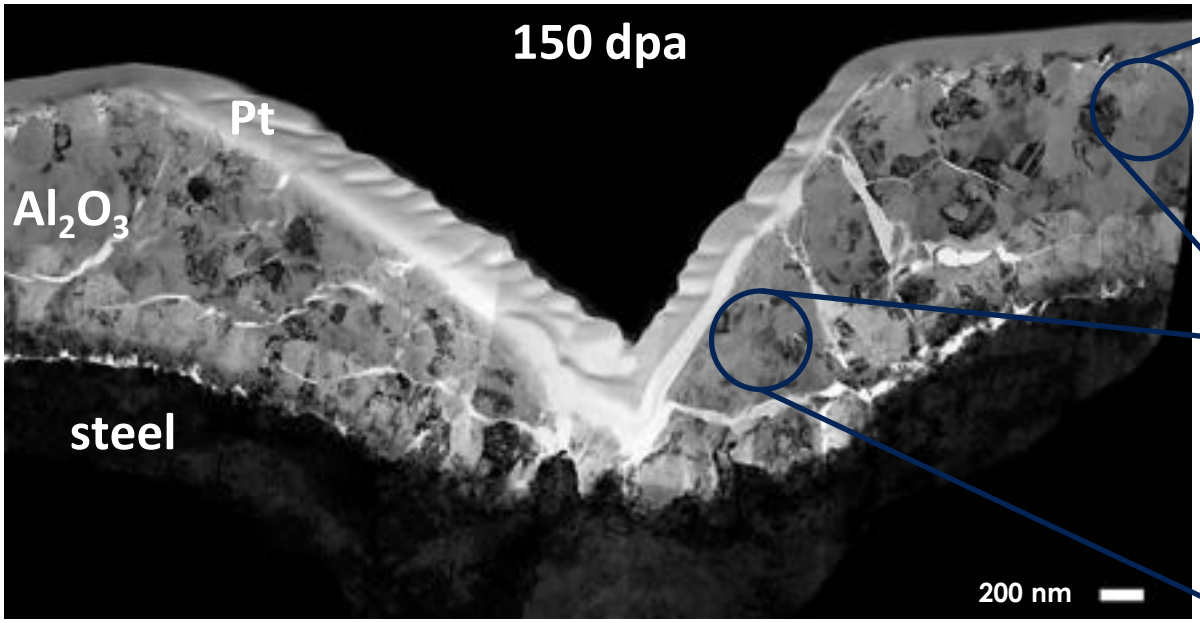
Impact energy is dissipated more efficiently in irradiated samples

Heavy ion irradiation (Au + W): nanoimpact – 10 mN

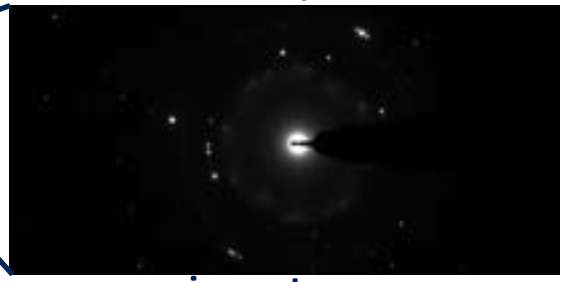




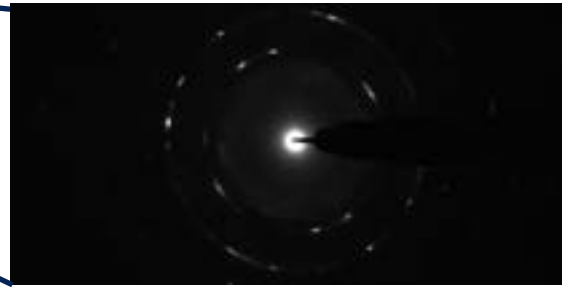
Heavy ion irradiation (Au + W): nanoimpact – 10 mN

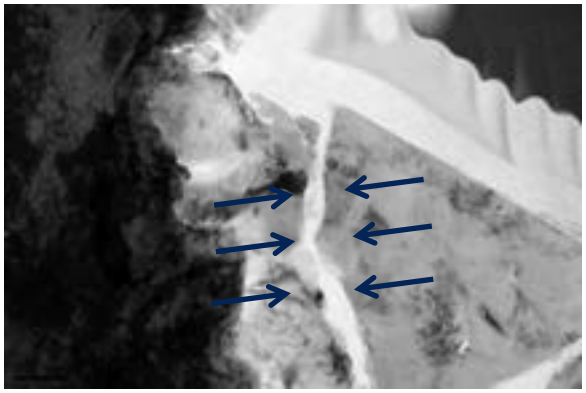


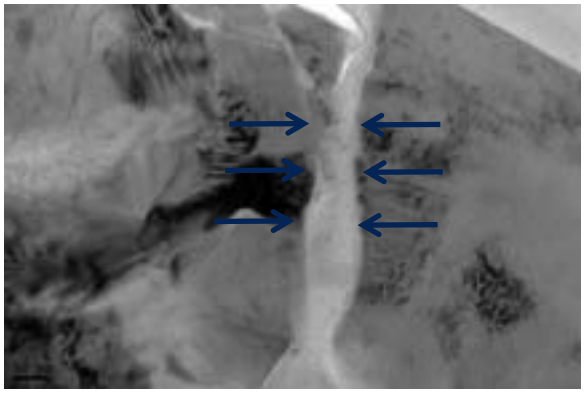
mechanically unloaded

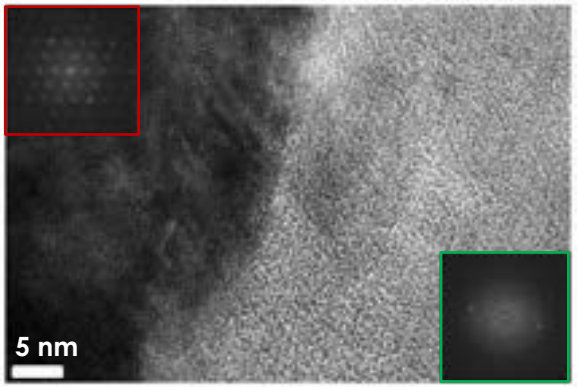


impact zone

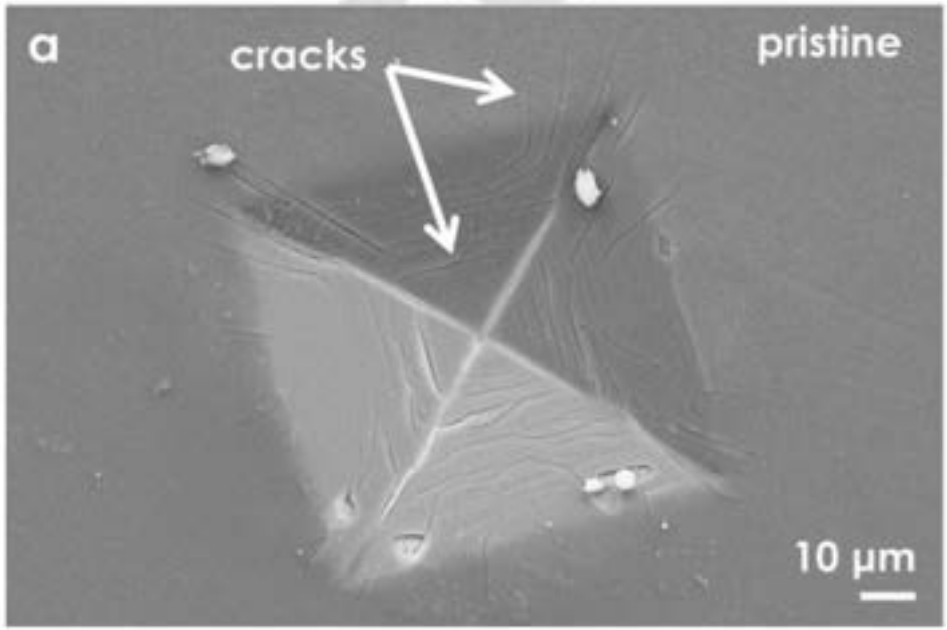


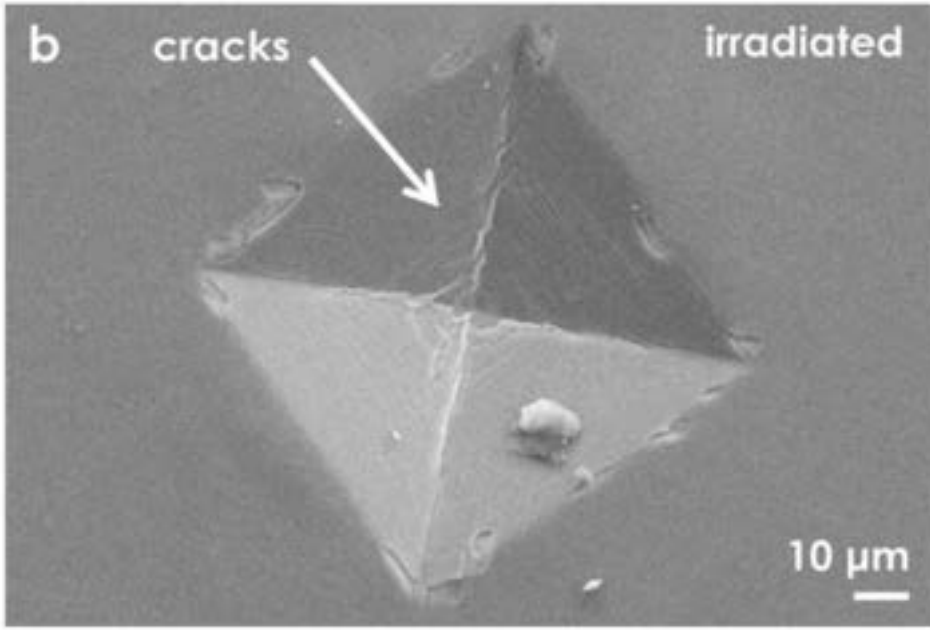






Microindentation



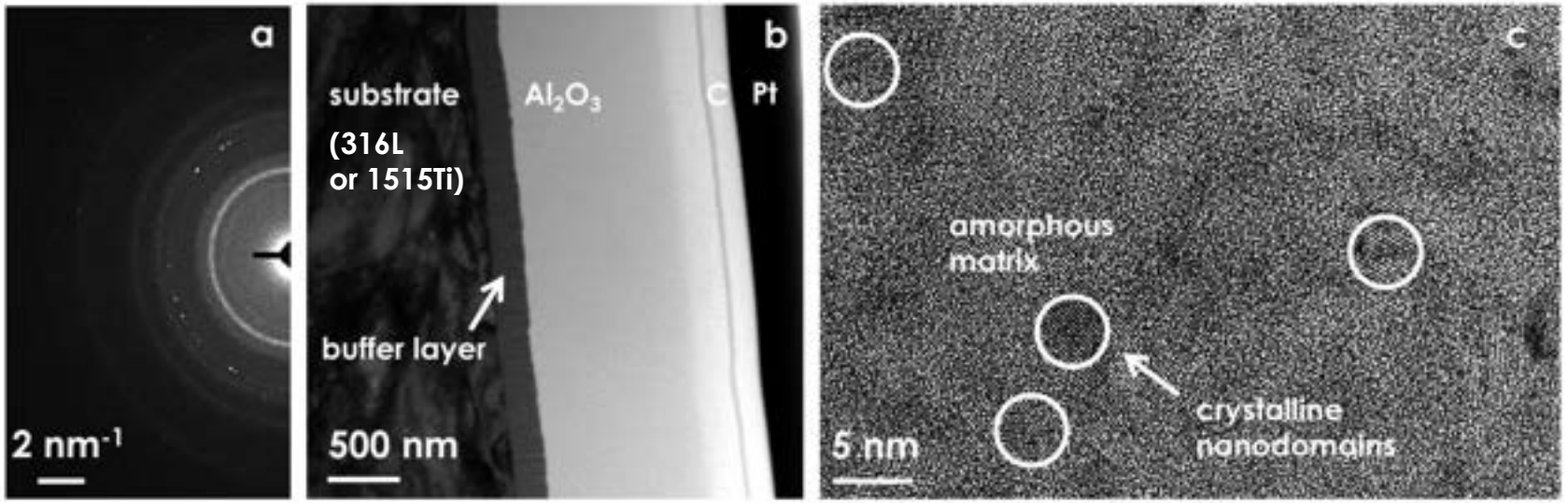


ntation imprints of the pristine (a) and the irradiated (b) coated 1515Ti plates. The cracks induced are more numerous and longer in the pristine
oughness is higher after irradiation.

Microindentation imprints of the pristine (a) and the irradiated (b) coated 1515Ti plates. The cracks induced are more numerous and longer in the pristine material, suggesting that the fracture toughness is higher after irradiation.

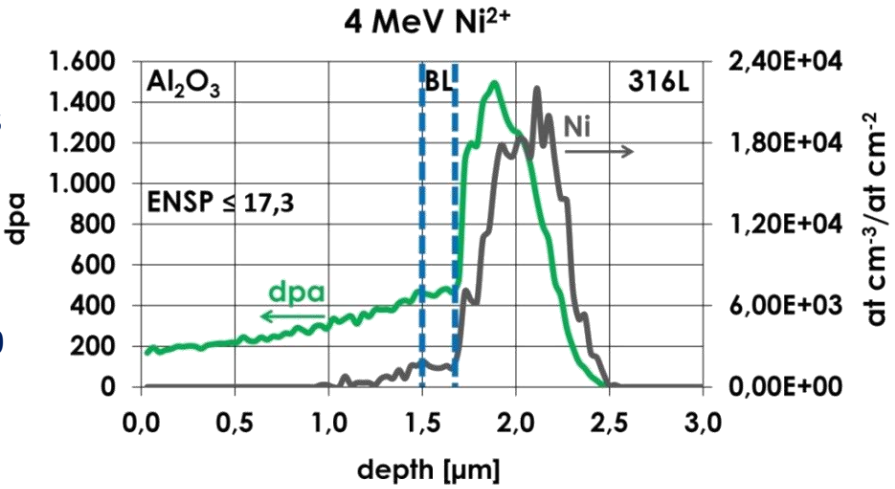
Heavy ion irradiation (Ni) of Al_2O_3

Ni ions up to 250 and 450 dpa @600°C

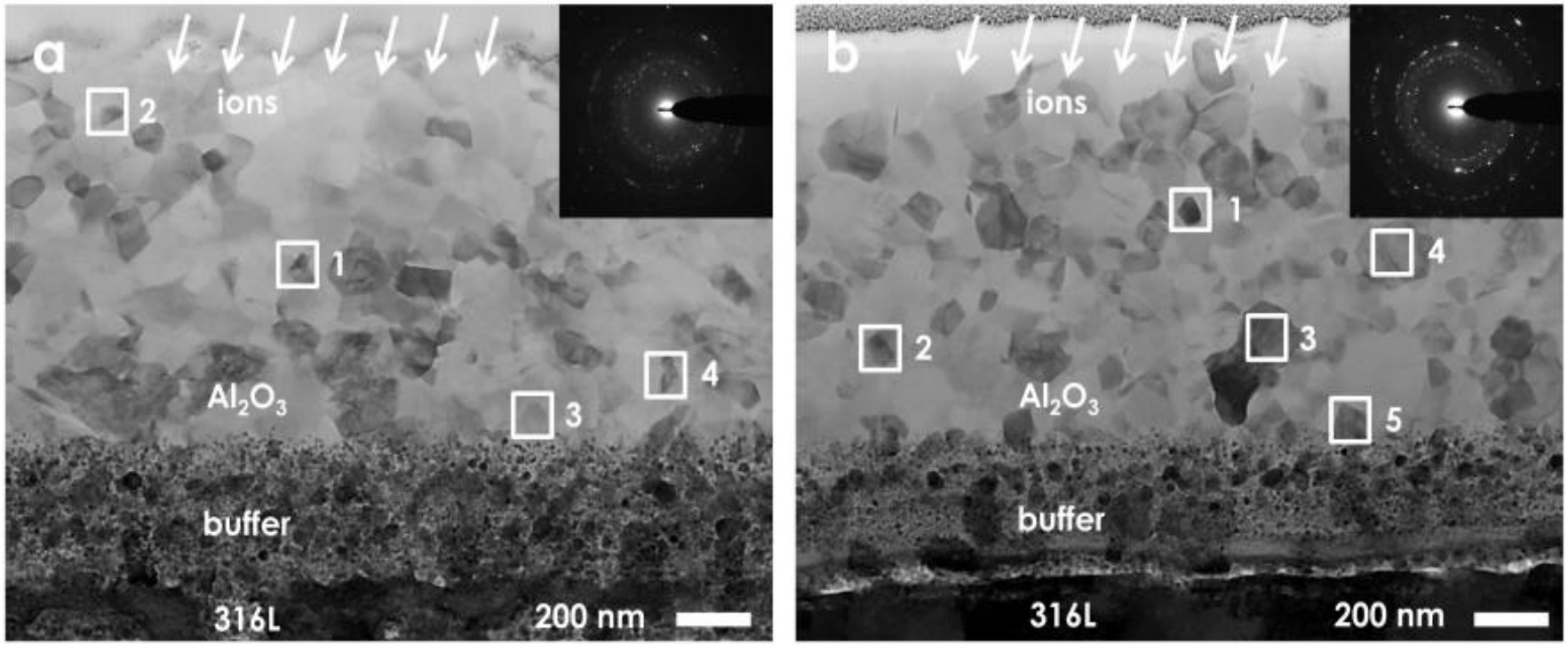


Main criteria

- Minimum coating thickness for nanoindentation: 1 µm
- Implantation beyond coating → negligible chemical effects
- Low ENSP ratio to simulate effect of neutrons
- Low enough absolute electronic stopping power to avoid single swift ion track formation (7 keV/nm vs ≈ 9,5 keV/nm threshold @RT)
- Different doses, corresponding to **20, 40, 150, 250 and 450 dpa** at the interface between Al_2O_3 and BL
- dpa calculated using SRIM (Kinchin-Pease)

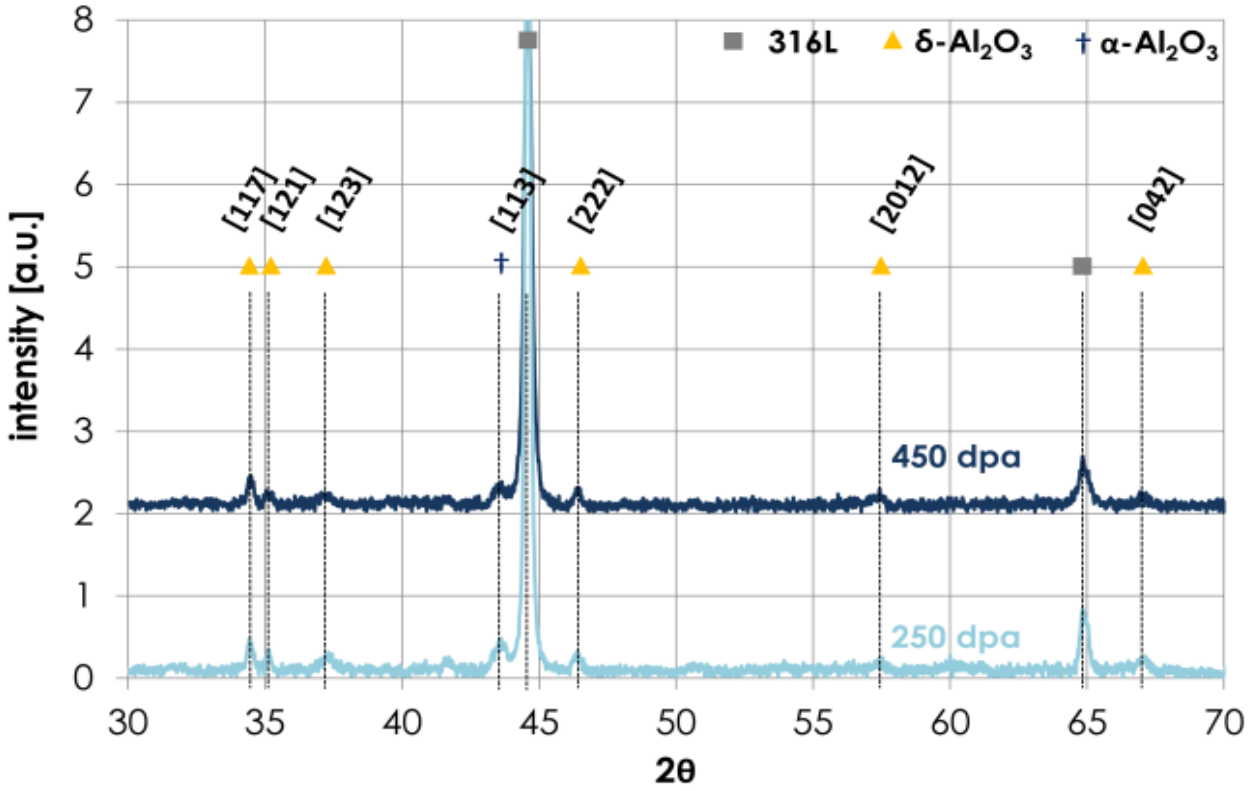


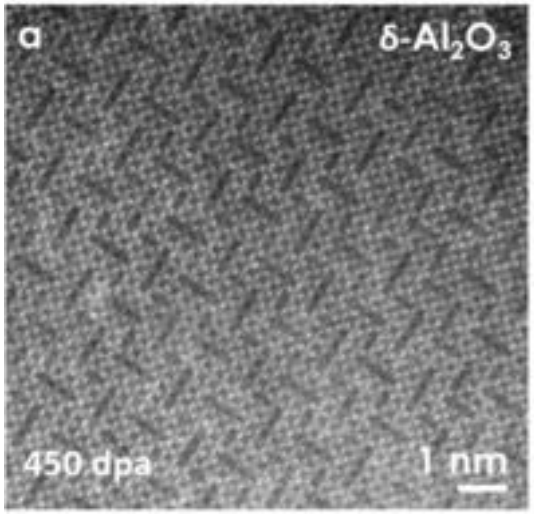
Heavy ion irradiation (Ni) of Al_2O_3

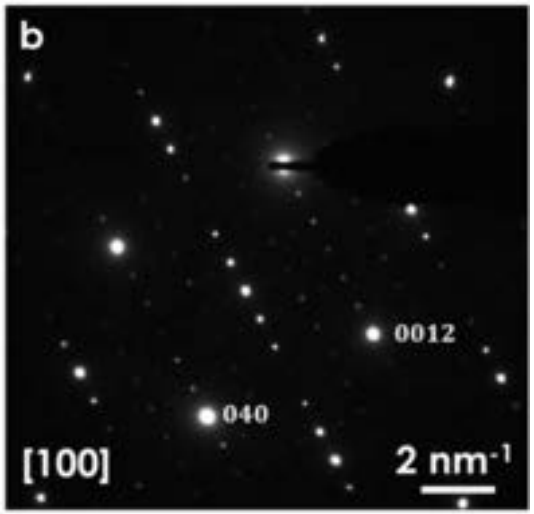


BF-STEM micrographs and DP insets of the Al_2O_3 nanoceramic thin films irradiated up to 250 dpa (a) and 450 dpa

Heavy ion irradiation (Ni) of Al_2O_3



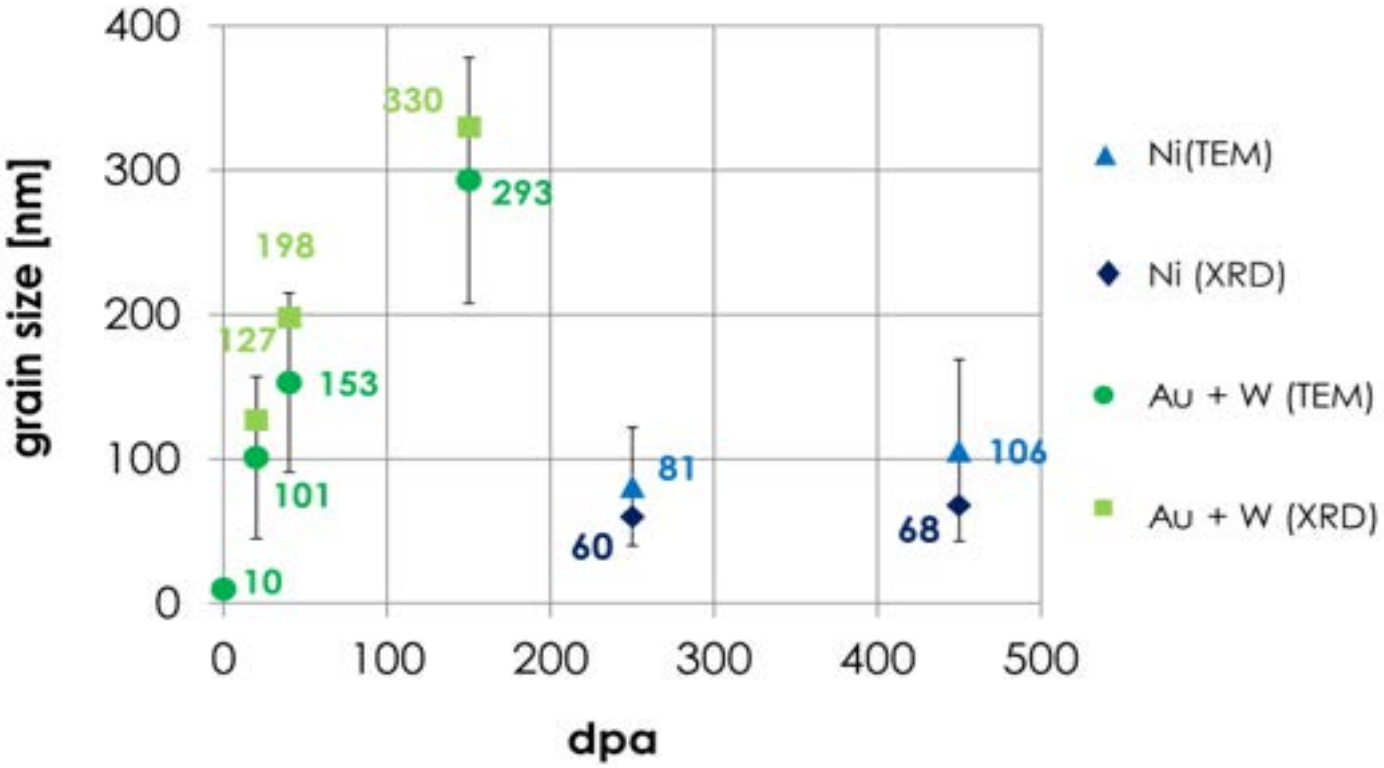


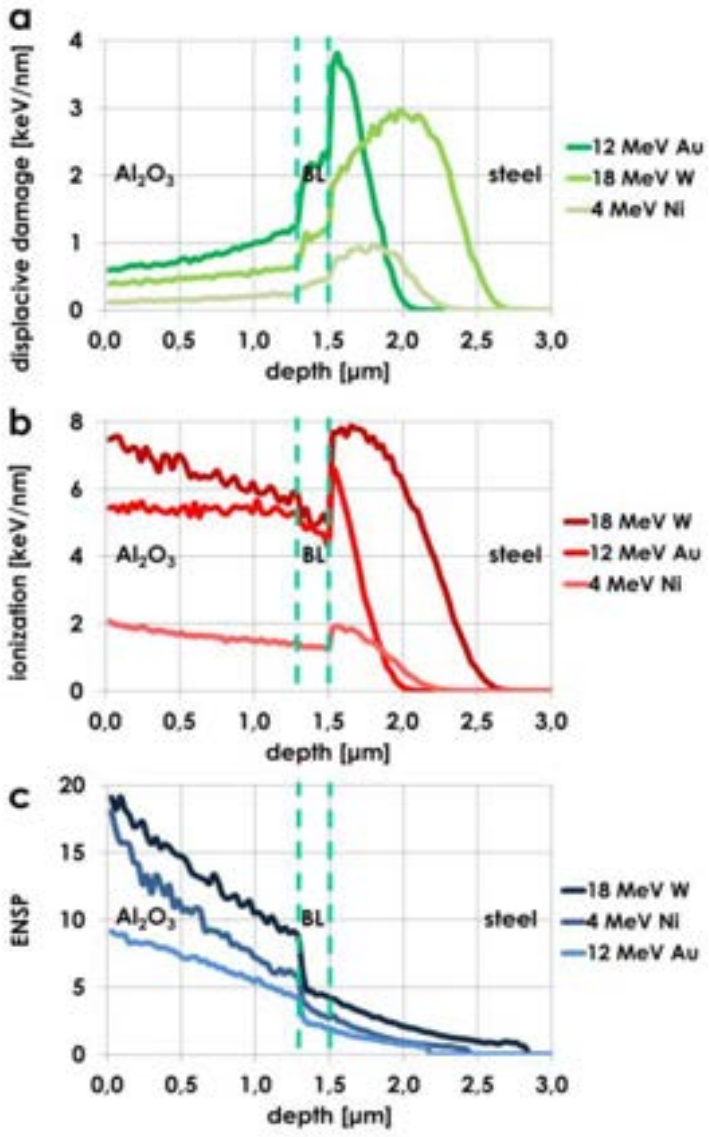


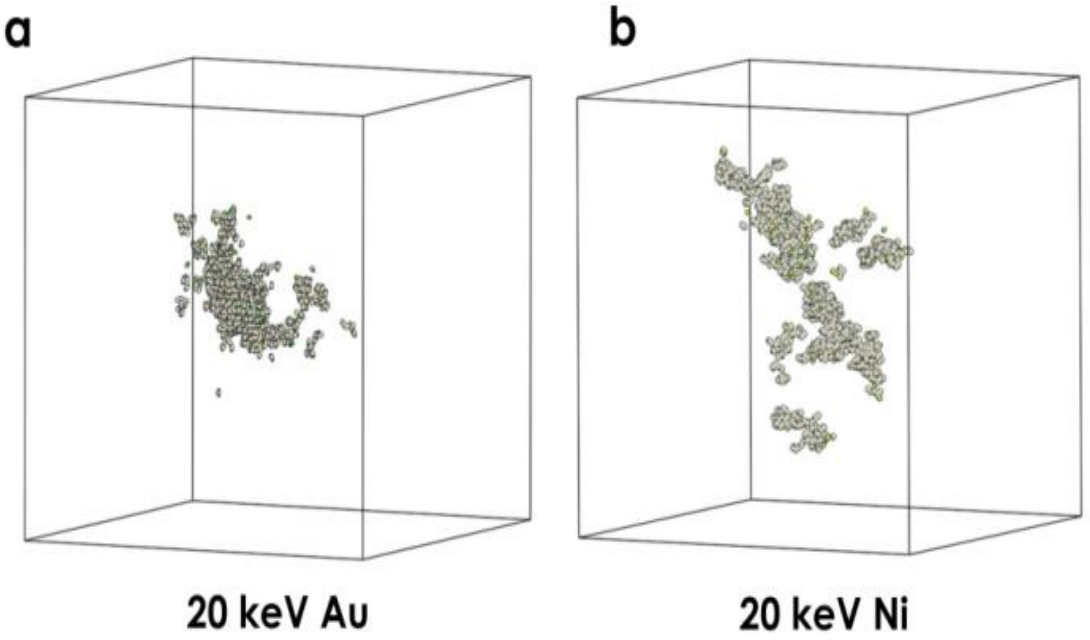
XRD phase evolution

HAADF-STEM micrograph (a) and DP (b) of δ-Al_2O_3 along the $[100]_\delta$ zone axis

Grain size evolution







MD by L. Van Brutzel, CEA

ISTITUTO ITALIANO
DI TECNOLOGIA

Pb compatibility of Al_2O_3 barrier coatings

fabio.difonzo@iit.it

Corrosion resistance, O_2 saturation

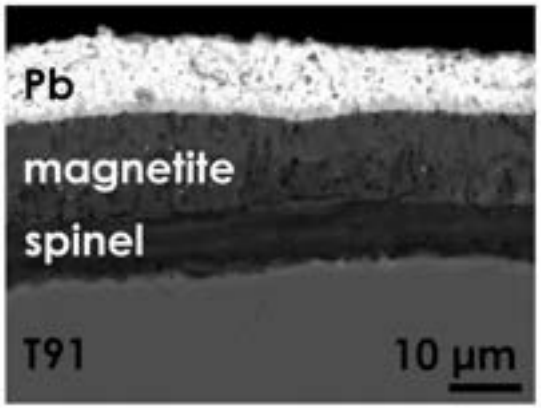
SS plates

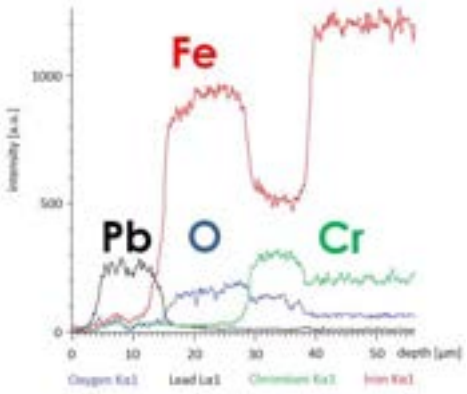
uncoated sample



heavy liquid metal corrosion

Oxidizing stagnant Pb test

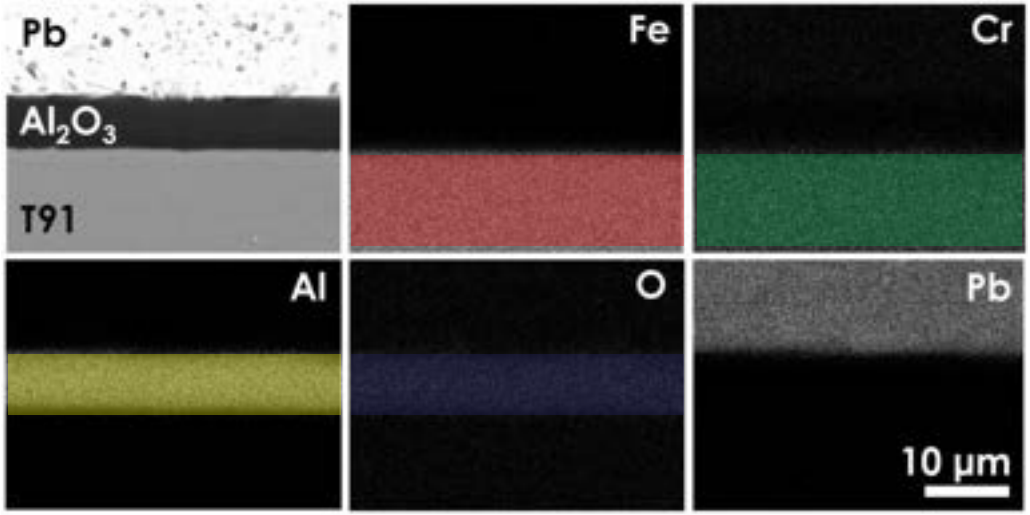




coated sample



protection



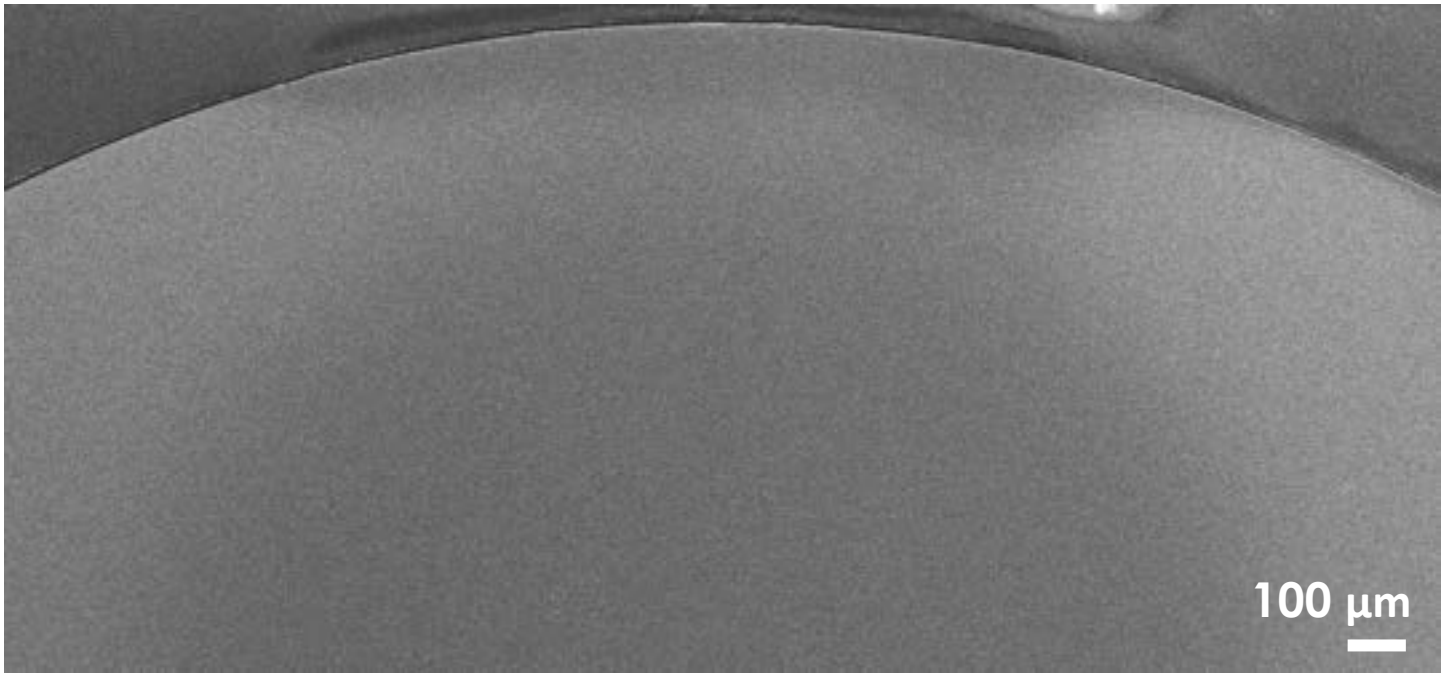
F. Garcia Ferré et al. – CORROS SCI – 2013

Corrosion resistance, O_2 depletion

1515Ti cylinder – 5000 h in stagnant Pb @550°C 10^{-8} wt.% oxygen

1 µm Al_2O_3 coating







before

No solidified lead on the 1515Ti cylinder

NO CORROSION

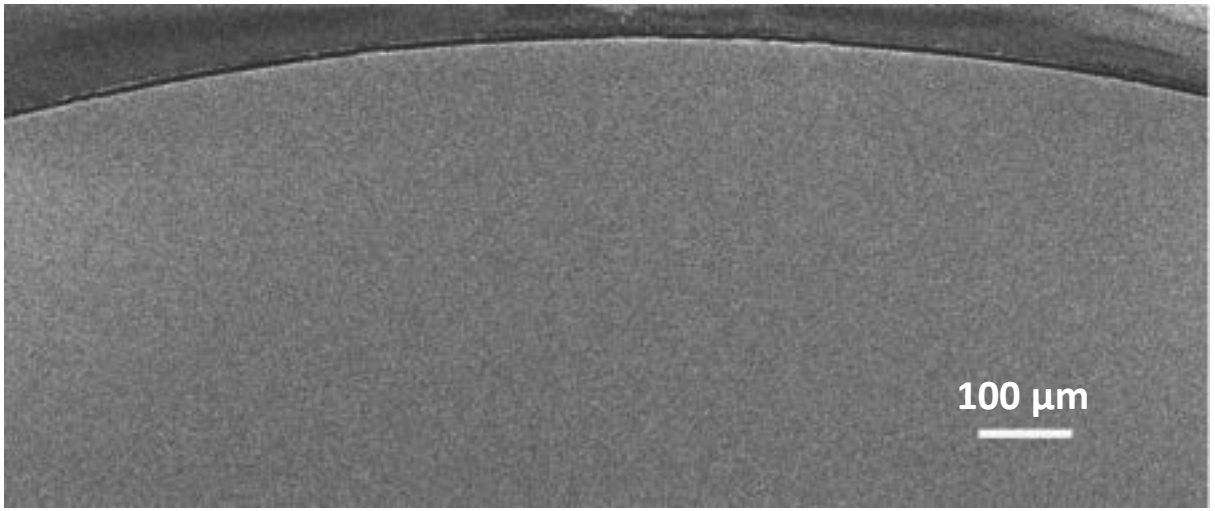
after

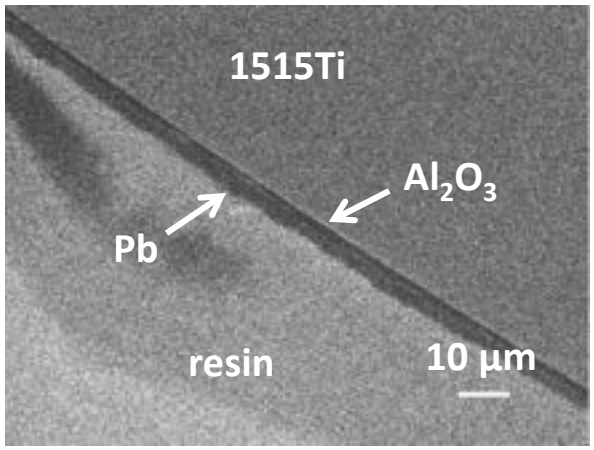
Corrosion resistance, O_2 depletion

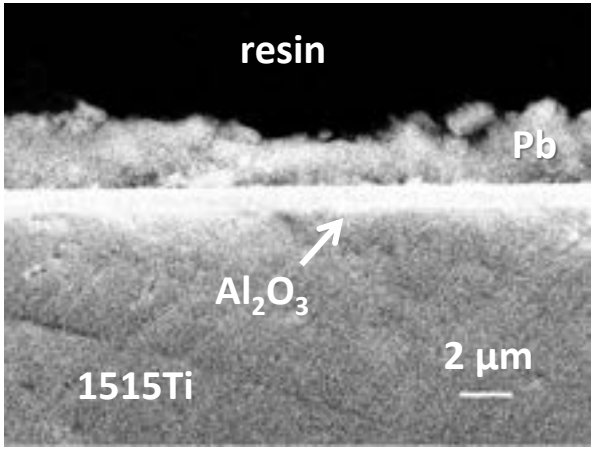
NO BL



BEFORE







NO BL



AFTER

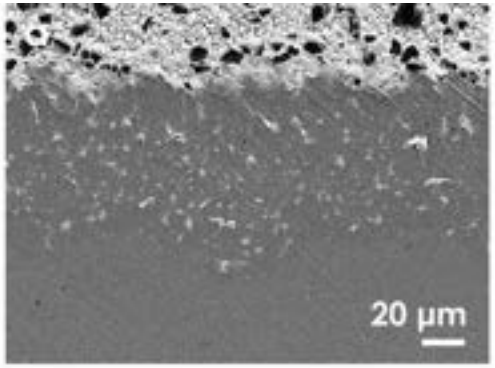
NO corrosion

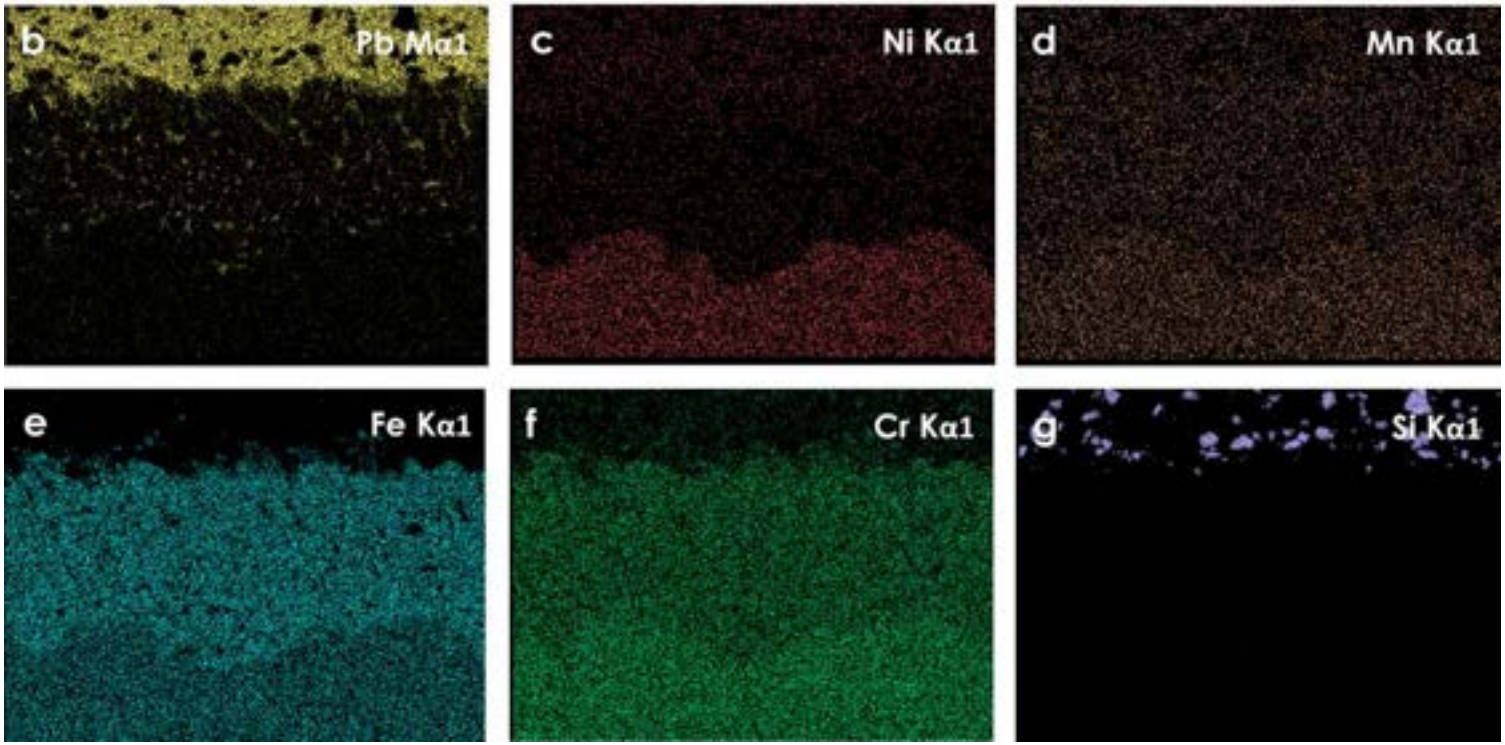
Corrosion resistance, O_2 depletion

Uncoated steel

5000 h in stagnant Pb

@550°C 10^{-8} wt.% oxygen



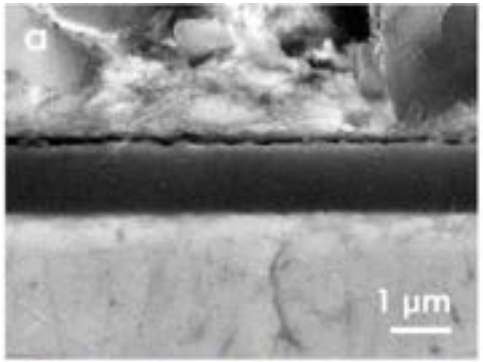


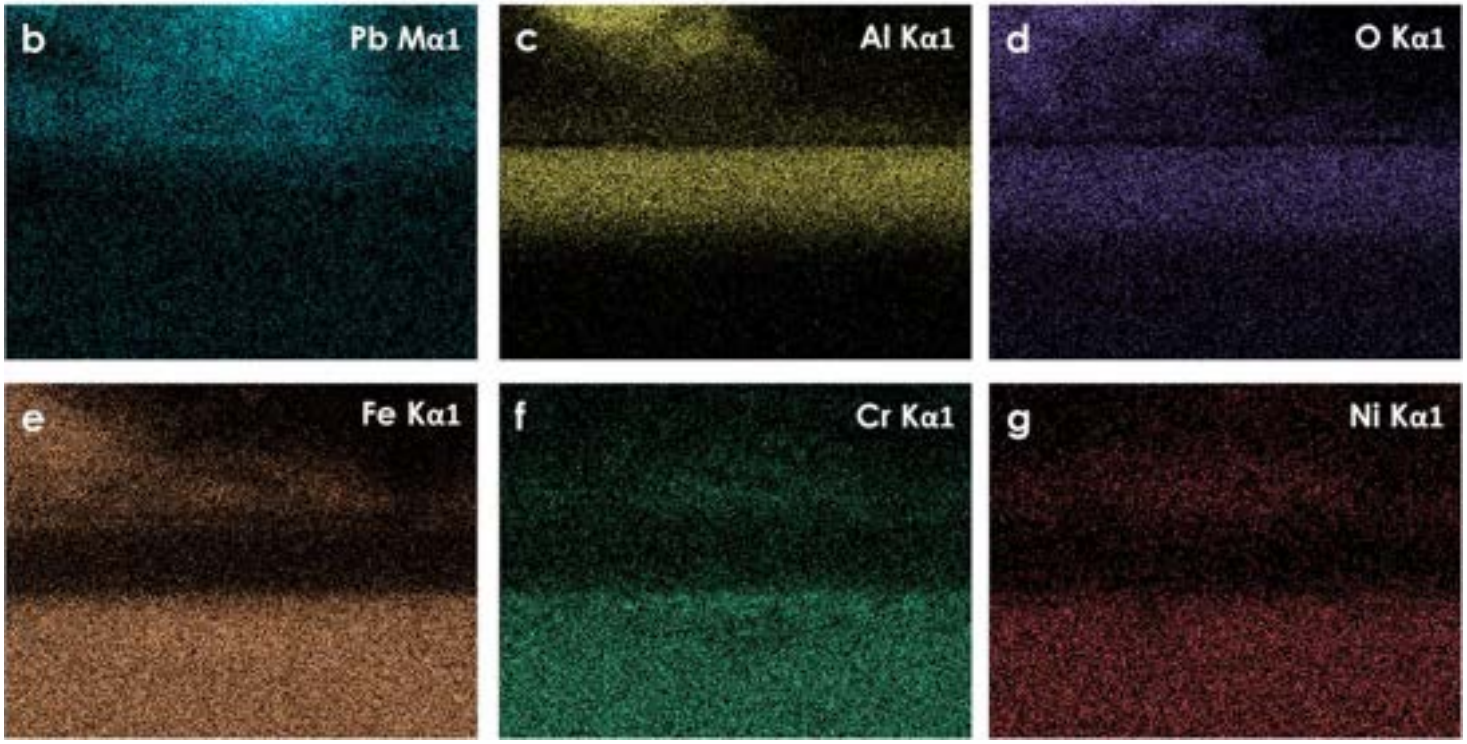
Corrosion resistance, O_2 depletion

Coated steel

5000 h in stagnant Pb

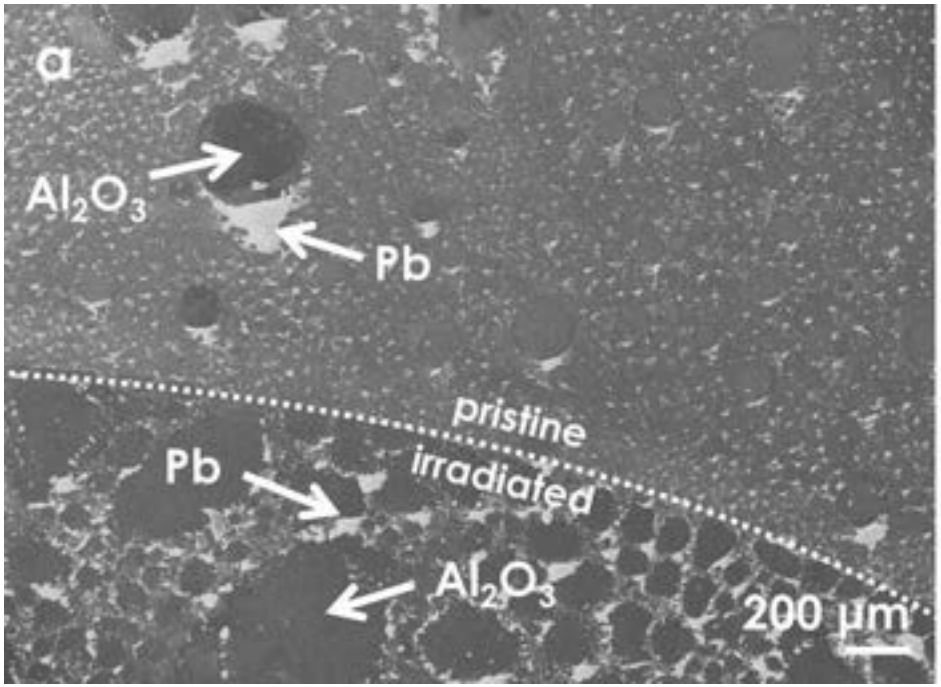
@550°C 10^{-8} wt.% oxygen

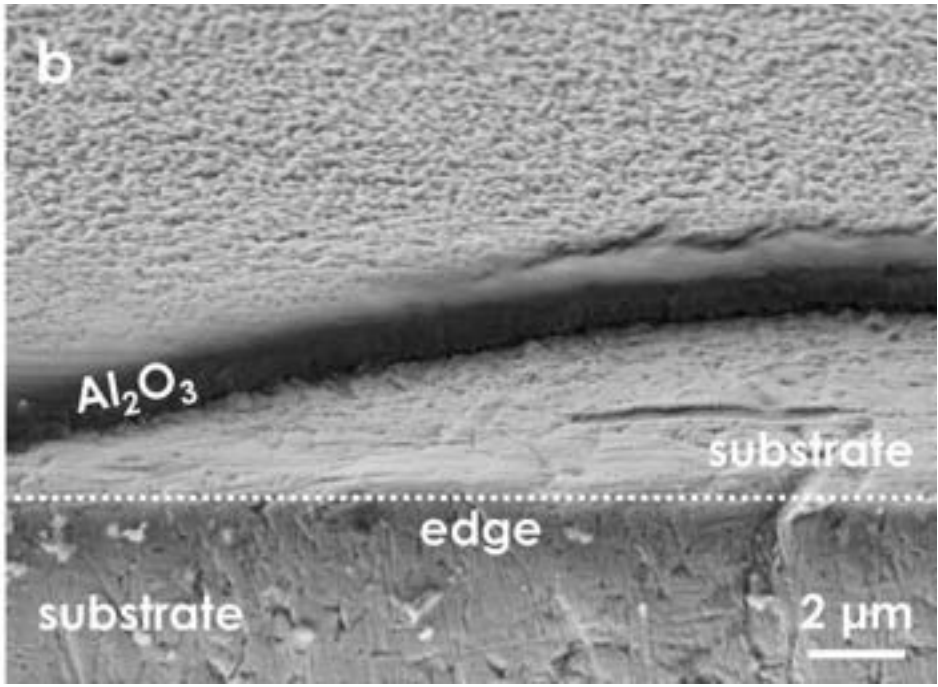




Corrosion resistance, O2 depletion

Irradiated sample, 1000 h in stagnant Pb @550°C 10^{-8} wt.% oxygen





Thank You
for your attention!

fabio.difonzo@iit.it

WORKSHOP TEMATICO

ACCORDO DI PROGRAMMA MISE – ENEA
PAR2016 – PROGETTO B.3.1. LP2

GENERATION IV
LEAD COOLED FAST REACTOR
STATO ATTUALE DELLA TECNOLOGIA E PROSPETTIVE DI SVILUPPO

ADP MiSE-ENEA (PAR2016-LP2)

Aula Magna
Scuola di Ingegneria e Architettura, Università di Bologna
26-27 settembre, 2017

Caratterizzazione microstrutturale e meccanica di ricoprimenti prodotti mediante tecnica di ablazione Laser



M. Bragaglia, F.R. Lamastra, F. Franceschetti; F. Nanni; G. Forasassi

CONTATTI:
Dipartimento di Ingegneria Impresa
Università di Roma "Tor Vergata"
Via del Politecnico, 1, 00133 Roma -Italia
Tel +39-06.7259.4496 - Fax +39-06.7259.4328

Indice dei contenuti

Caratterizzazione microstrutturale e compositiva

- Microscopia a scansione elettronica (SEM)
- Microscopia ottica (MO)
- Microanalisi EDS
- Diffrattometria dei raggi X (XRD)

Caratterizzazione meccanica

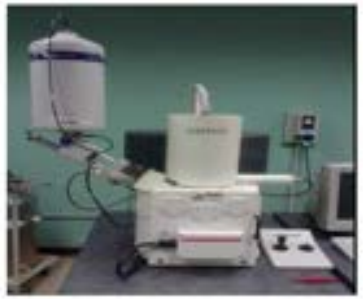
- Test di microdurezza Vickers
- Test di nanoindentazione
- Scratch test
- Prove di flessione
- Prove di usura ball crater

La valutazione delle proprietà meccaniche dei materiali è necessaria ogni qualvolta risulti necessario stabilire se una **struttura è in grado o meno di resistere alle combinazioni delle azioni di progetto** oppure con il fine di **determinare l'entità massima delle azioni, considerate nelle combinazioni di progetto previste, che la struttura è capace di sostenere con i margini di sicurezza richiesti.**

Caratterizzazioni Microstrutturali



MO



SEM/EDS



XRD

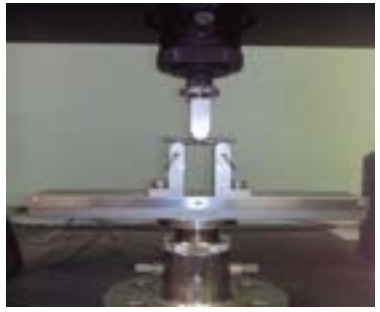
Caratterizzazioni Meccaniche



Prova di microdurezza
UNI EN ISO 6507-1:2005



Prova di nanoindentazione
UNI EN 14577/1-2



Prova di flessione a tre punti
ASTM-C1161



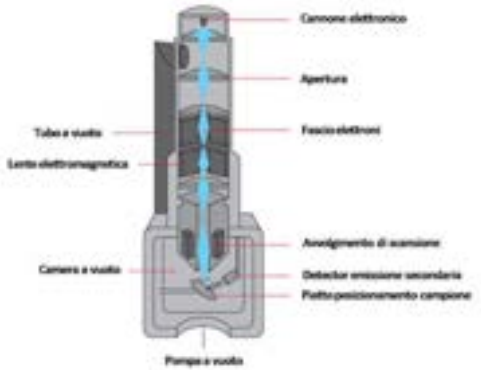
Scratch test
UNI EN 1071-3:2005

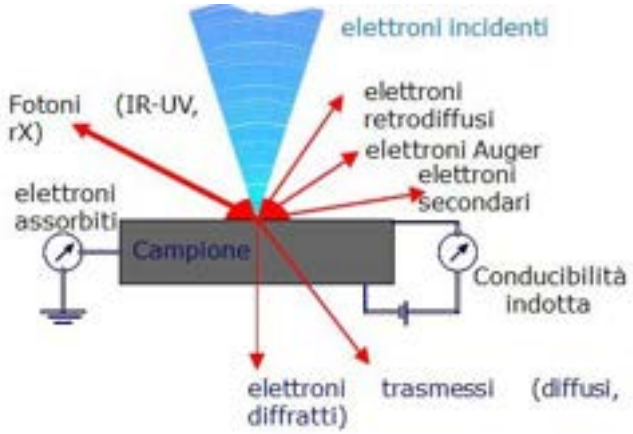


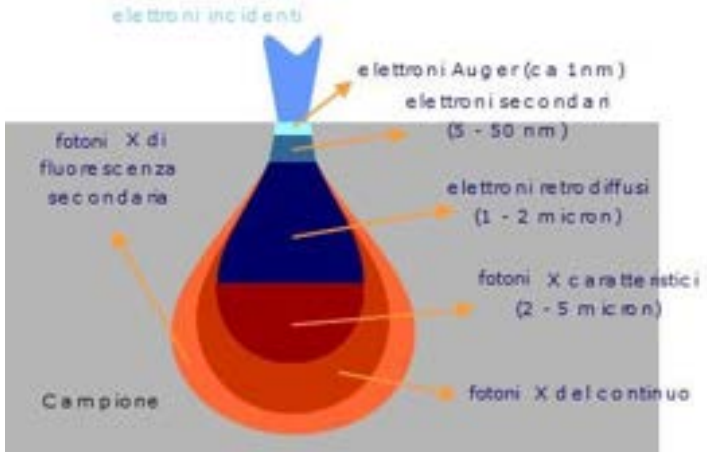
Ball Crater Test
BS EN 1071-6: 2007

Microscopia elettronica a scansione (SEM)

Il microscopio elettronico a scansione (SEM) sfrutta la generazione di un fascio elettronico ad alta energia focalizzato e deflesso da un sistema di lenti nel vuoto per scansionare un'area del campione.
L'interazione fascio-campione genera elettroni secondari e retrodiffusi. Questi sono raccolti da opportuni detectors e convertiti in segnali elettrici. Tali segnali vengono amplificati ed elaborati da un computer fino a formare un'immagine a livelli di grigio.



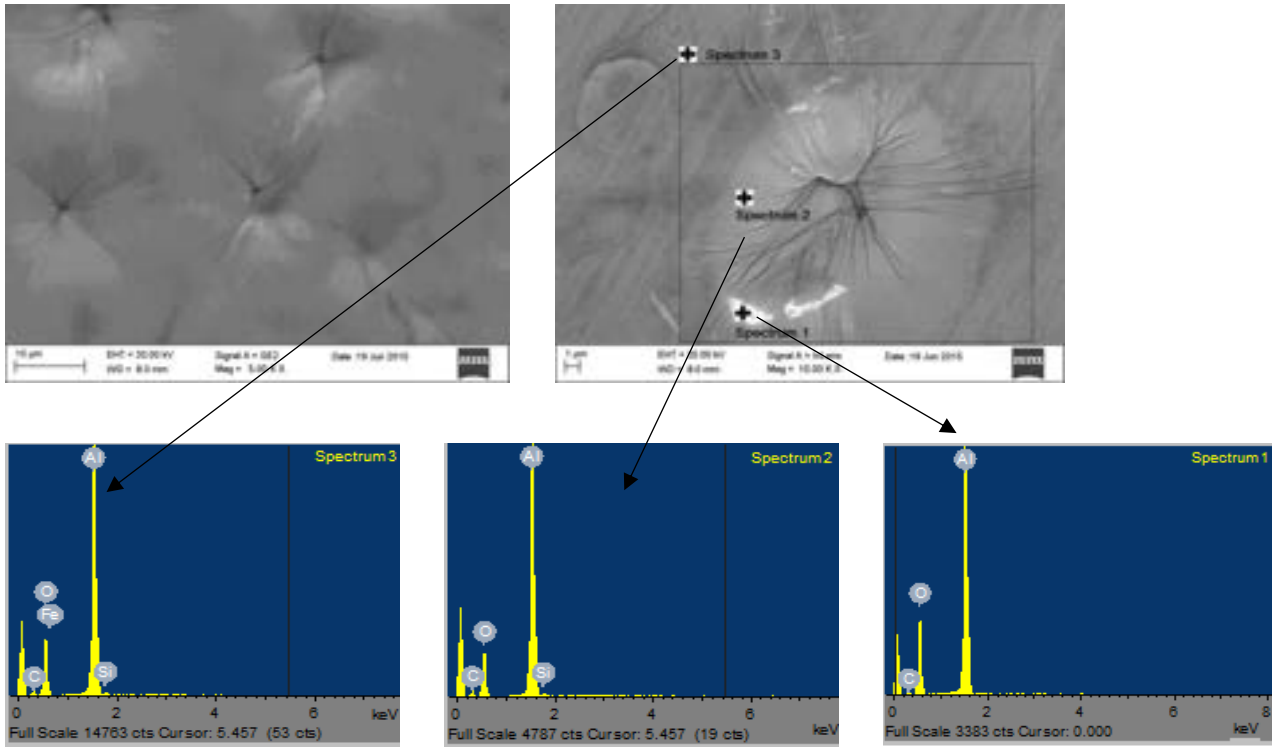




Permette:

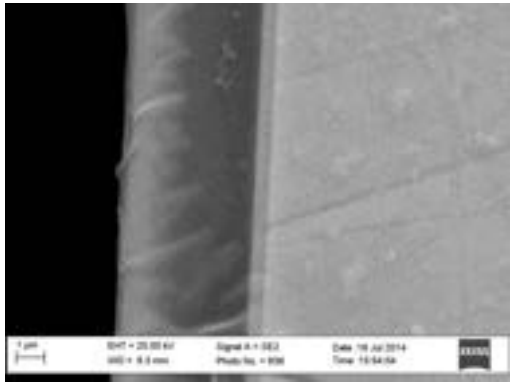
- Analisi morfologica della superficie del campione
- Analisi delle sezioni dei provini (compattezza film dimensioni)
- Analisi Elementare EDS (**Energy Dispersive Spectroscopy)**

Microscopia elettronica a scansione



5 µm Al_2O_3/500 nm FeCrAlY/lamina 316 post-irraggiamento (110 MeV Ni^{2+}-16 dpa-550 °C)

• Modifiche morfologiche e composizionali del rivestimento nelle zone di impatto degli ioni



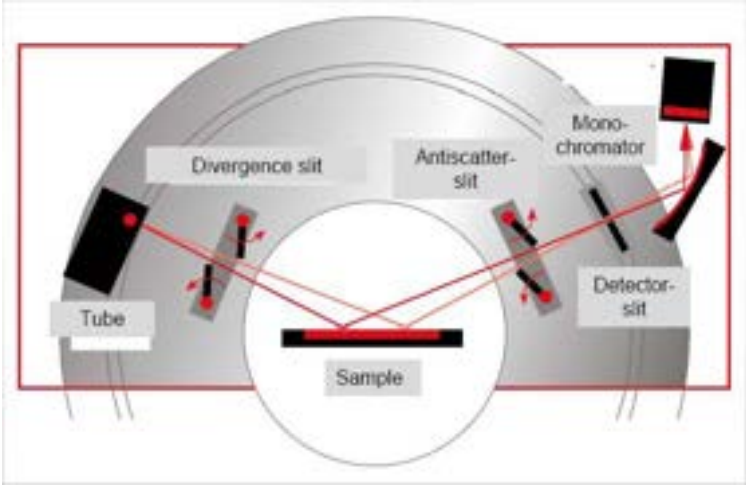
5 µm Al_2O_3/500 nm FeCrAlY/lamina 316 *as-deposited*

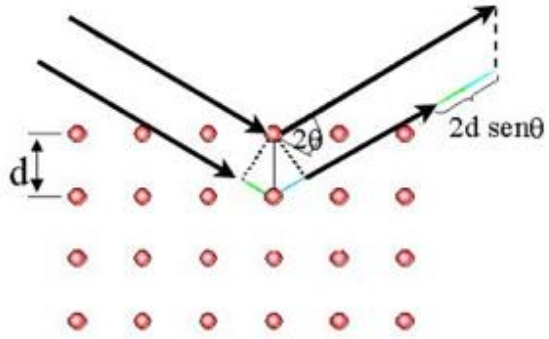
- Rivestimento compatto ed omogeneo buona adesione al substrato
- Presenza di bonding layer

Diffrazione raggi X

XRD: Processo di scattering elastico coerente dei raggi X da parte degli elettroni degli atomi disposti su piani paralleli ed equidistanti, che ha luogo quando vale la legge di Bragg.

Tecnica di analisi non distruttiva che misura gli effetti di interazione tra un fascio di raggi X e la materia cristallina.



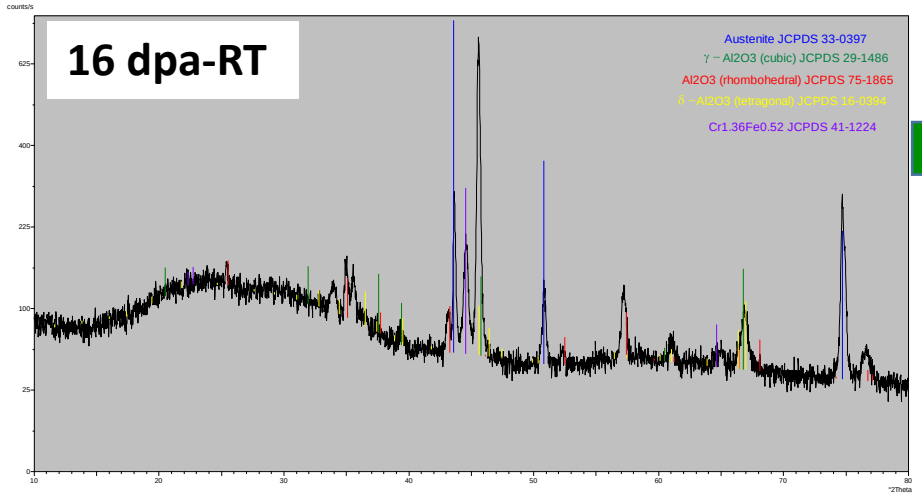


Legge di Bragg

nλ = 2d senθ

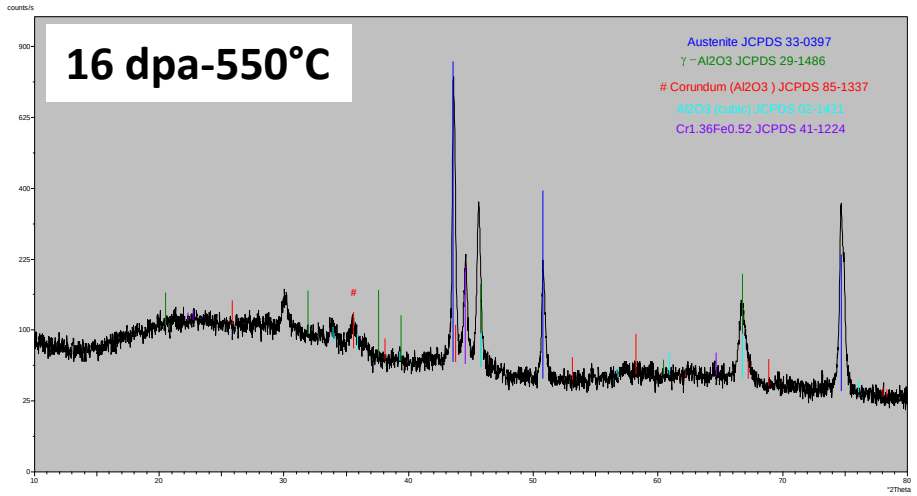
Variazioni delle fasi cristalline a seguito di processi termici o di irraggiamento

XRD



Fasi cristalline di allumina:

Al_2O_3 (romboedrica), - Al_2O_3 (cubica), δ- Al_2O_3(tetragonale)



Fasi cristalline di allumina:

Corindone (romboedrica), - Al_2O_3 (cubica), Al_2O_3 (cubica)

- Formazione di fasi cristalline di Al_2O_3 a seguito dell'irraggiamento ionico;
- Influenza della temperatura sulle fasi cristalline.

5 µm Al_2O_3/500 nm FeCrAlY/lamina 316 post-irraggiamento (110 MeV Ni^{2+}-16 dpa-RT e 550 °C)

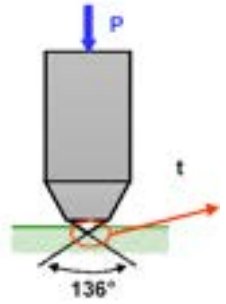
Microdurezza

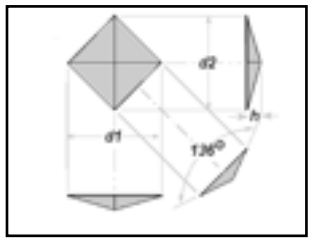
Durezza: resistenza di un materiale alla deformazione plastica localizzata.

Microdurezza Vickers: utilizzata per la caratterizzazione di materiali molto duri e tipicamente per il controllo dei trattamenti superficiali.

Modalità di prova: **ISO 6507-1:2005**

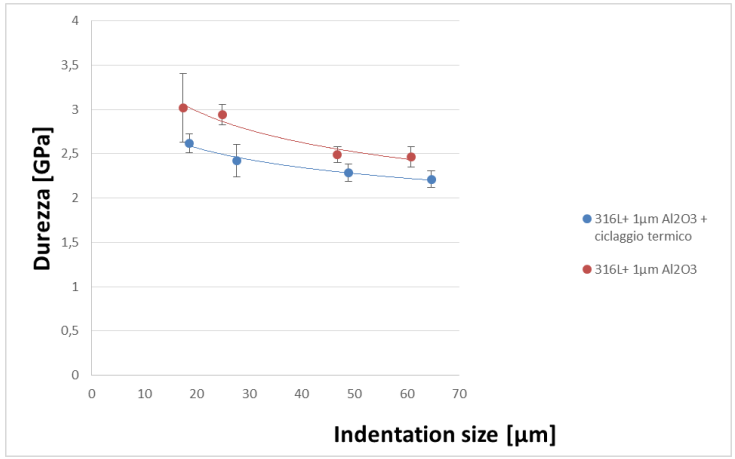
- ✓ Penetratore Vickers compresso ortogonalmente contro la superficie del provino applicando un determinato carico per un tempo stabilito (2000g – 10g).
- ✓ Rimozione dell'indentatore.
- ✓ Misura delle diagonali dell'impronta tramite microscopio ottico.
- ✓ Calcolo della durezza.

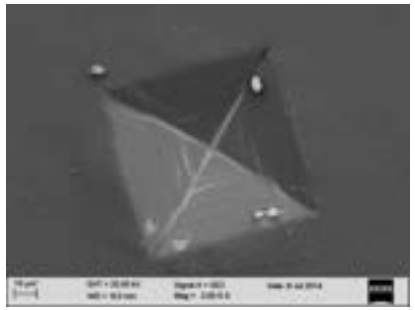




$$HV = \frac{P}{S} = 0.102 \frac{P \cdot sen(\frac{136°}{2})}{d^2}$$

Condizioni di prova:
- Indentatore Vickers
- Carichi: 2000 - 50 g
- Tempo: 30 s





Impronta Vickers Al2O3 su inox 1515-Ti (IIT)

Al_2O_3 PLD su tubi 316L: Influenza del ciclaggio termico (11 cicli in Ar tra 300 e 600°C) sulla microdurezza

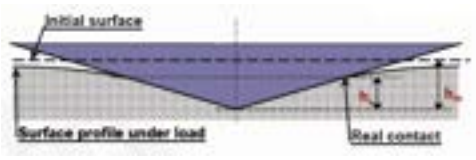
Dopo ciclaggio termico la microdurezza diminuisce di ≈ 0,3 GPa (Fenomeni di distensione del substrato)

Nanoindentazione

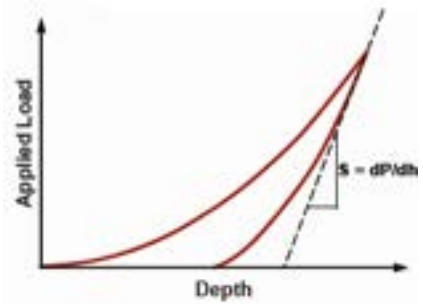
Funzionamento della prova: ***UNI EN 14577/1-2***
Lenta penetrazione di un indentatore piramidale Berkovich tramite l'applicazione controllata (e misura in controreazione) del carico normale ***P [mN]*** e la misura continua della penetrazione ***h***.
Si ottiene la curva ***P/h***
1 **Tratto di carico** (loading): si hanno deformazioni di tipo elasto-plastico, il cui ammontare relativo varia al variare del carico massimo applicato;
2 **Tratto di scarico** (unloading): si ha il recupero elastico del materiale a seguito della rimozione controllata dell'indentatore.

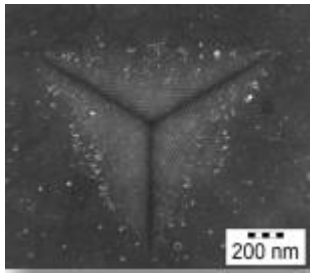
Estrapolazione delle proprietà meccaniche del rivestimento superficiale indipendentemente dalle proprietà del substrato (senza la sua influenza)
Modulo elastico del rivestimento E
Durezza del rivestimento

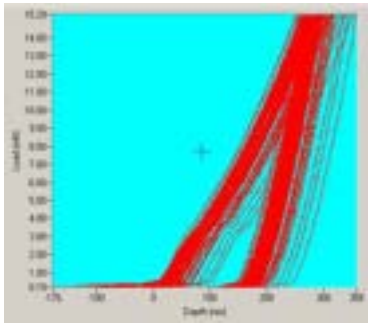
$$\frac{1}{E_r} = \frac{1-\nu_i^2}{E_i} + \frac{1-\nu_f^2}{E_f} \qquad E_r = \frac{\sqrt{\pi}}{2\beta}\frac{S}{\sqrt{A_p}} \qquad H = \frac{P_{max}}{A}$$









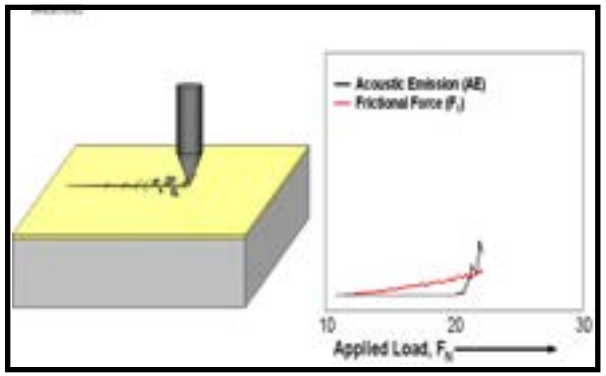


Campione	H (Al_2O_3) GPa	E (Al_2O_3) GPa
As-deposited	12.2±1.6	165
Irraggiato 150 dpa	12.7±3	152

L'irraggiamento non influenza in modo significativo durezza e modulo elastico del rivestimento di Al_2O_3

Scratch Test

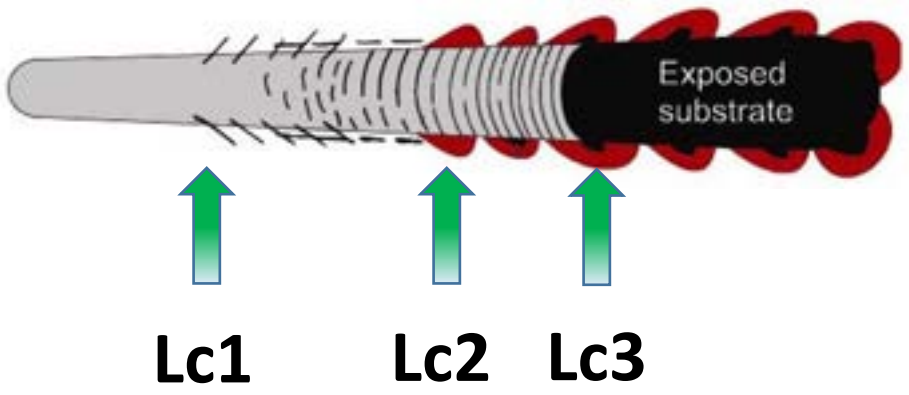
Consiste nel generare delle incisioni (scratch), su provini rivestiti, mediante l'utilizzo di un indentatore con profilo "Rockwell C" di diamante in moto relativo rispetto al provino sotto l'azione di un carico normale crescente.



Si definisce carico critico **Lc** (critical load) il carico per cui si manifesta per la prima volta uno specifico, ben riconoscibile e ben definito cedimento

Si definiscono tre carichi critici:

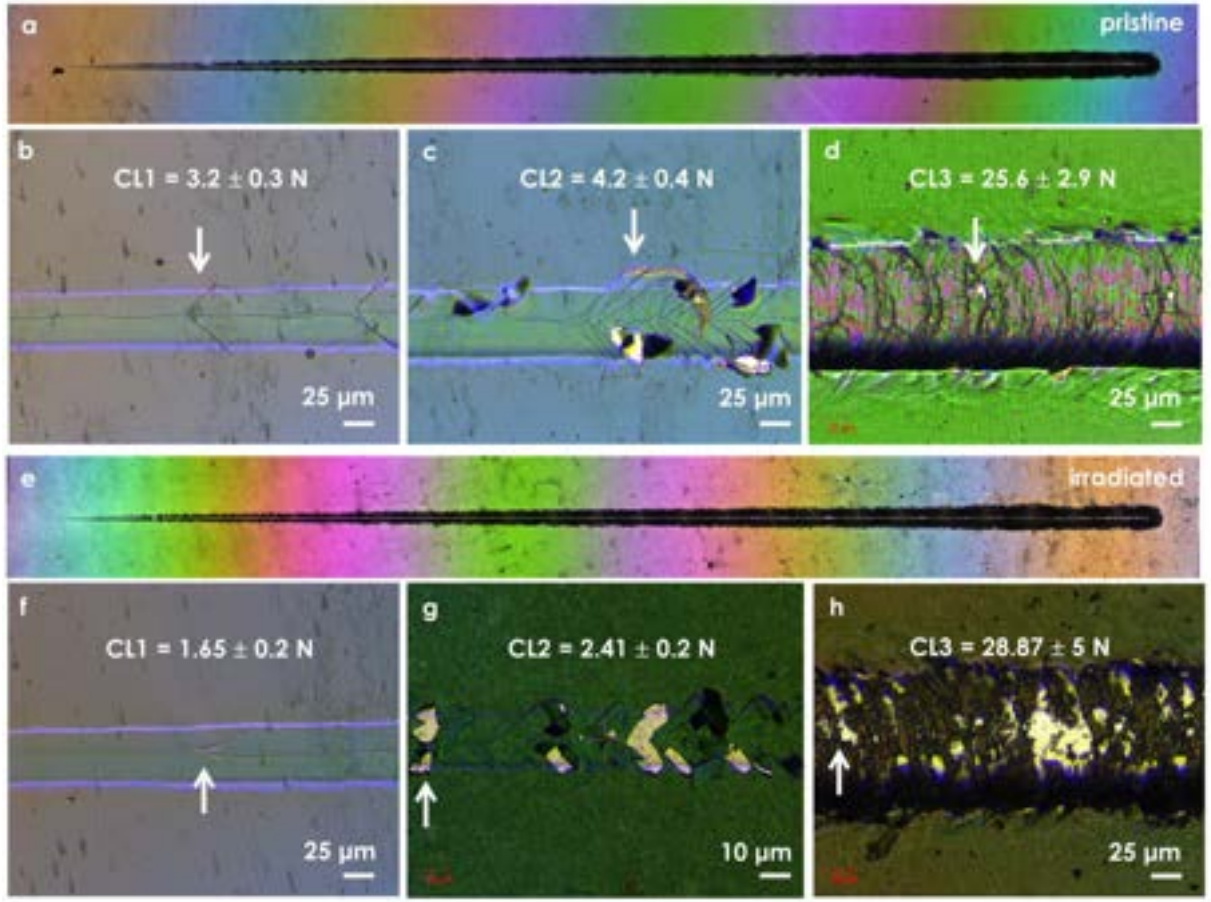
L_{c1}:primo cedimento coesivo all'interno del film, contraddistinto dalle prime cricche osservabili.
L_{c2}:primo cedimento adesivo,caratterizzato dal distacco del film con parziale esposizione del substrato.
L_{c3} :esposizione continua del substrato.



Parametri di prova:
-indentatore con profilo "Rockwell C" di diamante con raggio pari a 200 µm;
-lunghezza traccia 10 mm;
-carico progressivo da 0.03 N iniziali fino a 30 N finali;
-velocita relativa tra punta e provino 10 mm/min.

I carichi critici (Lc) dipendono dai parametri di prova e non vanno considerati in modo assoluto ma come valori comparativi dei diversi provini.

Scratch Test



CL1 and CL2 inferiori per campioni irraggiati, CL3 risulta maggiore.

< risistenza a rottura

> Tenacità a frattura del campione irradiato

Flessione a tre punti

Prove di flessione a tre punti (ASTM-C1161)



- Distanza coltelli 30 mm;
- Velocità di applicazione del carico 0,05 mm/min;
- Corsa 2 mm

Su tubi 316L rivestiti in Al_2O_3:

- spessori del film di Al_2O_3 1 e 5 µm;
-con o senza buffer layer in FeCrSi;
-*as deposited*
-dopo ciclaggio termico in Ar
(11 cicli tra 300 e 600°C)

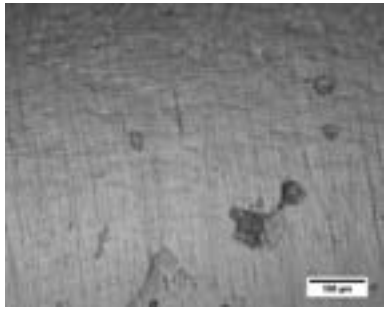
Caratterizzazione al microscopio ottico per osservare eventuale insorgenza di criccature o delaminazioni.



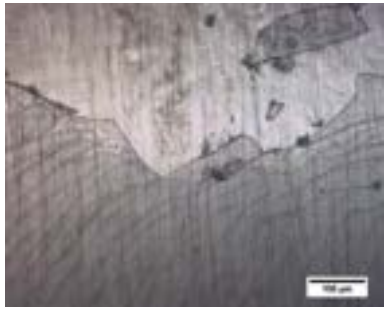
Influenza dello spessore, del *buffer layer* e del ciclaggio termico sull'adesione del rivestimento di Al_2O_3 al substrato

Flessione a tre punti

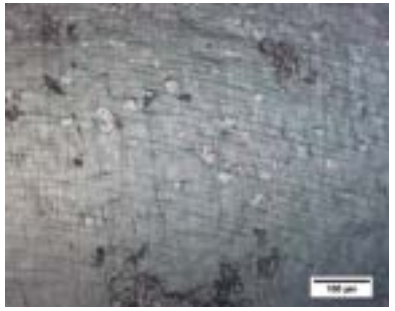
Influenza dello spessore, del *buffer layer* e del ciclaggio termico sull'adesione del rivestimento di Al_2O_3 al substrato



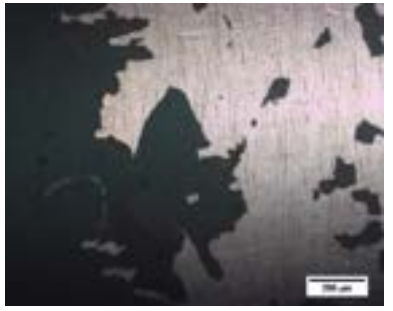
1 µm Al_2O_3/tubo 316L



5 µm Al_2O_3/tubo 316L



1 µm Al_2O_3/tubo 316L dopo ciclaggio termico



1 µm Al_2O_3/200 nm FeCrSi/tubo 316L dopo ciclaggio termico

- Cricche presenti in entrambi i provini in direzione parallela all'asse del tubo;
- Il provino con 5 µm Al_2O_3 mostra vaste zone di delaminazione.
- Cricche presenti in entrambi i provini in direzione parallela all'asse del tubo;
- Zone di delaminazione presenti nel campione ciclato termicamente.
- Nel campione con il *buffer layer* il rivestimento risulta in gran parte delaminato

La presenza del buffer layer influenza negativamente l'adesione del rivestimento al substrato

Prova di usura

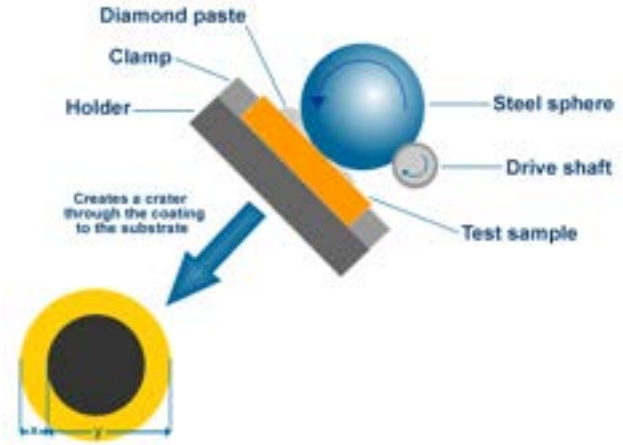
Consente di valutare il coefficiente di usura di un provino rivestito superficialmente e lo spessore del rivestimento.

Generazione di una depressione sferica detta cratere sul provino rivestito ponendo in rotazione una sfera, che preme sul provino, in presenza di un fluido abrasivo che viene fatto gocciolare nell'interfaccia tra provino e sfera. (Norma BS EN 1071-6: 2007)

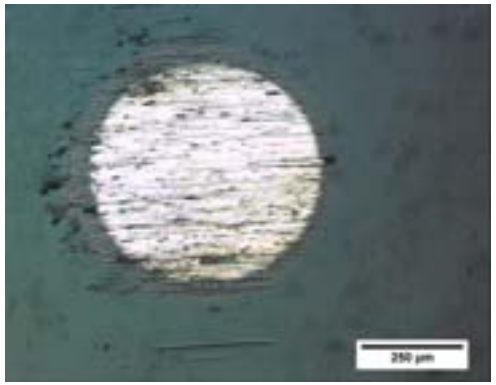
Misura dei diametri delle calotte sferiche generate tramite microscopia ottica.

Calcolo del Kf applicando le relazioni di Archard

$$Vs/Ks + Vf/Kf = s * Fn$$



Condizioni di prova:
- Fn agente sul provino: 0,2 N
- Granulometria dello slurry: d<5µm
- Diametro sfera: 2,5 cm



Conclusioni

Attraverso analisi microstrutturali e meccaniche è possibile ottenere le seguenti caratteristiche dei rivestimenti che ne vanno a influenzare le prestazioni in servizio

- Spessore Uniformità omogeneità e compattezza del rivestimento
- Influenza di trattamenti termici, di irraggiamento e corrosione in Pb fuso sulle fasi cristalline e sulla composizione
- Valutazione dell'adesione del rivestimento al substrato
- Proprietà meccaniche del rivestimento
- Reisistenza all' usura dei rivestimenti

Conclusioni per rivestimenti in allumina PLD

Rivestimenti PLD di Al_2O_3 su lamine 316

A seguito dell'irraggiamento:

- delaminazione parziale (RT) e modifiche morfologiche (550°C) del rivestimento; formazione di fasi cristalline dell'allumina;
- durezza e modulo elastico del rivestimento di Al_2O_3 non variano in modo significativo; peggiora leggermente l'adesione del film di Al_2O_3.

Rivestimenti PLD di Al_2O_3 su tubi 316L:

- la durezza dei tubi rivestiti aumenta con lo spessore di Al_2O_3 e in presenza del *buffer layer* in FeCrSi; la durezza diminuisce dopo ciclaggio termico;
- l'adesione rivestimento-substrato è minore aumentando lo spessore del film di Al_2O_3; dopo ciclaggio termico; in presenza del *buffer layer* in FeCrSi.

Tesi e pubblicazioni

Alessandro Merli
"Caratterizzazione microstrutturale meccanica e tribologica di rivestimenti PLD in allumina su acciai inox per applicazioni nucleari"
Laurea in Ingegneria Meccanica

Fabrizio Mario Ferrarese
"Caratterizzazione di film ceramici sottili per applicazioni nei reattori nucleari di quarta generazione"
Laurea in Scienza dei Materiali

Emanuele Rossi
"Caratterizzazione di rivestimenti FeCrAlY HVOF per applicazioni nei reattori nucleari di quarta generazione"
Laurea in Ingegneria Meccanica

Mario Bragaglia
"Caratterizzazione di materiali strutturali ricoperti per applicazioni nucleari"
Dottorato di Ricerca in Ingegneria Industriale

Paper Corrosion Science 2017
Radiation tolerant nanoceramic coatings for lead fast reactor nuclear fuel cladding
F. García Ferré, A. Mairov, M. Vanazzi, S. Bassini, M. Utili, M. Tarantino, M. Bragaglia, F.R. Lamastra, F. Nanni, L. Ceseracciu, Y. Serruys, P. Trocellier, L. Beck, K. Sridharan, M.G. Beghi and F. Di Fonzo



M.G. Beghi – E. Besozzi

Thermomechanical characterization of coatings for nuclear energy applications

POLITECNICO
MILANO 1863

ADP MiSE-ENEA --- PAR2016-LP2 --- 27/09/2017

Thermomechanical properties of coatings

In service behaviour of coatings strongly depends on thermomechanical properties.

Stresses at the interface:

- Are among the main causes of delamination or cracking
- Depend on the mismatch of
  - stiffness (elastic moduli)
  - thermal expansion (Coefficient of Thermal Expansion, CTE)

Thermomechanical properties of coatings:

- Depend on the deposition process
- Can be different from the bulk properties
- Require specific measurement techniques

Measurement techniques

CTE of coatings
by Sample Curvature (SC) method
(optical implementation)

Elastic moduli of coatings
by Brillouin spectroscopy
(optical technique to measure velocity of
bulk and surface ultrasonic waves
of sub-micrometric wavelength (GHz ÷ 100 GHz range)
combined with indentation

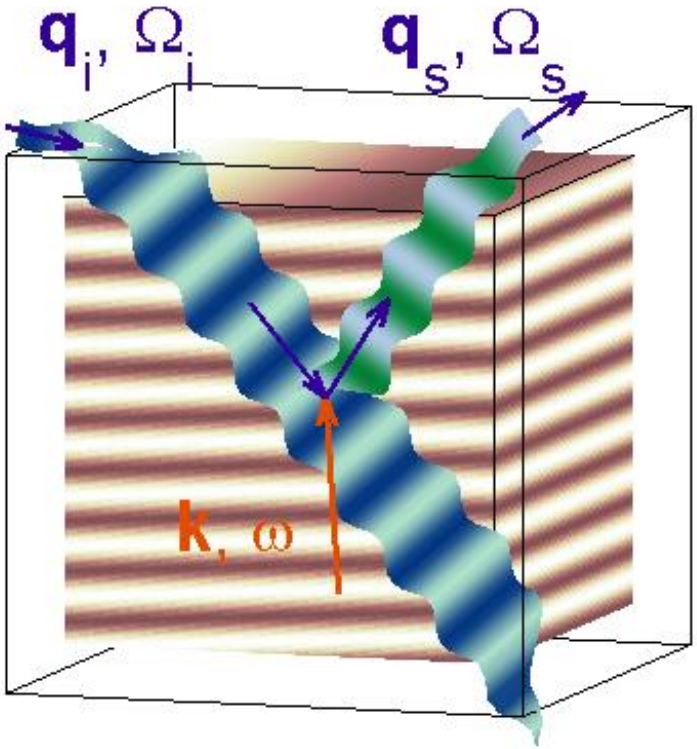
bulk longitudinal wave v_l $\sqrt{C_{11}/\rho}$

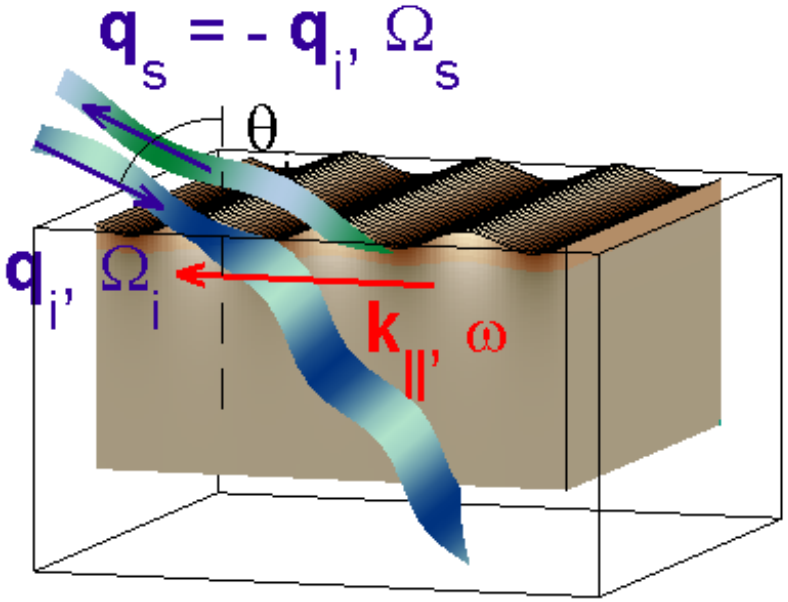
(isotropic media)

bulk transverse wave v_t $\sqrt{C_{44}/\rho}$

(surface) Rayleigh wave

v_R v_t v_l



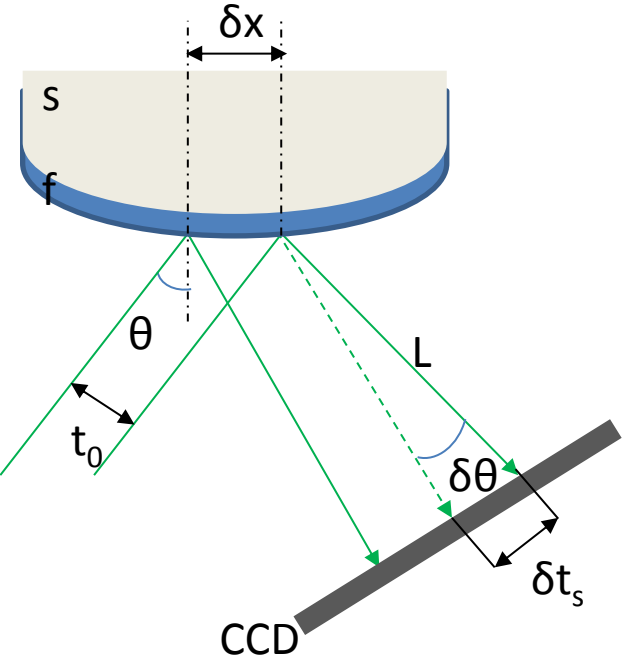


$q_s = q_i \pm k$

$q_{s\,||} = (q_i \pm k)_{||}$

$_s = \quad _i \pm$

Sample curvature: principles



Sample curvature evaluation

- **array of parallel laser beams** reflected by the coating / substrate surface and collected by a CCD
- **CTE mismatch** **bending upon heating**
- distance between laser beams $\mathbf{t_0}$ varied as $\boldsymbol{\delta t_s}$
- sample curvature obtained as

$$\frac{1}{R} = \left(\frac{\delta t_s}{t_0}\right)\frac{\cos\theta}{2L}$$

coating stress determined by **Stoney's eq.**

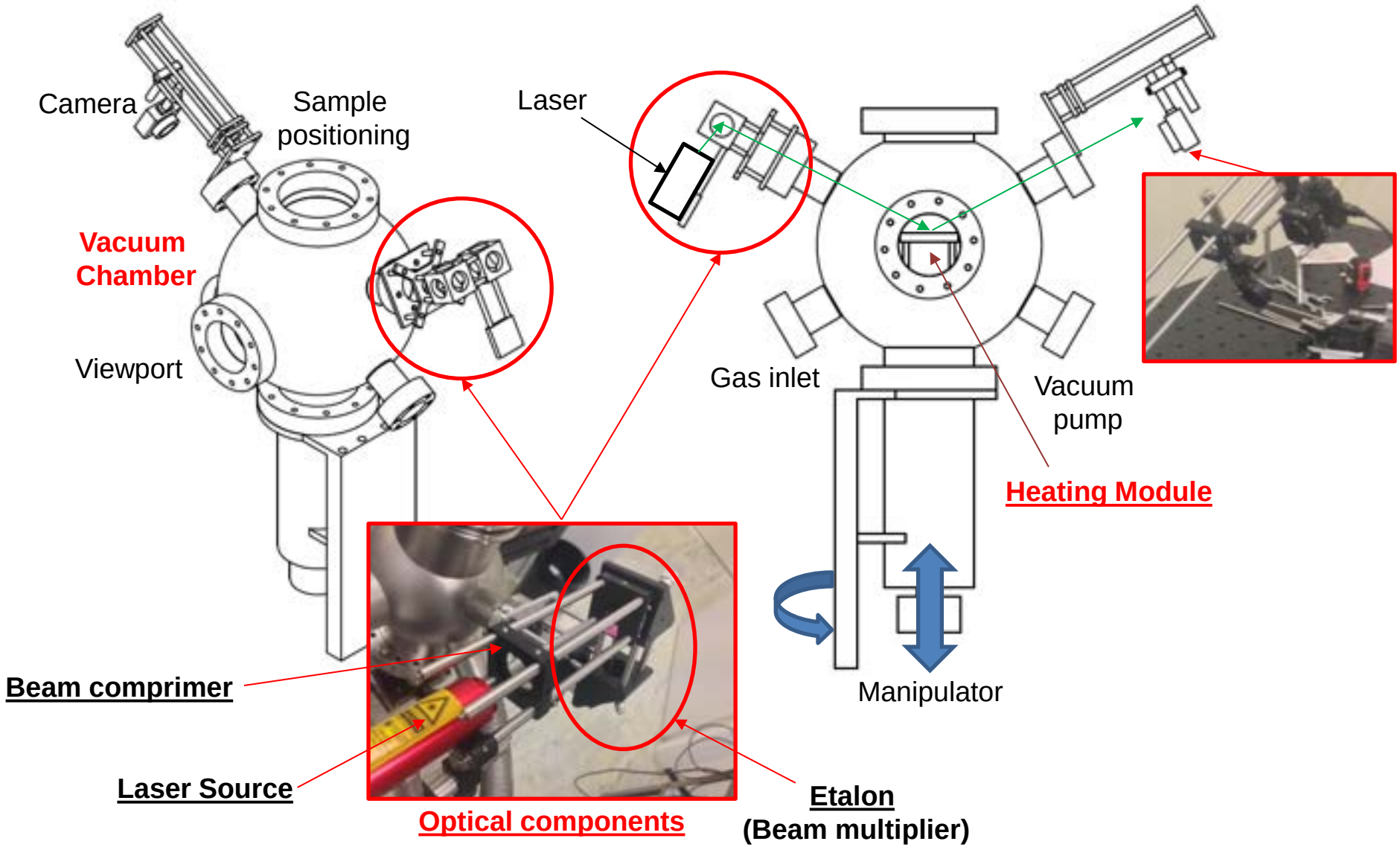
known substrate properties

$$\sigma_f = -\frac{E_s}{1-\nu_s}\frac{h_s^2}{h_f}\frac{1}{6R}$$

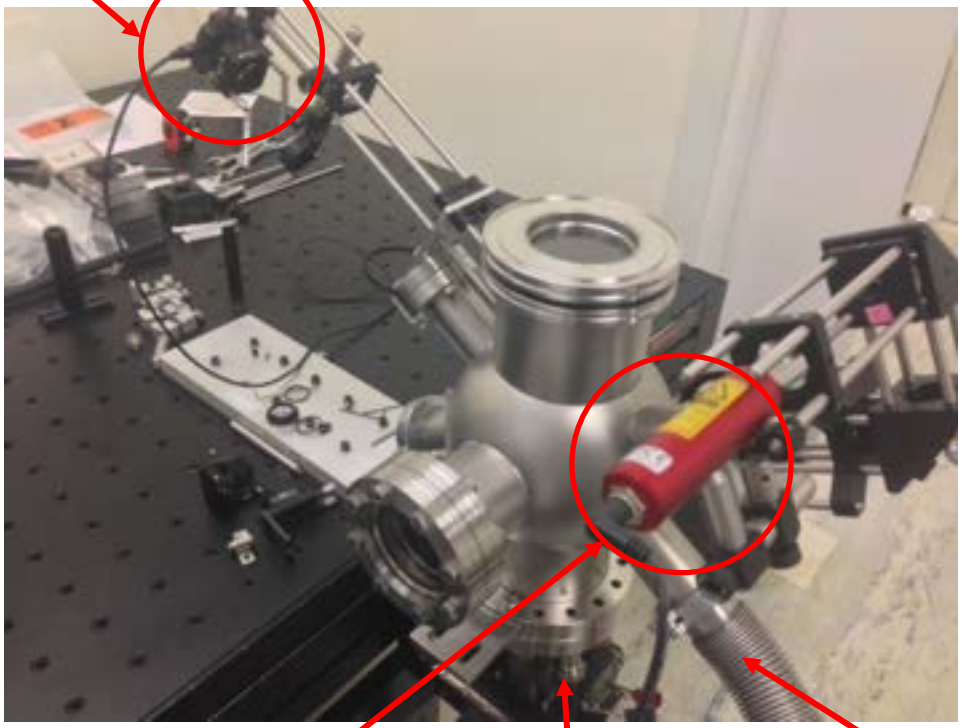
known thicknesses

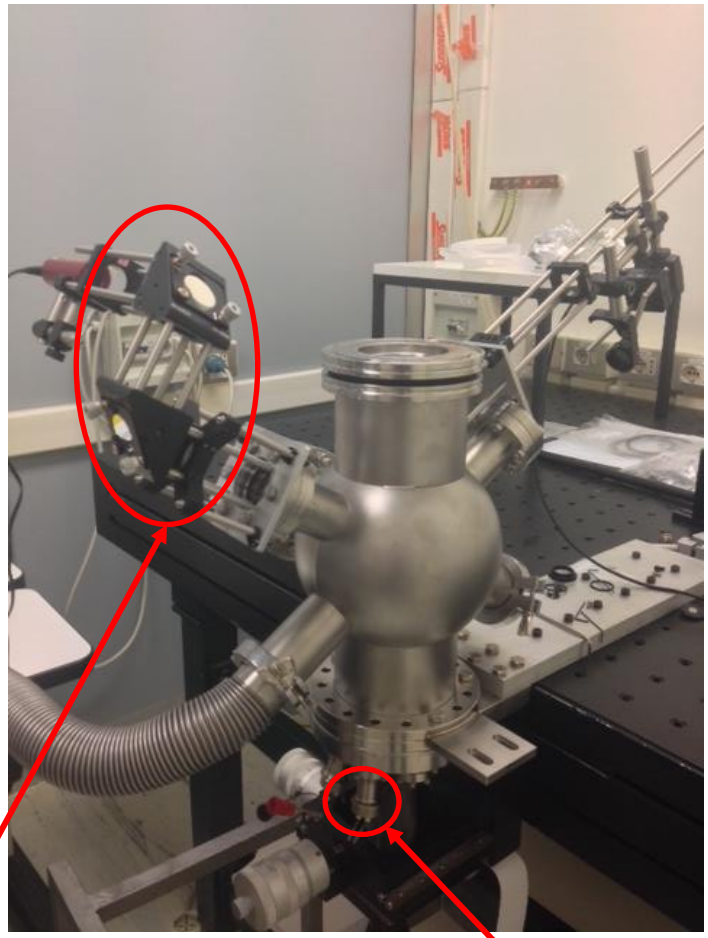
For **known elastic moduli** of the coating
the CTE can be derived

Sample curvature: experimental set-up



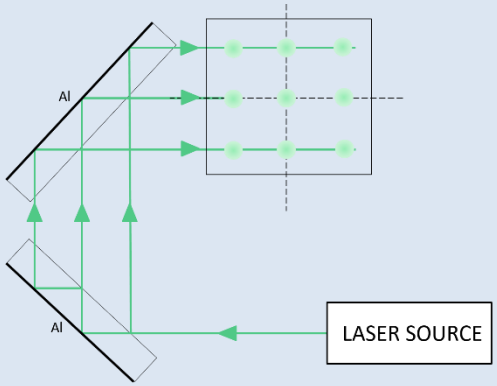
Sample curvature: experimental set-up





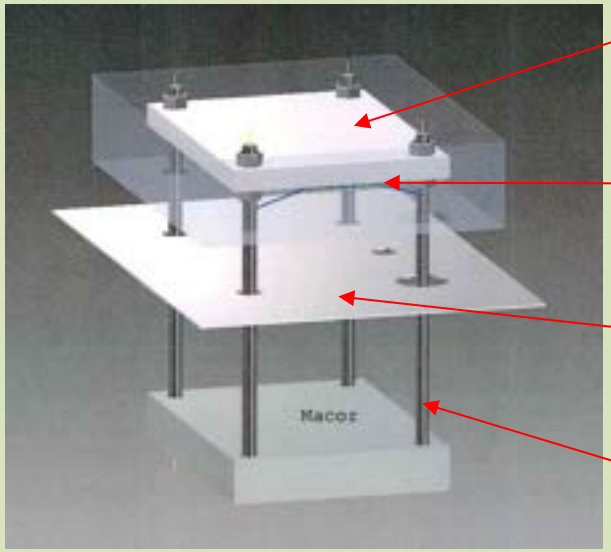
Sample curvature: experimental set-up

Beam multiplier



- Pair of **backside polished Al mirrors** 1”, 6 mm thick
- 2x2 / **3x3** laser beam array
- Total area ~ **1 cm²**
- Laser: **Nd:YAG, 1 – 5 mW**, 532 nm

Heating Module



Shapal holder

Tantalum wire

Molybdenum sheet

Molybdenum screws

Temperature up to 1200 °C

Vacuum (10^{-3} Pa) or controlled atmosphere (Ar, He) is necessary

- Avoid oxidation
- Suppress convection

Camera

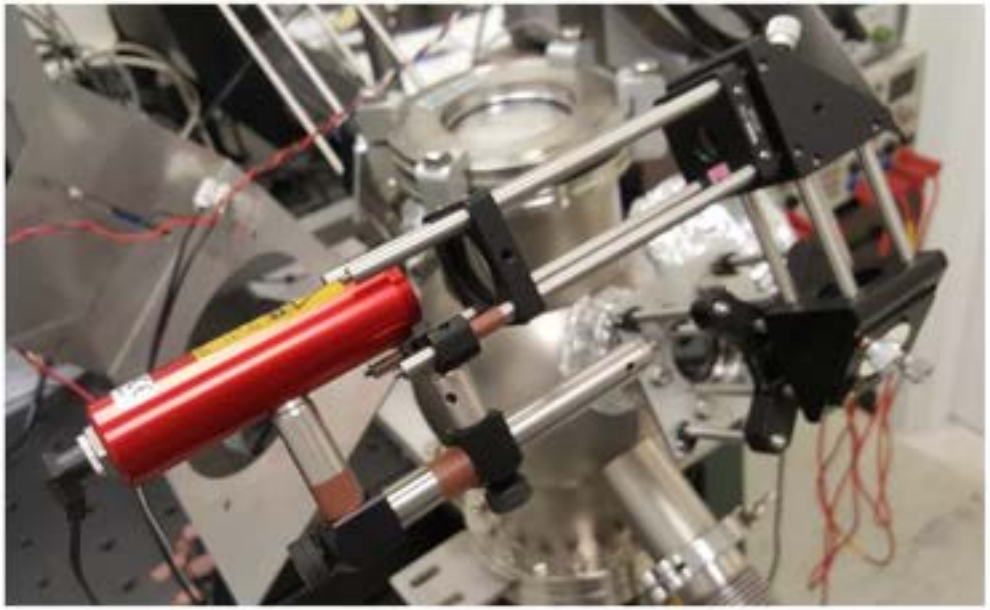


- 1280x1024, 1,4MPx
- Active area: **6.66 x 5.32** mm²

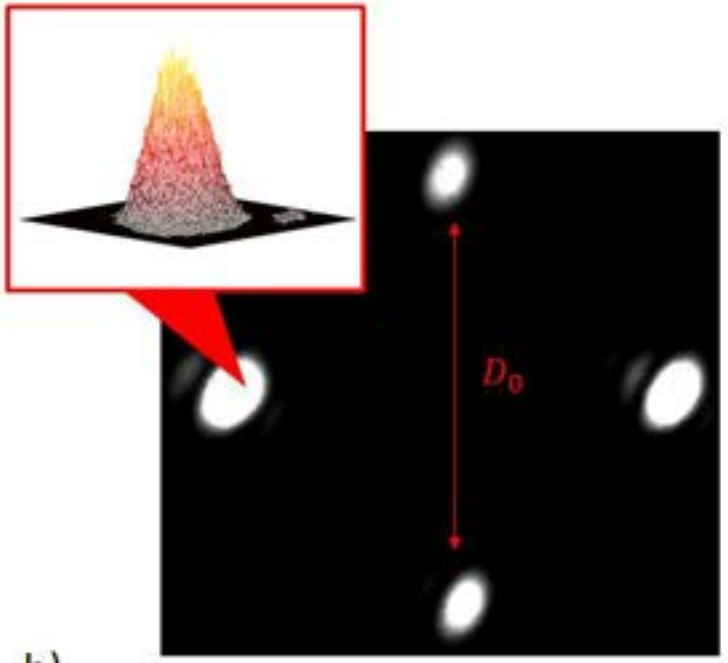
Need of reducing array size

- **25 fps up to 200 fps AOI**

Sample curvature: experimental set-up

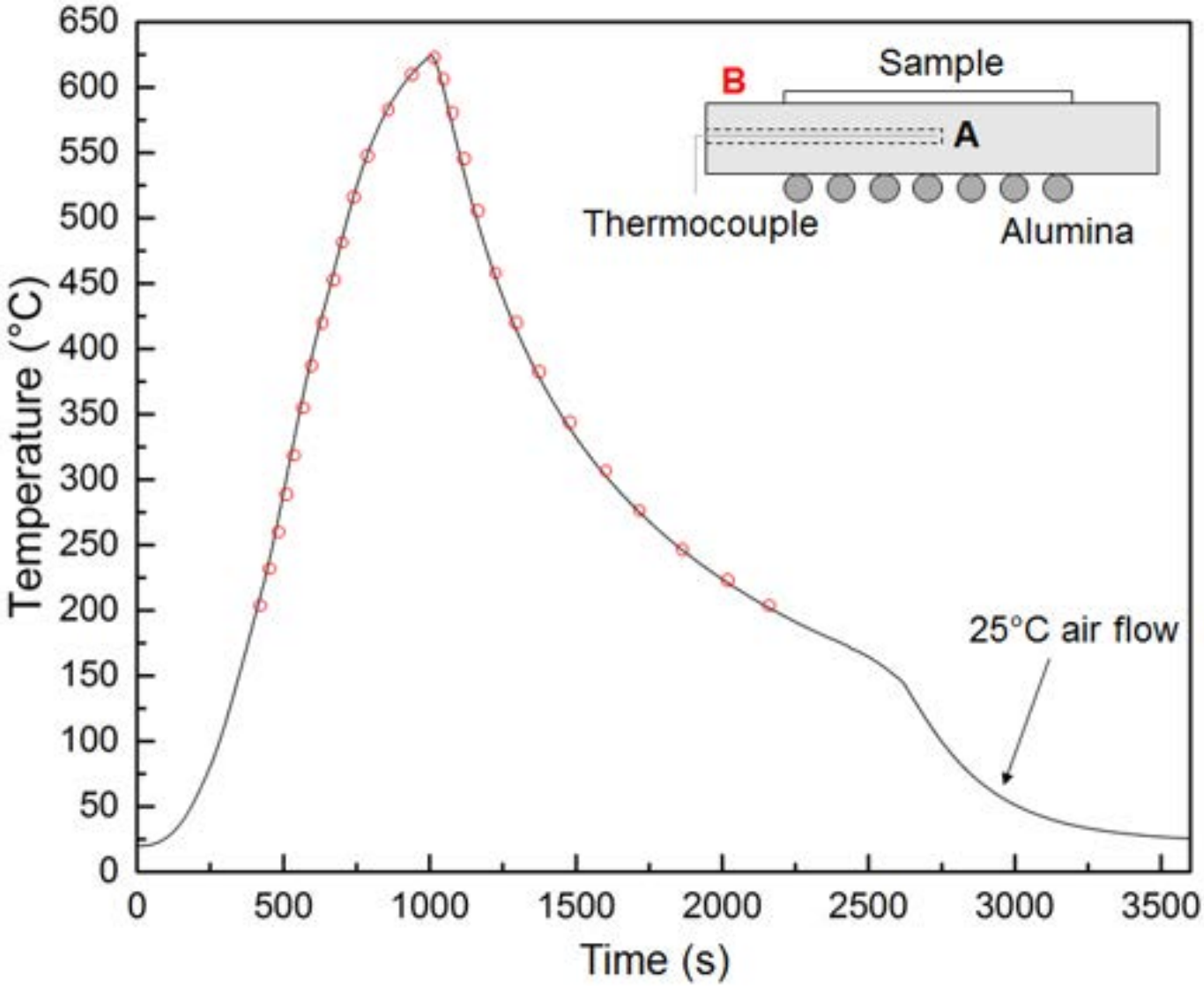


a)

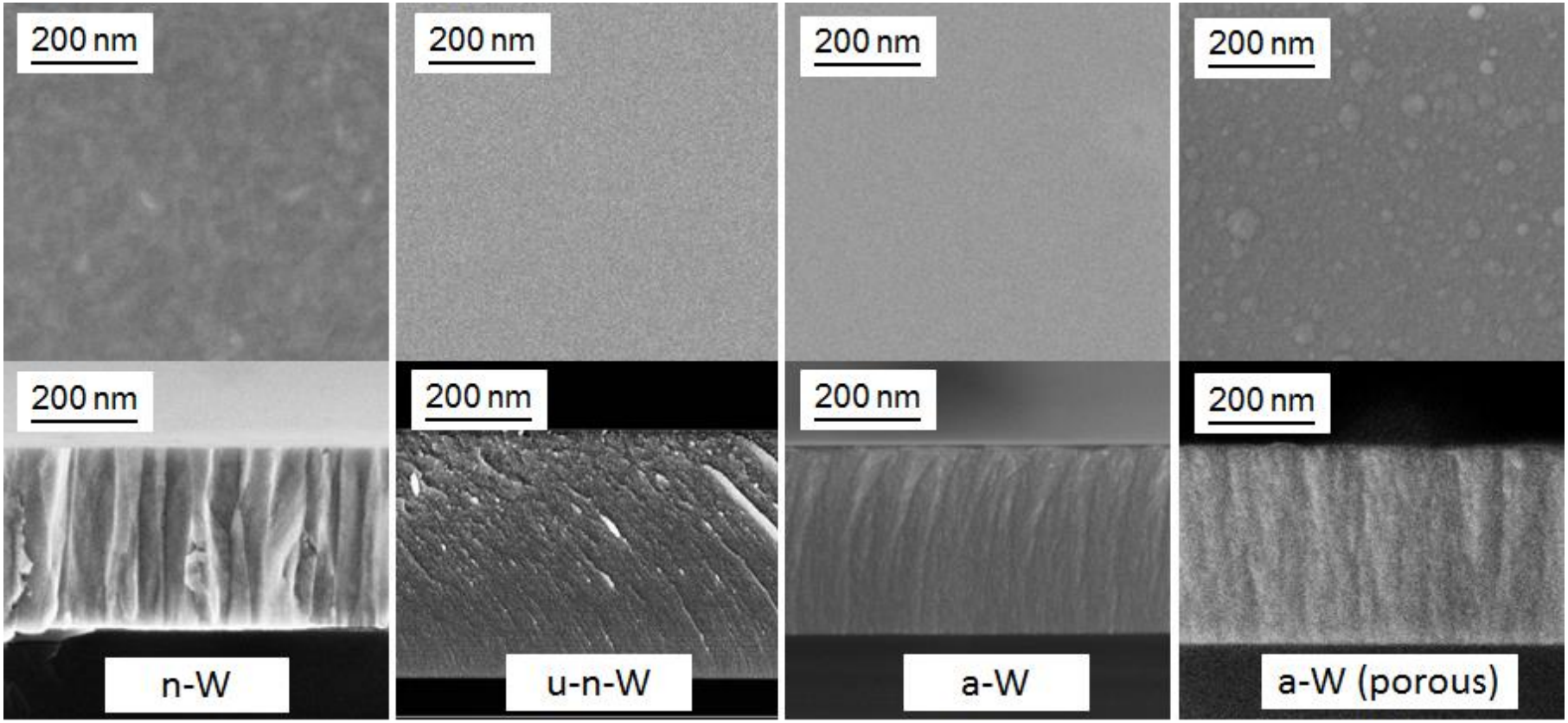


b)

Sample curvature: experimental set-up



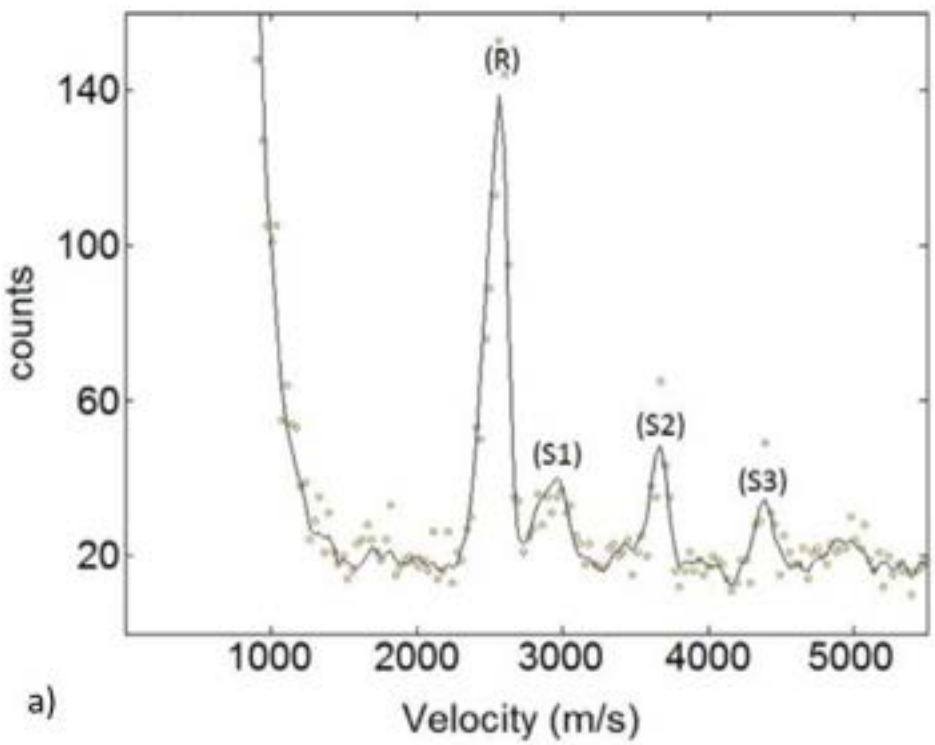
W-based films by Pulsed Laser Ablation (PLD)

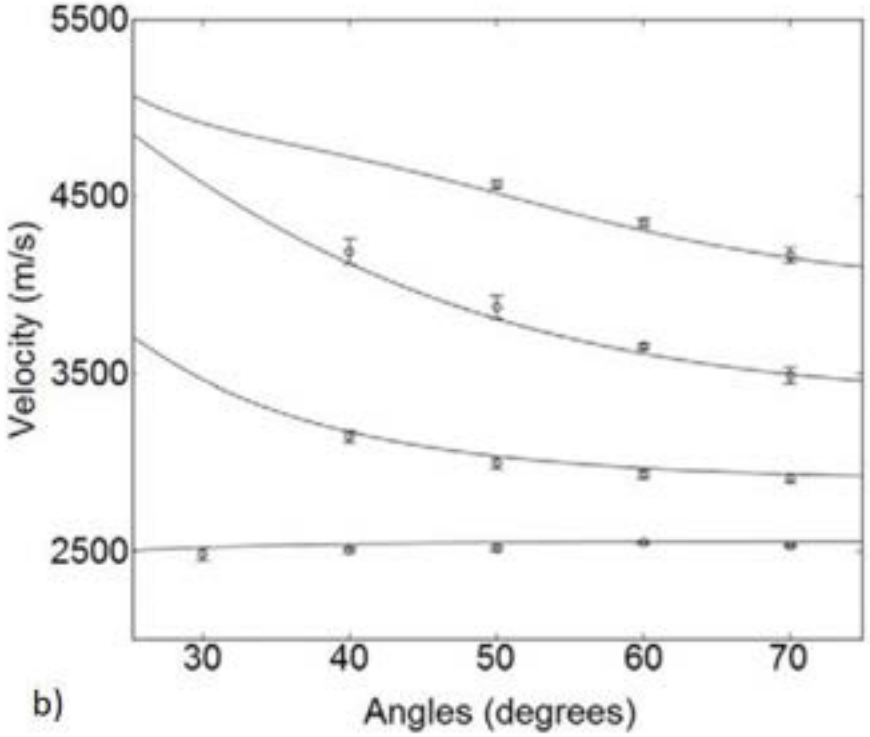


nanocrystalline (n-W)
ultra-nano-crystalline (u-n-W)
amorphous (a-W) (porous)

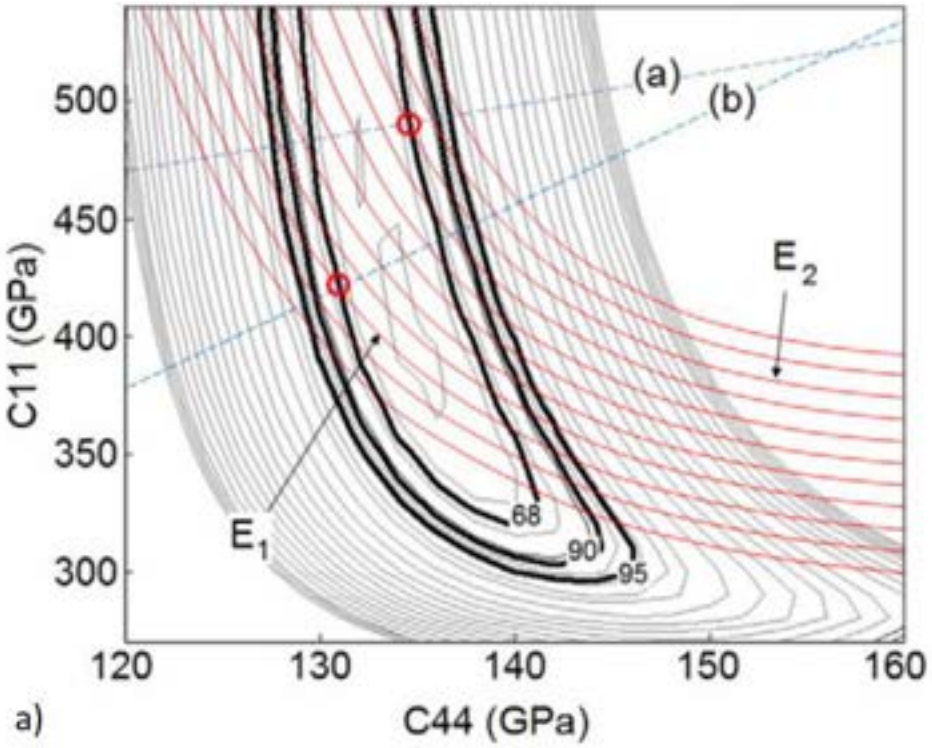
thicknesses: 200 nm ÷ 2 m

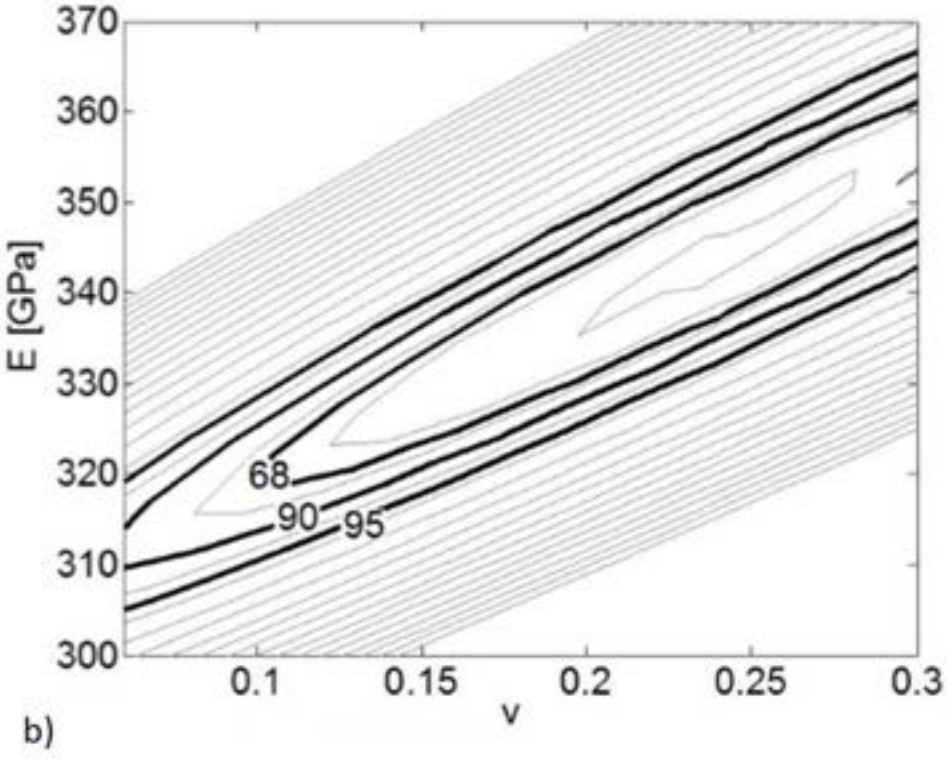
Brillouin spectroscopy



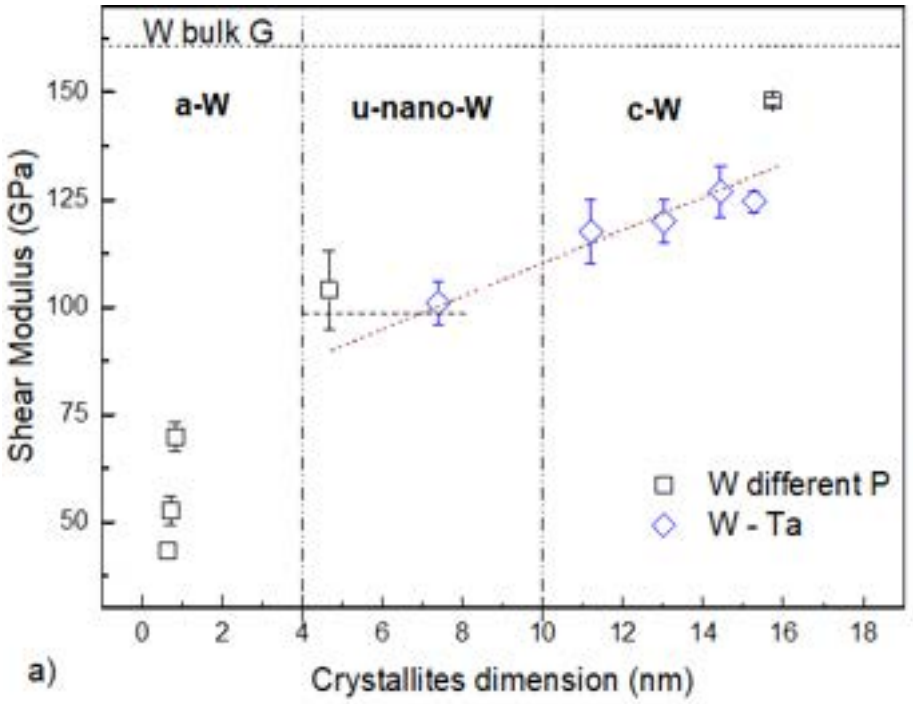


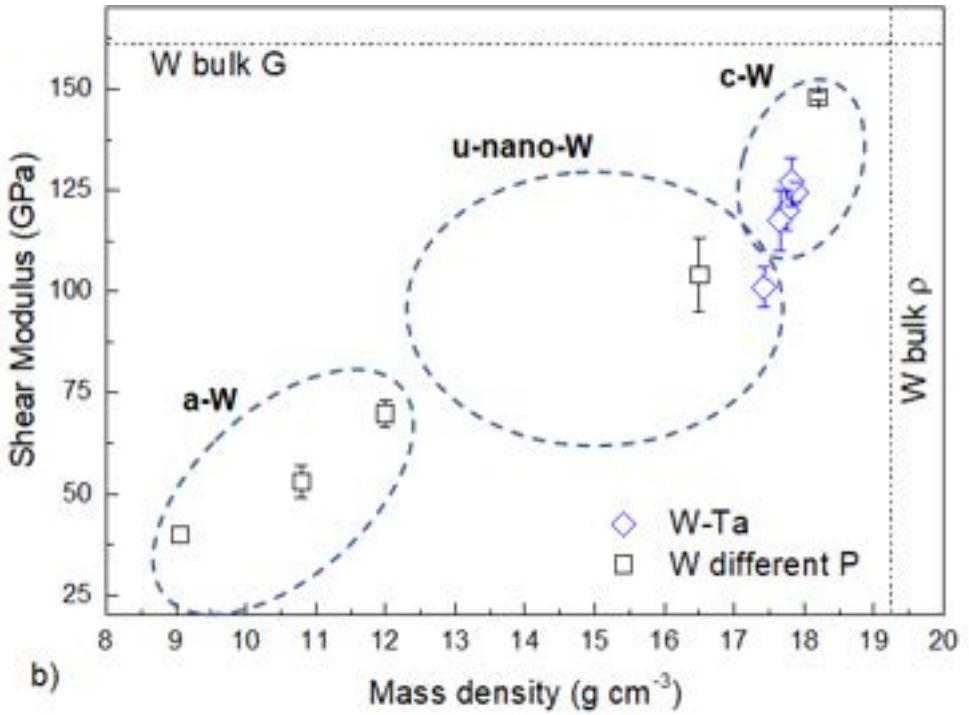
Brillouin spectroscopy: fit of the dispersion relations





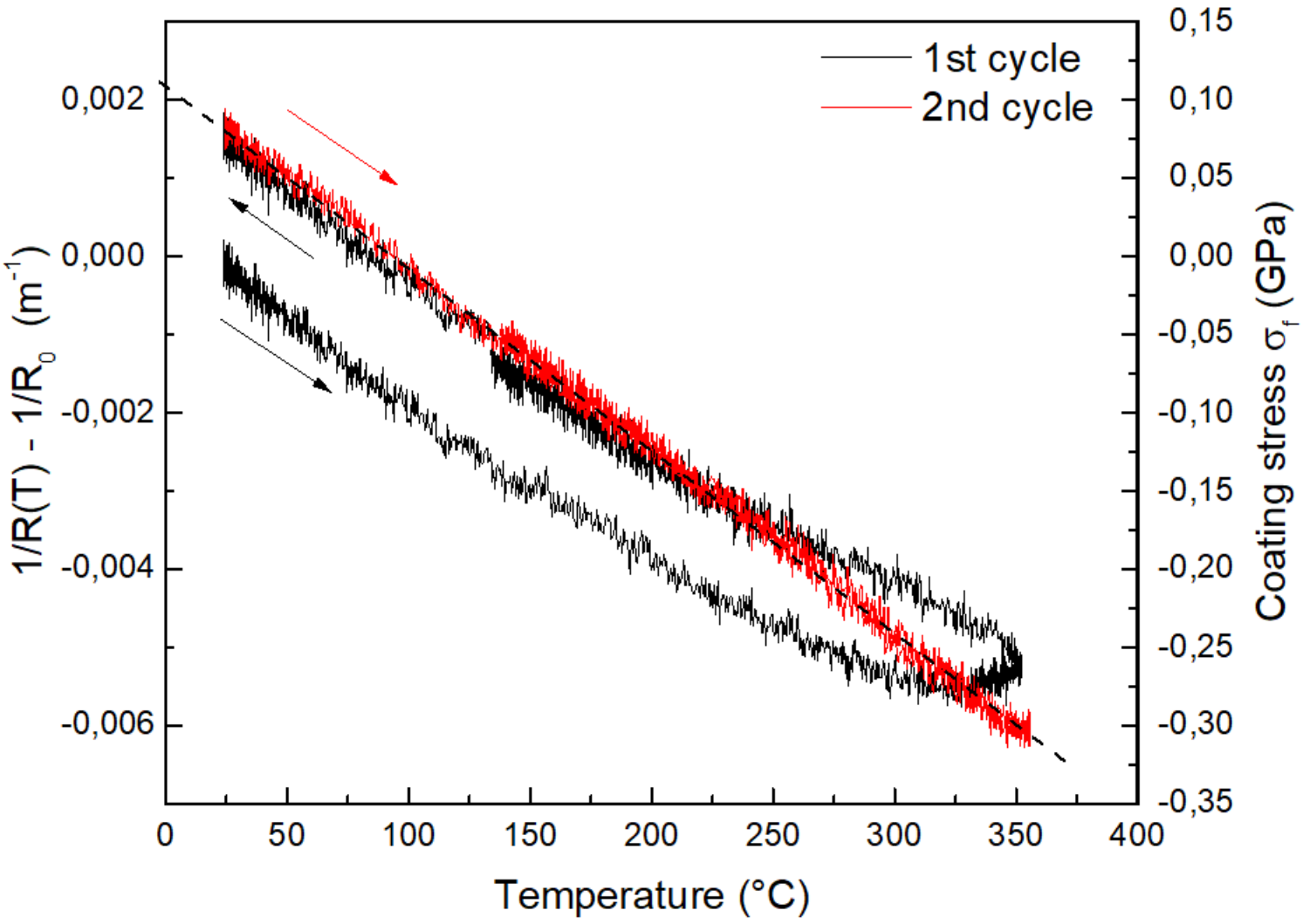
W-based films: stiffness vs. mass density vs. cryst. size



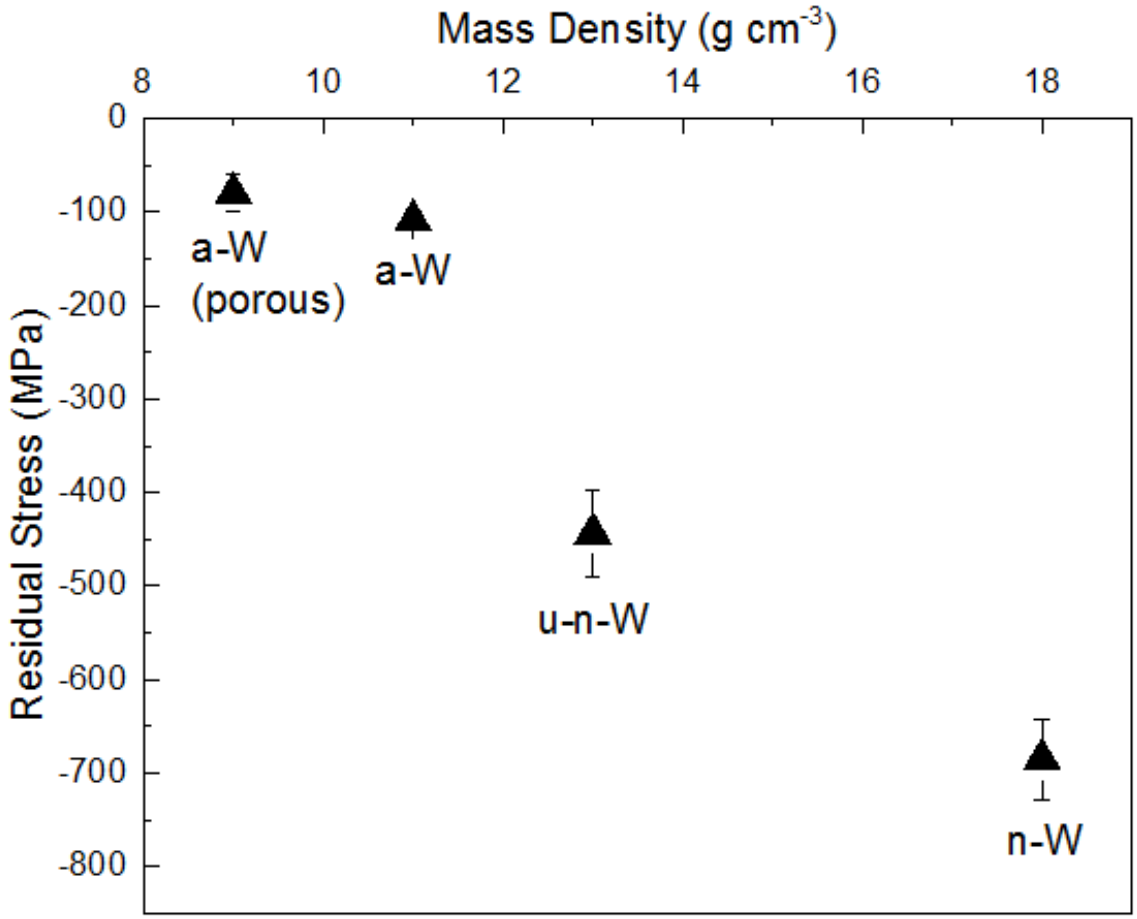


E. Besozzi, D. Dellasega, A. Pezzoli, C. Conti, M. Passoni, M.G. Beghi,
Amorphous, ultra-nano- and nano-crystalline tungsten-based coatings grown by Pulsed Laser Deposition: mechanical characterization by Surface Brillouin Spectroscopy
Materials and Design **106**, 14-21 (2016)

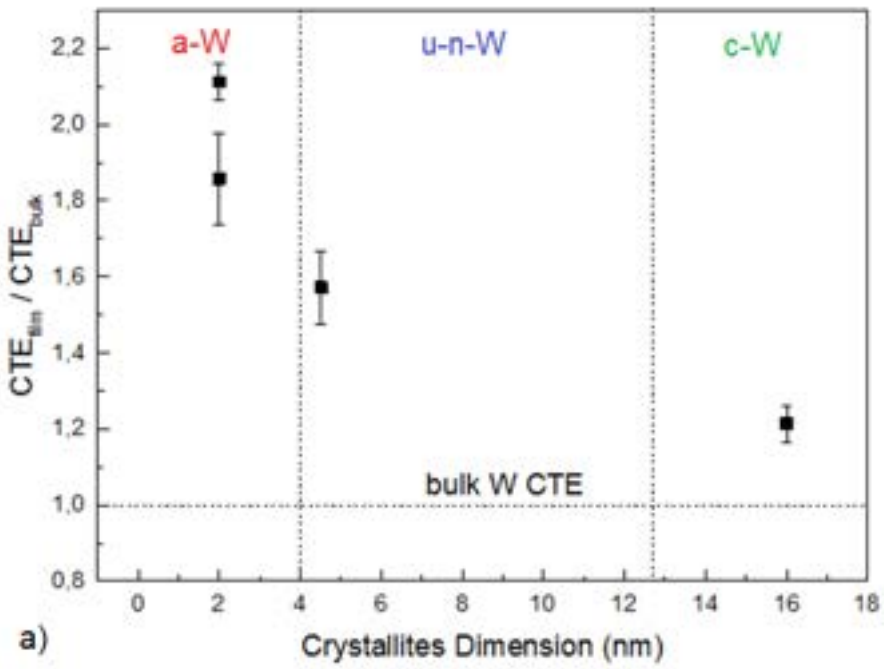
W-based films: thermal expansion

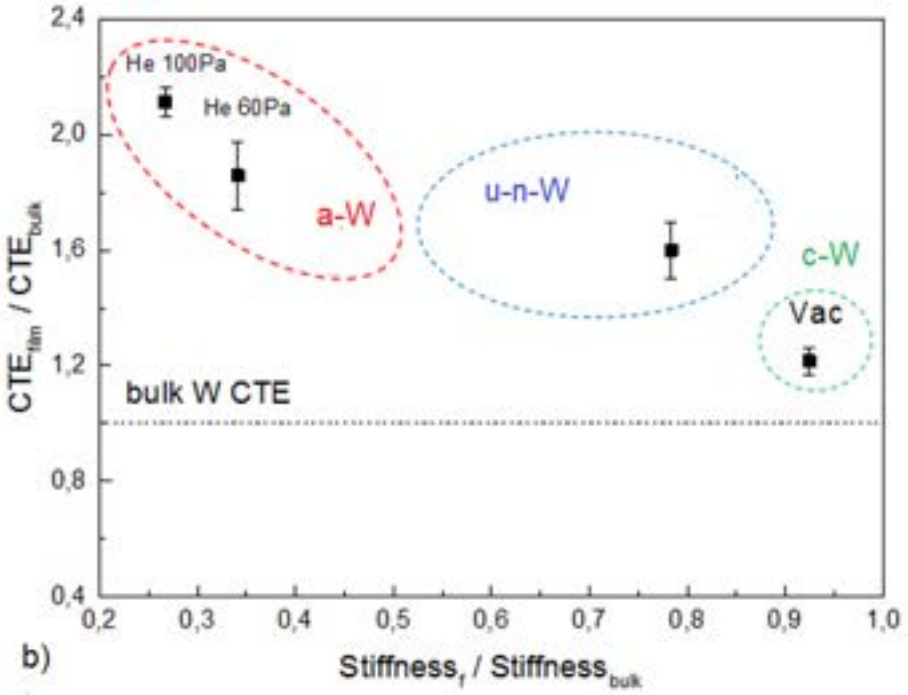


W-based films: residual stress vs. mass density

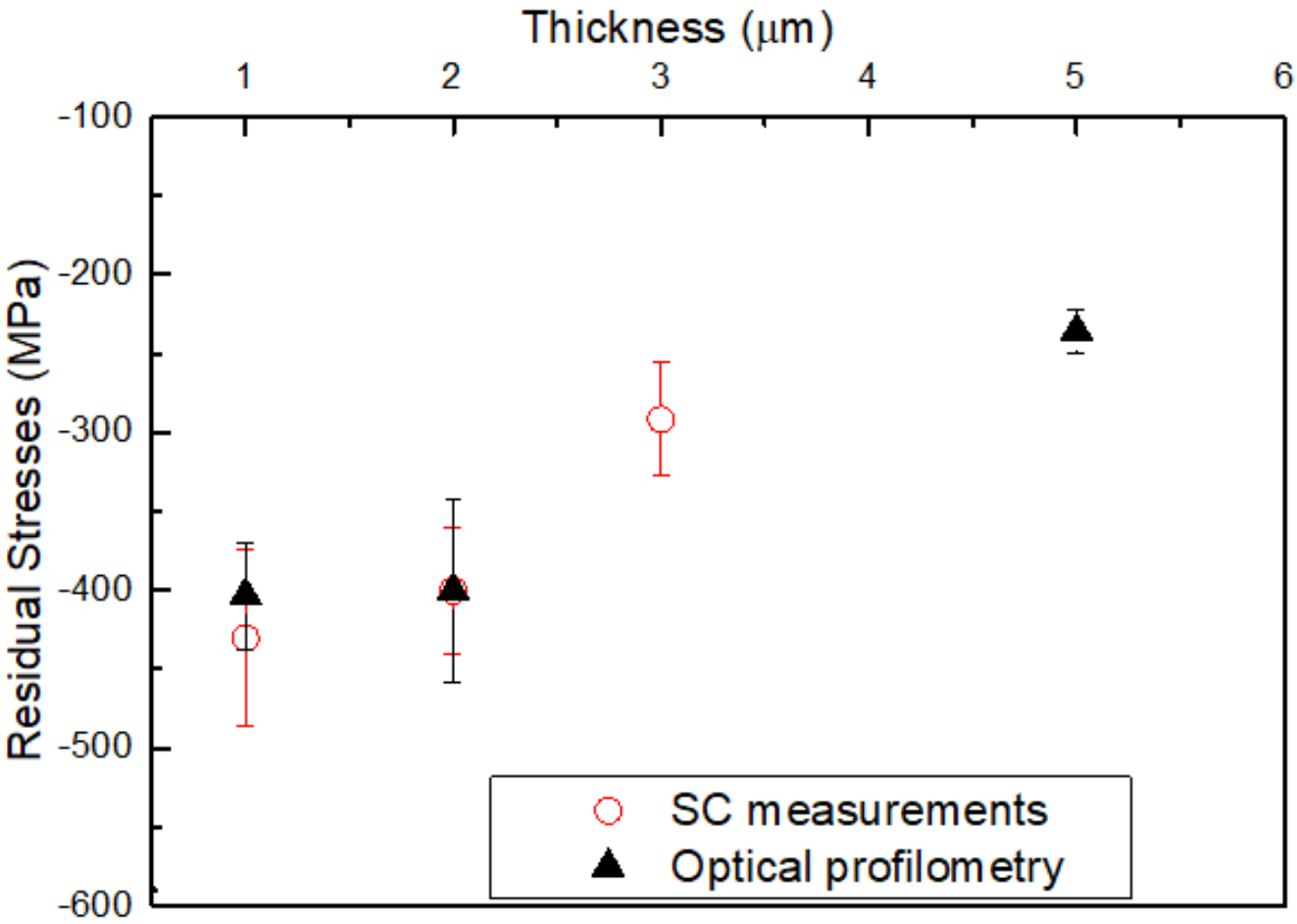


W-based films: CTE vs. mass density vs. cryst. size

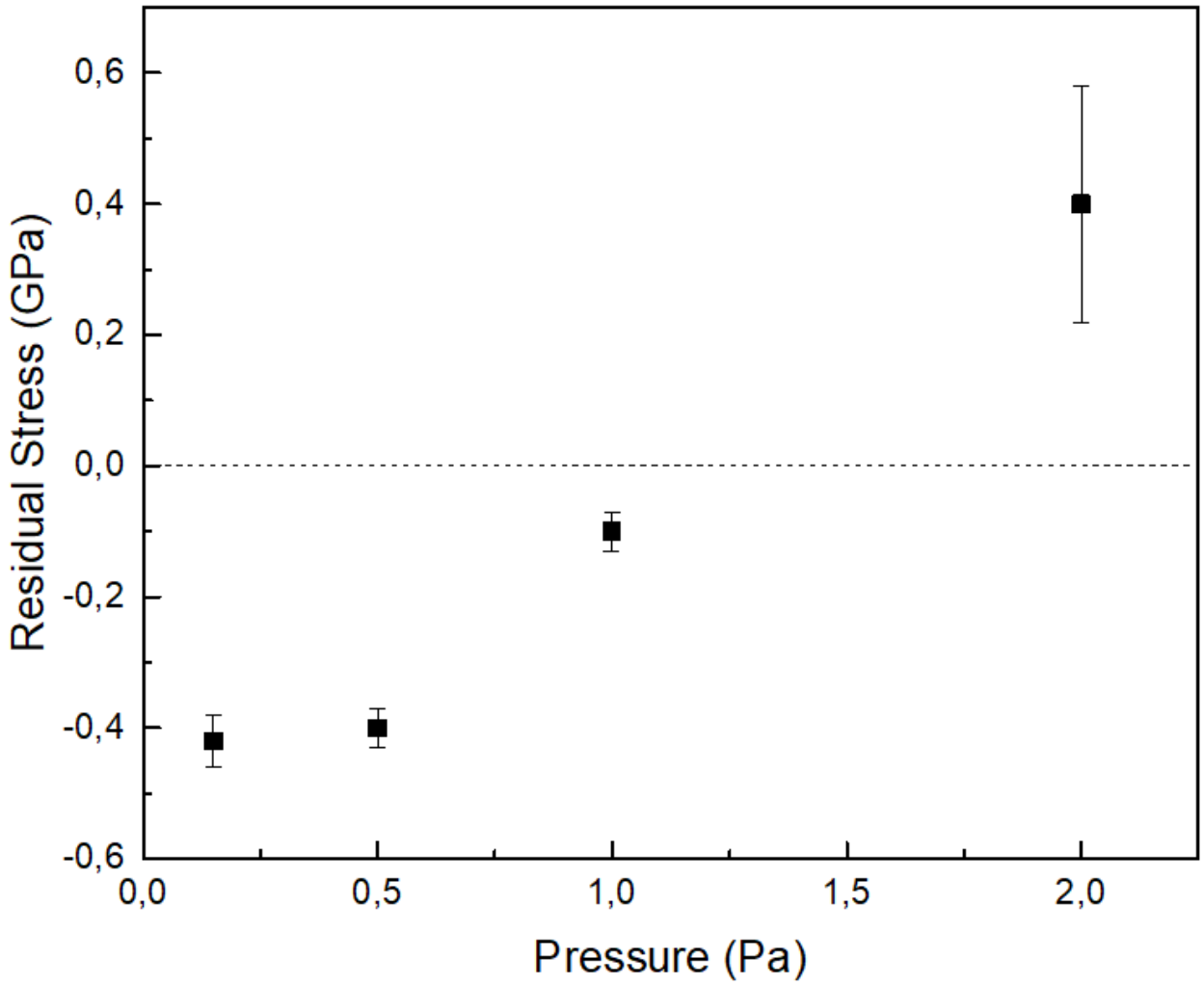




Alumina coating by PLD: residual stress



Alumina coating by PLD: residual stress



Conclusions

Thermomechanical characterization of coatings,
down to sub-micrometric thickness,

possible by combination of

Brillouin spectroscopy (possibly + indentation)
&
Sample Curvature (SC) method (optical implementation)

available for coating qualification

Thank you

Title

Title

Brillouin spectroscopy

Materials and Design 106 (2016) 14-21

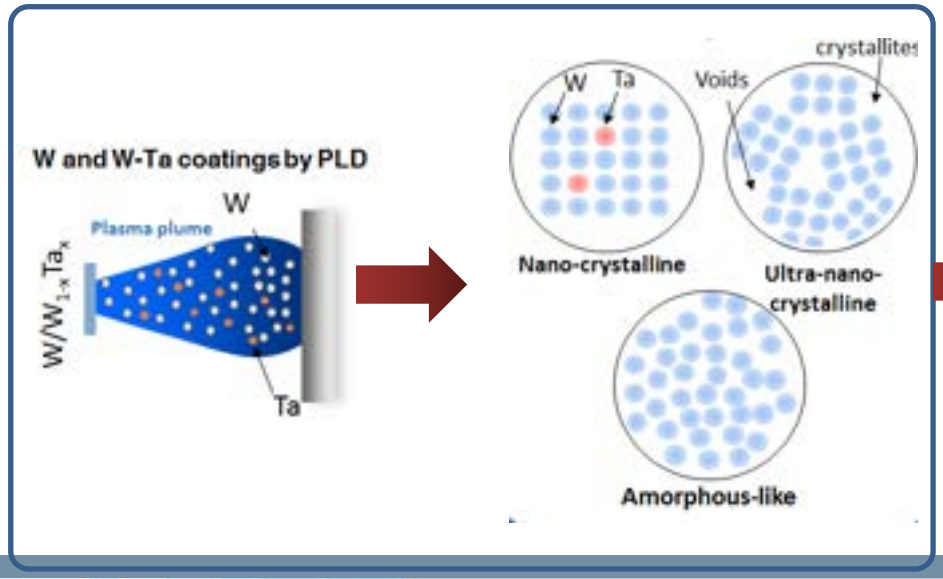
Contents lists available at ScienceDirect

Materials and Design

journal homepage: www.elsevier.com/locate/matdes

Amorphous, ultra-nano- and nano-crystalline tungsten-based coatings grown by Pulsed Laser Deposition: mechanical characterization by Surface Brillouin Spectroscopy

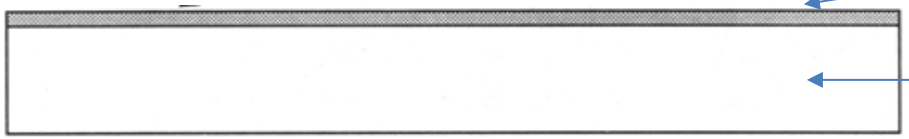
E. Besozzi [a], D. Dellasega [a,b], A. Pezzoli [a], C. Conti [c], M. Passoni [a,b], M.G. Beghi [a,*]



Different mechanical properties are expected for different nanostructures

MODEL

- Consider a film/substrate system



$h_f << h_s$

The film stress (σ_f) is constant along the thickness

Linear elastic, homogenous materials

Hooke's relation between σ and ε

Isotropic and biaxal state of stress

$$\sigma_f = \frac{E_f}{1-\nu_f}\varepsilon^*$$

- The mismatch strain ε^* between the layers produces stresses and may curve the specimen. It is defined as:

$$\varepsilon^* = \varepsilon^{thermal} + \varepsilon^{growth} + \varepsilon^{plastic}$$

f(T, geometry)

Function of T and the mismatch of α between f and s

Function of material combination and deposition process

Responsible of plastic flow, creep and stress relaxation

Moment balance → $\varepsilon^* = -\frac{1}{6}\frac{1}{m_r t_r} h_s K$

$m_r = M_f / M_s$

$t_r = h_f / h_s$

$$\sigma_f = -\frac{E_s}{1-\nu_s}\frac{h_s^2}{h_f}\frac{1}{6}K$$

Wafer curvature

Stoney equation

$(\sigma_f = \sigma^{th} + \sigma^{growth})$

$$\sigma^{th} = (\alpha_s - \alpha_f)\Delta T \frac{E_f}{1-\nu_f}$$

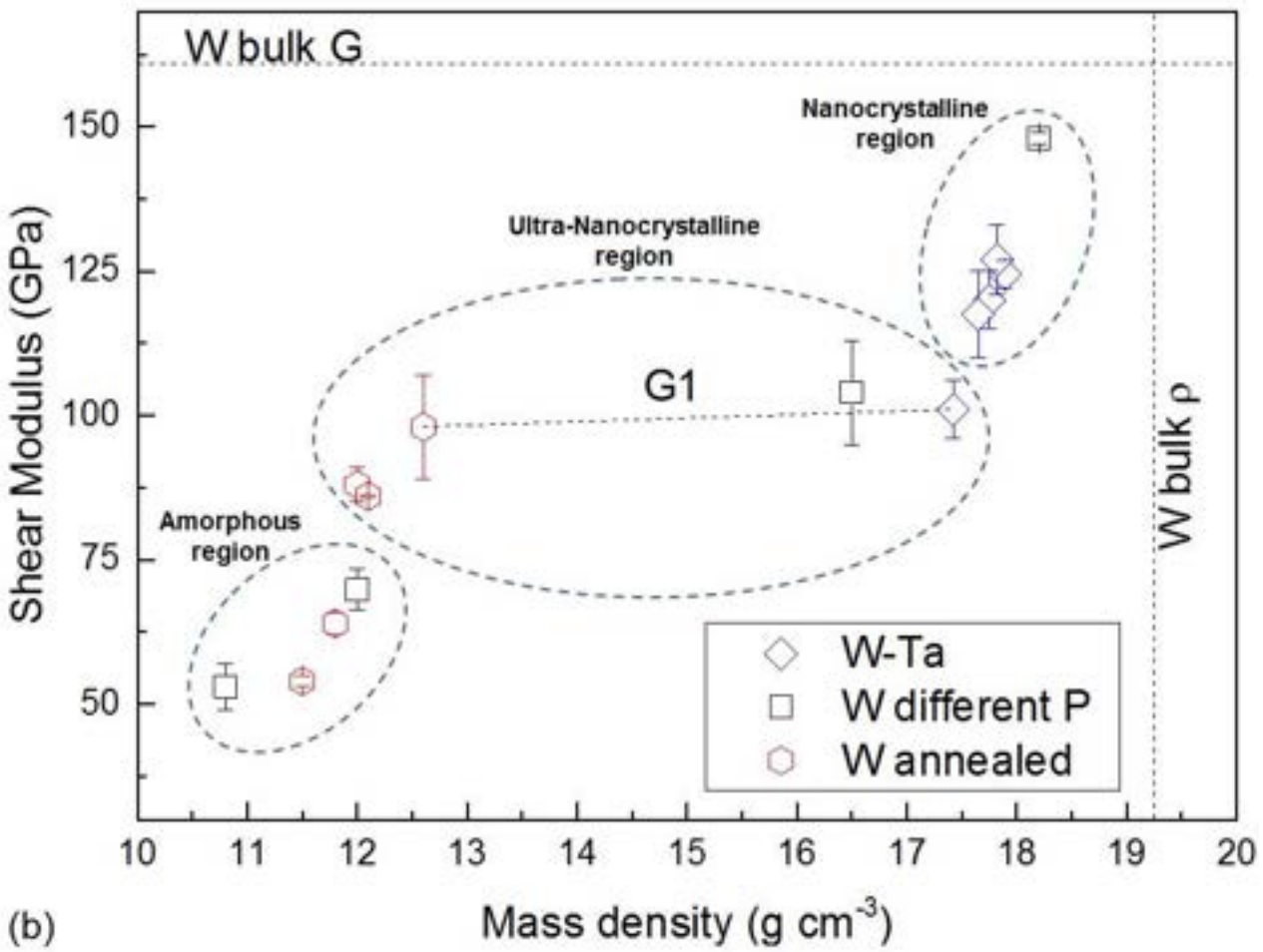
→ *How do we derive film CTE from σ_f measurement?*

- Once K as a function of T is measured, ε* can be derived

If α and ε^{growth} **<u>are not</u>** function of T → $\frac{d\varepsilon^*}{dT} = d$

$$\alpha_f = \alpha_s - d$$

W-based films: stiffness vs. mass density



E. Besozzi, D. Dellasega, A. Pezzoli, C. Conti, M. Passoni, M.G. Beghi,
Amorphous, ultra-nano- and nano-crystalline tungsten-based coatings grown by Pulsed Laser Deposition: mechanical characterization by Surface Brillouin Spectroscopy
Materials and Design **106**, 14-21 (2016)

Title

Title

Italian National Agency for New Technologies,
Energy and Sustainable Economic Development

Controllo della chimica del refrigerante nel reattore DEMO-LFR ALFRED

ADP MiSE-ENEA (PAR2016-LP2)

Aula Magna, Scuola di Ingegneria e Architettura, Università di Bologna
26-27 settembre, 2017

S. Bassini, A. Antonelli, I. Di Piazza (ENEA FSN-ING-TESP)
serena.bassini@enea.it

CHEMISTRY OF HLM (LEAD AND LBE)



Slag deposit in the circuit during circulation pump tests



Slag deposit in heat exchanger

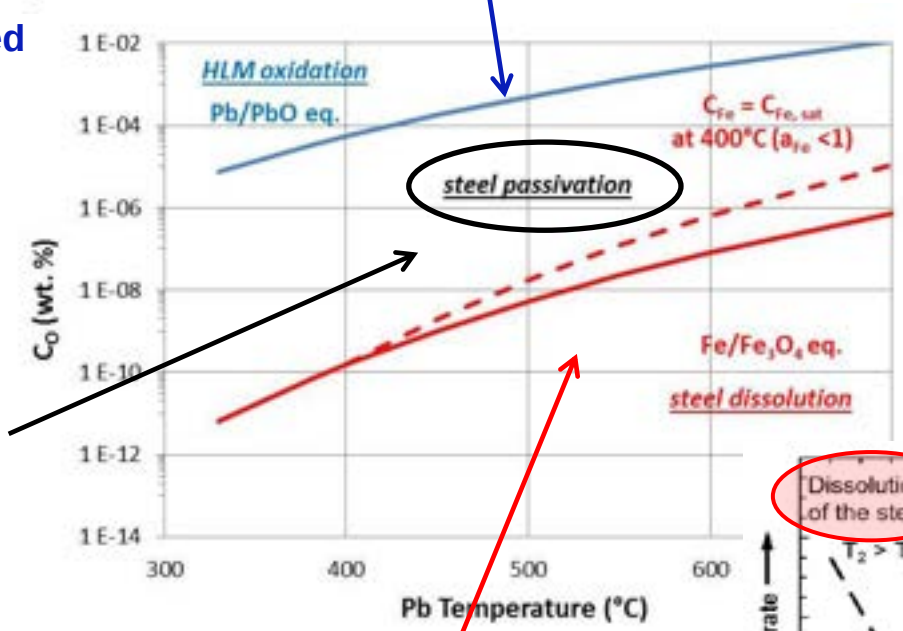
$$Pb_{liq} + O_{diss} \leftrightarrow PbO_{diss}$$

documento non esiste testo dello stile specificato.1

Oxygen saturation and PbO deposition

plugging in Pb-Bi cooled K-27 Russian Nuclear Submarine in 1960'

oxygen balancing for steel passivation and to avoid PbO formation: need of <u>oxygen sensors</u> and <u>oxygen control devices</u>



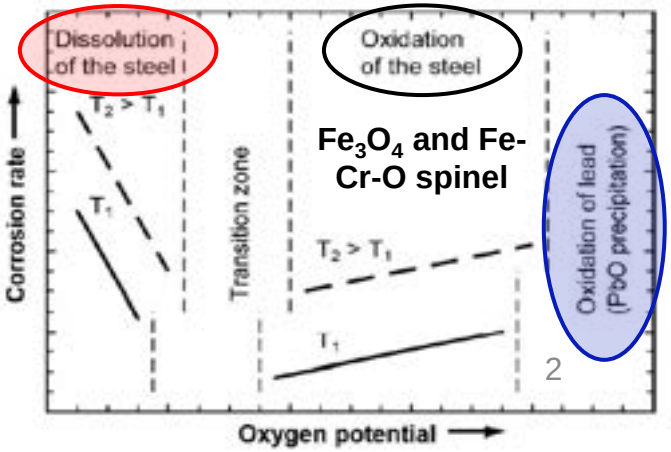
Steel corrosion at low oxygen content

Ni and Cr dissolution in 316L steel. Flowing LBE, 400°C, 10⁻⁶ wt% O_2, 1500 h.

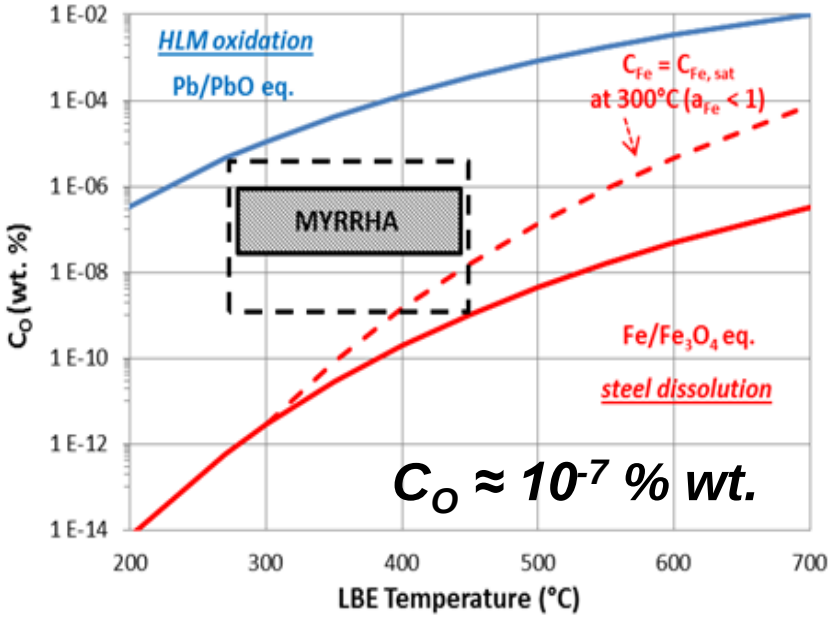


Benamati et al., J Nucl Mater 335 (2004) 169-173.

C. Schroer, Nucl Eng Des, 241 (2011) 4913-4923.

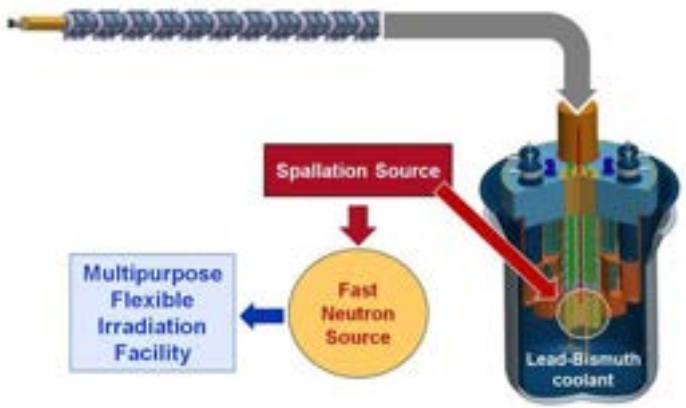


TARGET OXYGEN FOR OPERATION – MYRRHA (LBE)

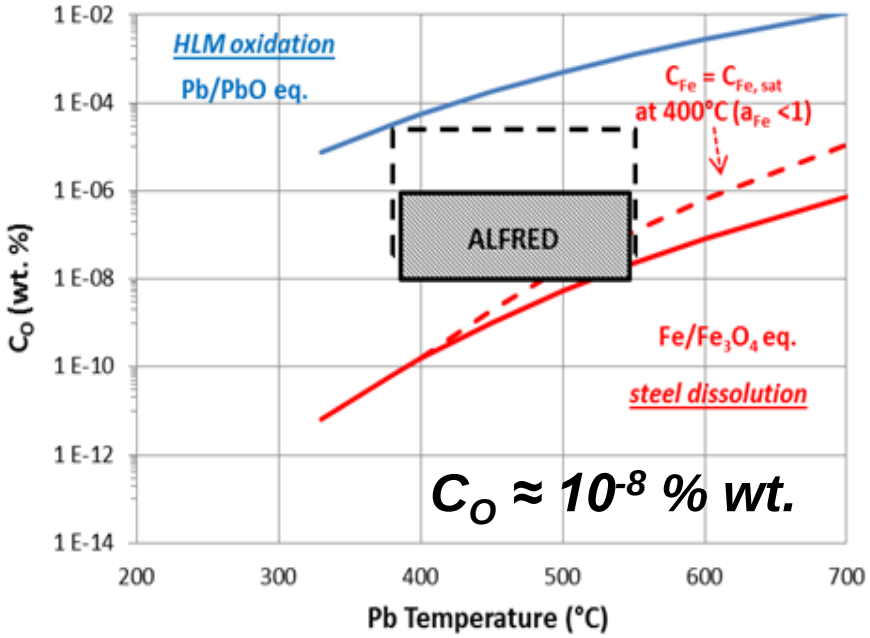


T (°C)	LBE	
	$C_{O,sat}$ (% wt.)	$C_{O,sat}$ (ppmw)
300	$1.1 \cdot 10^{-5}$	0.1
400	$1.3 \cdot 10^{-4}$	1.3
450	$3.5 \cdot 10^{-4}$	3.5
500	$8.2 \cdot 10^{-4}$	8.2
550	$1.7 \cdot 10^{-3}$	17

OK for steel passivation in the operative range 270-450°C. All components protected.

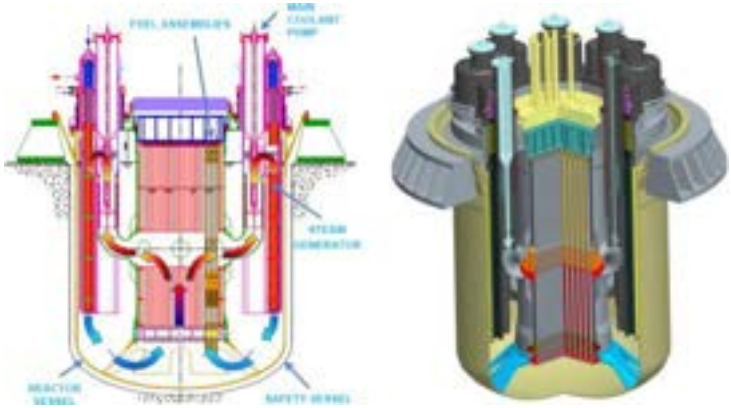


TARGET OXYGEN FOR OPERATION – ALFRED (Pb)



T (°C)	Pb	
	$C_{O,sat}$ (% wt.)	$C_{O,sat}$ (ppmw)
350	$1.4 \cdot 10^{-5}$	0.1
400	$5.5 \cdot 10^{-5}$	0.5
450	$1.8 \cdot 10^{-4}$	1.8
500	$5.1 \cdot 10^{-4}$	5.1
550	$1.3 \cdot 10^{-3}$	13

Steel passivation up to 450°C (vessel). Need of further protection in the range 450-550°C (fuel cladding & assembly, SG, pumps, inner vessels)



COATINGS FOR ALFRED PROTECTION

Materials and Coatings for low oxygen concentration ($C_O = 10^{-6}$ / 10^{-8} wt. %)

Component	*Min./Max Temp. Normal Operation (long term) (°C)*	*Max Temp. Accident Conditions (transient) (°C)*	*Max. Lead velocity (m/s)*	*Max. Radiation damage (dpa/y)*	*Max. Radiation damage (dpa)*	*Material*	*Coating*	*Notes*
Reactor Vessel	380÷430	500 (700 [1])	0,1	$< 10^{-5}$	0,0002 (40y)	**AISI316LN (ASTM)**	No	Back-up Liner of corrosion resistant steel (e.g. AFA)
Inner Vessel	380÷480	700 [1]	0,2	0,1	2,1 (20y)	**AISI316LN (ASTM)**	No Al diffusion coating by Pack Cementation	Back-up AFA steel
Diaphragm	380-480	700 [1]	0,2	0,1	(1,8) (20y)	**AISI316LN (ASTM)**	No	Al diffusion coating by Pack Cementation
Steam Generator	380÷480	700 [1]	0,6	$< 10^{-3}$	0,01 (20y)	**AISI316L (ASTM)** **15-15Ti (DIN 1.4970)**	No Al diffusion coating by Pack Cementation	Backup: AFA steel; Alloy 800 coated
Fuel cladding	380÷550	750	2	20	100 (5y)	**15-15Ti (AIM1)**	Al_2O_3 by PLD	No buffer layer (direct coating deposition over the bulk material)
FA Structures	380÷500	700	2	19	100 (5y)	**15-15Ti (AIM1)**	Spacer grids & wrapper (outside): Al_2O_3 by PLD Wrapper (inside): overthickness	Back-up (for wrapper tube): Al_2O_3 by ALD or PLD (**to be developed in-tube deposition**)
DHR Heat Exchanger	380÷430	700 [1]	0,2	$< 10^{-3}$	0,01 (20y)	**AISI316L (ASTM)** **15-15Ti (DIN 1.4970)**	No Al diffusion coating by Pack Cementation	Backup: AFA steel; Alloy 800 coated
Primary Pumps (impeller)	380÷480	700 [1]	15÷20	$< 10^{-3}$	0,01 (20y)	**AISI300 series**	Closed impeller: Al diffusion coating by Pack Cementation Open Impeller: Al_2O_3 by PLD	Backup (for open impeller ONLY): AlTiN coating by PVD

Substrate: 316L(N), 15-15Ti (DIN), 15-15Ti (AIM1, cold worked)

OXYGEN SENSORS FOR HLM

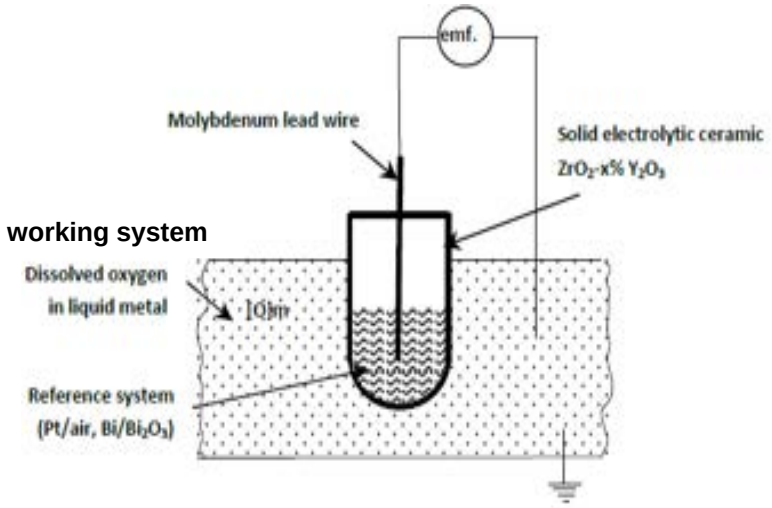
potentiometric sensor

$$E_{th} = \frac{RT}{4F} \cdot ln \frac{p_{O_2(ref)}}{p_{O_2(Pb,LBE)}}$$

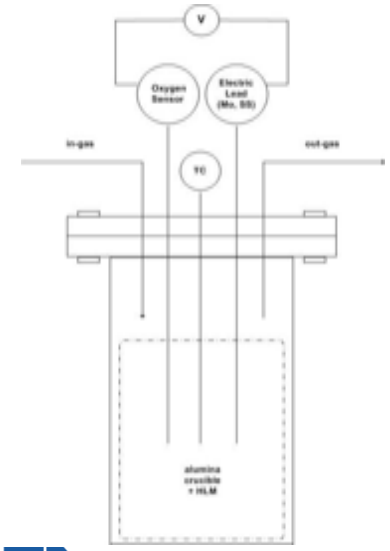
well-known (reference system)

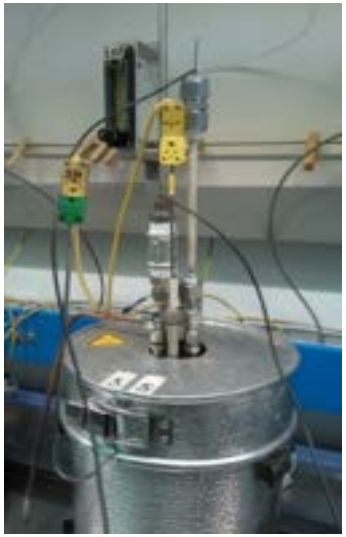
to be evaluated (working system)

+ ceramic solid electrolyte for O^{2-} conduction (*Yttria Stabilized Zirconia,* chemical compatibility with HLM)



set-up for oxygen sensor testing





V = high-impedance voltmeter
In-gas = flowing argon

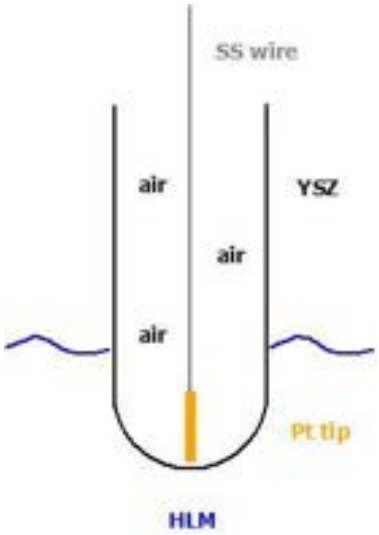
Reference systems
Pt-air, Bi/Bi_2O_3, Cu/Cu_2O

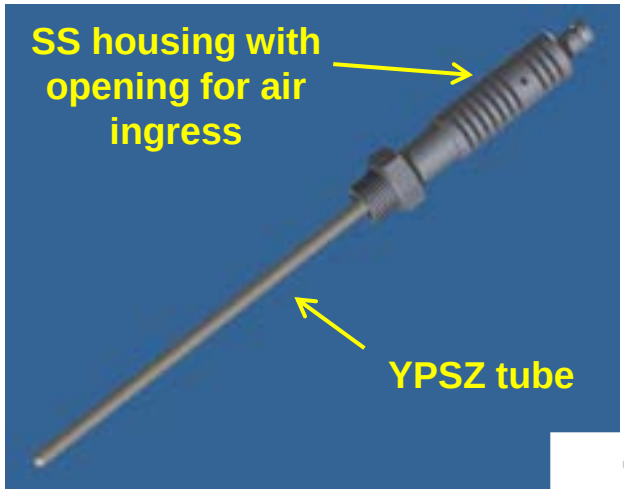
Calibration at oxygen saturation

Comparison of the experimental potential (E_{exp}) with the theoretical potential (E_{th}) expected in oxygen-saturated HLM (well-defined C_O) and at different T_{HLM}.

STUDY OF REFERENCE SYSTEMS: AIR

Influence of the reference on the min. reading temperature

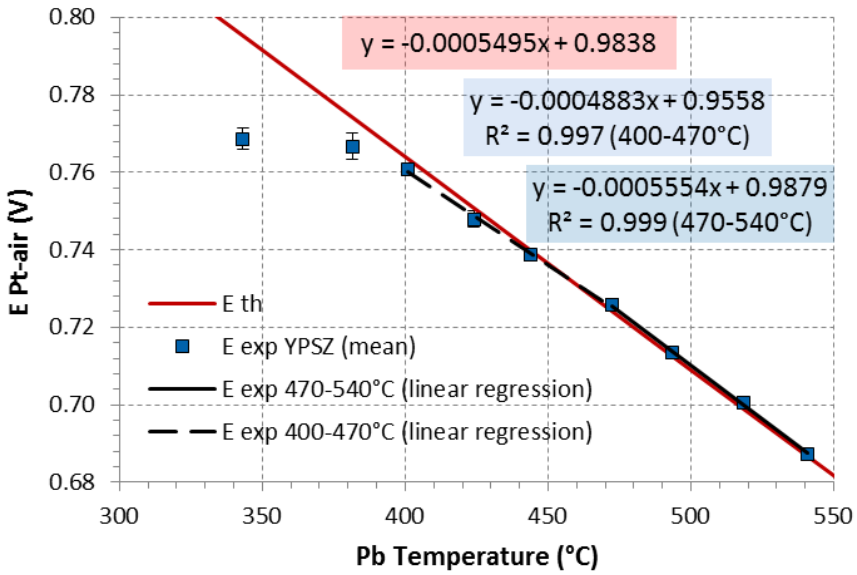




Pt-air sensor (KIT)
Solid electrolyte: YPSZ (Yttria Partially Stabilized Zirconia, 5 % mol of yttria)
Reference wire: 316Ti with Pt tip

Air reference

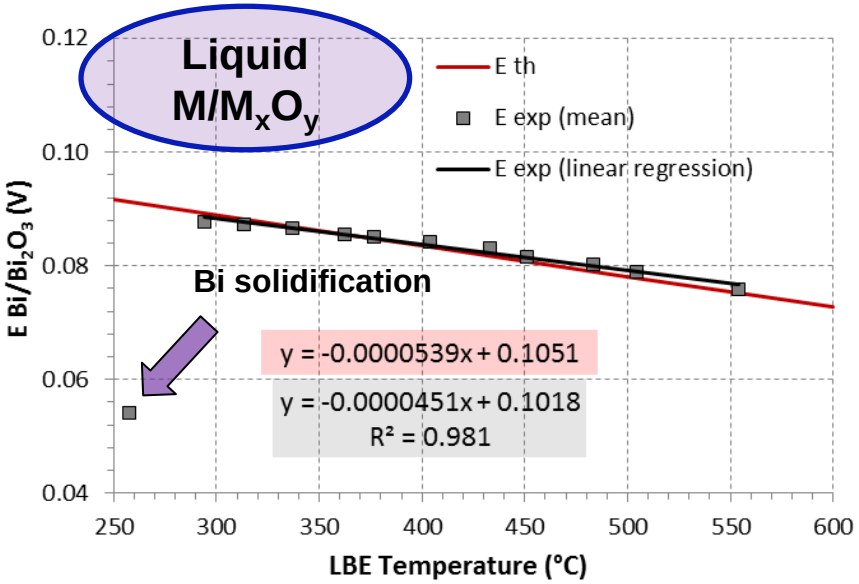
Pt-air
Min. reading T ≈ 400◦C
easy manufacturing, suitable for Pb system but not for LBE ones

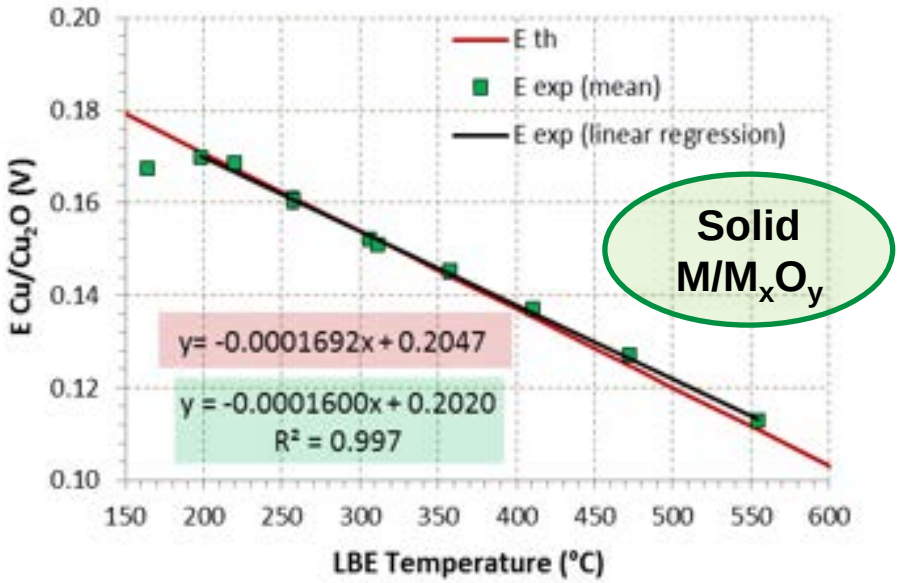


STUDY OF REFERENCE SYSTEMS: M/M_xO_y

Influence of the reference on the min. reading temperature







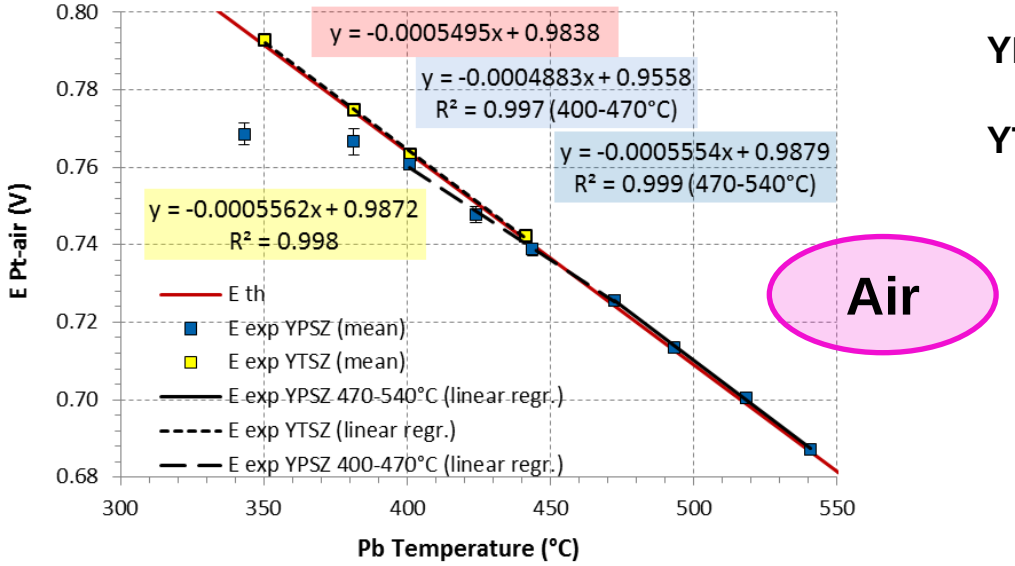
Bi/Bi_2O_3
Min. reading T ≈ 290◦C; tendency to crack due to Bi volume variation ($T_{m,Bi}$ =271◦C)

Cu/Cu_2O
Min. reading T ≈ 200◦C; tendency to powders sintering ($T_{m,Cu}$ =1085◦C)



STUDY OF SOLID ELECTROLYTES: YTSZ & YPSZ

Influence of the solid electrolyte on the min. reading temperature



Air

<u>ionic conductivity</u>: YTSZ > YPSZ

Max ionic conductivity for 8 % mol Y_2O_3

but <u>mechanical strength</u>: YTSZ < YPSZ

A. Mariën at al., *Solid electrolytes for use in lead-bismuth eutectic cooled nuclear reactors*, J Nucl Mater 427 (2012) 39-45

YPSZ = Yttria Partially Stabilized Zirconia
5 % mol of yttria
YTSZ = Yttria Totally Stabilized Zirconia
8 % mol of yttria

Pt-air + YTSZ
sensor reading down to 350◦C

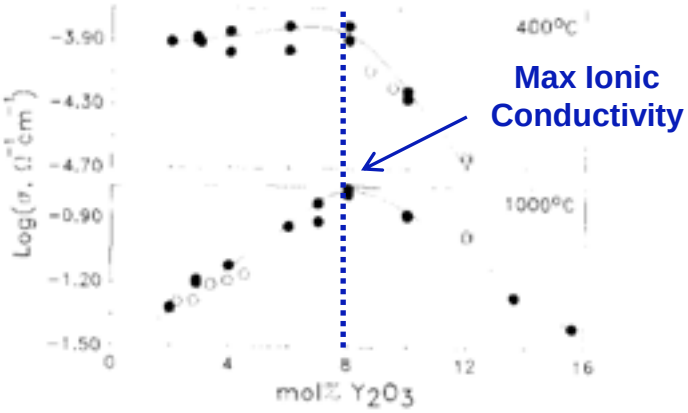
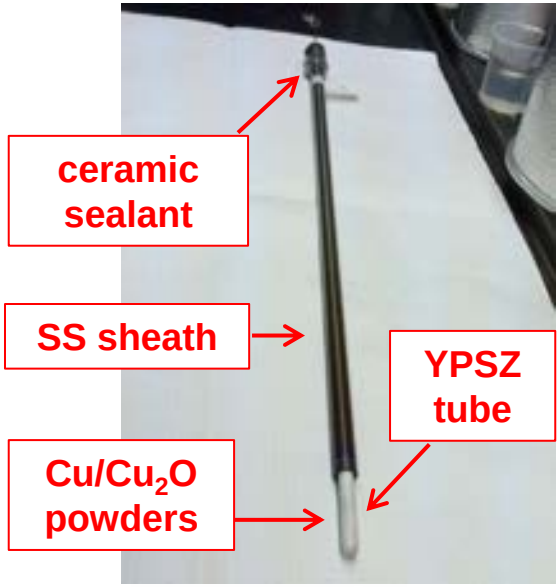


Fig. 2. Conductivity variation as a function of dopant content in Y_2O_3–ZrO_2. (○) single grain, (●) polycrystalline specimens.

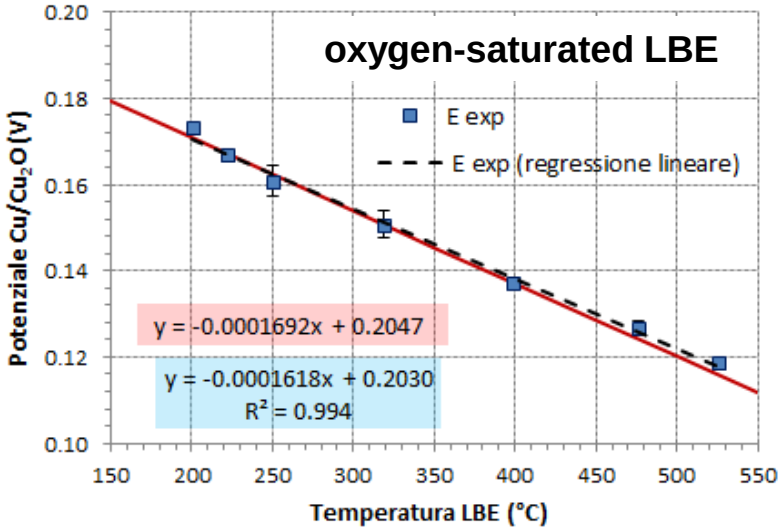
S.P.S. Badwal, *Zirconia-based solid electrolytes: microstructure, stability and ionic conductivity*, Solid State Ionics 52 (1992) 23-32

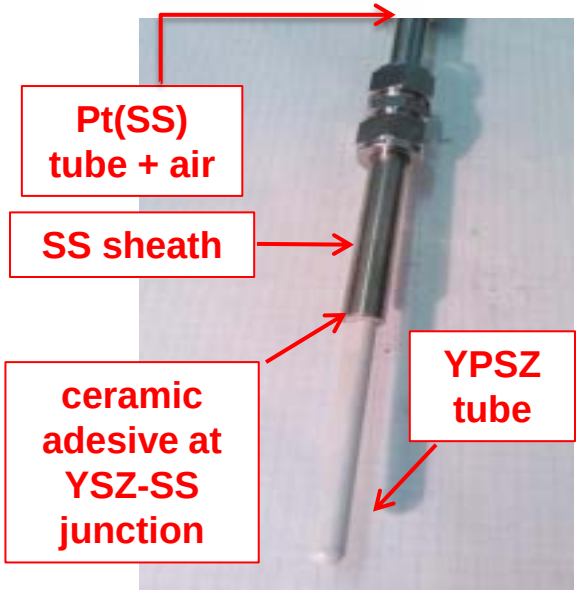
OXYGEN SENSOR FOR LOOPS & POOLS



Cu/Cu_2O sensor for NACIE-UP loop (LBE)
L= 600 mm
Position: expansion vessel,
T=200-400◦C

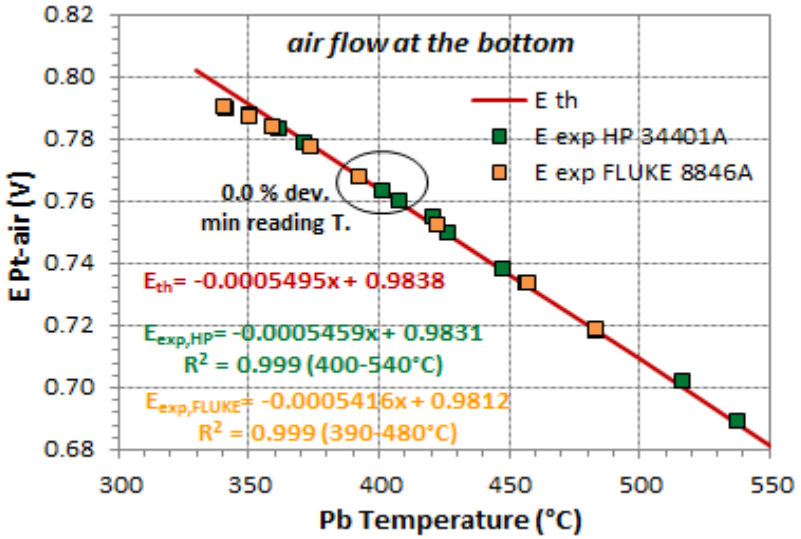
Min. reading T ≈ 200◦C
(but powder sintering)





Pt-air sensor for BID1 pool
L= 850 mm
T=400-550◦C

Min. reading T ≈ 400◦C

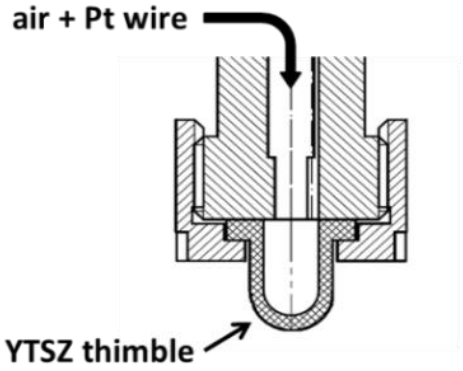


OXYGEN SENSOR FOR LARGE HLM POOL (1)



CIRCE facility
Main vessel: d= 1.2 m; L= 8.5 m;
70-90 ton of LBE, $T_{pool} \approx 300^{\circ}C$
application also in storage tank







Last Configuration

- Pt-air reference (with air dosing)
- YTSZ thimble (higher ionic conductivity) with a lateral step, pressed against a long steel tube by a perforated cap
- Total length = 1100 mm (to be adapted)

Technological requirements

1) ceramic protection to withstand the large pressures in pools or storage tanks;

2) reliable output at low T, e.g. at 300◦C for CIRCE pool.

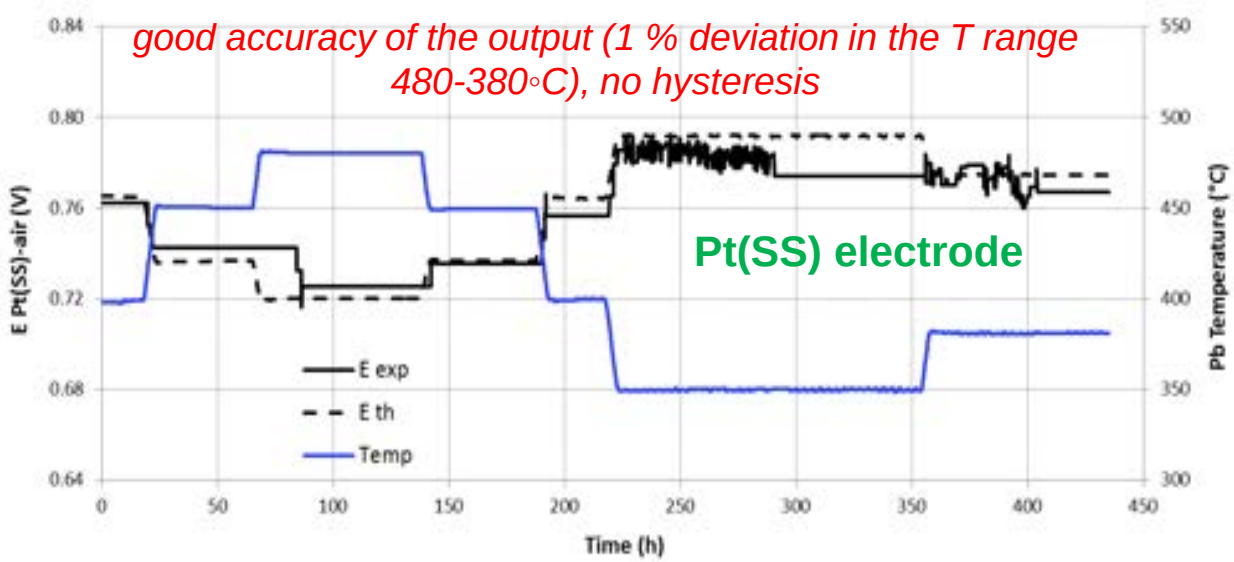
OXYGEN SENSOR FOR LARGE HLM POOL (2)



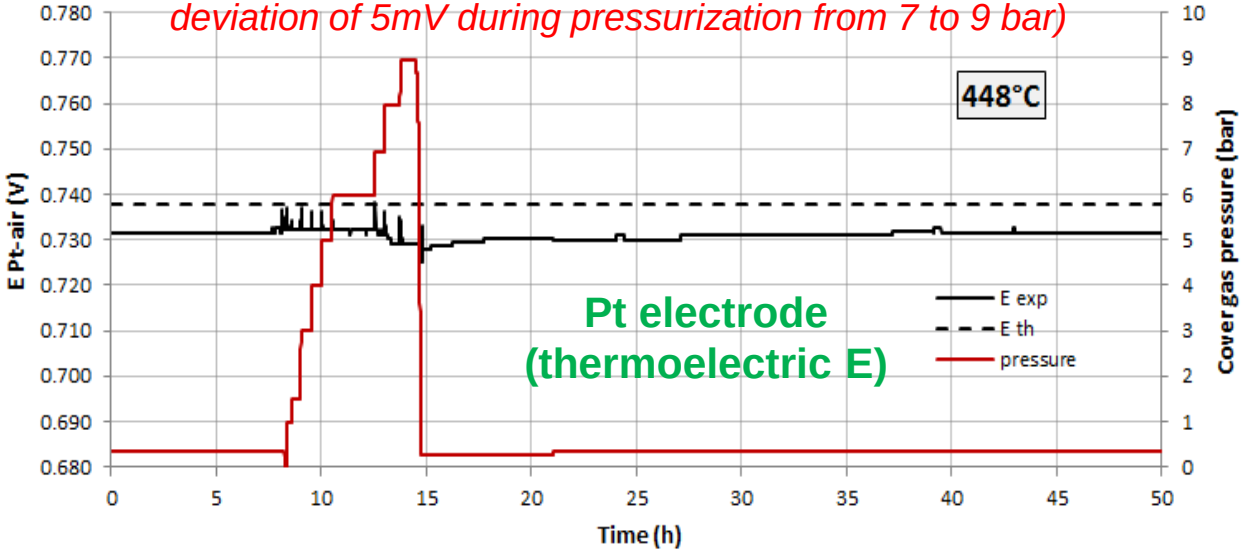
Calibration & Test at High Pressure in Pb storage tank

Min. reading T ≈ 380◦C , OK for storage tank application and Pb systems. Need of another reference for LBE systems

good accuracy of the output (1 % deviation in the T range 480-380◦C), no hysteresis



good tightness up to 9 bar of cover gas pressure (small deviation of 5mV during pressurization from 7 to 9 bar)



DEOXYGENATION WITH H_2: STATIC HLM, LAB SCALE



capsules for HLM chemistry & corrosion tests (750 g liquid Pb)

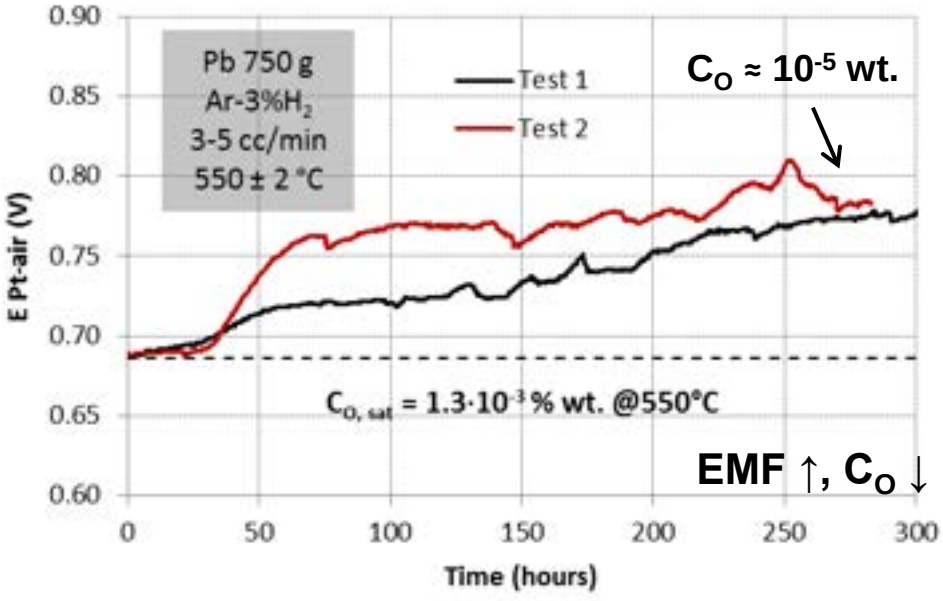




$$PbO_{diss.} + H_{2\,gas} \leftrightarrow H_2O_{gas} + Pb_{liquid}$$

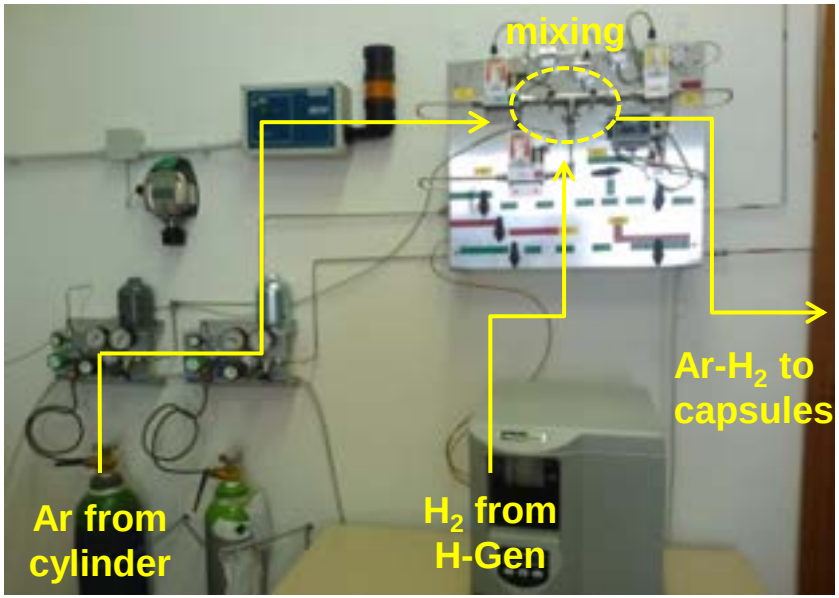
easy implementation, no HLM contamination (H_2O easily evacuated)

Target C_O = 10^{-7} - 10^{-8} % wt.

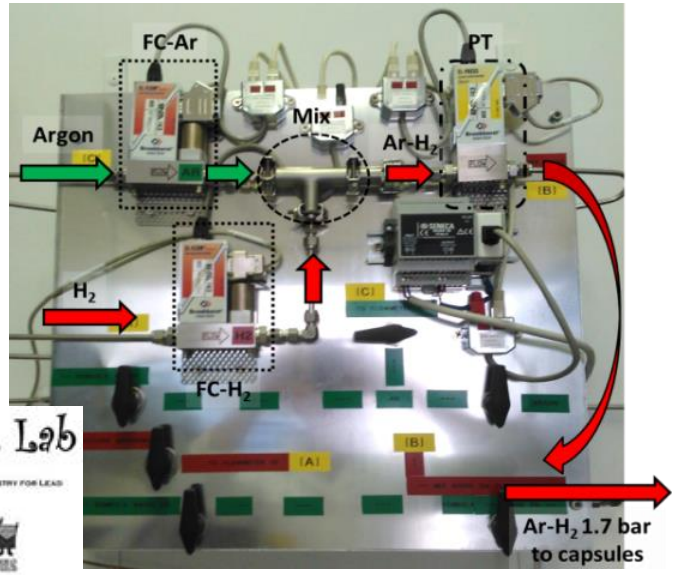


commercial Ar-3%H_2 gas mixture (bubbling) cannot provide efficient HLM deoxygenation in reasonable times → need of a dedicated gas control system

IMPLEMENTATION OF A GAS CONTROL SYSTEM



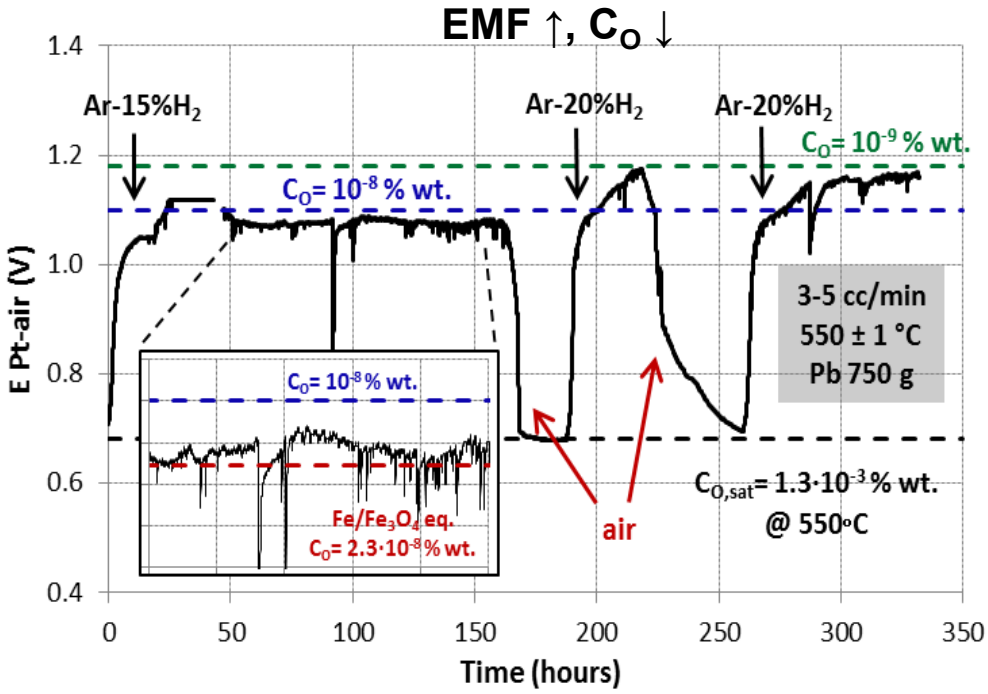
gas panel



Ar-H_2 gas mixtures with high H_2 % were obtained by mixing **pure Ar (cylinder)** and **pure H_2 (H-generator).**

Gas control system composed of:

- 2 digital mass flow controllers (1 for Ar + 1 for H_2)
- 1 mixing chamber
- 1 pressure transducer (to keep the gas line in pressure)

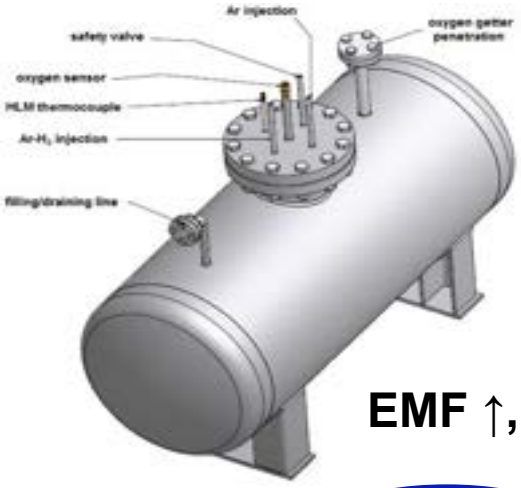


easy and fast HLM deoxygenation using Ar-H_2 gas mixtures with H_2 = 10-20 % vol.

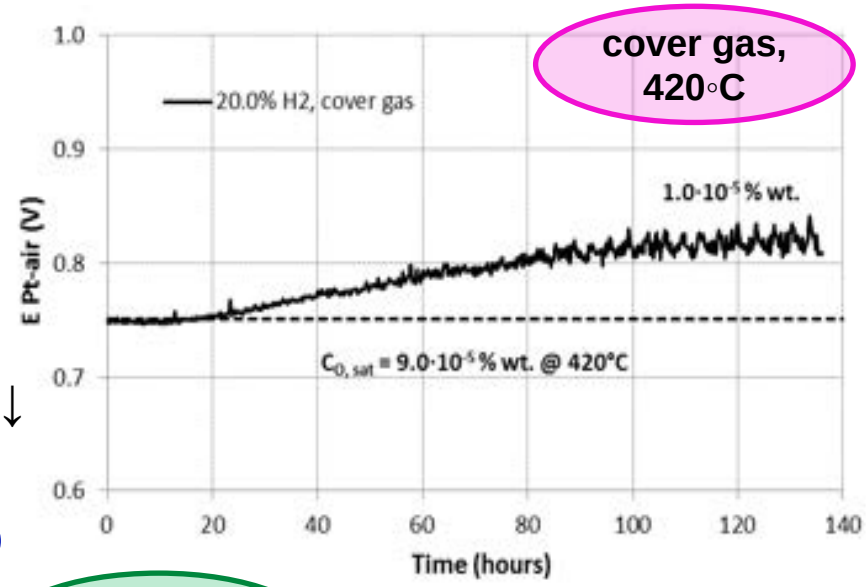
DEOXYGENATION WITH H_2: STORAGE TANK

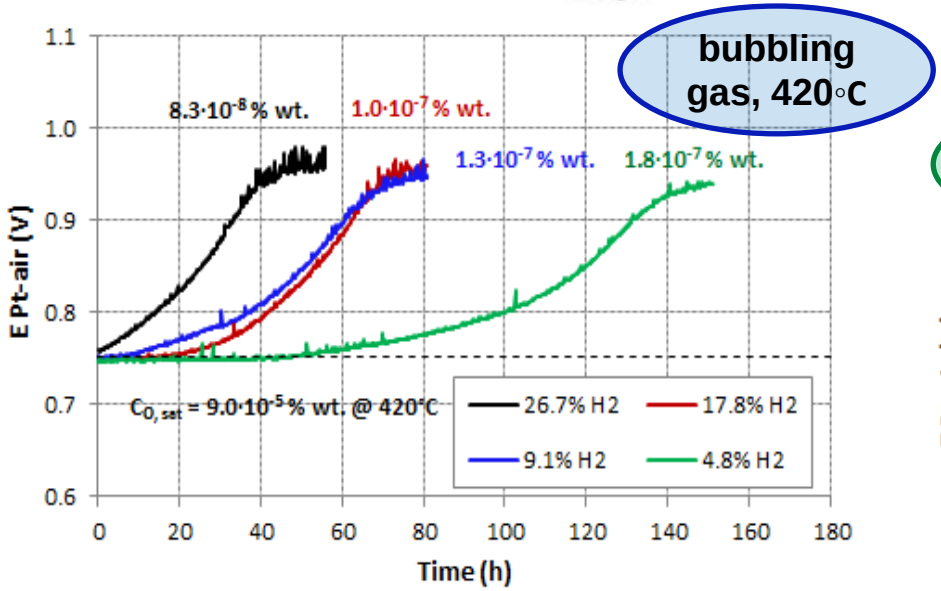


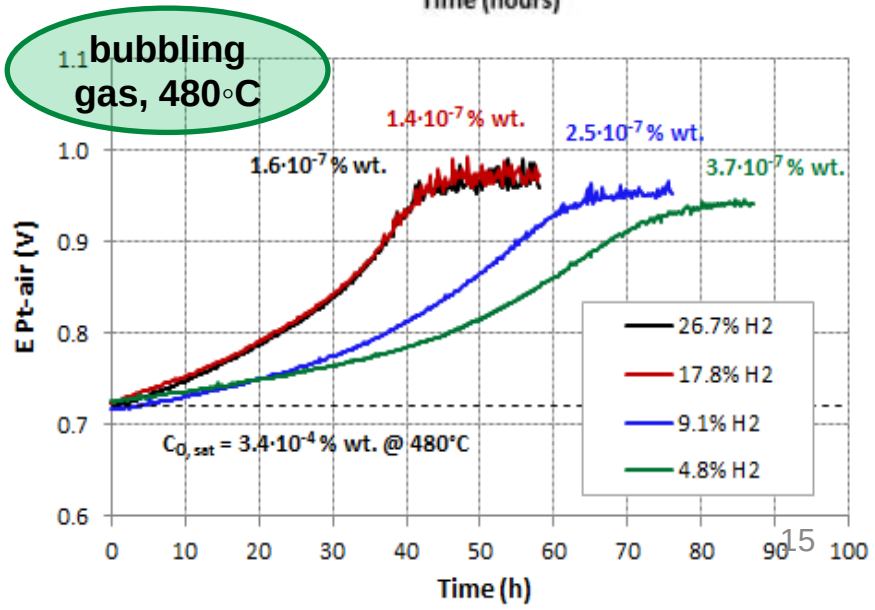
≈ 285 L of liquid Pb, gas control system implemented



EMF ↑, C_O ↓

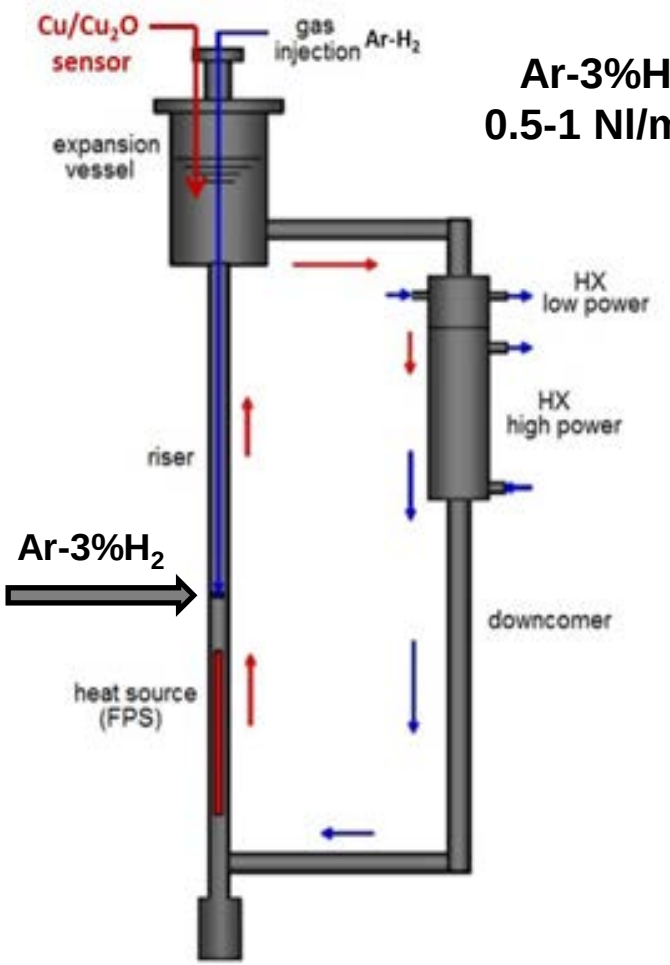






higher deoxygenation efficiency for higher T_{HLM}, H_2 %, and HLM mixing (i.e. bubbling)

DEOXYGENATION WITH H_2: LOOP FACILITY



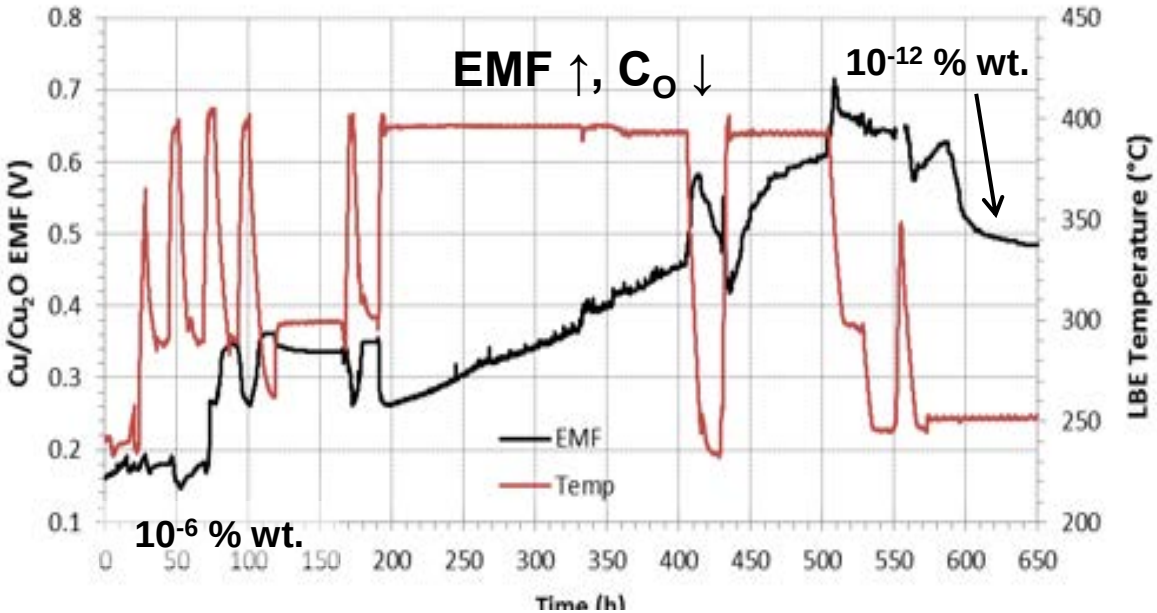
Ar-3%H_2
0.5-1 Nl/min



multi-holes gas injector in the raiser column (5 m long)



Cu/Cu_2O sensor



thermal-hydraulic NACIE-UP loop
LBE inventory ≈ 200L
200-400◦C

high deoxygenation efficiency even with Ar-3%H_2 thanks to the forced HLM circulation → too low C_O reached → need of oxygen supply (e.g. Ar-O_2 injection)

QUALITATIVE INTERPRETATION

$$PbO_{\,diss.} + H_{2\,gas} \leftrightarrow H_2O_{\,gas} + Pb_{\,liquid}$$

- ✓ H_2 absorption with chemical reaction
- ✓ hypothesis: fast reaction in the HLM phase occurring at the G/L interface

Enhancement factor
(Perry's Chemical Engineers' Handbook, 7th ed.)

$$E = \frac{K_L}{K_L^\circ} = \sqrt{\frac{D_{H_2}}{D_O}} + \sqrt{\frac{D_O}{D_{H_2}}} \cdot \left(\frac{C_O^{HLM}}{C_{H_2}^I}\right)$$

K_L = mass-transfer coefficient with chemical reaction
K_L° = mass-transfer coefficient without chemical reaction
D_{H_2} = H_2 diffusion coefficient
D_O = O_{diss} diffusion coefficient
C_O^{HLM} = C_O in the HLM bulk
$C_{H_2}^I$ = $C_{H_2,sat}$ at the G/L interface

$D_{H_2} \approx D_O \approx 10^{-6}$ cm²/s (400-1000◦C)
$C_O^{HLM} \approx 10^5 \cdot C_{H_2}^I$ (425-810◦C)

E ≈ 10^5

The reaction is fast, takes place at the G/L interface and enhances H_2 mass transfer in the HLM phase.

main controlling resistance:
O diffusion towards G/L interface

effect of HLM fluid-dynamic conditions (mixing, turbolence)

OXYGEN GETTER SCREENING

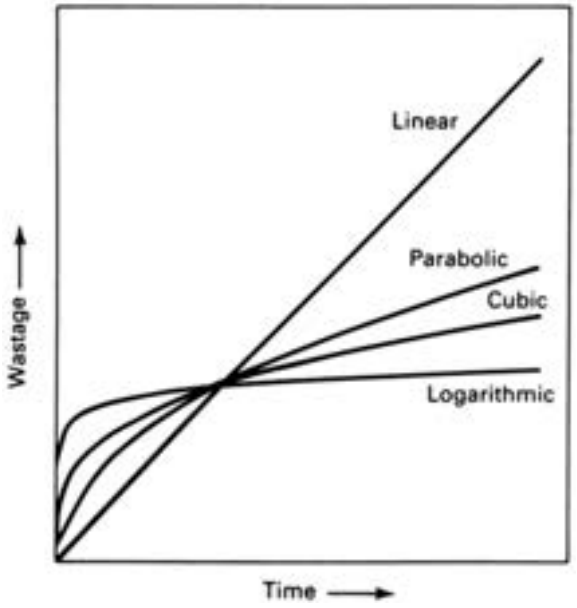
$Mg_{(s)} + PbO_{(diss)} \rightarrow MgO_{(s)} + Pb_{(l)}$

$Ti_{(s)} + 2PbO_{(diss)} \rightarrow TiO_{2(s)} + 2Pb_{(l)}$

$Zr_{(s)} + 2PbO_{(diss)} \rightarrow ZrO_{2(s)} + 2Pb_{(l)}$

$2Ta_{(s)} + 5PbO_{(diss)} \rightarrow Ta_2O_{5(s)} + 5Pb_{(l)}$

kinetics

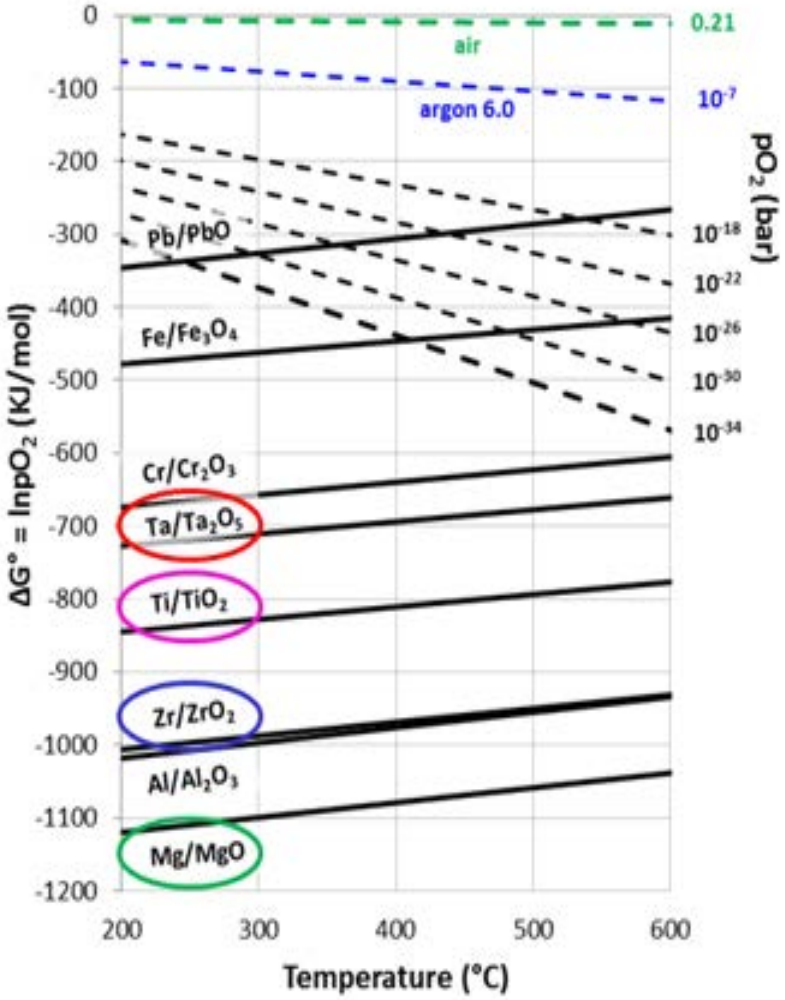


$\Delta m = k \cdot t$
Mg, Ta, Nb, Mo, W

$(\Delta m)^2 = k \cdot t$
Fe, Ni, Ti, Zr

$\Delta m = k \cdot Lnt$
Al, Cr

thermodynamics



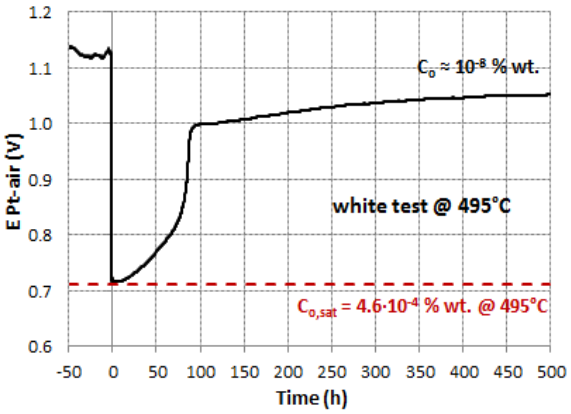
DEOXYGENATION WITH OXYGEN GETTERS

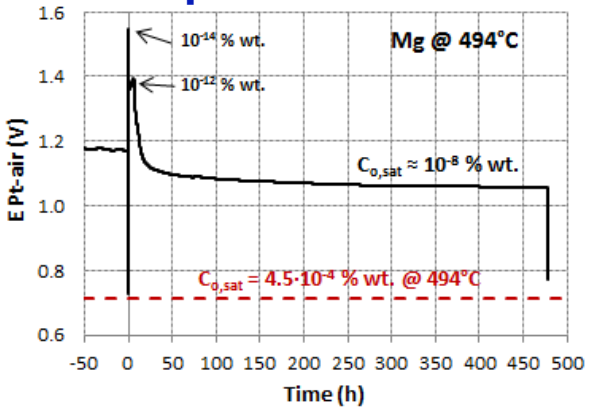




Pb ≈ 780 g, OG wire 35 mm (Mg, Ta, Ti and Zr)

lab scale: steel capsules





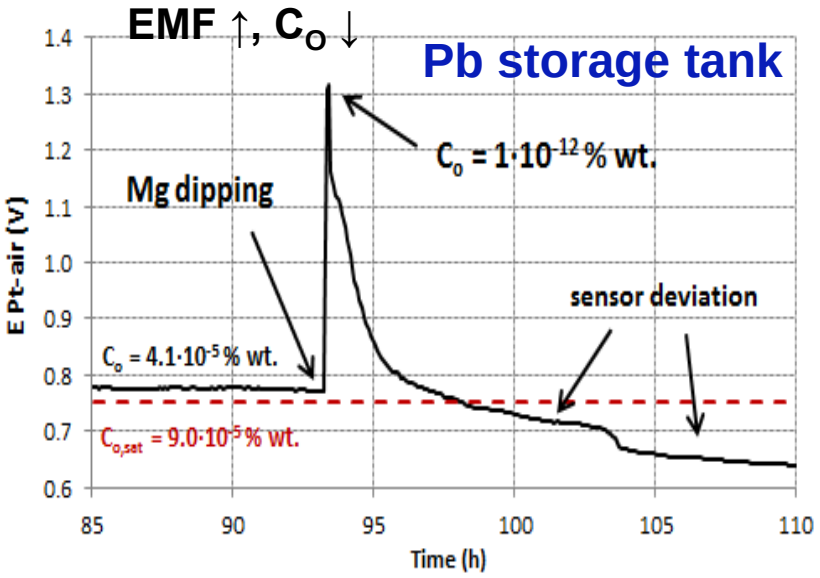
Mg showed some reactivity in Pb inside steel capsules. For Ta, Ti and Zr no difference with white test (competitive reaction with steel walls?)





Pb ≈ 285 L Mg pellets ≈ 98.4 g inside meshed cartridge 150 µm mesh

Pb storage tank





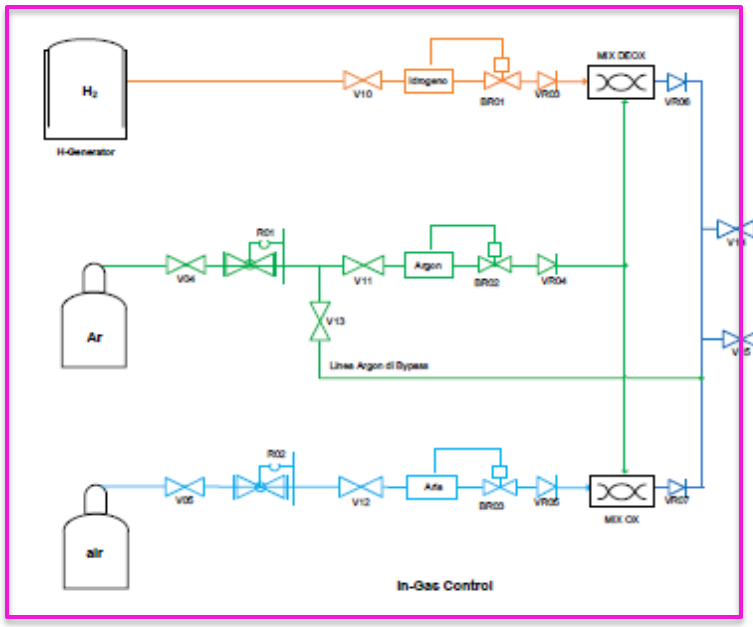
slug formation and sensor fouling. high reactivity of Mg due to fast evaporation.

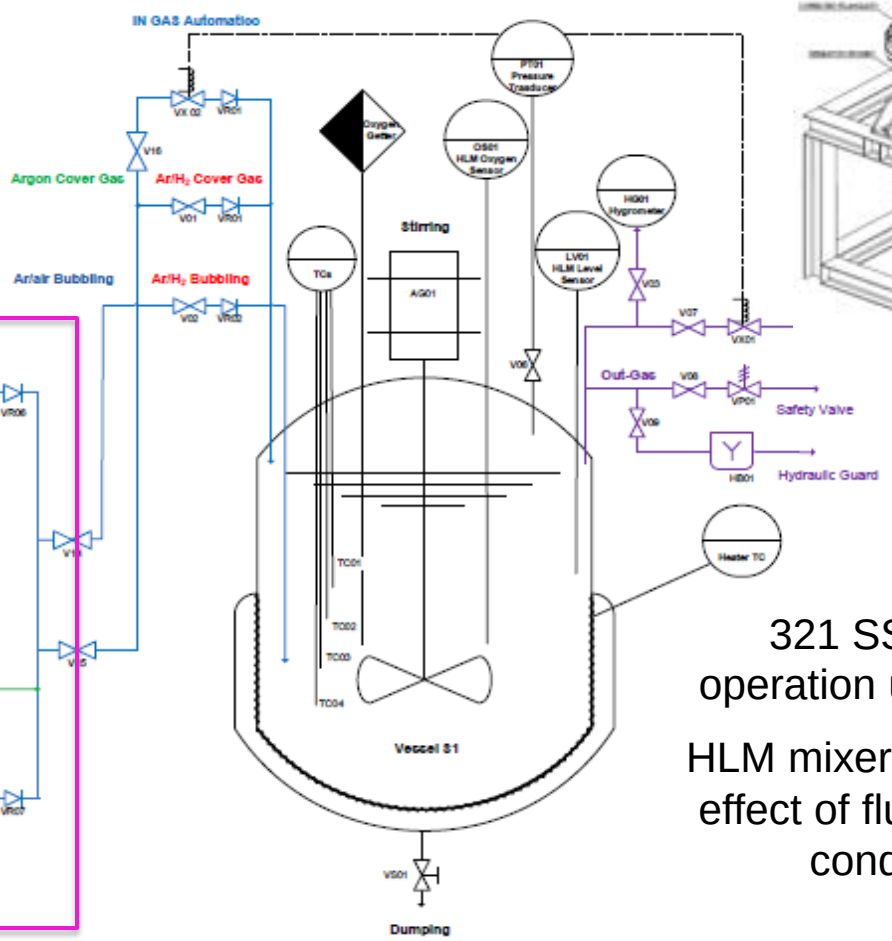
BID1 SMALL POOL (Pb)

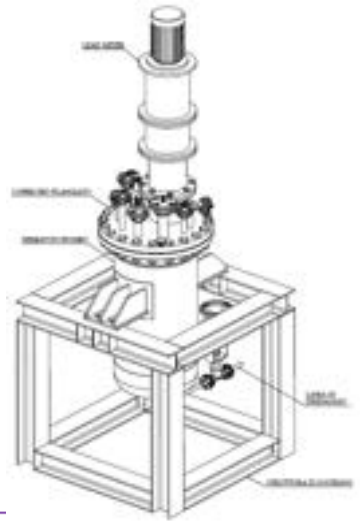
BID1 “Brasimone gas Injection Device”

Small pool (Pb ≈150 L) to test oxygen control methods:

- H_2 and O_2(air) injection
- oxygen getters
- buffer H_2/H_2O cover gas
- oxygen sensors performance







321 SS for the operation up to 550◦C

HLM mixer to study the effect of fluid-dynamic conditions

OCS with Ar-H_2 + Ar-O_2 injection foreseen also for NACIE-UP and LECOR loop

SUMMARY

- **Oxygen sensors** and **oxygen control devices** are essential instruments in LFR and ALFRED to avoid PbO formation and reduce corrosion of unprotected components.
- **Baseline study** on different **oxygen sensors** was carried out. The **min. reading T** is mainly influenced by the **reference system**:

  Min. reading T: Pt-air (400◦C) > Bi/Bi_2O_3 (300◦C) > Cu/Cu_2O (200◦C)
  Cu/Cu_2O is subjected to powder sintering → addition of inert powders, e.g. YSZ or GDC
  Also the solid electrolyte has influence (YTSZ vs YPSZ)

- **Oxygen sensor prototype for large HLM pool** was developed and tested with success. Current Pt-air configuration has a **min. reading T ≈ 380◦C**, ok for the application where T > 400◦C (storage tank and Pb systems).
- **HLM deoxygenation** was successfully achieved in **small capsules, storage tank and loop facility** with **Ar-H_2 gas** and using developed sensors. A dedicated **gas control system** was implemented.

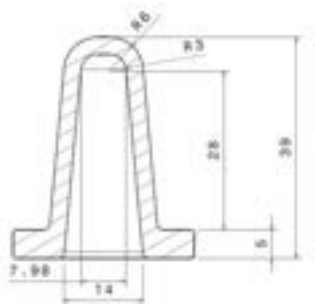
  Main limiting step in HLM deoxygenation with H_2 is related to oxygen diffusion in HLM bulk and poor HLM mixing. The increase of H_2 % or T_{HLM} promote the process with minor effect.

- Between **Mg, Ta, Ti and Zr** elements, only **Mg exhibited oxygen getter capability** in Pb during screening tests in steel capsules. **Mg slug formation** was observed in Pb storage tank. Mg reactivity (very fast) is likely related to **evaporation**.

NEXT STEPS

- Test of new **reference systems for oxygen sensor** is required to have a reliable detection capability at low T (e.g. modified Cu/Cu_2O or air-perovskite system).
- Test of long **oxygen sensor up to 8 m long** in CIRCE pool, implementation with **different reference systems** and new **solid electrolyte**.

New design of the solid electrolyte in YPSZ (in place of YTSZ) to improve mechanical resistance →



- Implementation of the gas control systems for loops to have both **H_2 and O_2 injection,** to balance correctly the oxygen concentration and compensate for strong deviations (as occurred in NACIE-UP loop).
- Tests of H_2 and O_2 injection in **BID1 small pool,** conceptualized and designed to test various oxygen control methods.
- **New tests for oxygen getter screening** (new set-up to be arranged considering factors such as new shape of getter (powders?), new fluid-dynamic conditions (Pb flowing or mixed?) or the use of inert system (quartz capsules?).

S. Bassini, *"Coolant Chemistry Control in Heavy Liquid Metal cooled Nuclear Systems"*, PhD Thesis, UniBo, 2017.

A. Graldi, *"Heavy liquid metal deoxygenation with hydrogen gas mixtures in experimental facility storage tank"*, Master Thesis, UniBo, 2017.

S. Bassini, A. Antonelli, I. Di Piazza, M. Tarantino, *"Oxygen sensors for Heavy Liquid Metal coolants: Calibration and assessment of the minimum reading temperature"*, J. Nucl. Mater. 486 (2017) 197-205.

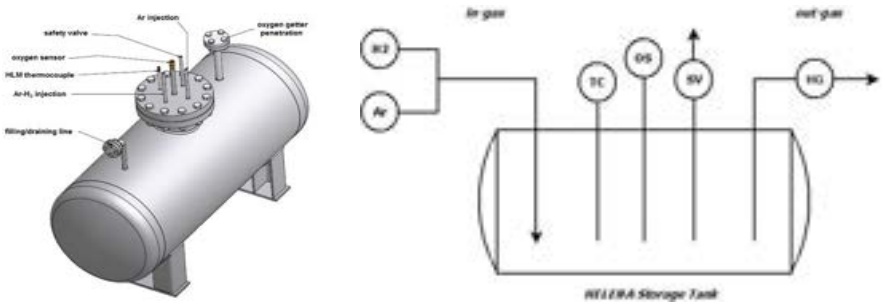
RACHEL Lab

REACTIONS AND ADVANCED CHEMISTRY FOR LEAD

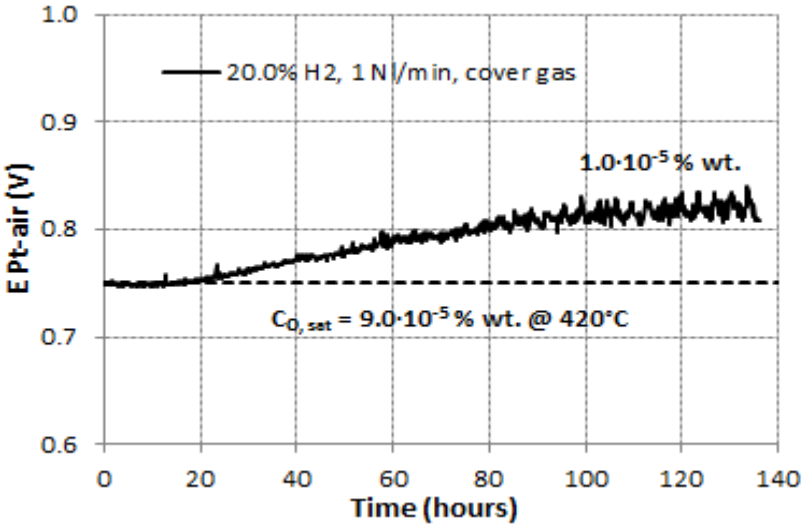


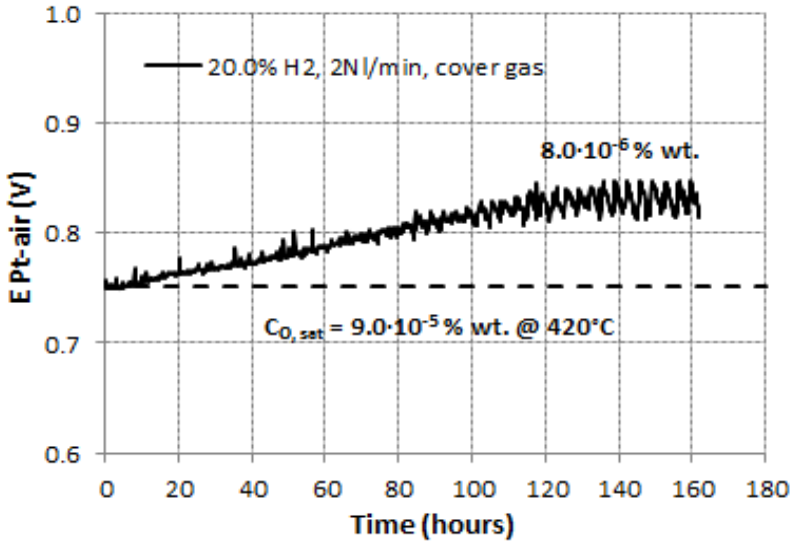
THANK YOU FOR THE ATTENTION

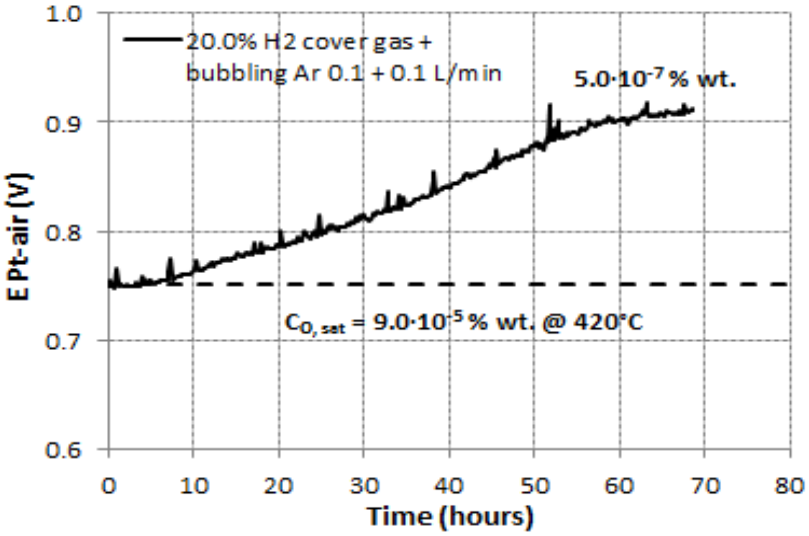
DEOXYGENATION WITH H_2: STORAGE TANK (COVER GAS MODE)



Mode	T_{Pb} (°C)	H_2 (% vol.)	Gas flow rate (NL/min)
Cover	420	20.0 ± 0.3	1
Cover	420	20.0 ± 0.1	2
Cover + Bubbling Ar	420	20.0 ± 0.1	2 + (0.1 + 0.1 bubbling Ar)



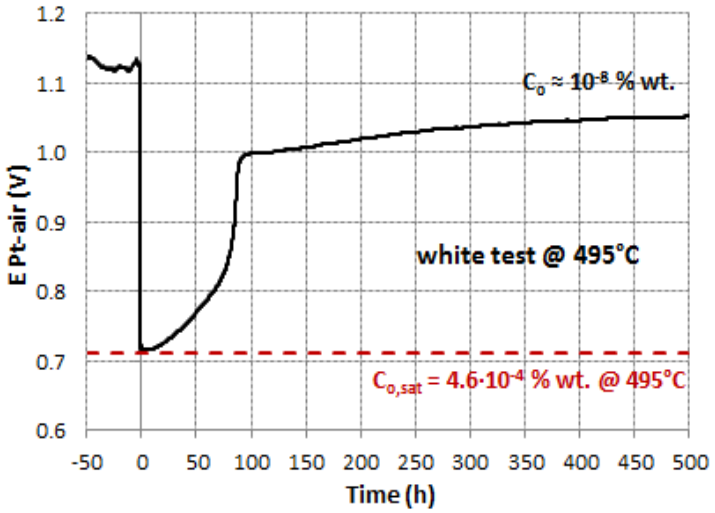


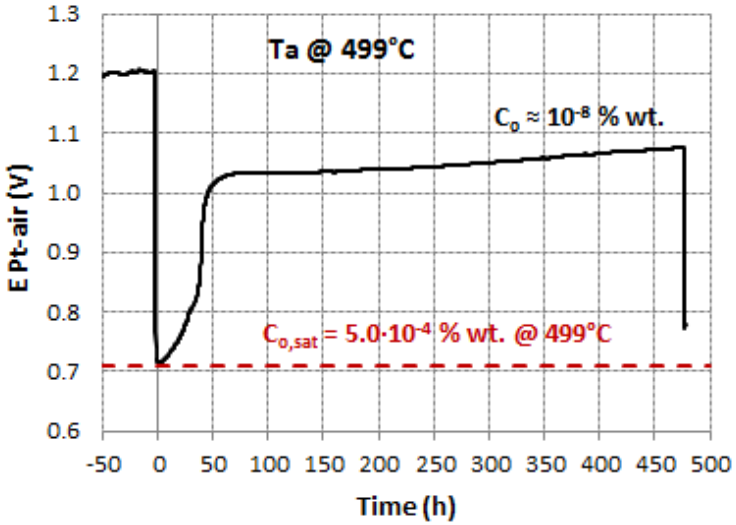


OXYGEN GETTER SCREENING (LAB SCALE, STEEL CAPSULES)

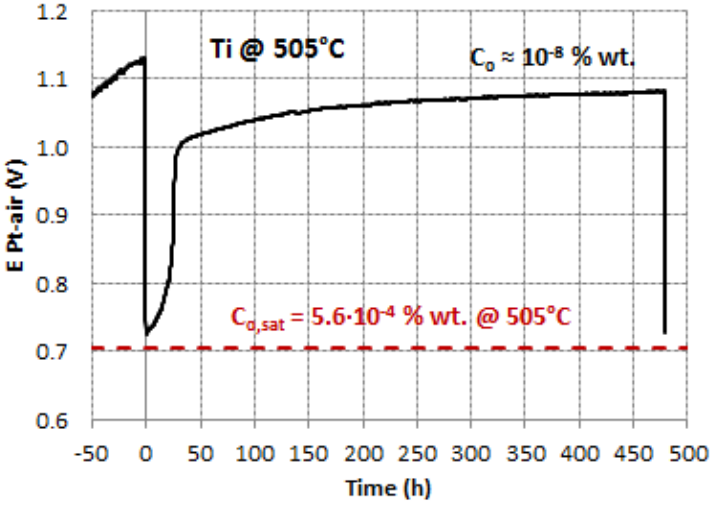


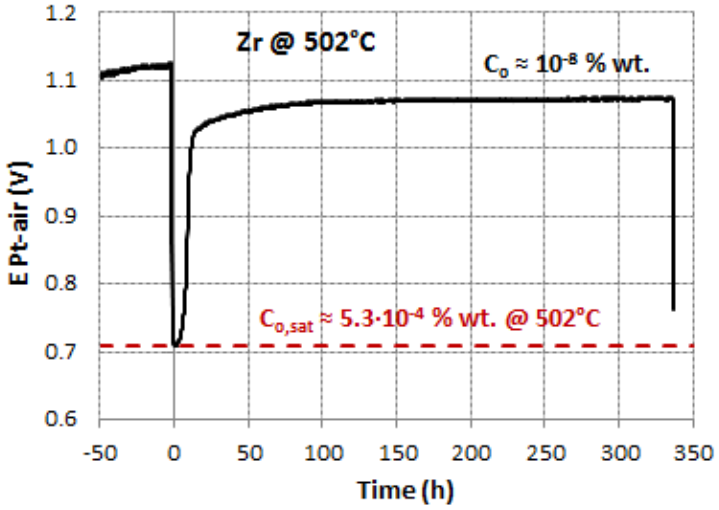






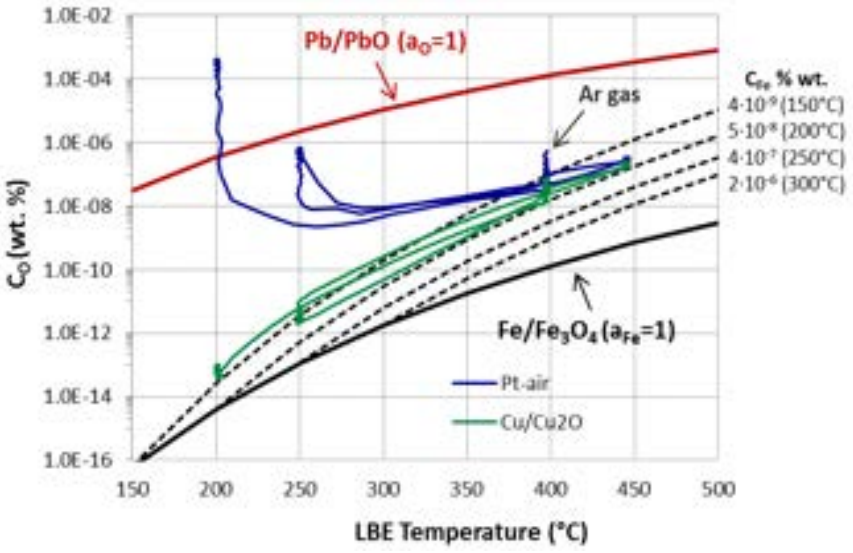
Pb ≈ 780 g, OG wire 35 mm





no weight change observed for Ta, Ti and Zr

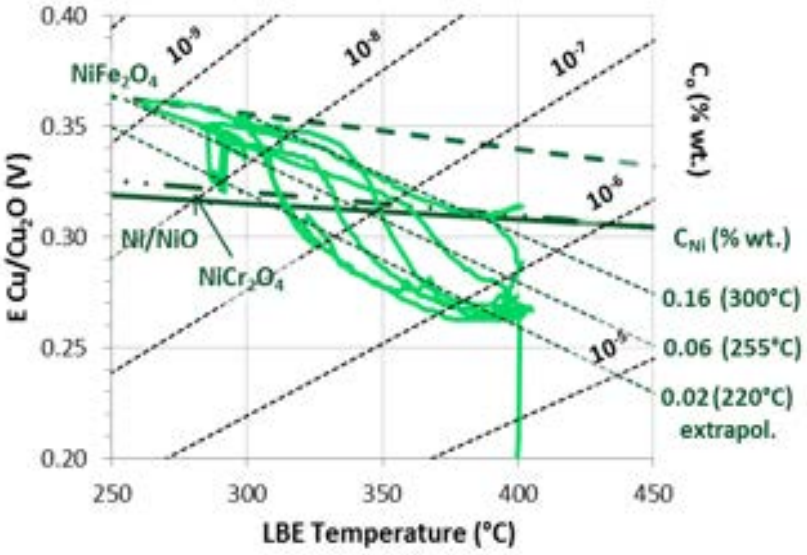
EFFECT OF METAL IMPURITIES ON OXYGEN CONTROL



C_O monitored by Cu/Cu_2O sensor during a test in static fresh LBE, T=200-450◦C identified equilibrium (impurity):

$$\frac{3}{4}Fe_{\,solid} + PbO_{\,diss} \leftrightarrow \frac{1}{4}Fe_3O_{4\,solid} + Pb_{\,liq}$$

with $a_{Fe}=1$



analysis of Cu/Cu_2O sensor output during deoxygenation in LBE loop, T=250-400◦C hypothesis of equilibrium (corrosion product):

$$\frac{3}{4}Ni_{solid} + \frac{1}{2}Fe_3O_{4\,solid} + PbO_{diss} \leftrightarrow \frac{3}{4}Fe_2NiO_{4\,solid} + Pb_{\,liq}$$

with $a_{Ni}=1$

formation of a M_xO_y from dissolved metal M involves oxygen consumption during HLM cooling → effect on the control of the oxygen concentration → need of (i) a quantitative prediction of corrosion products formed and (ii) design of a cold trap

Italian National Agency for New Technologies,
Energy and Sustainable Economic Development

GENERATION IV LEAD COOLED FAST REACTOR
STATO ATTUALE DELLA TECNOLOGIA E PROSPETTIVE DI SVILUPPO
ADP MiSE-ENEA (PAR2016-LP2)

Scuola di Ingegneria e Architettura, Università di Bologna
26-27 Settembre, 2017

Produzione e caratterizzazione dell'acciaio di guaina 15-15 Ti

M. Angiolini

massimo.angiolini@enea.it

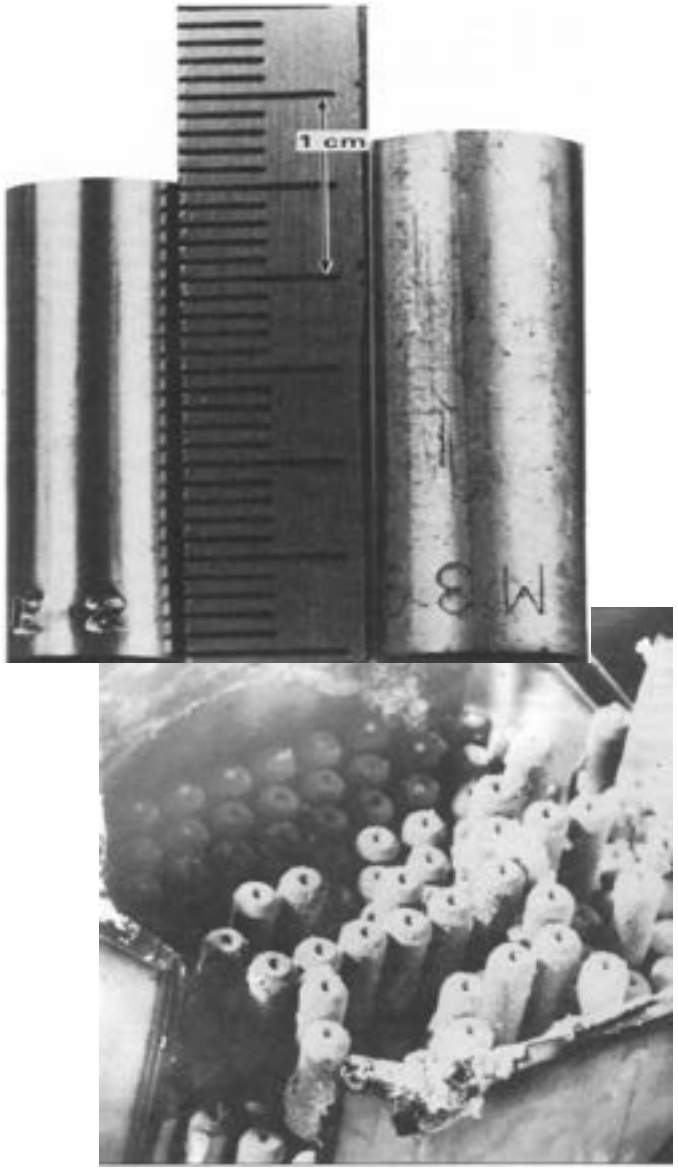
Introduction

- ✓ AIM1 is at present the reference material for the realization of ASTRID and benefits from a large feed-back from the previous French SFRs
- ✓ Able to resist in Na at 480-700°C & 110 dpa (swelling)
- ✓ PLD alumina coated 15-15 Ti AIM1 steel is the reference material for the realization of the core internals of the ALFRED reactor (550° 80 dpa)
- ✓ Qualifying the materials regarding the specificities of the ALFRED core
- ✓ Testing of the AIM1+PLD Al2O3 coating
  - ❖ Resistance to irradiation
  - ❖ Corrosion
  - ❖ Creep
  - ❖ Fretting
- ✓ Restore the production know-how

Swelling

Swelling is a form of irradiation induced dimensional instability associated to the nucleation and growth of vacancies voids

- ✓ general increase of the size of components
- ✓ structure distortions due to gradients in dose, dose rate and temperature
- ✓ affect transport and thermal hydraulics
- ✓ embrittlement

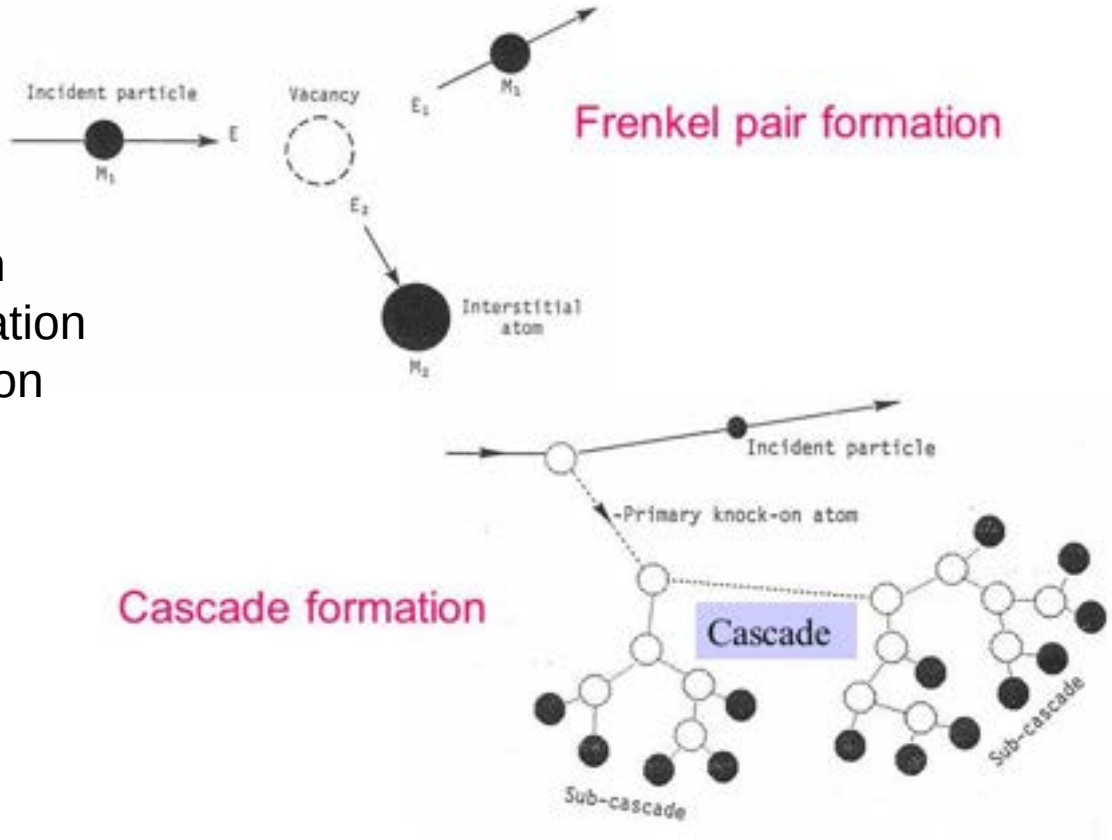


Neutron radiation damage

- Neutrons impact the material's atoms (PKA) that in turn produce displacement cascades i.e. interstitial atoms and vacancies (Frenkel pairs)
- Vacancies and interstitial in part recombine, but part of them diffuse in the lattice

- Flank loops
- Dislocations
- Voids
- Radiation enhanced diffusion
- Radiation enhanced precipitation
- Radiation induced precipitation

- Swelling
- Embrittlement
- Loss of ductility



Development of radiation resistant steels

The AIM1 steel is the result of the optimization of composition and thermo-mechanical treatments starting from 316 SS

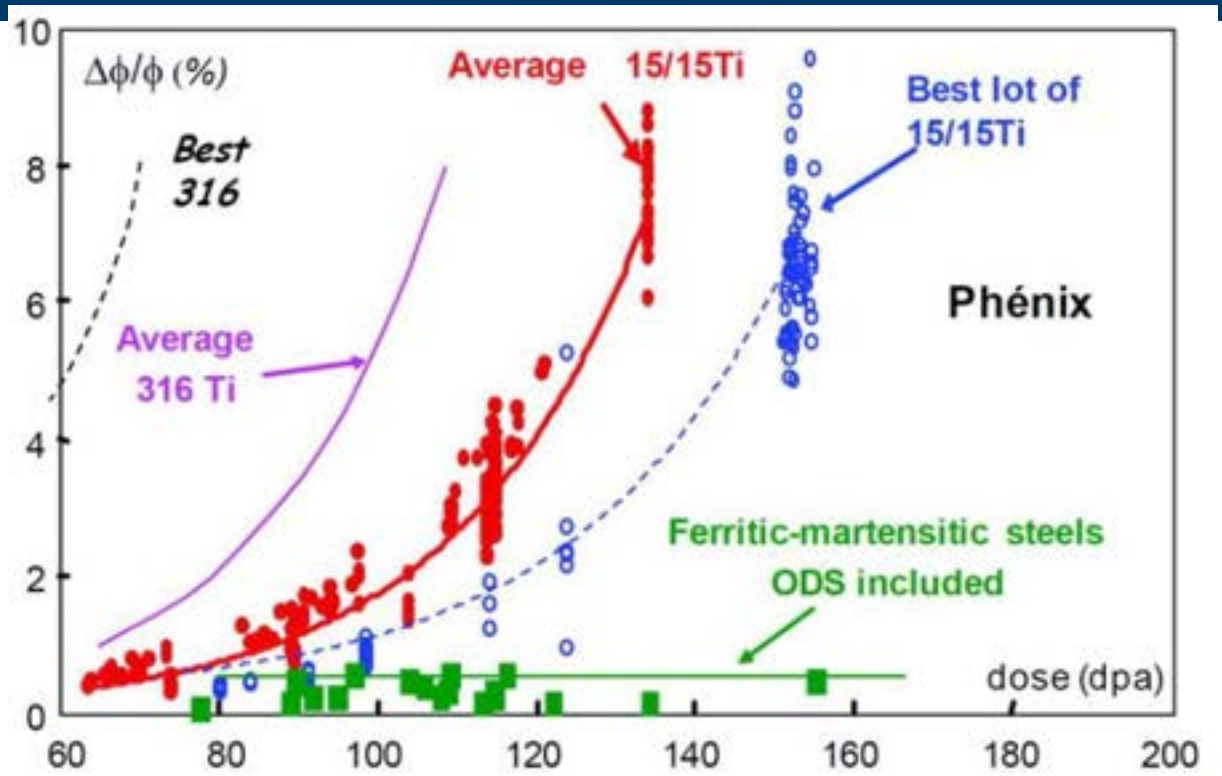
- to improve the resistance to irradiation swelling
- maintain suitable mechanical properties

The twofold objective is achieved by an alloy design with account for the following factors as demonstrated by the improvements obtained during the last decades:

- Optimization of the solid solution concentration of alloying (Cr Ni)
- Optimization of impurity elements (C, Ti, B, Si, P etc.) that form “point defect-impurity” complex
  - act as recombination centres
  - change the diffusion characteristics of the point defects
- Phase instability leading to secondary “in-service” precipitation, highly effective in
  - stabilizing the microstructure
  - influencing the process of point defects aggregates nucleation and growth
- Optimization of the density of dislocations acting as point defect sinks and effective in retarding the onset of intensive voids formation

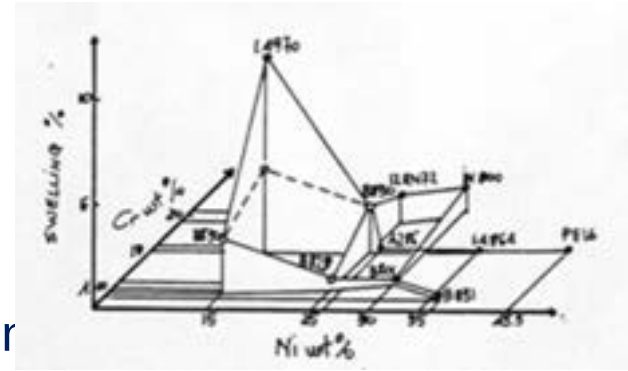
Development of radiation resistant steels

	SA 316	316 Ti	15–15Ti	Si-mod. 15-15 Ti
C	0,055	0,050	0,096	0,085
Cr	17,00	17,00	14,70	14,90
Ni	13,00	14,00	14,70	14,80
Mn	1,50	1,50	1,60	1,50
Mo	2,30	2,70	1,15	1,50
Si	<0,5	0,50	0,43	0,95
Ti	-	-	0,43	0,50
Fe	bal.	bal.	bal.	bal.



Δ / % vs dpa.
SA 316 => CW 15-15 Ti
increased by a factor 3 the subassembly life time

- Cold working
- Ni/Cr ratio optimization
- Minor element contents (C, Ti, Si, P) optimization



[Ni],[Cr] wt% vs. ΔV/ Δ %

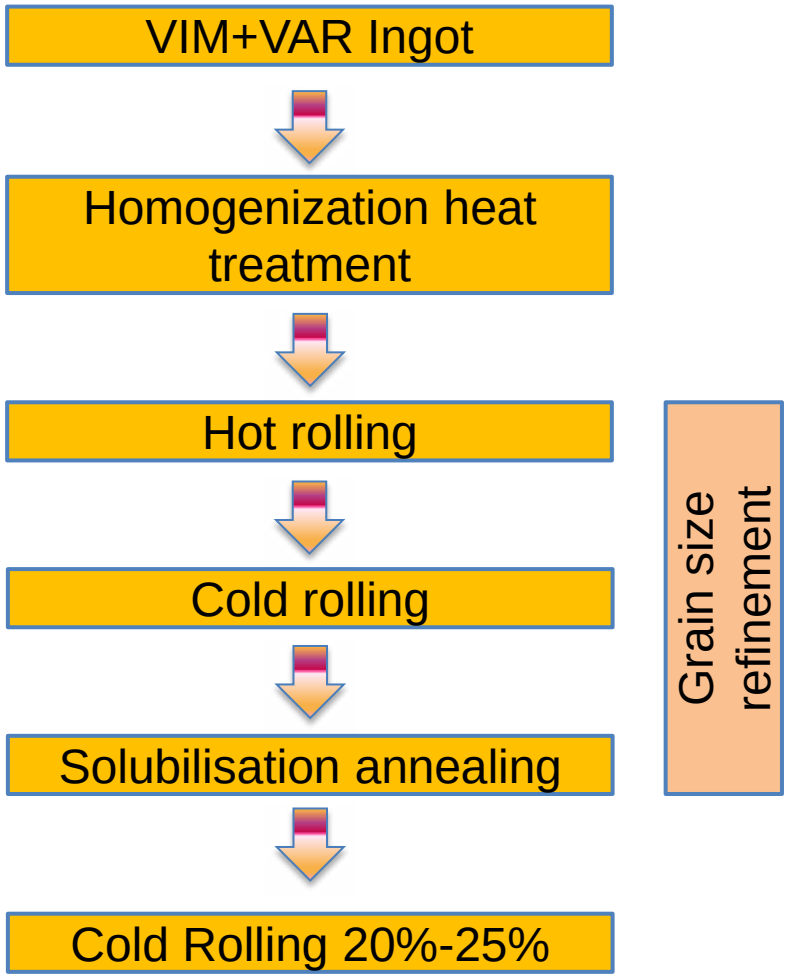
Development of radiation resistant steels

No Primary precipitation
- Reduce N content (0% ideal)
- Stabilization ratio [Ti]/[C]

Uniform distribution of the alloy components
- Solubilisation heat treatment
- Quenching

Optimal dislocations density
- Cold Work @20%-25%

Optimal grain size
- $6 \leq G \leq 9$



AIM1 Chemical composition

Wt %	Ottimale	Wt %	Ottimale
0,08 ≤ C ≤ 0,10		Zr ≤ 0,03	A.L.A.P.
14,0 ≤ Cr ≤ 16,0	14,5	W ≤ 0,03	‘’
14,0 ≤ Ni ≤ 16,0	15,5	V ≤ 0,03	‘’
1,0 ≤ Mn ≤ 2,0		Cu < 0,03	‘’
1,3 ≤ Mo ≤ 1,7		Co ≤ 0,03	‘’
0,30 ≤ Ti ≤ 0,5	(Ti/(4 C)) ≥ 1,0	Ca ≤ 0,02	‘’
Nb + Ta ≤ 0,03		Sb ≤ 0,005	‘’
0,70 ≤ Si ≤ 0,9	0,85	Sn ≤ 0,005	‘’
0,003 ≤ B ≤ 0,007	B ≥ 0,004	O ≤ 0,01	‘’
0,03 ≤ P ≤ 0,05	0,045	Fe il resto	
N < 0,015	A.L.A.P.		
S ≤ 0,01	‘’		
Al < 0,015	‘’		

VIM + VAR Fusione in forno ad induzione sotto vuoto seguita da rifusione in forno ad arco sotto vuoto

AIM1 thermo-mechanical processing

- ✓Trattamento termico di omogeneizzazione in fornace a 1200 ≥ T ≥ 1250 ° C per un tempo da ottimizzare (microstruttura 100% austenitica)

- ✓Laminazione a caldo @ T > 1000 ° C per la riduzione dello spessore
- ✓Laminazione a freddo
- ✓Ricottura di solubilizzazione a 1100 ≤ T≤ 1200 ° C per un tempo da ottimizzare

Ottimizzazione grain size 6 ≤ G ≤ 9 AFNOR NF/A 104- 02

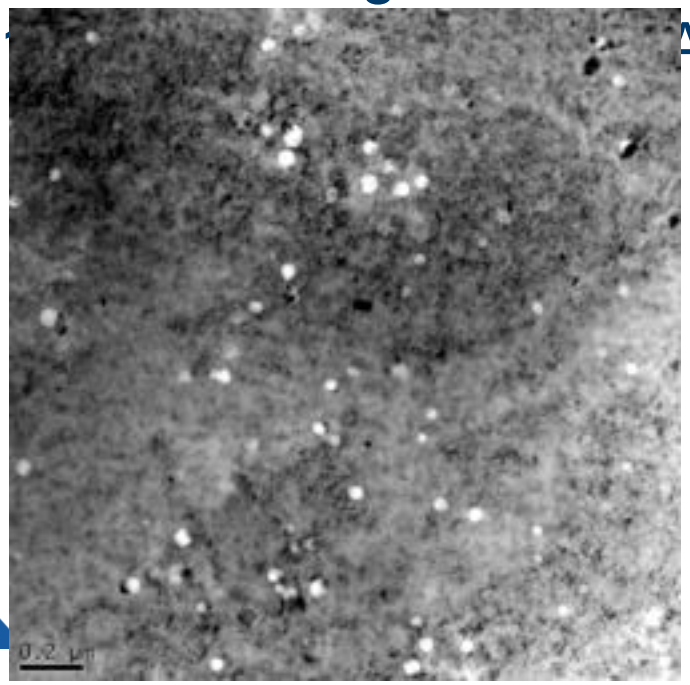
- ✓Tempra con velocità di raffreddamento tale da passare dalla temperatura di ricottura a 500°C in meno di 10 minuti primi
- ✓Laminazione a freddo per ottenere piastra incrudite al 20-25% dello spessore finale di 15 mm

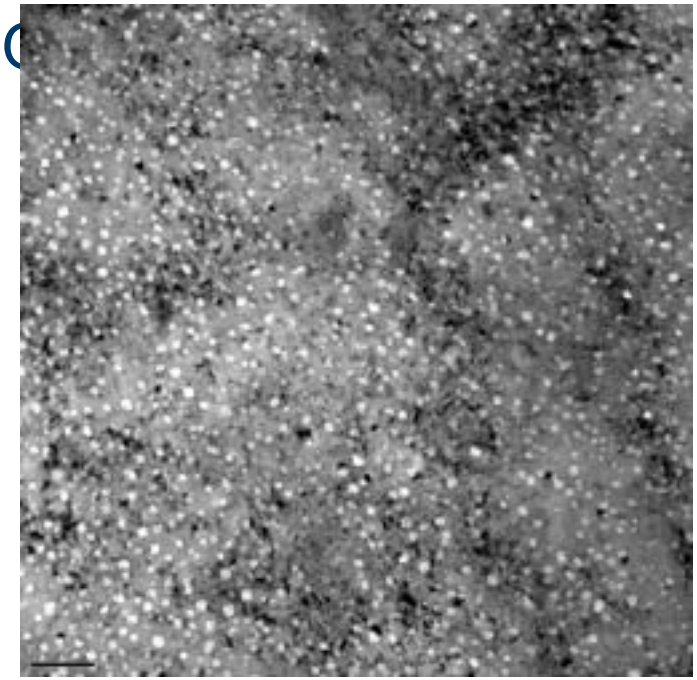
Prodotto finale con caratteristiche simili ai tubi di guaina incruditi

AIM1 specifications

CARATTERISTICHE DELLE PIASTRE DOPO LA LAMINAZIONE A FREDDO

- ✓100% Austenitic microstructure.
- ✓Grain size 6 ≤ G ≤ 9 in agreement with AFNOR NF/A 104-02
- ✓620 ≤ $Rp_{0,2}$ ≤ 840 MPa in agreement with AFNOR NF/A/ 49-851
- ✓Rm ≥ 760 MPa in agreement with AFNOR NF/A/ 49-851
- ✓Atot ≥ [illegible] AFN[illegible]





Sommario

- Nell'ambito delle attività di R&D collegate alla realizzazione del reattore ALFRED si è proceduto all'approvvigionamento di acciaio di tipo AIM1
- L'AIM1 è un acciaio resistente all'irraggiamento messo a punto nello sviluppo dei reattori al sodio
- E' al momento il candidato per la costruzione delle camicie del combustibile del reattore ASTRID
- L'AIM1 ricoperto con allumina PLD è anche il materiale di riferimento per le camicie del combustibile e le scatole esagonali di ALFRED
- Il materiale verrà impiegato per attività di testing e qualifica dei componenti rivestiti con allumina PLD
- Rappresenta un primo passo per ristabilire la filiera produttiva di questo acciaio in vista della realizzazione di ALFRED

Grazie per l'attenzione

massimo.angiolini@enea.it

Structural Material Development & Qualification for ADS/Fast Reactor Application

C. Cristalli, L. Pilloni, S. Storai (ENEA)

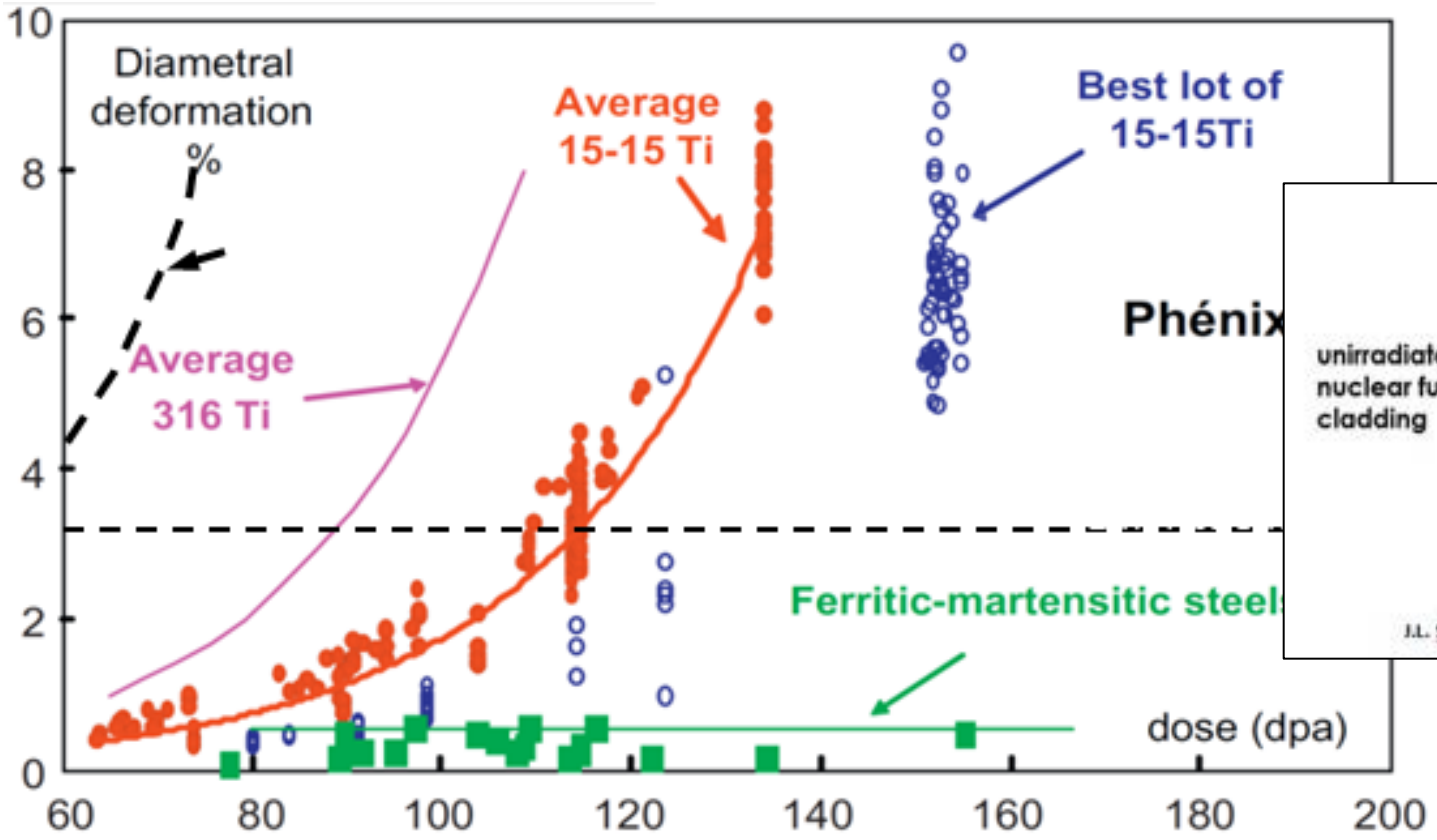
Workshop tematico
Bologna, 27th Settembre 2017

Contents

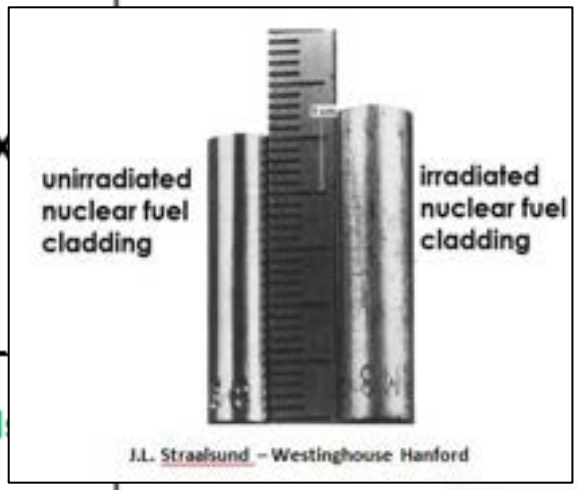
- Introduction about the challenge of swelling reduction and the development of the DS steels
- Neutron irradiation results (1988, Saclay)
- Production of a new DS4 plate(2014, ENEA-CSM)
- Status of the on going characterization of the new plate (ENEA-Brasimone)

Introduction

The challenge of swelling reduction; beyond 15-15 ?



[Séran et al.]



Introduction

At the beginning of the ‘80s, within an experimental program carried out at the Saclay Center, the under electrons irradiations (1 MeV) have shown the effectiveness of the simultaneous presence of Ti and Nb on the swelling resistance of 316 and 15 Cr-15 Ni matrix.

Development of the **First Generation** of Double Stabilized Steels:

316DS

15-15DS

In the first generation double stabilized steels the annealing temperature used, 1125° C, didn’t result sufficient to obtain a good solubilization of “free” Ti and Nb also because of the high stabilization ratio.

Revision of the composition

Stabilization Ratio :

$$R = \frac{[Ti] + [Nb] - [N]}{[C]}$$

Birth of the **2nd Generation** Double Stabilized steels:

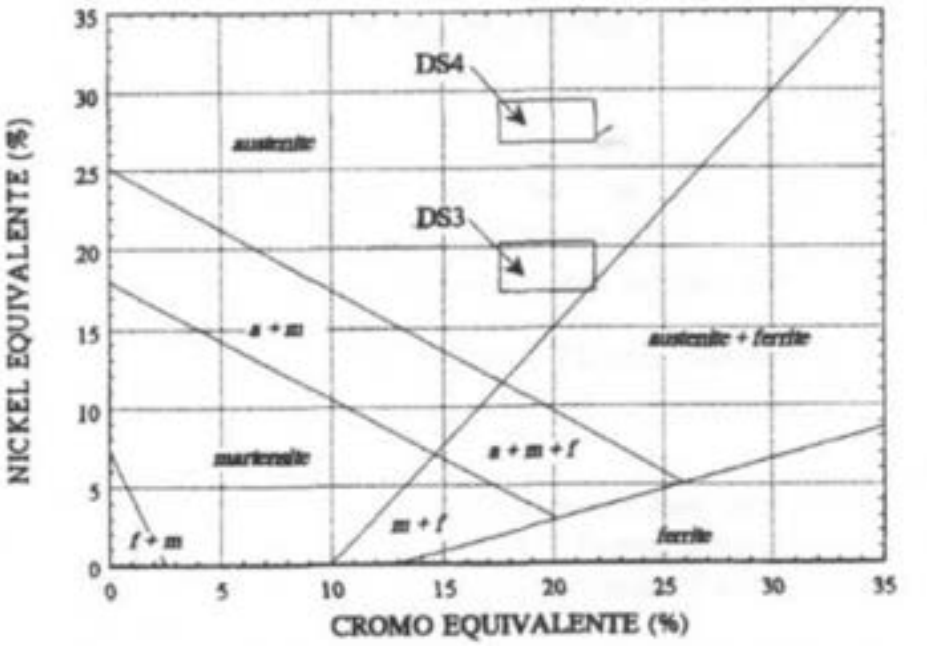
DS3 (15Cr-15Ni)

DS4 (15Cr-25Ni)

DS5(15Cr-25Ni)

Production of the first batch of DS alloys (2nd gen) in the late 80s

Position into the Shaffler's diagram



Manufacturing Details

Two kinds of products realized:

- rods (external diameter 8 mm)
- cladding pipes (ext. diam. 6,55 mm, internal 5,65)

The rods and the pipes were **cold-worked** with a final section reduction ratio of **20%**.

Annealing temperature before final cold-working : **1100° C** (5 minutes in Argon atmosphere), followed by air cooling.

Mechanical Characterization (1990): tensile & creep

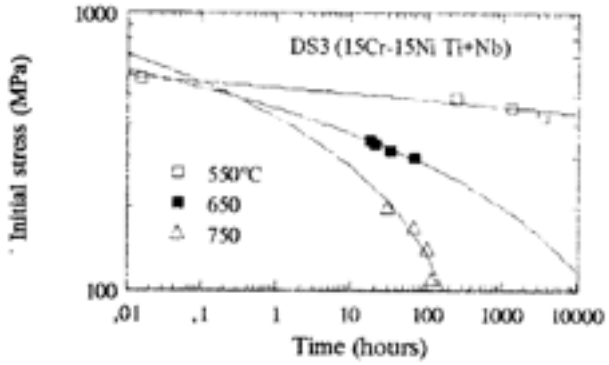
Fitting of data

Fitting function:

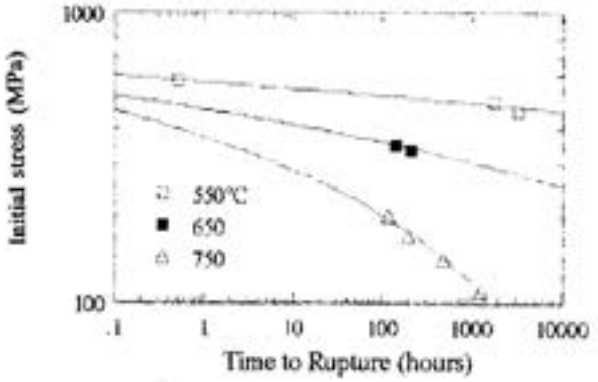
$$t = K \cdot exp(-\gamma \cdot \sigma)$$

G. Filacchioni, L. Pilloni and oth. «Mechanical and structural behaviour of the second double stabilized steels generation», B.N.E.S. London,1990

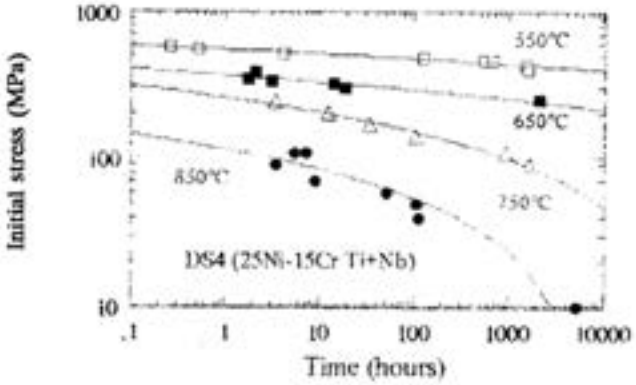
Time to obtain 0.2% of creep strain; DS3



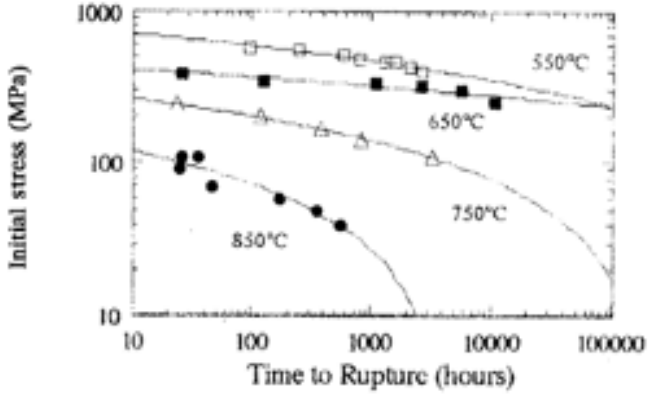
Time to failure; DS3



Time to obtain 0.2% of creep strain; DS4



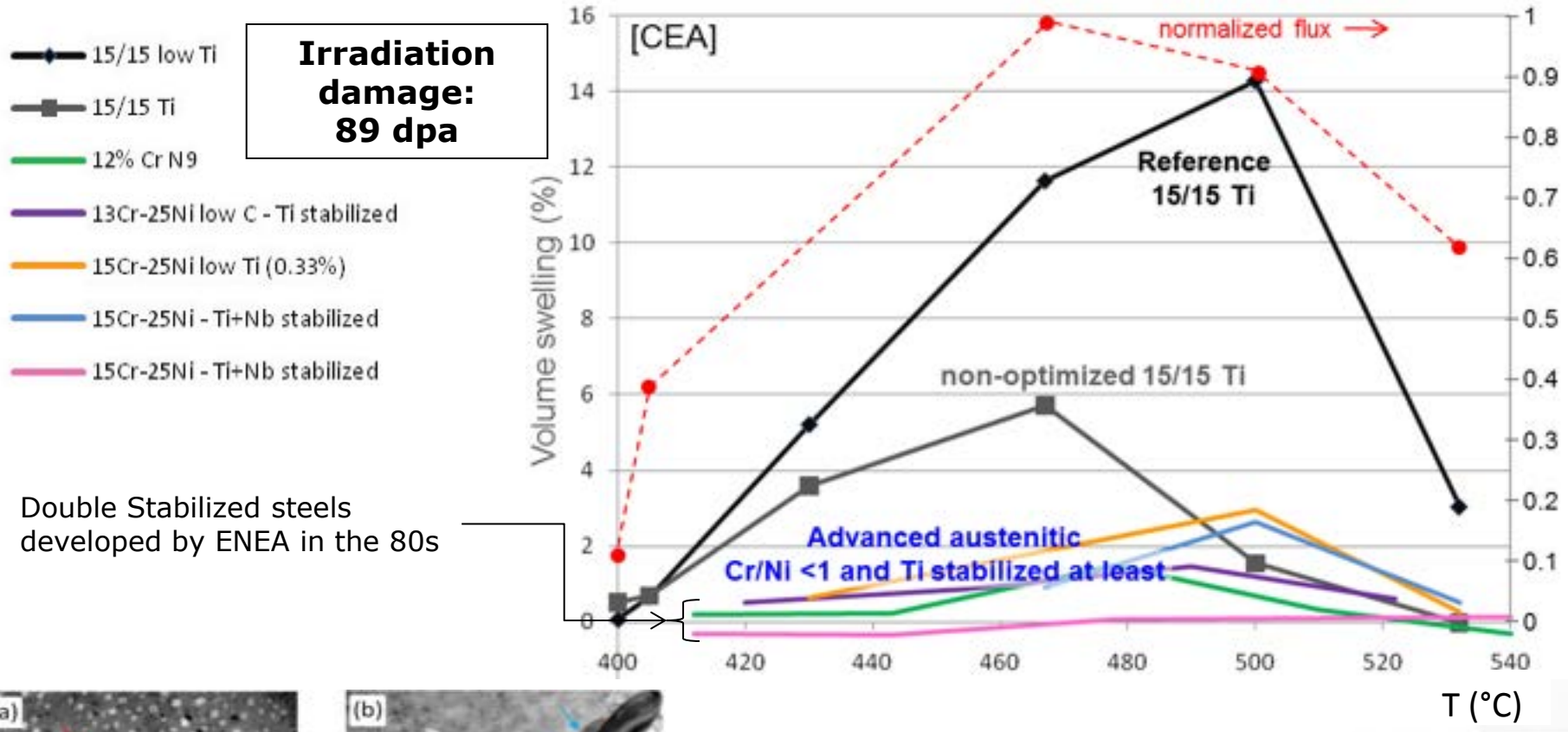
Time to failure; DS4



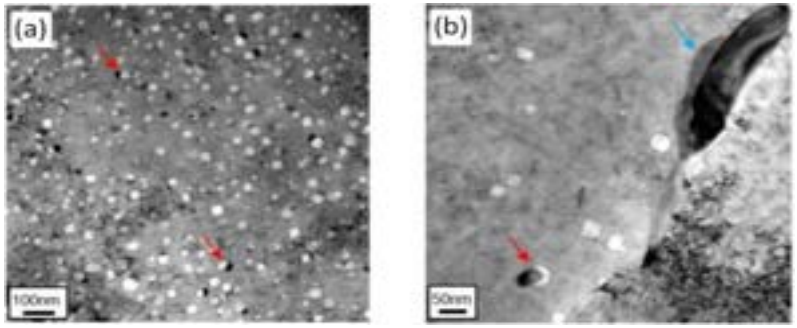
Irradiation Results

Irradiation Tests at Saclay: the results of the experience « Supernova »

Irradiation damage: 89 dpa



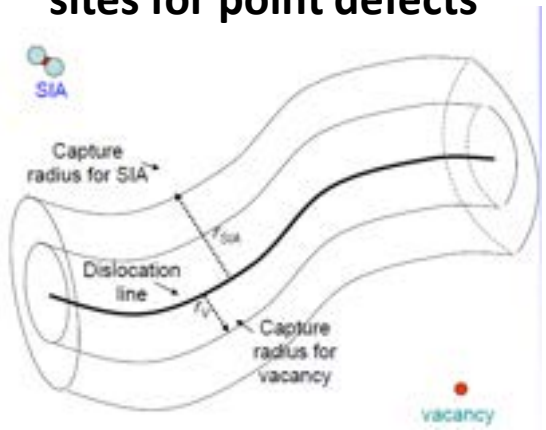
Double Stabilized steels developed by ENEA in the 80s



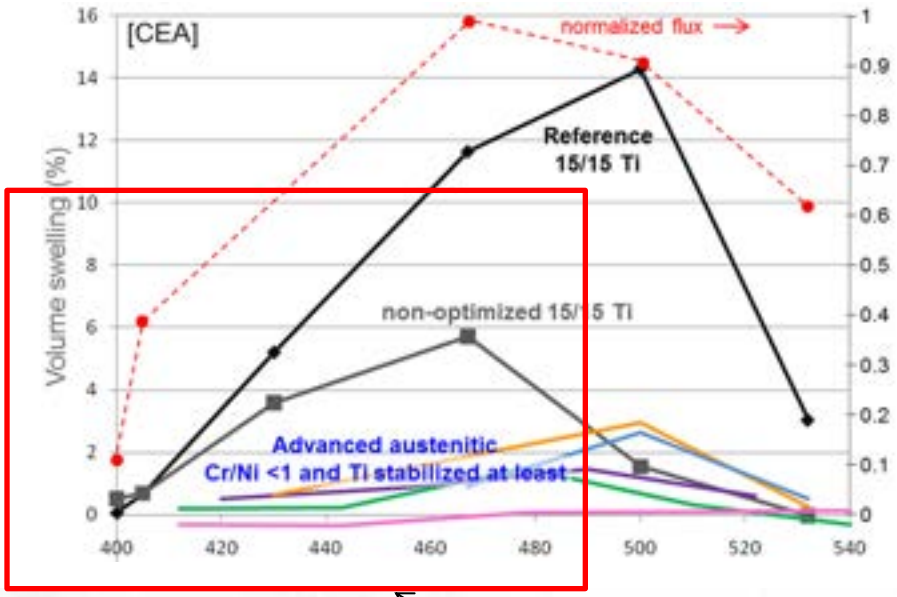
Low amount of cavities in the advanced austenitic stainless steel (b) if compared to the non-optimized 15-15 Ti (a)

Factors affecting swelling reduction

Beneficial effect 1: Dislocation act as sinks; recombination sites for point defects



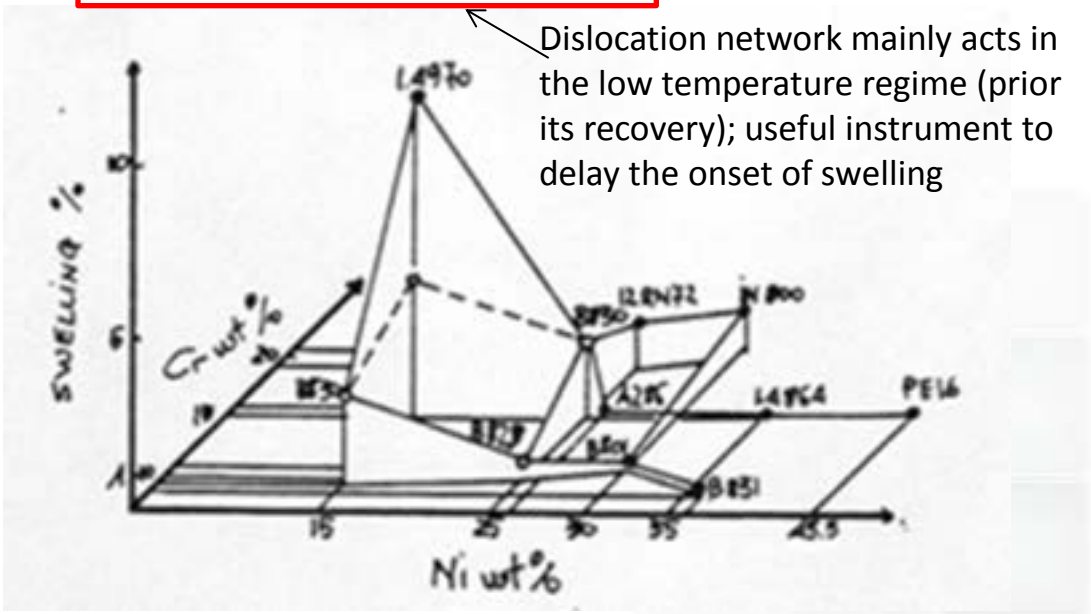
20% c.w.



Dislocation network mainly acts in the low temperature regime (prior its recovery); useful instrument to delay the onset of swelling

Beneficial effect 2: Effect of Ni content on swelling

25% Ni

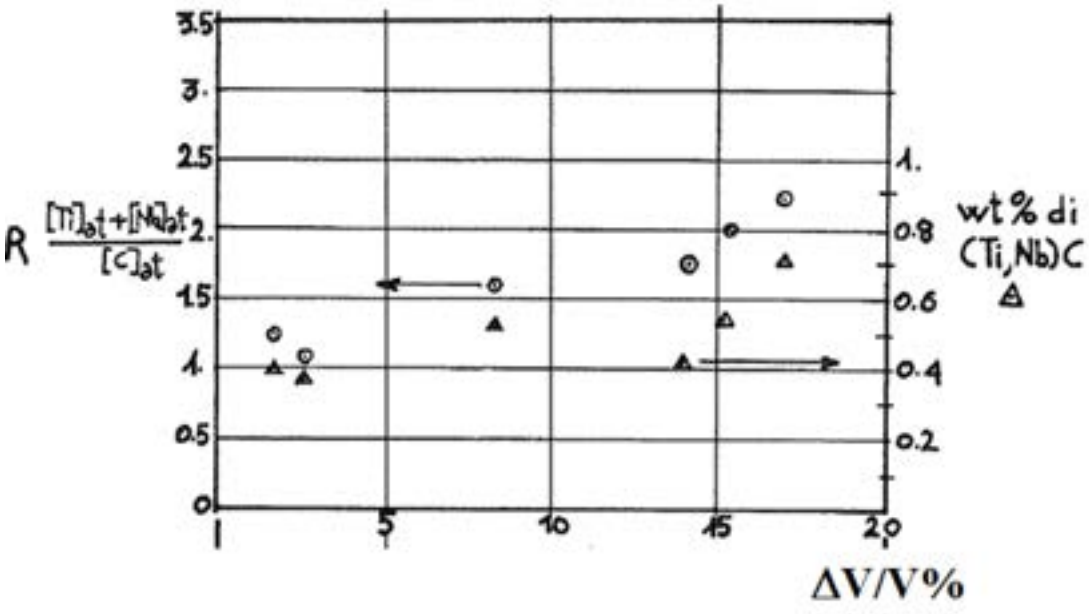


Factors affecting swelling reduction

Beneficial effect 3: Double Stabilization; how primary and secondary precipitation of carbides affect swelling

A good high temperature creep resistance for an austenitic steel is essentially due to microprecipitation of carbides which result finely dispersed on the dislocations network;

- Primary precipitation, the one occurring during the annealing heat treatment of the steel. Low primary precipitation means sufficient "free" contents of Carbon, Ti and Nb in solid solution in order to allow a secondary (in service) beneficial precipitation.
- Secondary, so-said "in-service" precipitation, occurring during operation inside the reactor. This sort of "in-service" precipitation is highly effective as movement inhibitor for linear defects..

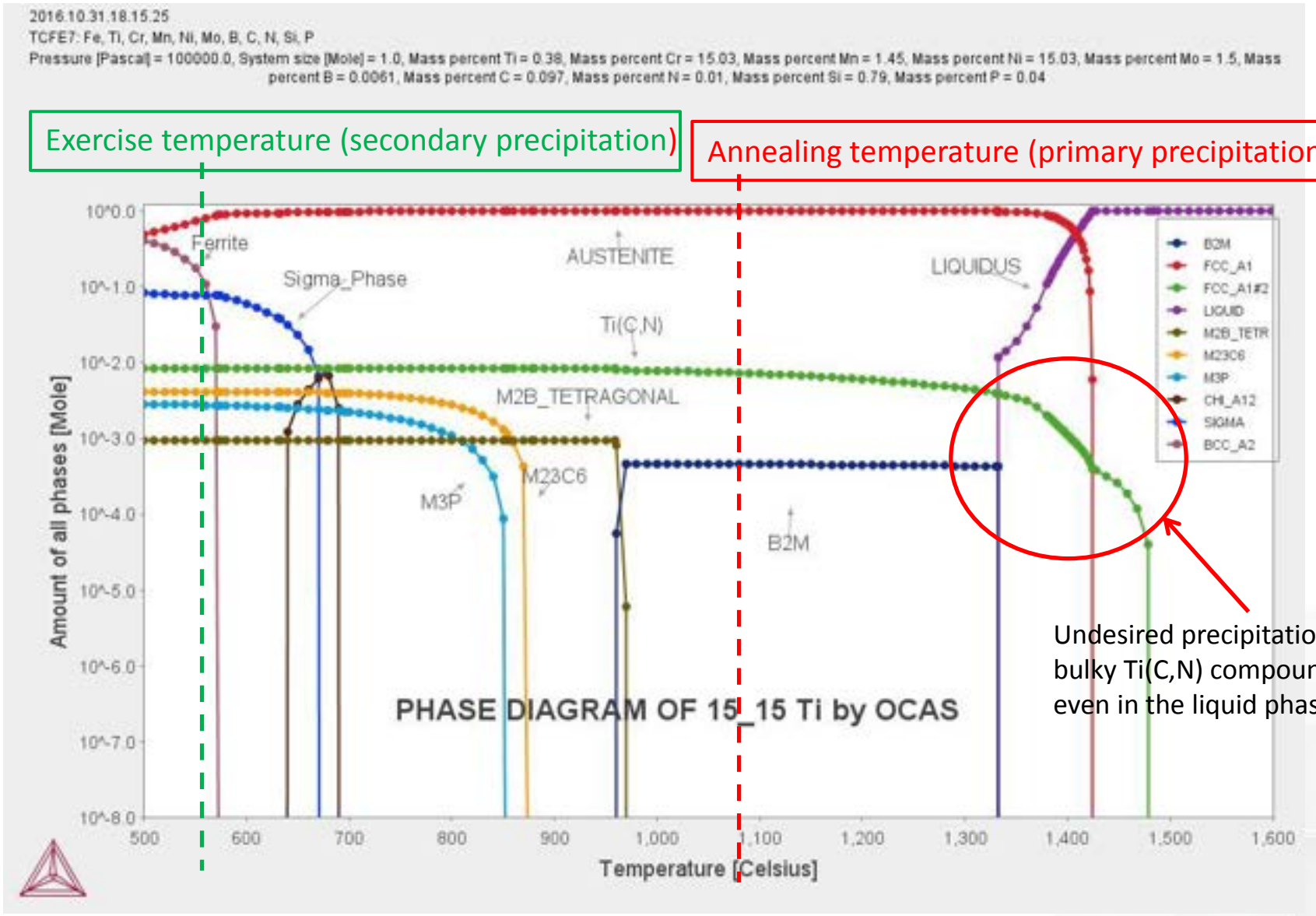


15-15DS; 105dpa, Tirr=450° C

The precipitation of carbides doesn't only act on the creep resistance of the material; it also has positive effects on the stability under irradiation. Here's a graphical investigation of the first 90's about the dependence of swelling attitude on the primary precipitation and on the stabilization ratio for a 15Cr-15Ni matrix. As long as the primary precipitation is kept low (keeping the stabilization ratio close to 1) the secondary (highly desirable) precipitation is fostered and the limited swelling attitude is a consequence.

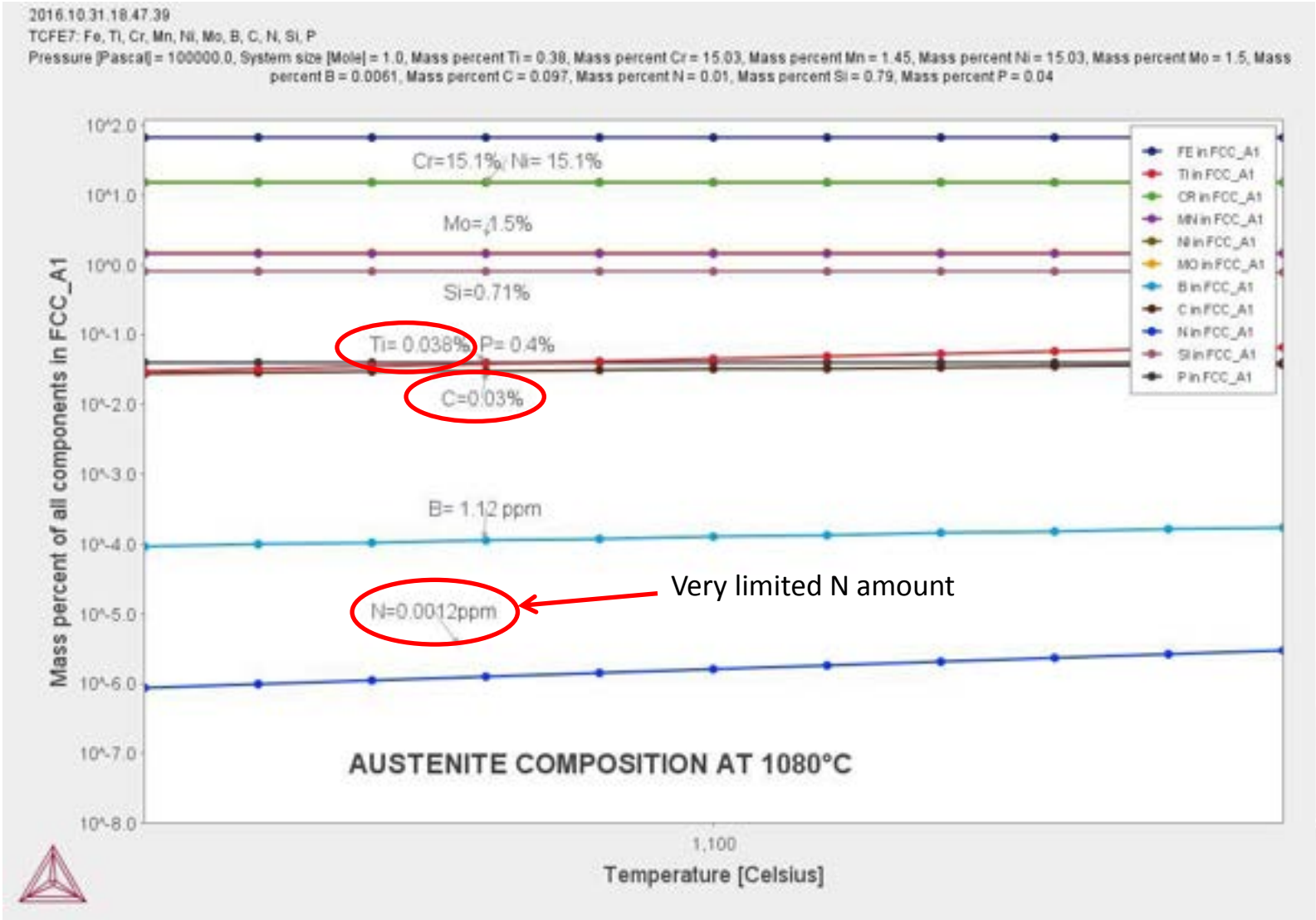
L. Pilloni; internal ENEA report, restricted distribution

15-15 Ti; Phase Diagram according to Thermocalc

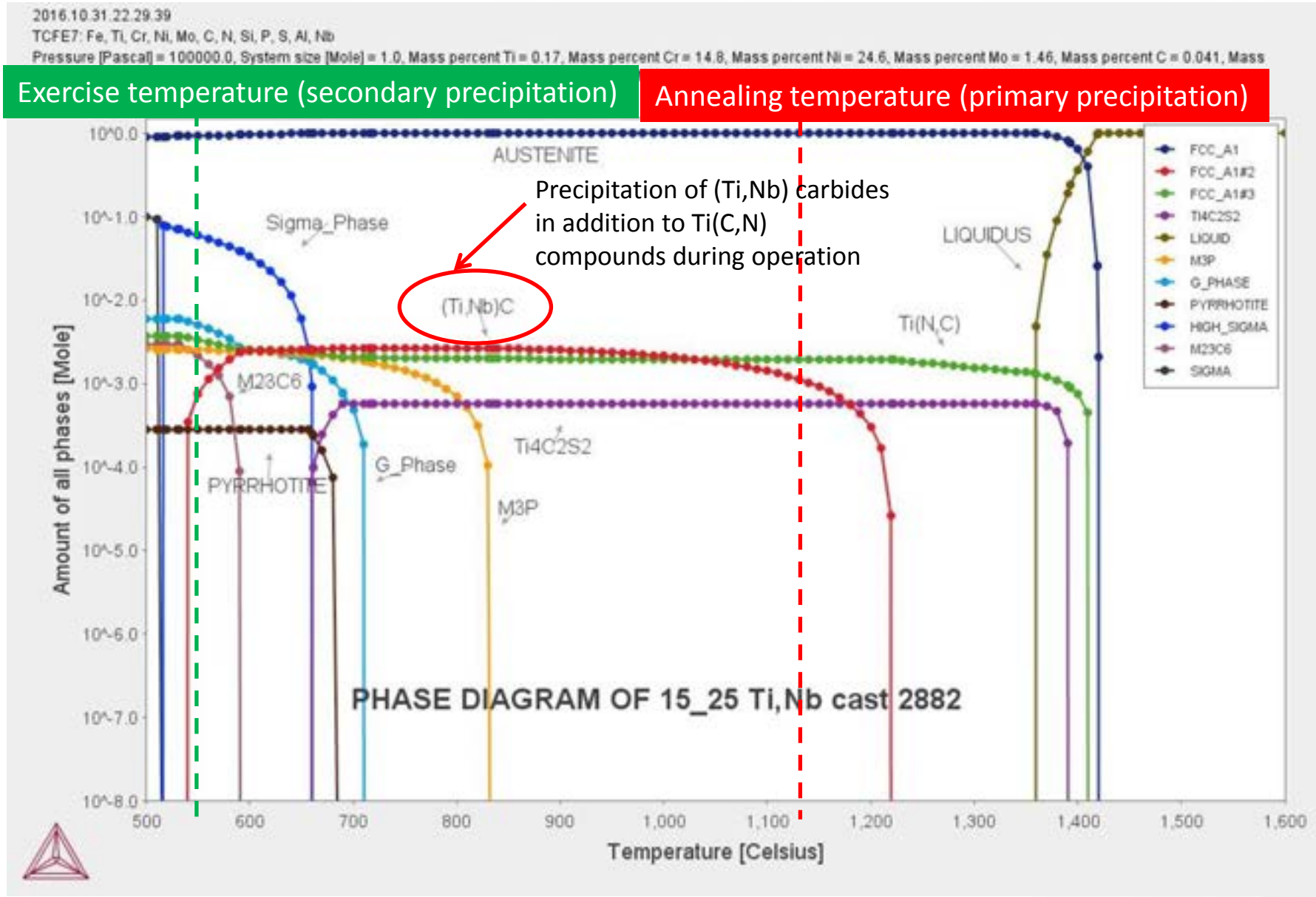


15-15 Ti; Phase Diagram according to Thermocalc

Available contents of carbo-nitride forming elements in the Austenite phase at the annealing temperature (1080 ° C)

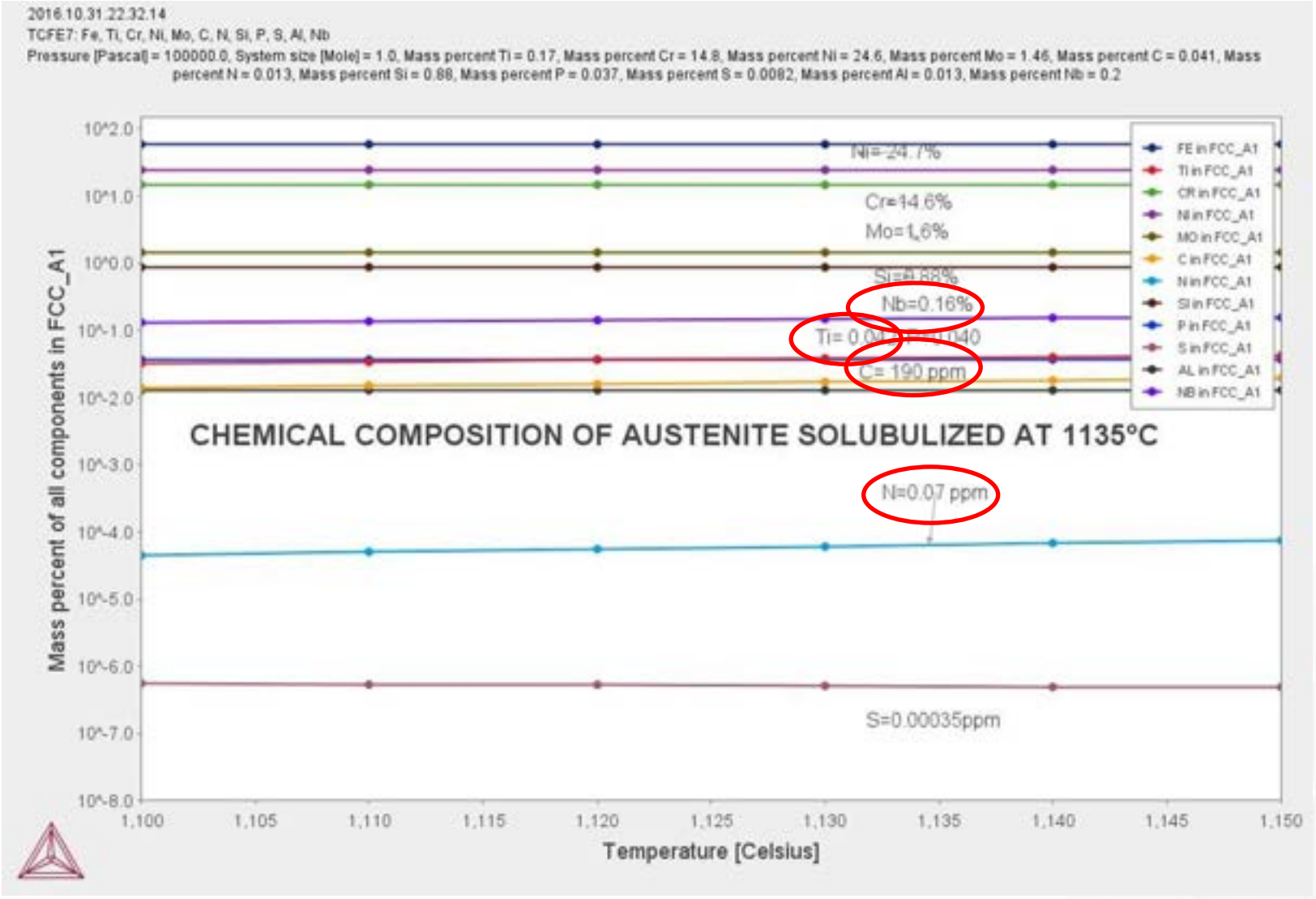


DS4; Phase Diagram according to Thermocalc



DS4; Phase Diagram according to Thermocalc

Increased available contents of carbo-nitride forming elements in the Austenite phase at the annealing temperature (1135 ° C)



2014 - Production DS4 plate



Production of a new DS4 ingot in 2014



Hot rolling of the ingot (Pre-heating -1200° C)



After last hot rolling stage (919° C) 20 mm thickness

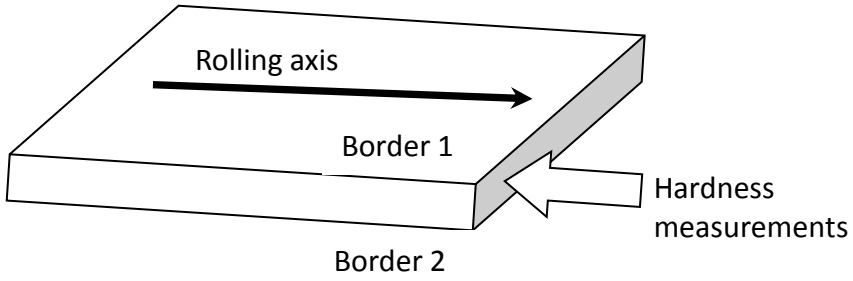
Solubilization annealing 1135° C

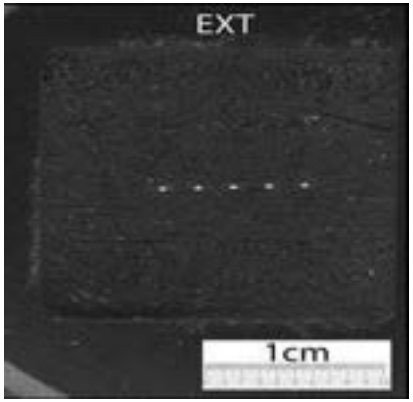
Cold working up to 15 mm thickness



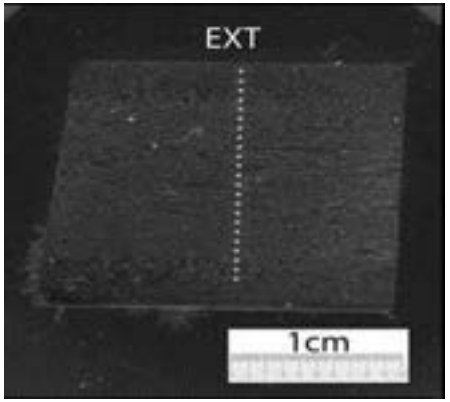
«waving» on the rolling direction due to 20% c.w.

Production of DS4 plate; Hardness measurements

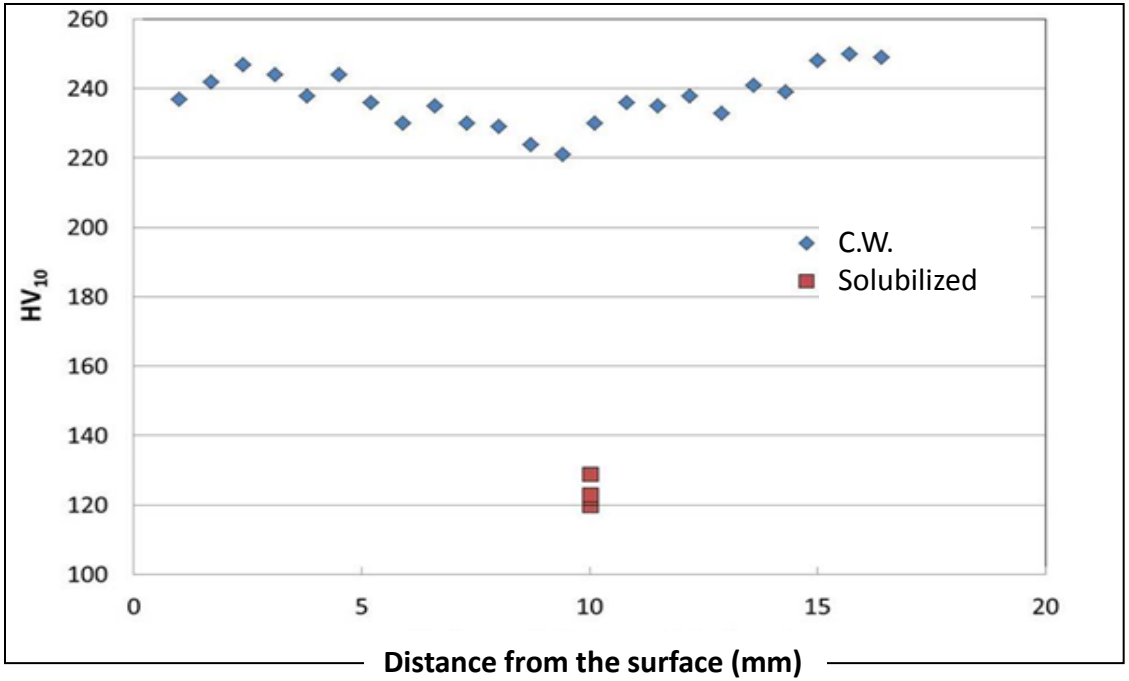




solubilized
(T-L direction)



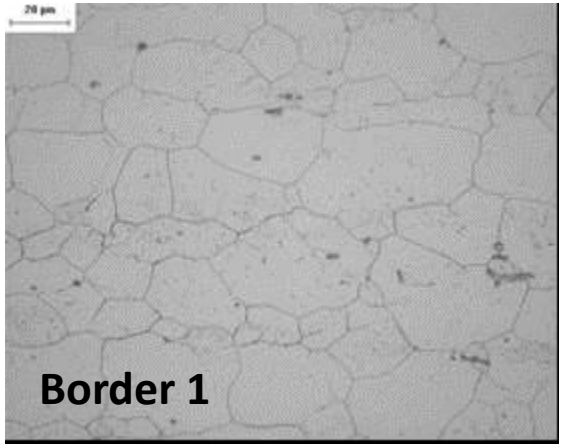
Cold worked
(L-T direction)

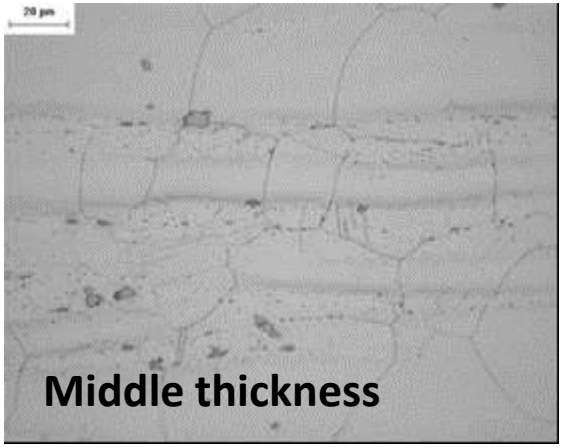


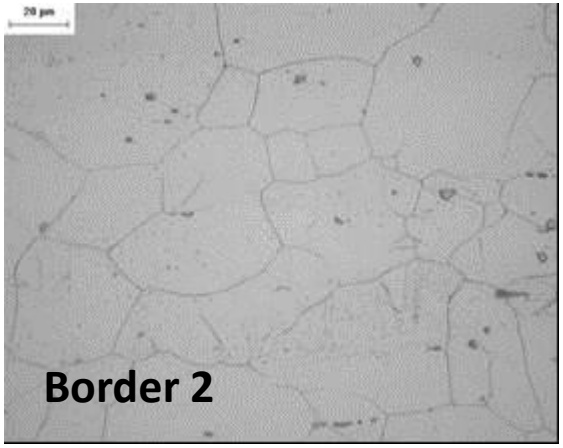
80s batch (DS4): 260 HV

Grain Size (32-45 m in the 80s batch)

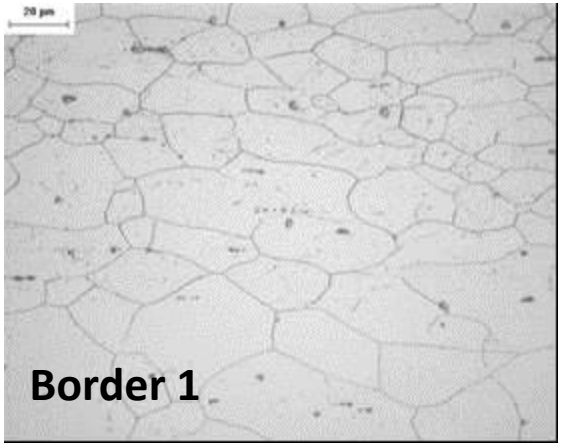
After solubilization

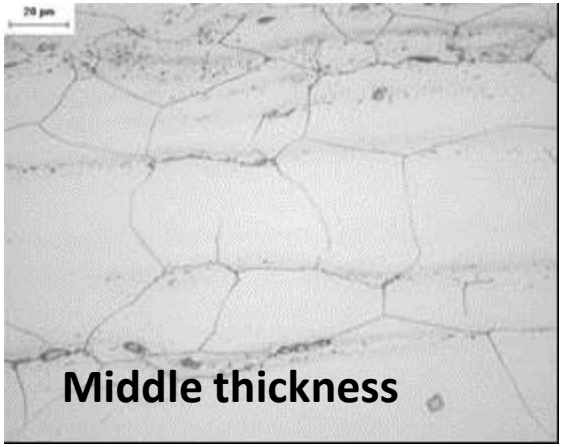


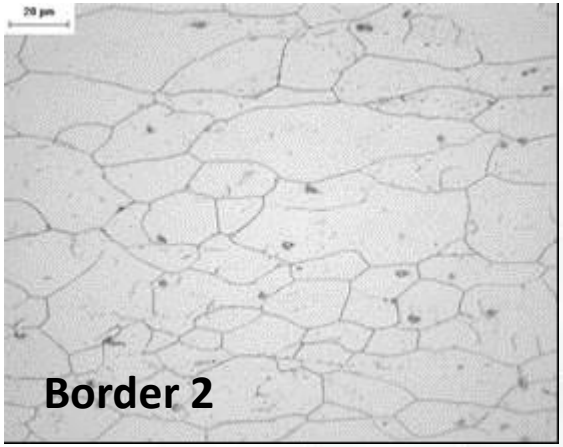




After 20% c.w.

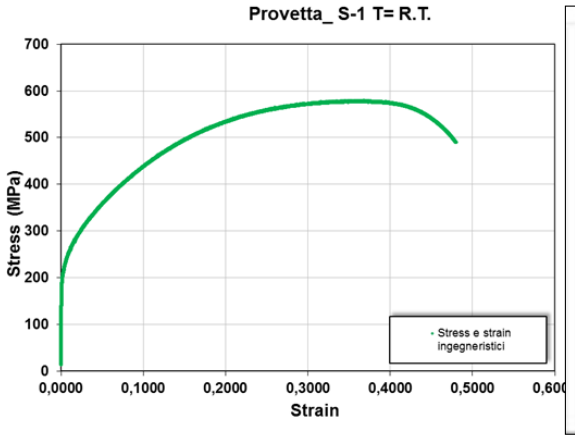


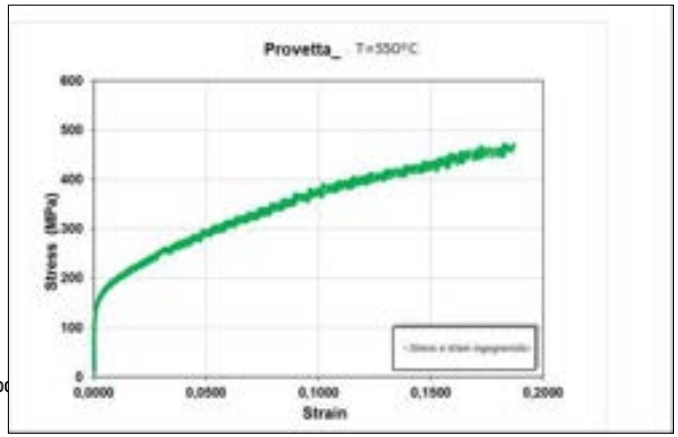


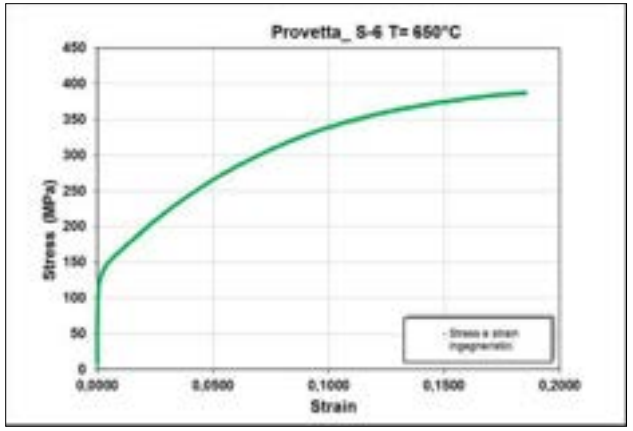


Tensile Properties; qualitative comparison

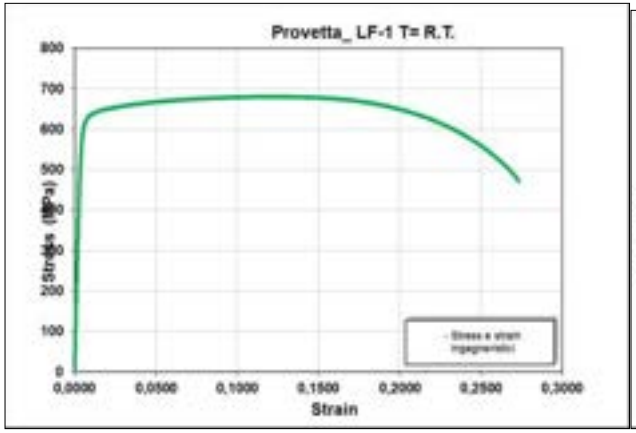
Solubilized Material (RT, 550° C, 650° C)

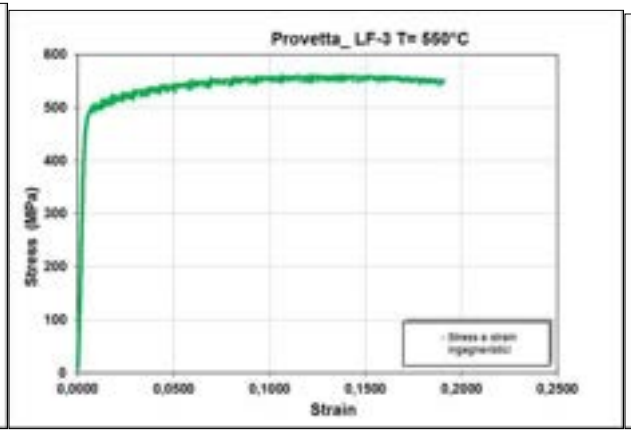


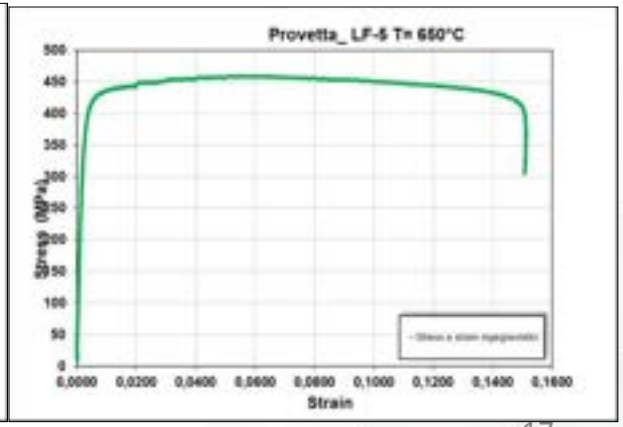




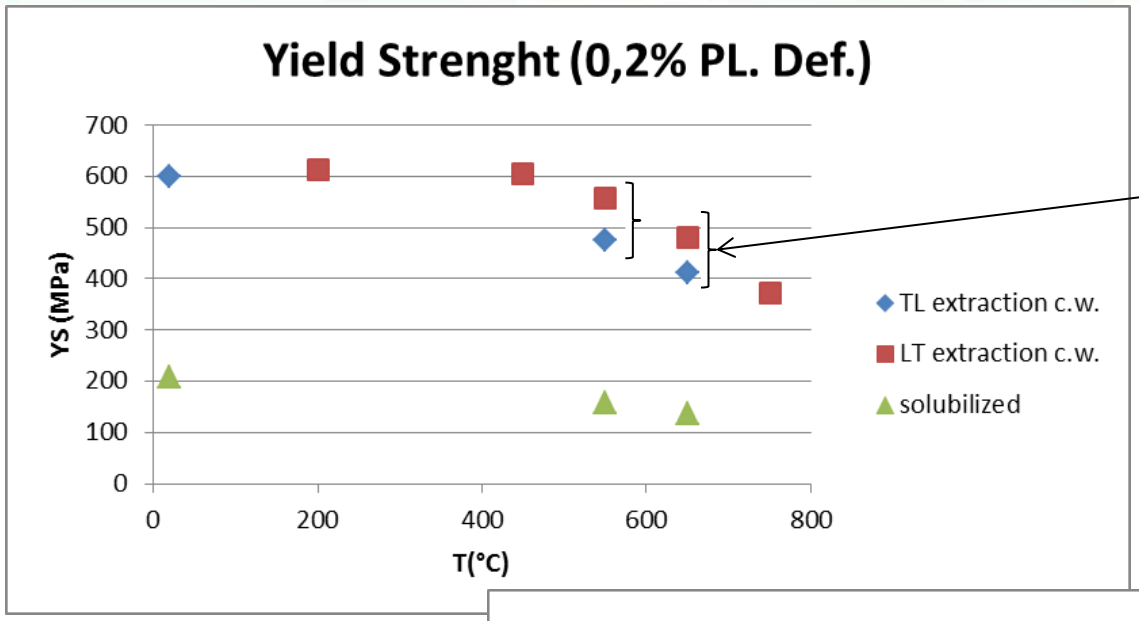
20% C.W. material (RT, 550° C, 650° C)



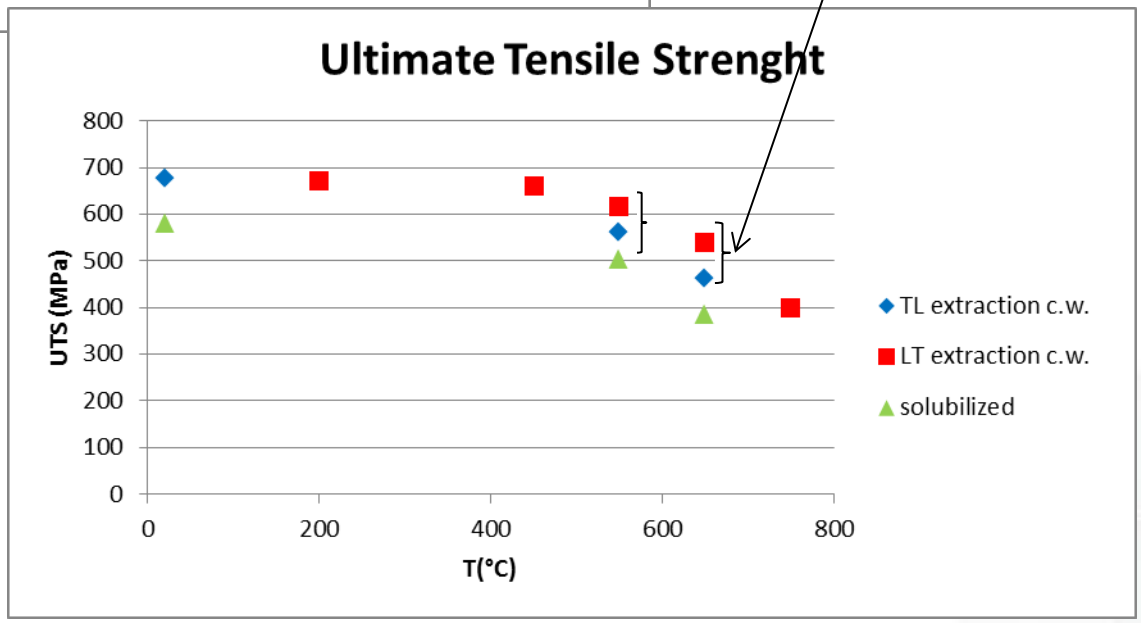




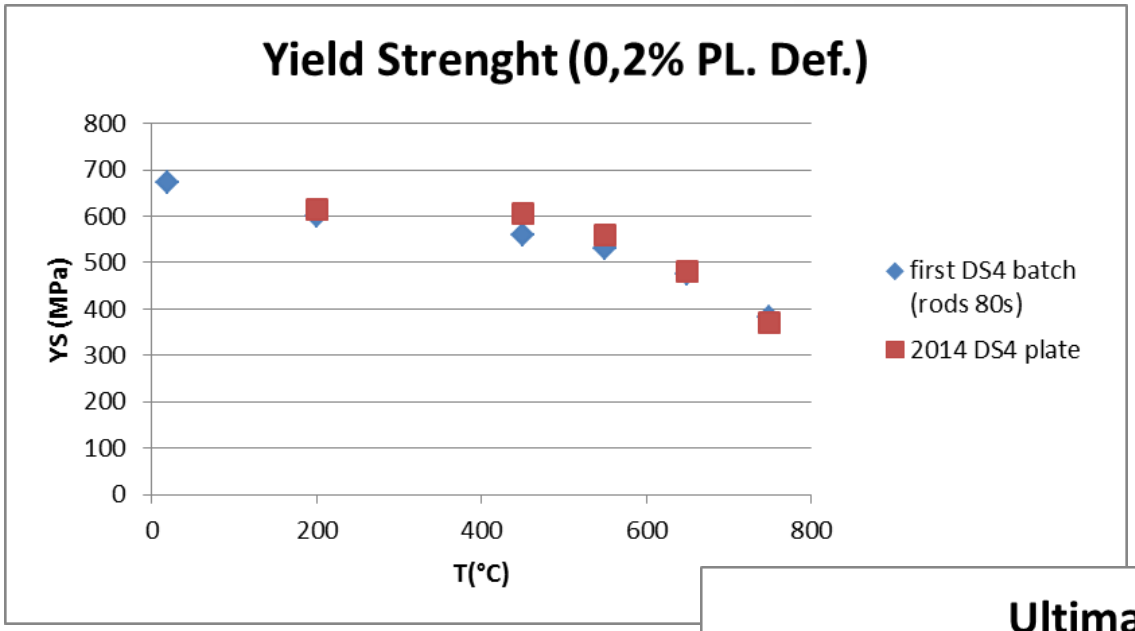
Anisotropy of the material; comparison between extraction directions



Anisotropy of the produced plate



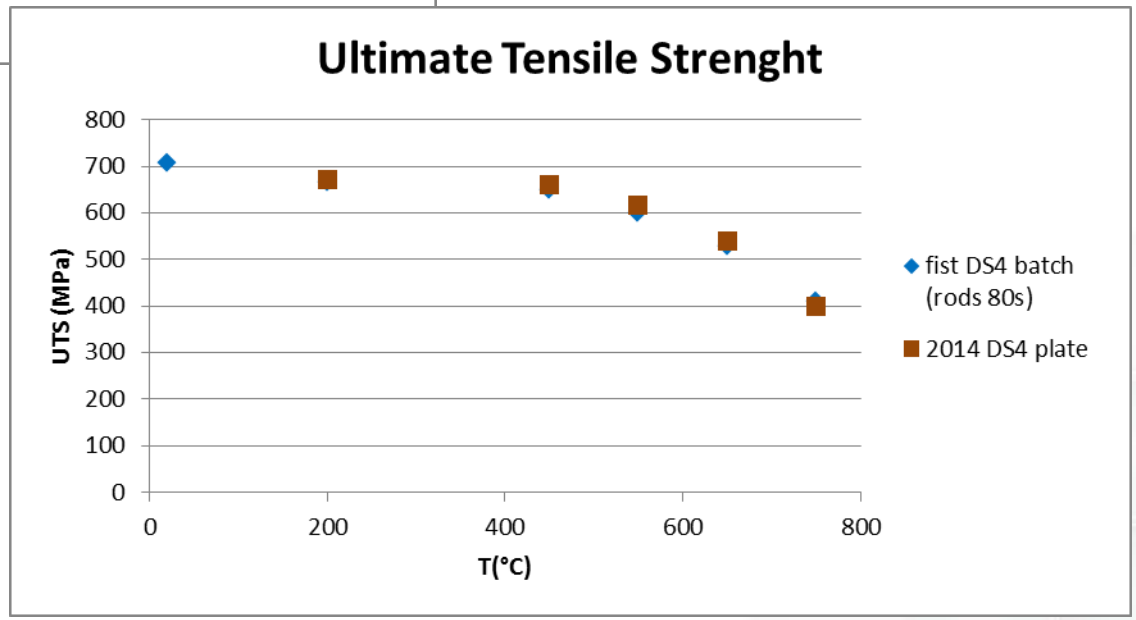
Comparison DS4; rods 90s vs 2014 plate



Data 90s:

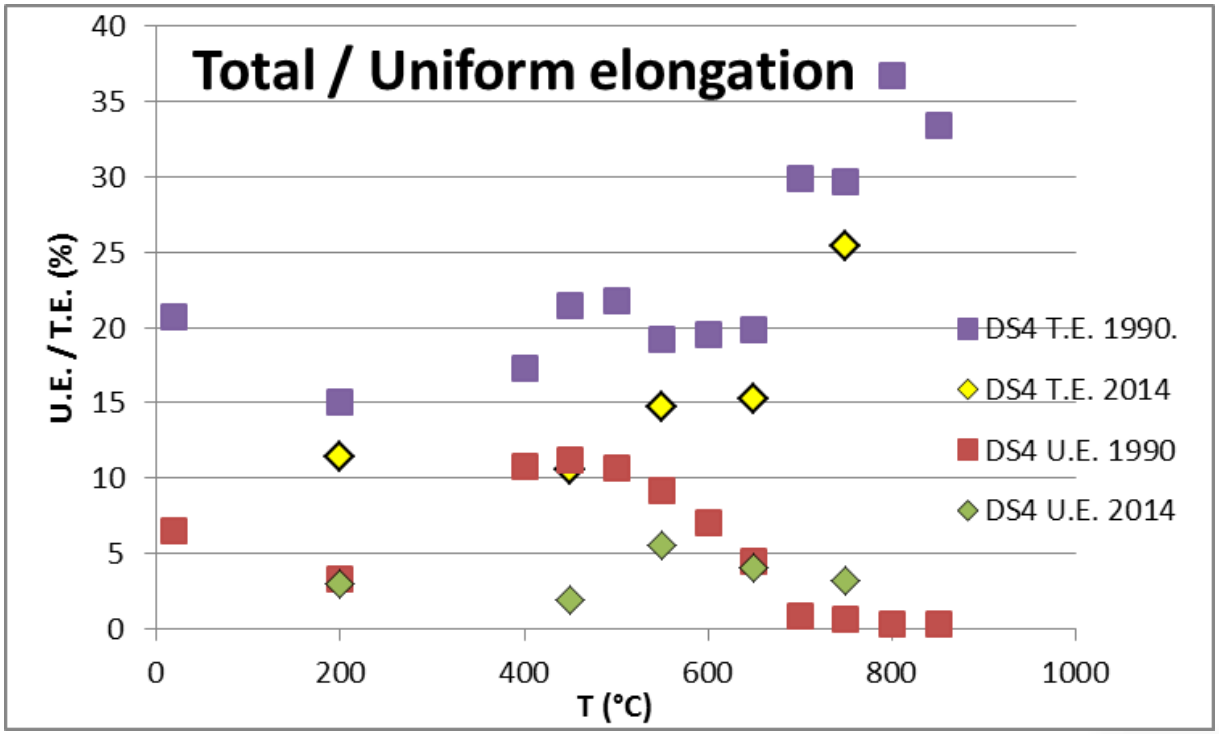
G. Filacchioni, U. de Angelis, D. Ferrara, L. Pilloni / Proceedings B.N.E.S., London, 1990

Comparable mechanical properties of the new plate with respect to the rods characterized in the 90s



Total Elongation; Comparison





Concerning the uniform elongation DS4 behaviour was excellent. In the interval between 400 and 600-650° C the steel performs values that are almost twice respect to those of the other steels. This behavior, similar to the best ones for the stainless steels with high yield strength, is symptomatic of good characteristics of stretchiness, performing delayed onset of mechanical instability. The values of the deformations, comparing the new batch to the former one, appear averagely less performing.

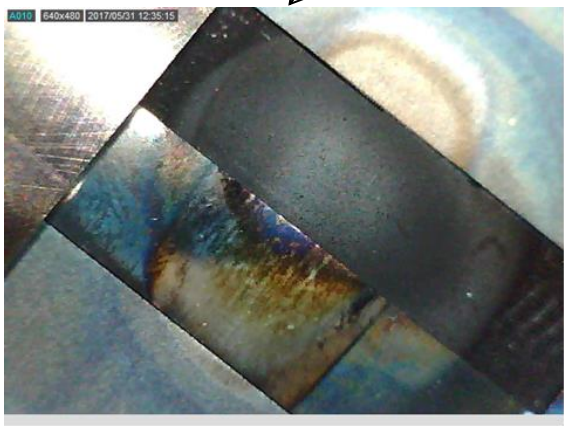
Running activities: Ion-Irradiation

Irradiating in LNL (Laboratori Nazionali di Legnaro, INFN, Padova);
5 irradiation sessions (two days each) in order to achieve the 100 dpa target dose; start: July 2015, end: March 2017

- Geometry of the sample: 20mm x5mm x1,3 mm; polished surfaces



Inside the test section, after 4 irradiation sessions (approx. 80 dpa)



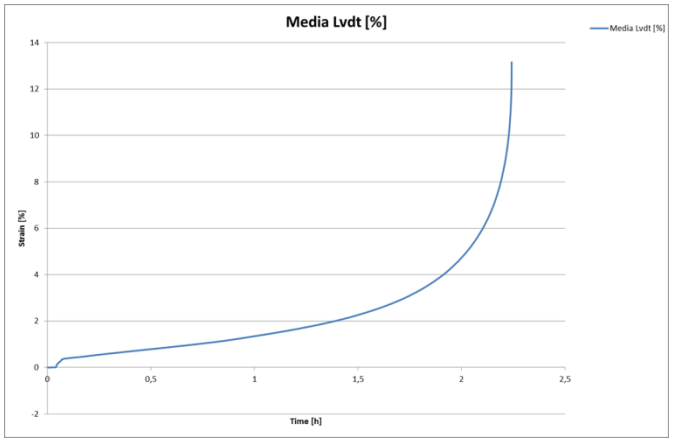
- Target: 100 dpa
- Heavy ions: 58 Ni
- 110 MeV

In progress … (four sessions completed, last session postponed due to the rupture of the "laddertron" of the TANDEM facility)

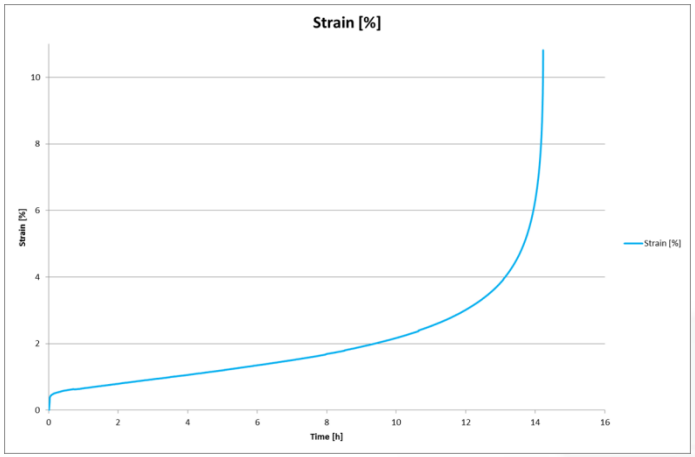
Experimental activities in progress …

- **Corrosion Tests (flowing lead)**; 1000 hrs exposure completed (flowing Pb, 10^-5 wt% O_2); waiting for SEM analysis ;
- **Ion irradiation**; target: 100 dpa (58 Ni, 110 MeV). In progress (four sessions completed, one additional session to achieve the target dose);
- **Creep tests;** experimental campaign temporarily interrupted due to safety issues; 2015 results

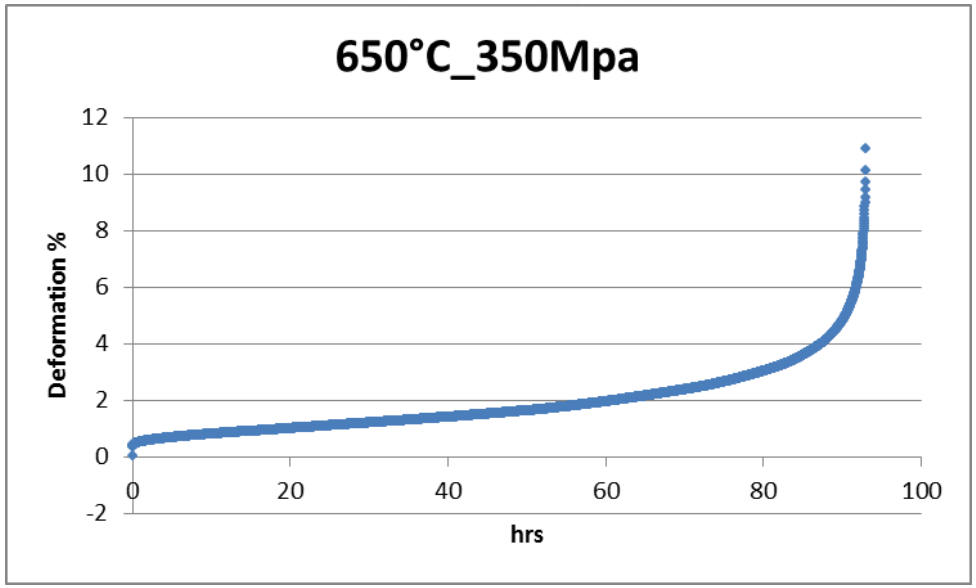
Test 650° C – 415 Mpa (Yield Stress)



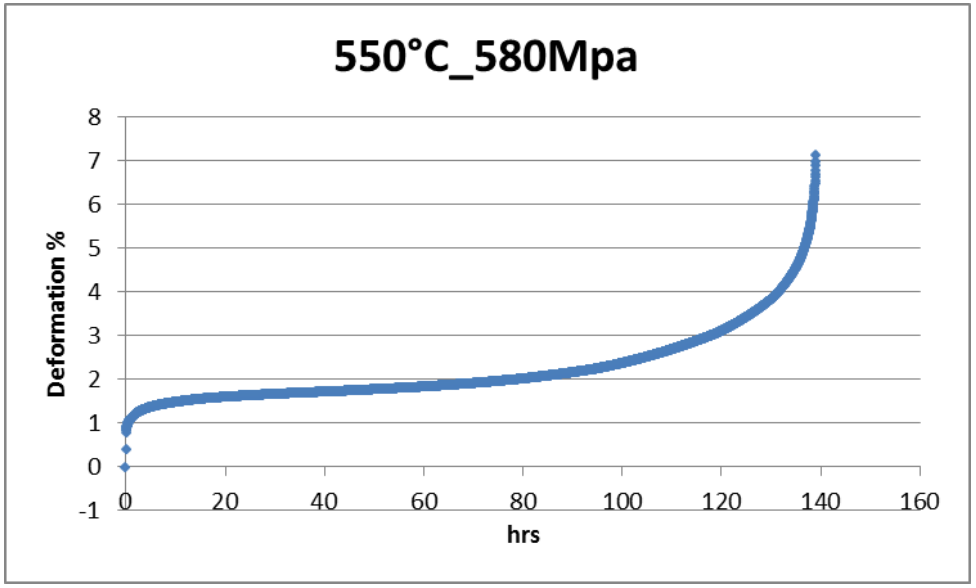
Test 650° C – 390 Mpa



Creep characterization in progress ; 2017 Results

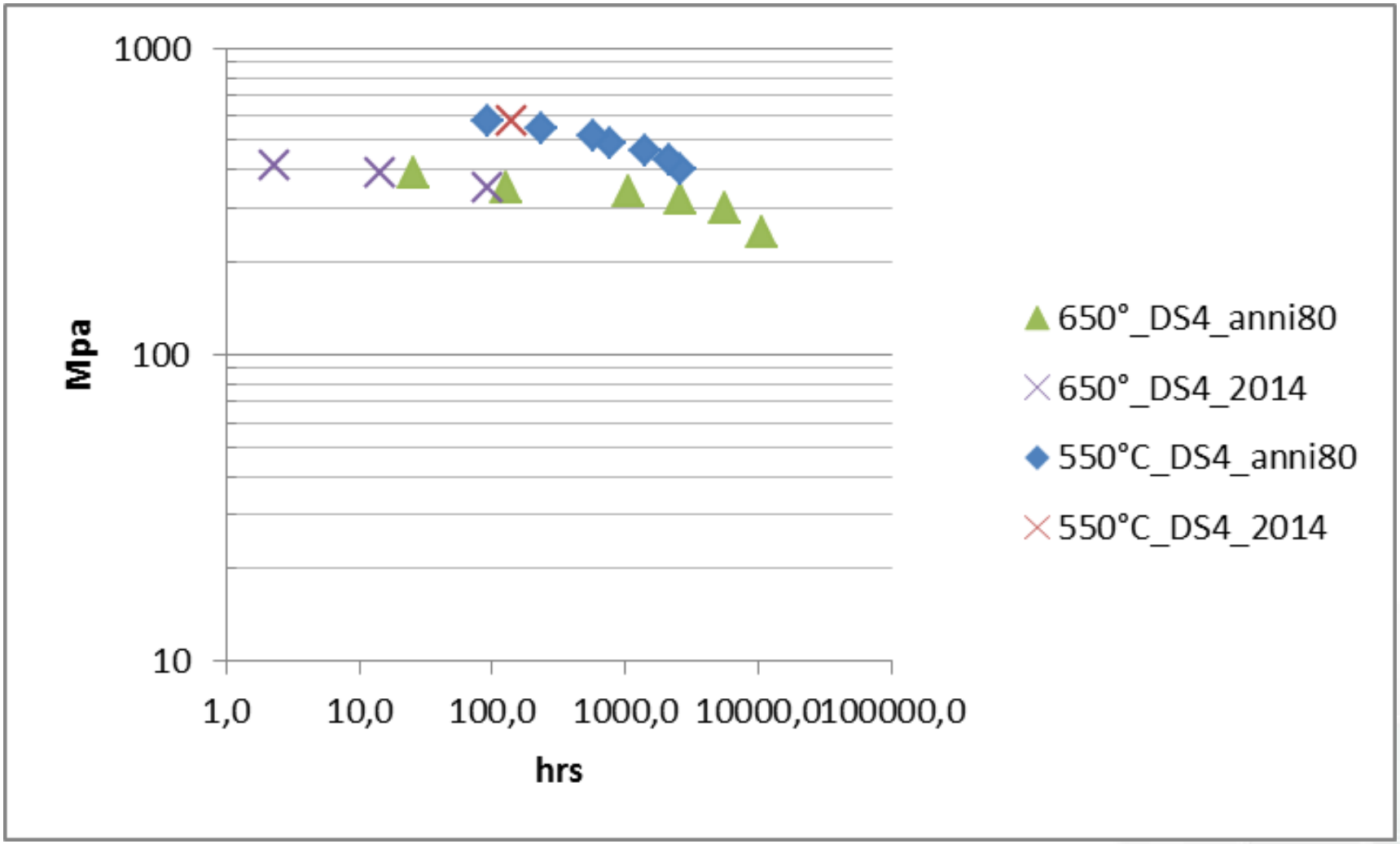








Creep characterization in progress …



Conclusions

Double stabilized steels appear very promising because of the following reasons:

- the long term properties are nearly the best among the austenitic stainless steels (improved creep properties);
- the common C.E.A.-E.N.E.A. irradiation programme, the Supernova rig loaded in Phenix FBR at the beginning of May 1988, demonstrated the good swelling resistance;
- The features affecting the good swelling behaviour of these alloys are thought to be the high c.w. rate, the increased Ni content and the double stabilization (addition of Ti and Nb) which grants the possibility to tune up the precipitation of primary and secondary carbides in order to reduce the swelling;
- A new DS4 plate has been produced in 2014 and the tensile properties appear superposed to the ones of the former DS4 batch (namely the “Supernova” rods). Lower values of Uniform and Total Deformations of the new cast when compared to the ones of the former batch (irradiated in Supernova).

Thank you for your attention

ADP ENEA-MSE, PAR2016

SVILUPPO MATERIALI E CHIMICA DEL REFRIGERANTE

''Prove di CREEP-RUPTURE su materiali strutturali ricoperti per applicazioni in sistemi LFR''

Bologna 27 Settembre 2017 *A. Coglitore, A. Strafella.*

ENEA – SSPT-PROMAS-TEMAF

Dipartimento Sostenibilità dei sistemi produttivi e territoriali (SSPT)

Divisione Tecnologie e processi dei materiali per la sostenibilità (PROMAS)

Laboratorio tecnologie di materiali Faenza (TEMAF)



1. **Ricerca e Sviluppo Tecnologie e Nuovi Materiali**
2. **Qualificazione ed Ingegnerizzazione di Materiali e componenti**
3. **Servizi**

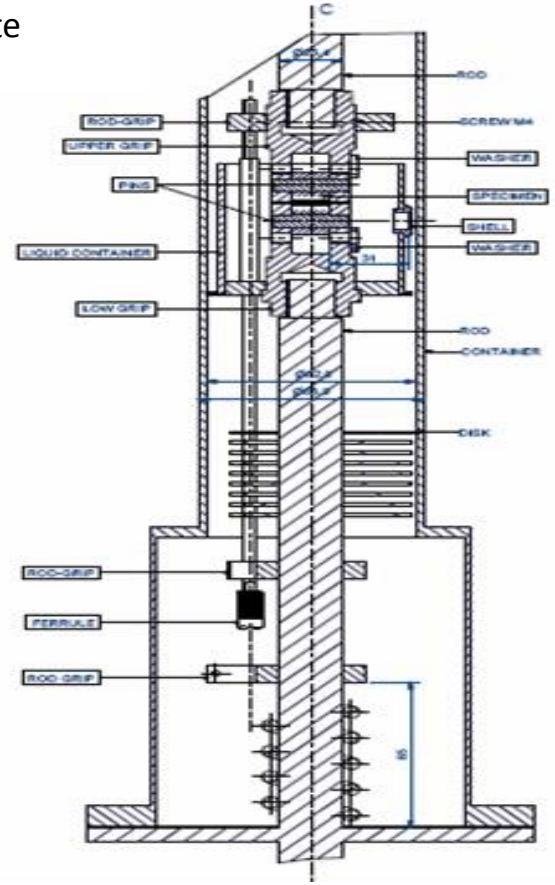
PAR2012 LP2 B1: Messa a punto di prove meccaniche in piombo liquido stagnante per la caratterizzazione di materiali strutturali ricoperti per applicazioni nucleari

Nell'ambito della campagna sperimentale di caratterizzazione dei rivestimenti realizzati nella precedente annualità sono state avviate le prove di creep-rupture in piombo liquido stagnante

- **Substrati :** AISI 316L , T91, 15-15 Ti (mod. Si, 20% CW)
- **Rivestimenti:** TiN (PVD), Fe(67wt%)Al(33wt%) (PVD), Fe Cr (18-20 wt%)Al(8-10 wt%) (PVD), Ta (CVD))
- **Test preventivati : 96**

Questa attività ha richiesto modifiche ed implementazioni alla strumentazione presente presso i laboratori di caratterizzazione termomeccanica "Creep" presenti nei Laboratori ENEA di Faenza

- Realizzazione di una linea di gas inerte/riducente dedicata ad ogni singola macchina di prova
- Modifiche alla linea di carico del campione per il contenimento del piombo liquido per poter utilizzare le termo-camere da vuoto in dotazione
- Progettazione e realizzazione di un nuovo sistema di acquisizione (Hardware/Software)



Disegno complessivo della facility di prova

PAR2013 LP2.b1_h: ''Prove di CREEP-RUPTURE su materiali strutturali ricoperti per applicazioni in sistemi refrigerati a metallo liquido pesante''

- Sono stati realizzati i particolari dei disegni CAD per la progettazione finale dell'attrezzatura di prova per i test in metallo liquido
- È stato individuato come materiale prioritario il [15-15 Ti(Si)]
- Sono state eseguite delle prove preliminari nelle seguenti condizioni:
  - 550°C; 300MPa; in aria
  - 550°C; 400MPa; in aria
- Sono stati elaborati risultati delle prove
- I risultati sono stati confrontati con quelli di un acciaio austenitico analogo, disponibili in letteratura.
- Si è provveduto a identificare un adeguato sistema di aspirazione (come richiesto da normativa vigente, a causa della presenza di vapori di Pb durante i test)

PAR2014 LP2.b1_h: ''Prove di CREEP-RUPTURE su materiali strutturali ricoperti per applicazioni in sistemi refrigerati a metallo liquido pesante''

- Realizzazione dell'attrezzatura di prova per i test in metallo liquido

- Sono state eseguite delle prove nelle seguenti condizioni del materiale di riferimento individuato nel ADP ENEA-MSE PAR2013 LP2.b1_h (15-15 Ti (Si)):
  - 550°C; 400MPa; in aria
  - 550°C; 558MPa; in aria
  - 550°C; 576MPa; in Pb

- Sono stati elaborati risultati delle prove .

PAR2015 LP2.b1_h: ''Prove di CREEP-RUPTURE su materiali strutturali ricoperti per applicazioni in sistemi refrigerati a metallo liquido pesante''

- E' stato individuato come materiale da testare il [T91].
- E' stata eseguita la prove preliminare nelle seguenti condizioni:
  - 550°C; 280MPa; in aria.

- Sono attualmente in corso i test nelle seguenti condizioni:
  - 550°C; 250MPa; in aria;
  - 550°C; 210MPa; in aria;
  - 550°C; 210MPa; in Pb.

- Sono state eseguite delle elaborazioni preliminari dei test.

Nell'ambito del ADP ENEA-MSE PAR2016:

- Sono attualmente in corso i test nelle seguenti condizioni:
  - 550°C; 265MPa; in aria;
  - 550°C; 250MPa; in aria;
  - 550°C; 250MPa; in Pb;
  - 550°C; 210MPa; in aria;
  - 550°C; 210MPa; in Pb.
- Sono state eseguite delle elaborazioni preliminari dei test.

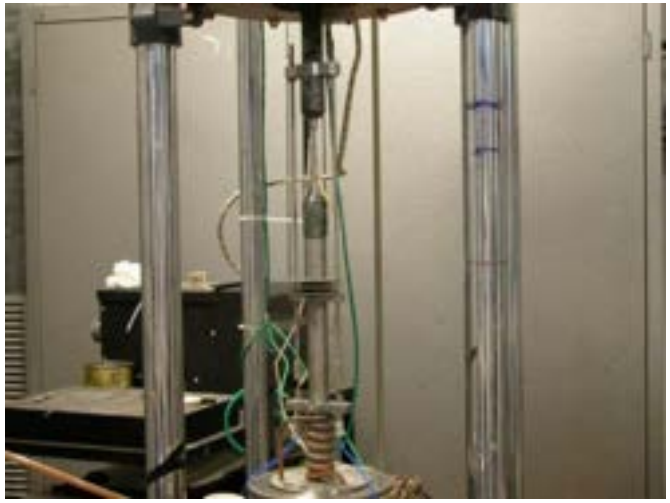
Particolari montaggio attrezzatura per prove in Pb



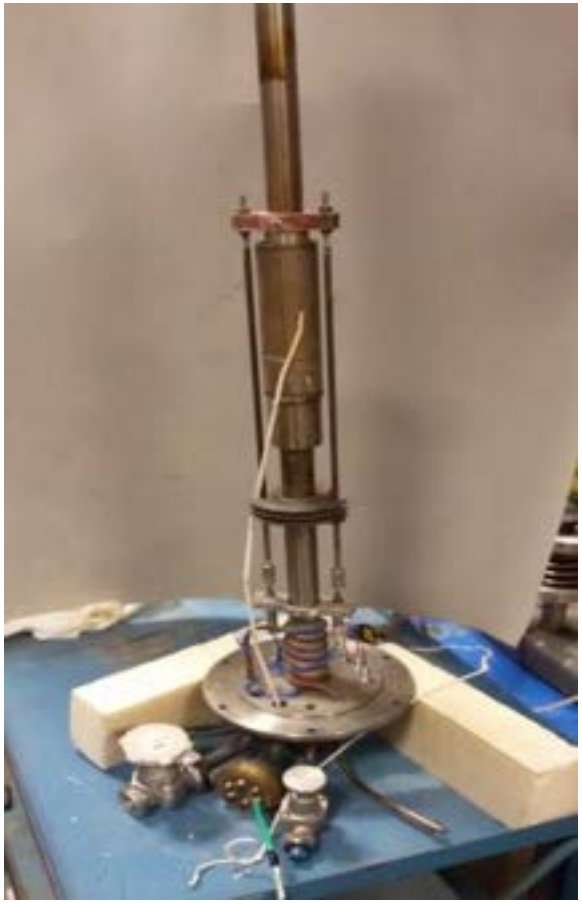




Particolari di campioni in aria ed in Pb

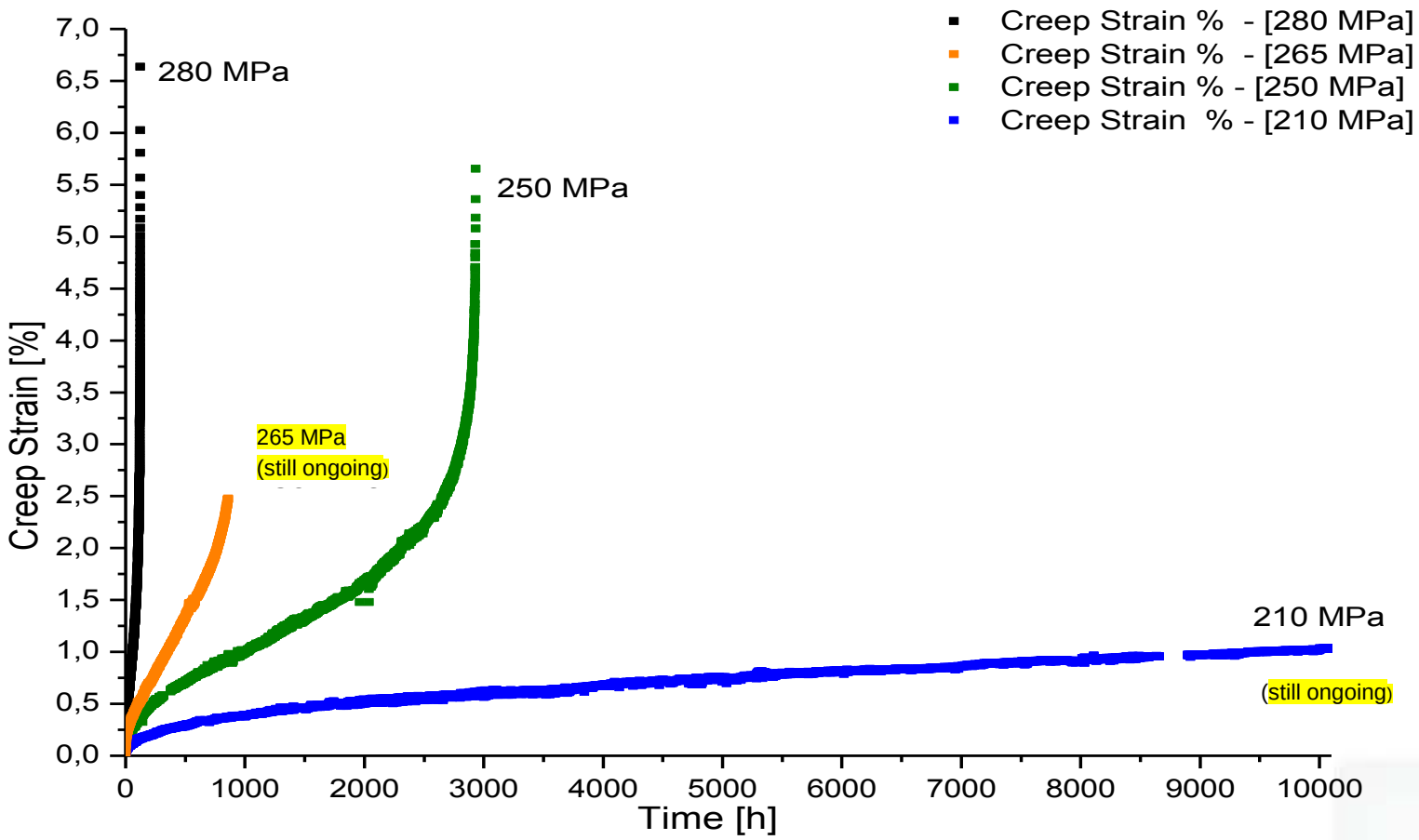




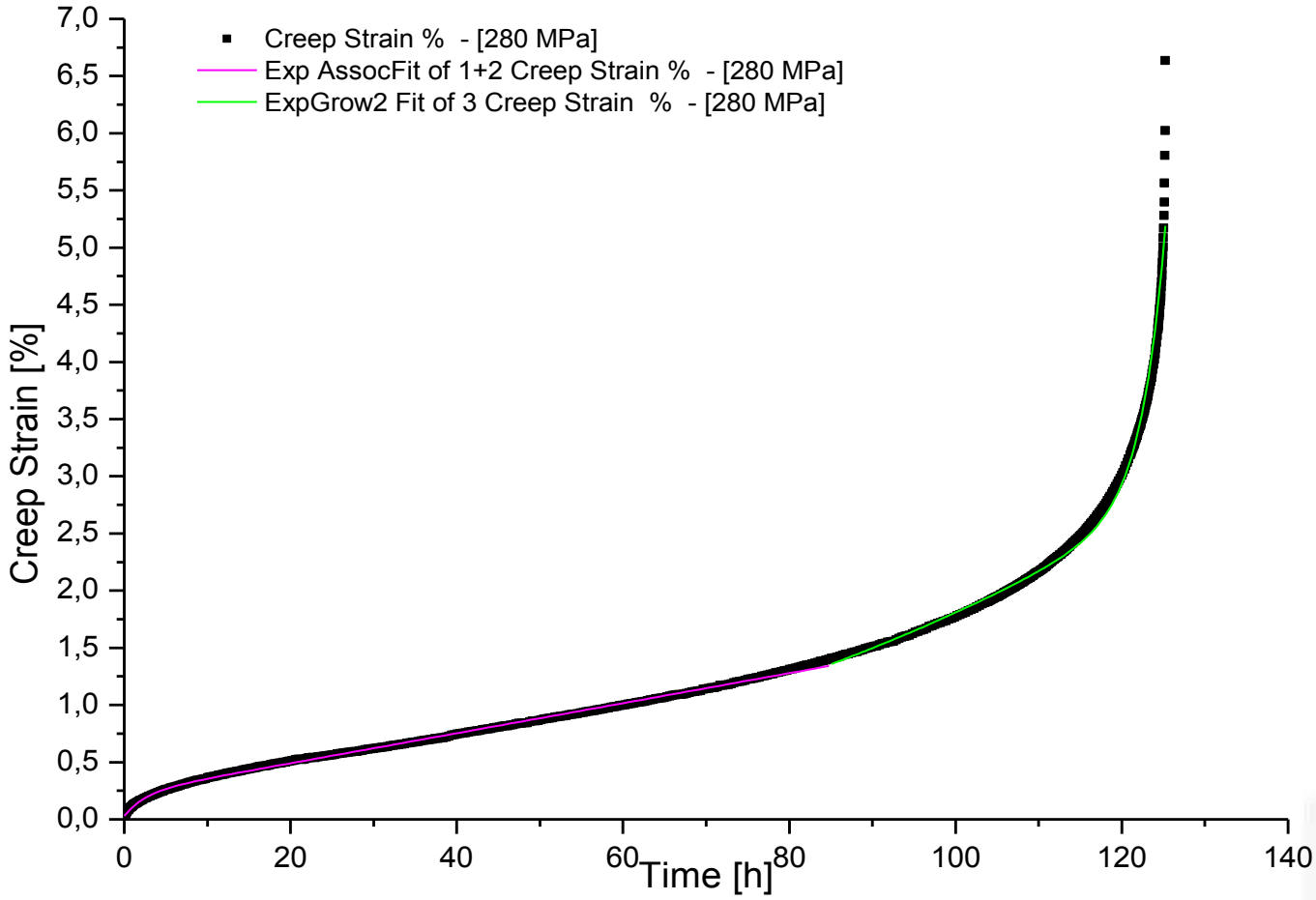




Confronto curve Creep Strain test T91 in aria



Curva Creep Strain test T91 a 280 MPa in aria



Particolare di campione in aria dopo rottura



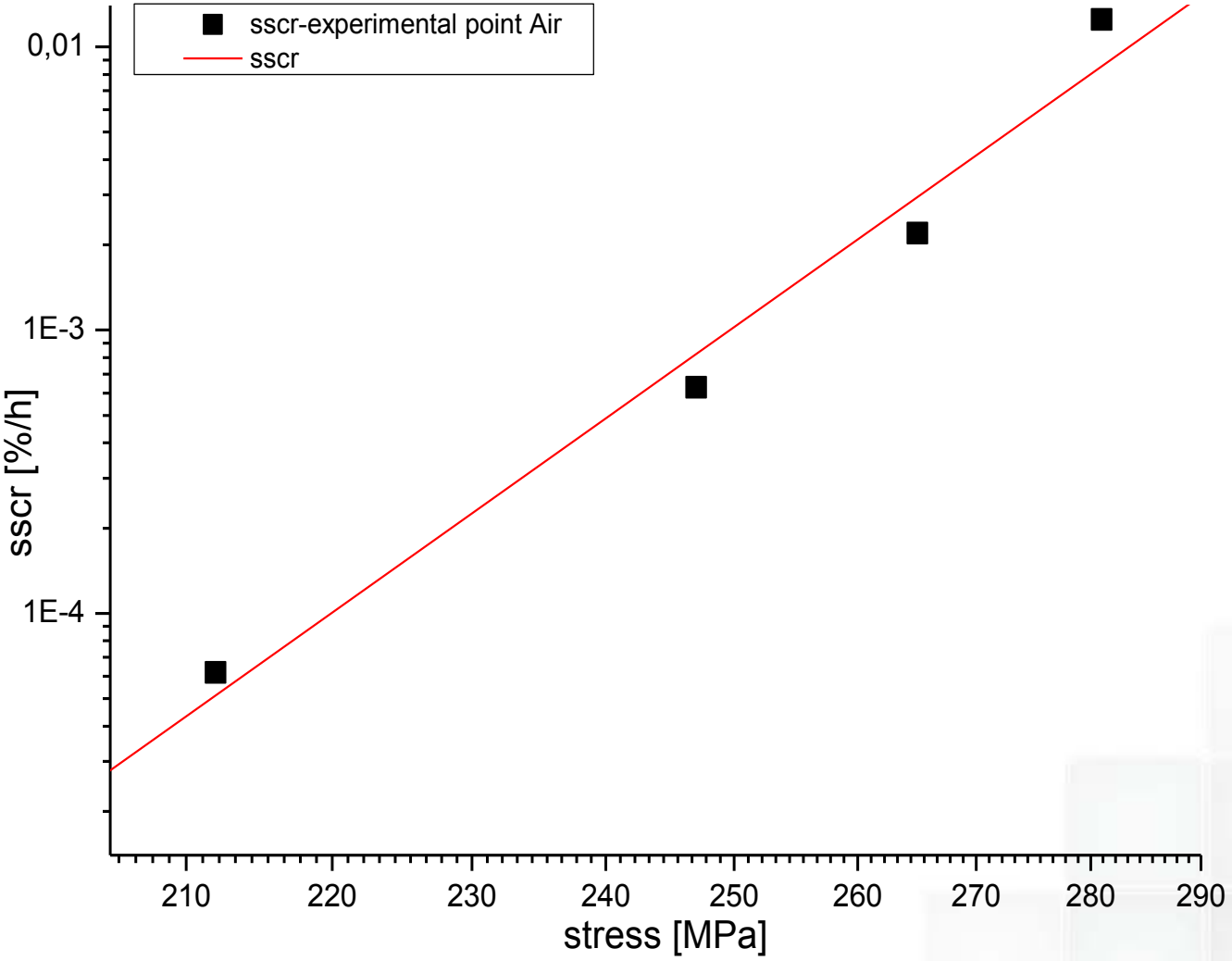




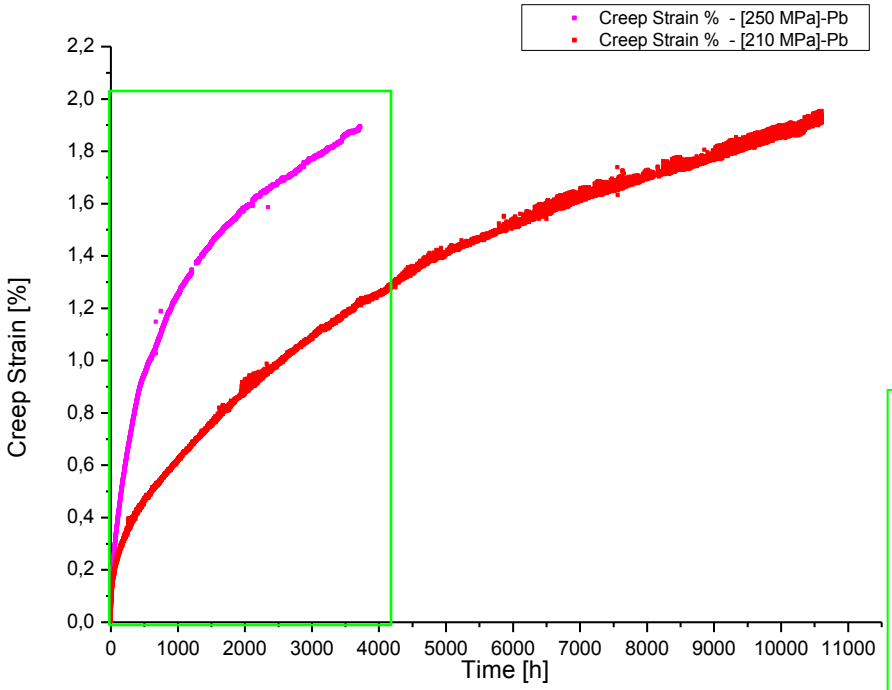
Ipotesi di analisi delle steady-state creep rate (sscr)

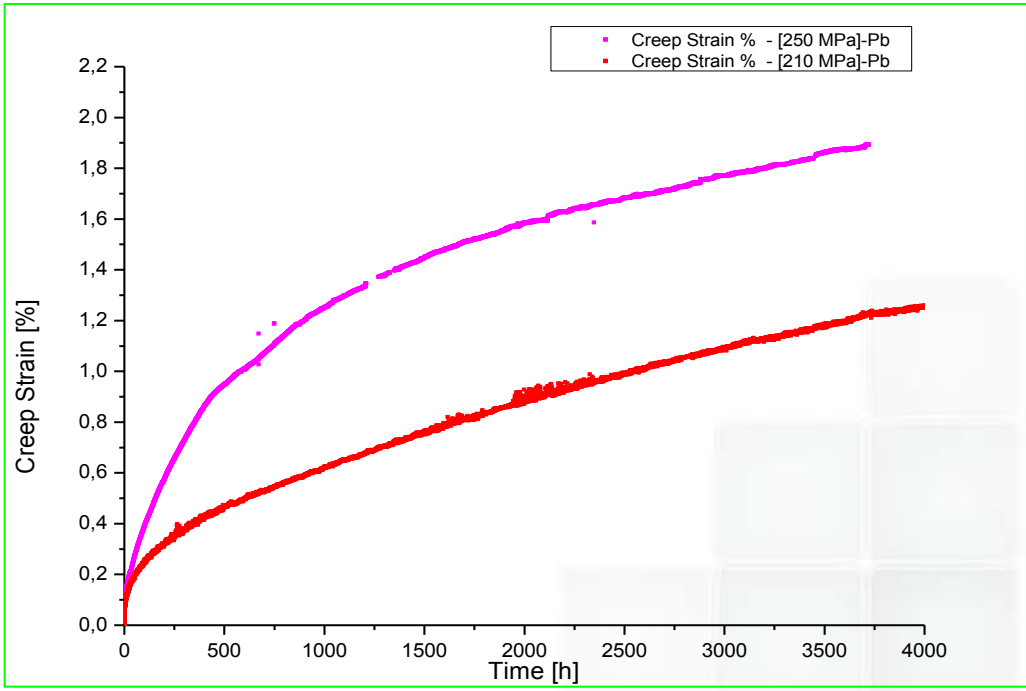
$$sscr \quad A^{\,n}$$

A	n
$2{,}98*10^{-47}$	18,15

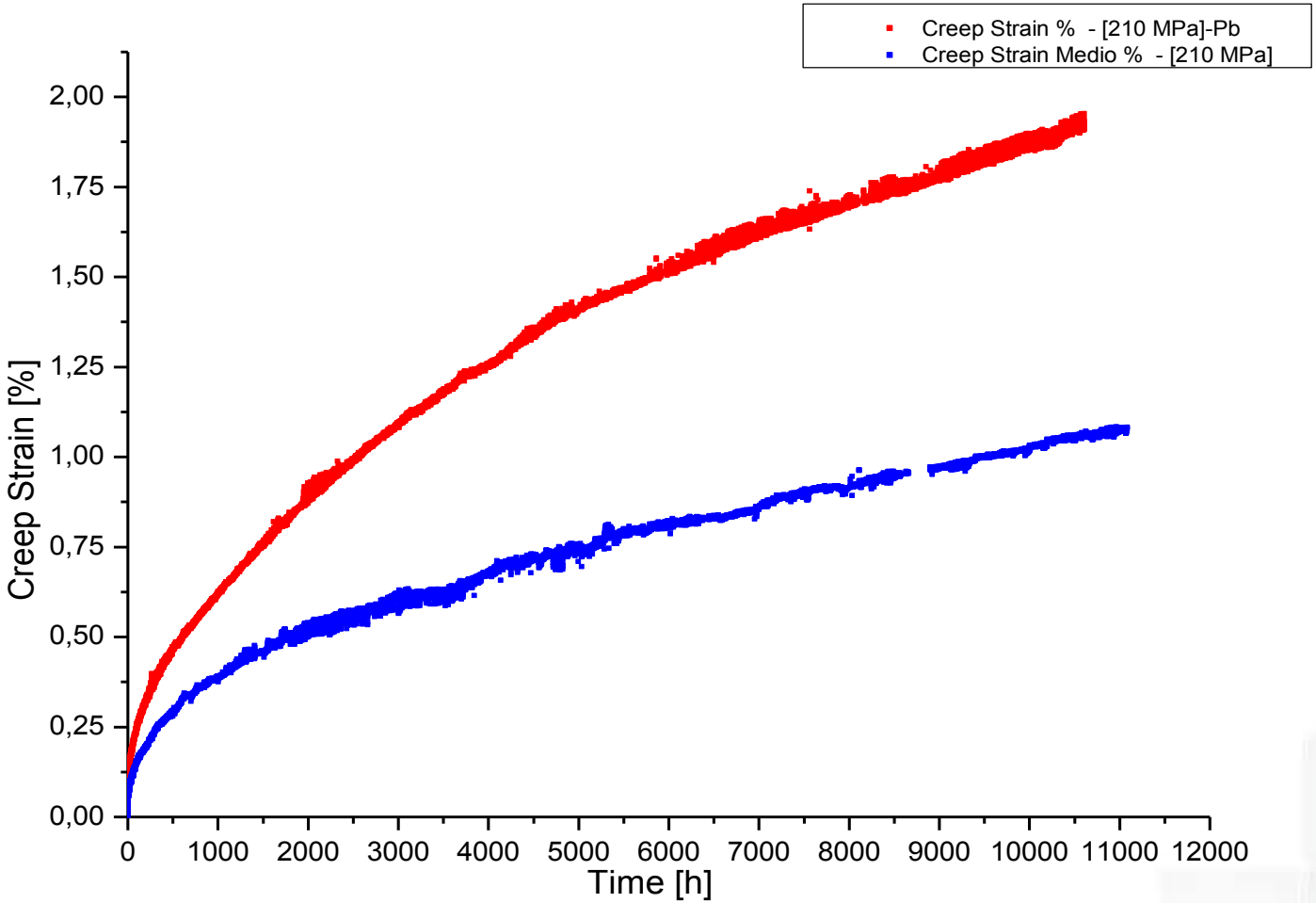


Curva Creep Strain test T91a 210 e 250 MPa in Pb

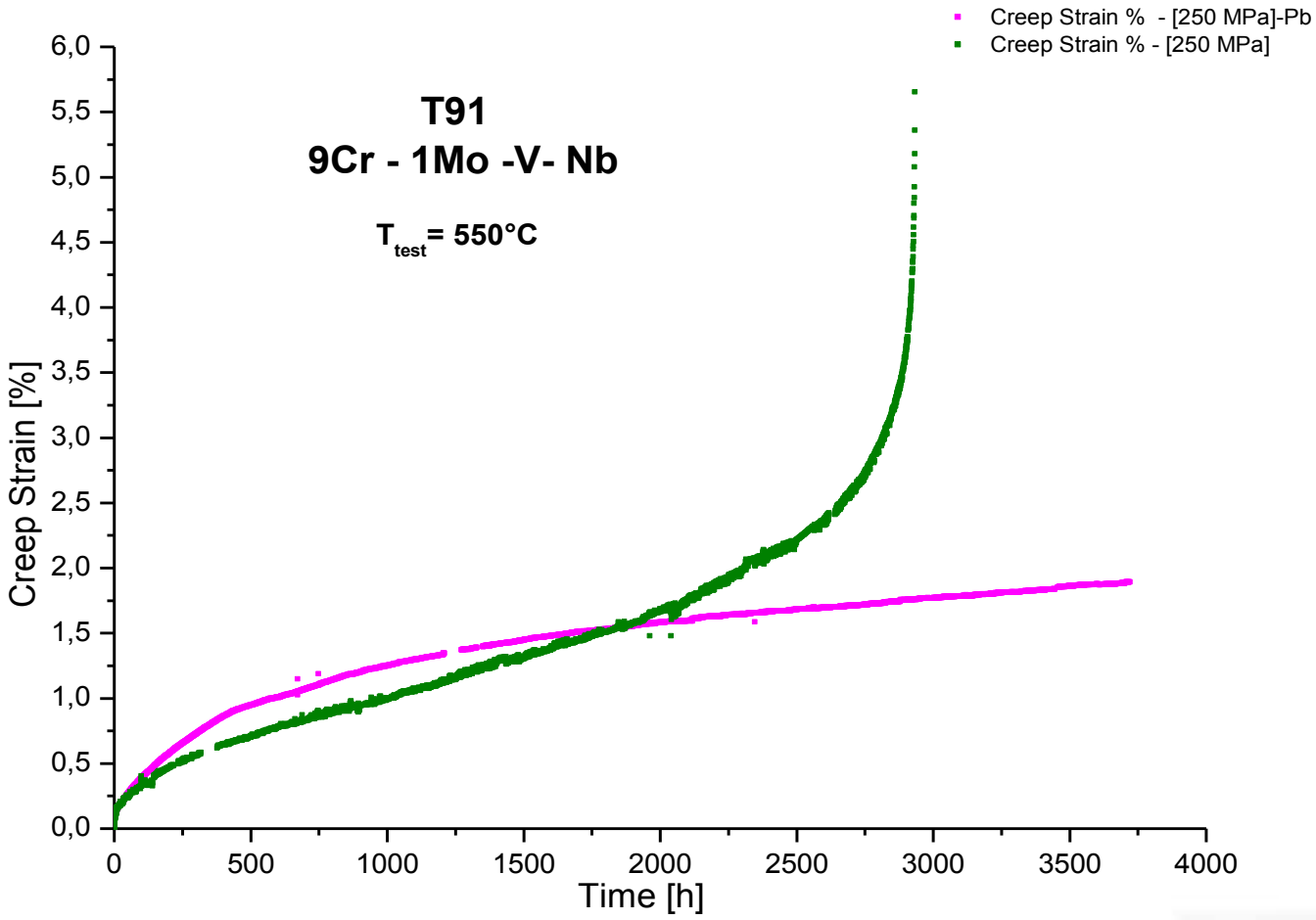




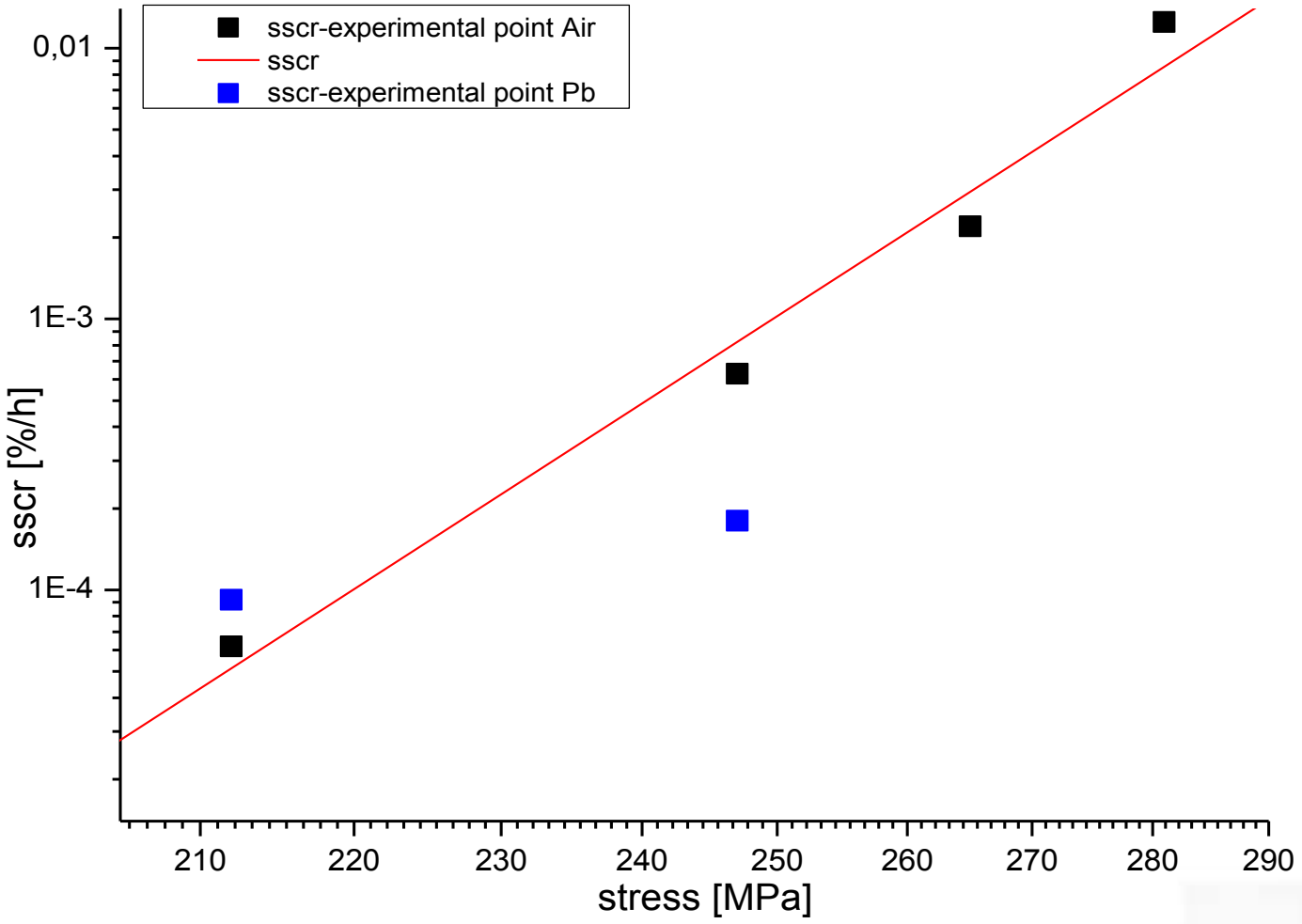
Confronto curve Creep Strain test T91a 210 MPa in aria e in Pb



Confronto curve Creep Strain test T91a 250 MPa in aria e in Pb

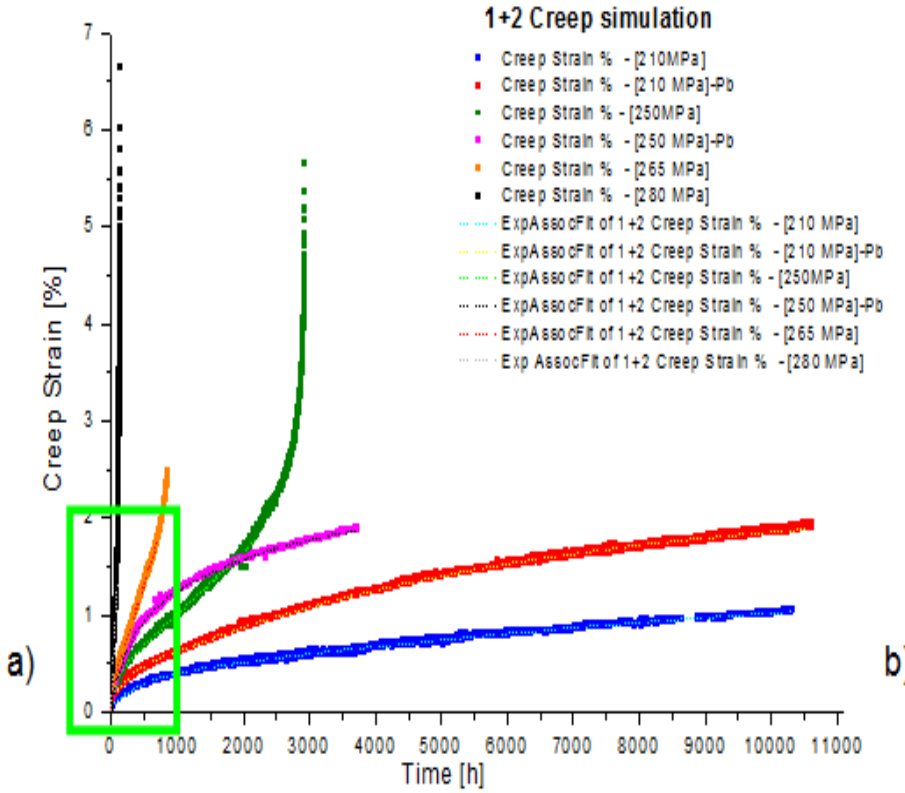


Ipotesi di analisi delle steady-state creep rate (sscr)

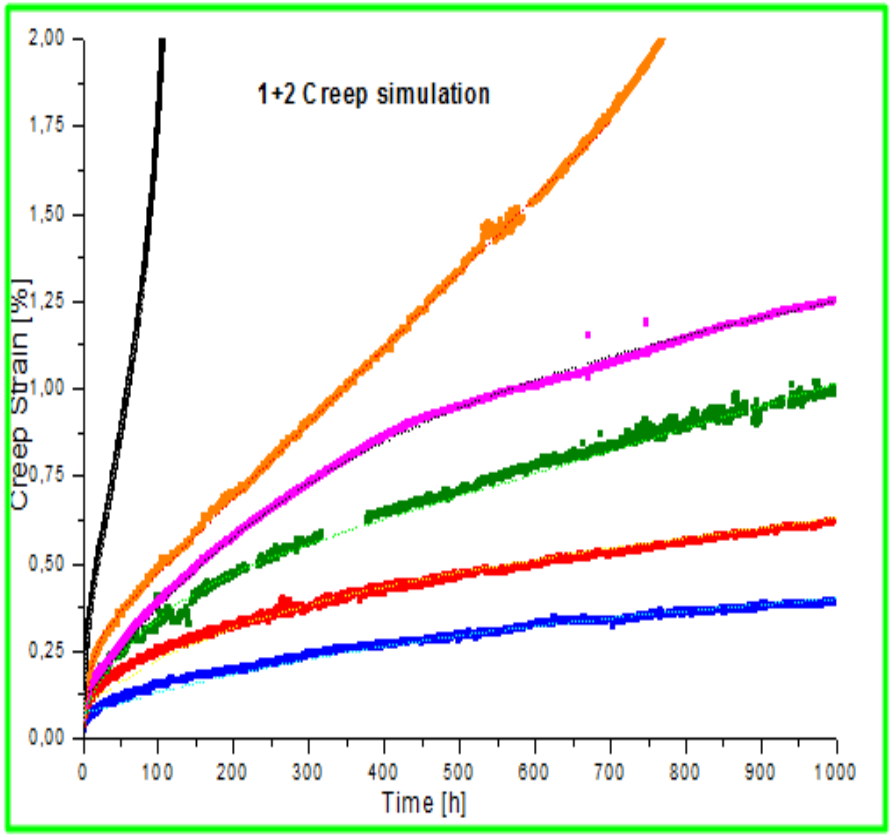


Confronto curve Creep Strain test T91 in aria ed in Pb

a)



b)



CONCLUSIONI

Nell'ambito del ADP ENEA-MSE PAR2016 sono attualmente in corso le seguenti attività:

- Test di CREEP in aria di un acciaio martensitico [T91] a due differenti livello di carico (210, 250 e 265MPa);
- test di CREEP in piombo di un acciaio martensitico [T91] a 210 e 250MPa;
- confronto preliminare dei risultati ottenuti;
- determinazione preliminare dei parametri del secondario per i test in aria, in accordo con la legge di Norton;
- programmazione di un test di CREEP in piombo di un acciaio martensitico [T91] a 265MPa;
- programmazione di test di CREEP in piombo di un acciaio martensitico [T91] in controllo d'ossigeno.

FINE

Italian National Agency for New Technologies,
Energy and Sustainable Economic Development

NACIE Fuel Assembly and System Experiments

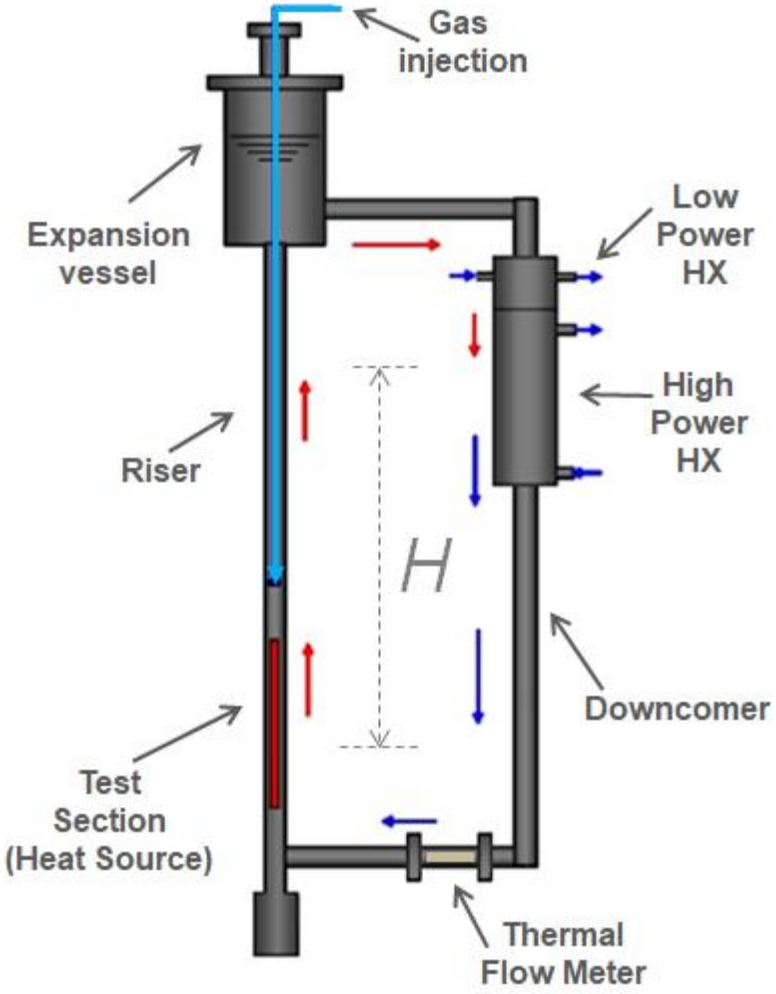
Scuola di Ingegneria e Architettura
Università di Bologna 26-27/09/2017

M. Angelucci (Università di Pisa)
I. Di Piazza, V. Sermenghi, G. Polazzi (ENEA FSN-ING-TESP)

Workshop tematico ADP MiSE-ENEA (PAR2016-LP2)
Generation IV Lead Cooled Fast Reactor: Stato Attuale Della Tecnologia E Prospettive Di Sviluppo

Summary

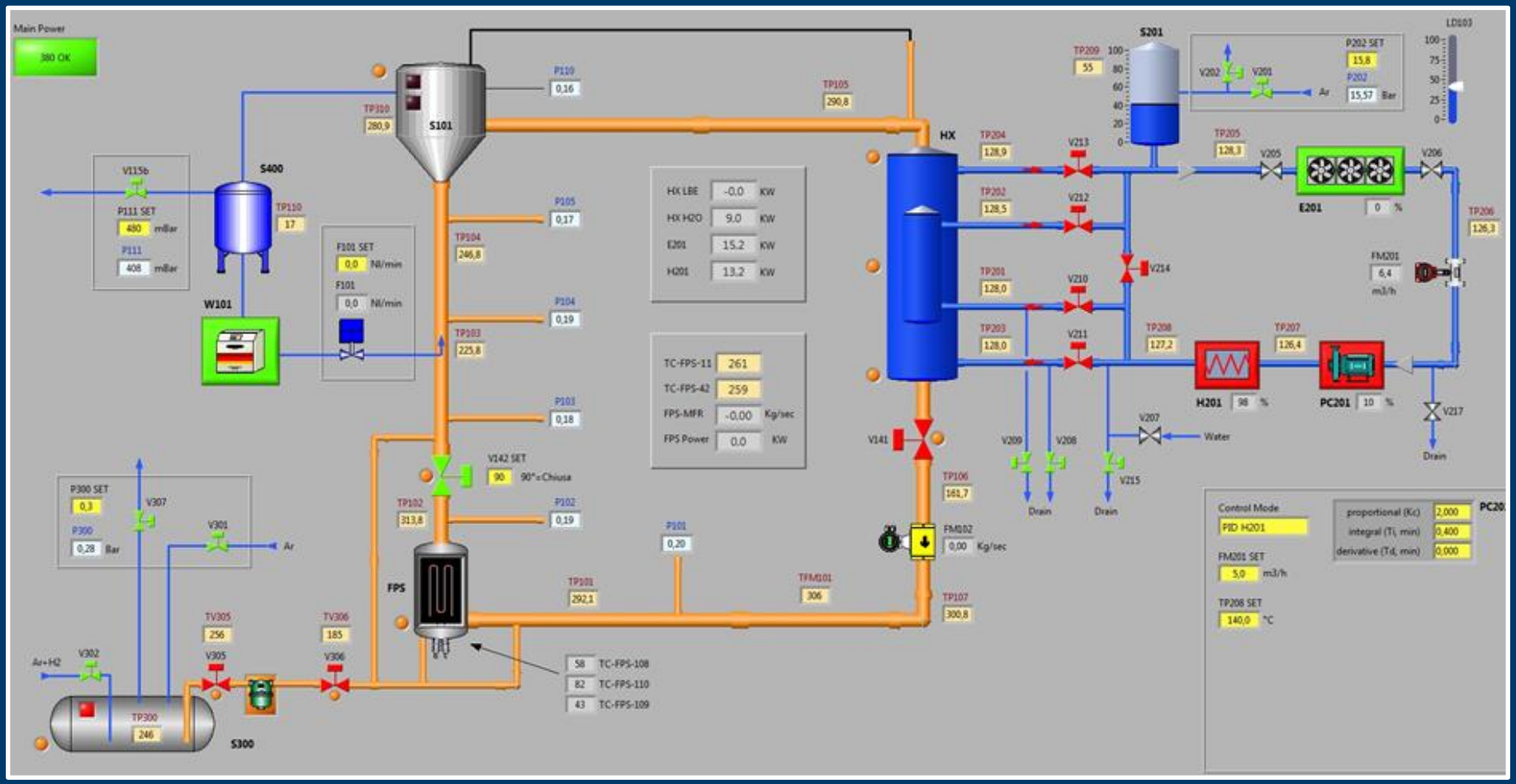
- NACIE-UP facility
  - Fuel Pin Bundle Simulator
- Experimental test matrix
- Experimental results
  - Comparison between ADP10 & ADP06
  - FPS temperature - Test ADP07
- Conclusions





NACIE-UP Facility – Primary loop

Composed by heat source (FPS), heat sink (H_2O Hx), expansion vessel, prototypical thermal flow meter

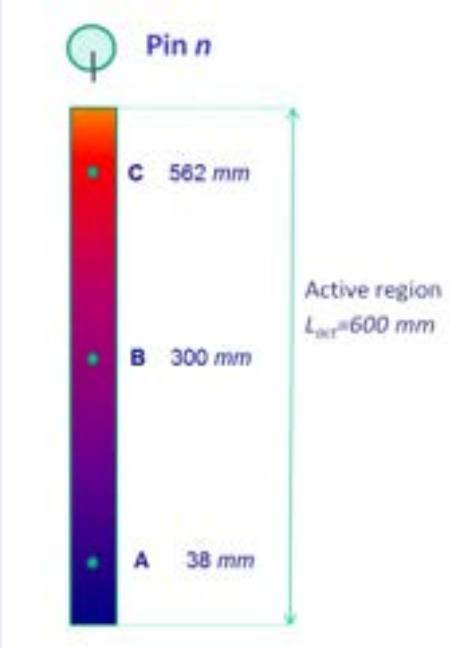


NACIE-UP PLC

Schematic layout of the primary (LBE) and secondary (H_2O)systems, of the gas system and of the fill & drain system

The Fuel Pin bundle Simulator



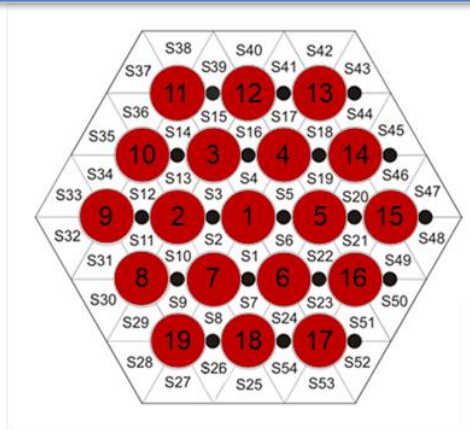


D_{pin}	6.55 mm
P	8.4 mm
P/D	1.2824
d	1.75 mm
P_{wire}	262 mm
L_{tot}	2000 mm
L_{active}	600 mm
$D_{H,nom}$	3.84 mm
q''_{max}	1 MW/m^2

- **11 instrumented pins**
- **52 TCs** (0.35 mm thick) - **wall embedded thermocouples location**
- **15 TCs** (0.5 mm thick) - **5 instrumented sub-channels**
- Instrumentation distributed along three axial positions (A, B, C): **z = 38, 300, 562 mm** from the beginning of the active length
- Pin 3 instrumented with wall embedded TCs every 43.66 mm (13 TCs)

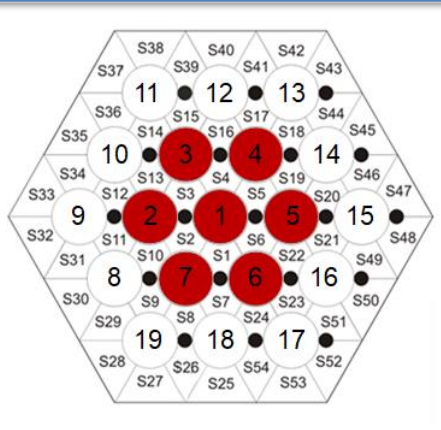
Experimental test matrix

TEST ADP 10



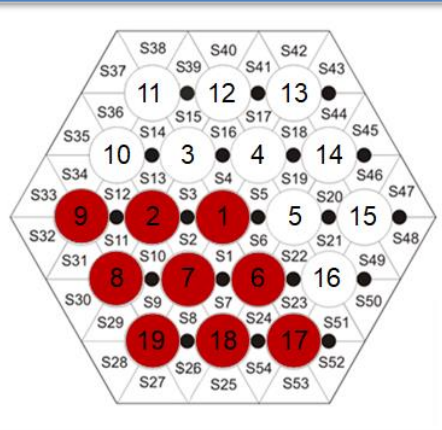
- **19** active pins
- FPS power **30 kW**
- $\dot{q}''_w \approx$ **127.9 kW/m²**
- $\dot{m}_{gas}$ **= 10 Nl/min**
  → 0 Nl/min
- $\dot{m}_{H_2O}$ = 10 m³/h
- $T_{in,\,H_2O}$ = 170 °C

TEST ADP 06



- **7** active pins
- FPS power **30 kW**
- $\dot{q}''_w \approx 347.1\ kW/m2$
- $\dot{m}_{gas}$ **= 10 Nl/min**
  → 0 Nl/min
- $\dot{m}_{H_2O}$ = 10 m³/h
- $T_{in,\,H_2O}$ = 170 °C

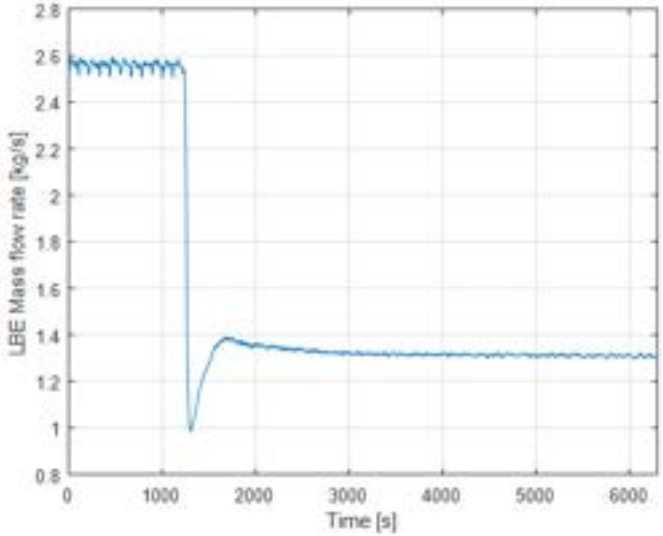
TEST ADP 07



- **9** active pins
- FPS power **38 kW**
- $\dot{q}''_w \approx 342.0\ kW/m2$
- $\dot{m}_{gas}$ **= 10 Nl/min**
  → 0 Nl/min
- $\dot{m}_{H_2O}$ = 10 m³/h
- $T_{in,\,H_2O}$ = 170 °C

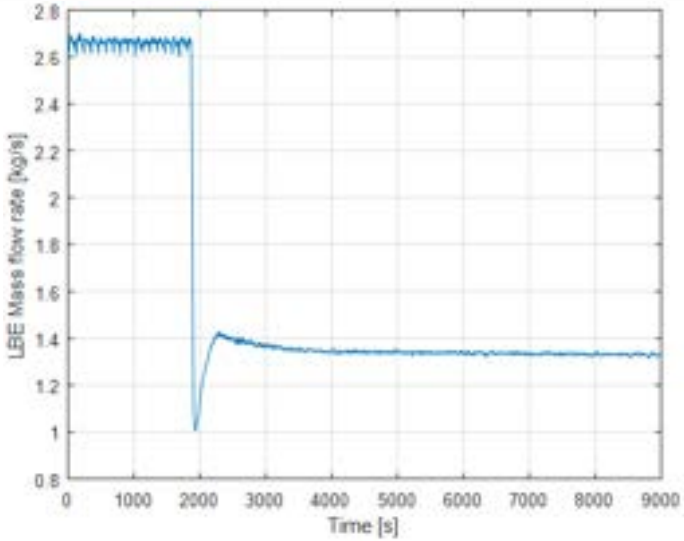
Experimental results - LBE mass flow rate

TEST ADP 10



Test ADP 10	Steady state 1		Steady state 2	
Variable	Data	σ [%]	Data	σ [%]
M_{gas} [Nl/min]	10.0	5.0	0.1	2.8
M_{lbe} [kg/s]	2.56	2.9	1.31	2.9
ΔT_{FPS} [°C]	72.0	0.9	140.6	0.2
Q_{nom} [W]	3.00E+04	0.2	3.00E+04	0.1
Q_{eff} [W]	2.71E+04	3.9	2.70E+04	3.7
Q_{pre} [W]	2236	18.0	2339	9.3
Q_{tfm} [W]	1915	0.2	1644	0.3

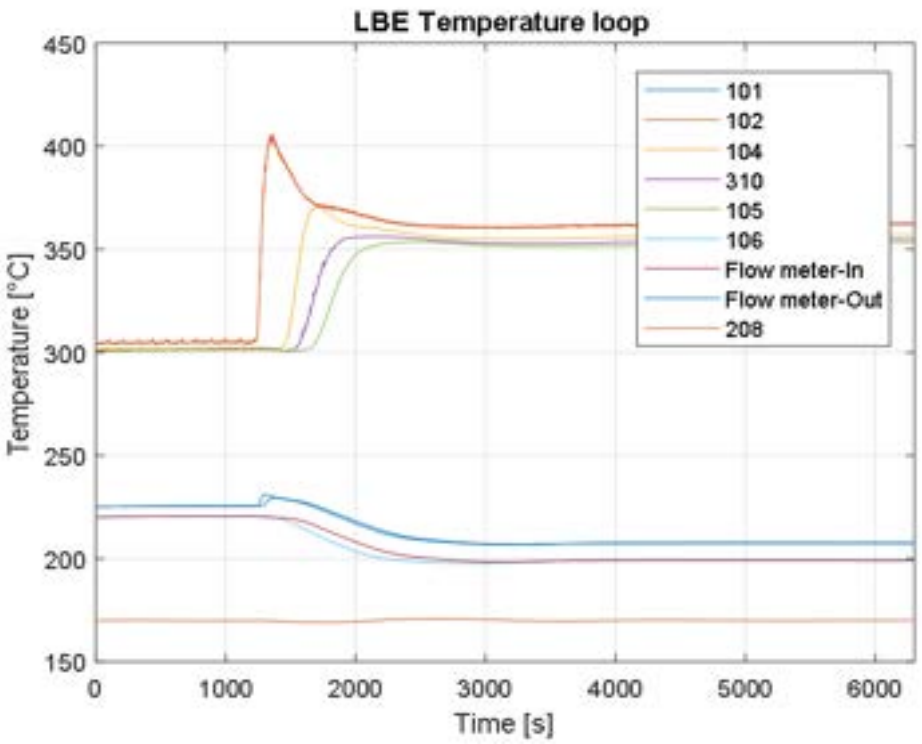
TEST ADP 06



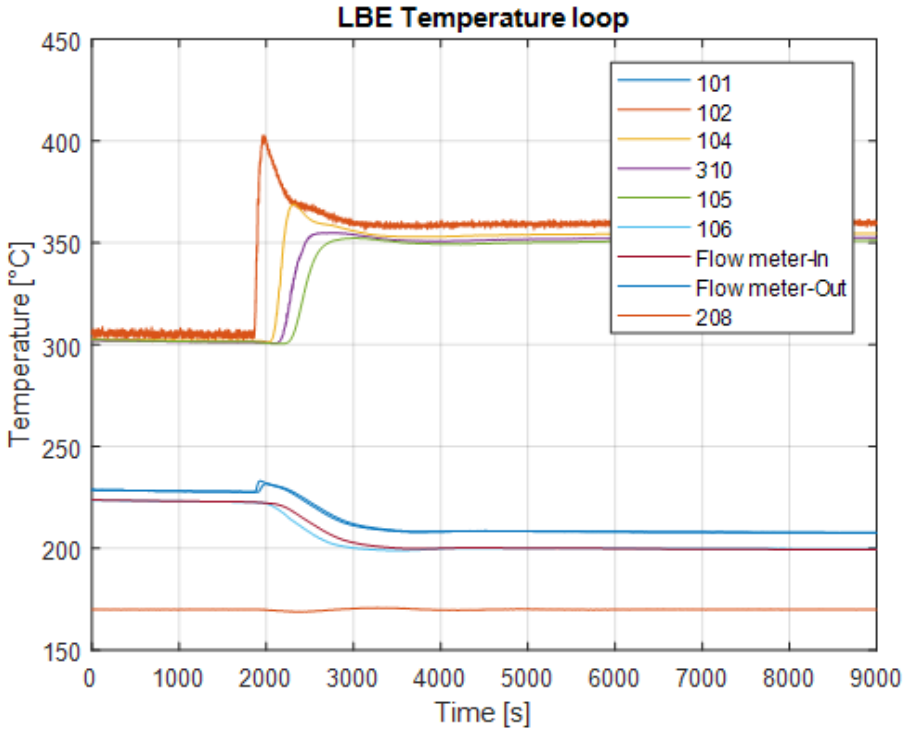
Test ADP 06	Steady state 1		Steady state 2	
Variable	Data	σ [%]	Data	σ [%]
M_{gas} [Nl/min]	10.0	5.0	0.0	2.8
M_{lbe} [kg/s]	2.66	2.9	1.33	2.9
ΔT_{FPS} [°C]	68.4	1.1	130.1	0.4
Q_{nom} [W]	3.00E+04	0.2	3.00E+04	0.2
Q_{eff} [W]	2.68E+04	3.9	2.54E+04	3.7
Q_{pre} [W]	2508	17.5	2675	8.6
Q_{tfm} [W]	1933	0.2	1652	0.3

Experimental results – LBE temperature

TEST ADP 10

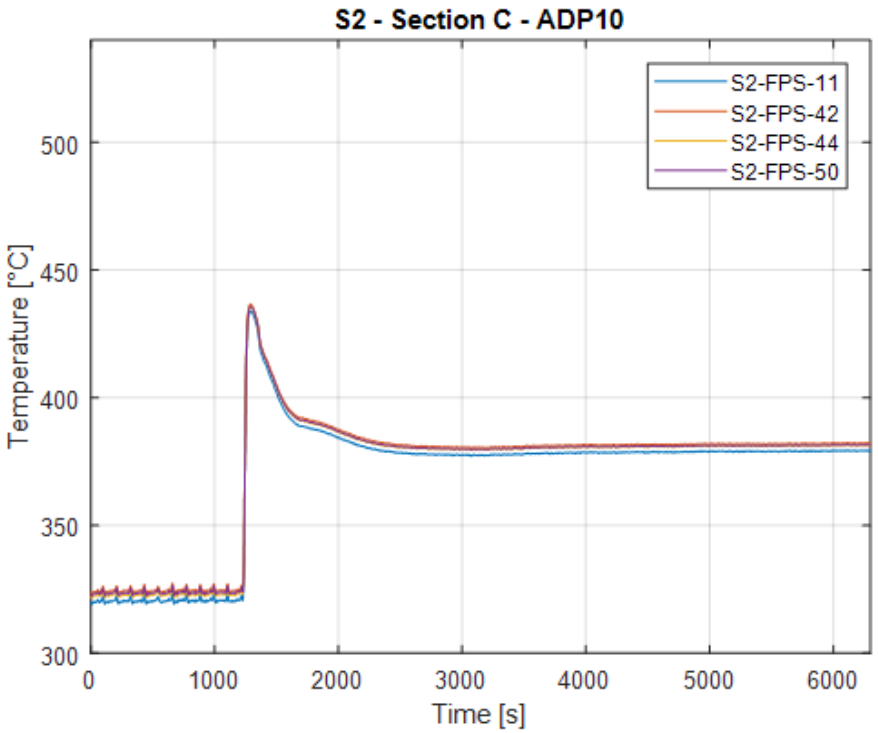


TEST ADP 06

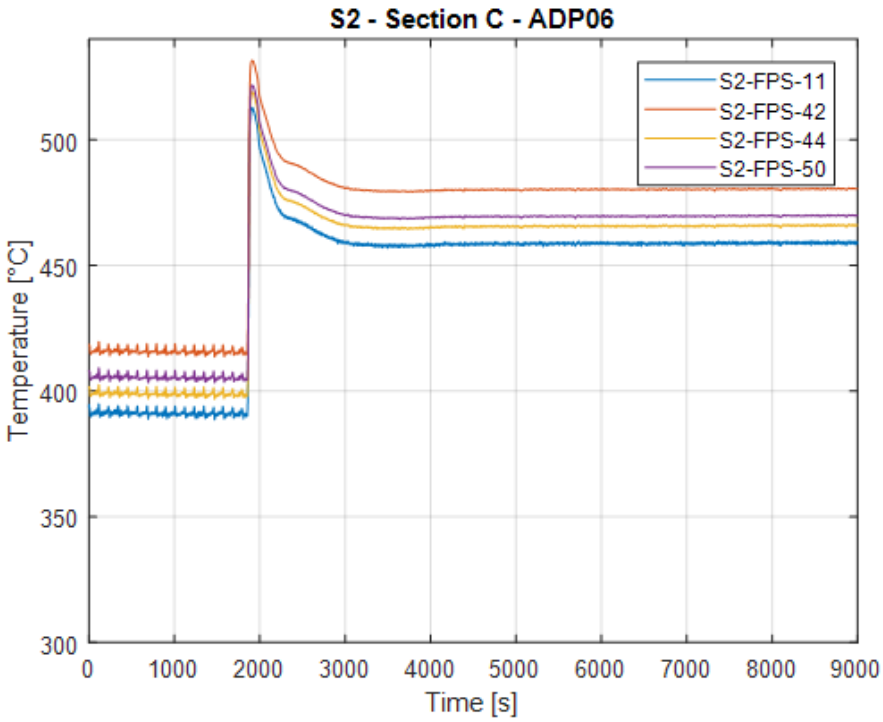


Experimental results - FPS temperatures S2

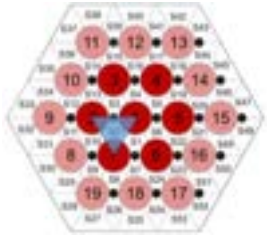
TEST ADP 10



TEST ADP 06

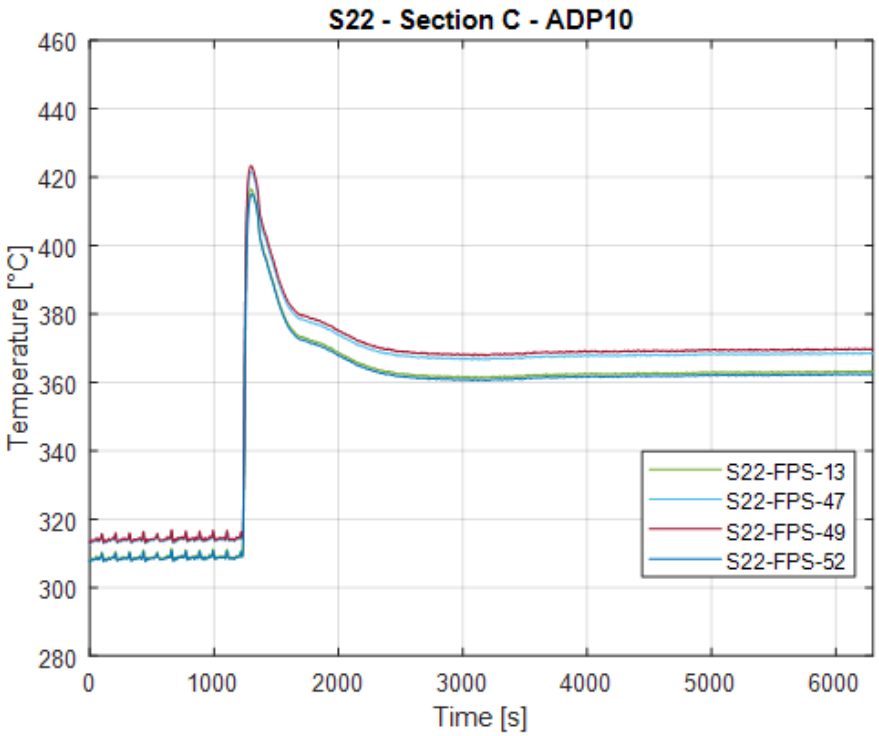


z = 360mm

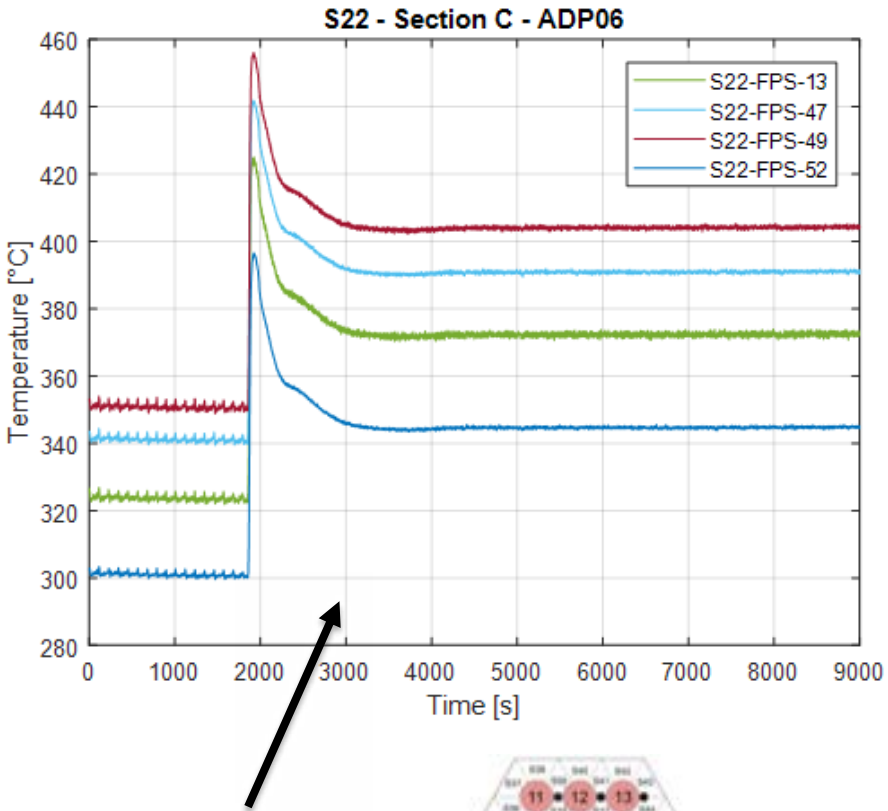


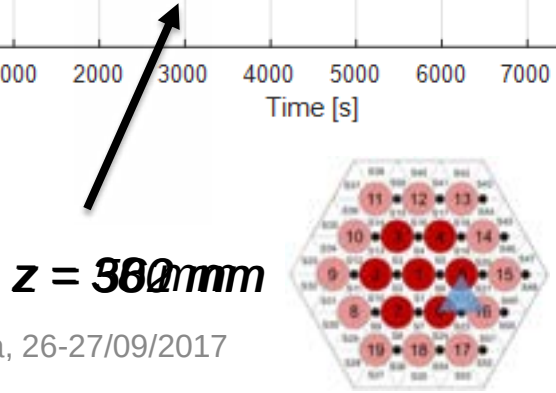
Experimental results - FPS temperatures S22

TEST ADP 10



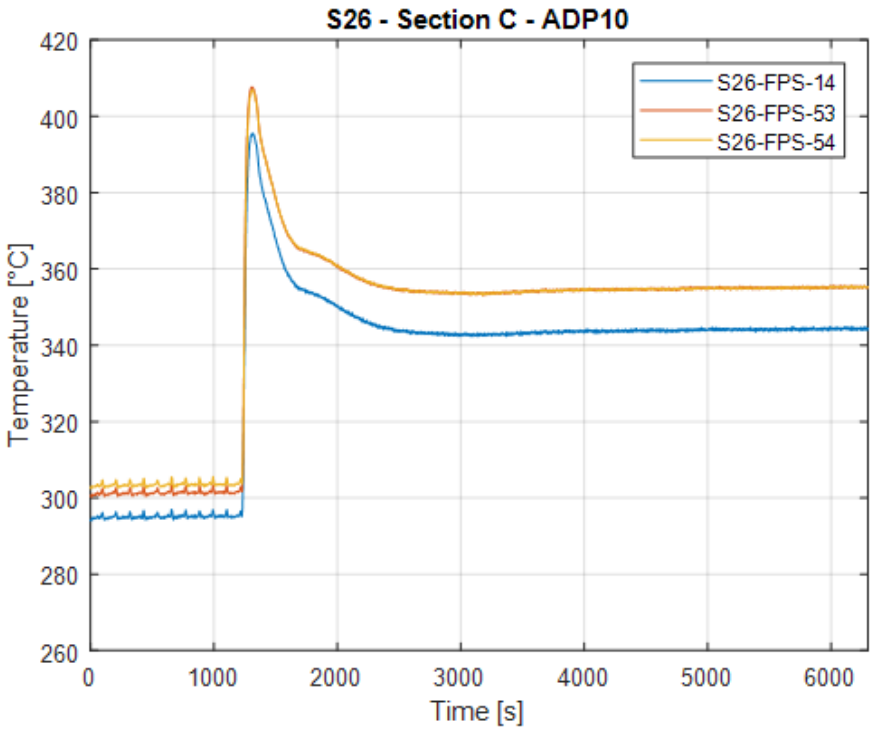
TEST ADP 06



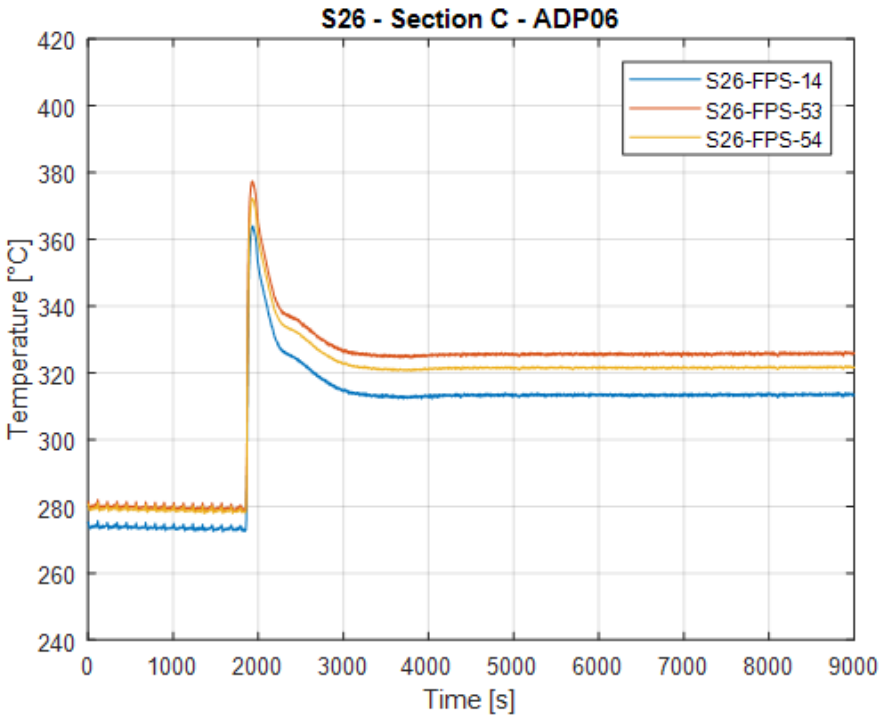


Experimental results - FPS temperatures S26

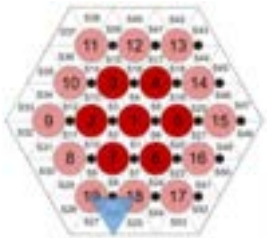
TEST ADP 10



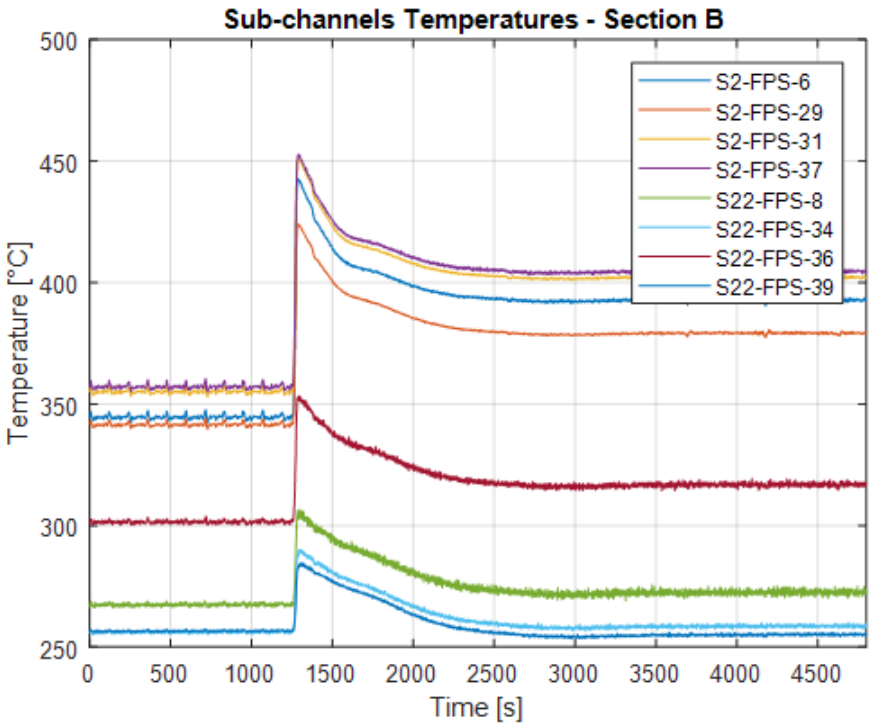
TEST ADP 06



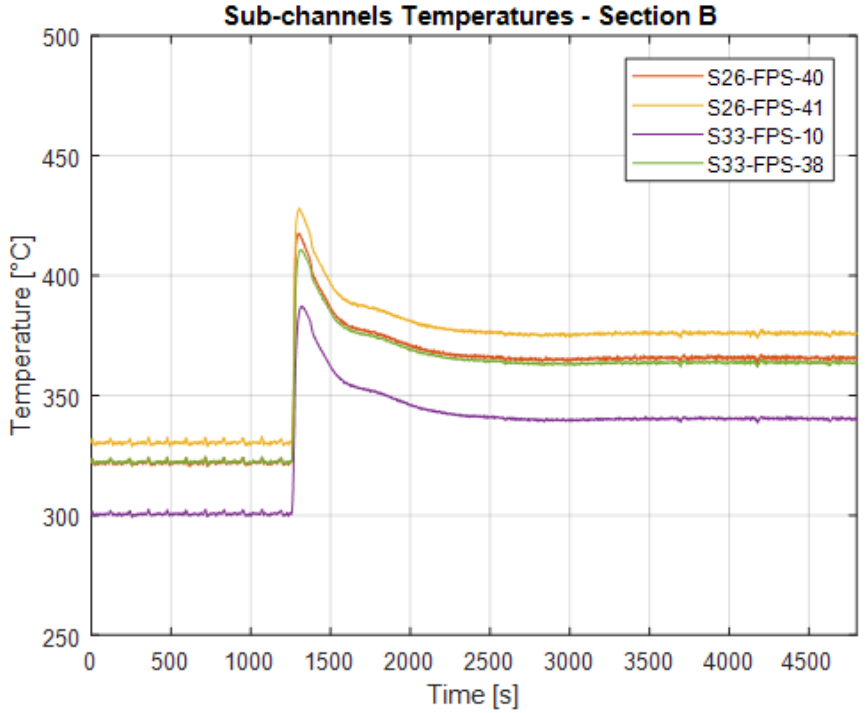
z = 300mm



Experimental results - ADP 07

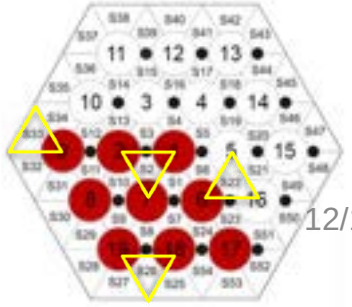


Internal sub-channels S2 & S22



External sub-channels S26 and S33

z = 300 mm



Conclusions

- Experimental tests with gas flow rate transition have been performed in NACIE-UP facility;
- A first reference test was characterized by all 19 pins on;
  - Lower local Nu in external sub-channels (S26 and S33)
  - Higher values in the inner sub-channels (S2, S5 and S22)
- A second test, characterized by the same power distributed in among the 7 central pins (higher wall heat flux) was compared to the reference one;
  - Same integral parameters between the two tests
  - S2, S5 and S22 were hotter in the second test, S26 and S33 colder (off during the second test)
- A third test was characterized by power distribution localized in a limited part of the bundle (triangular sections), with pin-wall heat flux comparable with the second test;
  - FPS temperature distribution affected by the power distribution
  - Non-conventional behaviour was noticed in S2
- Obtained experimental data was used to characterize bundle (by computing the heat transfer coefficient). The collected system data can be used to qualify STH codes, whereas the local fuel bundle data (especially the ones from dissymmetric tests) can be useful for the validation of CFD codes and coupled STH/CFD methods for HLM systems.

Morena Angelucci
PhD Student
University of Pisa
Dipartimento di Ingegneria Civile e Industriale
+39 050/2218080

morena.angelucci@for.uinpi.it

Experimental Characterization of Bubble Detection in liquid metal pool

A. Del Nevo, M. Tarantino [ENEA]
M. Eboli, N. Forgione [UNIPI]
D. Mazzi, F. Giannetti [SRS]

WORKSHOP TEMATICO: Gen. IV - LFR
ADP MiSE-ENEA (PAR2016-LP2)
Aula Magna - Scuola di Ingegneria e Architettura, Università di Bologna
26-27 Settembre, 2017

List of contents

- Objectives
- Introduction to LIFUS5/Mod3
- Description of LIFUS5/Mod3 – Test Section Small Leak (S1_A)
- Execution of the experiments – Test series C
- Summary and Follow-up

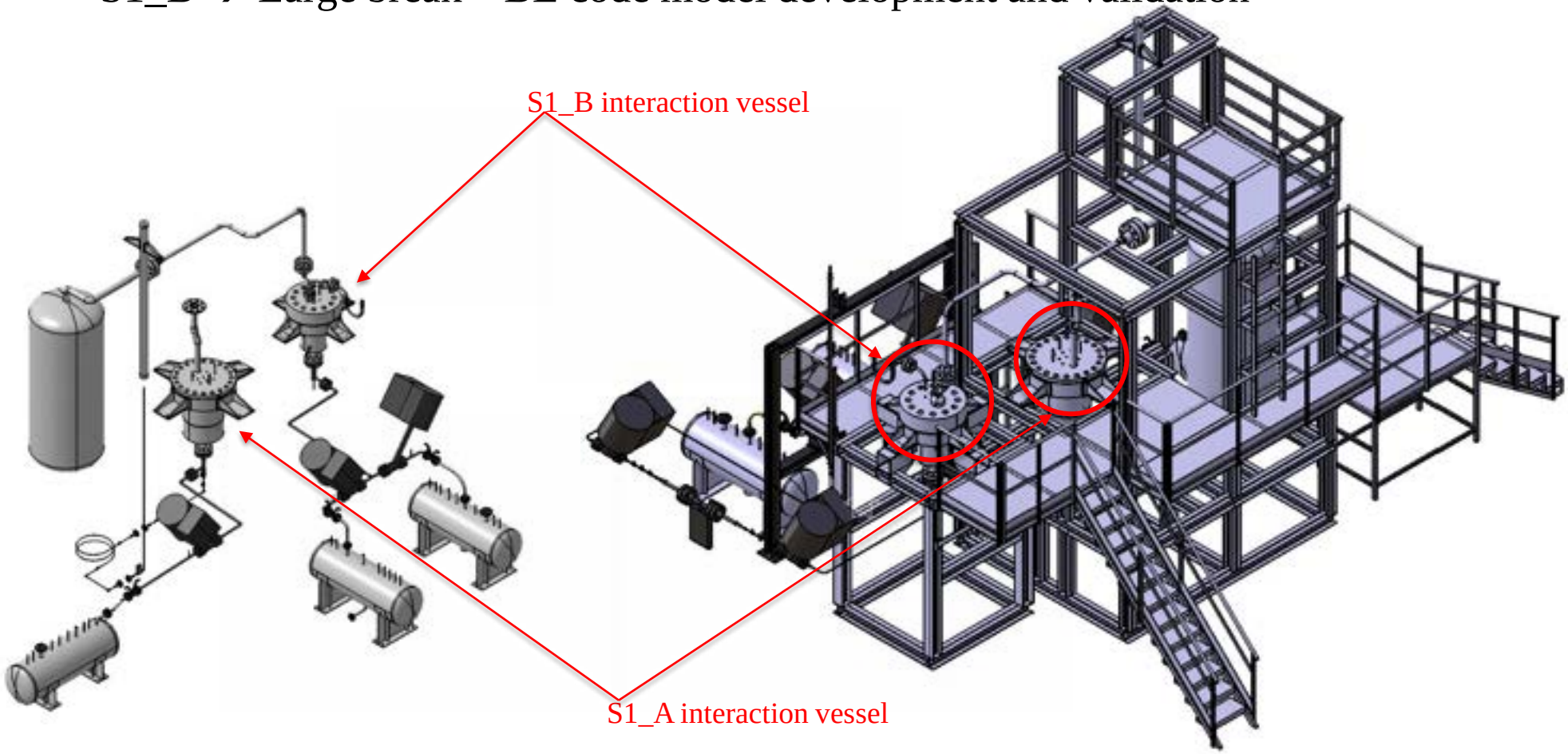
OBJECTIVES

The goal is to implement an experimental activity, supported by the numerical simulations, that will **characterize the leak rate and bubbles sizing through typical cracks** occurring in the pressurized tubes

- Basic tests in LIFUS5/Mod2 facility will be carried out to correlate the flow rates of the leakage through selected cracks with signals detected by proper transducers
- Different crack sizes and geometries will be analyzed, while the injection pressure and the temperature will be recorded
- A detection system will detect the bubbles migration through the free level

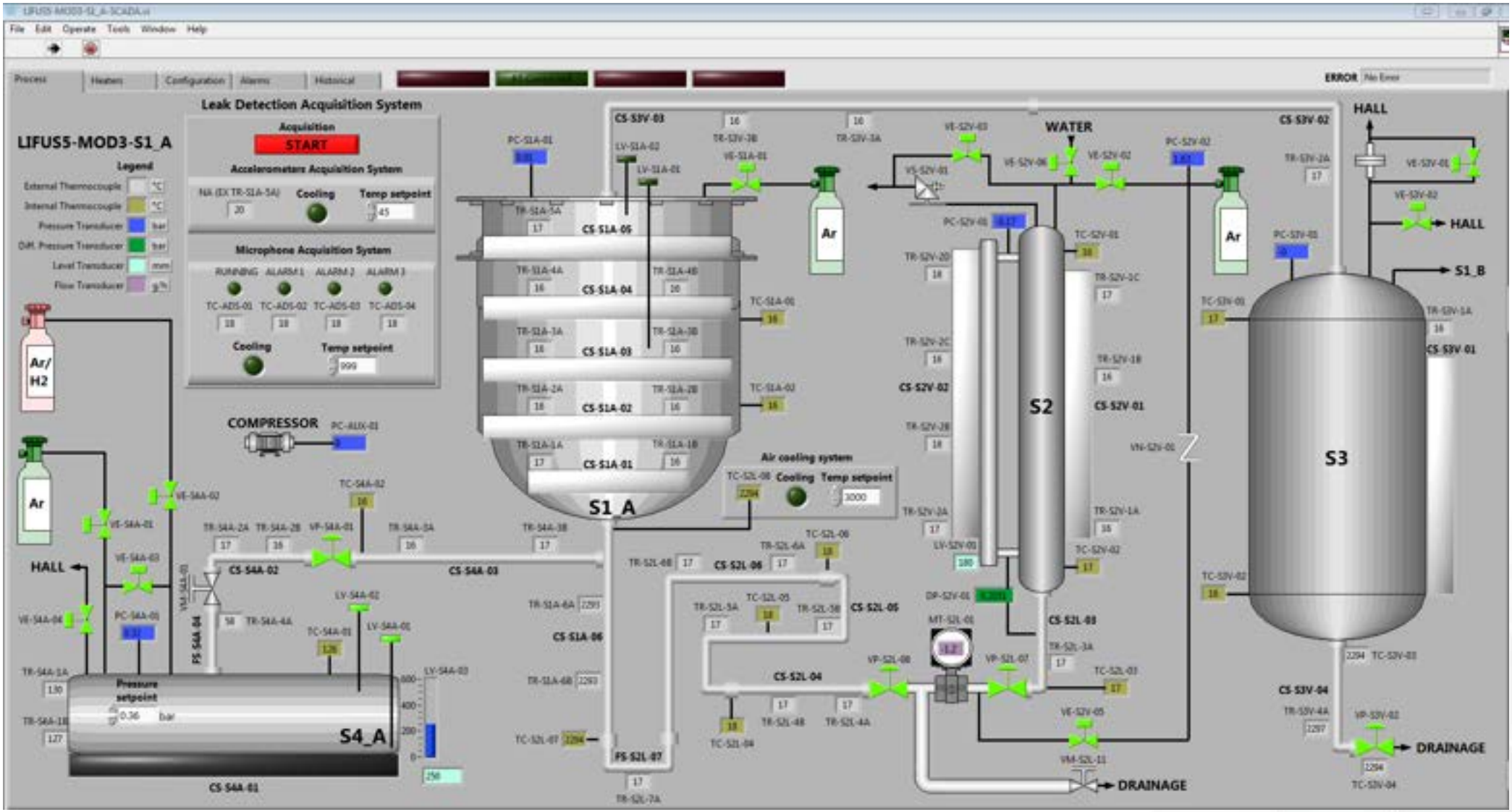
INTRODUCTION TO LIFUS5/MOD3

- LIFUS5/Mod3 (*the third refurbishment*) is a multi purpose facility
  - experiments related the HLM (i.e. PbLi, LBE, Pb) and water interaction /reaction
    - ✓ S1_A → Small Leak detection
    - ✓ S1_B → Large break – BE code model development and validation



LIFUS5/MOD3: TEST SECTION SMALL LEAK

- LIFUS5/Mod3-S1_A synoptic (control system and data recording based on NI / Labwiew)
  - Two additional PCs are in charge of the leak detection systems (NI and DAWEsoft)



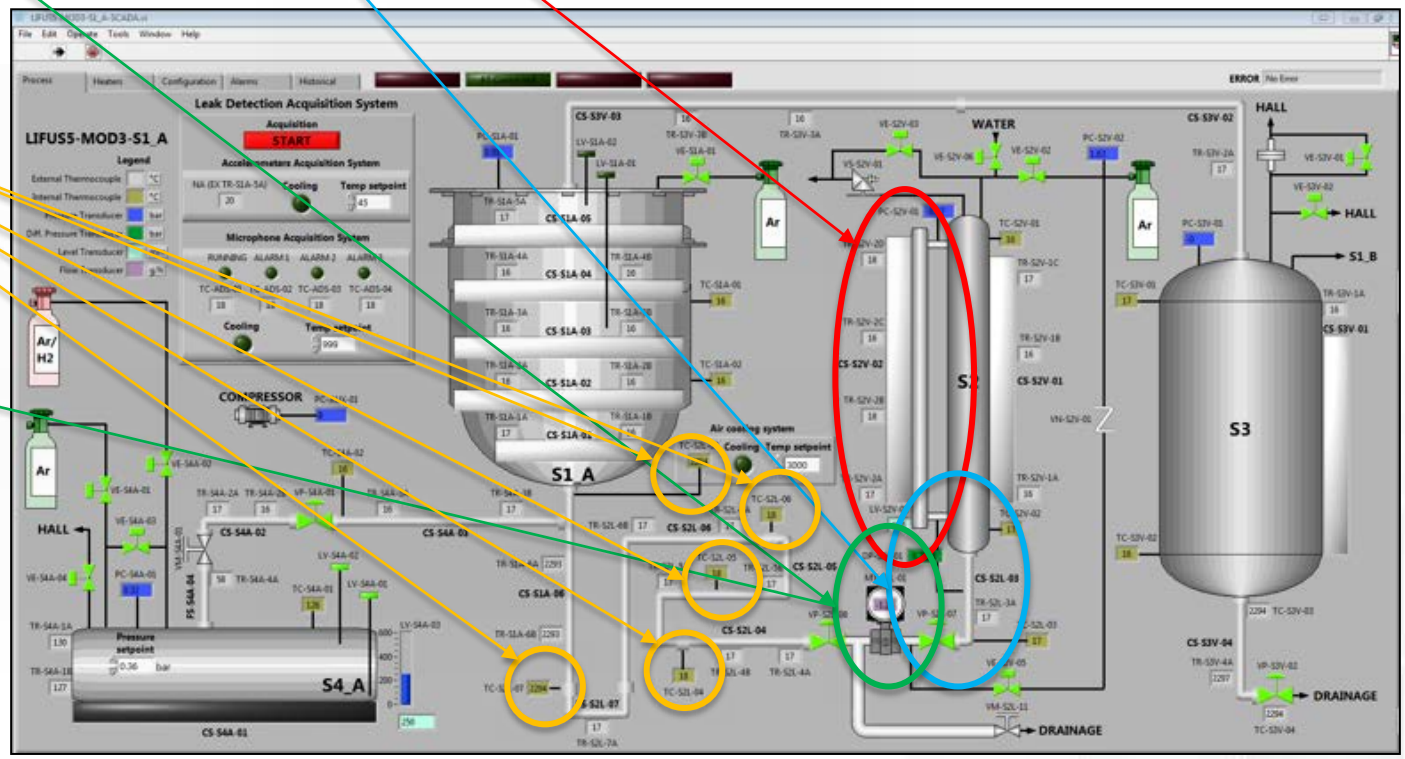
LIFUS5/MOD3: TEST SECTION SMALL LEAK

Injection system acquisition (1 Hz)

- S2 filled with “cold” water at 16 bar
- Mass of water injected monitored through
  - the level meter (resolution 5mm)
  - DP meters (resolution < 1 mm)
  - Coriolis flow meter



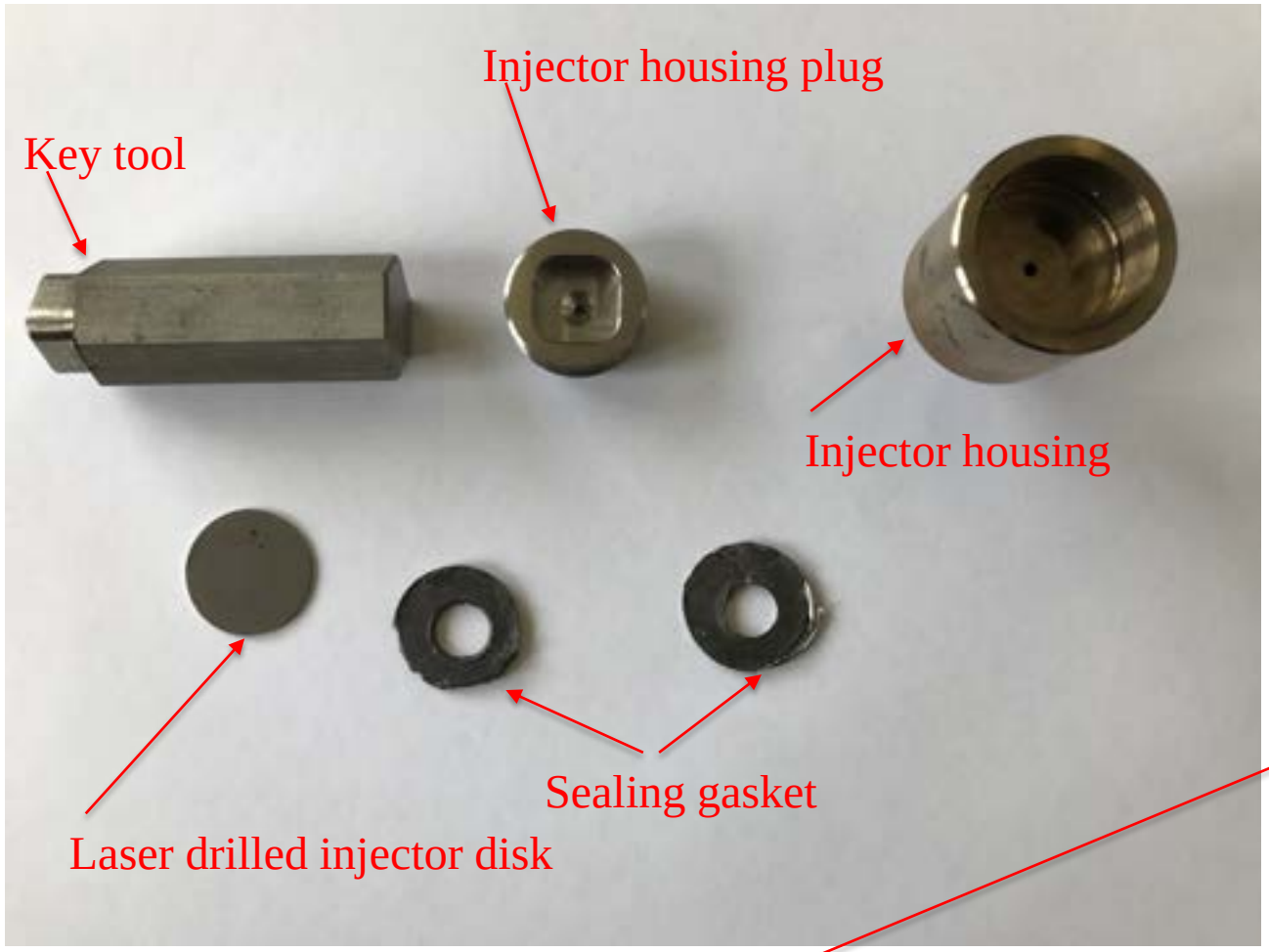




LIFUS5/MOD3: TEST SECTION SMALL LEAK

- Injector disk hole design: nominal orifice diameters

Description	T#1	T#2	T#3	T#4	T#5	T#6	T#7	T#8	T#9
Orifice diameter [mm]	0.005	0.010	0.020	0.040	0.060	0.080	0.10	0.15	0.20





Injector system device

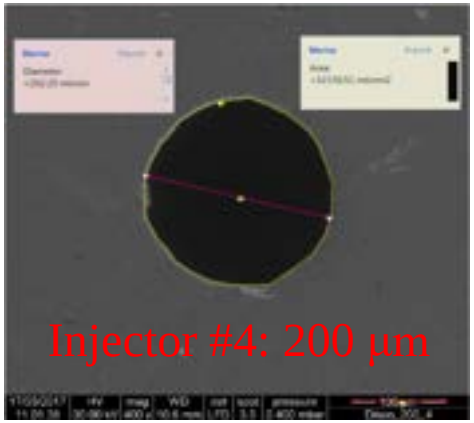
LIFUS5/MOD3: TEST SECTION SMALL LEAK

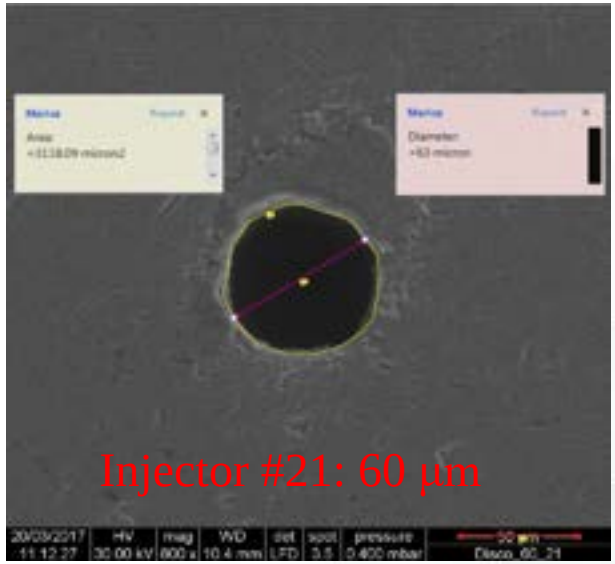
- Injector disk holes characterization



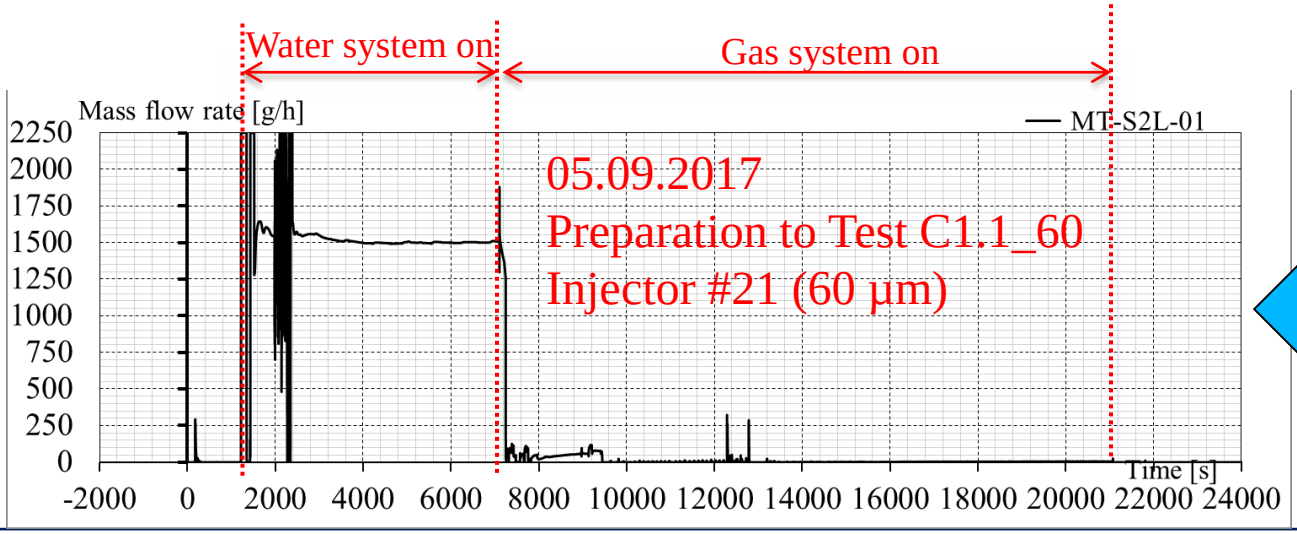
Hole dimensions is characterized using SEM in CR Bologna (A. Gessi)





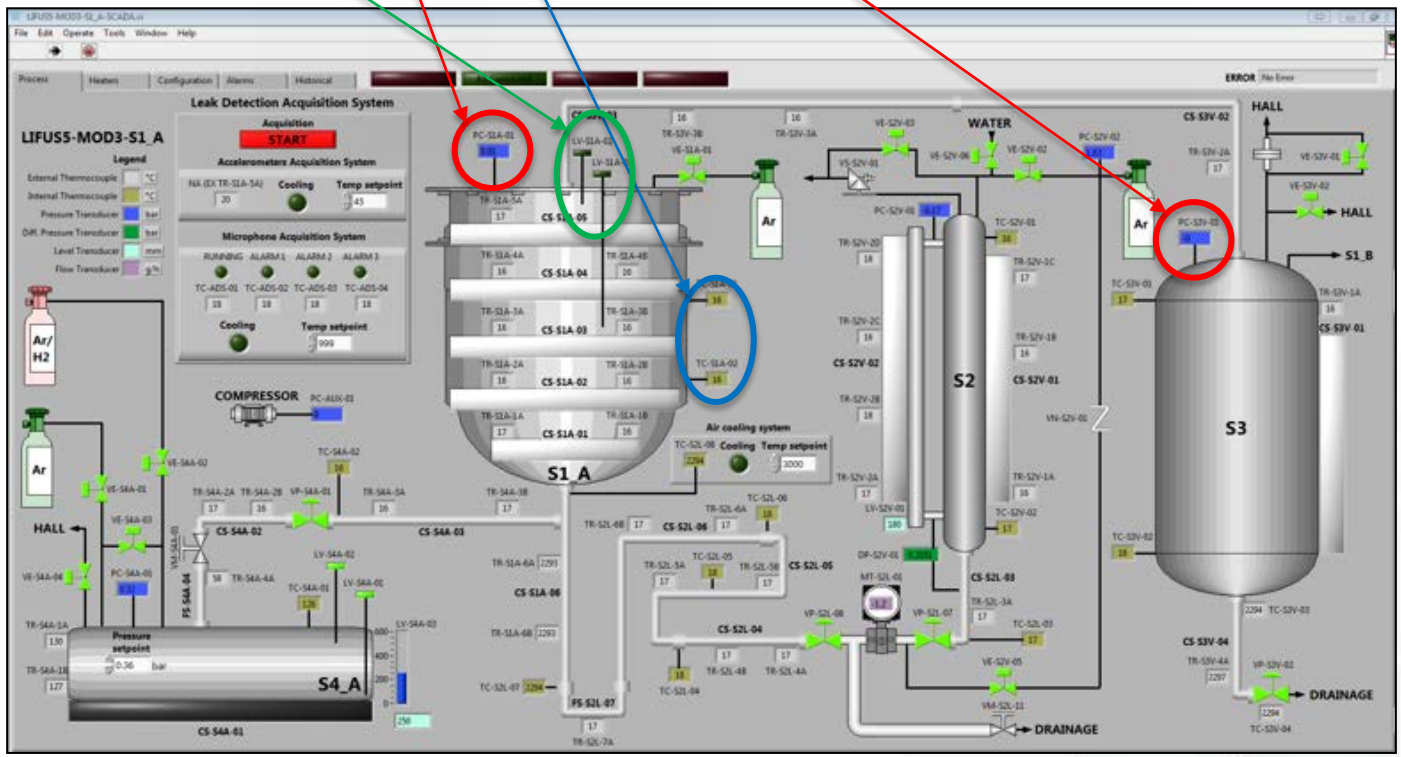


Injection performance is characterized prior-to-test in cold and hot conditions



LIFUS5/MOD3: TEST SECTION SMALL LEAK

- S1 filled with LBE @ 1 bar - S3 connected
  - Absolute pressures in S1 and S3
  - LBE temperature monitored by 2 TC
  - 2 Level ON/OFF
  - 6 strain gauges on the vessel wall @ 10kHz (**<u>OFF during the first 2 tests</u>**)
  - Small leak detection system



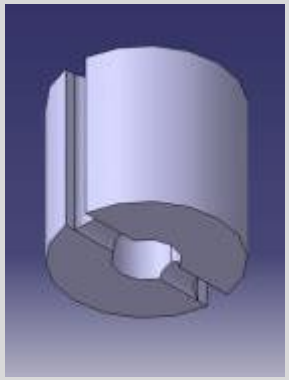
LIFUS5/MOD3: TEST SECTION SMALL LEAK

Primary proposed detection system

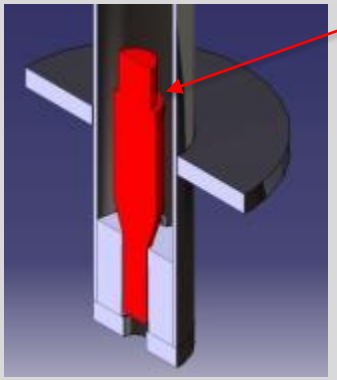
Acoustic Detection (AD) with dedicated hardware and software (i.e. real time acquisition system)

- Acquisition at @ 20 kHz
- Data analysis on real time (8 channels)
- 5 microphones on the cover flange

AD support and cooling system of Low T acoustic sensors



Ceramic support



AD support and cooling system

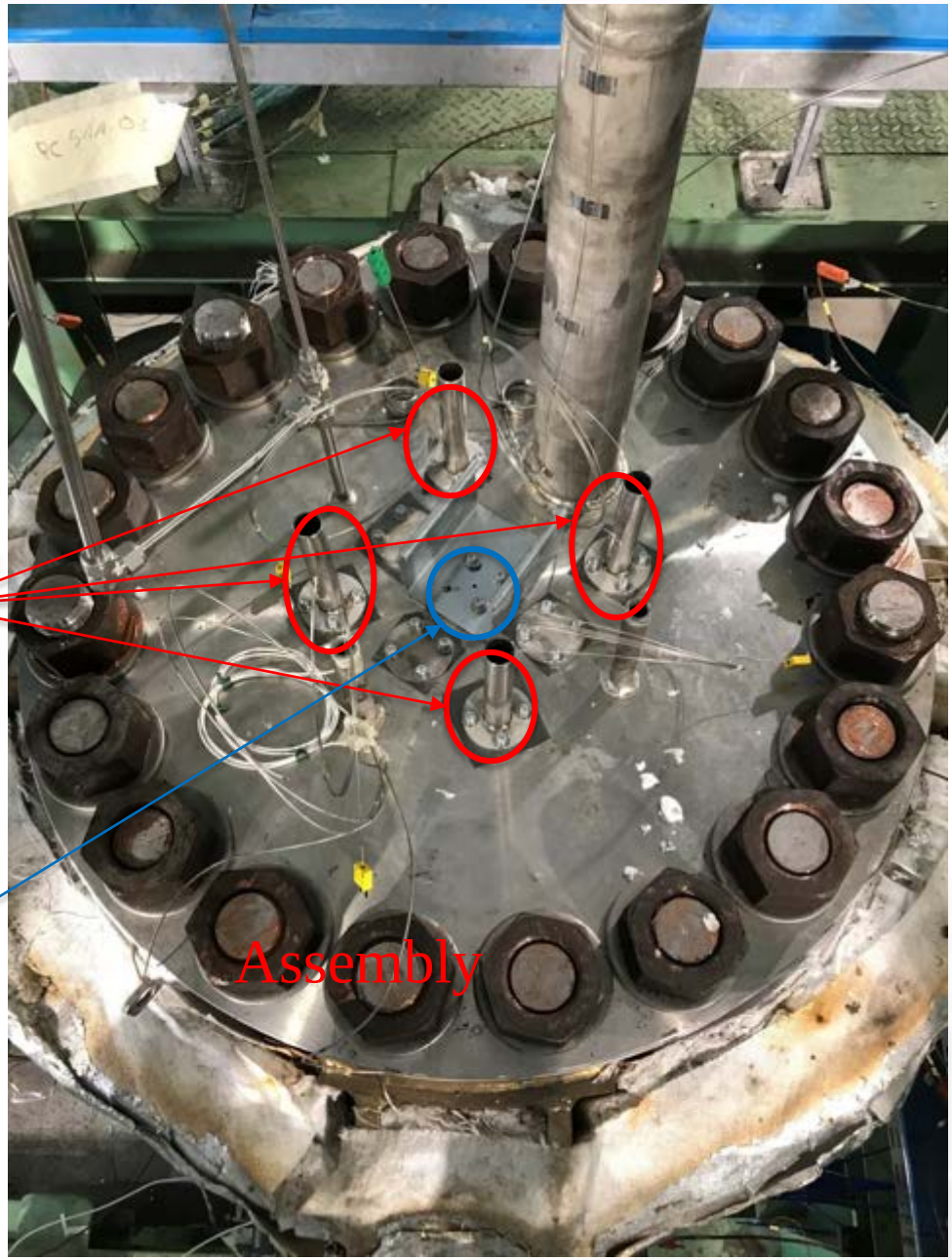
Temperature is monitored (TC) and Ar gas cooling thanks the lateral grooves in the ceramic support



#4 → Model 130E20 (low temperature)



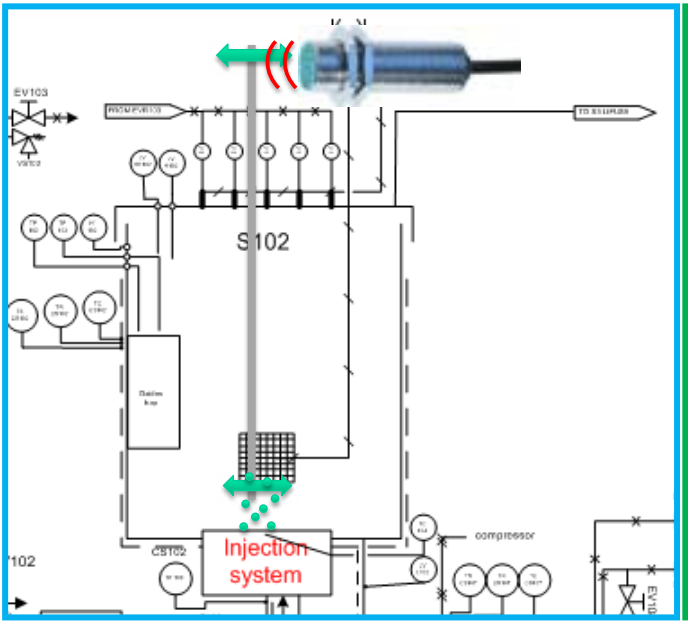
#1 → Model 377B26 (high temperature)



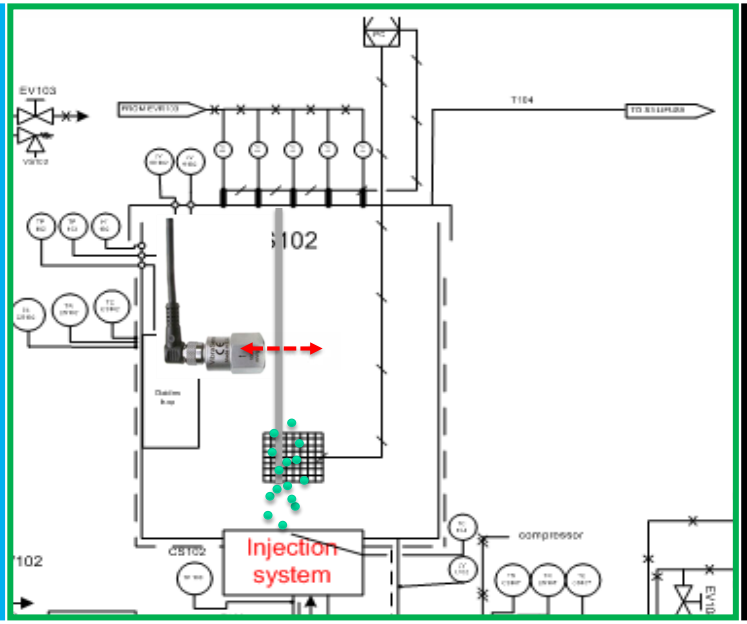
LIFUS5/MOD3: TEST SECTION SMALL LEAK

Alternative (*promising*) identified detection systems

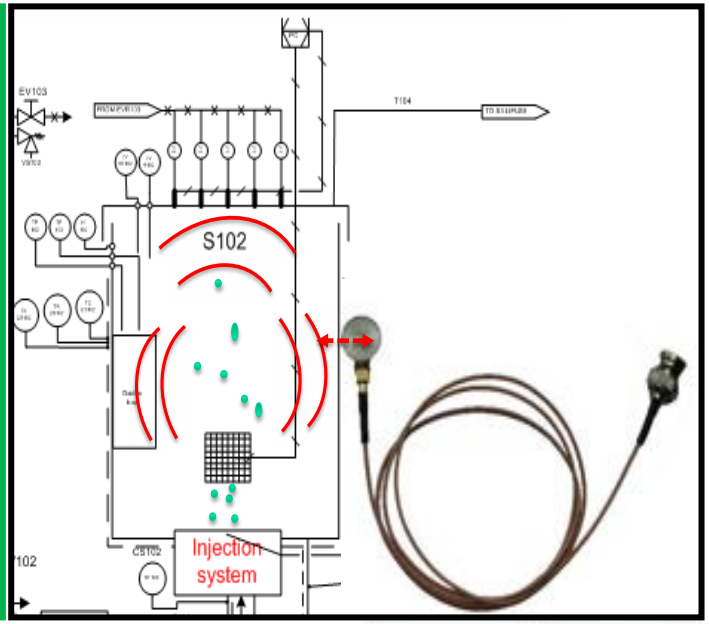
1. Inductive proximity sensor (i.e. High Sensitivity Accelerometer – **HSA**) installed outside the vessel
2. Accelerometer sensors installed inside the vessel (i.e. High Temperature Accelerometer – HTA) installed on a metallic support
3. Acoustic Emission (**AE**) sensor installed outside the vessel, measuring the high frequency signals



High Sensitivity Accelerometer – **HSA**



High Temperature Accelerometer – HTA



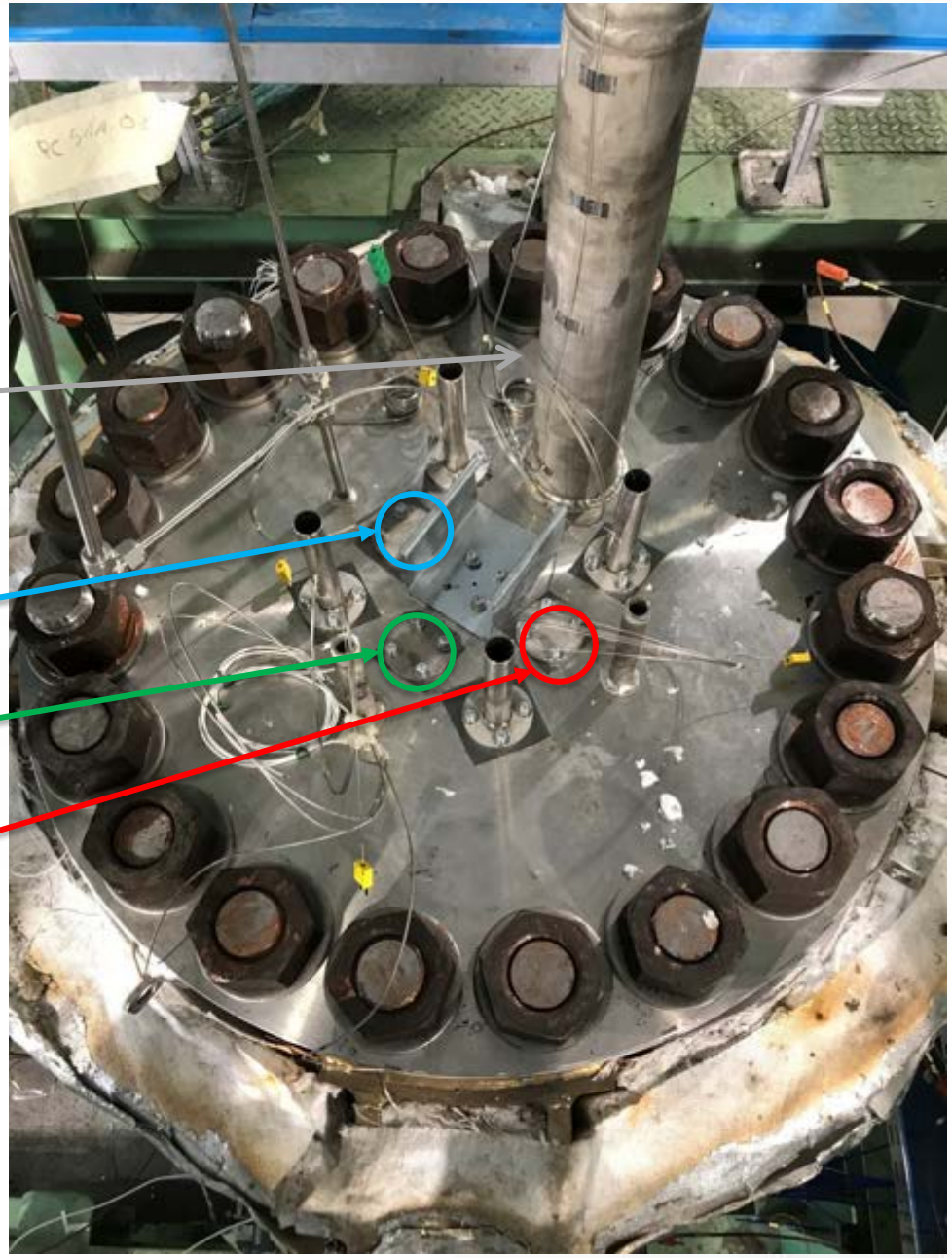
Acoustic Emission – **AE**

LIFUS5/MOD3: TEST SECTION SMALL LEAK

Alternative (*promising*) identified detection systems

1. High Sensitivity Accelerometer – **HSA**
2. High Temperature Accelerometer – HTA
3. Acoustic Emission (**AE**)



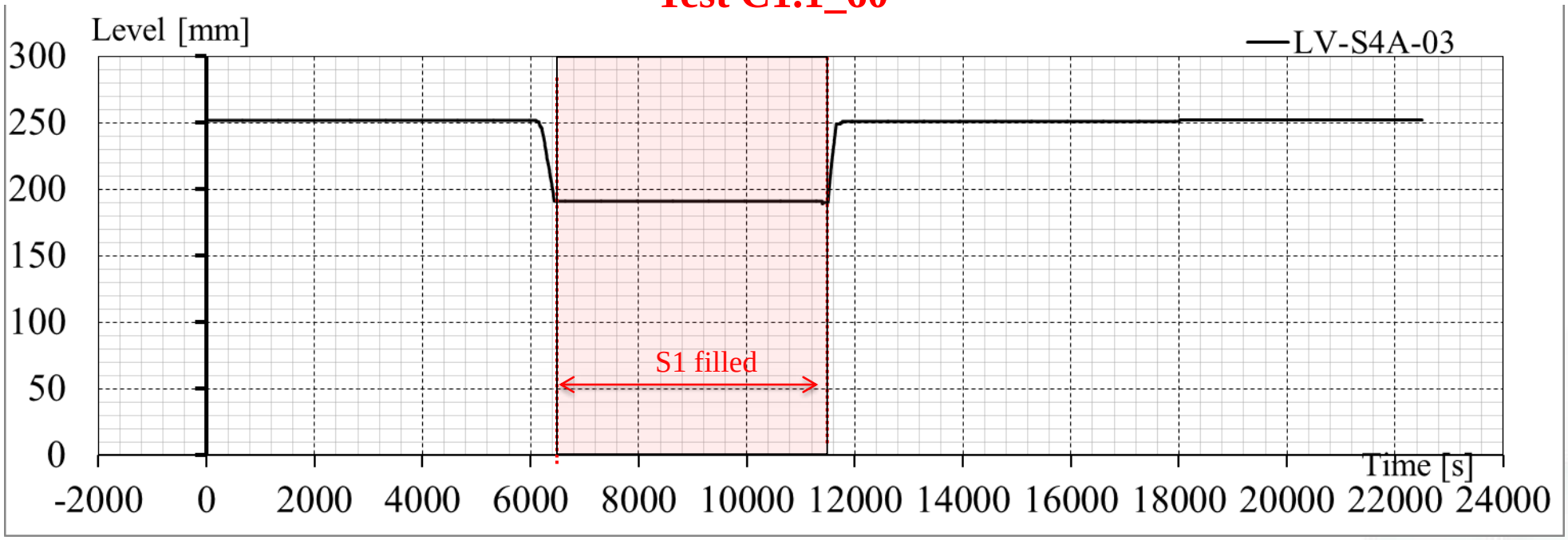


EXECUTION OF EXPERIMENTS – TEST SERIES C

Two tests executed (*analyses of data still in progress*)

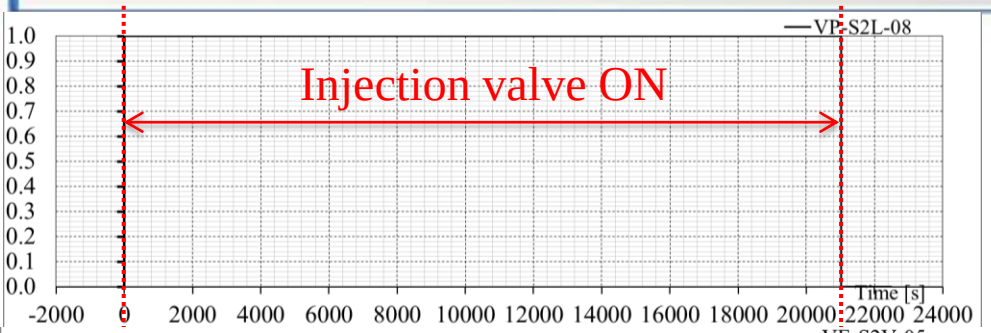
- Test C1.1_60 (*06.09.2017*)
- Test C2.1_80 (*13.09.2017*)

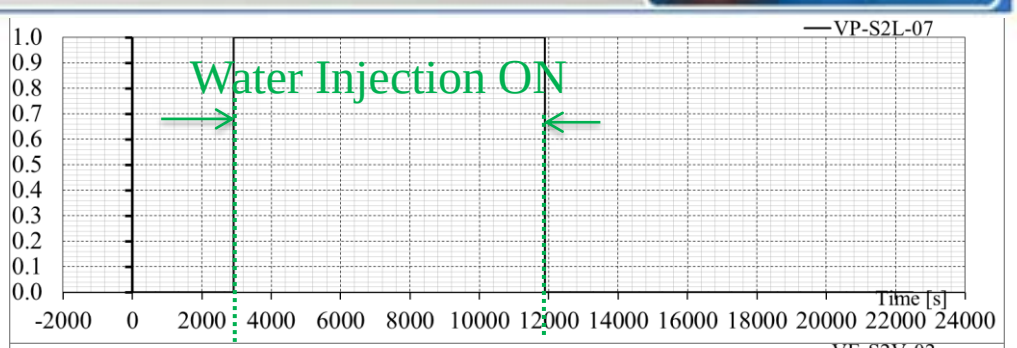
Test C1.1_60

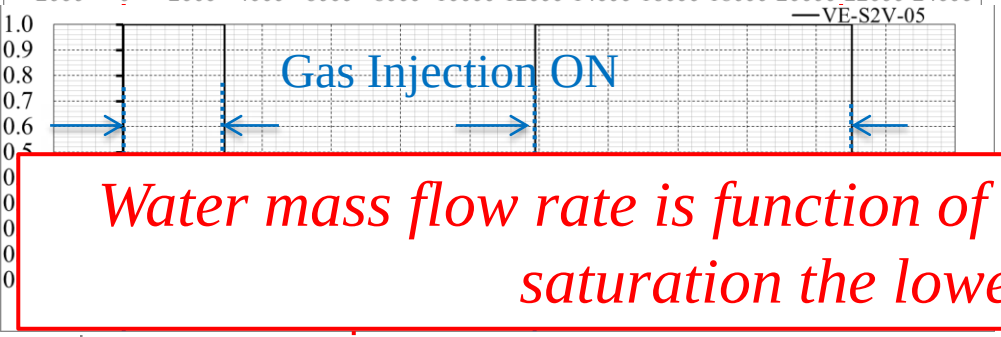


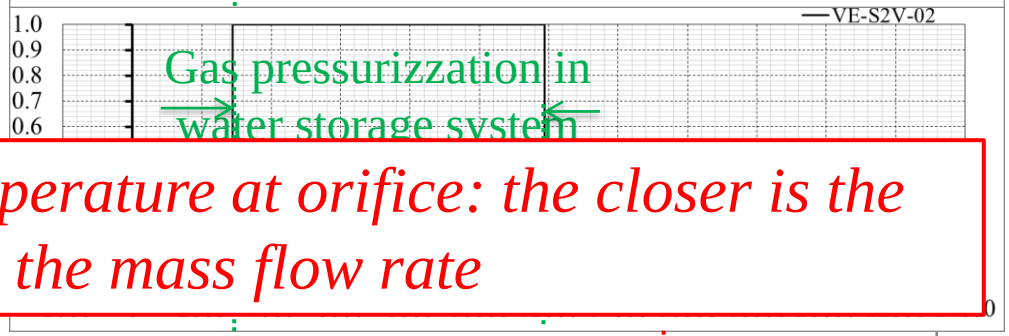
Storage tank level

TEST C1.1_60

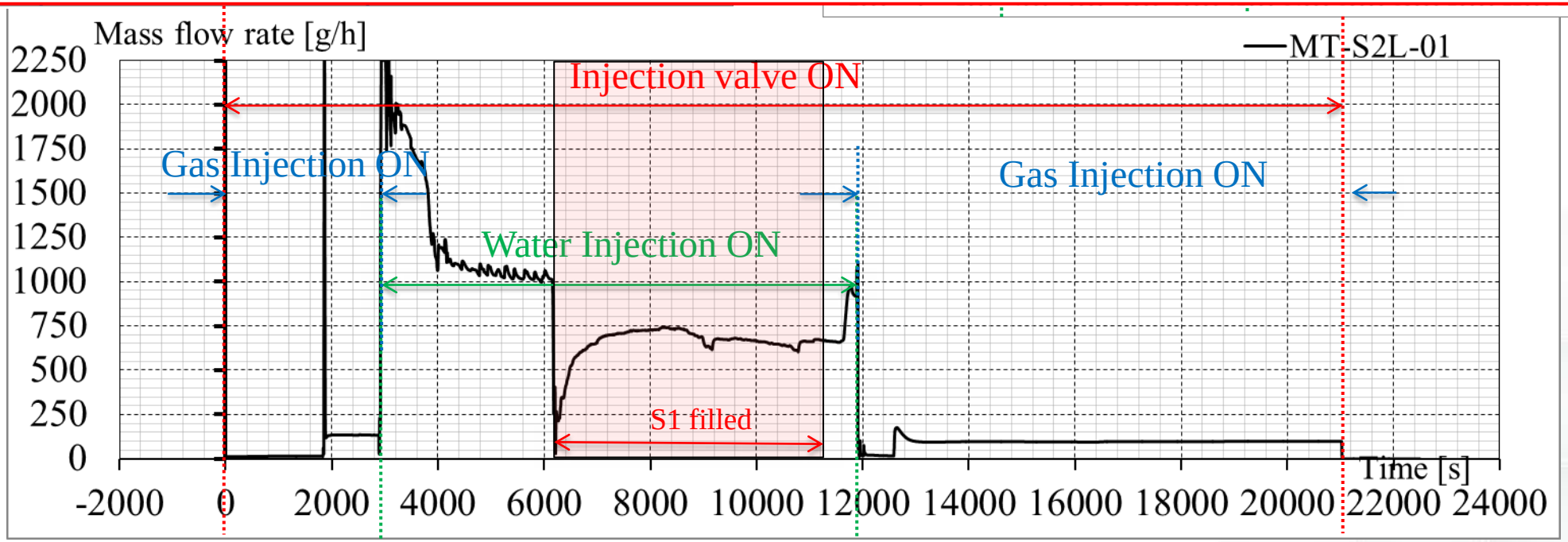








Water mass flow rate is function of temperature at orifice: the closer is the saturation the lower is the mass flow rate

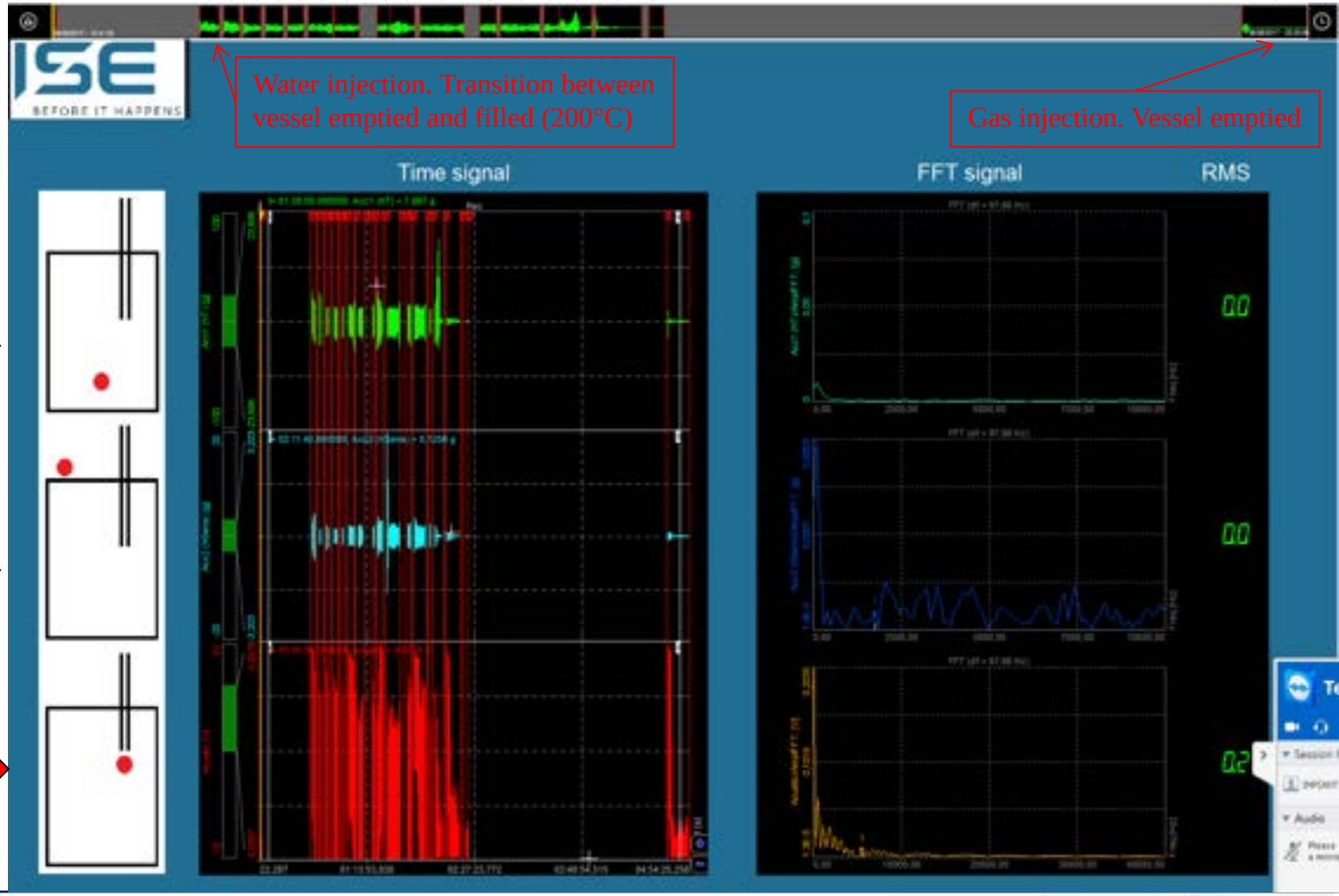


TEST C1.1_60

It seems possible to distinguish the phases: ⟹ *Analyses of data is not yet done*

1. Water injection w/o LBE in S1A
2. Water injection w LBE in S1A
3. Gas Injection

Acquisitions in intervals from time 16.31 to 20.35 – about 30GB of compressed data



High Temperature Accelerometer – HTA

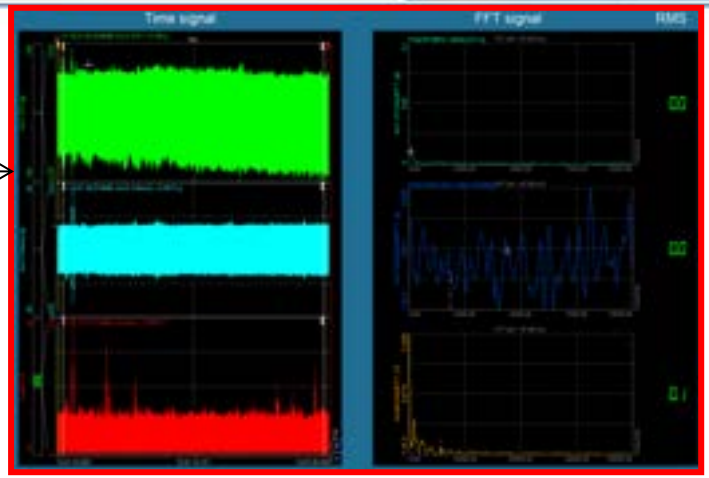
High Sensitivity Accelerometer – **HAS**

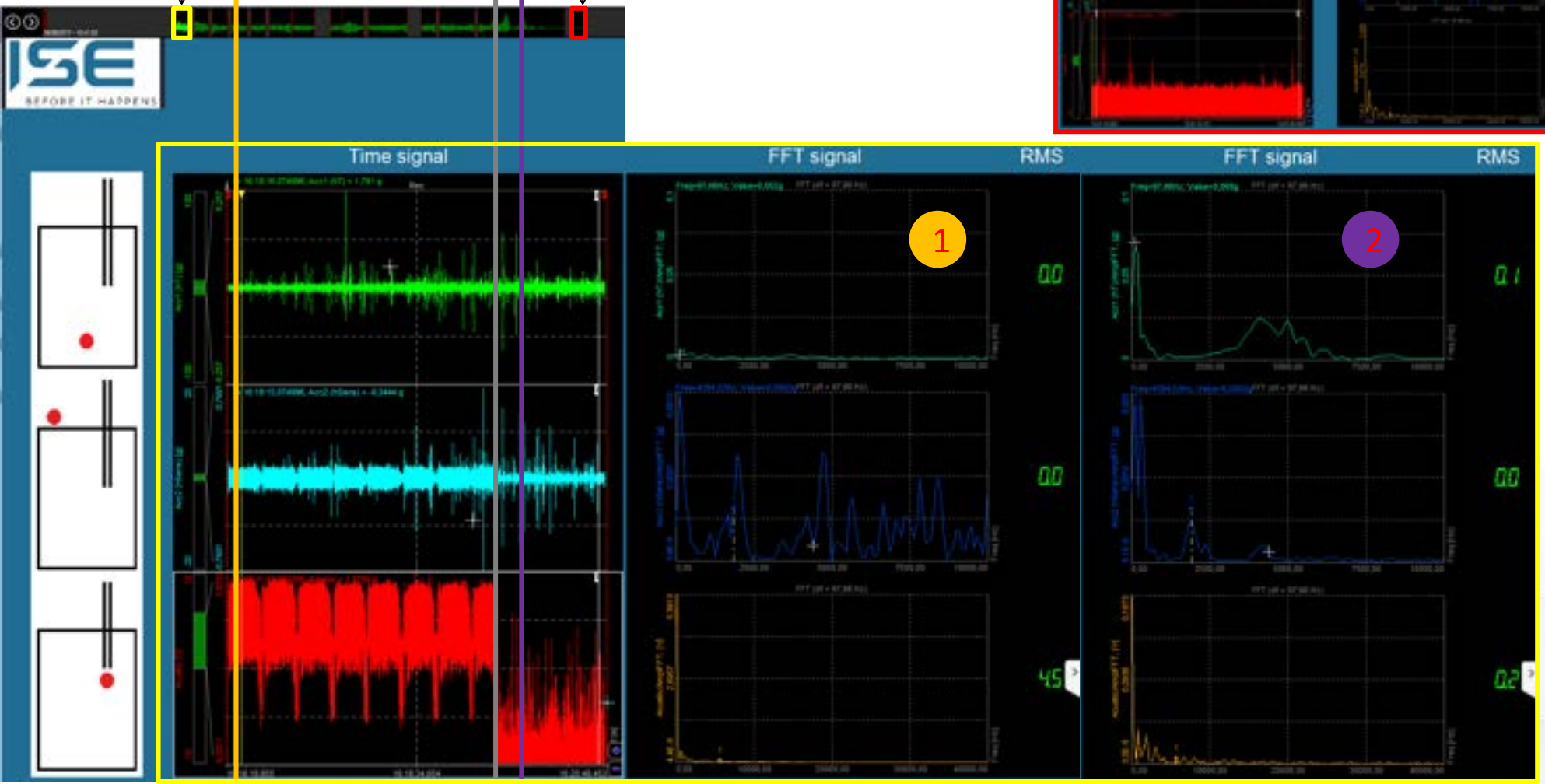
Acoustic Emission (**AE**)

TEST C1.1_60

Water injection. Transition between vessel emptied and filled

Gas Injection





SUMMARY AND FOLLOW-UP

- An experimental activity for characterizing the leak rate through typical cracks occurring in the pressurized tubes has been implemented
- 50 laser drilled disks have been manufactured and characterized for simulating the leak
- A primary proposed detection system – Acoustic Detection (AD) – has been installed and tested
- Alternative (promising) identified detection systems, supported by the PAR2016, have been also identified and installed. They are: 1) High Sensitivity Accelerometer; 2) High Temperature Accelerometer; and 3) Acoustic Emission (AE)
- Two (i.e. C1.1_60 and C2.1_80) out of ten (planned) tests have been executed
- Preliminary evaluation of data seems to demonstrate that is possible to distinguish the different phases of the experiment. Analysis of data is in progress
- Analyses of the experimental data and the preparation of the EDTAR are in progress

GENERATION IV
Lead cooled Fast Reactor
Stato attuale della tecnologia e prospettive di sviluppo

Bologna, 26-27 Settembre 2017



SAPIENZA
UNIVERSITÀ DI ROMA

Pre-test analysis of protected loss of primary pump transients in CIRCE-HERO facility

V. Narcisi, F. Giannetti, A. Del Nevo, M. Tarantino, G. Caruso

OUTLINE

➢ GOAL OF THE ACTIVITY

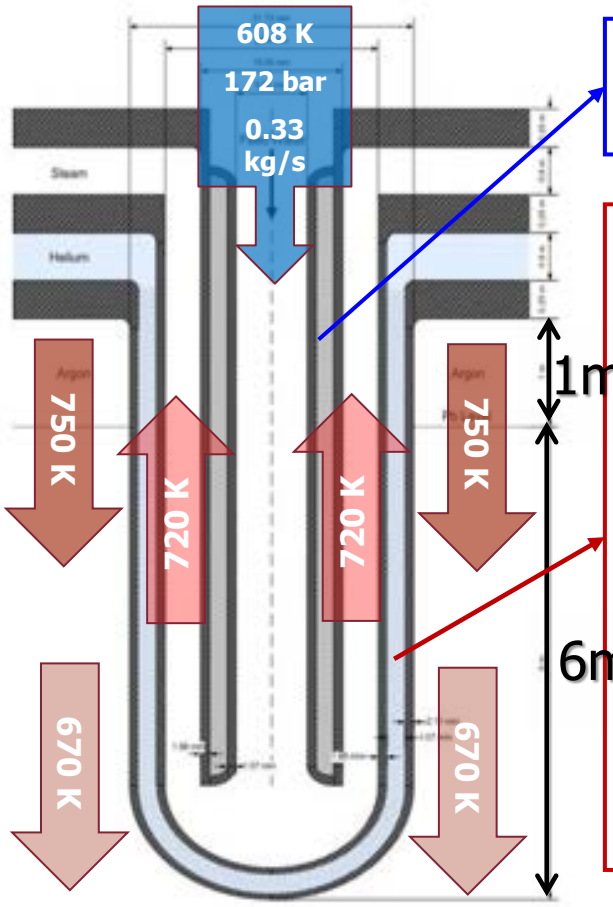
In the framework of **Horizon 2020 SESAME project**, the activity aims to perform pre-test simulations to provide the preliminary test-matrix for the realization of the validation benchmarck

➢ OVERVIEW

- CIRCE-HERO Test Section
- CIRCE-HERO: Thermal-Hydraulic model
- Pre-Test Analysis
- Conclusions

CIRCE-HERO Test Section

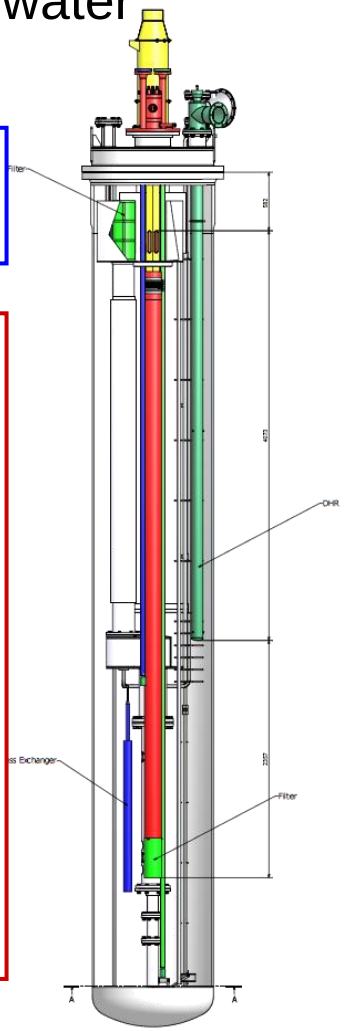
CIRColazione Eutettico – Heavy liquid mEtal-pRessurized water cOoled tube



- **Insulator layer** in order to **prevent** the **steam condensation**
- To investigate a bundle of

Gap pressurized with **Helium and filled** by **high thermal conductivity powder** to

1. Avoid **lead-water interaction** in case of tube rupture (double physical separation).
2. **Detect tube leakages** thanks to monitoring the He pressure
3. **Enhance the heat exchange** capability thanks to the powder medium.

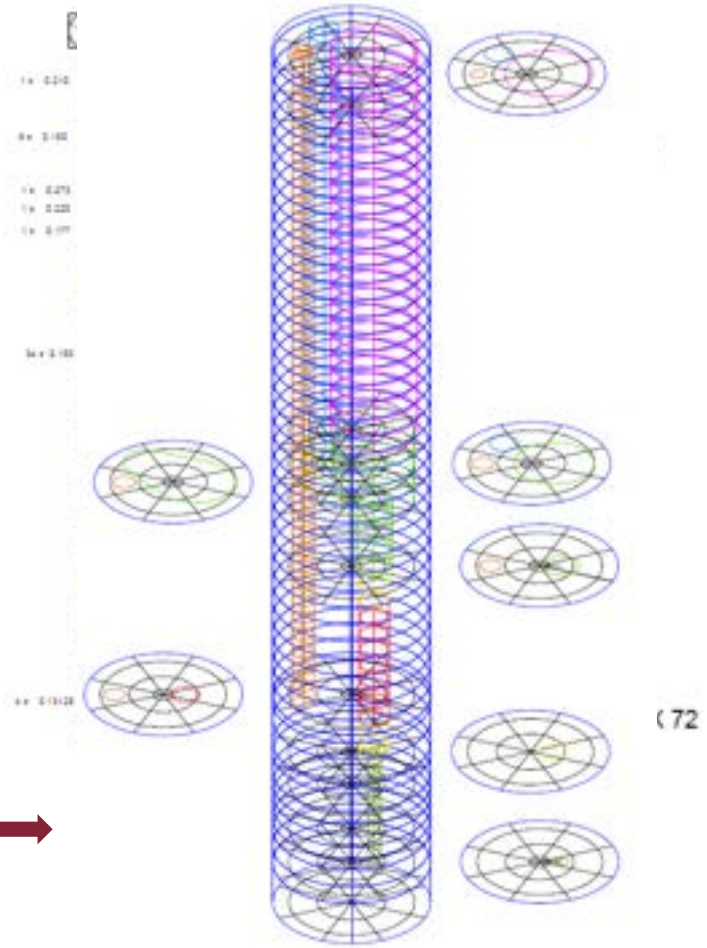


CIRCE-HERO: Thermal-Hydraulic Model

The validated thermal-hydraulic model of **CIRCE-ICE**, developed using **RELAP5-3D© ver. 4.3.4**, has been upgraded to reproduce the **HERO test section**

- **Region #1** main differences:
  - The full **CIRCE-HERO** model consists of:
    - **2942** hydrodynamic volumes
    - **7565** junctions
- **Region #2**: the **3D component** is the same. The only difference is the volume occupied by the HX
  - **21153** heat transfer nodes

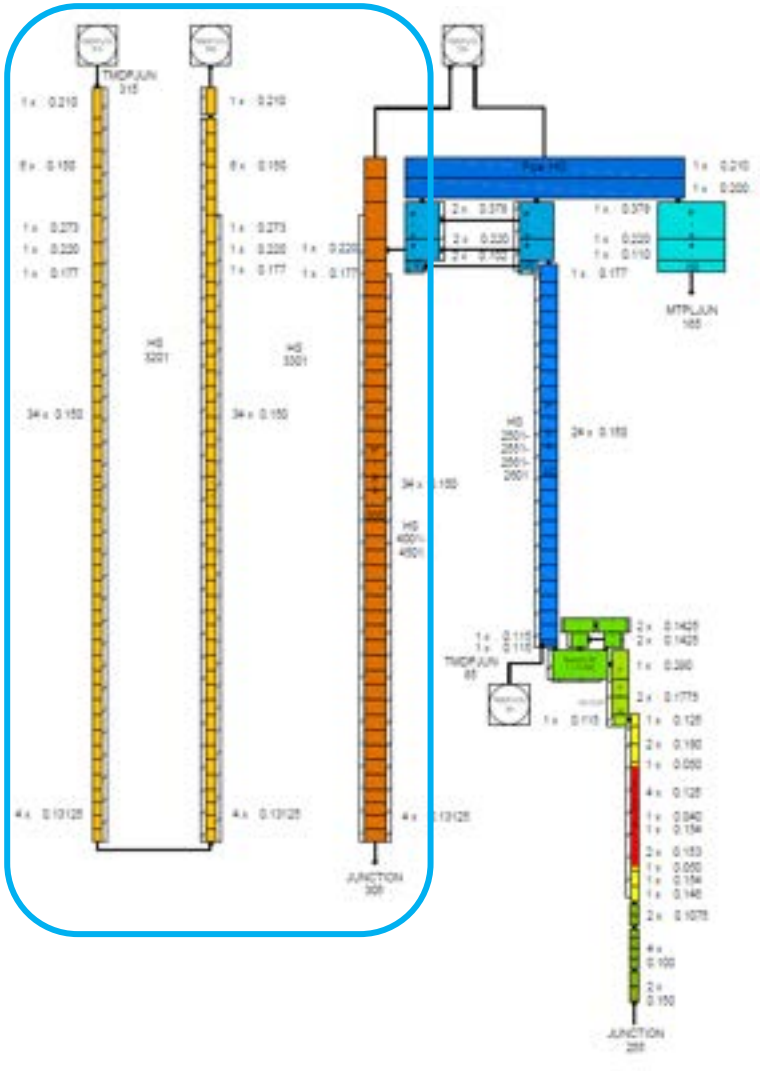
- The **HERO SG-1** substitutes the previous HX; 6 m of active length and 500 kW of nominal power
- The test section is not equipped with the **DHR**; this function will be performed by **HERO SG**, reducing FW mass flow rate



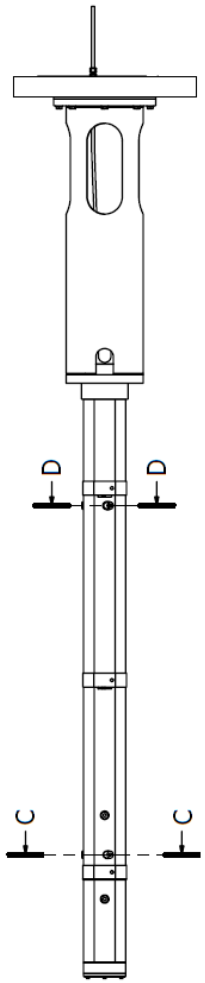
Thermal-Hydraulic Model: HERO SGBTs

- **LBE side**: a single equivalent tube composed of 43 volumes; 3 junctions connect the component to the separator, the upper plenum and the pool
- **Steam/water side**: 2 pipes for a total of 96 volumes
- 4 **heat structures** model thermal behavior of the unit:
  - HS 3201: 48 axial structures and 20 radial meshes (AISI 3016 + insulator gap)
  - HS 3301: 41 axial structure and 31 radial meshes (AISI 316 + helium and high conductivity powder)
  - HS 4001 and 4501: 39 axial structure and 24 radial meshes
- Calibrated **fouling factor** as the ratio between **Ushakov** and **Todreas&Kazimi** HTC correlation, in the range of the SG temperatures and assuming the predicted flow conditions: 1,01





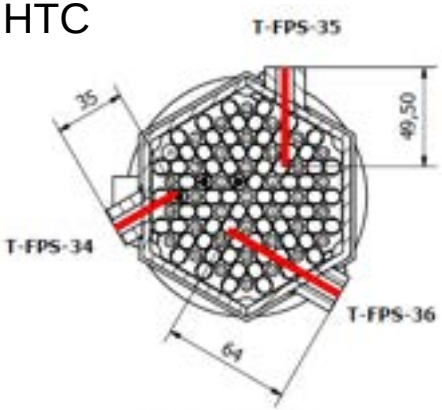
Thermal-Hydraulic Model: FPS



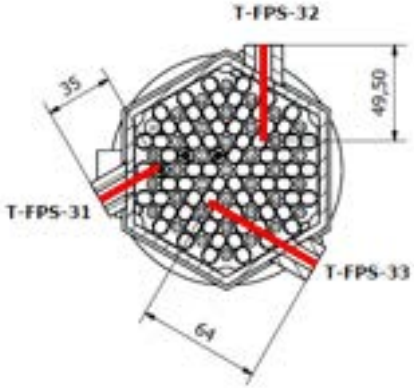
The **FPS** is analyzed subchannel by subchannel: the model consists of **72 parallel pipes** (15 control volumes for each pipe), which simulates the sub-channel, **5760 heat structure nodes** reproducing the thermal power supplied by the 37 pins and **1728 heat structure nodes** to models the heat dispersion through the hexagonal wrapper. **1536 cross junctions** link the 72 pipes.

The unit is equipped with several TCs to measured the LBE temperature across the HS. The model is obtained to compare the temperature in the **exact position of the TCs**. The grids are simulated with pressure loss coefficients, dependent on the flow conditions and evaluated with **Rheme correlation**.

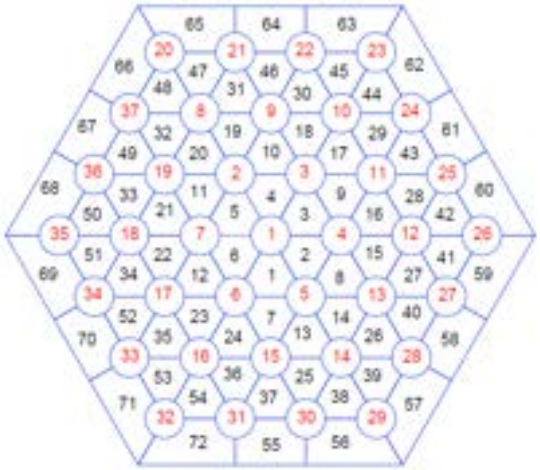
A calibrated fouling factor is evaluated as the ratio between **Ushakov (*p/d=1.8)*** and **Todreas&Kazimi (*p/d=1.6)*** equal to 0.86 in order to better reproduce the HTC



D-D (1 : 2)



C-C (1 : 2)



Pre-Test analysis

The pre-test simulations have been organized in two phases:

- **Phase 1**: assessment of **Steady State (SS) Full Power Conditions**, in order to determine initial conditions for transient
- **Phase 2**: transient simulations

PHASE 1

For the identification of the initial conditions of the transient tests, 12 different SS condition are analysed:

- **Case #1**: setting to achieve a constant temperature drop across the FPS equal to 80 K in the range of about 673-753 K, representative of the temperature drop across the **ALFRED core**; duration 3000 s, FPS power 450 kW, pool initial temperature 690 K, Ar mass flow rate 1,28 Nl/s, feedwater mass flow rate 0.3308 kg/s;
- **Case #2, #3, #4, #5, #6, #7**: as **Case #1** except pool initial temperature: 670, 675, 665, 662, 660, and 655 K;
- **Case #8**: as **Case #3** except Ar mass flow rate: 2,354 Nl/s. Case #8 has been set to achieve LBE mass flow rate across the SGBT section equal to 44,7 kg/s (representative of the scaled down **SG of ALFRED**);
- **Case #9, #10, #11, #12**: as **Case #3** except Ar mass flow rate: 2,242 Nl/s, 2,13 Nl/s, 1,85 Nl/s, 1,79 Nl/s.

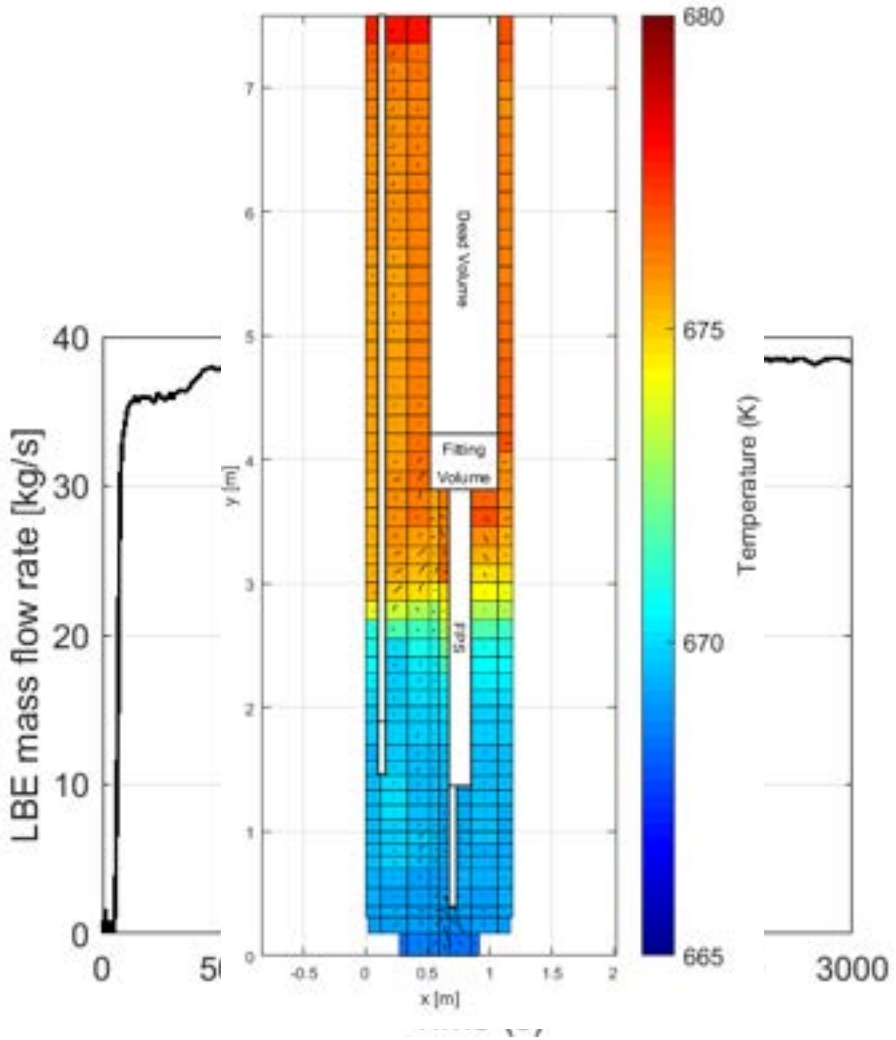
Pre-Test simulations: SS initial conditions

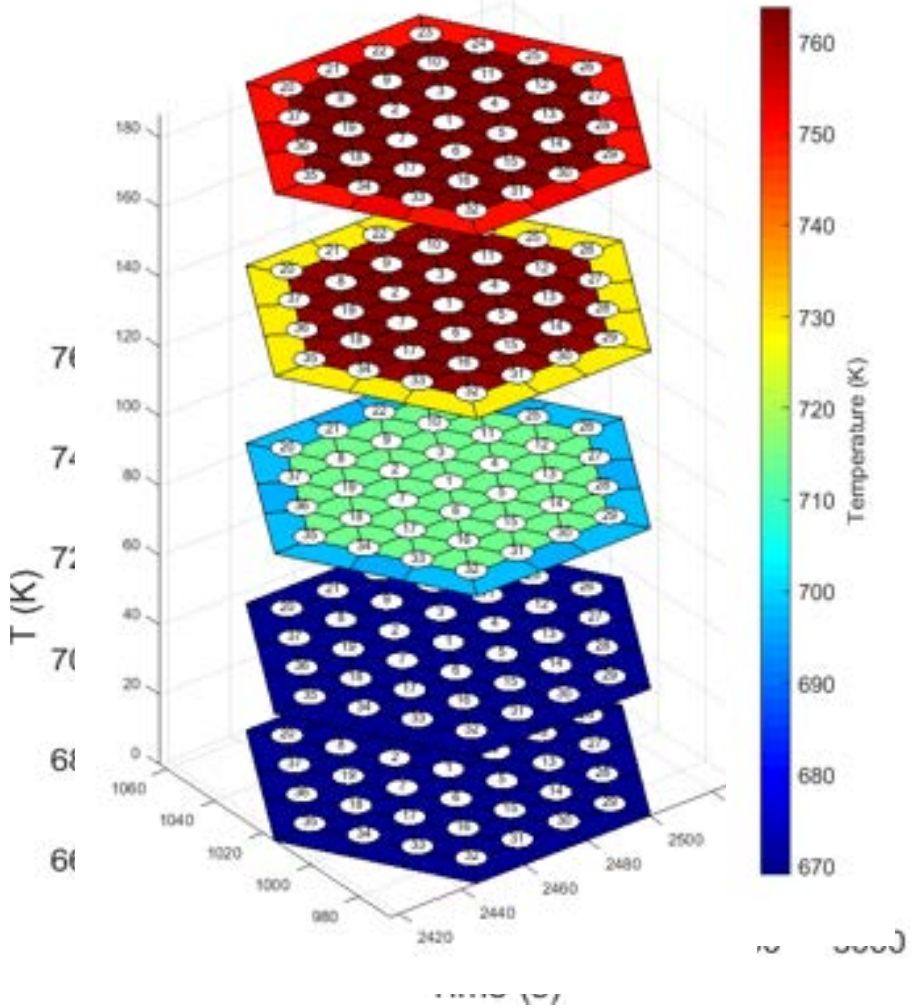
Description		Case 1	Case 2	Case 3	Case 4	Case 5	Case 6	Case 7	Case 8	Case 9	Case 10	Case 11	Case 12
Initial conditions	FPS power [kW]	450.0	450.0	450.0	450.0	450.0	450.0	450.0	450.0	450.0	450.0	450.0	450.0
	Pool initial T [K]	690	670	675	665	662	660	655	675	675	675	675	675
	Ar mass flow [Nl/s]	1.28	1.28	1.28	1.28	1.28	1.28	1.28	2.354	2.242	2.13	1.85	1.79
	Feed-water pressure [bar]	172.0	172.0	172.0	172.0	172.0	172.0	172.0	172.0	172.0	172.0	172.0	172.0
	Feed-water inlet T [K]	608	608	608	608	608	608	608	608	608	608	608	608
	Feed-water mass flow [kg/s]	0.331	0.331	0.331	0.331	0.331	0.331	0.331	0.331	0.331	0.331	0.331	0.331
	Heat losses [kW]	15.0	15.0	15.0	15.0	15.0	15.0	15.0	15.0	15.0	15.0	15.0	15.0

Pre-Test simulations: SS main results

Description		Case 1	Case 2	Case 3	Case 4	Case 5	Case 6	Case 7	Case 8	Case 9	Case 10	Case 11	Case 12
Results at steady state	FPS inlet T [K]	673.5	668.5	669.4	667.3	662.2	665.6	663.8	672.5	672,3	672,1	671.5	671.2
	FPS outlet T [K]	754.3	749.8	751.0	748.5	747.5	746.9	745.2	740.9	741.4	742.0	743.8	744.3
	LBE - HERO inlet T [K]	745.2	739.0	740.6	737.1	735.3	733.7	732.9	732.3	733.2	733.6	734.7	734.9
	LBE - HERO outlet T [K]	671.9	668.4	667.5	665.7	665.9	665.5	664.2	671.5	671.2	671.2	670.5	671.1
	LBE mass flow HERO inlet [kg/s]	37.6	37.5	37.5	37.5	37.4	37.4	37.3	44.5	43.9	43.4	42.1	41.7
	Power removed by HERO [kW]	421.0	405.0	409.7	400.2	398.1	395.0	389.0	410.0	409.1	409.1	407.9	410.0
	Steam max temp T [K]	663.5	657.9	659.1	682.9	654.7	656.6	653.1	659.2	659.1	659.1	659.1	658.8

Pre-Test simulations: SS Case #4





Pre-Test analysis

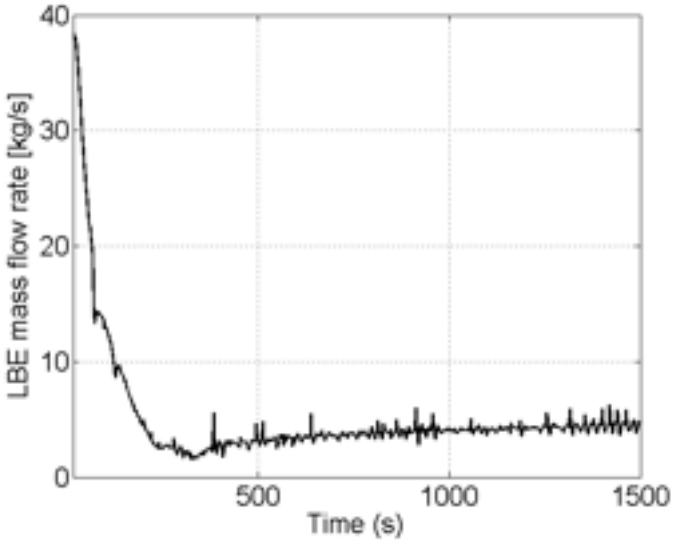
PHASE 2

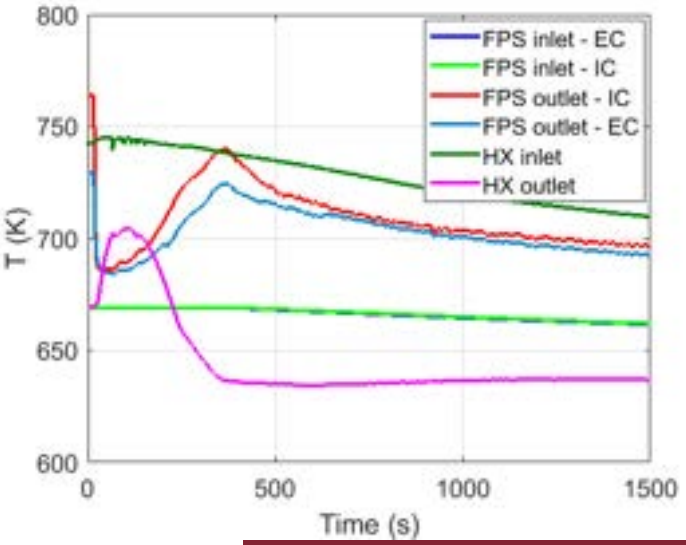
The starting point for transient tests (TrT) is considered **Case #4**.
Seven tests are studied:

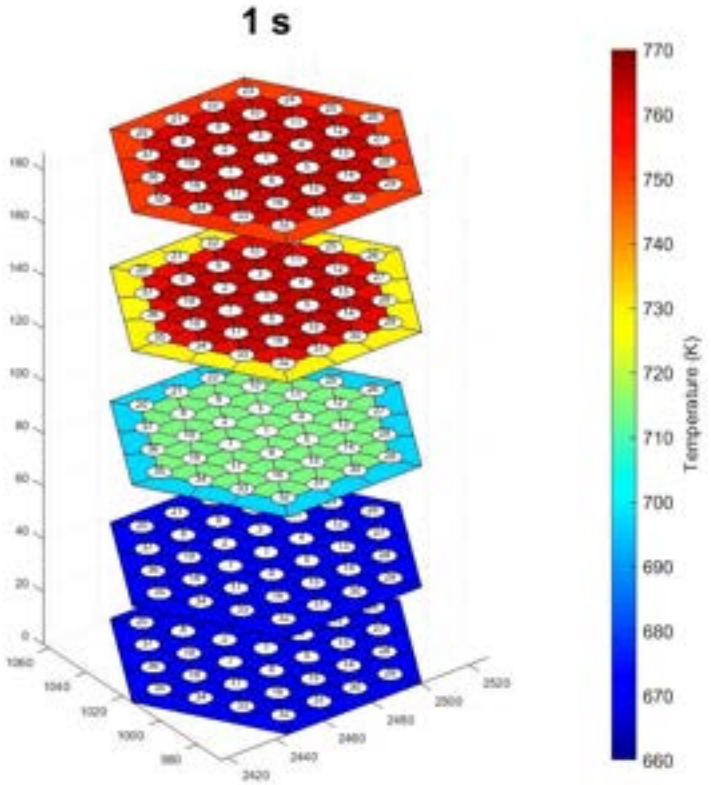
- **TrT #1**: it consists of a **protected loss of LBE pump**.
  - **FPS power** decrease down to the compensated decay heat value;
  - **Ar mass flow rate injection** decrease to 0 simulating presence of a pump flywheel;
  - **Feedwater mass flow rate** is set at 10% of nominal mass flow to simulate activation of DHR system;
- **TrT #2, #3, #4, #5, #6**: as **TrT #1** except feedwater mass flow rate: 15%, 20%, 3%, 2%, 1% of the nominal mass flow rate;
- **TrT #7**: as **TrT #1** except feedwater mass flow rate, which decrease to 0 in order to simulate a **loss of DHR function in hot conditions**.

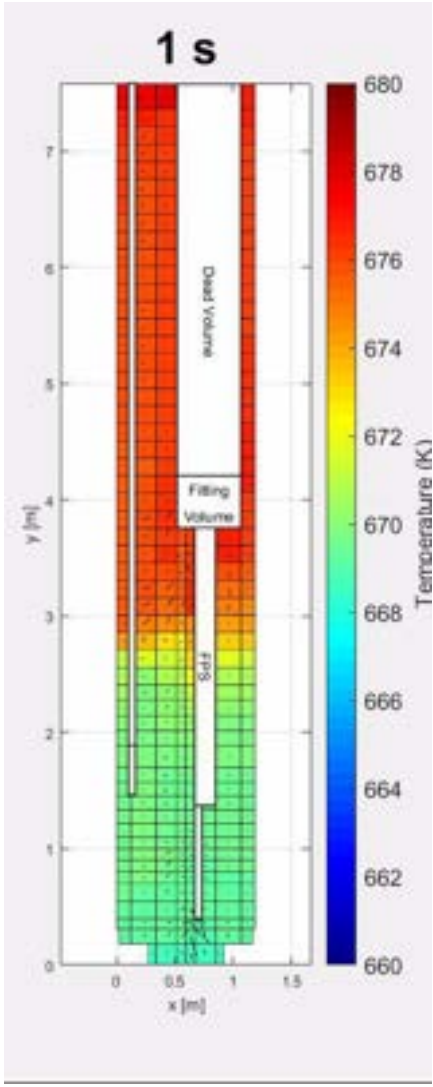
For all transient test simulations, **FPS power simulates a decay heat curve**, scaled down by a typical curve for fast reactors.
Decay heat power is increased with the value of heat losses at the end of SS in order to **compensate thermal heat losses** through main vessel.
The FPS power decreases in 900 s to the compensated one.

Transient Test #1: main results





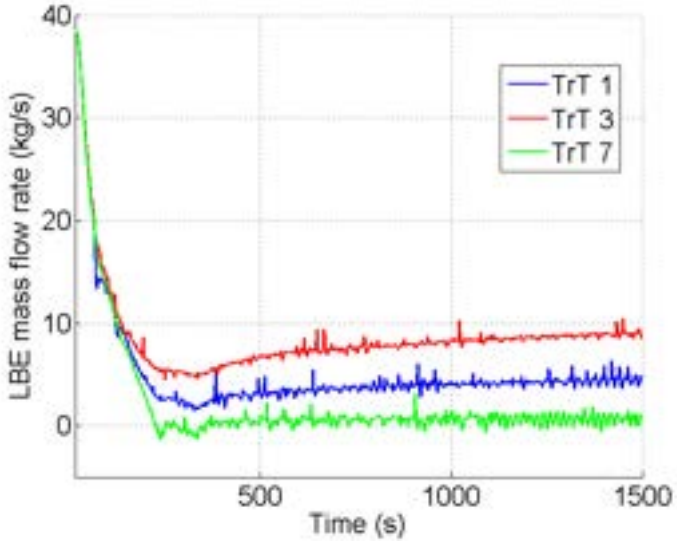


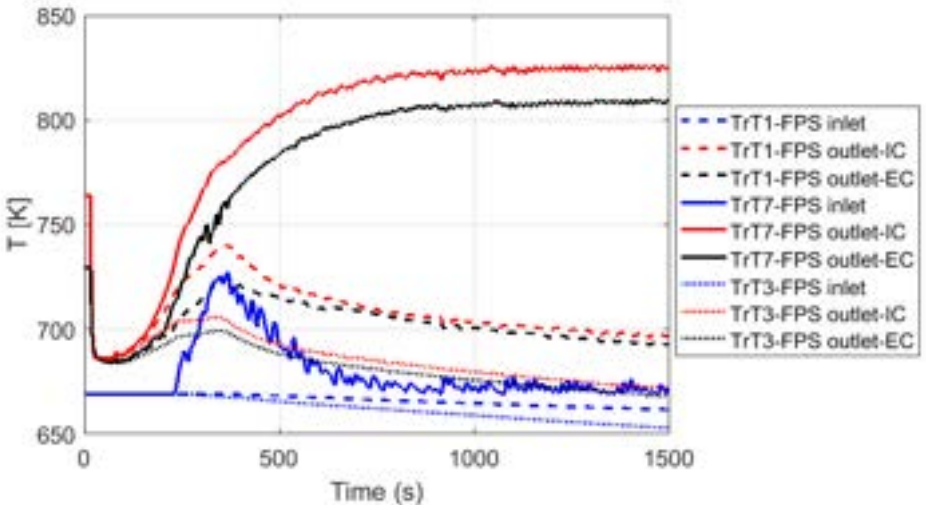


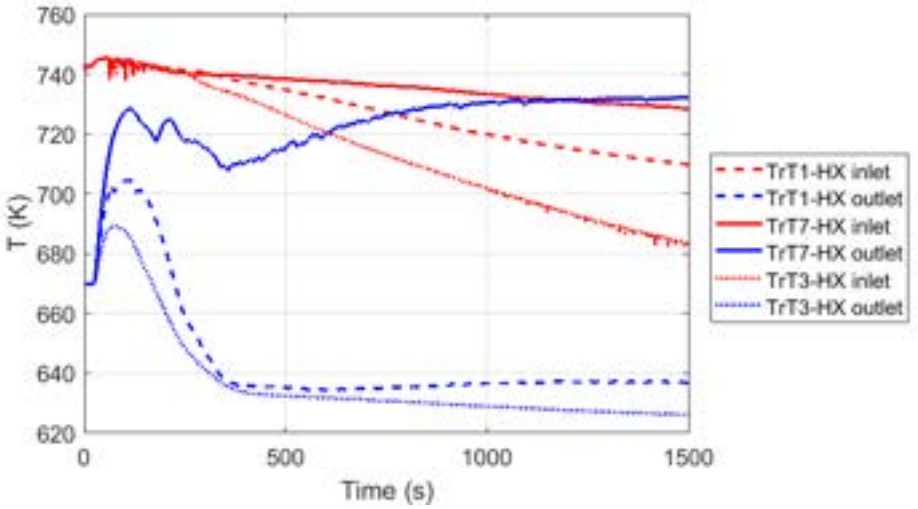
Transient Test #1: time schedule

Time (s)	Event description
0	Start of transient sequence (Protected loss of LBE primary pump)
40	Temperature at HERO inlet section reaches maximum value of 745 K
55	Temperature at the outlet section of FPS reaches minimum value of 685 K. At this time, thermal power has nearly reached the value of the compensated decay power; LBE mass flow rate is close to 50%. It results in the minimum value of ΔT at the FPS section
95	Temperature at HERO outlet section reaches maximum value of 705 K. Feed-water mass flow rate decrease after 2 s the beginning of the transient event; LBE mass flow rate is enhanced by the pump wheels simulation system and the hot fluid pass through the HX without decreasing only slightly the temperature
97	Temperature of the pool downstream HERO outlet section reaches the maximum value of 685 K
240	Temperature at HERO outlet section reaches lower values than pool temperature
335	LBE mass flow reaches minimum value
370	T FPS outlet section reaches the maximum value of 732 K. At this time LBE mass flow has the minimum value and the temperature drop at FPS reaches the maximum value
350 - 1500	End of transient event. The thermal stratification level is shifted downward of about one meter compared with the initial conditions

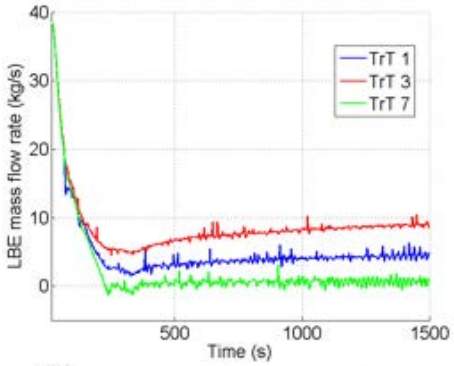
Transient Test: compare #1 #3 #7

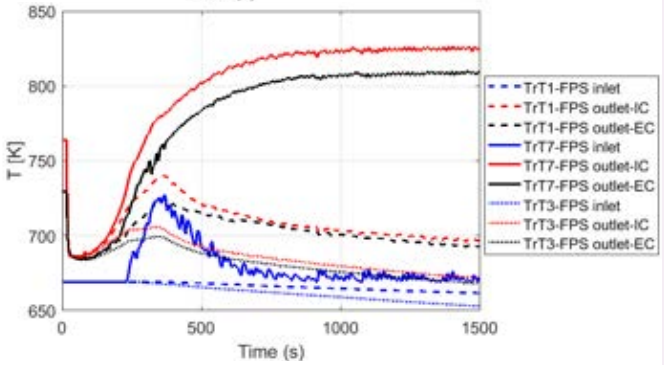


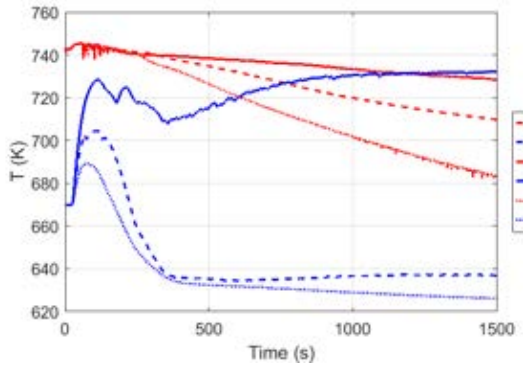


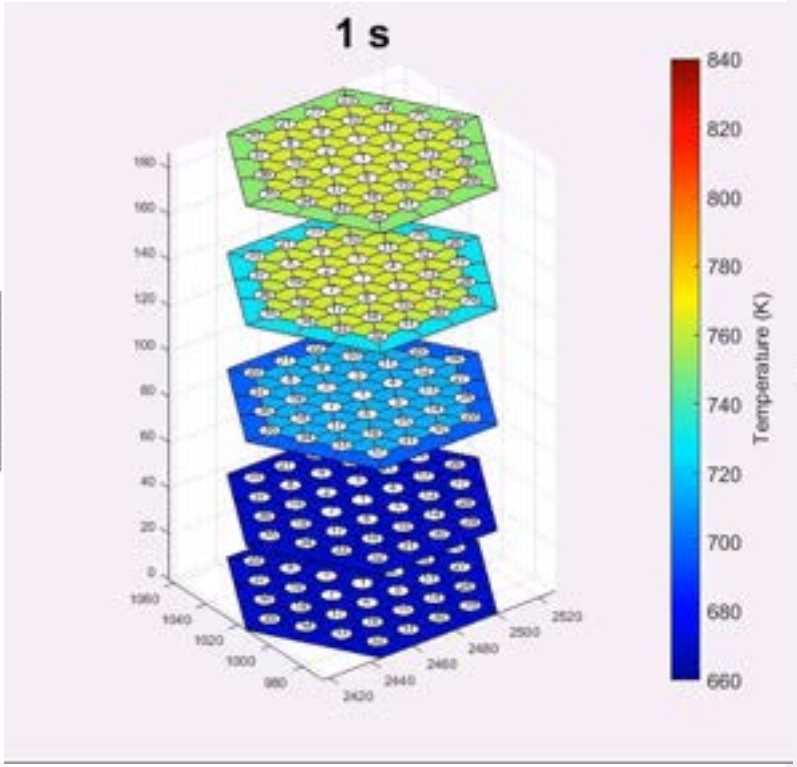


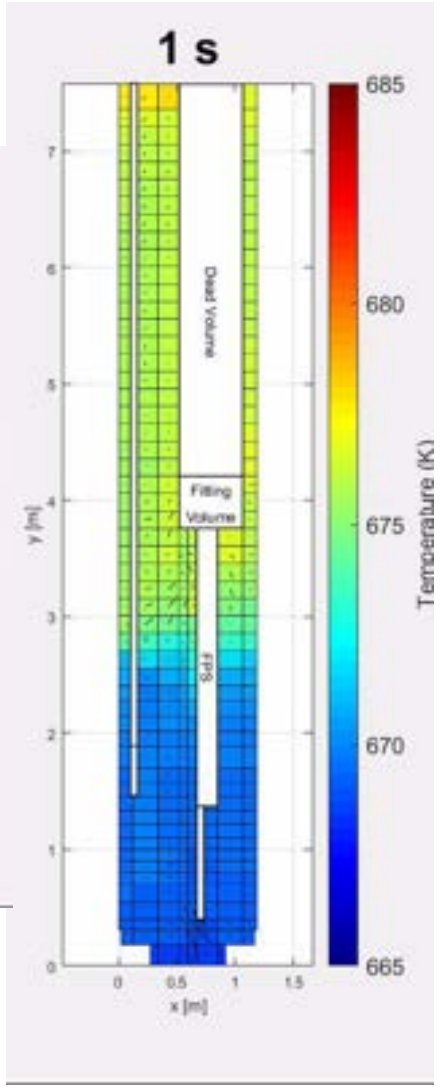
Transient Test: compare #1 #3 #7





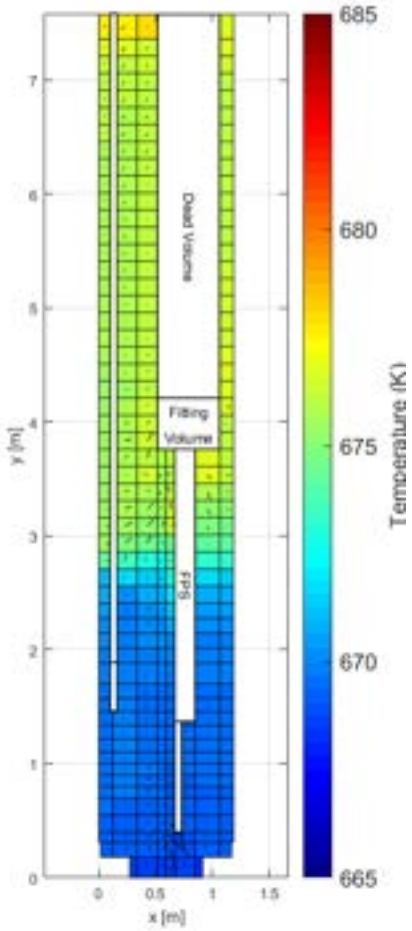




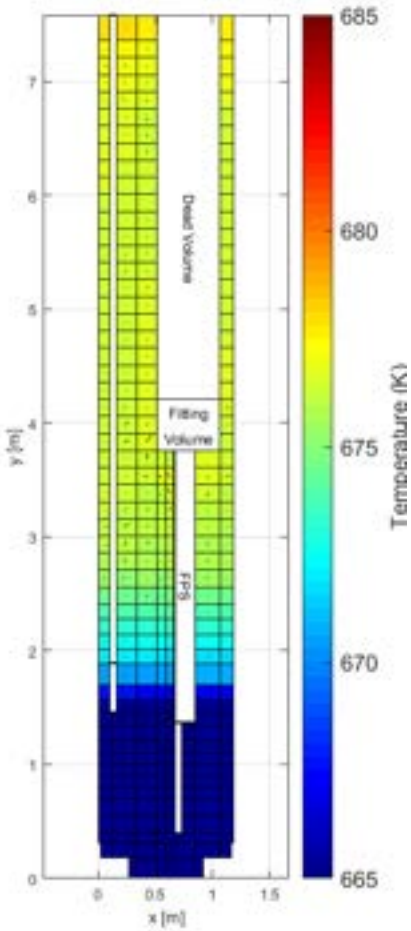


Thermal Stratification phenomena

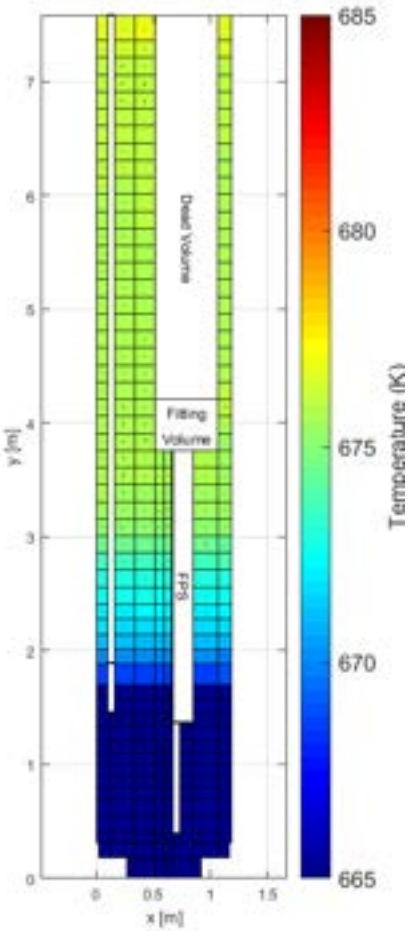
SS 4



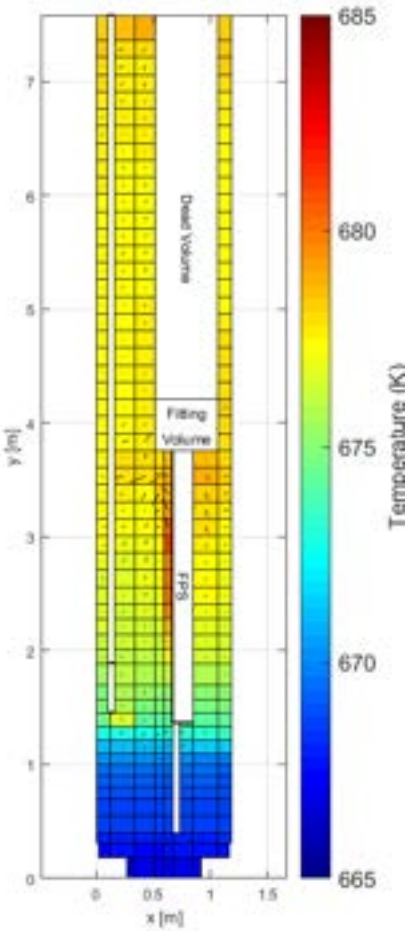
TrT 1



TrT 3



TrT 7



CONCLUSIONS

- **CIRCE-HERO RELAP5-3D©** model has been developed and calibrated comparing previous **CIRCE-ICE** simulations results with experimental data
- **Sensitivity analysis** has been performed in order to determine the reference steady state conditions
- The transient test simulations have highlighted that **low natural conditions** take place into **HERO test section**. When feed-water mass flow rate decreases to value under 2% of the nominal value, code predicts a **reverse flow** of the primary coolant. Further investigations are necessary in order to confirm that.
- Further investigations are needed to verify the physical feasibility of compensate power shutdown curve and pump flywheel curve with technical instrumentation.

THANKS FOR YOUR ATTENTION

ITALIAN NATIONAL AGENCY FOR NEW TECHNOLOGIES, ENERGY AND SUSTAINABLE ECONOMIC DEVELOPMENT

GEN-IV LFR

STATO ATTUALE DELLA TECNOLOGIA E PROSPETTIVE DI SVILUPPO

SGTR event in HLM pool and Post Test Analysis

A. Pesetti, M. Tarantino, P. Gaggini, G. Polazzi, V. Sermenghi
(alessio.pesetti@for.unipi.it)

Scuola di Ingegneria e Architettura, Università di Bologna, 26-27 settembre 2017

List of contents

- Introductory remarks
- CIRCE facility and MYRRHA-PHX
- Experimental campaign objectives
- Test Section design, instrumentation and assembly
- Experimental campaign (test SGTR-B)
- Post-test analysis (SGTR-B) by SIMMER-IV code
- Conclusive remarks

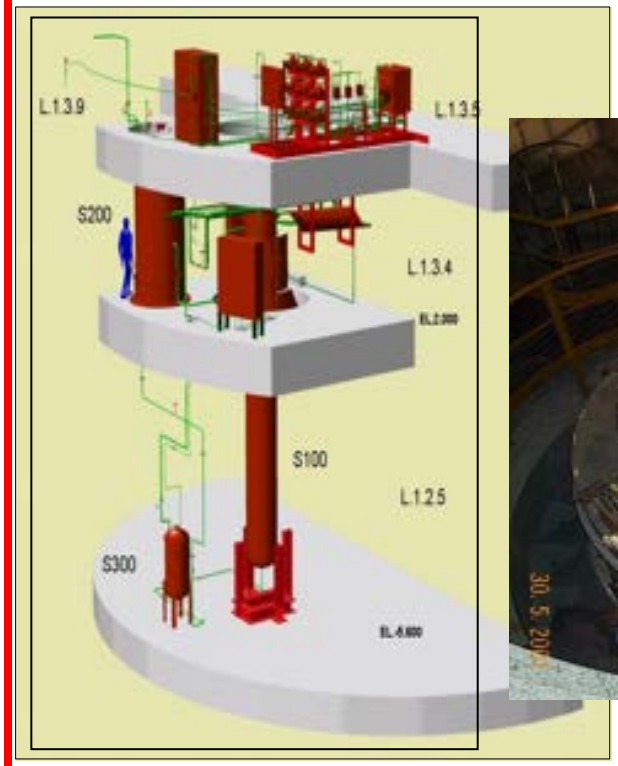
Introductory remarks

- The SGTR scenario needs to be analysed in the integrated pool type HLMFRs configuration, aiming to predict the hazardous consequences of the SG/PHX tube rupture taking place in the HLM pool (pressure wave propagation and cover gas pressurization, domino effect, steam dragged into the core, primary system pollution and slug formation)

- The SGTR event was experimentally investigated (4 tests) in a relevant configuration for MYRRHA reactor, implementing, in the large scale pool facility (CIRCE at ENEA CR Brasimone), a test section oriented to simulate a full scale portion of the PHX tube bundle of MYRRHA reactor

CIRCE Facility and MYRRHA-PHX

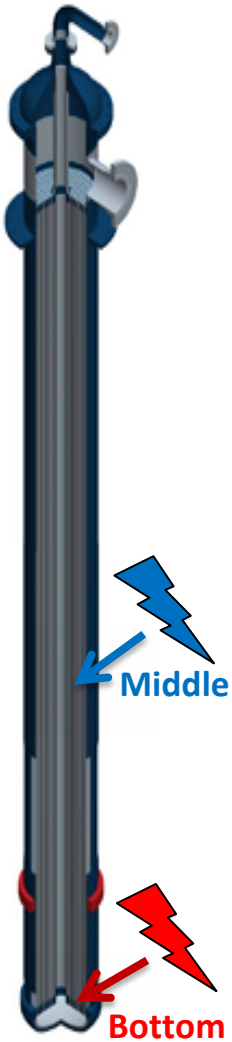
CIRCE facility (ENEA Brasimone CR)





Main Vessel S100	
Outside Diameter	1200 mm
Wall Thickness	15 mm
Material	AISI 316L
LBE Inventory (max)	90 tons
Height	8-10 m
Design Pressure	**16 bar**
Design Temperature	450°C

MYRRHA-PHX



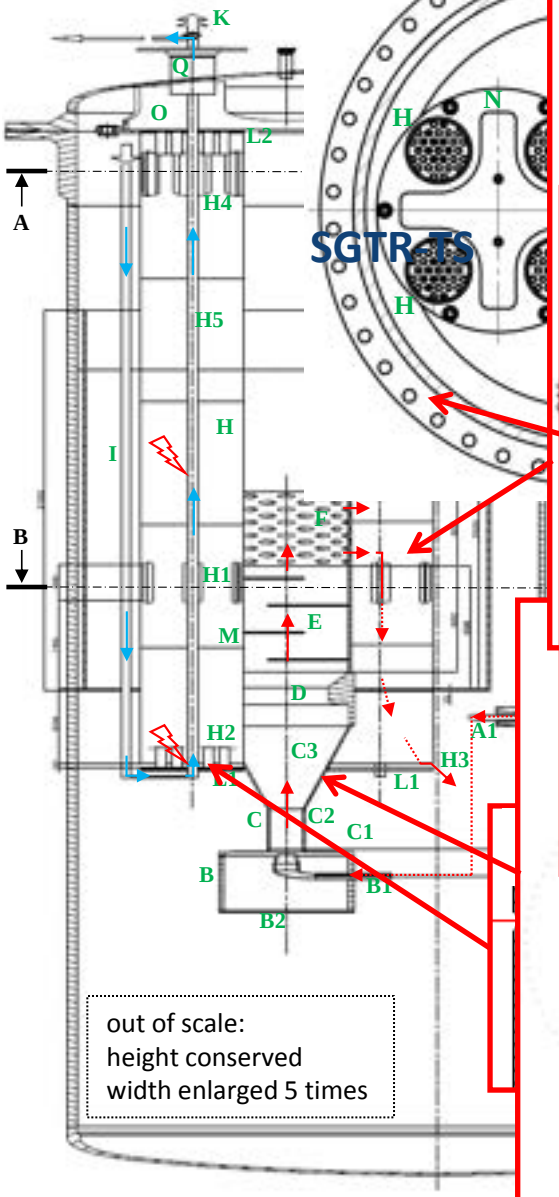
Parameter	Unit	Value
Power of one HX	MW	27.5
Shroud external diameter	mm	~850
Shroud internal diameter	mm	~800
Feed water pipe external diameter	mm	~200
Number of water tubes	-	684
External diameter of water tubes	mm	16
Internal diameter of water tubes	mm	14
Thickness of water tubes	mm	1
Length of water tubes	mm	~8500
HX LBE inlet temperature	**° C**	**350**
HX LBE outlet temperature	° C	270
HX LBE mass flow rate	Kg/s	~2500
HX water inlet temperature	**° C**	**200**
HX water outlet temperature	° C	201.6
HX water mass flow rate	Kg/s	~47
HX water pressure	**bar**	**16**

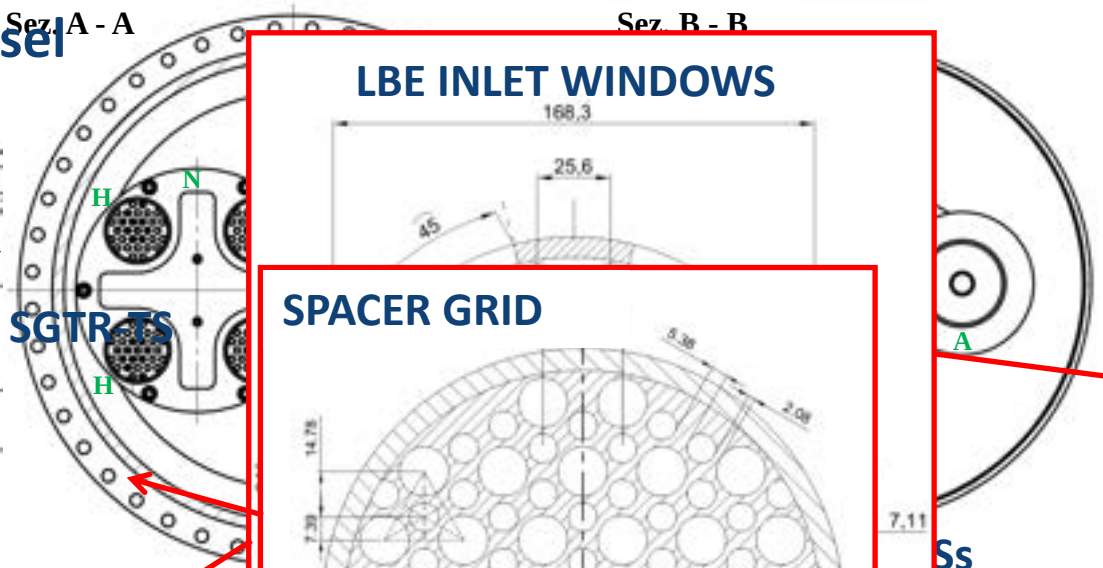
Experimental campaign objectives

- Tube rupture propagation in the HX-tube bundle
- The vapour flow path in the tube bundle
- Pressure waves propagation into the HX-tube bundle and damping effect of the HX-shell towards the surrounding structures
- Assessment and performance evaluation of the safety-guard devices (rupture disk) aiming to mitigate the effects of the SGTR event
- Investigation on the solid impurities formation after the SGTR event, accompanied by a quantitative qualification of filtering performance in the pool
- Qualitative characterization of the LBE particulate discharged by water and rupture disk discharge lines

Test section design

CIRCE vessel

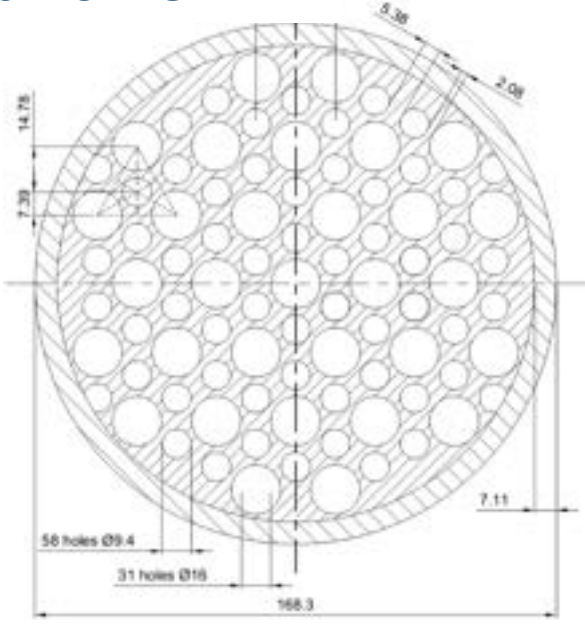


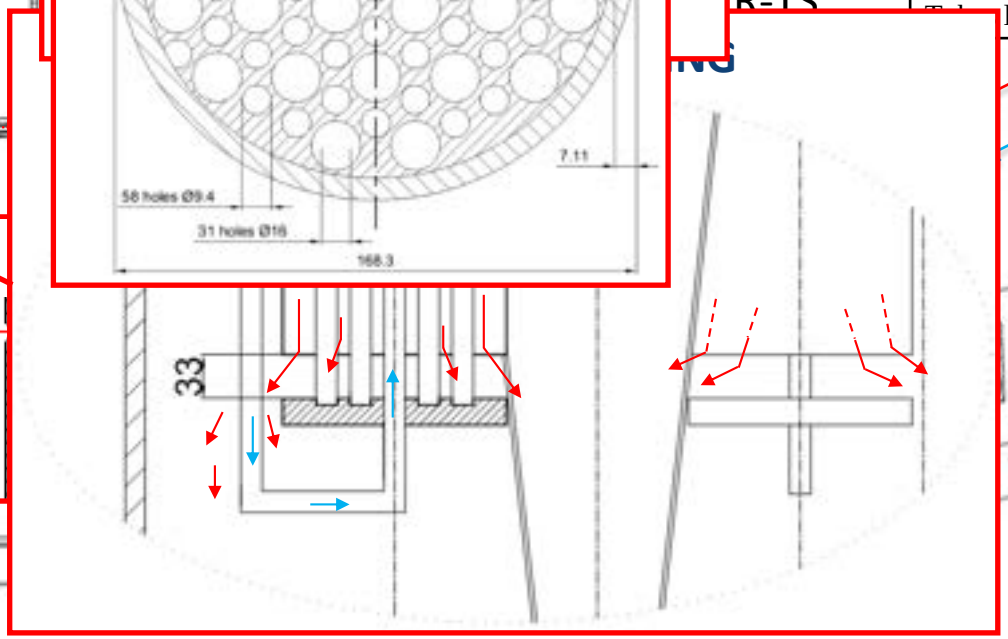


SGTR-TS

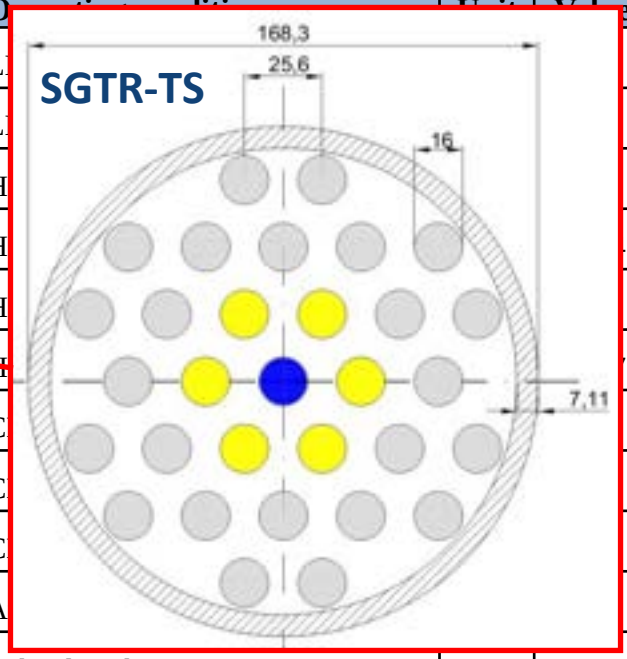
LBE INLET WINDOWS

SPACER GRID





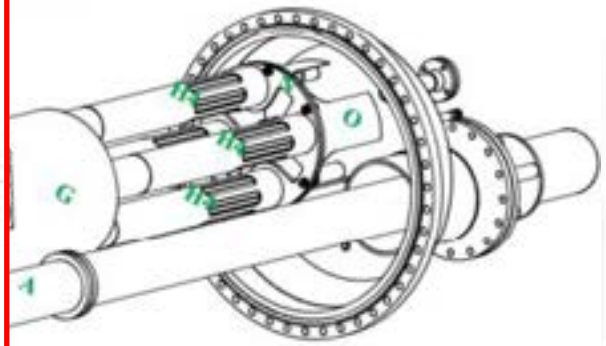
SGTR-TS



length	mm	~5200

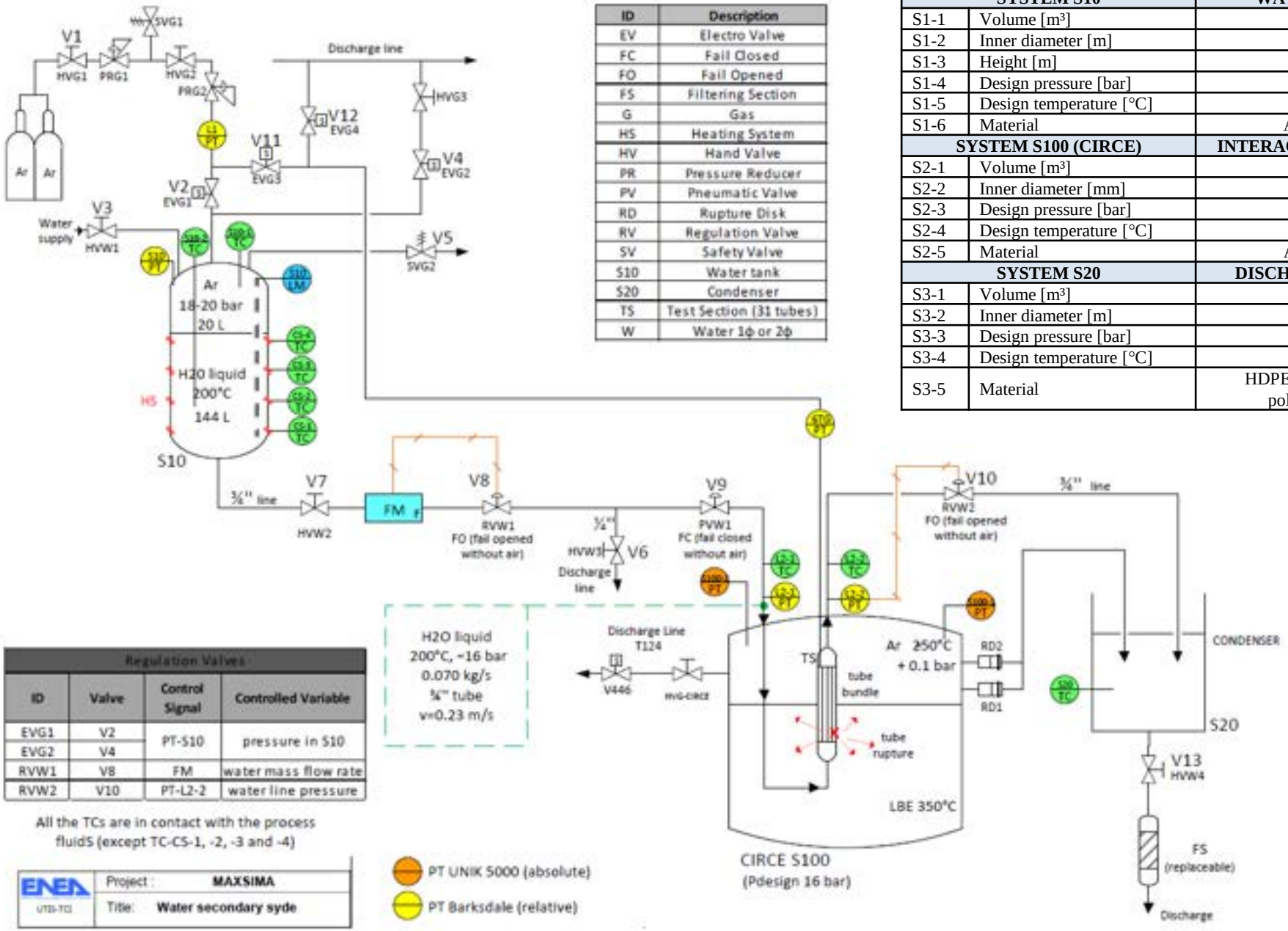
LBE flow path

Water flow path



Test Section

P&ID of the secondary circuit



ID	Description
EV	Electro Valve
FC	Fail Closed
FO	Fail Opened
FS	Filtering Section
G	Gas
HS	Heating System
HV	Hand Valve
PR	Pressure Reducer
PV	Pneumatic Valve
RD	Rupture Disk
RV	Regulation Valve
SV	Safety Valve
S10	Water tank
S20	Condenser
TS	Test Section (31 tubes)
W	Water 1ϕ or 2ϕ

SYSTEM S10		WATER TANK
S1-1	Volume [m³]	0.165
S1-2	Inner diameter [m]	0.355
S1-3	Height [m]	1.8
S1-4	Design pressure [bar]	25
S1-5	Design temperature [°C]	300
S1-6	Material	AISI 316
SYSTEM S100 (CIRCE)		**INTERACTION VESSEL**
S2-1	Volume [m³]	8.5
S2-2	Inner diameter [mm]	1170
S2-3	Design pressure [bar]	16
S2-4	Design temperature [°C]	500
S2-5	Material	AISI 316
SYSTEM S20		**DISCHARGE TANK**
S3-1	Volume [m³]	1.5
S3-2	Inner diameter [m]	1
S3-3	Design pressure [bar]	-
S3-4	Design temperature [°C]	80
S3-5	Material	HDPE (high density polyethylene)

Regulation Valves			
ID	Valve	Control Signal	Controlled Variable
EVG1	V2	PT-S10	pressure in S10
EVG2	V4		
RVW1	V8	FM	water mass flow rate
RVW2	V10	PT-L2-2	water line pressure

All the TCs are in contact with the process fluidS (except TC-CS-1, -2, -3 and -4)

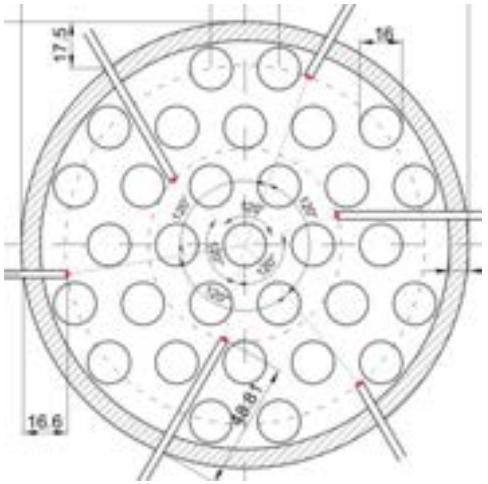
PT UNIK 5000 (absolute)

PT Barksdale (relative)

ENEA UTIS-TCI	Project: MAXSIMA
	Title: Water secondary syde

Test section instrumentation

~200 **Thermocouples**
~45 in each SGTR-TS
6 TCs at level (two level below, one level at and 5-6 levels above the rupture position)
N 6 tubes 3x1 mm, 6'' tube drilled
Vapour path propagation



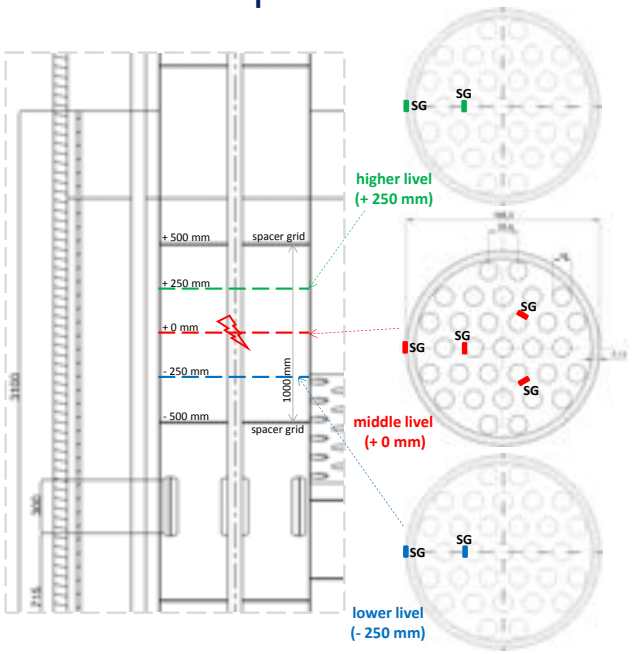
Ultrasonic flow meter



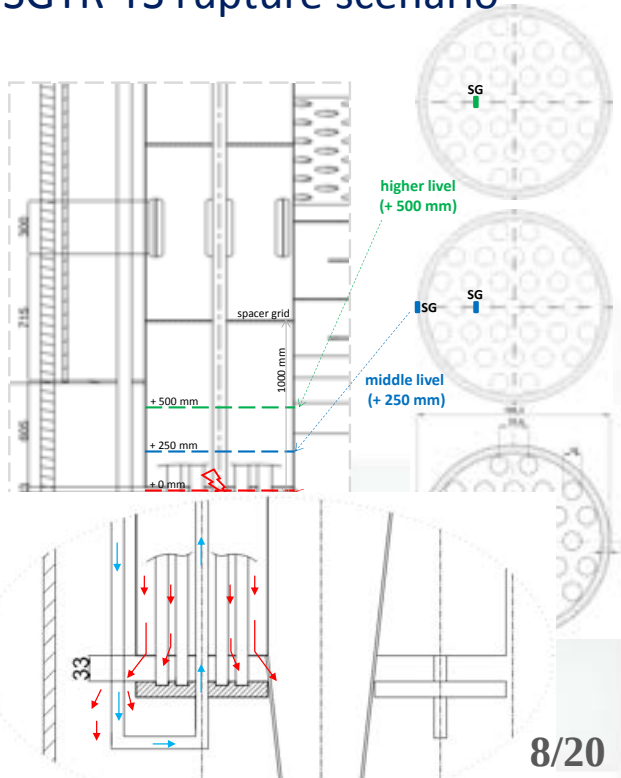
S10 level meter



8 Strain Gages in the **middle** SGTR-TS rupture scenario



6 Strain Gages in the **bottom** SGTR-TS rupture scenario



7(8) **fast Pressure Transducers** (transient pressure)
12 **Bubble Tubes** (level, mass flow rate and stationary pressure)

30 Strain Gages

Test Section assembly

SGTR-TS







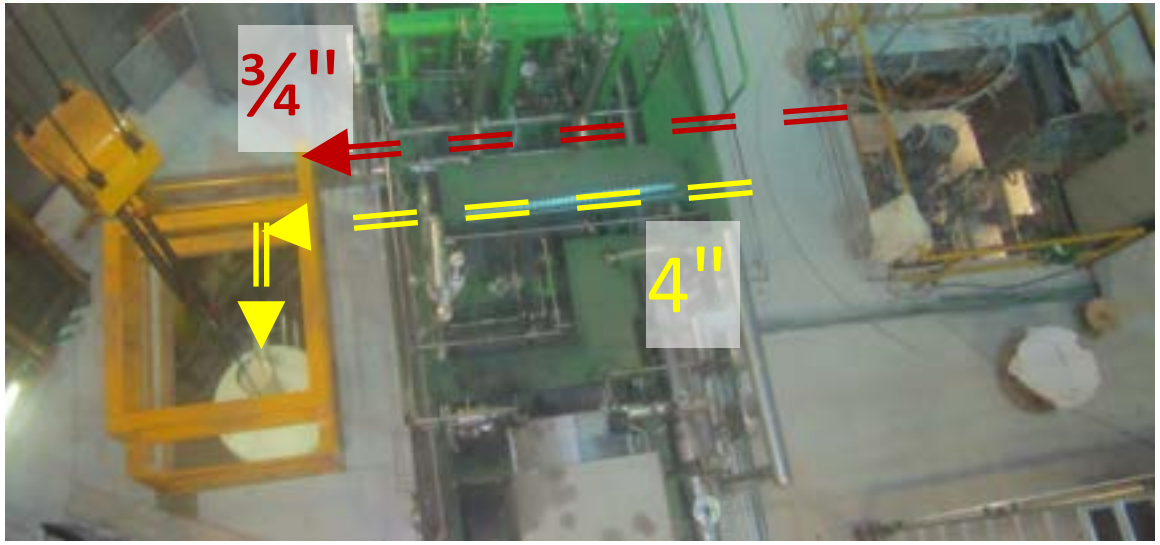


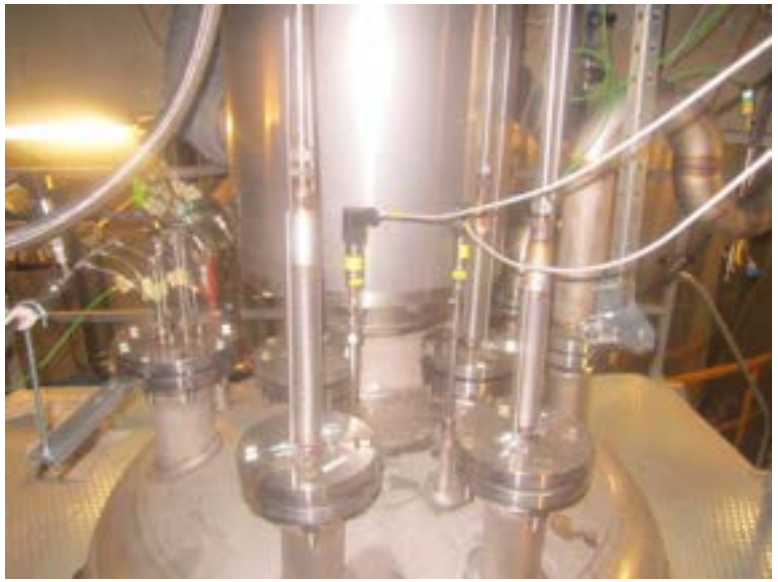


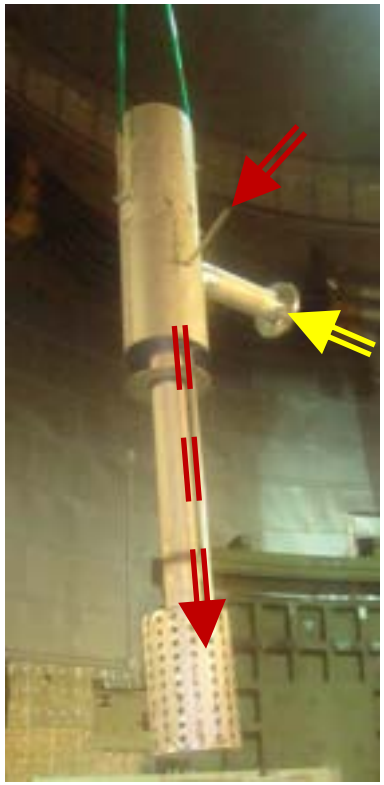




Two discharge line assembly



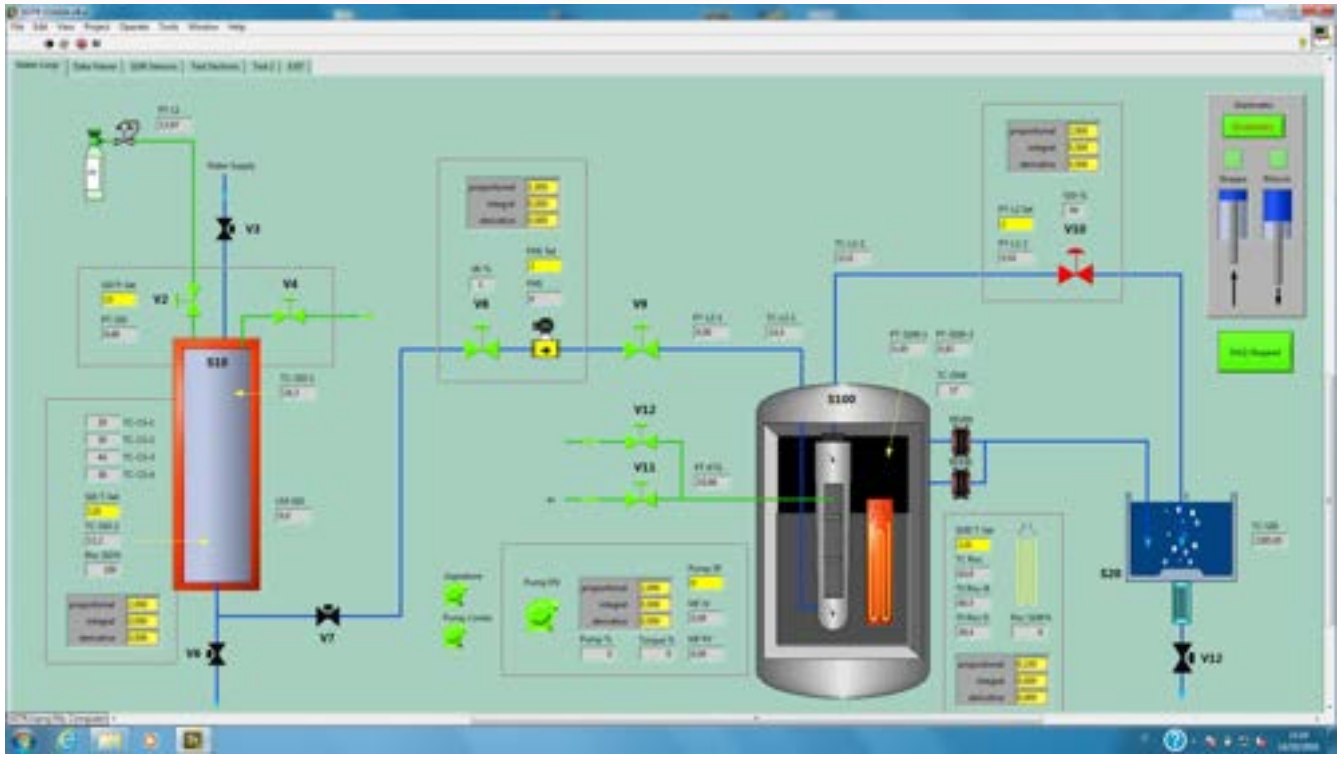


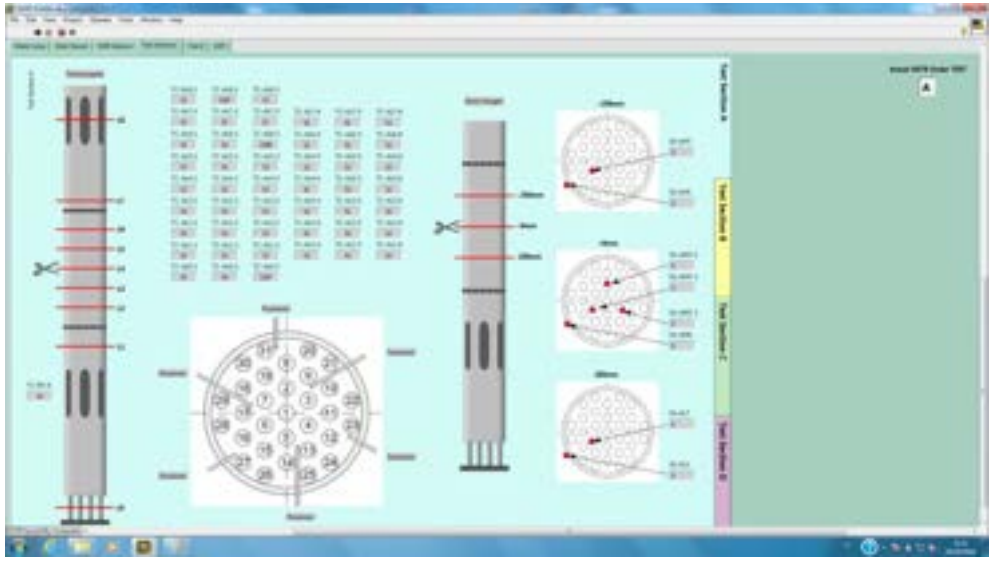


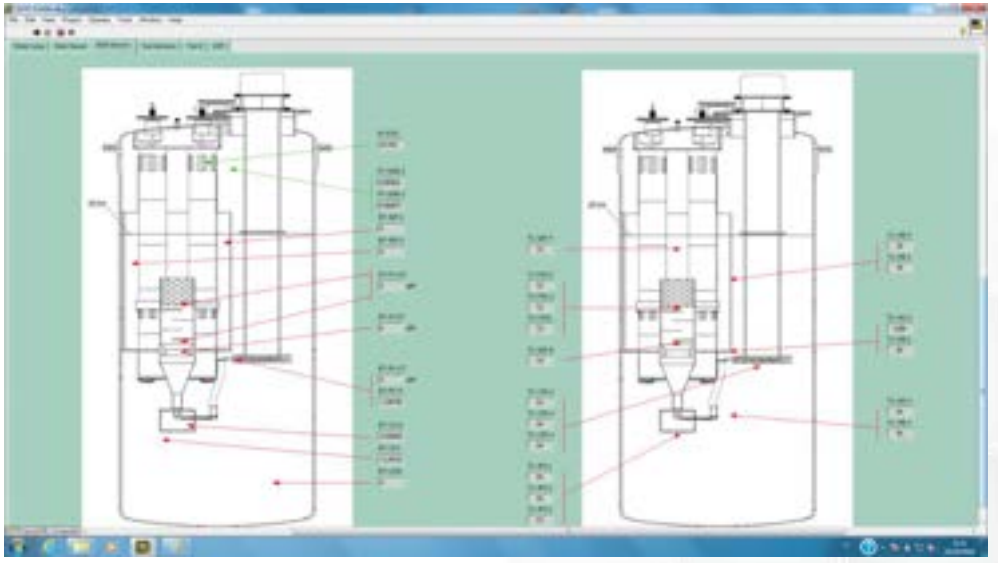




DACS in LabVIEW environment

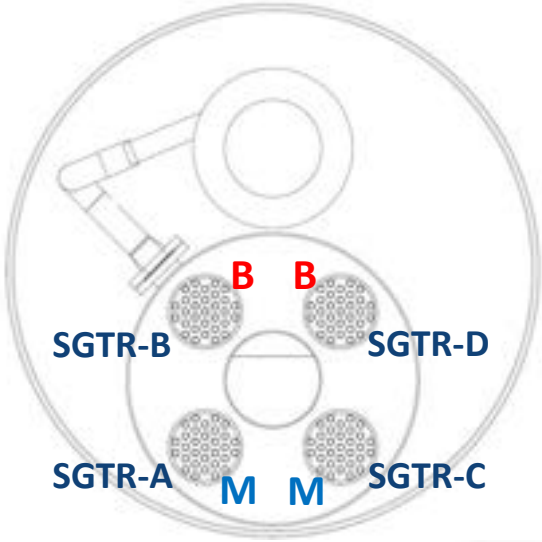




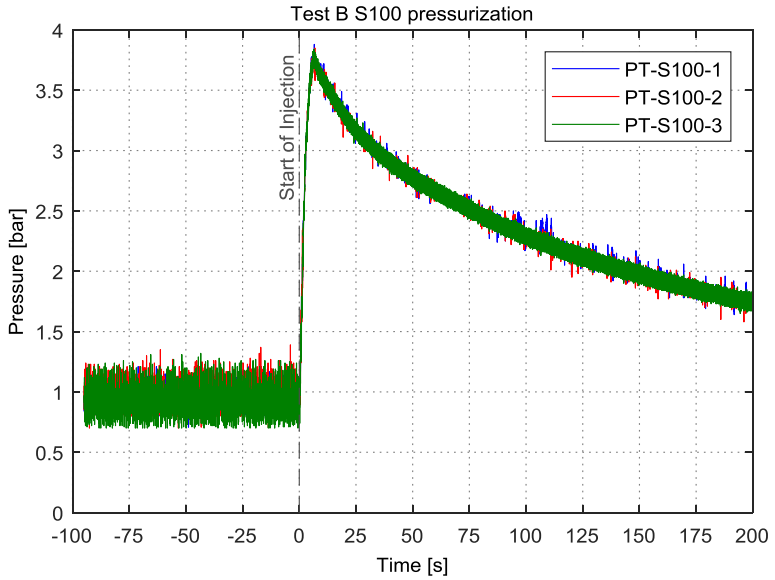


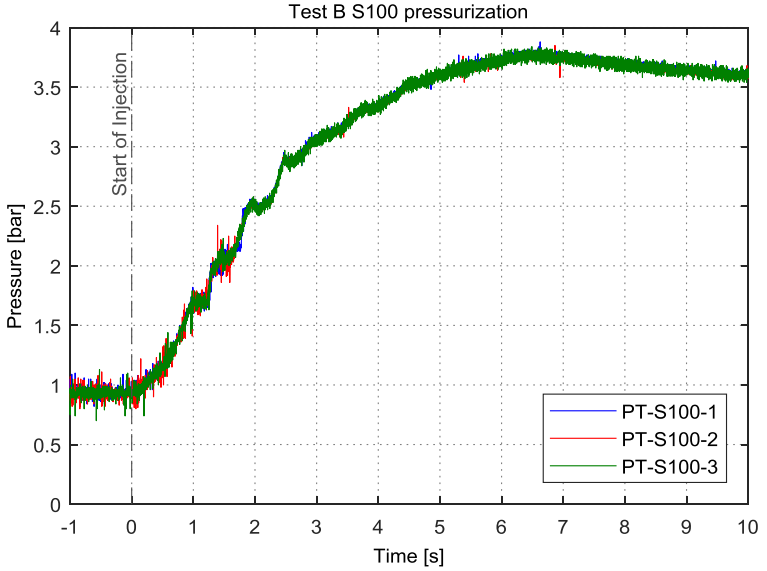
Experimental results

	Test #1 SGTR-A	Test #2 SGTR-C	Test #3 SGTR-B	Test #4 SGTR-D
LBE temperature [°C]	350	350	350	350
LBE cover gas pressure [bar]	0.05	0.05	0.05	0.05
LBE flow rate (kg/s)	60-65	75	80	75
Water temperature [°C]	182	190	192	195
Water pressure [bar]	16.3	17	16.5	16.9
Water flow rate (g/s)	70	70	70	70
Centrifugal pump head [bar]	2	2.2	3.1	2.7
Rupture position	Middle	Middle	Bottom	Bottom
Rupture occurrence in right position (by TC analysis)	Yes	Yes	Yes	Yes
Injection time [s]	5	5	5	5
Max water mass flow rate [g/s]	120	130	130	135
Max CIRCE pressurization [bar]	2.6	2.7	3.6	3.7
Rupture disc activation	Yes	Yes	No	No
LBE in 3/4 inch discharge line	No	No	Yes	Yes

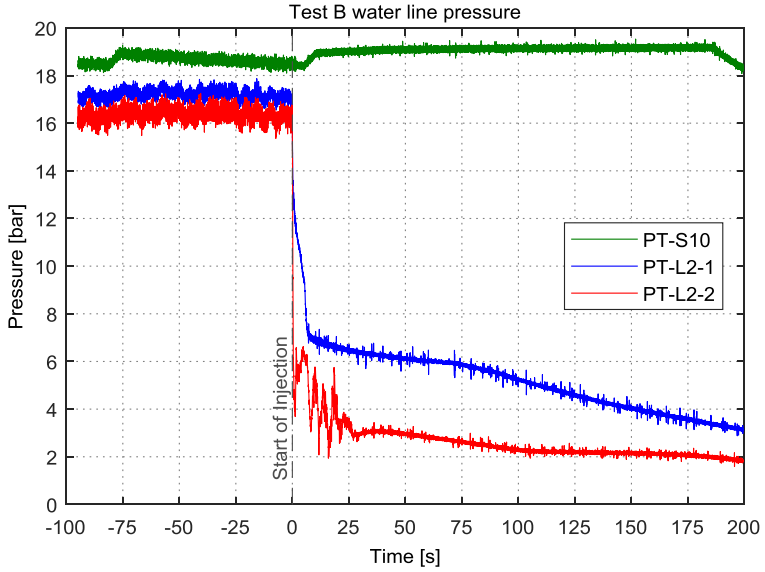


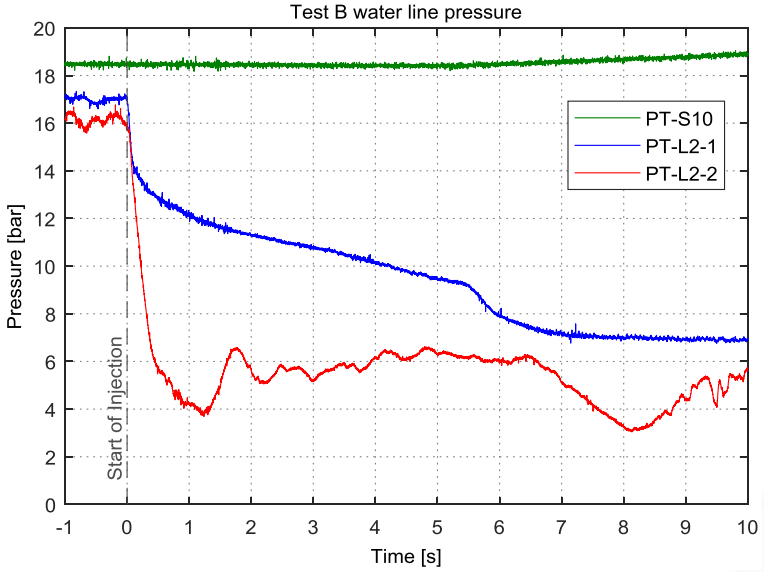
Test SGTR-B data post-processing





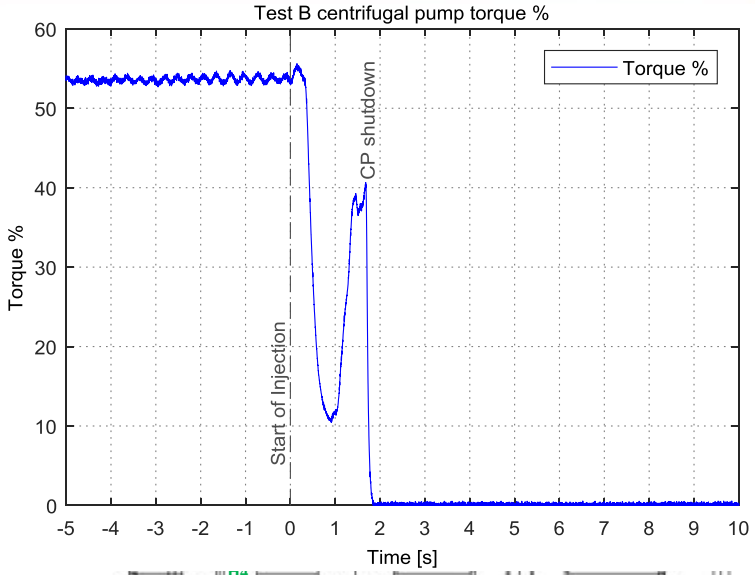
Test B pressure time trends in S100 cover gas (zoom on right)

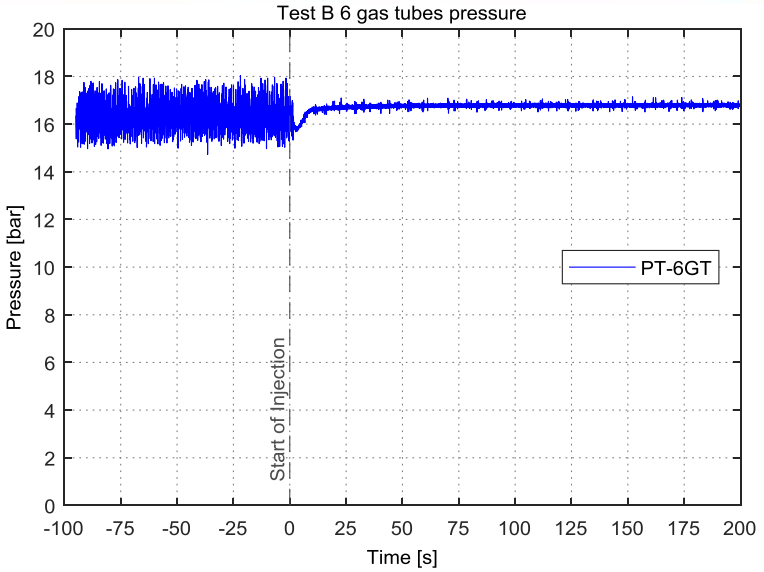


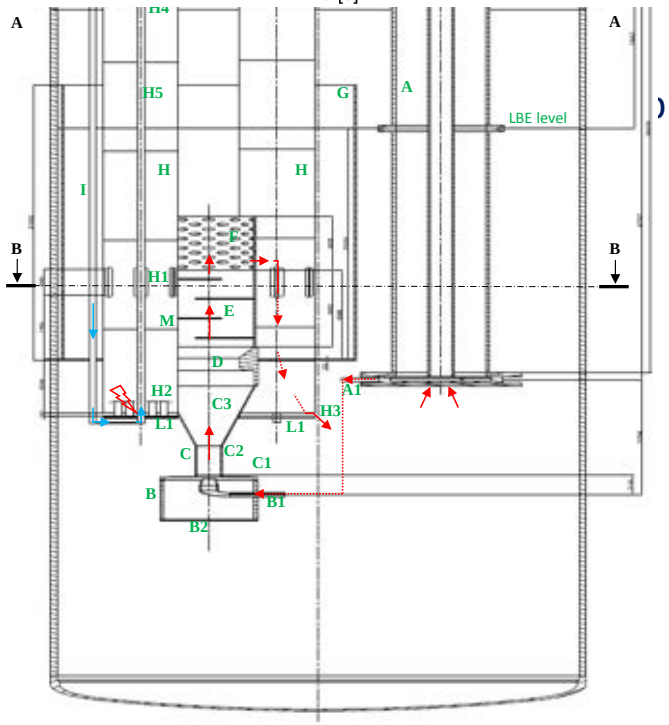


Test B pressure time trends in S10 and injection line (zoom on the right)

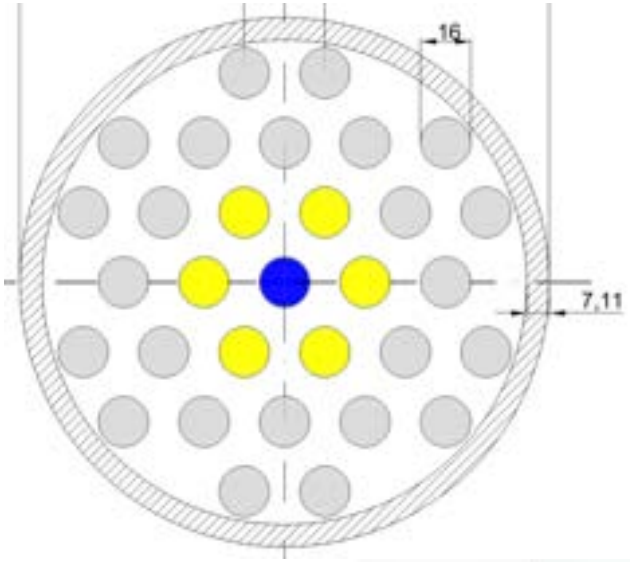
Test SGTR-B data post-processing



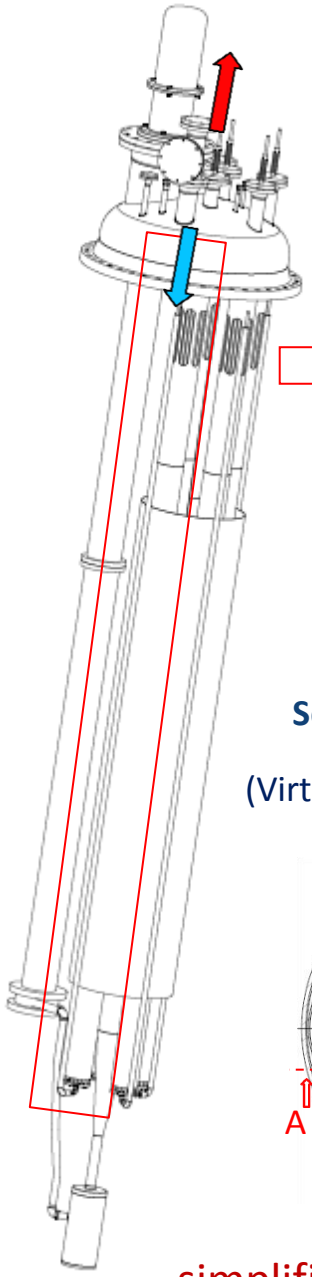


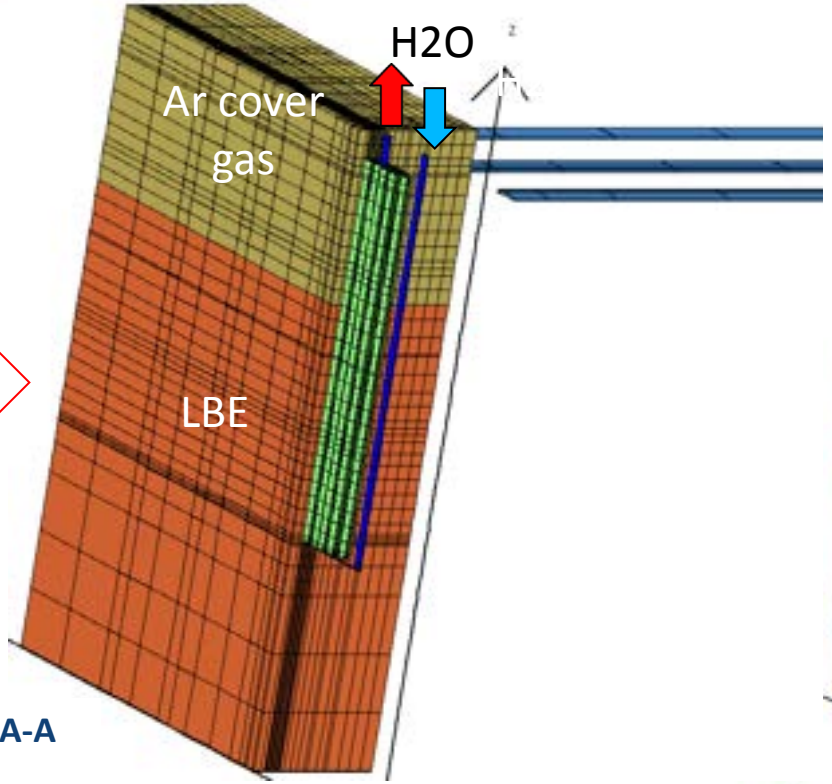


› torque (left) and pressure in first rank of tubes (right)



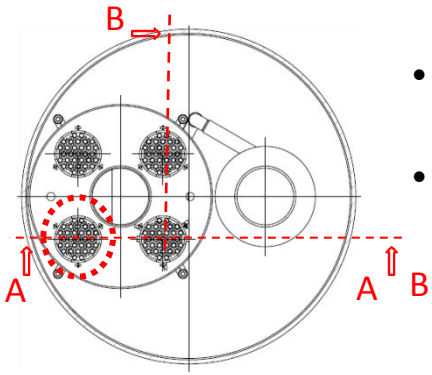
Post-test analysis by SIMMER-IV



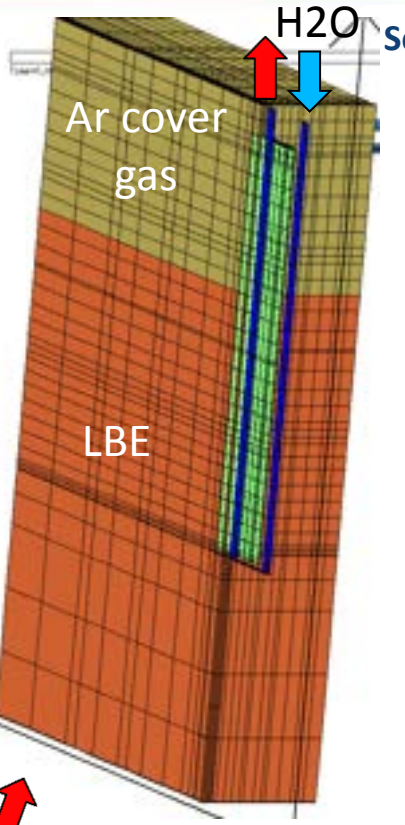


Section A-A

(Virtual walls are not shown in 3D views)

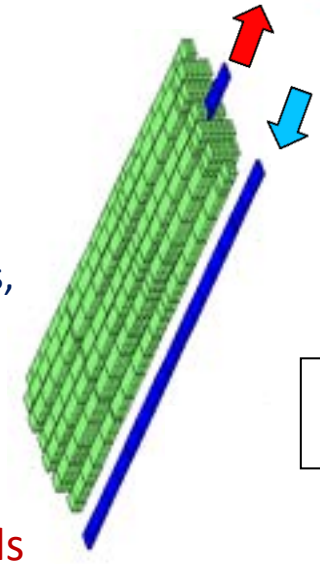


- Flowing areas conserved
- Mass flow rates, temperatures, conserved

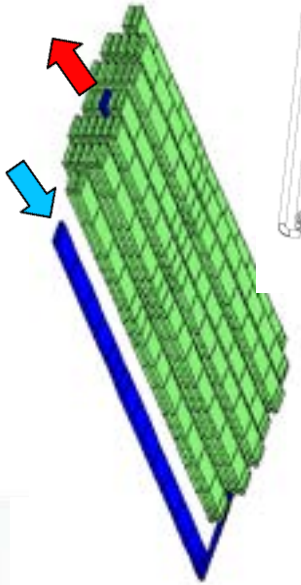


Section B-B

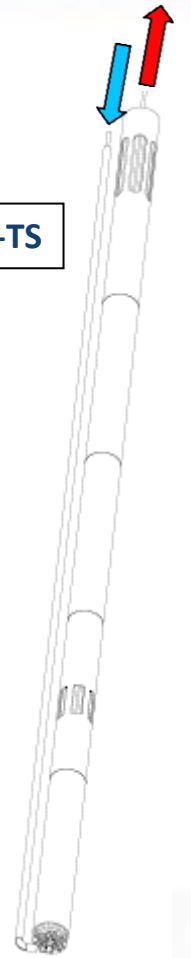
SGTR-TS



SGTR-TS

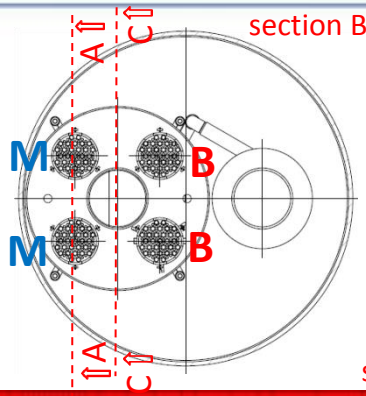


30 dummy tubes
1 water tube

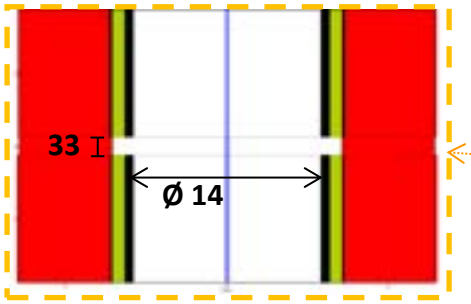


simplified model (30x27x42cells) 34020 cells

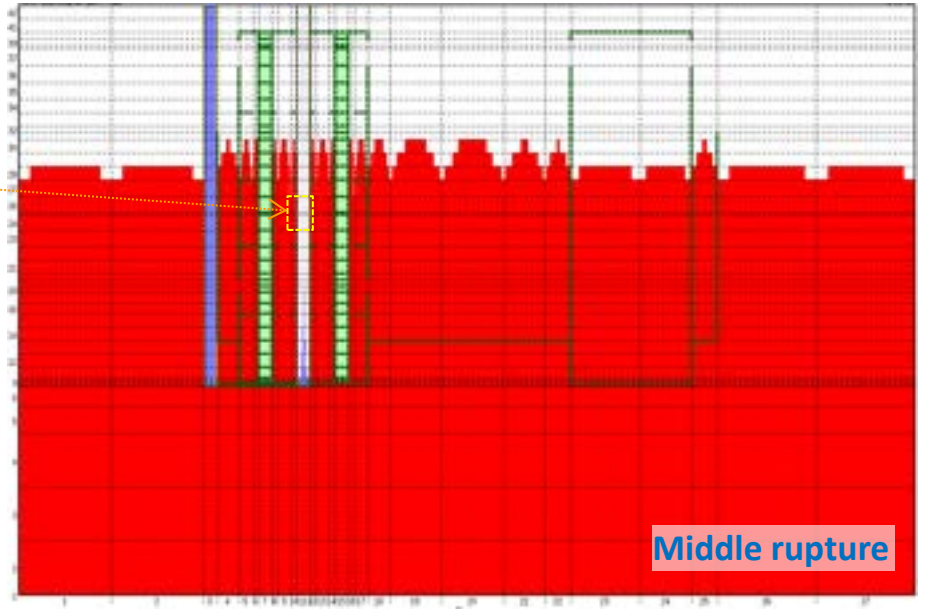
Post-test analysis by SIMMER-IV



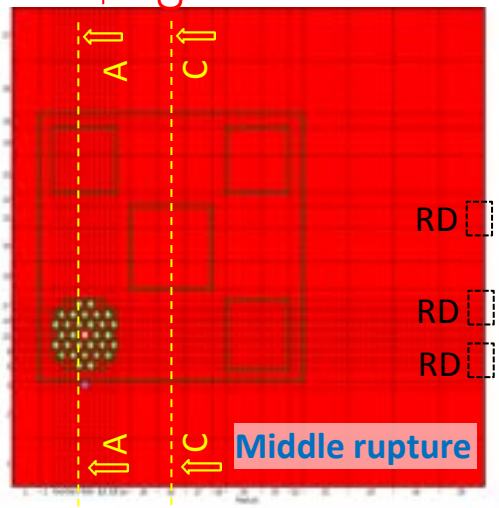
model (30x27x42cells) 34020 cells

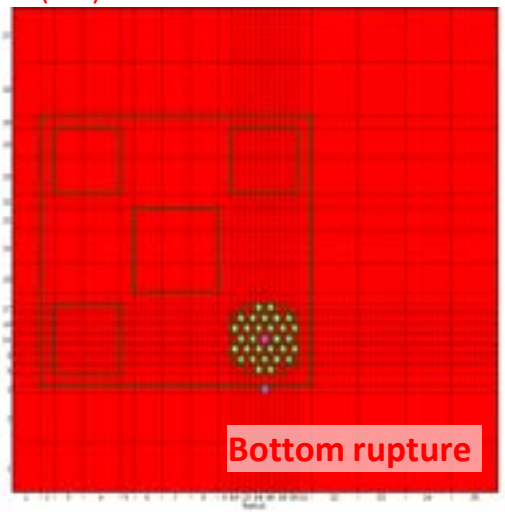


section A-A

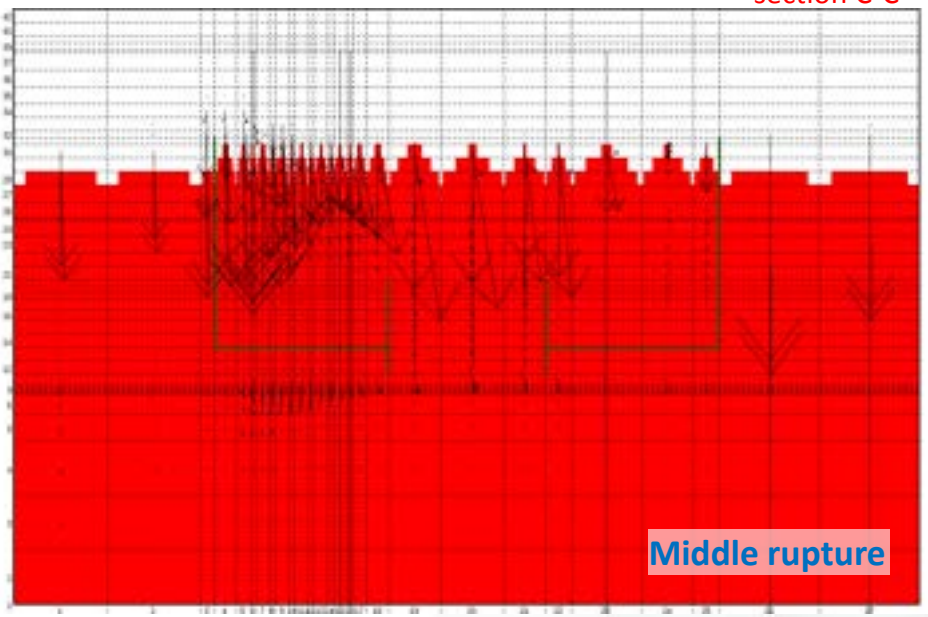


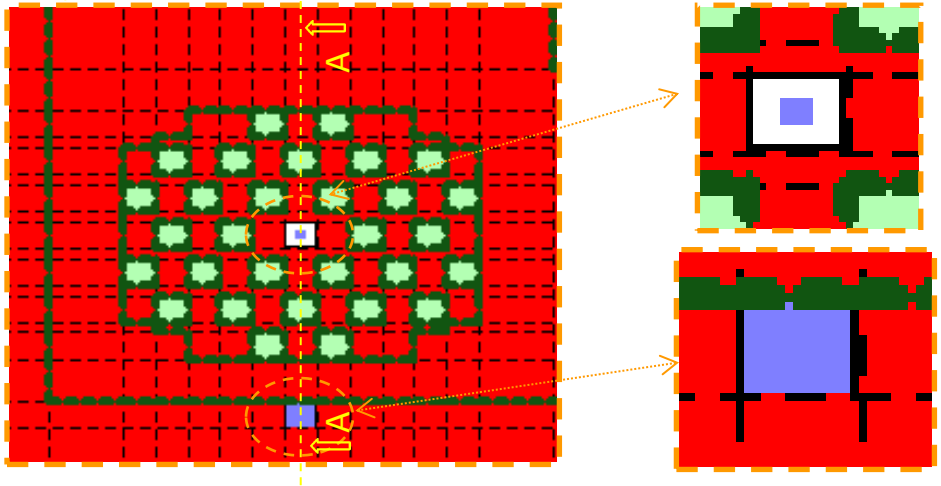
section B-B (J15)





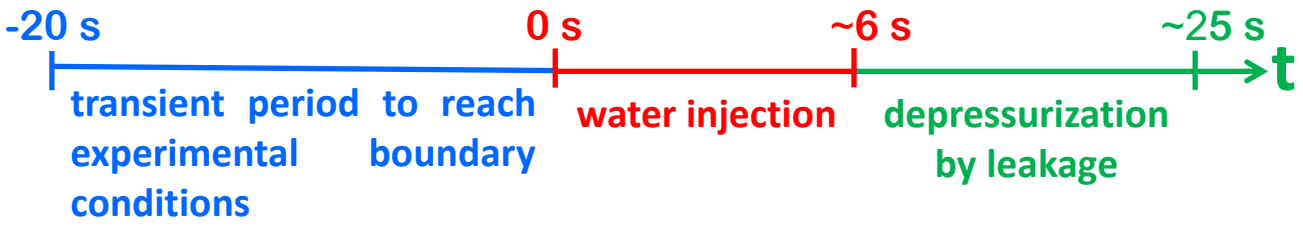
section C-C

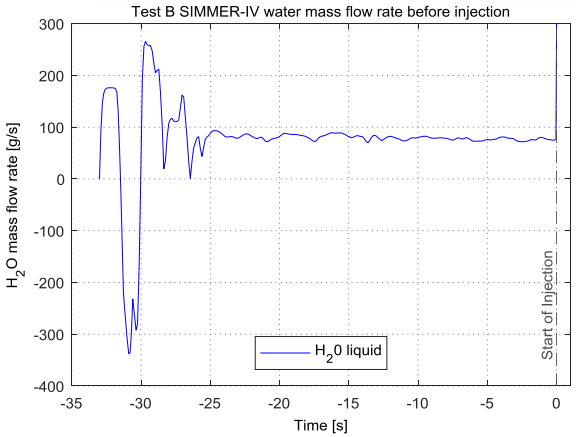




Test SGTR-B post-test analysis

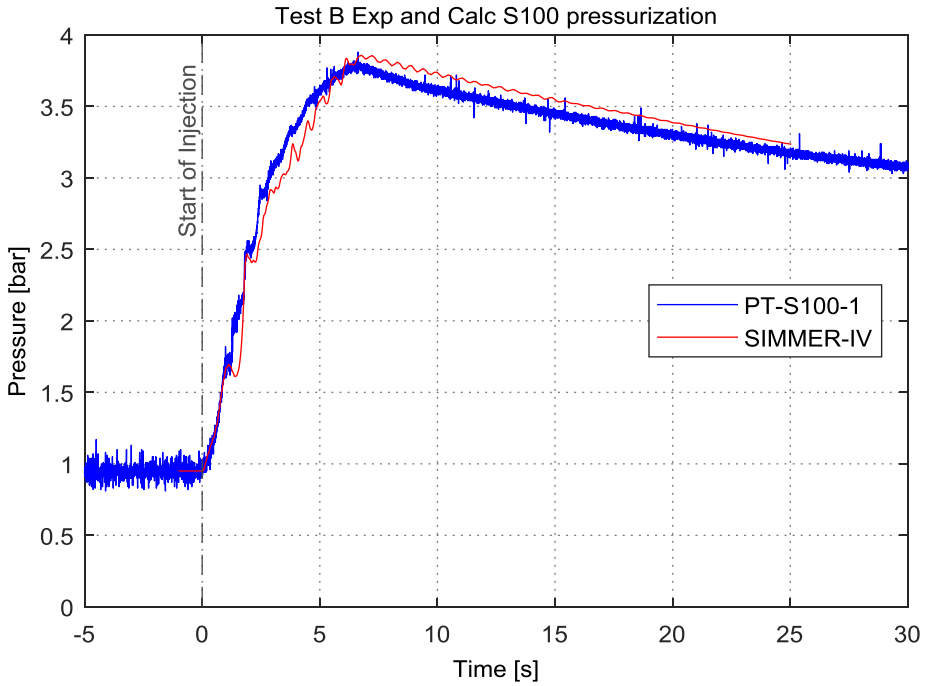
Test B temporal phases of SIMMER-IV calculation

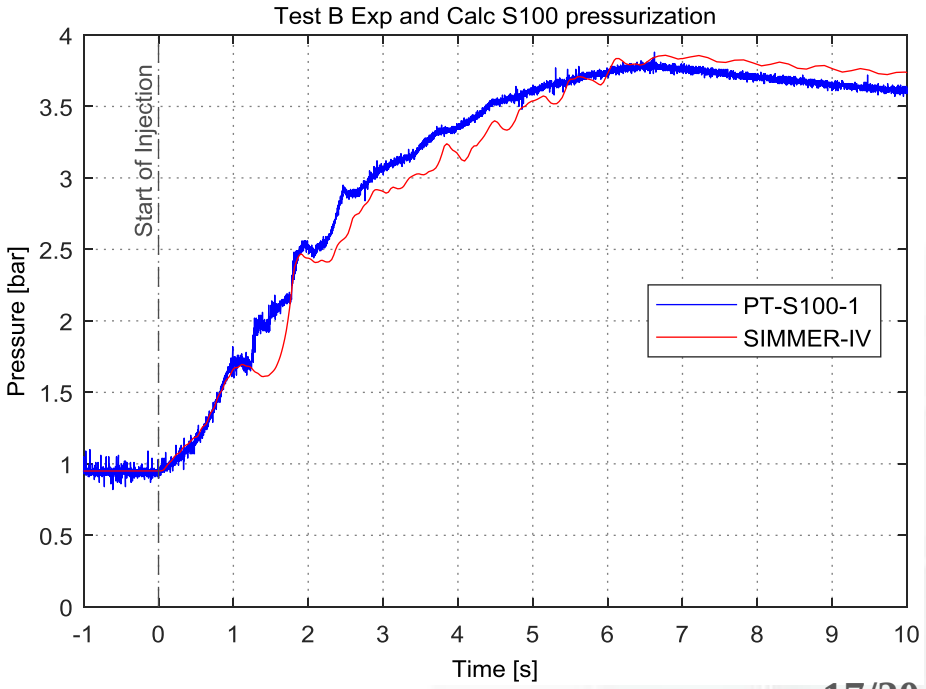




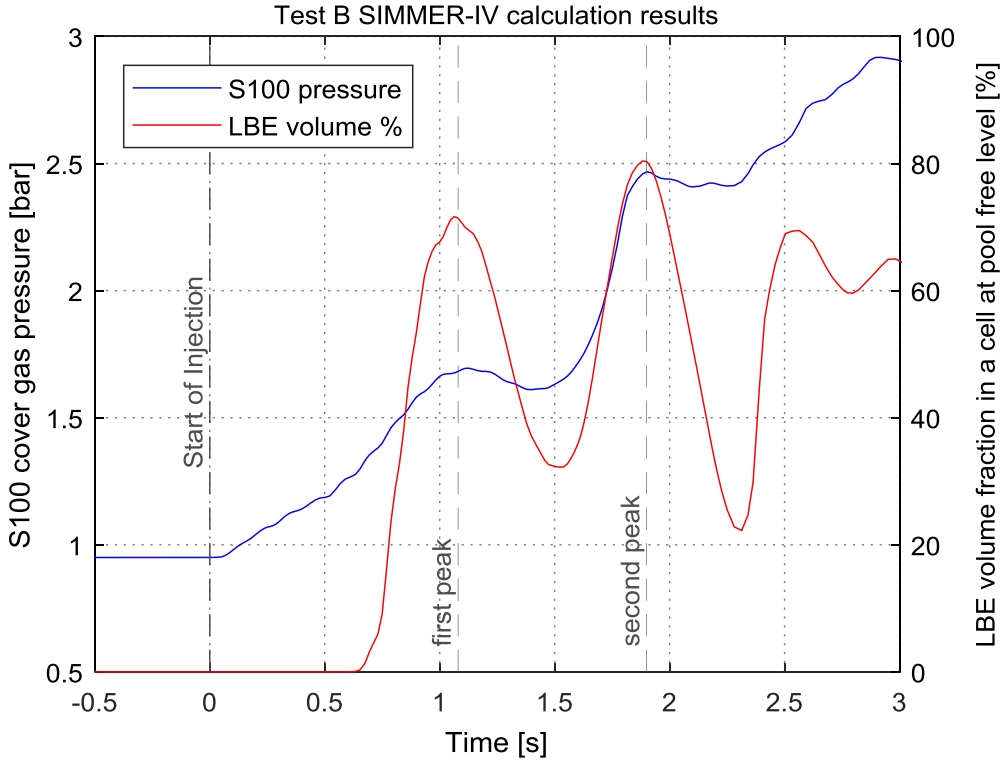
Test B water mass flow rate before tube rupture, by SIMMER-IV

Test B calculated and experimental pressure time trends in S100 cover gas

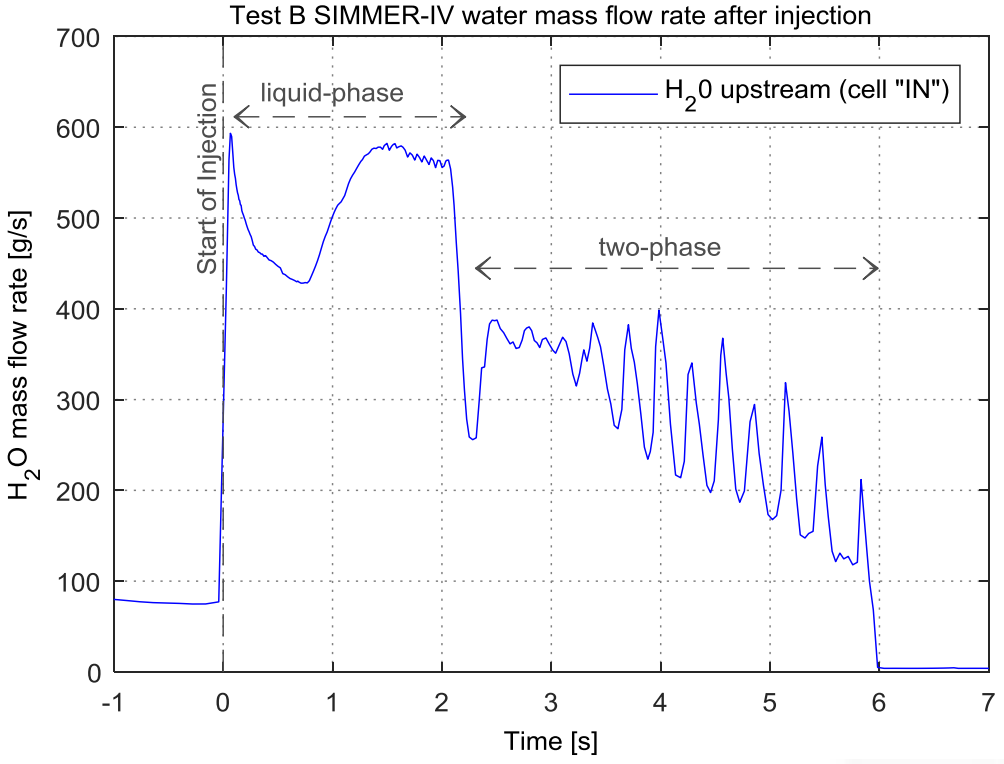




Test SGTR-B post-test analysis



Test B comparison of S100 pressurization and LBE free level oscillations, sloshing effect



Test B water mass flow rate time trend entering upstream water line

Conclusive remarks

- A dedicated test section was designed (supported by preliminary and detailed pre-tests), assembled, instrumented and implemented in CIRCE facility for SGTR test relevant for MYRRHA
- Four SGTR tests were successfully performed, two tests for both middle and bottom rupture scenarios (B/ICs coherent with MYRRHA, good repeatability)
- About 140 signals were acquired in each test (pressure, temperature, mass flow rate, strain, valves position …)
- Visual inspection of tubes surrounding the rupture did not show permanent deformation
- 6 pressurized tubes (surrounding the injector one) maintained their integrity during injection
- Post-test analysis by SIMMER-IV of SGTR-B (bottom rupture) showed good agreement with exp data (as for other tests)
- Wide database formation for code validation model development

Conclsive remarks

THANK YOU FOR YOUR ATTENTION

ALFRED

Conclusioni e Sviluppi futuri

Workshop Tematico: Gen-IV LFR: Stato Attuale della Tecnologia e Prospettive di Sviluppo - Bologna, 26-27 Sett. 2017

Michele Frignani

Mariano Tarantino

ALFRED

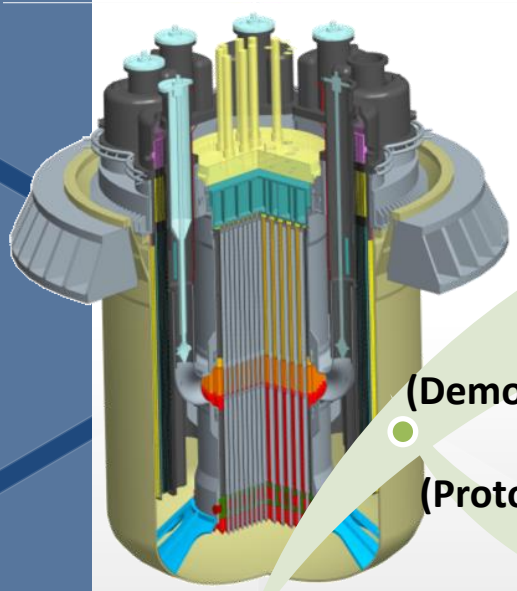
Outline

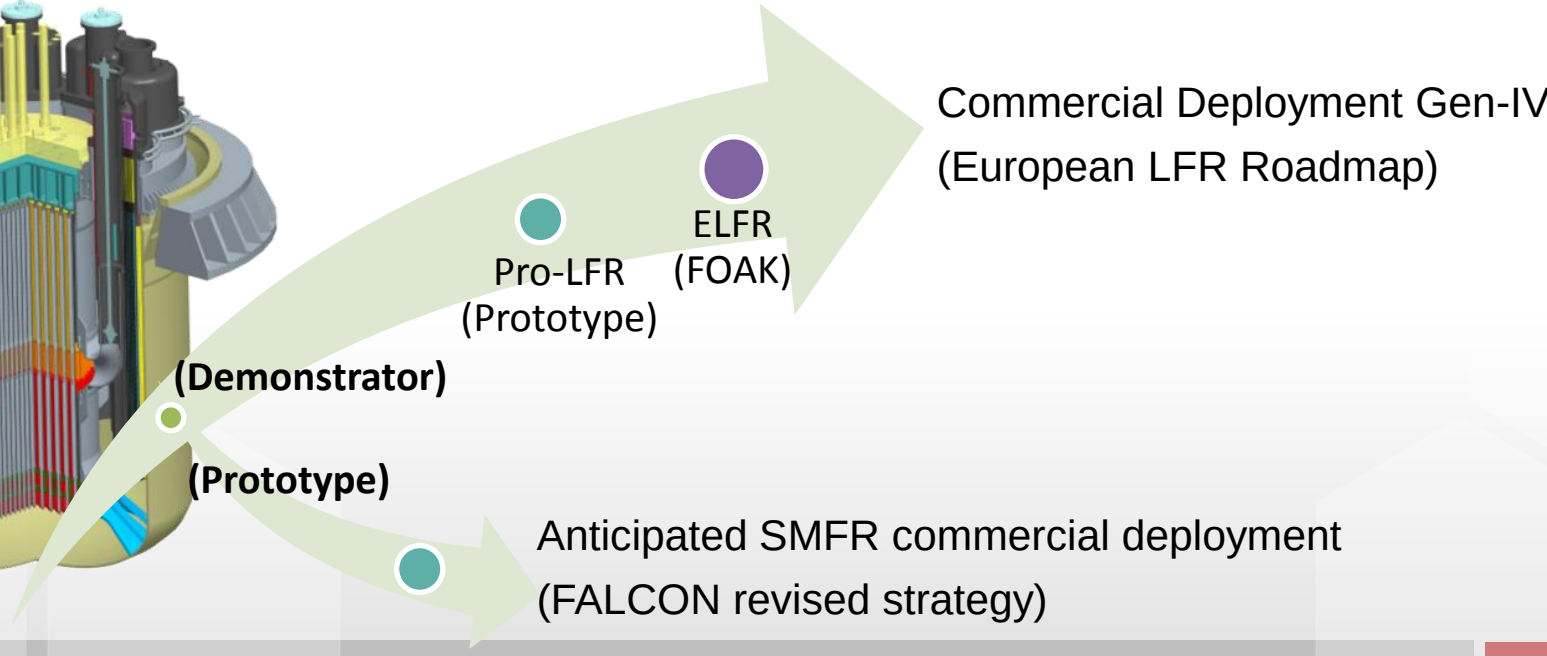
- The objective
- The drivers
- The challenges
- The roadmap
- Conclusions



ALFRED as LFR demonstrator with SMR-oriented features

- Deployment of a Lead-cooled Fast Reactor Demonstrator, having
  - SMR-oriented features, aimed at being a competitive option for the future Nuclear Power Plants
  - longer-term potentialities to demonstrate that the LFR technology can meet the goals set out by GIF for Generation-IV reactors





Outline

- The objective
- The drivers
- The challenges
- The roadmap
- Conclusions



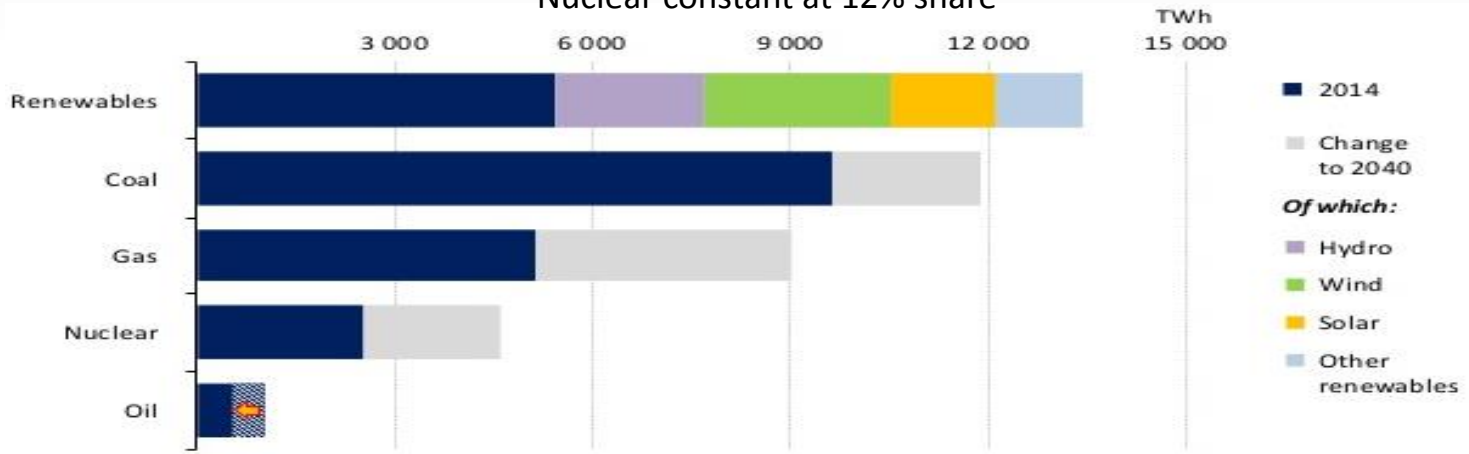
ALFRED

Energy needs and Nuclear power

FALCON

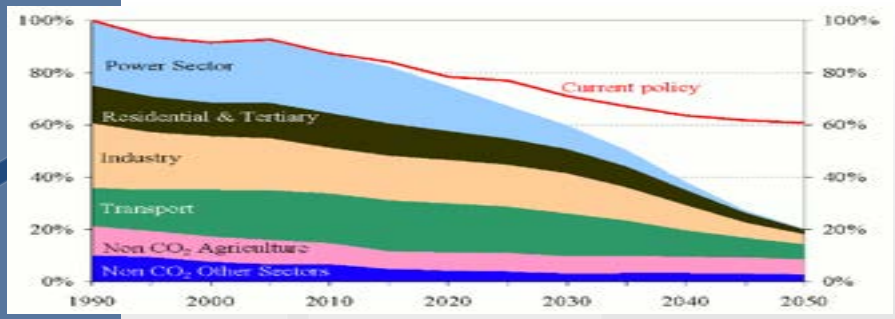
World Energy Outlook 2014, IEA (2014)

- +37% energy demand by 2040
- Nuclear constant at 12% share



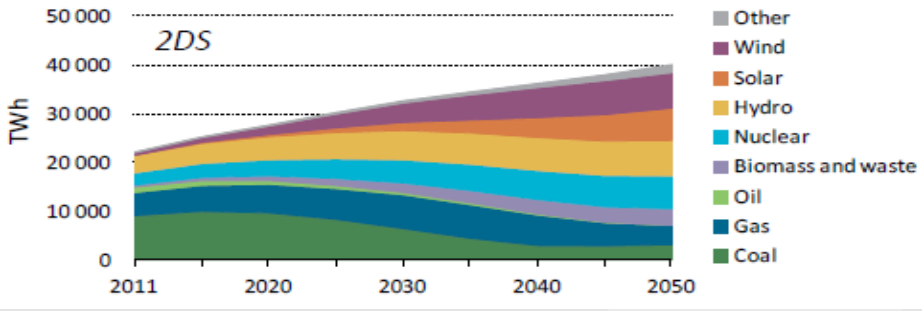
Energy Roadmap 2050, EC (2012)

- By 2050, greenhouse gas emissions by 80-95% with respect to reference levels of 1990



Technology Roadmap, IEA (2015)

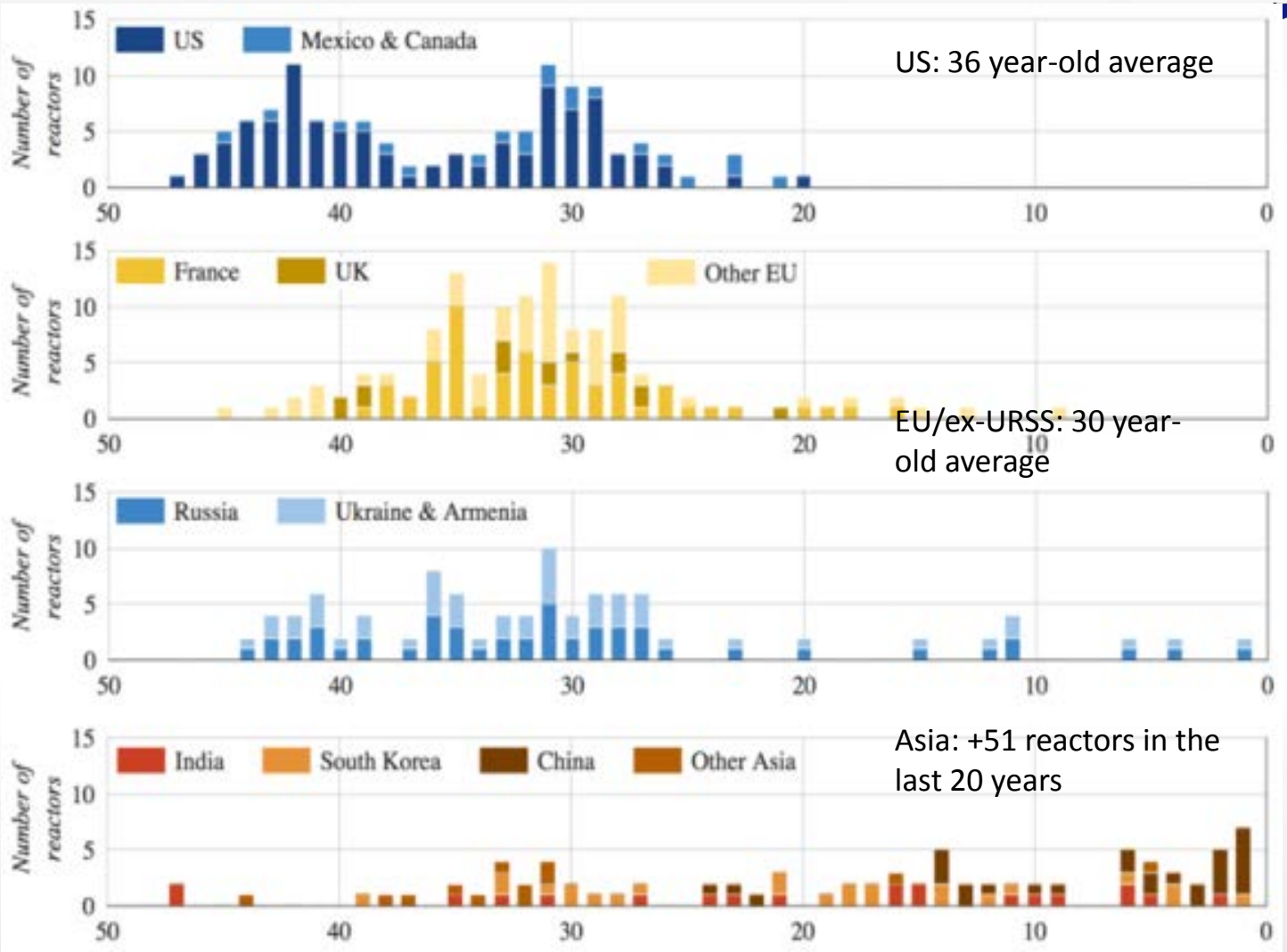
- Nuclear capacity in 2014: 396 GW
- Projections by 2050: >930 GW



Plant aging and retirement

World Energy Outlook 2014, IEA (2014)

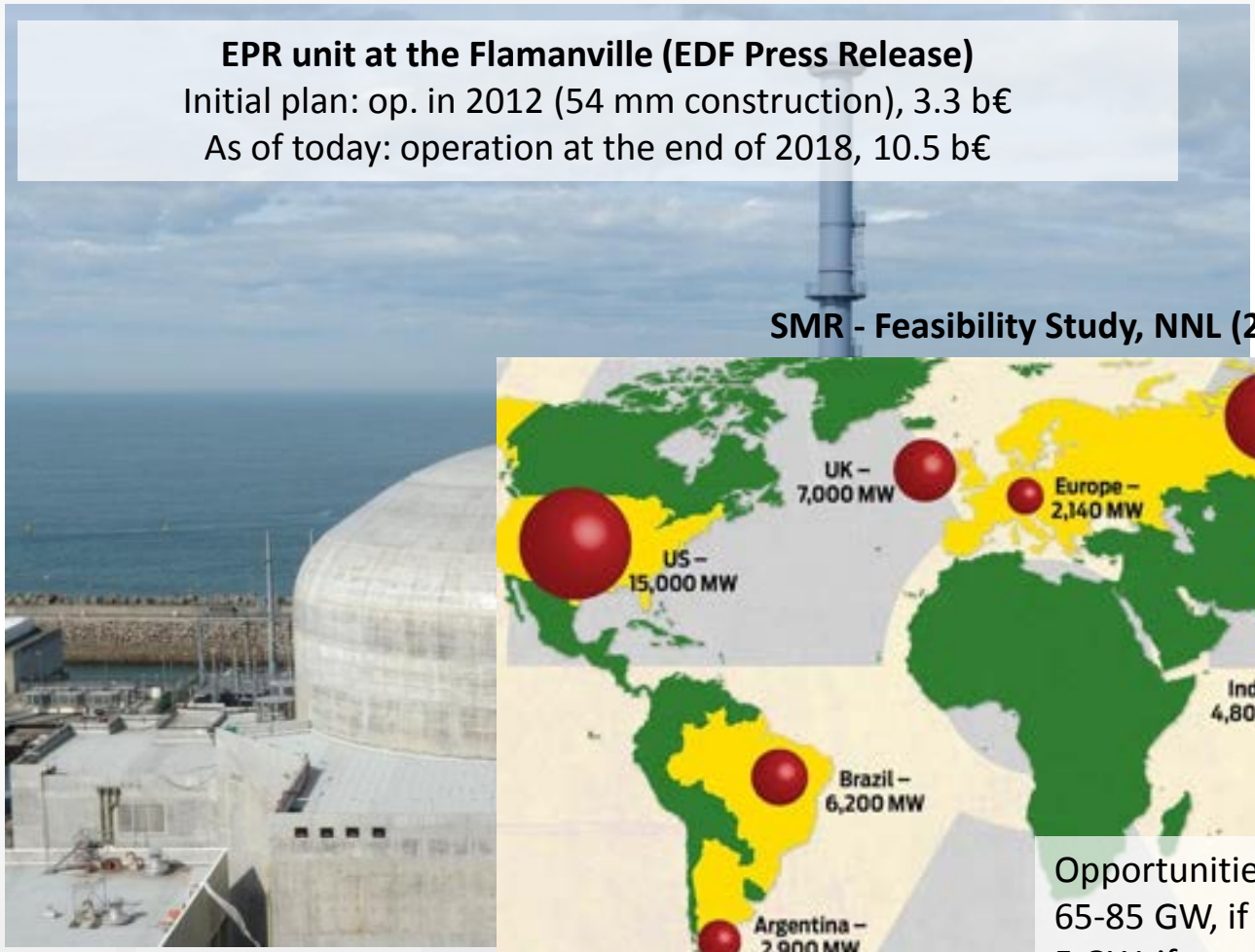
38% of today's capacity expected to retire by 2040



Challenges to the "economy of scale"

FALCON

EPR unit at the Flamanville (EDF Press Release)
Initial plan: op. in 2012 (54 mm construction), 3.3 b€
As of today: operation at the end of 2018, 10.5 b€

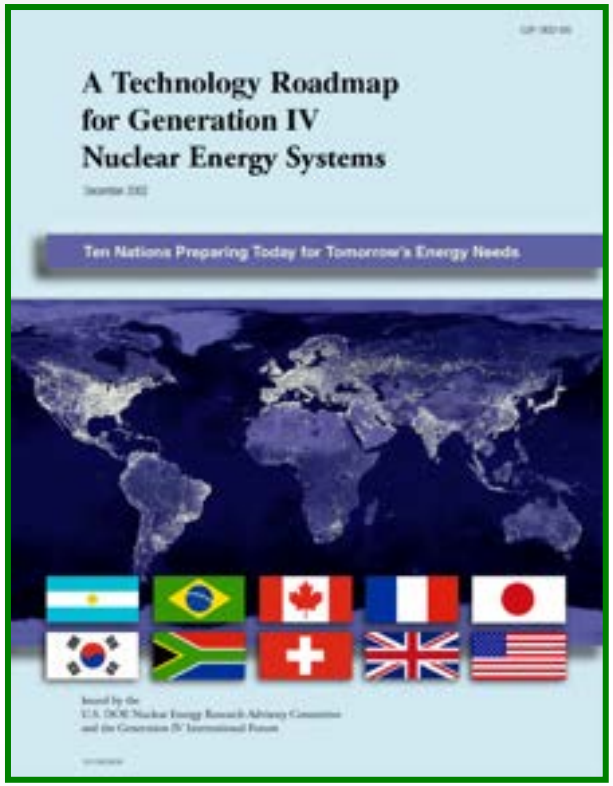


SMR - Feasibility Study, NNL (2014)



Opportunities by 2035:
65-85 GW, if cost-competitive
5 GW, if not

Advanced reactors and Generation-IV goals





The **industrial interest** will decrease if the time-frame is too far

Outline

- The objective
- The drivers
- The challenges
- The roadmap
- Conclusions



Design

- Challenges
  - Applicable design **codes and standards**
    - accepted basis for the **design verification** of any technical solution implemented in a nuclear facility
    - **innovative** coolants and selected candidate materials not fully covered
  - **Technology readiness** for main components
    - steam generators and primary pumps are **prototypical**
    - **tested** on small scale in experimental facilities
    - need for supporting **qualification** campaigns
- Actions
  - **Researchers** shall identify **short term options** affected by minimum associated risk
  - **Designers** shall keep sufficient **flexibility** to integrate new promising options into the design as soon as sufficient experience is gained

Safety

- Challenges
  - Unknowns concerning **design extended conditions**
    - very unlikely events or sequence of events imposed to be **postulated**
    - **over-complicate** design provisions to mitigate consequence
  - **Verification and validation** of computational codes and nuclear data
    - Extensive **benchmarking** for t/h codes, but dedicated verification and validation program is needed
    - **uncertainties** on nuclear data and their propagation under investigation
- Actions
  - **Designers** shall implement technical choices aimed at increasing the safety **margins** against the allowable limits in the most representative environment
  - Achieving a **robust design** will provide the necessary basis for the final safety demonstration and will further improve knowledge (for researchers, designers, operators, licensing bodies, utilities) in a safe and secure way

Operation

- Challenges
  - Availability of non-nuclear **research facilities** on HLM
    - most of the **operational experience** gathered through experimental facilities
    - selected technological choices not always **scalable** and/or applicable
  - **Delays** in nuclear supporting infrastructures based on HLM
    - original LFR roadmap mined by the lack of **financial and political support**
    - limited **return of operational experience** for the timeframe of interest
- Actions
  - **Designers** shall identify the target performances of an industrial scale reactor and assess the maximum credible **scaling factor** that could be achieved with a relatively low risk
  - **Researchers** shall define the roadmap and **necessary infrastructures** to achieve the objective

Licensing

- Challenges
  - Lack of experience on **non-LWR technology**
    - experience of safety authority and TSOs typically related to LWR or HWR
    - regulatory framework usually **prescriptive** and strongly oriented to LWR
  - Difficulties in engaging **early dialogues**
    - for well-known technologies, general **trend** towards **COLs** to reduce overall risk
    - general difficulty in getting a "**licensability review**" as first step
- Actions
  - **Researchers** and **designers** shall enhance **early dialogues** with Safety Authorities and TSOs, in order to have preliminary feedback to re-orient the design
  - Due to uncertainties related to licensing of a first LFR in western countries, **designers** shall address **safety concerns** through design solutions or increased margins against uncertainties

Financing

- Challenges
  - Difficulties in estimating the **up-front** necessary investment
    - different approaches providing **apparently coherent** estimates
    - **questionable** reliability (in general, see ongoing conventional projects)
  - Difficulties in guaranteeing any **return of investment**
    - **uncertainties** related to the reliability of not yet proven technologies
    - business case to demonstrate the installation is **financially worthwhile**
- Actions
  - A **shorter term** opportunity based on technologies of **higher readiness level** might attract additional investments, thanks to the lower initial investment, the added flexibility, and the shorter implementation of lessons learned
  - **Private investors** could be attracted by different perspectives and play a **leverage role** at national level, if a strategic vision on competitiveness is shared

Outline

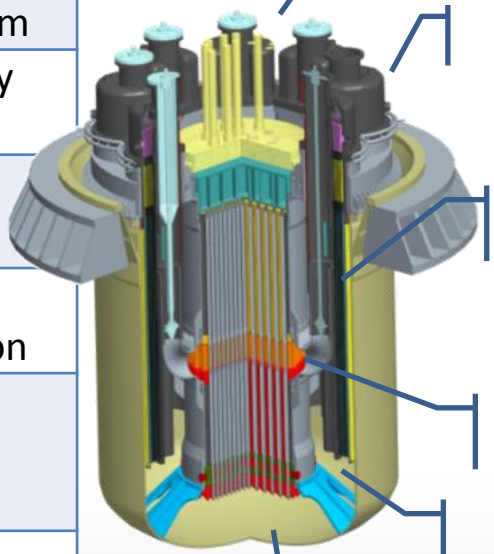
- The objective
- The drivers
- The challenges
- The roadmap
- Conclusions



ALFRED to address the challenges

FALCON

	LFR Demonstrator
Size	Order of few hundreds of MWth
Target rationale	Easily scalable Similar technological solutions Solutions not optimized
Design	Design focusing on short-term R&D in parallel targeting longer-term
Safety	Reasonable power to address safety concerns/unknowns with margins
Licensing	Means to improve the regulatory framework to be used later
Operation	Gain operational experience Staged commissioning and operation
Financing	Shortened time-to-market Strengthening synergies and opportunities of PPP
Schedule	7-10 years for licensing and construction 5+ years of operation Commercialization may require 15+ years



Relatively low power (300 MWth)

Compact design
Removable components
Proven technologies

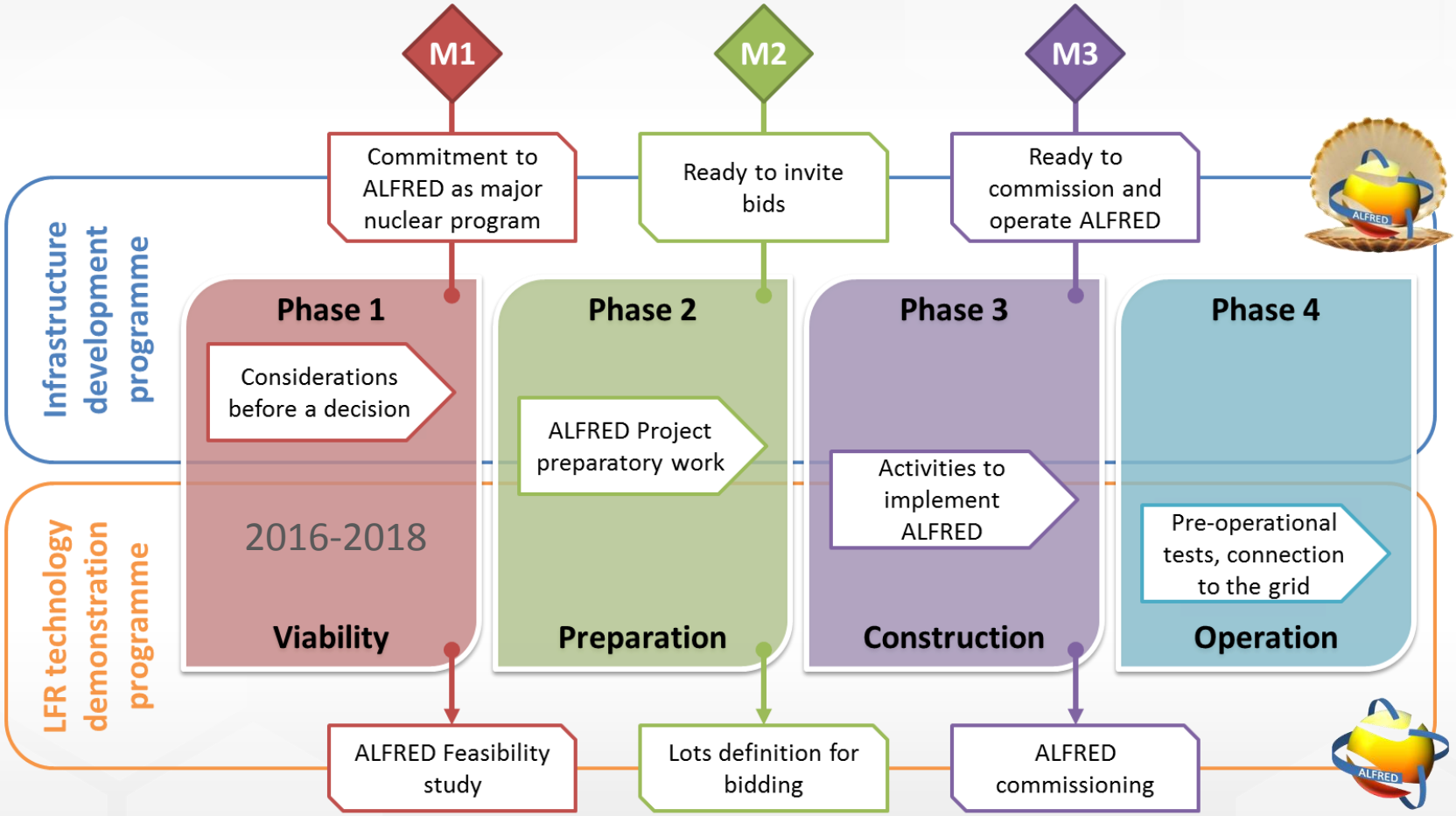
Simple flow path
Efficient natural circulation

Inner vessel
Enclosing hot pool

Molten lead as coolant
Excellent intrinsic prop.
Manageable neg. prop.

Pool type Primary System

ALFRED General Roadmap



Outline

- The objective
- The drivers
- The challenges
- The roadmap
- Conclusions









Conclusioni e Priorità

- Progettazione di Sistema e Analisi di Sicurezza
- Sviluppo e Validazione di Codici e Modelli Multi-fisici per Analisi di Sicurezza di Reattori Veloci di IV Generazione
- Sviluppo Materiali e Chimica del Refrigerante
- Termofluidodinamica dei Sistemi LFR

- Maggiori comunicazioni tra progettisti e ricercatori
- Programma sistematico di R&D
- Attenzione al Quality Management System
- Attenzione alle soluzioni per lo short term, senza dimenticarsi del long-term nell'ottica della nuova strategia e visione per ALFRED

ALFRED

Grazie a tutti per la partecipazione!

FALCON

Short-term



Long-term

